The influence of particle shape on bedload transport in coarse-bed river channels

Demir, Tuncer

THE INFLUENCE OF PARTICLE SHAPE ON BEDLOAD TRANSPORT IN COARSE-BED RIVER CHANNELS

by
Tuncer Demir

Doctor of Philosophy

Department of Geography
University of Durham
June 2000

ABSTRACT

This thesis investigates the influence of bed material shape on sediment transport in gravel-bed rivers. The approach involves a combined series of field and laboratory experiments. Magnetic tracing experiments were carried out at three experimental sites in two Pennine gravel-bed streams. The specific aim of these experiments was to quantify the selective transport of different shapes of coarse river gravel and determine their spatial sorting within a natural stream channel. A total of 900 tracers in three size groups (32- 64 mm, 64-128 mm and greater than 128 mm) and four shape classes (spheres, blades, rod and discs) were prepared for each of the three sites. In the laboratory, tilting table experiments were carried out to clarify the mechanistic behaviour of different particle shapes, sizes and orientations on a variety of artificial and naturally formed bed roughnesses. Using strobe-light photography visualisation experiments were undertaken with natural and artificially-moulded gravel-size particles of differing shape, size and weight in order to investigate the influence of shape on settling, grain impact, initial motion and transport paths of gravel-size particles.

Results of the magnetic tracing experiments showed that there was both size and shape selectivity in bedload transport. Preferential movement occurred in the small and medium particle size classes with tracers concentrated along the channel thalweg. Sphere-shaped particles were transported the greatest distance and in greatest numbers. Rods also moved preferentially, while discs showed a lesser degree of transport and blades hardly moved at all.

Results from the tilting table experiments highlight the importance of roundness as well as particle form and particle orientation in controlling thresholds of entrainment. In terms of size, friction angle was found to depend on the ratio of the diameter of the test particle to be moved to that it rests upon (d/D). Shape and orientation were found to be important parameters influencing friction angles. On a given bed roughness and for a constant size non-spherical test particles showed greater friction angles than spherical ones. A very clear difference was found in friction angle distributions between sphere, transverse rod and other flat-shaped particles, namely, blades with parallel and transverse orientations, disc, and rod with parallel orientations.

Visualisation experiments indicated that shape is an important particle characteristic that has a significant effect on settling rates and also the mode of near bed transport. These effects increase with greater particle sizes. The departure of a particle from a sphere leads to a decrease in its settling velocity. Experiments, across a range of test sizes showed that when compared to a sphere of equivalent weight and density, sphere and rod-shaped particles tend to settle the fastest and move by rolling. Discs and blades showed slower settling rates and, in most instances, moved by sliding. Experiments carried out with irregularly-shaped, natural particles show greater variability in settling behaviour and irregular patterns of motion. For every size group, sphere and rod shaped particles have lower critical angles of initial motion than blade and disc-shapes. Regardless of shape, greater bed roughness, or decreasing particle size results in an increase in the critical angle for motion.

ACKNOWLEDGEMENTS

My particular thanks to the Turkish Government and the Harran University for funding this research. During the course of this study period I greatly acknowledge the support and advice given to me by several people to whom I wish to offer my sincere thanks. First and foremost I would like to thank my supervisor Dr. Jeff Warburton for his guidance, enormous support, enthusiasm and hospitality throughout this study. I wish him and his wife Dr. Christine Warburton and lovely daughter Isabel Maya all the very best. I am also grateful to David Bridgland, my second supervisor, for his friendly advice, support and direction during the study period. I have received much help and friendly approach from the all the technical stuff, i.e. Derek Coates, Ian Dennison, Stella Henderson, Andrew Hudspeth, Derek Hudspeth, Michele Johnson, Eddie Million and Brain Priestley, to whom I owe my sincere thanks. I wish to express my thanks and appreciation to Dr. Muzaffer Bakirci, Dr. Mustafa Cin, Melanie Danks, and Richard Johnson for their unforgettable help and companionship during those rainy, windy, cold and dark days of fieldwork in Moor House. Lots of thanks to Joe Holden and Andy Mills for helping me to improve my poor mathematics. Lots of thanks to Richard Johnson and John Thompson because of their great hospitability for inviting me to their summer time (!) traditional-barbeque parties. I had also the pleasure of meeting many unforgettable friends, Richard Bromiley, Dr. Helen Dunsford, Sarah Hamilton, Vicky Holliday, Eleanor Rocksborough-Smith during my stay in Durham.

I owe my greatest thanks to Meryem for her help, encouragement, and support throughout every stage of my study period.

I expressed my thanks and appreciation to my cousin Dr. Savas Demir who made all the necessary communication and arrangements for my entry into British Universities at a time when I was unable to speak or read English. Finally I would like to thank every member of my family to whom I owe an enormous depth of gratitude: for their continuous backing throughout my life, for endless love, and support.

This thesis is dedicated to the memory of ***Dr. Savas Demir*** *who passed away in his early age of life.*

I confirm that no part of the material presented in this thesis has previously been submitted by me or any other person for a degree in this or any other university. I all cases, where it is relevant, material from the work of others has been acknowledged.

Signed: 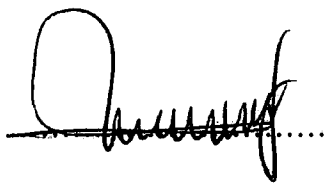

Date: 18.8.2000

TABLE OF CONTENTS

CHAPTER 8: Conclusions

LIST OF FIGURES

LIST OF TABLES

LIST OF APPENDICES

CHAPTER 1

1.1 INTRODUCTION

Construction and operation of major engineering works have seriously affected many river systems. Examples include the development and management of water resources, navigation, power generation, flood control schemes, land use changes and modifications to drainage systems (especially in agriculture and forested areas). Besides these, in some areas channels have been dredged and straightened; banks raised and protected; natural vegetation removed or changed; channel flow modified; and water quality altered. Such changes have had marked effects on river systems and their natural dynamics, either causing instability or adversely affecting the ecological and environmental characteristics of the channel (Lewin, 1981; Hey *et al.,* 1982). Ever since scientists have become aware of these problems, many researchers, especially hydrologists, engineers, and geomorphologists have begun to investigate flow hydraulics, channel morphology and dynamics in order to better understand the processes and morphology of rivers.

Sediment transport is an extremely important process in fluvial geomorphology. Despite a considerable body of literature on sediment transport, there are still many problems in river management arising from the inadequate prediction of sediment behavior during flood flows. This is because the mechanisms of entrainment and transport of sediment are complex and governed by many categories of variables. Some of these variables have been attributed to the composition and arrangement of the particles that make up the channel bed (Reid *et al.,* 1997; McEwan, 1999), the importance of hydraulic condition and the characteristics of individual moving particles (Hassan and Church, 1990; Ferguson and Asworth, 1992).

Although there have been considerable advances in the understanding of transport mechanisms of small-size particles, the measurement and assessment of bedload transport still remains an extremely difficult task. Indeed many investigators have shown that even for steady discharge, bedload transport rates are unsteady and uneven across the stream. Some difficulties are associated with measurement

techniques, because existing techniques are relatively few and sometimes unreliable. Therefore no single apparatus or procedure, whether it be theoretical or empirical, has been universally accepted as completely adequate for the determination of bedload discharge.

Because of the practical difficulties encountered in the direct and indirect measurement techniques, some investigators have concentrated on developing a series of empirically calibrated bedload equations (Lechalas, 1871; du Boys, 1990; Bagnold, 1980; Agostino and Lenzi, 1999). Given information, such as stream velocity, discharge or stream power and measures of bed material size and sorting, bedload transport rates may be calculated rather than directly measured. Some of these equations involve prediction of transport rates in terms of excess shear stress above the threshold value at which transport starts. Some involve computation of total sediment transport rates rather than the bedload alone. However, no theoretical formula has been found to offer a completely satisfactory estimation procedure, although in the absence of field measurement theoretical data may be the only data available.

1.2 DEFINITION OF BEDLOAD AND DIFFERENCES BETWEEN COARSE-BED UPLAND STREAMS AND LOWLAND RIVERS

The sediment load transported by a stream consists of two parts: solution load (dissolved load) and solid load. Solution load that is derived largely from bedrock weathering is dispersed throughout the flow. Solid load consists of two types: suspended load and bed material load. *Suspended load* is of fine calibre and includes all particles prevented from falling to the channel bed by the upward momentum imparted by eddies within turbulent flows (Knighton, 1998). The finest fraction of suspended load, consisting of very small clay-sized particles, is termed *wash load* and is able to stay in permanent suspension as long as some flow is maintained. The actual volume of wash load moved may be limited by supply, but there is always a supply of bed material available for transport according to the capability of the river. *Bed material load*, on the other hand, consists of coarse clastic materials, normally occurring in the channel bed, which are sporadically moved, usually along the bed, during high flow events (Church and Gilbert, 1975, Gomez, 1991, Reid *et al.*, 1997).

Two major mechanisms have been identified for clastic sediment movement: (a) movement of material in suspension, that is, the weight of the sediment is supported by

water currents, and (b) movement of material as *bedload*, that is by rolling, sliding, or skipping along the stream bed (Bagnold, 1966, 1973). The proportions of load vary greatly, controlled by climatic and structural factors. For rivers, bedload usually amounts to less than 10 percent of total sediment transport.

Rolling and sliding are primary modes of bedload transport in gravel bed rivers, while saltation, in which grains hop over the bed in a series of low trajectories, is largely restricted to sand and fine gravel (Knighton, 1998). Once shear stresses just exceed the critical level necessary for entrainment, movement will probably occur by sliding or rolling of particles. In such circumstances, the submerged weight of the particle is largely borne by the bed of the channel (hence the term *bedload* is used to describe it). Depending on flow conditions, during transport material may intermittently lose contact with the bed by bouncing.

Although in most environments, particularly in lowland zones, the bed material load is the least important of the three components of transport, in mountainous environments, where the supply of coarse material from the slope system is high, it may be greater than the combined dissolved and suspended loads (Lane and Borland, 1951; Simons and Senturk, 1977; Hayward, 1980; Lauffer and Sommer, 1982; Thompson *et al.*, 1992). In general, bedload will rarely include sediment that is finer than 0.1-0.2 mm in diameter, because once disturbed these fine particles tend to go directly into suspension (Sundborg, 1956).

Although there is a considerable body of literature on sediment transport in lowland rivers, less is known about the pattern of sediment transport in coarse-bed upland streams. Studies have shown that there are significant differences between upland and lowland gravel-bed rivers (Simons and Simons, 1987). Bathurst (1987) stressed that bedload transport rates in mountain rivers are higher than those in lowland rivers and the actual mechanisms of bedload transport are poorly understood. Lack of understanding is attributed to difficulties in the field measurement of bedload transport and associated hydraulic conditions in steep, coarse-bed channels (Carling, 1989). Some of these differences are summarised by Newson (1981). He points out several important characteristics of mountain and piedmont streams. For example, mountain streams have steep channels and side slopes without an intervening floodplain. The dominant bed material consists of coarse bedload. Flow resistance is complex and generally controlled by large-scale roughness elements and the local characteristics of the bed material (such as shape, size and density). Under conditions of steady flow there is a wide scatter in the

relationship between hydraulic variables and bedload transport in coarse-bed mountain rivers. Several factors have been identified as causing this scatter in the sediment transport relationship. These include sedimentological characteristics of the bed (e.g. microform bed roughness elements) (Jackson & Beschta, 1982; Parker & Klingeman, 1982; Hoey, 1989; Reid *et al.*, 1992), the progressive construction of an armour layer during waning flood flows (Proffitt and Sutherland, 1983; Gomez, 1983), variable cementation of the gravel framework by interstitial matrices (Frostick *et al.*, 1984; McEwan, 1999), characteristics of individual moving particles (e.g. size shape, density, etc.) (Hassan and Church, 1990) and pool-riffle sequences (Robert, 1990).

Another important aspect is associated with sediment supply and the energy levels of geomorphic processes in mountain streams as compared with their lowland counterparts. Newson (1981) points out that due to high residual proportion of coarse-bed material the majority of sediment transport occurs as bedload. This transport requires quite high thresholds of critical tractive velocity, therefore bedload transport is restricted largely to periods of flood. Indeed many investigators, such as Davies and Pearce (1981), emphasise that sediment supply and transport processes in mountain areas are highly episodic. Erosion processes are often accelerated, and sediment supply to the stream channels increases, during extreme climatic events or following marked changes in land use. Pearce and Watson (1983) also state that the residence time of sediment in mountain rivers is on the order of decades or less because the transport capacity of steep streams often greatly exceeds the mobility of material under normal or even extreme conditions. Newson (1979) indicated that the sensitivity and the quick response to erosion processes in uplands rivers means that it is quite usual to study river processes over relatively short periods in upland areas, whereas the same processes might take a lifetime of research in the lowlands. In addition, Carson and Kirkby (1972) and Newson, (1981) have pointed out that the rate of erosion increases with relief and in upland streams the amount of transported bedload is higher than in the lowlands.

1.3 IMPORTANCE OF BEDLOAD TRANSPORT IN UPLAND STREAMS

Bedload transport in upland streams and rivers has gained the attention of earth scientists and engineers for the following reasons:

(a) Sustained interest in bedload transport was initiated directly as a consequence of the need to determine the quantity of bed material transport in navigable channels (Du Boys, 1879; Davis, 1900).

(b) Bedload transport provides the major process linking channel form and hydraulics. Morphological change (including bank erosion) in rivers is largely governed by bedload transport (Gomez, 1991).

(c) Engineering projects require an understanding of sediment movement in rivers or channels transporting predominantly coarse-bedload and sand. This is because the movement of river bed material as bedload is often responsible for problems associated with shifting channels, with loss of reservoir capacity and with local difficulties that arise in water abstraction, flooding, loss of agricultural land and navigation (Reid *et al.*, 1985).

(d) Bedload material is an important component of ancient geomorphological cycles because a significant proportion of the geological column consists of alluvial sandstones that contain particles coarser than 0.5 mm in diameter (Meade *et al.,* 1990) hence knowledge of bedload processes is important in geological studies.

More specifically, in the UK, land use changes, such as afforestation, livestock changes and engineering constructions in upland areas frequently produce increases in bedload transport which, via erosion or sedimentation, can destabilise activities in river systems and cause serious problems for river management (Newson, 1979). The decline in the use of river gravel for building roads during the last century in Britain has already had an impact on bedload channels and Clayton (1951) has indicated that it has been a major factor in creating problems of aggradation in some Lake District streams. In some areas of Britain, however, commercial extraction of sand and gravel continues and it has been estimated, for example, that over 130000 tonnes of material has been removed from the upper Clyde (Fleming, cited in Lewin, 1981).

Although coarse material transport is an important part of many fluvial problems, geomorphologists and engineers have only relatively recently attempted to examine sediment production and transport processes in coarse-bed rivers in upland areas. Transport mechanisms of coarse-bedload in mountain rivers with irregular beds are still relatively poorly understood (Ergenzinger and Custer, 1983).

1.4 FACTORS AND PROCESSES GOVERNING BEDLOAD TRANSPORT

Movement of bedload is a complex phenomenon and it is controlled mainly by three principal categories of variables and their interactions (Hassan and Church, 1990) (Ferguson & Ashworth, 1992; Figure 1) These are sedimentological characteristics of the bed (e.g. texture, packing, armouring, bed forms), hydraulic condition of the flow (e.g. discharge, velocity, duration), and characteristics of individual moving particles (e.g. size, shape, roundness). Figure 1.1 shows interrelationships between form, flow, and bedload in gravel-bed rivers and indicates that unsteady discharge through a system of highly non-uniform channels with rough beds produces a complicated spatial pattern of water velocity that changes over time. The vertical velocity gradient at any point determines the shear stress on the bed and this together with sediment availability governs the size and amount of bed material that can be moved. Bedload transport either maintains the existing size, shape and pattern of channels or alters the morphology by scour, fill and lateral migration. It may also alter the existing texture and structure of bed sediments by selective entrainment and deposition (Ferguson and Ashworth, 1992; Figure 1).

Knighton, (1998) also pointed out variables that influence the process of bed material transport. He classified the basic problems in bedload transport studies into two groups; (1) to understand the dynamic of material movement and (2) to establish a reliable relationship between sediment transport rate and relevant properties of the flow, fluid and sediment (Table 1.1).

Table 1.1 Variables related to bedload transport (After Knighton, 1998)

Flow properties	**Fluid properties**	**Sediment properties**	**Others**
Discharge	Kinematic viscosity	Density	Gravity (g)
Velocity	Density	Size	Planform geometry
Flow depth	Temperature	Sorting	
Width	Wash load concentration	Fall velocity	
Slope			
Resistance			

The movement of bedload is generally accepted to be the most difficult mode of sediment transport to measure. The difficulty arises from the fact that movement occurs at relatively high flow velocities when bedload particles are intermittently transported by the means of sliding, rolling or skipping along in almost continuous contact with the stream bed. Direct measurements are therefore relatively few and possibly unreliable. Although there have been many studies concerning the prediction of bed material transport rates in coarse-bed channels, most of these do not correspond well with actual transport rates (Naden, 1988; Gomez and Church, 1989a). This is because most of these studies are based on either a over-simplifying assumptions, such as steady flow, uniform bed roughness conditions, approximated or uniform distribution of shear stress in the cross profile, or uniform particle shape and size.

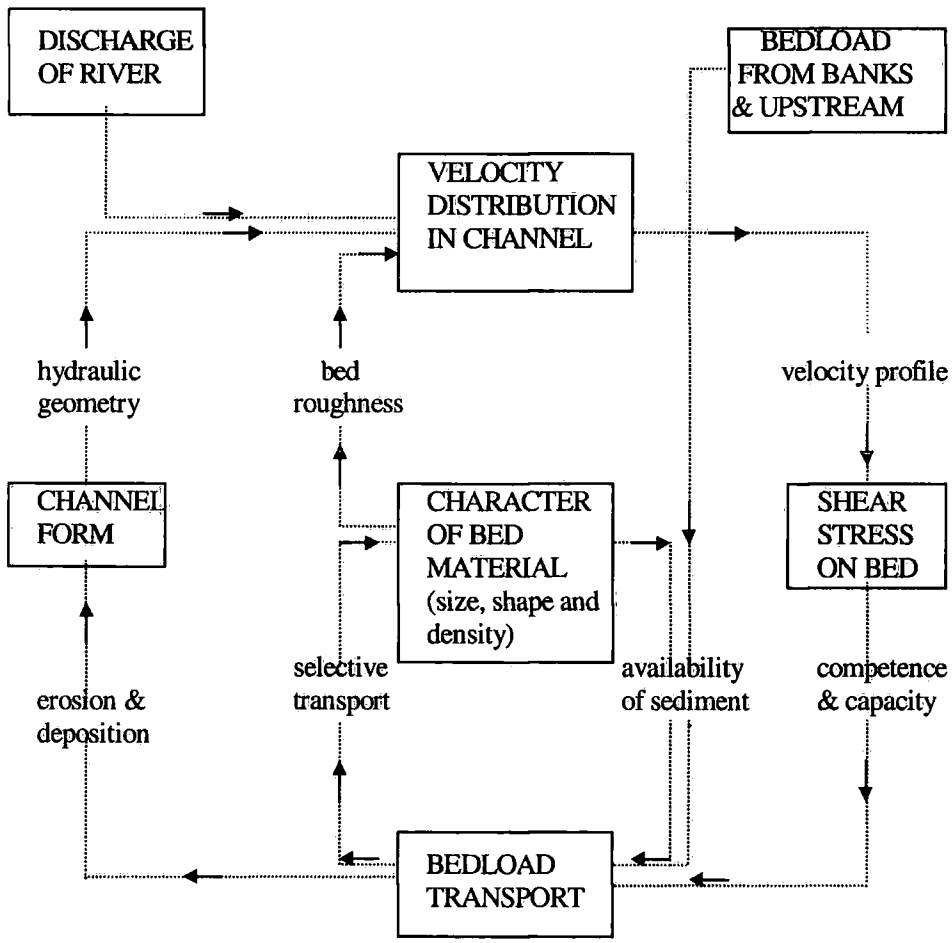

Figure 1.1 Interrelationship amongst form, flow, and sediments in active gravel-bed rivers (After Ferguson & Ashworth, 1992).

1.5 BEDLOAD SHAPE

Understanding of transport mechanisms of coarse-bedload in fluvial geomorphology has grown considerably in the last two decades as a result of improved theoretical comprehension and carefully conducted field and laboratory experiments (Wiberg and Smith, 1987; Ashworth and Ferguson, 1989; Gomez, 1991; Carling *et al.*, 1992). However, these studies have mainly tended to focus on bedload processes: equations to model thresholds of bedload movement and bedload transport rates (Bagnold, 1941, 1980; Wilcock, 1988; Wilcock and Southard, 1989); bedload sampling and measurement methods (Hubbel, 1964; Helley and Smith, 1971; Bathurst, 1987); measures of bedload character such as sorting, etc. (e.g. Waddell, 1932; Cailleux, 1947; Krumbein, 1941a) bedforms and their dynamics such as riffles, pools, bars, etc. Although extensive research has been carried out with regard to different aspects of bedload dynamics, it is rather surprising that the importance of bed material shape in influencing sediment transport in coarse-bed streams has received little attention.

Shape is thought to be significant factor because, all other factors being equal, the entrainment and hydraulic behavior of a particle depends on its shape, orientation and its relative projection above the mean bed level. Changes in dynamic conditions of transport, are reflected by changes in the shape-sorting, size and packing of deposits. However, despite its importance the exact mechanisms of how shape influences sediment transport are not fully understood and there are some conflicting results from existing studies. It is therefore timely that a systematic study should be directed at improving the understanding of bedload transport mechanisms in terms of particle shape.

1.5.1 Importance of bed material shape in bedload transport studies

In general, particle shape is analysed for three purposes: (a) to describe sedimentary materials, (b) to understand past events and the history of the materials, (c) as a basis for measuring present-day processes (Briggs, 1977).

The importance of shape in sediment transport is demonstrated by the fact that shape is one of the three properties that control bedload transport and settling. Shape, size and density are of fundamental importance in the hydrodynamic behaviour of the

particles. Different conditions of transport produce changes in the size, shape-sorting, and packing of deposits. Furthermore, the ratio of surface area to particle volume is important in controlling the response of particles to lifting forces, so that particles of low sphericity may behave differently from particles of high sphericity during transport. King (1966) stated that the analysis of pebble shape and its character is important in interpreting the origin of a deposit and may also provide evidence concerning the nature of transport. For example the ratio of length to breadth to height can be used to determine the probable movement of a pebble by rotation or sliding. Bed material shape characteristics, especially angularity or roundness, are particularly important for palaeoenvironmental reconstruction. This is because the shape of bed material is related to process, transport, degree of weathering (e.g. frost action) and other environmental factors. Thus shape may give some significant clues for the correlation and differentiation of deposits (Bridgland, 1986). Several studies, including both field and laboratory experiments, have shown how different particle shapes exert an influence on bedload transport in coarse-bed rivers (e.g. Wentworth, 1919; Krumbein, 1942; Unrug, 1957; Sneed and Folk, 1958; Bradley *et al.*, 1972; Komar and Li, 1986; Schmidt and Ergenzinger, 1992; Carling *et al.*, 1992; Schmidt and Gintz, 1995). Although shape is recognised as an important factor in bedload transport, there have been few systematic investigations into the transport of different particle forms. Many earlier studies, based on laboratory experiments using tumbling barrels, mills or circular flumes, mainly focused on effects of abrasion or sorting processes on particles of various shapes and sizes (e.g. Daubree 1879; Wentworth 1919; Marshall, 1927, Krumbein, 1941a; Rayleigh, 1942, 1944; Sarmiento, 1945; Potter, 1955; Kuenen, 1956; Bradley, 1970; Bradley *et al.*, 1972; Moriwaki *et al.*, 1985; Kodama, 1992). Early field investigations described the distribution of bed material shape and size characteristics along the long profile of streams and rivers (e.g. Plumley, 1948; Unrug, 1957; Sneed & Folk, 1958; Bradley, 1970: Bradley *et a.,* 1972; Brierley and Hickin, 1985; Knighton, 1980, 1982; Dawson, 1988; Shih and Komar, 1990; Komar and Carling, 1991). Only a few previous studies have investigated the hydraulic behaviour of different particle sizes and shapes during transport (e.g. Krumbein, 1942; Leopold *et al.,* 1966; Keller, 1970; Laronne and Carson, 1976; Carling *et al.,* 1992; Schmidt and Gintz, 1995). Thus until now very few systematically collected data sets have been available to show how particle shape influences bedload transport.

However, more recently the number of investigations into bedload transport involving the hydraulic behaviour of various bedload shapes and sizes has increased due to the applications of new techniques (e.g. Bunte and Ergenzinger, 1989). Most of these studies are either concerned with laboratory measurements and flume experiments (e.g. Komar and Reimers, 1978; Komar and Li, 1986; Lee and Komar, 1986; Kirchner *et al.*, 1990; Buffington *et al.*, 1992; Carling *et al.*, 1992) or field observations (e.g. Schmidt and Ergenzinger, 1992; Schmidt and Gintz, 1995). Few of these studies have focused on a combined field and laboratory investigation. This is significant, because many investigators have pointed out that due to over-simplifying assumptions such as: steady flow; uniform bed roughness; uniform distribution of shear stress in the cross profile; uniform particle shape, size and packing; most of the laboratory models and experiments are often unreliable and the nature of the bedload transport process is not fully characterised. Field investigators have also expressed difficulties in obtaining accurate data from mountain rivers with irregular beds of coarse material. These facts emphasise the need for a systematic study to determine the effect of bed material shape on bedload transport in gravel-bed rivers. A study focusing on both laboratory measurements as well as field investigations, and combining and comparing the results, will provide a better understanding and improve knowledge in this little-studied area. Therefore the importance of particle shape in bedload transport in coarse-bed river system can be viewed in four contexts relating to the hydrostatic and hydrodynamic effects of particle shape:

1. Particle shape influences the entrainment of individual particles: Particle shape both influences the local force field and also the mode of transport (rolling or sliding) along with the geometry of the particle–surface pocket relationship (Komar and Li, 1986).

2. The interaction of different shaped particles is important in producing microforms on the surface of river beds (Reid *et al.*, 1992).

3. Apart from other factors there is a strong relationship between bed material shape and imbricate structures that control particle entrainment. Surface roughness is affected by bed configuration (Kirchner *et al.*, 1990; Carling *et al.*, 1992).

4. The importance of shape in sediment transport is demonstrated by the fact that shape is one of the three properties that control settling. The ratio of surface area to particle volume is important in controlling the response of particles to lifting forces, so that particles of low sphericity may behave differently from particles of high sphericity during transport.

1.6 AIMS AND OBJECTIVES

It has been suggested that in order to understand and model the nature of bedload transport, the shape and size of particles needs to be investigated in detail. It is surprising that, although there have been extensive studies of particle size of bedload and bed material, the effects of bed material shape on bedload transport have received considerably less attention. This thesis focuses on bed material shape in the bedload transport process. The aim of this thesis is to investigate through a series of field and laboratory-based experiments, the influence of particle shape on the transport of coarse fluvial gravel. The objectives of this study are:

1. To determine experimentally the influence of particle shape on the dynamics of bedload motion.
2. To determine the travel lengths of particles in different shape and size classes after particular flow periods.
3. To examine the influence of bed topography on travel lengths and transport of different shape and size classes.
4. To determine variability in friction angles and mechanistic behaviour of particles of different size, shape, orientation and roundness on beds of varying gravel roughness.

1.7 THESIS STRUCTURE

The remainder of this thesis is organised as follows. Chapter 2 focuses on a literature review concerning all aspects of bedload shape in bedload transport and also importance and use of magnetic tracing techniques in bedload transport studies. Chapter 3 sets out the research design of the thesis and describes the methods and techniques used. Chapter 4 describes the main physical characteristics of the field study sites and

catchments where the main fieldwork was carried out. Chapter 5 presents the results of the magnetic tracing experiments carried out during a range of storm events in the experimental reaches. Chapter 6 explains the results of tilting table experiments of measurements of the friction angles of particles of different shape and size, on both artificial and naturally-formed gravel stream bed of varying roughness. Chapter 7 gives results of photographic visualisation experiments that were carried out with particles of various shapes and sizes. Chapter 8 summarises the results of the field and laboratory experiments and attempts to integrate the results, and assess the significance of shape, in bedload transport studies.

CHAPTER 2: REVIEW OF THE INFLUENCE OF BED MATERIAL SHAPE ON SEDIMENT TRANSPORT AND TECHNIQUES FOR MEASURING COARSE-BEDLOAD TRANSPORT

2.1 INTRODUCTION

It is generally known that during bedload transport, sedimentological characteristics, hydraulics of flow, and characteristics of the bed material, which are mainly size, density and shape (form, roundness, sphericity and flatness) have an influence on transport. Studies have shown that the entrainment of a particle sitting on a rough bed depends on its shape, size, density, orientation, and relative exposure to the incident flow (Sneed and Folk, 1958; Schmidt and Ergenzinger, 1992; Carling *et al.*, 1992). Thus in order to understand bedload transport mechanisms in detail, attention must be given to the different aspects of bed material characteristics in coarse-bed upland rivers.

A comprehensive review of all aspects of bedload transport is beyond the scope of this chapter. Instead the focus will be on how bedload shape influences sediment transport and tracer techniques for measuring bedload movement. Firstly bedload shape is defined and the importance of bed material shape in bedload transport studies considered. This leads to a description of the processes governed by bed material shape. Explanation of the parameters describing the shape of particles is given and there is a discussion of various shape indices, which include *two-dimensional* (e.g. angularity, elongation and roundness) and *three-dimensional* (form, sphericity and flatness) *shape indices.* Case studies of laboratory and field experiments on bedload shape are then reviewed. The final two sections deal with techniques for tracing bedload transport and case studies using tracer techniques in different aspects of bedload transport investigations. Methods of tracing using artificial magnetic enhancement, natural magnetic tracers and their automatic detection (Pebble Transmitter System (PETSY)) are considered.

2.2 BEDLOAD SHAPE

The fundamental properties of sedimentary particles are mineralogical and chemical composition, specific gravity, volume or the size of the true nominal diameter, sedimentological shape (sometimes the crystallographic form) and the roundness of the corners and edges (Wadell, 1935). One important property is shape, which is the expression of external morphology, which for some is synonymous with form (Gary *et al.*, 1972; Barrett, 1980). However, Sneed and Folk (1958) used the term form specifically for overall particle shape, obtained from the measurement of the three orthogonal axes, and plotted on a form triangle.

2.3 FACTORS AND PROCESSES DETERMINING BED MATERIAL SHAPE

Many investigators have pointed out that the shape of particles is controlled by one or more of the following factors (e.g. Krumbein, 1941b; Sneed and Folk, 1958; Bridgland, 1986; Gale and Hoare, 1991).

- The shape of the particles as liberated from the parent rock.
- Lithology: the physical and chemical character of the particles (e.g. mineralogy, chemistry, structure e.t.c.).
- The nature of the sedimentary processes,
- The period and/or distance of transport,
- Sorting,
- Particle size.

These factors are responsible for some of the wide shape variations between particles of essentially similar composition and transportation history (Figure 2.1).

The influence of the first factor, "shape of the particles as liberated from the parent rock", may be illustrated by comparing the effect of different rocks. For example highly-jointed rocks may produce angular particles, frequently subcubic in shape; highly-cleaved rocks may yield bladed or platy particles; deeply-weathered rocks give rise to sub-rounded particles in the form of residual corestones (Gale and Hoare, 1991). Smalley (1966) used probability theory to predict that, for a totally isotopic lithology, 11 % of the particles released from the rock would posses a. b, and c axes of similar length, 22 % would be blades and the remaining 67 % would be made up of disc and rods.

Sneed and Folk (1958) found that the most important single factor governing

pebble morphology is lithological composition. Particle lithology has a significant influence on the shape of the resultant particles. For example after a similar transport distance, limestone tends to be soft and soluble and will therefore be rounded rapidly, while slates are usually brittle and possess close cleavage planes and are therefore angular and platy (Sneed and Folk, 1958; Knighton, 1982; Gale and Hoare, 1991). In addition, the initial shape of weathered particles is affected by mineralogy: micas tend to platy, feldspars are often tabular, and quartz tends to be equant.

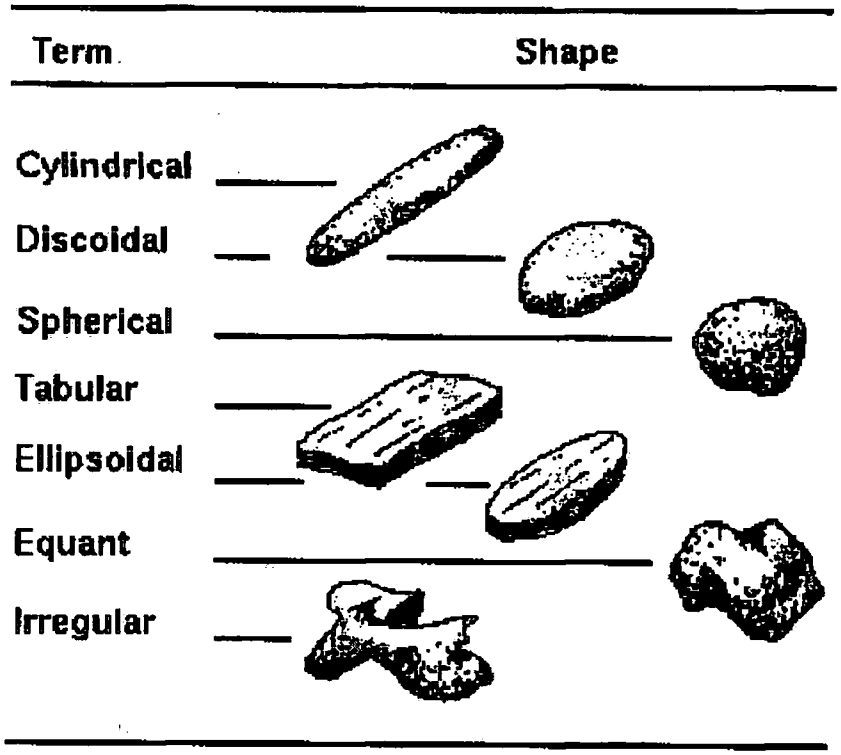

Figure 2.1 Descriptive terms applied to particle shape classification. (Source: Internet, date of download: 22.02.2000. Title: Particle shape. Address: Department of Geological Sciences, University of Saskatchewan, 114 Science Place, Saskatoon, SK, Canada, STN 5E2).

The nature of sedimentary processes exerts different influences on particle shape. There have been a great number of investigations determining what processes that give rise to specific shapes from different environments (e.g. Dobkins and Folk, 1970; Stratten, 1974; Gale, 1990). A detailed investigation by Dobkins and Folk (1970) on the shape of river and beach gravels showed that river gravels have higher mean

sphericity values than marine beach gravels. Stratten (1974) and Gale (1990) supported Dobkins and Folk's findings stating that mean sphericity of fluvial gravels is between 0.67 and 0.77, while the range is between 0.53 and 0.64 in beach gravels. Dobkins and Folk (1970) also found that modified Wentworth roundness of river gravels is less than for low energy beach gravels.

Boulton (1978) carried out another study on boulder shapes and grain size distribution of debris as indicators of transport paths through a glacier. It was found that different modes of glacial transport of gravel result in different particle shape. Plots of roundness in contrast with sphericity clearly distinguished between boulders transported supraglaciallly and englacially, boulders transported as traction load and boulders found in lodgement till (Gale and Hoare, 1991).

Many investigations have proved that distance of transport has a significant influence on bedload shape (e.g. Krumbein, 1941a; Kuenen, 1956; Sneed and Folk, 1958; Mills, 1979; Knighton, 1980). In particular, there is usually a strong relation between particle roundness and its transport distance. With increased distance, particles become more abraded and rounded. Water is the most effective transport medium for rounding coarse particles. A detailed review on transport distance and bedload roundness has been written (Mills, 1979) and also on marine transport (Andel *et al.*, 1954), beach transport (Grogan, 1945 and Emery, 1960), and glacial transport (Drake, 1972 and Bergesen, 1973).

In terms of sorting, certain particle shapes may be preferentially transported and deposited. However, shape sorting is more problematic since shape has not been easily correlated with entrainment, transport, or deposition. Conflicting evidence exits as to whether spherical (Krumbein, 1942; Sneed and Folk, 1958) or platy (Bradley *et al.*, 1972) shapes are preferentially transported. Some studies have shown consistent aspects of hydraulic behaviour of different shaped particles during transport. Indeed at high transport rates some particles become entrained in the water column and hydrodynamic effects may become important as particle settle. Sneed and Folk (1958) stated that particle settling velocity is governed by the volume of particle, which affects the downward force, and surface area of motion, which provides an upward resistive force. Thus the sphericity value of a particle may indicate its behaviour during transport. In other words high-sphericity particles may settle more rapidly than those of low sphericity. For instance, at high flow, assuming equal volume and density, spherical particles carried by rivers will have a higher settling velocity and will tend to be

deposited rapidly as the velocity of flow decrease, while platy particles will tend to remain in temporary suspension and be carried further downstream. On the other hand, spherical and rod-like particles will tend to roll along the channel, while discoid and bladed particles will tend to remain behind (Krumbein, 1941b; Sneed and Folk, 1958; Bradley 1972; Schmidt and Ergenzinger, 1992).

In terms of particle size, investigations have proved that particles of different size have different hydraulic behaviour during fluvial transport. For example, regardless of their shape, smaller particles may be transported continuously in suspension rather than as bedload. But as particle size increases the effect of particle volume and the surface area of particles become important factors that will probably lead to selective transport. In other words particles of different sizes may experience widely differing conditions of transport, which may result in their acquiring different shapes or being sorted by shape in different ways. Particle size has an important effect on shape change (roundness, sphericity) during transport. Although smaller particles are transported further downstream, they do not show an equivalent change in shape as does coarser material. Larger particles tend to be transported by rolling, sliding or saltating close to the bed. This means they are more affected by the abrasion processes which include: splitting, crushing, chipping, cracking (superficially), and grinding. On the other hand smaller sizes include fragments broken off larger particles (Krumbein 1941a; Kuenen, 1956). Thus, over an equal distance, particles in the larger size ranges tend to be more rounded than those of smaller sizes (Krumbein, 1942; Kuenen, 1956; Bluck, 1969). All these factors indicate that, especially in gravel-bed rivers, where a wide range of particle sizes exists size must be taken into account in bedload shape studies. Sneed and Folk (1958) also indicate that grain size is significantly correlated with sphericity, implying that particle behaviour is only consistent over restricted size ranges.

2.4 PARAMETERS FOR DESCRIBING THE SHAPE OF PARTICLES

There are many parameters for describing particle shape, but none of these has been universally accepted. Confusion appears to exist over what the various parameters of shape actually measure and how they are related (Barrett, 1980). Conventionally shape is expressed in three main ways (Table 2.1). Form is the measurement of the three relative lengths of three major orthogonal axes of a particle. Particles can be classified

as spheres, blades, rods and discs (Zingg, 1935), although some other investigators have used different classifications (e.g. Wentworth, 1922a; Wadell, 1932; Cailleux, 1947; Sneed and Folk, 1958; Benn and Ballantyne., 1993). Sphericity is a measure of how equal in length are the three major axes of a particle (Wadell, 1932; Krumbein, 1941b; Aschenbrenner, 1956; Sneed and Folk, 1958). Roundness is a measure of the smoothness and lack of angularity of a particle's surface (Wentworth, 1919, 1922b; Wadell, 1932; Russell and Taylor, 1937; Krumbein, 1941b; Cailleux, 1947; Kuenen, 1956; Dobkins and Folk, 1970). Although surface texture is characterised as the range of features which may be found on the surface of particles (Gale and Hoare, 1991), it is often not considered in discussions of shape, since it cannot be easily recognised in the projected outline of a particle and it also gives rise to some difficulties in the measurement of shape (Whalley, 1972).

Table 2.1. Main parameters used to characterise different aspects of shape of particles.

Property	Parameters
Form	Elongation and Flatness (Wentworth, 1922a; Zingg, 1935; Cailleux, 1947) Form ratio (Sneed and Folk, 1958).
Sphericity	Wadell, 1932; Krumbein, 1941; Sneed and Folk, 1958.
Roundness	Wentworth, 1919; Wadell, 1932; Russell and Taylor, 1937; Krumbein, 1941; Cailleux, 1947; Pettijohn, 1949; Powers, 1953; Kuenen, 1956; Dobkins and Folk, 1970; Swan, 1974.

2.5 SHAPE INDICES

The purpose of shape indices is to give a single descriptive term or value that will define or classify different particles. Many shape indices have been suggested, but unfortunately considerable ambiguity has arisen in the literature about the terms used to describe them (Briggs, 1977). Briggs (1977) made the distinction between indices

related to the two-dimensional shape of a particle and those referring to the three-dimensional shape. He stated that the main reason for the distinction is that the two-dimensional shape of a particle is controlled largely by the type and extent of weathering and wear during transport, while three-dimensional shape is more closely related to the structure of the material. Two-dimensional definitions include roundness, angularity and elongation, while three-dimensional ones include form, sphericity and flatness (Figure 2.2).

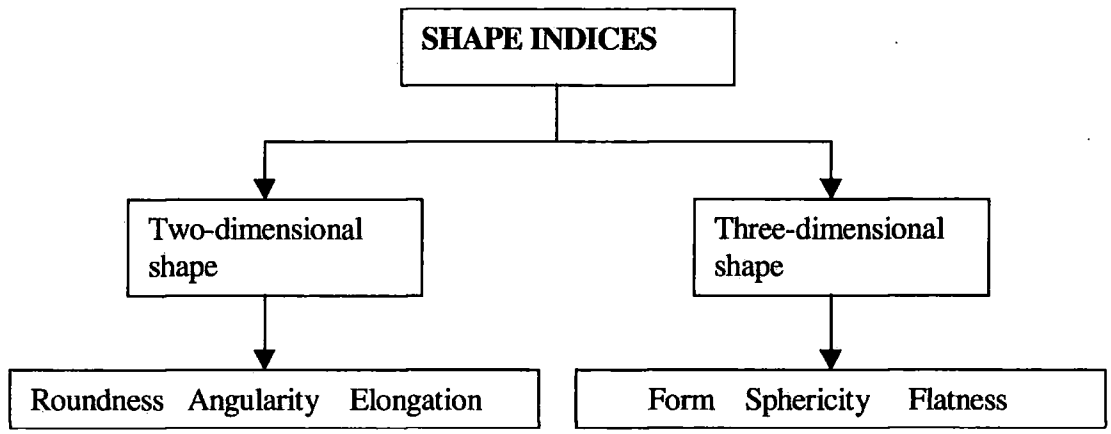

Figure 2.2 A simplified representation of two and three dimensional shape indices (Briggs, 1977)

Many shape studies have shown independence of form, roundness and surface texture. A large change in one property may not necessarily affect the other two (e.g. Krumbein, 1941a; Sneed and Folk, 1958; Barrett, 1980). Barrett (1980) stated that form, roundness and surface texture can be distinguished at least partly because of their different scales with respect to particle size, and this feature can also be used to order them (Figure 2.3). Thus, he identified form as a first order property that reflects variations in the proportions of the particles, while roundness, which is the second order property, reflects variations at the corners. In other words, variations superimposed on form. Surface texture, which is the third order effect, is superimposed on the corners, and is also a property of particle surfaces between corners.

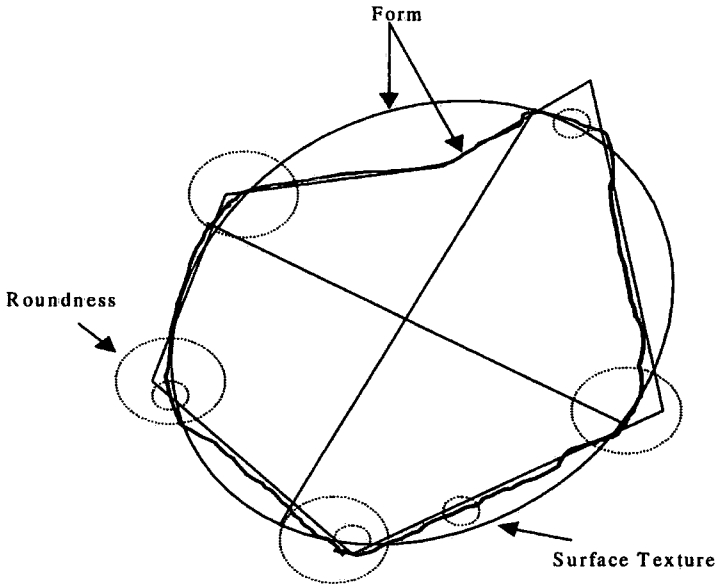

Figure 2.3. A particle outline (light solid line) with its component elements of form (light solid line, two approximations shown), roundness (dashed circles) and texture (dotted circles) identified (Redrawn from Barrett (1980).

The importance of different aspects of particle shape in bedload transport studies and various parameters to estimate particular aspects of shape are discussed below. Barrett (1980) pointed out that there are at least two properties that parameters should have. (1) Each parameter should represent one aspect that has some physical meaning, so that they can be related to the processes that determine particle shape. (2) Each should represent a combination of measurements from the same aspect of shape, that is, from the same hierarchical level.

2.6 TWO-DIMENSIONAL SHAPE

Two-dimensional measurement methods involve the assessment of roundness or angularity (Figure 2.1). Using these methods the particle is usually compared with the properties of a circle.

2.6.1 Angularity:

The irregularity of outline of the particle or its image, essentially the inverse of roundness (Briggs, 1977).

2.6.2 Elongation

This parameter is based on ratio of different axes of a particle. Schneiderhohn (1954) described the elongation index as the ratio of the greatest width to the greatest length of a particle:

$$\text{Elongation index: } \frac{b}{a}$$

Where b is the length of the intermediate axis and a is the length of the long axis. Another method which was described by Folk (1968) based on least projection widths (which is the two-dimensional form of a particle when viewed along the a-axis) and lengths of a particle. Table 2.2 shows the classes and indices derived by Folk.

$$\text{Elongation index: } \frac{b_p}{a_p}$$

Where and a_p and b_p are the least projection length (a_p) and b width (b_p)of the particle.

Table 2.2. Elongation classes and indices (After Folk, 1968)

Elongation classes	Elongation indices
Very equant	> 0.75
Equant	0.75 - 0.72
Subequant	0.72 - 0.69
Intermediate	0.69 - 0.66
Subelongate	0.66 - 0.63
Elongate	0.63 - 0.60
Very elongate	0.60

Briggs (1977) also described the elongation as the ratio between the longest (a) and shortest (c) axes of a particle.

$$\text{Briggs's elongation index: } \frac{a}{c}$$

2.6.3 Roundness

Roundness is a valuable sedimentological parameter. Along with other shape parameters (e.g. sphericity, form), roundness influences the hydrodynamic behaviour of a particle and may yield information about transport distances (Diepenbroek *et al.*, 1992). Roundness is the relationship of the outline or image of the particle to a circle, often defined as the ratio between the radius of curvature of the particle and that of an inscribed circle (Briggs, 1977). Roundness is usually taken to refer to the curvature of

the extremities on a particle. Its measurement is generally carried out in order to determine quantitatively the amount of wear undergone by a particle as a result of processes operating in a transporting environment (Shakesby, 1980). An increase in roundness is an expected consequence of the abrasion sustained by the stone in moving downstream, but it does not have much effect on form. On the other hand, a change in form significantly affects roundness, because fresh surfaces are exposed, and new corners appear.

2.6.4 Factors affecting roundness

Many studies have shown that, apart from distance of transport, there are many other factors that affect roundness. Shakesby (1980) reviewed some of these factors:

1) The nature of the particle on leaving its source will affect roundness at the point of deposition.
2) Lithology of a rock is an important factor in determining susceptibility of a particle to abrasion (Kuenen, 1956).
3) The nature of the transporting medium is significant in determining the particle roundness. As King and Buckley (1968), Bergesen (1973) and Gregory and Cullingford (1974) pointed out, particles in different transporting modes showed different roundness characteristics.

4. The size of a particle at all stages during its transport is an important factor. Particles of different sizes respond in different ways to processes acting in the same environment (e.g. Zingg, 1935; Russel and Taylor, 1937; Plumley, 1948; Sneed and Folk 1958 and Sorby, 1980).

5. The distance of transport and the effectiveness and duration of processes acting during transportation also affect the roundness of a particle, such as chipping caused by the impact of a particle against an obstacle.

2.6.5 Techniques in roundness measurement

An ideal measurement technique should be both accurate and rapid. Available techniques are either accurate but time consuming or rapid but inaccurate and, therefore, there is no single technique or apparatus that is capable of fulfilling both aims (Shakesby, 1980). Although, many different techniques have been used to assess particle roundness (Dobkins and Folk. 1970), these techniques have been traditionally

classified into two groups; (1) subjective techniques which generally include (a) visual description (b) visual comparison charts and (2) direct measurement techniques.

Subjective Techniques

a) Visual description: The operator verbally describes grain morphology from visual observation of the grain or grain facsimile. Visual descriptions are subjective and their level of efficiency is poor unless there is a specified set of standards for comparison (Orford, 1981). Allen (1982) gives a list of British Standard shape descriptions which apply to fine sediment. Roundness estimates are not encouraged, as the level of efficiency (replication) is low due to subjective assessments. Orford (1981) suggested that this type of description should be considered only as a superficial field statement when samples are unobtainable for further analysis. Standard verbal description of roundness and angularity have been developed by Russel and Taylor (1937), Pettijohn (1957) and Schneiderhonn (1954; in Pryor, 1971) (Table 2.3).

Table 2.3 Verbal description of roundness/angularity classes, modified from Schneiderhohn (1954, in Bridgland, 1986).

1. Well rounded	No flat faces, corners or reentrants discernible; a uniform convex particle outline.
2. Rounded	Flat faces nearly absent, with corners all gently rounded. Small reentrants absent and large reentrants only suggested.
3. Sub rounded	Poorly developed flat faces with corners well rounded. Few small and gently rounded reentrants; large reentrants weakly defined.
4. Sub angular	Strongly developed flat faces with incipient rounding of corners. Small reentrants only suggested.
5. Angular	Strongly developed faces with sharp corners. Sharply defined, large reentrants with numerous small reentrants
6. Very angular	As 5, but corners and edges very sharp, with no discernible blunting. [This class was added to the visual charts by Powers (1953) (Figure 2.5), although only for sand grains. For pebbles it may be reserved for frost-fractured and other freshly broken particles.]

b) Visual comparison charts: The operator views the actual grain or grain facsimile and compares it to a standard reference. Methods of this type prove to be most popular when dealing with fine sediments (<4 mm; *b axis*) and especially with sand-sized material, where direct measurement of particle axes is difficult.

Roundness analysis using visual comparison charts is less precise than the methods of direct measurements. This is because, when using visual comparison charts

it is normally impossible to distinguish subtle differences in particle rounding. In this method each particle is compared with a set of images and assigned to the particle form it most closely corresponds. Although several charts are available (e.g. Russel and Taylor, 1937; Pettijohn, 1957; Krumbein and Sloss, 1955), the most widely used are those Krumbein's (1941a) visual comparison, Rittenhouse's (1943) sphericity and Powers's (1953) roundness comparison charts. These methods of analysis are simple and rapid to use. Powers's chart, generally intended for sand grains, is perhaps the most frequently used. Powers (1953) included six classes in his chart, having added a new class 'very angular' to Russell and Taylor's (1937) five classes of roundness (Figures 2.4 and 2.5). The data is collected on a ordinal scale, but may be transformed by assigning each category a value in an interval scale, thus allowing statistical analysis. Powers also made the divisions of his classes intentionally coarser for classes depicting more rounded particles than for those representing angular ones, since he considered that the eye can more readily distinguish differences of roundness when the roundness values are low (Shakesby, 1980).

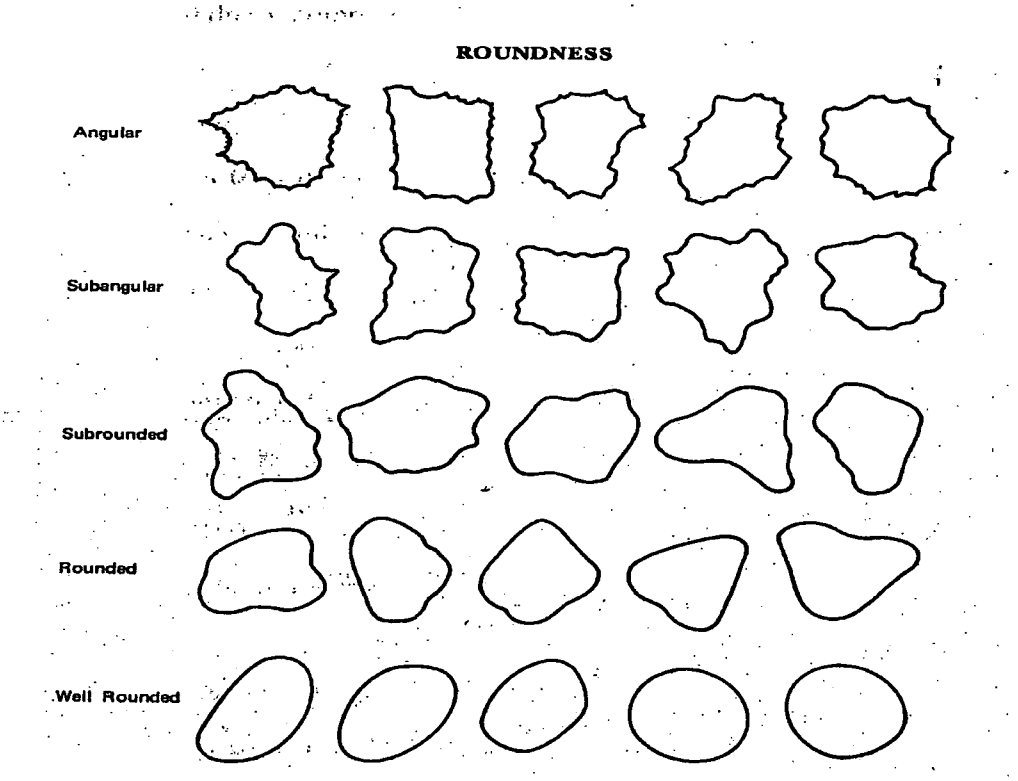

Figure 2.4 Roundness chart of Russell and Taylor (after Pryor, 1971)

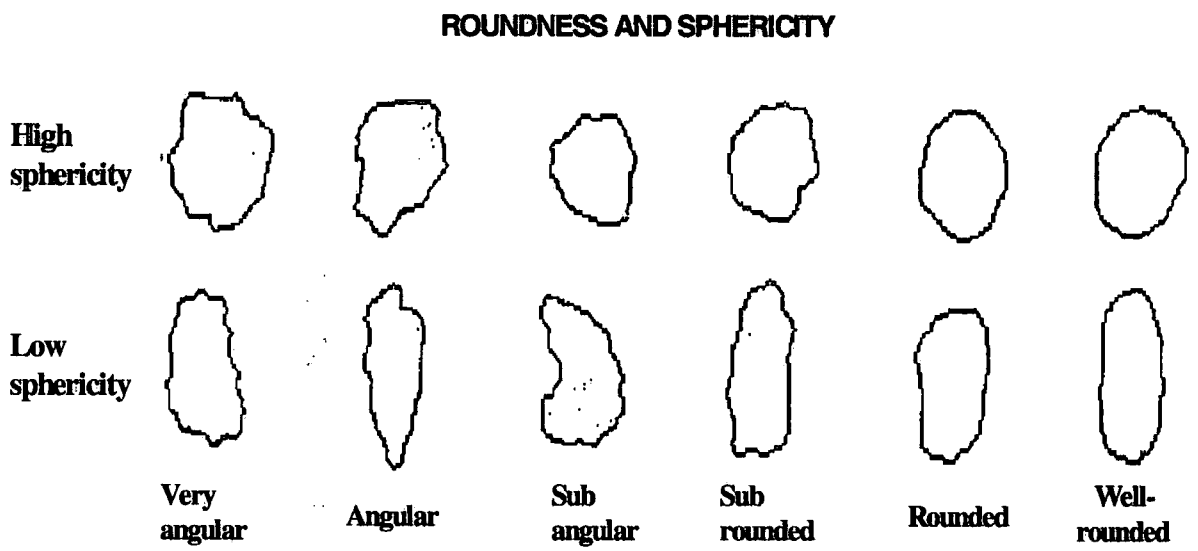

Figure 2.5 Powers roundness comparison chart. Each roundness class is shown with two particles, one with a fairly high sphericity, and one with a rather low sphericity (After Powers, 1953).

Krumbein's chart is based on visual comparison of individual grains with silhouettes to determine roundness values. In other words a pebble is compared with standard images of known roundness, and a roundness value assigned to it. His classification is based on ten sets of standard images, with long axes of about 25mm (Figure 2.6). The standard images vary in roundness from 0.1 to 0.9. In this classification he also included a set for broken pebbles to indicate effects of breakage on roundness. By enlarging or reducing the images photographically, similar sets may be made for any size range. This method was criticised by Powers on the basis that the method is rather slow and somewhat tedious. This is because divisions between Krumbein's ten classes were too fine, making it difficult to decide which roundness value to assign to a particle.

Lees (1964) developed a new method for determining the angularity of particles. He considered angularity as not simply the absence of roundness but a distinct concept. Lees regarded his chart as representing degrees of angularity rather than roundness but the resulting chart is similar to those of Powers and Krumbein. His divisions were based on 16 classes, however, this means it is more difficult to decide to which class a particle most closely corresponds. On the other hand Reichelt (1961) developed a chart based on

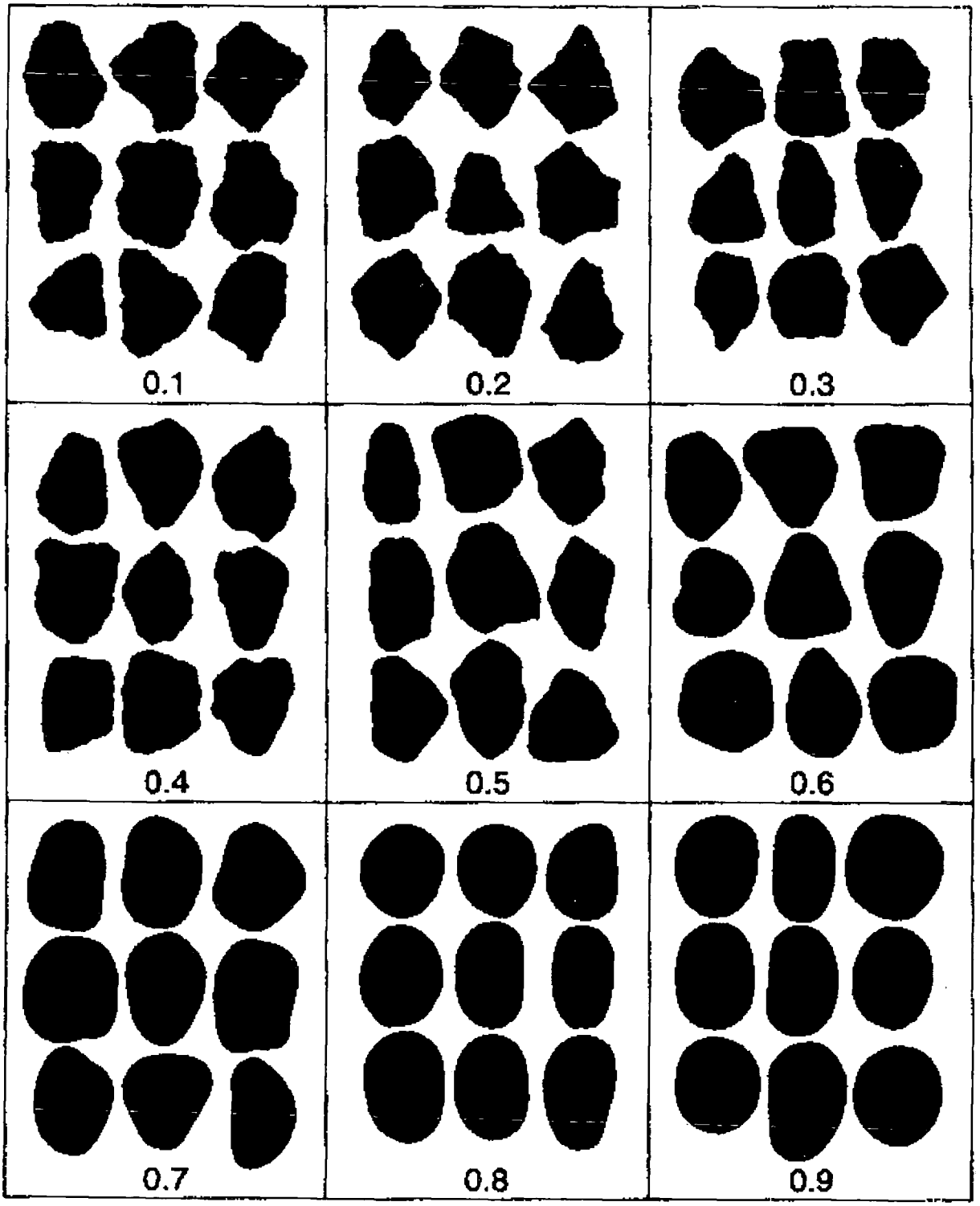

Figure 2.6 Pebble imges for visual roundness (Krumbein, 1941b). The images should lie within the size range of the particles being measured. If gravels to be examined lie outside the size range of the images, the figure should be enlarged or reduced correspondingly.

only four classes of roundness, but it has not been used by British or North American workers, it has mainly been used in Europe (Shakesby, 1980). There is no universally accepted visual comparison chart for roundness estimation.

c) Curvatures estimation methods: Using these methods proportions of particle surfaces can be estimated as flat, convex or concave. One of the well known method in this area is the Scadeczky-Kardoss curvature estimation method (Sames, 1966). The main advantages of this method is that results can be shown directly on a triangular graph, and thus allowing small variations between samples to be seen relatively clearly. Despite the advantages, disadvantages of the method include its highly subjective nature, which permits personal bias to influence the results, and the strong chance that the ratios of concave, convex and flat sections will depend more on the rock lithology and structure than on environmental processes that effect the particle.

Table 2.4 Subjective techniques for assessing the roundness of particles (revised from Shakesby, 1980)

References	Number of classes	Type of display
Visual comparison charts		
Krumbein (1941)	10	silhouettes
Powers (1953)	6	photographs of clay models
Lees (1964)	16	silhouettes
Reichelt (1961)	4	photographs of particle
Curvature estimation		
Szadeczky-Kardos (1933)	—	—

Direct measurement techniques

In general, direct measurement techniques are attractive mainly because they reduce much of the subjectivity, and thus the possibility of intuitive tendency, which is the major problem with visual comparison charts. Apart from some techniques that require expensive equipment (e.g. Wadell, Schwarcz and Shane and Wainberg

methods), direct measurement techniques are also relatively rapid and can be carried out using simple and inexpensive devices e.g. Cailleux (1947) and Wentworth (1919) methods (Table 2.5). The operator makes dimension measurements of the actual grain or grain facsimile and values are inserted into a roundness formula.

Techniques for the quantitative determination of roundness may be subdivided in to two groups. (1) Those that are theoretically desirable but practically difficult to use (e.g. Wadell, 1932; Schwarcz and Shane, 1969; Ehrlich and Wainberg, 1970). (2) Those that are less complex and more practical, but the degree of accuracy may be less (e.g. Wentworth, 1919; Cailleux, 1947; Dobkins and Folk, 1970; Swan, 1974) (Table 2.5). The practicality of the latter four techniques is achieved by sacrificing a degree of accuracy in order that measurement in the field of a large number of particles is possible within a reasonable period of time (Shakesby, 1980). Virtually all these techniques are based on intercept or curvature measurements. The particles are usually viewed in outline in each case, although Dobkins and Folk (1970) demonstrated how roundness may be obtained three dimensionally (Swan, 1974).

Table 2.5 Direct measurement techniques for assessing particle roundness (After Shakesby, 1980)

Reference	Formula	Definition	Remarks
1) Wadell (1932)	$\frac{\sum r_n / N}{R_i}$	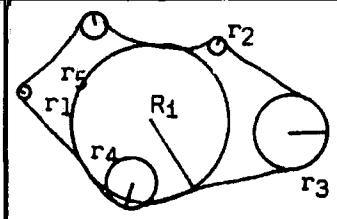	Judged to be theoretically commendable but too tedious for use in the field. It is used to provide the numerical divisions in visual comparison charts of Krumbein (1941) and Powers (1953).
2) Wentworth (1919)	$\frac{2r_m}{a}$	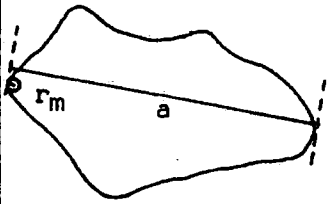	Not often quoted by European workers though it resembles very closely the technique later proposed by Cailleux (1947)
3) Cailleux (1947)	$\frac{2r_m}{a} X\ 1000$	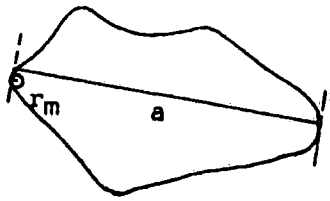	The most popular direct measurement technique in Europe. It has been used by many workers (e.g. King and Buckley, 1968; King, 1969; McCann and Owens, 1969; Hollerman, 1971; Dugdale, 1972; Gregory and Cullingford, 1974; Orfold, 1975).
4) Kuenen (1956)	$\frac{2r_m}{b} X\ 1000$	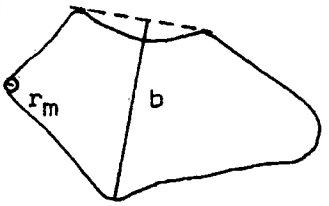	Kuenen considered that the b-axis was a better index of size and less influenced by shape than the a-in Cailleux's formula.
5) Dobkins & Folk (1970)	$\frac{r_m}{R_i}$	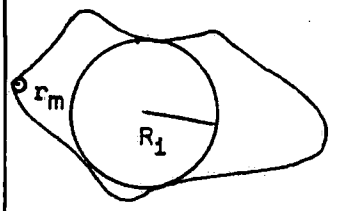	Effectively a measure that combines aspects of the techniques suggested by Wentworth and Wadell. The authors referred to it as the "modified Wentworth technique" (Flemming, 1965; Griffiths, 1967).
6) Swan (1974)	$\frac{r_1 + r_2}{2} / R_i$	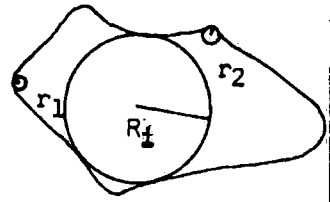	Swan considered that Wadell's technique was "the most representative of roundness" but that it appeared too complex. As a simplification, he suggested selection of the two sharpest corners (r1 and r2) rather than all the corners as in Wadell's technique

One common index (e.g. Wentworth (1919) and Cailleux (1947)) uses the radius of curvature of the sharpest corner in the maximum projection plane and divides this value by the length of the long axis. This index was originally used by Wentworth (1919) (Table 2.5). Wentworth later changed the divisor to the average of the long and short diameter of the particle in the plane of projection (Wentworth, 1922a). This method was later reinvented and popularised by Cailleux, 1947. Wentworth suggested two indices of roundness. His formula of 1922 is given here as:

$$2r_1/D \tag{2.1}$$

where r_1 is the radius of the sharpest curvature and D is the mean diameter of the particle, D equalling:

$$3\sqrt{a.b.c}$$

Where *a*, *b* and *c* are the length, breadth and thickness of a particle respectively.
In 1933, he simplified this by eliminating consideration of the third intercept. His revised formula is given as:

$$r_1/R \tag{2.2}$$

where r_1 is the radius of the sharpest curvature; with R equalling the mean radius of the particle which is determined as:

$$\frac{a+b}{4} = R \tag{2.3}$$

Where a is the longest dimension, and b is the greatest width of the particle at right angles to a.

Wadell expressed roundness as the ratio between the radius *r* of the sharpest corner of the particle and the radius R of the largest inscribed circle, both in the maximum projection of the particle. Wadell (1932, 1935) calculated the degree of roundness by dividing the mean of the radii of curvature of the corners by the radius of the maximum inscribed circle,

$$\frac{\Sigma r_n / n}{R_i} \tag{2.4}$$

where n refers to the number of corners. Wadell (1932) defined a corner as "every such part of the outline of an area which has a radius of curvature equal to or less than the radius curvature of the maximum inscribed circle of the same area" (Swan, 1974) (Table 2.5). The measurement of roundness in this way is lengthy and time consuming, therefore Krumbein (1941a) produced a chart for visual determination of roundness by comparison with pebble images, the roundness of which has been measured by Wadell's method. The agreement between both methods of determination is acceptable, when the number of pebbles is greater than 25. The values range from 0 to 1, the latter representing perfect roundness, whatever the shape may be (Andel, *et al.*, 1954).

Cailleux's roundness index is based on measurement of the radius of curvature of the sharpest corner of the particle, in the plane of maximum projection. The plane of maximum projection is defined by inspection, and the sharpest corner in this plane located. The pebble is then placed on a series of concentric semicircles of known radius so that the sharpest corner just encloses a semicircle. The radius of the semicircle is the radius of curvature of the corner. The length of the longest axis is then 1. (Briggs, 1977). In reality, most sedimentary particles fall between 0.3 and 0.9. Caulleux's rounding index is as follows:

$$\frac{2r_m}{a} \cdot 1000 \qquad (2.5)$$

In 1947, Cailleux also used the measurements of the curvature of the second and third order indices. He pointed out that these measurements were made in order to determine which the sharpest corner really was. Cailleux (1947) also emphasised that comparison of roundness, where his formula was employed, was possible only among particles of similar sizes (Swan, 1974). According to Blenk (1960), Cailleux's roundness index is as good as others that have been proposed subsequently and it has the advantage that many studies have made use of it, so results are comparable. The measures suggested by Kuenen produce similar values. Therefore it seems reasonable to use Cailleux's method for determining the shape of pebbles. Tonnard (1963) also tested the various indices proposed to assess the shape of sand and concluded that Cailleux's index was the most satisfactory.

Cailleux's (1947) method has been criticised by Kuenen (1956), Dobkins and

Folk (1970), Swan (1974) and Folk (1977). They state that it confuses both roundness and form in the same measure. Kuenen modified the Cailleux formula by replacing the long axis with the intermediate axis, whereas Dobkins and Folk suggested using the largest inscribed circle, and Swan proposed a modification of the Dobkins and Folk procedure by averaging the diameters for the two sharpest corners (Barrett, 1980). Kuenen's (1956) suggested formula is:

$$2r_1/1 \qquad (2.6)$$

Where r_1 is the radius of the sharpest curvature as in Wentworth's and Cailleux's formula, and '1' is the largest diameter at right angles to the greatest length. '1' is identifiable as approximately twice R1 of Wadell's formula and more or less the same as the width of the particle.

In terms of pebble shape analysis Dobkins and Folk (1970) promoted a method which they called the "*Modified Wentworth Index*". Their formula is given as:

$$\frac{r_m}{R_i} \qquad (2.7)$$

This method involves a combination of the measurements proposed by Wentworth and Wadell. Dobkins and Folk (1970) also measured only the radius of curvature of the sharpest corner (r_m) in the a-b plane which eliminated the most tedious aspect of Wadell's method. They used the largest inscribed circle because the a-axis may tend to be influenced by morphometric properties other than roundness (Shakesby, 1980). Dobkins and Folk (1970) suggested that *The Modified Wentworth roundness* is more objective and quantitative than any other procedure for measuring roundness, including Wadell's, but in both respects it is no better and no worse. The greatest problem is recognising corners. They demonstrated that the sharpest corner provided the best measure of roundness, because it best reflects the amount of rounding going on in the latest environment. This applies to river pebbles, although in other situations, such as beneath glaciers, the level of rounding attained rather than roundness change since the last breakage, may be of most interest (Barrrett, 1980).

Comparison of the Wadell-Krumbein index and Cailleux index shows that both techniques give values of 1.0 for spheres, but the Wadell-Krumbein index generally

gives higher roundness values than the Cailleux index. Mills (1979) pointed out that this difference can be attributed to two factors. First, the diameter of curvature averaged over all corners usually will be greater than the diameter of curvature of the sharpest corner. Second, the diameter of the maximum inscribed circle will, in most cases, be smaller than the long axis. He also concluded that modifications of the Cailleux index employing the intermediate axis or mean axis will decrease the differences between the two methods due to the second factor, but not that due to the first. As a result, using different techniques in direct comparison may lead to some difficulties.

Shakesby (1980) made the following observations concerning measurement of curvature of corners on particles. First, corners may approach segments of parabolas or hyperbolas rather than a true circle, and thus it may be difficult when considering such corners to decide which reference circle offers the closest match. Second, with decreasing size and rounding the accuracy of the technique diminishes (Andel, *et al.*, 1954; Whalley, 1972). Third, there is a problem of parallax when comparing the corners of particles with the reference circles so that the operator tends to overestimate the value of **r** (Dobkins and Folk, 1970). Fourth, for techniques where the radius of curvature of the sharpest or two sharpest corners is needed, not all operators select the same corner to measure (Folk, 1972)

2.7 THREE-DIMENSIONAL SHAPE

Three-dimensional shape indices generally include measurement of sphericity, form, and flatness. Form and sphericity have a direct influence on the hydraulic behaviour of particles whereas two dimensional shape such as roundness does not effect the behaviour to the same degree. In this respect, three-dimensional shape indices are considered an important measure for bedload transport studies.

2.7.1 Form

The form of a particle determines its mode of transport, its abrasion, point of deposition and its effect on the resulting sedimentary rock (Flemming, 1965). Form is the relationship of a particle to a formal shape such as a sphere, disc, rod, cube, or prism. Almost all parameters of particle form are based on the longest, intermediate and shortest orthogonal axes. The simplest form methods are generally based on direct measurement of a particle's three major axes (a, b, and c) taken orthogonally but not

necessarily intersecting at the same point (Orford, 1981). Given three axial values, then the elements of shape and sphericity can be determined.

One of the earliest attempts to standardise the classification of particle shape was made by Zingg (1935) (Figure 2.7). The Zingg classification is based on ratios of the three principal axes; the long (a), intermediate (b) and short (c) axes. The a axis is the longest, the b axis is the maximum diameter at right-angles to it, and the c axis is the maximum diameter of the third, in a mutually right-angled plane. In Zingg diagram b:a is plotted against c:b. In this diagram, four rather distinctive shapes are distinguished by following ratios:

Sphere (Equant)	$b/a \geq 0.67$	$c/b \geq 0.67$
Blade (Bladed)	$b/a < 0.67$	$c/b < 0.67$
Rod (Prolate)	$b/a < 0.67$	$c/b \geq 0.67$
Disc (Tabular)	$b/a \geq 0.67$	$c/b < 0.67$

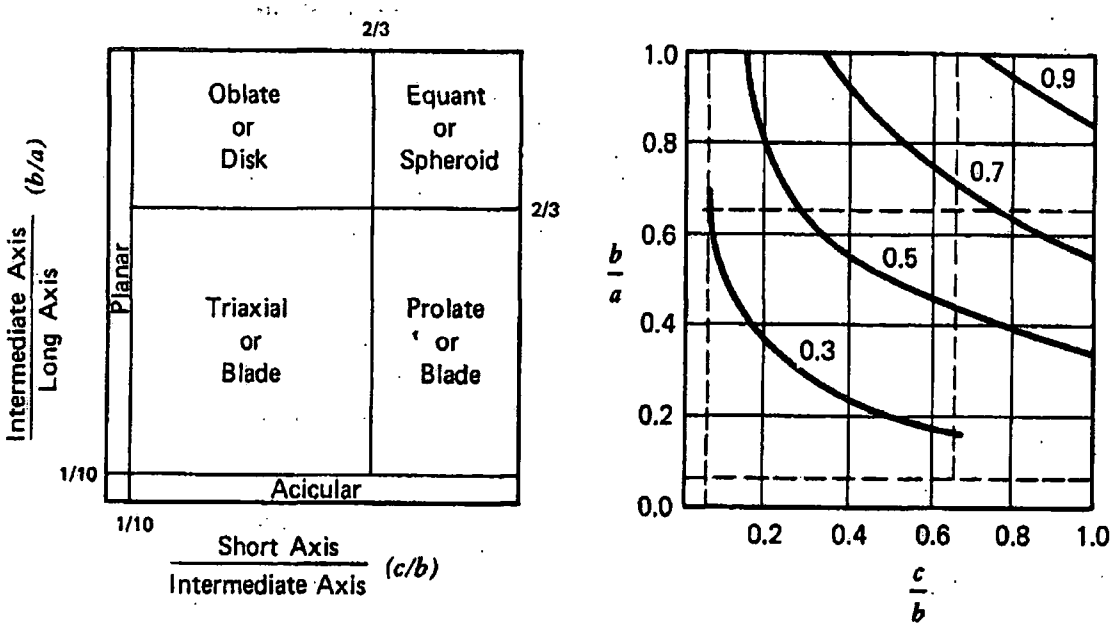

Figure 2.7 Zingg shape classes based on ratios of specific axes and relationship of sphericity to the shape classes (From, Krumbein, 1941b, and Brewer, 1964 cited in Pryor, 1971).

On this basis any particle can be assigned to any of these categories relating to a formal shape (Briggs, 1977). Zingg's classification scheme, including modifications by Krumbein (1941) and Brewer's (1964), is shown in Figure 2.7. Although this approach

is popular, Zingg diagrams possess disadvantages that limit its usefulness. The advantage of this scheme is that it gives an objective and swift measure of the particle form but particles are only assigned to categories, and not given numerical shape values. Consequently analysis of shape using the Zingg method provides only nominal data; which limits the range of statistical analysis. Another important disadvantage is that b:a and c:b ratios are not necessarily the most powerful indices for the characterisation of any particular data set. Both may vary little between particle populations that have widely differing transport histories (Ballantyne, 1982; Benn and Ballantyne, 1993). Indeed, most other shape indices plot on Zingg diagrams as families of curves, including the important and useful c:a and (a – b):(a – c) indices. Another disadvantage is that almost half of the Zingg diagram is occupied by shapes that are rarely represented in naturally occurring particles. This reflects the fact that particle shape invariably falls between three extremes and hence is most appropriately represented on triangular diagrams (Benn and Ballantyne, 1993). Sneed and Folk (1958) also pointed out several similar weaknesses with the Zingg classification chart of particle form. They stated that first, there are only four form classes, which makes it inadequate for any detailed work. Second, the classes defined by Zingg divide the field of variations very unequally (Figure 2.7). Thus, in contrast to Zingg's classification, Sneed and Folk (1958) made 10-way division of pebble form that has been used more commonly in recent years (Figure 2.8). Their compactness measurement is based on the ratio of c/a, which is plotted against elongation in order to give a verbal description of the form of the pebble. Where c is the length of the shortest principal axis, b is the length of the intermediate principal axis and a is the length of the longest principal axis. These three principal axes are mutually perpendicular to each other and determined in the order a-c-b for any particular pebble.

$$\frac{a-b}{a-c} \tag{2.8}$$

Sneed and Folk (1958) combined maximum projection sphericity with the intercept ratios of c:a and (a – b):(a – c). Thus particle shape in Sneed and Folk classification may vary between the three end members, defined in terms of their three orthogonal axes on a form triangle. In their proposed triangular diagram, (designed for

plotting pebble form) the three poles representing platy, elongated and compact pebbles (Figure 2.8). Given the a, b, and c measurements, the location of a point is determined by the value of the apex end member-compactness, measured by c/a, and a proportion (as ratios 2.8) measured parallel to the base, which divides pebbles into three classes, platy, bladed and elongated. The diagram emphasises the fundamental character of these shapes, and the way in which they converge on a single type, compact (Barrett, 1980).

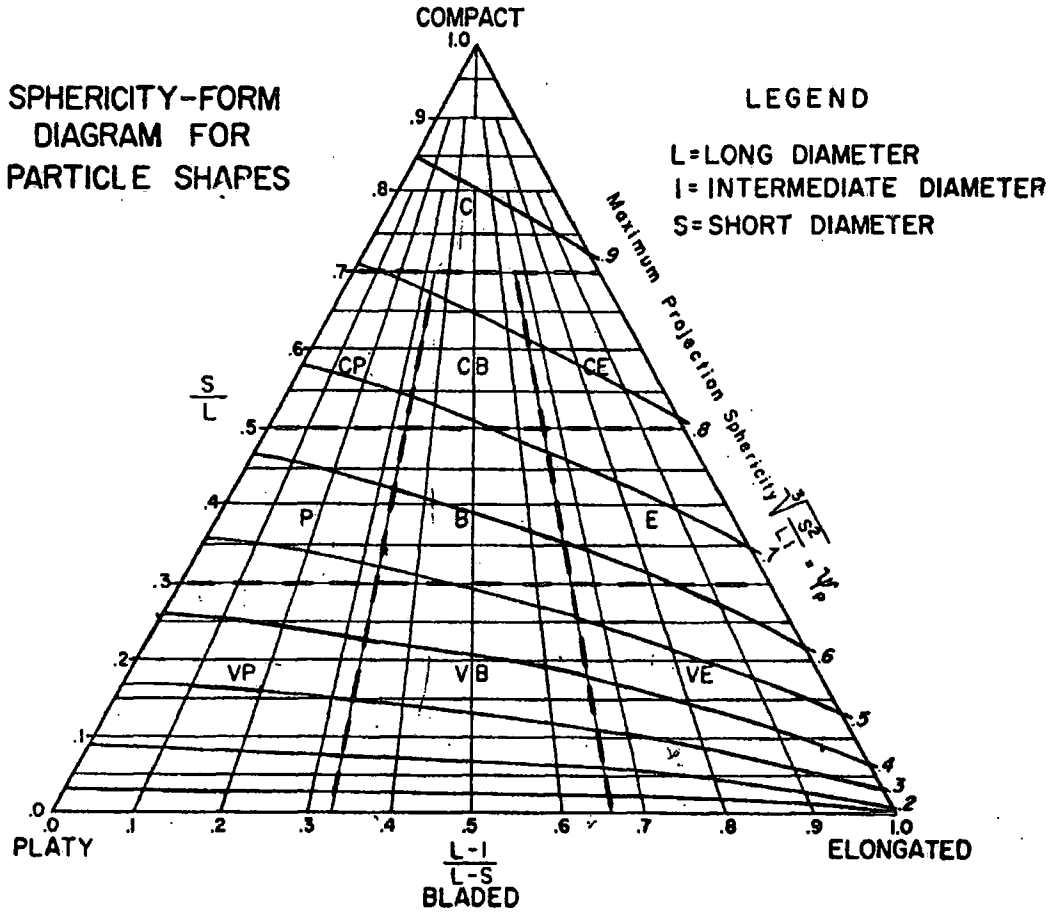

Figure 2.8. Form triangle showing the relationship of sphericity to form (Redrawn from Sneed and Folk, 1958).

2.7.2 Sphericity

Although form classification of pebble shapes allocates particles to formal categories, the concept of sphericity represents a different aspect of shape. Sphericity gives a numerical shape value for each individual particle that enables higher statistical analysis to be carried out. In general, sphericity provides a quantitative value illustrating

the departure of a body from equidimensionality. Sphericity is the relationship of a particle to a sphere, often defined as the ratio between the surface area of the particle and that of the inscribed sphere. Sphericity is an important factor producing sorting of particles in traction by rolling, because spherical particles roll faster than non-spherical ones. When dealing with bedload particles the sphere may therefore appropriately be taken as the standard for comparison. However, when dealing with particle settling velocity, the expression of shape must theoretically be seen from another angle, such as the area of the grain surface. A sphere has the greatest relative volume with the smallest surface area and, therefore, has a great settling velocity than any other shape of the same volume and density. Progressively greater departure from spherical shape means progressive increase of surface area without change of volume and, therefore also, a decrease of the settling velocity of the solid (Wadell, 1932).

Some particles may have similar numerical sphericity values, but they may have different ratios between their three dimensions, such as one may be a disc and another may be a rod (Figure 2.8). For example disc-shaped and rod-like particles may have the same sphericity, despite the fact that they have very different shapes and probably will have different hydraulic behaviour during transport and deposition (Krumbein, 1941a). Because of these differences the use of sphericity values in bedload studies does not always permit the complete evaluation of the influence of shape (Andel *et al.*, 1954).

One of the earliest measures of equidimensionality was the Wadell (1934) sphericity formula, which is the cube root of the ratio between the actual volume of a particle (originally obtained by immersion in water) and the volume of the smallest sphere that will just enclose the particle. Wadell expressed the sphere as a reference form, and considered that deviations were best represented by ratios of particle volume to the volume of the circumscribing sphere (Andel *et al.*, 1954; Barrett, 1980).

Wadell's definition of sphericity (ψ) can be shown as follows:

$$\Psi = \sqrt[3]{\frac{Volume\ of\ the\ particle}{Volume\ of\ the\ circumscribed\ sphere}} \qquad (2.9)$$

He expressed the volume of the particle in terms of a sphere that had the same volume; the diameter of the corresponding sphere is the " nominal diameter" (d) of the particle. On this basis, the volume of the particle is $(\pi/6)\ d^3$. The volume of the circumscribed sphere is based on the longest axis (a) of the particle. Thus, the volume of this sphere is $(\pi/6)\ a^3$. By substituting these values in the equation above, Wadell's sphericity

reduces to the ratio of the nominal diameter of the particle to its longest diameter

$$\Psi = \sqrt[3]{\frac{(\pi/6)d^3}{(\pi/6)a^3}} = \sqrt[3]{\frac{d^3}{a^3}} = \frac{d}{a} \tag{2.10}$$

Barrett (1980) pointed out that Wadell's sphericity is sensitive to roundness as well as form. Therefore Wadell's sphericity is not a parameter of form alone, but includes a quantity of roundness, making it a difficult parameter to deal with, conceptually.

Following Wadell's method, more recent investigations have been based on measurements of actual particles or particle projections. These include Krumbein's (1941a) "Intercept Sphericity" and Sneed and Folk's (1958) "Maximum Projection Sphericity" (Bridgland, 1986).

Differences between the procedures of Zingg and Wadell for describing particle shape were modified by Krumbein (1941a). Krumbein's definition of sphericity can be explained as follows: He used the same basic definition as Wadell, but the volume of the particle was expressed in terms of a triaxial ellipsoid having the three diameters, a, b, and c, where $a > b > c$. The volume of such an ellipsoid is expressed $(\pi/6)\,abc$. This is because the volume of the circumscribed sphere is still $(\pi/6)\,a^3$. Thus, these two volumes are substituted as follows:

$$\psi = \sqrt[3]{\frac{(\pi/6)\,abc}{(\pi/6)\,a^3}} = \sqrt[3]{\frac{bc}{a^2}} \tag{2.11}$$

This equation then is simplified by cubing both sides, to eliminate the radical sign:

$$\psi = \frac{b\,c}{a^2} \tag{2.12}$$

Sneed and Folk (1958) also pointed out that Wadell's measure of equidimensionality is not a behavioristic parameter in relation to the dynamics of particles under natural conditions. They stated that assuming two spheroids of identical volume and identical Wadell number (such as one is a rod measuring 100 x 10 x 10 cm and the other a disc of 100 x 100 x 1 cm) the disc is the more inequidimensional of the two particles and it would have sliding motion and settle more slowly than the rod in water, although they have precisely the same Wadell sphericity values. Thus, they

suggest that sphericity of particle should express its behaviour in a fluid. In other words a more behavioristic measure of sphericity is obtained by comparing the volume of the particle with its maximum projection area i.e., the surface area opposed to the direction of motion. Their measurements simply compare the maximum projection area of the particle itself (defined as the product of large and intermediate axes) with the maximum projection area of a sphere of the same volume as the particle. The maximum projection sphericity of a particle is defined as the ratio of the maximum projection area of a sphere of the same volume as the particle to maximum projection area of the particle.

$$\text{Maximum Projection Sphericity } (\psi_p) = \sqrt[3]{\frac{c^2}{a \cdot b}} \qquad (2.13)$$

In this formula, the particle is assumed to approximate to a triaxial ellipsoid with axes *a* (long), *b* (intermediate) and *c* (small)

The maximum projection area of the particle is defined as: $\frac{\pi}{4}(ab)$ (2.14)

The volume of the particle and also the equivalent sphere is $\frac{\pi}{6}(abc)$

The general formula for the volume of a sphere is $\frac{\pi}{6}d^3$ Therefore, $d^3 = abc$ and the diameter of the equivalent sphere, *d*, will equal $\sqrt[3]{abc}$ The maximum projection area of this sphere will equal $\frac{\pi}{4}(\sqrt[3]{(abc)^2}$. The maximum projection sphericity (ψ_p) then equals:

$$\frac{\frac{\pi}{4}(\sqrt[3]{(abc)^2}}{\frac{\pi}{4}(\sqrt[3]{(ab)^3}}, \text{ which reduces to } \sqrt[3]{\frac{a^2b^2c^2}{a^3b^3}} = \sqrt[3]{\frac{c^2}{a\ b}} = \Psi_p \qquad (2.15)$$

In reality the formula for Sneed and Folk's measure is very close to that of intercept sphericity of Krumbein (1941a), which it was designed to replace. The only difference is that for maximum projection sphericity the short axis is used as a reference, whereas intercept sphericity uses the long axis. Barrett (1980) noted that the two formula can be equally valid measures of sphericity from a conceptual point of

view and he also stated that the relationship between Sneed and Folk's form triangle and maximum projection sphericity is similar to that between Zingg's diagram and intercept sphericity. This similarity is attributed to the fact that each of the four methods derives from the same basic data (the lengths of the three principal axes).

Particle settling can at times be an important aspect in the transport of bedload in a river. The settling velocities of the particles governing whether they are transported as rolling close to the bed, saltation or temporary suspension during the high flow period. Several investigators have shown that there is a relationship between sphericity of a particle and its settling velocity. The departure of a particle from a spherical shape results in a decrease in its settling velocity within a fluid. The more non-spherical the particle the greater the departure from the settling velocity of a spherical particle of the same weight (Krumbein, 1942; Komar and Reimers, 1978). In order to study the effect of Wadell sphericity on both setting velocity and traction transport in a flume, Krumbein (1942) conducted a very helpful series of experiments with differing shapes (discs, blades, rods and spheres) hand-moulded from concrete mortar. All particles were of the same density and same volume. He found that although there is a wide degree of scatter, there is a general correlation, in that the high-sphericity particles settle more rapidly. It was found that all the rod-like particles settle about 6 cm s^{-1} faster, and the discs about 6 cm s^{-1} slower, than their sphericity values would predict. In his flume experiments similar differences were also observed. For example, it was found that disc-shaped particles moved more slowly and rods more rapidly than the predicted values. It was also shown that for equal volume and density, "rollers" have faster velocities than corresponding discs. Thus Krumbein showed that Wadell's concept of sphericity is related to the dynamic behaviour of various shaped particles, but apparently sphericity alone is not the only controlling factor. The results from prove that the difference in behaviour of rollers and discs is due to an additional factor in shape, not clearly included in Wadell sphericity.

Sneed and Folk (1958) stated that the differences in behaviour of rollers and discs are due to the maximum projection plane that Wadell did not include in his sphericity determination. In other words they indicated that Wadell sphericity measure is not behavioristic, because it takes no account of the manner in which particles actually settle, that is, with the maximum projection plane horizontal. In order to compare settling velocity of particles as a function of maximum projection sphericity and of Wadell sphericity, Sneed and Folk (1958) used Krumbein's (1942) experimental

data and recalculated the lengths of the three axes of each of the modelled forms from Krumbein's figure 1. From these data the maximum projection sphericity could be computed. Maximum sphericity was then plotted against the settling velocity and Wadell sphericity (Figure 2.9), and thus, it was found that the agreement with experimental hydraulic data was greatly improved. Comparison of correlation coefficient values in settling velocity also showed significant difference between two measures (for Wadell measure 0.76 and maximum sphericity measure 0.97).

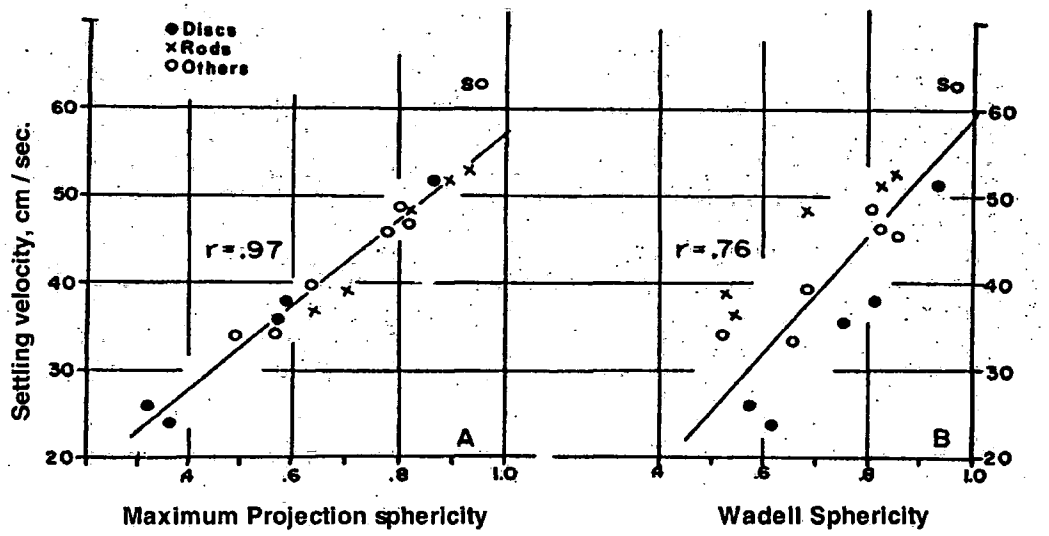

Figure 2.9 Settling velocity of particles as a function of maximum projection sphericity (A) and of Wadell sphericity (B) (From Sneed and Folk, 1958). Comparison of both plots clearly shows that there is almost perfect correlation between maximum projection sphericity and particles settling velocity (r = 0.97), while there is no similar correlation with Wadell sphericity (r = 0.76). Thus maximum projection sphericity method provides a better representation of the actual hydraulic behaviour of particles than that of Wadell's sphericity.

They also compared rolling velocities of particles as a function of maximum projection sphericity and Wadell sphericity (based on the same data). By plotting maximum projection sphericity and of Wadell sphericity data against rolling velocity a significant agreement was found between maximum sphericity data and rolling velocity of particles (Figure 2.10). In other words maximum projection sphericity gives a much better prediction of rolling than Wadell sphericity.

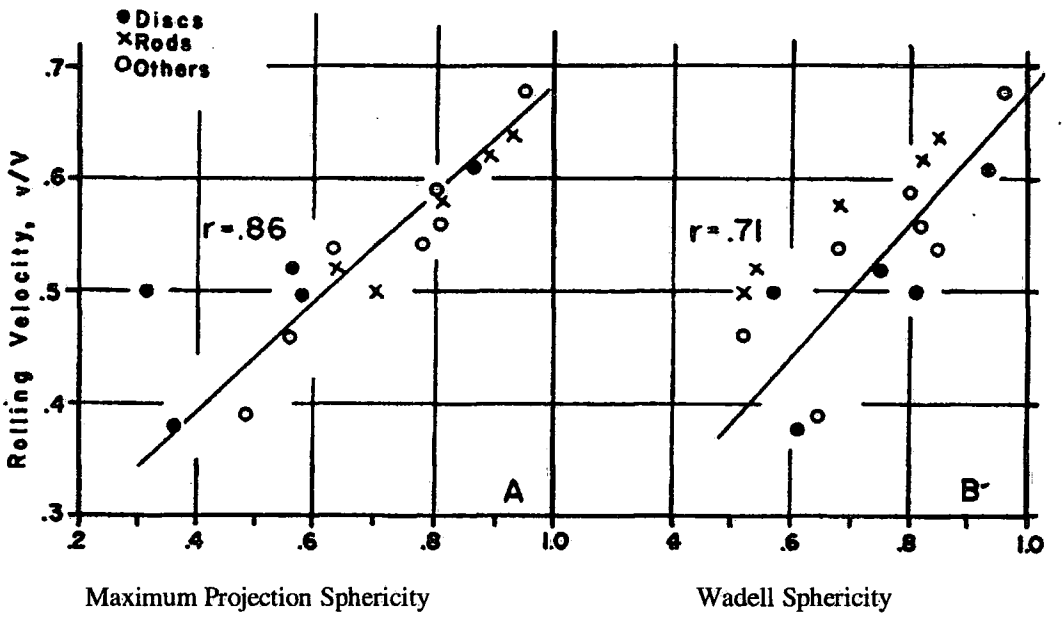

Figure 2.10. Comparison of rolling velocity of particles as a function of maximum projection sphericity (A) and of Wadell sphericity. (B) The rolling velocity expresses the ratio between the speed of a water current (V) and the speed with which a body in that current is rolled along the bottom of a flume (v) (After Sneed and Folk, 1958).

Sneed and Folk (1958) showed that in flume experiments the maximum projection sphericity measure showed a much closer correlation with actual hydraulic behaviour (Figure 2.10). For rolling velocity, the correlation coefficient with maximum projection sphericity was 0.86 as against 0.71 for the Wadell sphericity. Extreme rod-like and extreme disc-like forms fall directly on the same trend line when maximum projection sphericity is plotted, compared with their systematic displacement when Wadell sphericity is used. It was concluded that correlation coefficients for rolling velocity are lower than those for settling velocity because rolling velocity is influenced more by sharpness of edges (brick-shaped and cylindrical forms of the same sphericity do not have the same rollability).

Apart from direct measurement techniques, there are also some visual estimation charts for determining the sphericity of particles. Owing to their ease of operation, large numbers of particles can be quickly classified. Particles are compared with a standard visual comparison chart and a decision is made relative to the sphericity classification of the particles. Krumbein and Sloss (1955) produced a grain silhouette chart showing four

classes of sphericity in combination with five classes of roundness (Figure 2.11). This chart enables both sphericity and roundness of particles to be estimated simply and speedily.

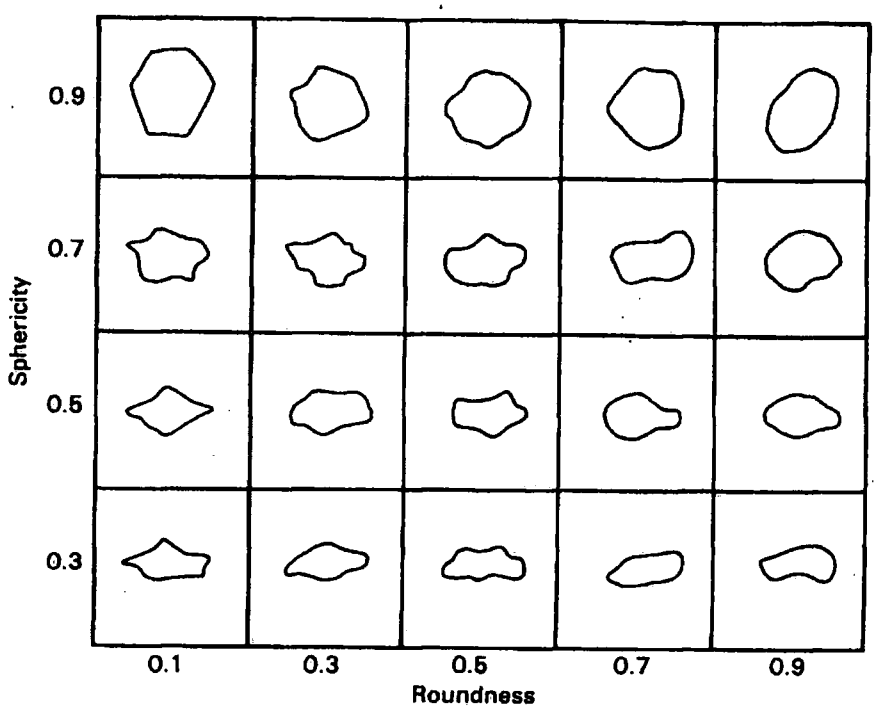

Figure 2.11. Chart for visual estimation of roundness and sphericity. (from Krumbein and Sloss, 1955).

However, this chart has been much criticised in the use of sphericity, because the chart is two-dimensional. The instructions should perhaps include the need to rotate the particle in directions at 90° of each other and take an average.

2.7.3 Flatness

Clast flatness has an important influence on hydraulic behaviour and also on mode of motion. There is an inverse relation between the rolling and particle flatness. The flatter the particle the more likely it is to move by sliding. Flatness also has a significant influence on particle settling velocity (Wilde, 1952; Alger, 1964; Romanovskij, 1966; Komar and Reimers, 1978; Baba and Komar, 1981a and 1981b; Halllermeier, 1981; Hottovy and Sylvester, 1979). When compared with a sphere of the same volume and density, flatter particles settle slower due to a larger cross sectional area to volume, and hence higher flow resistance (See Chapter 7).

In terms of three-dimensional characterization of a particle, Cailleux (1947), following Wentworth (1922a, b), suggested a flatness index which has a very high inverse correlation with Sneed and Folk's sphericity (r = ⁻ 0.981) (Orford, 1975). Again this index is based on the relationship between the three principal axes:

$$F = \frac{a+b}{2c} \cdot 100 \qquad (2.16)$$

The index ranges from 100 to infinity. The minimum value relates to a perfectly equidimensional particle, and the flatter the particle the higher is the flatness index. This is also essentially the inverse of Krumbein's sphericity (Briggs, 1977).

Differences between roundness and sphericity

Roundness should not be confused with sphericity. Wadell (1932) pointed out that roundness value gives a summary expression for certain detail characteristic of the solid, while the sphericity value expresses the shape. Thus sphericity and roundness together express the image of the solid. Sphericity is a measure of the degree to which particles are equidimensional. For example a particle may have a maximum degree of roundness and still not be a sphere. Conversely a particle (e.g. a perfect cube) may have a high degree of sphericity and a low roundness value (Figure 2.12) (Wadell, 1932). This is because, as Kuenen (1956) pointed out, the initial shape of particles often has an important effect regardless of the rounding accomplished by wear. Similarly a cube has the best chance of approximating a sphere as a result of the attrition, whereas a particle with a plate or rod-like initial shape has little chance of achieving a spherical form.

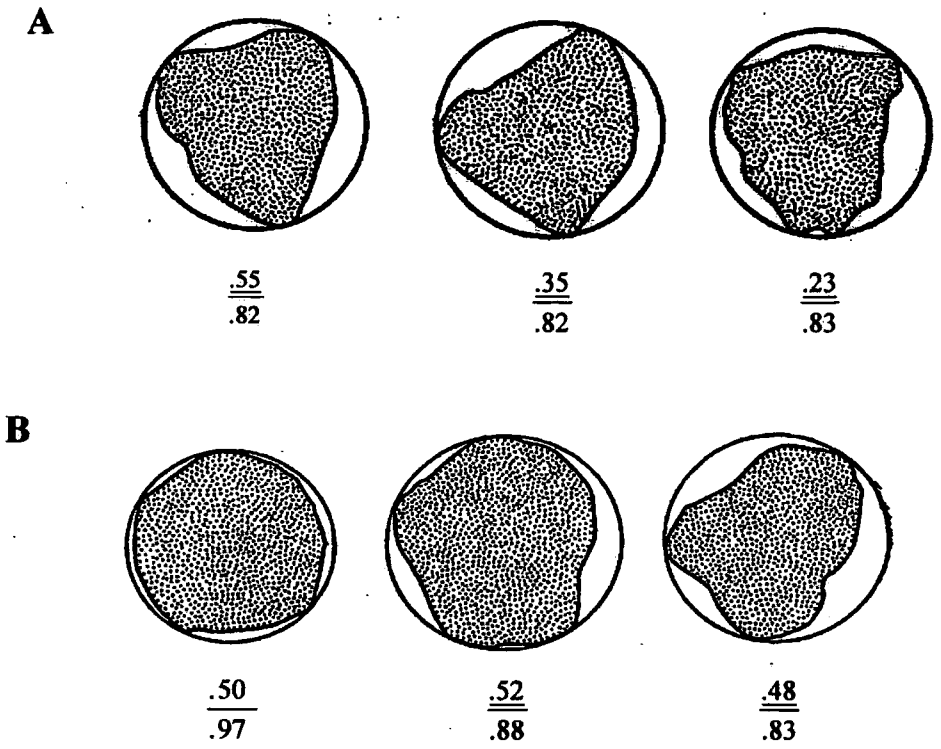

Figure 2.12 Particles of the same sphericity but differing roundness (A), particles of the same roundness but of differing sphericity (B) (After Wadell, 1932). The circles around the particles facilitate the impression of sphericity. The top and bottom numbers of the first particle indicate 0.55 degree of roundness and 0.82 degree of sphericity. The first and second particles from the left in the upper row have the same sphericity, but different roundness values. The third particles in the top and bottom rows are of the same sphericity, but show noticeable difference in sharpness.

Wadell (1932) described rounding as a special type of disintegration created by attrition and solution. Fracturing and chipping destroy or diminish the roundness. Krumbein (1941a) also pointed out that roundness is extremely sensitive to abrasion, and angular particles change rapidly in their roundness during movement. After the initial stages of rounding the process is much slower. Whereas during abrasion, shape is relatively stable, and the original form is often reflected in the pebble even after considerable wear. Under impact breakages mean shape may change rapidly.

Wadell (1932) was the first to show that there is a fundamental difference between shape and roundness and that these properties are geometrically independent

variables. It was stated that roundness was a matter of the sharpness of the corners and the edges of a particle, whereas shape has to do with the form of the particle independently of the sharpness of its edges. In other words a particle may be perfectly spherical in shape but completely angular, or perfectly rounded but far from spherical. Indeed although several geometrical solids such as cube, tetrahedron, dedocahedron, have different shapes, their corners are equally sharp, thus radius of curvature of the corners is zero. In terms of hydraulic behaviour of a particle in a fluid flow, some studies have shown that the shape of a particle influences its behaviour during transport and deposition. There is a direct relationship between the degree of particle sphericity and the velocity at which a particle of a particular volume will roll along a bed or will settle in a fluid. The more spherical the particles the more it moves in a rolling mode (e.g. Krumbein, 1942; Sneed and Folk, 1958; Bradley *et al.*, 1972; Gale and Hoare, 1991; Schmidt and Ergenzinger, 1992). Therefore sorting may be controlled partly by shape, whereas roundness of a particle does not effect its hydraulic behaviour or settling rate as much as sphericity does. In other words it has less effect on sorting or transport as compared with sphericity. In essence, influence of roundness on mode of movement becomes important for the particles that are more spherical or rod-shaped. A sphere or rod-shaped particles with greater roundness value can roll easier than those that are more spherical (cube) or cylindrical but less round. On the other hand, for flat particles, such as blade and disc, roundness has no significant effect on their sliding. Roundness is mainly influenced by rigour of wear and distance of transport. As a result it can be concluded that the definition of roundness and sphericity are almost independent and it is generally assumed that only very great changes in one may effects the other (Pettijohn, 1949). Thus, due to its significant influence on the hydraulic behaviour of a particle, sphericity is considered the most significant measure for bedload transport studies compared to roundness.

2.8 OTHER TECHNIQUES IN GRAIN SHAPE ANALYSIS

Over the last two decades there have been great advances in shape determination technology due to the development of the of automatic image analysers and associated computer software. Advances in video-picture capture and digital transformation as well as in the data storage and memory have increased speed and accuracy of shape measurements. Allen (1981) reviews some of the specific methods of automatic and

semi-automatic grain counting, which enable shape indices to be generated from particle size data collected rapidly from large grain samples.

2.8.1 Image analysis techniques

Most of the image analyses techniques decompose the video picture into an array of picture elements (pixels), each one of which records a digital value related to the grey scale registered at each pixel. By setting a grey-scale threshold that identifies a two tone range (black and white), each picture element can then be set to 1 or 0 depending on whether or not the particle's image overlies that particular position. In this way the outline of the particle can be detected at the boundary between 1 and 0 in the picture elements (Orford and Whalley, 1983). Pye (1994a) pointed out that most of automated image analyses techniques have been based on two-dimensional images. Basically, once the grain outlines are digitised and converted to a series of x, y coordinates. These data are then analysed using techniques such as Fourier analysis (Ehrlich and Weinberg, 1970; Ehrlich, *et al.*, 1974, 1980; Mazzullo *et al.*, 1986, 1992) and fractal analysis (Mandelbrot, 1967, 1977; Orford and Whalley, 1983, 1991; Clark, 1981, 1987; Diepenbroek, *et al.*, 1992).

2.8.2 Fourier analyses

In Fourier analyses, the maximum projected grain profile is compartmentalised into a series of standard shape components that converge to reproduce the natural grain shape. The grain perimeter is expressed as Fourier series expansion of the grain radius as a function of the polar angle about the centre of gravity of the grain;

$$R(\theta) = R_o + R_n \cos(n\theta - \theta_n)$$

where R_n is the harmonic amplitude, θ is the polar angle, R_o the grain radius, n the harmonic number, and θ_n is the phase angle. The lower order harmonics (1-5) reflects the broad form characteristics of the grain, while the higher order harmonics (usually up to 23) provide information about the grain roundness and, to a limited extent, surface texture. Data may be presented graphically by plotting the frequency of occurrences as a function of each harmonic amplitude. The interval boundaries in these shape-frequency histograms are then defined by the maximum entropy concept, and the most informative harmonics identified by relative entropy analyses (Pye, 1994a).

Results of two-dimensional Fourier grain-shape analysis have been shown to be

influenced by preferred grain orientation but these techniques have been applied successfully in a wide range of provenance and sediment transport studies (e.g. Mazzullo *et al.*, 1983, 1986; Kennedy and Enrich, 1985; Dowdeswell *et al.*, 1985; Haines and Mazzullo, 1988; Diepenbroek, *et al.*, 1992). Pye (1994a) pointed out that difficulties appear when grain outlines show a very high degree of irregularity, such as in the case of highly weathered or diagenetically altered grains. In these circumstances, fractal analyses may provide a more suitable alternative (Orford and Whalley, 1983, 1991; Kennedy and Lin, 1991). Boon *et al* (1982) stressed that use of Fourier coefficients as a means of identifying scale components of form is a technique of considerable importance to form studies.

Most of the previous conventional roundness determination methods have failed to separate the influence of sphericity from roundness and, consequently, a systematic error is introduced in the higher roundness grades. An increase in elongation or eccentricity of the ellipsoid results in a decrease of the corresponding roundness values. Using a Fourier analyses method which is called "Closed-form Fourier analyses" (which was originally developed by Ehrlich and Weinberg (1970)) Diepenbroek, *et al* (1992) were able to avoid this error by relating the roundness of a given particle to the best inscribed ellipsoid. The method basically evaluates the curvatures of the complete outline of a particle and takes the position of these curvatures on the particle surface into account. Diepenbroek, *et al* (1992) stated that tests on more than 30000 fluvial and coastal gravel clasts proved the reliability and sensitivity of the method. Even small roundness changes during transport along short mountain rivers were detected by the method.

2.8.3 Fractal dimension

Fractals provide an alternative integrated index of form which is appropriate for any regular or irregular particle (Mandelbrot, 1982; Orford and Whalley, 1983). Although Mandelbrot regards the fractal dimension as being singular for any particle, some investigators (e.g. Kaye,1978; Orford and Whalley, 1983; Whalley and Orford, 1983) showed that natural and artificial particles may have three fractal dimensions: structural and textural values that reflects the two major scales of edge variation appropriate to macro-form and edge texture respectively, and an overall fractal value that integrates all scale changes of form.

2.9 CASE STUDIES ON BEDLOAD SHAPE AND SIZE

Although there is a considerably body of literature on bedload transport in gravel-bed rivers, there have been relatively few studies investigating the effects of bed material shape on bedload transport. Many previous investigations concentrated on the effects of abrasion, selective entrainment, grain pivoting and friction angles, and downstream changes in bed material shape (roundness, sphericity, etc.). Far less is known about the hydraulic behaviour of different shape of particles during bedload transport. Much of the existing work on shape selective transport is based on laboratory experiments and thus there is a lack of field-based studies. The scope of the following section is to summarise the laboratory and field studies that have investigated the influence of bedload shape and size on bedload transport in gravel bed rivers. In considering laboratory experiments, friction angle measurements based on mechanistic behaviour of particles in relation to particle shape, size and bed roughness are discussed. Field based studies, on the other hand, summarise downstream changes in bed material shape (roundness, sphericity, flatness) and influence of shape on bedload transport dynamics.

2.9.1 Laboratory experiments

Many early laboratory experiments concentrated on the effects of abrasion and sorting processes on bedload shape and size, (e.g. Daubree 1879; Wentworth 1919; Marshall, 1927, Krumbein, 1941a; Rayleigh, 1942, 1944; Sarmiento, 1945; Potter, 1955; Kuenen, 1956; Bradley, 1970; Bradley *et al.*, 1972; Moriwaki *et al.*, 1985; Kodama, 1992). In addition to the abrasion processes, several attempts have been made to describe the physics of bedload transport. For example, some laboratory studies have examined selective entrainment in relation to particle size and shape on various bed roughnesses. The laboratory or flume-based approaches are justified because of complexity of the field setting. Streambed roughness varies from place to place within a given channel due to (a) differences in shape, size, roundness, mineralogical particle composition, surface texture and orientation of a individual bed material; (b) local hydraulic conditions (e.g. discharge, velocity) and; (c) sedimentological characteristics of the bed (e.g. texture, packing, armouring, bed forms). Thus, the combined affects of these factors results in at a point-to-point variation in the processes that control the

critical shear stress of each individual grain (Kirchner *et al.,* 1990). A second difficulty is that the movement of bedload is accepted to be the most difficult mode of sediment transport to measure. The difficulty arises from the fact that movement occurs at relatively high flow velocities when bedload particles are intermittently transported by the means of sliding, rolling or skipping along in almost continuous contact with the streambed. Because of these difficulties, direct measurements of bedload movement are still relatively few.

Friction angle measurements

One of the most important problems in describing the physics of bedload transport involves constructing a force balance for individual grains on a rough bed. There are two significant factors that affect the force balance. These are the friction angle and the relative protrusion of the grain above the bed (figure 2.13). The first factor indicates the resistance to movement of the particle by the flow, while the second factor affects exposure to the flow (Kirchner *et al.,* 1990). Studies have shown that variability in friction angles and relative grain protrusion above a given bed affect critical shear stress, the relative mobility, selective entrainment of different sediment sizes (Komar and Li, 1986, 1988) and the mechanics of bedload transport (Iseya and Ikeda, 1987; Whiting *et al.*, 1988). It has been clearly demonstrated by several investigators that both grain protrusion and friction angle vary with the shape, size, and orientation of the individual particles, as well as the shape, size, orientation, and packing arrangement of the particles comprising the local bed (Kirchner *et al.*, 1990).

Friction angles have been measured by several investigators and it has been stated that the mechanics of grain movement from a bed of mixed sediment involves a consideration of the pivoting of the grain about its contact point with an underlying grain (White, 1940; Bagnold, 1941; Slingerland, 1977; Komar and Wang, 1984; Li and Komar, 1986; Komar and Li, 1986). Initiation of movement occurs as the drag force of the flowing fluid, tipping the grain out of its resting position, exceeds the particle's weight. This threshold process mainly depends on the magnitude of the pivoting angle of the particle (Li and Komar, 1986) (Figure 2.13). Although some investigators have equated this pivoting angle to the angle of repose, which is about 33^0 for sand-sized sediments (Shields, 1936; Allen, 1969, 1982; Carrigy, 1970), in coarse-bed rivers, because of the various grain shape and sizes, it is impossible to determine a standard pivoting angle representing all bed material. Where this has been attempted, friction

angle measurements were restricted to uniform sand-sized, sphere-shaped particles (e.g. Chepil, 1959; Miller and Byrne, 1966). Recent investigations (e.g. Li and Komar, 1986) have shown that for a similar size range, friction angles measured with different test particles showed great variance. Compared to ellipsoid and angular particles, sphere-shaped test particles showed lower friction angles on beds of varying roughness. This is because particles of different shape have different contact point with the underlying bed roughness elements. Another factor is that in many of the earlier experiments, artificially-formed, uniform bed roughnesses were used. However, the bed roughness of a coarse-bed river varies from place to place within a given channel reach (Hoey, 1992). Due to this spatial variation, on a natural bed roughness different friction angle measurements would be expected.

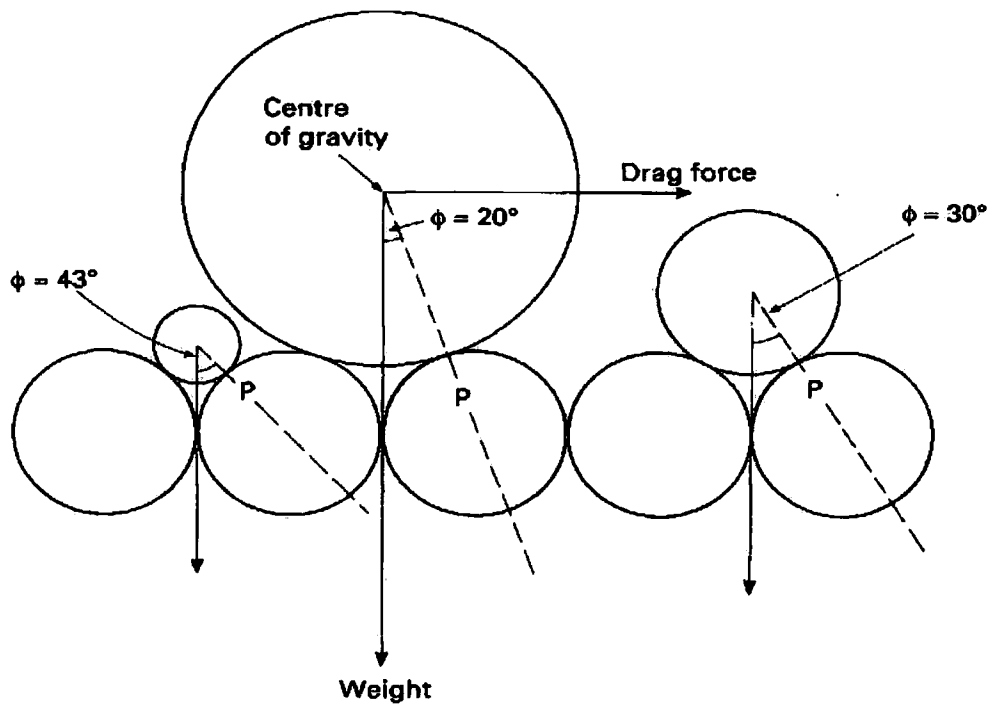

Figure 2.13 Schematic two-dimensional diagram showing the dependence of the pivoting angle on the relationship between the size of a spherical particle (D) and the size of the particles on which it rests (K). P is the pivot point (After Pye, 1994)

Several investigators have shown how the pivoting angle will differ for the various particle shapes and sizes within a bed of mixed grains. The pivoting angle depends on the ratio of the diameter of the grain to be moved to those it rests upon; The

larger the ratio, the smaller the value of the pivoting angle and the more easily the grain can be pivoted out of position during entrainment (Li and Komar, 1986) (Figure 2.13). This dependency in pivoting angle has been noted as a significant factor in the selective entrainment of gravel in rivers (Slingerland, 1977; Komar and Wang, 1984).

Previous friction angle measurements

Most of the earlier friction angle measurements were carried out for a variety of gravel surfaces whose grains were arranged by various artificial means, rather than by the action of flowing water. The majority of these measurements also illustrated the influence of particle size on the friction angle. For example, Eagleson and Dean (1961) made a series of friction angle experiments to determine the threshold of particle movement. Friction angles for a spheres of different size resting on two beds of uniform natural sands (one 1.83 mm and the other 0.79 mm in diameter) were measured. Their experiments mainly based on various relative roughness values (D/K ratios), where K is the bed-particle diameter and D is the diameter of the single particle resting on the bed. It was found that the average friction angle (Φ) decreased with increasing D/K. (Figure 2.13). They also compared their measurements with the theoretical relationship for the pivoting angle of a sphere of diameter D resting on a bed of uniform size K.

$$\tan \Phi = \frac{y}{\sqrt{(D/K)^2 + 2\,(D/K) - \frac{1}{3}}} \qquad (2.17)$$

In order to achieve this comparison the bed grains were arranged into equilateral triangles as in the cannon-ball tetrahedron: the volume of the y coefficient depends on whether the upper grain pivots directly over the top of a base particle ($y = 2/\sqrt{3}$) or through the lower saddle between two base particles ($y = 1/\sqrt{3}$). Equation 2.17 predicts that pivoting angle decrease with increasing D/K value but the measurements of Eagleson and Dean showed poor agreement with this theoretical relationship. The average values of friction angles (φ) were found about 10-20° larger than theoretically expected from the geometry of a regular triangular packing of uniform spheres. In other words the data fell parallel to the predicted curve, but were systematically displaced to higher values. For the special case of uniform grains (D/K=1), this equation predicts that pivoting angle is 35° for grain-top rotation and 19.5° for saddle rotation, on the

order of the angle of repose; the measurements of Eagleson and Dean gave pivoting angle equal to 50°.

Miller and Byrne (1966) also studied the dependence of the pivoting angle on relative roughness. Their measurements were carried out with sand-sized spheres, with natural beach sands, and with crushed angular quartzite sand. Using a binocular microscope, individual grains pivoting out from fixed grains, were observed. It was found that the measurements with spheres agreed with the data of Eagleson and Dean (1961), but not with the theoretical equation. Thus Miller and Byrne (1966) proposed an empirical relationship to describe the mean friction angle.

$$\Phi = {}^{\alpha}(D/K)^{-\beta} \tag{2.18}$$

Where α is a coefficient which changes with grain shape (shape parameter), β depends on the effects of sorting of the bed grains (sorting parameter) and K is the average diameter of the bed grain (Miller and Bryne, 1966). Fitting equation 2.18 to the measurements on uniformly sized and poorly sorted beds of spheres, a positive relationship was found between the degree of sorting and β coefficient, while the α coefficient was found relatively insensitive to sorting. By using equation 2.18, it was found that the measured pivoting angles were significantly greater than the angle of repose or avalanche angle of 50° for spheres of uniform size, 61° for the natural beach-sand and 70° for the crushed quartzite sand. Using typical bed particles as test grains, Φ and $D/\overline{K}$ were compared for three beds of various grain shape but almost identical size distributions. It was found that although α was sensitive to shape, the same sensitivity was not observed for β. In other words there is an inverse relation between values of α (and thus Φ) and sphericity and roundness, but a similar relation is not true for β.

Eagleson and Dean's (1961) and Miller and Byrne's (1966) studies were mainly limited to sand-sized grains, spheres, and natural sands. Although these studies, to some extent, demonstrate how the friction angle is affected by grain size (D/K) and grain shape, they were not able to clarify fully why the measured angles are significantly greater than the angle of repose and why average values of Φ were larger than the theoretically expected relationship (equation 2.17). In order to have a clear idea of the dependency of size and shape on the friction angle it also seems reasonable that the effect of these parameters should be investigated on a bed of natural mixed sediment

rather than uniform grain size and shape. This may be an important factor in selective grain entrainment.

Li and Komar (1986) attempted to resolve these uncertainties, and provide an improved assesment of how grain pivoting depends on grain shape (rollability and angularity); relative roughness and on factors such as imbrication. The major focus of their study involved pivoting angle measurements for natural pebbles. The measurements were carried out on gravel-size particles. For the experiments naturally formed gravel-sized spheres and angular crushed basalt pebbles were used.

The experiments undertaken with spheres provided a direct test of theoretical equation (2.17) and it was found that although the data also depart systematically from the theoretical equation (2.17) (a similar relationship as discussed previously), the maximum departure is at most $3\text{-}4^0$ and average close to 1^0. This is much lower than studies of Eagleson and Dean (1961) and Miller and Byrne (1966) that depart by about $10\text{-}20^0$. Thus unlike the previous experiments with sand-sized spheres, large gravel-sized spheres showed reasonable agreement with the theoretical equation (2.17) for the dependence of Φ on D/K.

Effect of grain shape on friction angle

Li and Komar (1986) carried out further experiments with ellipsoidal gravel to analyse the effects of particle shape and size on pivoting angles. In these experiments the grains were placed with their long axes transverse to the slope and small axes perpendicular. It was shown that apart from grain size there is also a significant relationship between grain shape and Φ. In other words friction angle was found to depend on grain shape, particularly on the D_c/D_b ratio of axial diameters (ratio of the particle shortest axis D_c to its intermediate axis D_b). In relation to a particle's D_c/D_b ratio different motions occurred during the experiments. The flatter ellipsoidal pebbles moved by sliding rather than pivoting and rolling. Sliding grains also tend to show higher Φ, while the rolling grains had lower values. Differences in motion were dependent on D_c/D_b, or in other words the grain's ability to roll or slide. Thus it was shown that as D_c/D_b increases (towards a circular cross-section) Φ decreases and particle tends to roll (pivoting occurs), whereas sliding occurs at low D_c/D_b values. Using the ellipsoidal grains Li and Komar clearly showed that pivoting angle depended on grain shape as well as on grain size. No relation was found between the pivoting angle and particle elongation D_b/D_a (D_a is the longest axis of particle).

Effects of particle imbrication and orientation on friction angle

Several investigators (e.g. Church and Gilbert, 1975; Laronne and Carson, 1976; Petts, 1983; Li and Komar, 1986; Hassan and Reid, 1990) have clearly shown that as well as particle shape and size, pebble imbrication, which is primarily related to pebble shape, also controls particle entrainment (Laronne and Carson, 1976; Li and Komar, 1986; Gomez, 1991). On a gravel bed the stable resting position of a particle depends on its shape and also on the concentration of gravels in the bed. It is generally accepted that there is a close link between bed material shape and imbrication, leading to spatial and temporal variability in the pattern of bedload transport, even during near constant flow conditions (Laronne and Carson, 1976; Gomez, 1991).

Imbrication in gravel-bed channels is known as one of the controlling factors in bedload transport. Gravels in streams tend to imbricate, especially if the grains are relatively flat. Particles in discontinuous transport as part of the bedload present the greatest resistance to movement when tilted upstream (Laronne and Carson, 1976; Gomez, 1991). Most particles will also tend to be oriented with their long axis parallel to current, minimising the cross-section presented to the current and increasing stability. Thus, imbrication develops in response to the flow of water impinging on the bed particles. Orientation of the plane of maximum projection to dip upstream was found the most stable position for closely packed particles because the force of the flow presses the particle to the bed. Petts (1983), however, pointed out some aspects of the mechanisms of imbrication development in terms of pebble shape. He stated that "imbrication is particularly well developed by *disc-shaped* particles transported as bed-load and sufficiently well sorted to permit the particles to come out into contact with each other to become imbricated".

Li and Komar (1986) carried out several experiments to investigate the effect of imbrication on grain pivoting and entrainment. They used ellipsoidal pebbles in order to develop imbrication. Two experiments were carried out. All measurements were made with the pebbles in a grain-top pivoting arrangement. In the first experiment pebbles were arranged parallel to the slope, while in the second experiment, the same pebbles were placed in an imbricated pattern with a 23° dip and the measurements were repeated. It was shown that Φ values increased when the pebbles were in an imbricated situation. Li and Komar (1986) clearly demonstrated that imbrication (mainly because of flatter shaped bed material) creates a very different geometry for grain pivoting and movement. This must be considered as a important factor in studies of the effect of

particle shape on Φ angles and entrainment.

Experiments with angular gravel have shown that friction angles are greater than for smooth, ellipsoidal pebbles and spheres (Li and Komar, 1986). This was due to the interlocking of angular grains.

Friction angle experiments with "natural" beds

These experiments discussed so far have demonstrated the dependence of friction angle affected on many factors, including grain shape, relative grain size (D/K) and bed grain-packing arrangements. However, none of the studies have been based on naturally formed fluvial gravel surfaces. Previous friction angle studies (e.g. Miller and Byrne, 1966; Li and Komar, 1986) were limited to artificially manufactured surfaces. More recently investigators have begun to investigate the friction angle properties of water-worked, flume-based or natural streambed surfaces with a variety of grain shapes and sizes. The surface topography of natural water-worked sediments is complex and friction angles, grain protrusion and estimated critical shear stress will therefore vary widely among individual grains, even for a narrow range of grain shapes and sizes of a natural bed. Individual grains may vary greatly in their entrainability, depending on their exact location on the bed (Kirchner *et al.,* 1990). On natural beds, with more complex structural arrangements, interlocking of irregular-shaped particles and impacts of mobile particles on static bed particles may also be very important for initial motion (McEwan *et al.*, 1999). As Kirchner *et al* (1990) observed, artificial beds have looser packing arrangements with many pore spaces that are large enough to trap small and medium grains. However, with water-worked natural beds, because of active transport, such pores would trap grains and thus close themselves and smooth the surface.

Kirchner *et al* (1990) presented some of the first measurements of friction angles and grain protrusion distributions for water-worked sediments. Results, based on a flume study, compared unworked and water-worked beds. These comparisons clearly show that the friction angle distributions of the two surfaces differed greatly. Friction angles measured on the unworked bed were significantly greater than those for the water-worked bed. Differences increase with decreasing test grain size. The difference was mainly attributed to grain packing geometry. In addition, Kirchner *et al* (1990) also determined two main factors causing variability on the water-worked surface. First, a water-worked mixed-grain surface is characterised not by a single friction angle, but by a wide distribution of friction angles due to the local variability in the pocket geometry

and from variation in the shape and orientation of individual test grains. Secondly, as with previous studies, there is a very significant inverse relation between the D/K ratio (ratio of test grain size to the median bed grain size) and measured friction angles. Kirchner *et al* (1990) were able to show the critical shear stress of a single grain size on a rough bed is not a single value, but instead a probability distribution which becomes broader with decreasing grain size and increasing bed roughness.

Comparison of unworked and water-worked beds also showed that even when grain shape and sorting are held constant, variations in packing geometry can create significant differences in friction angles (Kirchner *et al.,* 1990). On the other hand, by controlling for both grain packing geometry and sorting, Li and Komar (1986) found that particles of different shape had a different influence on friction angle. These two studies clearly suggest that more experimentation is required to better understand the relationship between different grain shapes and friction angles. Following Kirchner *et al* (1990), Dietrich and Kirchner (1992) presented the first friction angle data from naturally-formed gravel streambeds. These data showed a dependency of friction angle on degree of surface sorting. Similar to the previous studies, it was found there was an inverse relationship between friction angle and relative grain size, and lower friction angles are associated with poorer sorting. In addition, the probability distributions of critical shear stress for different grain sizes on a given bed surface showed a common origin, but otherwise a divergence with larger grains having narrower and lower ranges of critical shear stresses.

Kirchner *et al* (1990) and Dietrich and Kirchner (1992) made several important points about mechanistic behaviour of particles on natural bed surfaces but the effect of different particle shapes on the friction angle has been somewhat neglected. Particle shape must also be considered in friction angle measurements.

In a series of experiments with a recirculating glass-walled flume, Carling *et al* (1992) examined the initial motion of particles of similar weight but different shape and orientation on three beds of differing roughness. They demonstrated that for a particular size range, particle shape and orientation on a given bed roughness are as important as is the mass of the particle (defined by weight or diameter) in determining initial motion. In these experiments, three artificial stable bed roughnesses were used with three sizes of particle (16-32 mm, 40-64 mm, and 125-250 mm). Four concrete well-rounded particles of similar weight (1 kg) and density (2.69) were compared. These test particles were a rod, an ellipse, a disc, and a spheroid. Three particle orientations were considered; long

axis parallel to flow, transverse and oblique. The entrainment characteristics of a sphere and a cuboid of similar weight (2.4 kg) and density (2.65) were also compared on various bed roughness types.

In terms of the mode of initial motion, particles of different shape and orientation showed different hydraulic behaviour. On the smoothest bed the ellipse and rod placed parallel or oblique to the flow, swivelled to a transverse attitude before rolling out of place. Sphere-shaped particles were entrained in all orientations. Rolling about the *a* axis was commonly observed, and was the main mode of transport for all shapes. At the highest velocities, disc, could roll about any of the three axes or slide. On the smoothest bed the most stable position was for an ellipse was with the *a* axis positioned parallel to the flow, while the least stable was the rod, positioned transverse to the flow. These experiments clearly demonstrated that particle orientation is as important as particle shape and relative mass in dictating the critical threshold of motion. Orientation alters the cross-sectional area of the particle that is exposed to main stream-line and to a lesser extent affects particle stability with regard to the contact points of the particle with underlying particles. Because of their movement by rolling as well as sliding, rod-shaped pebbles commonly have their a axis orientated perpendicular to streamflow. A rod-shaped pebble may become lodged at one end so that it swings round to become orientated parallel to the current. Such particles in isolation in a mixed sand and gravel bed, however will, be rolled around their longer axis and arranged perpendicular to the flow direction. Once a pebble has come to rest on the stream bed a circular depression is excavated at its upstream end whilst the deposition of material on the downcurrent side supports the downstream end. Eventually the pebble becomes tilted at low angle $< 20^0$ and dips upstream in a position of equilibrium, with its a-axis remaining more-or-less horizontal. The threshold shear velocity for the parallel rod was found to be more than double that for the transverse rod.

Increasing the bed roughness result in moving the pivot points further apart and provided an opportunity for the test particles to take-up more stable rest positions. Thus, pivot angles increase. On the smoothest bed the parallel rod was the most stable, while on the rougher bed it was the parallel ellipse. On rougher beds oblique particles tended to become less stable and easily rolled to a transverse orientation. The typical mode of movement for the sphere was rolling. Comparison of the entrainment characteristics of a sphere and a cuboid of similar weight demonstrated that the cuboid-shaped particle moved at a higher shear velocity than the sphere. On smooth bed site sphere was very

unstable but stability increased with increasing roughness. However, because cuboid particles did not sit in the col between the bed particles, but tended to bridge across the gap and sit on the top of the bed particles, differences between critical values for sphere and cube decreased with increasing bed roughness (Carling *et al.*, 1992).

On the roughest bed Carling *et al* (1992) found that shortening the c axes of test particles caused the initiation of imbrication that also enhanced bed stability. Only rods were observed to be entrained from any orientation without imbrication occurring, while spheroids rotated into an imbricated position before entrainment. In contrast to smooth and intermediate bed roughnesses on the roughest bed oblique particles required lower threshold values than the parallel and transverse particles.

Carling *at al* (1992) showed that variation in particle shape, orientation and different bed roughness are important factors for the initial motion of bedload. The potential for a particle to become imbricated was found primarily to depend on the test particle shape and size with respect to roughness of the bed material. They also stated that, even in a laboratory situation, there could be a wide range of critical flow conditions for a particle of given size due to variations in bed material shape, orientation, and also bed roughness. However, on natural beds, with more complex structural arrangements, interlocking of irregular-shaped particles and the impacts of mobile particles on static bed particles such variability would be even greater. They concluded that variation in the size range of particles entrained for given flow condition would depend primarily on particle size, shape, and packing arrangement of the bed materials.

In terms of particle travel velocities on beds of varying roughness, it was found that particles with different shapes responded differently. On the smoothest bed all particles moved close to the bed primarily by rolling, but rods move faster and tended to twist about obstacles and achieve greater acceleration as the end of the rod protrudes into the higher velocity flow. On rougher beds, peak velocities increased as particles began to bounce into higher velocity flow. As a result, selective transport became more significant among different shapes of particles. Oblate and flat particles move more easily (possibly with enhanced lifting) and directly over the roughness elements, while the spheroids meander around obstacles and thus lengthen the transport path. Transport of spheroid-shaped particles on the rougher beds was retarded by the roughness of the bed more than for any of the other shapes. The decreasing orders of transportation (fast to slow) were found to be disc, rod, ellipse, and spheroid.

Work by Meland and Norman (1966), and Steidtmann (1982) also found that sphere-shaped particles on a very rough bed in high-velocity flows show different hydraulic behaviour than at low velocities. The relative movement (velocity) decreases as the bed is roughened. Francis (1973) stated that different bed roughness and flow velocities control the hydraulic behaviour of particles. He pointed out that on a rough bed, spheres meander around obstacles at low flows and thus extend their transport paths, however, at higher flows they may shorten their transport paths and increase their velocity by bouncing or rebounding. Investigators such as Krumbein (1942) and Meland and Norman (1969) noted that, due to rolling, spheres can move easily even at low flow velocity on a bed with low roughness, while oblate particles do not. In high velocity flow and over rough beds, flat particles outrun sphere or rod-shaped particles (Bradley, 1972; Johansson, 1976).

These laboratory experiments have demonstrated that as well as factors such as pebble size and bed structures (e.g. imbrication), variations in pebble shape and orientation for a given bed roughness are important in controlling bedload transport. However, results from laboratory experiments are different from the naturally formed gravel beds. Several investigators (e.g. Laronne and Carson, 1976; Schmidt and Ergenzinger, 1992) have pointed out the influence of river bed morphology on bedload transport which Carling *et al* (1992) did not consider in their experiments. In fact, using different shapes of particle in their field experiments, Schmidt and Ergenzinger (1992) found that although particle shape has an absolute influence on transport length, most laboratory studies do not consider bed morphology (e.g pool-riffle, sinuosity) which also has a significant controlling effect on particle initiation motion and transport. It was found that the critical unit discharges along the river are dependent significantly on river bed (pool-riffle, bar, etc.) morphology. For example, in steps, bedload needs higher unit discharges to be entrained. Once entrained, the transport of bedload is stochastic in nature and single particle transport is controlled by the step lengths and the duration of rest periods. Thus they concluded that spatial variability is one of the main factors in gravel bed rivers and must be taken into account in bedload transport studies.

Therefore laboratory studies (flume-based and mechanical analysis) can shed light on only some bedload transport mechanisms. They cannot represent the exact nature of bedload transport mechanism. Thus in order to better understand actual mechanisms, laboratory results must be integrated with field based experiments.

2.9.2 Field studies

In terms of particle shape, early field studies generally focused on factors and processes that influence changes in bed material character in a downstream direction (e.g. Sneed and Folk, 1958; Bradley, 1972; Knighton, 1980-1982). However, in recent years, due to advances in tracer techniques, there have been several field-based studies which have considerably enhanced understanding of particle shape on transport mechanisms of coarse bedload (Ergenzinger and Schmidt, 1990; Schmidt and Ergenzinger, 1992; Schmidt and Gintz, 1995).

Field studies based on downstream changes in bed material shape (roundness, sphericity, flatness).

The downstream variation of bed-material characteristics observed at any one time reflects the cumulative impact of many processes and events which have operated over an indefinite time period (Knighton, 1980). The factors and processes responsible, which have been considered by many authors (e.g. Wentworth, 1919; Krumbein, 1941b; Sneed and Folk, 1958; Bradley *et al.*, 1972; Mills, 1979; Knighton, 1980, 1982; Kodama, 1992; Hoey and Ferguson, 1994; Ferguson *et al.*, 1998) are summarised below:

a) Lithological factors that affect the initial shape and size of bedload particles, their ease and pattern of breakage and their resistance to abrasion.

b) Bedload source factors, including the range of sources and calibre of material supplied, the downstream pattern of inputs and their spatiotemporal variability.

c) River channel processes, including sorting, abrasion and breakage.

d) The influence of tributary inputs on the bed material characteristics of the main stream.

e) Flow variables.

f) Inherited geomorphological characteristics of a catchment (e.g. slope).

An early study undertaken by Unrug (1957) investigated size and shape variation in granite boulders and pebbles along the Dunajec River, Tatra Mountains (Poland). High rates of size reduction were attributed to the combined effect of abrasion and selective transport enhanced in the lower reaches due to the low gradient. In terms of particle shape, it was found that mean sphericity and roundness first increased along

the upper and middle river course but then decreased in the lower river section. It was concluded that the initial high rate of increase in sphericity and roundness resulted from transport of pebbles within the steep Tatra stream valleys over a distance of 8 km. The decrease of mean sphericity and roundness along the lower river course was attributed to the action of sorting controlled by shape, rather than pebble breakage or abrasion. Pebble sphericity was found to be inversely proportional to size.

Sneed and Folk (1958) studied the effect of transportation on roundness, sphericity and form of pebbles derived from three rock types of markedly different physical properties (quartz, chert, and limestone) along the Colorado River. They found that pebble size has a greater effect on sphericity and form than 320 km of fluvial transportation. Large pebbles of limestone retain low sphericity (produced by the bedding of the limestone) and show no significant change with distance. In contrast, quartz and chert pebbles are of similar sphericity and form near the source, regardless of size. However, because large and small sizes wear by different mechanisms, there is increasing divergence in sphericity and form between large and small quartz and chert pebbles as they are carried farther from their source. In short, it was shown that sphericity depends most importantly on the inherent abrasional properties of the different rock types. It is a function of size as well as distance, and is little affected by selective sorting. In terms of pebble roundness it was found that quartz rounds markedly downstream for 432 km but then appears to approach an asymptotic limiting roundness. Chert shows no significant change in roundness between upstream and midstream because of the continuing supply of fresh chert along the river course. At the downstream stations, however, roundness increases significantly. In contrast, there is no statistically significant change in roundness of limestone particles.

Mills (1979) attempted to provide tentative answers to the question of how rock particles become more rounded as they are carried downstream. He analysed data from several studies of downstream change in pebble roundness by computing simple correlation coefficients and regression equations for the relationship between distance and roundness for individual streams. In 20 out of 30 cases examined, there were statistically significant downstream increases in roundness. In 13 of these 20 cases the downstream change was described better by logarithmic or semi logarithmic functions than by linear ones. He also found that in terms of downstream changes in roundness the slopes tend to be steepest for limestone, flattest for quartz, and intermediate in steepness for other lithologies. He attributed differences between studies not only to lithological

factors, but also to: (a) operator variance and the use of different techniques by different studies, (b) differing initial values of roundness of bedload source material and (c) variability in initial roundness of inputs along stream channels.

Knighton (1982), argued that the shape and size of bed material observed at any one time and place depends on two sets of factors: (1) the characteristics of the initial input, which are strongly related to the bedrock, lithology and structure; and (2) the nature and rate of subsequent modifications to that input, either in place or during transport. He argued that because the flow conditions that influence the rate of movement vary with distance downstream, systematic changes in the size and shape of bed material can be expected in that direction.

It was generally found that for gravel-bed rivers, grain size decreases and roundness increases in a downstream direction. Many investigators (e.g. Krumbein, 1941a; Kuenen, 1956; Pettijohn, 1957; Knighton, 1982, Parker, 1991a, b; Hoey and Ferguson 1994; Ferguson *et al.*, 1998) have attributed both grain size reduction and the increase in roundness to a combination of two important processes: (a) abrasion and (b) sorting, in which finer grains are preferentially transported further downstream.

Knighton (1982) investigated longitudinal changes in the size and shape characteristics of the River Neo, a fifth-order stream in north Derbyshire and found three regimes in which different processes are dominant.

1) Abrasion and size sorting in the headwater area.
2) Shape and size sorting in the middle reaches.
3) Sorting and breakage towards the downstream end of the stream.

He acknowledged also that these processes are interrupted by tributary inflows, the main effects of which are to increase grain size and flatness below junctions.

As a part of size-selectivity experiments in gravel bed rivers, Ashworth and Ferguson (1989) examined downstream changes in bed material size in Allt Dubhaig River Feshie and Lyngsdalselva (Norway). They found a strong downstream size fining in all the three rivers. This size decrease was attributed to a strong size selectivity rather than abrasion processes.

Field studies based on examining the influence of particle shape on bedload transport

There have been relatively few field-based investigations on the influence of particle shape on bedload transport (e.g. Bradley *et al.*, 1972; Ashworth and Ferguson,

1989; Gintz and Schmidt, 1991).

One of the earliest studies was carried out by Lane and Carlson (1954), who analysed bed material shape and weight in the beds of Colorado drainage canals. They found that pebbles were sorted by both size and shape. In a given sample of bed pebbles the disc-shaped pebbles had substantially smaller volumes than the more spherical pebbles. This indicated that spherical pebbles rolled more easily and were more easily set in motion than disc-shaped pebbles, which tended to assume more stable, imbricated orientations on the bed. Comparisons showed that on the average the discs are of the same suspectibility to movement as spheres that have weights 2.5 times as large.

In order to study the transport velocity of particles of various shapes, Pashinskiy (1964) carried out a series of experiments in a natural stream in the Psezuapse River on the southwestern slopes of the Main Caucasian mountains. For these experiments, particles of various shapes were used, namely, spherical, elliptical, flattened, prismatic and angular. It was found that the particles with regular shapes, approaching a sphere and an ellipsoid, had the straightest course of movement. The course of movement of a particle of prismatic and angular shape frequently had the appearance of a winding or a zig-zag line. The strongly flattened well-worn particle was found to have a trajectory with an angular loop-like form. In terms of velocity of movement and of saltation velocity, it was noted that particles of equal size and of different shapes are relatively different. Spherical and elliptical particles are streamlined better than angular particles

Bradley *et al* (1972) studied coarse sediment transport by flood flows of the Knik River, Alaska. They found that the size and elongation of bed material are both exponential functions of distance travelled in the events. In terms of shape sorting, they found that platy particles outrun all others, because they are light and travel more easily in suspension; elongated particles outrun lighter, more compact particles, apparently because of the way they wobble as they move. It was also found that coarse particle size decreases by 87 percent and the quartz and greywacke particles become progressively more elongated downstream. They attributed the downvalley changes in size and shape of coarse gravel mainly to sorting processes, but aided by frost-splitting.

Ashworth and Ferguson (1989) investigated weight shape and size selectivity of bedload using over 3700 painted pebbles in the several reaches of two streams in the Scottish Highlands, (Allt Dubhaig and River Feshie) and Norway (Lyngsdalselva). In terms of weight selectivity, The results clearly showed unequal mobility of different size, weight and shape of bedload. In eight of the nine reaches, where tracers had been

introduced, distance moved by the tracers varied inversely with weight. In terms of shape, it was also found that, despite a considerable variation in results, a statistically significant relation was found between tracers sphericity and transport distances. In other word, spherical particles moved further than flat ones. The influence of particle size on entrainment showed that for sizes coarser than the local D_{50} moved indicated a clear decrease in mobility with increasing particle size.

Schmidt and Ergenzinger (1992) and Schmidt and Gintz (1995) examined the effect of different particle shapes and their resistance to transport and erosion using artificial magnetic tracers in the Lainbach, a steep-pool mountain river in Bavaria, Southern Germany. 480 artificial cobbles of nearly constant weight (950-1000g) were measured and classified into 4 shape categories, compact bladed (CB), very bladed (VB), very elongated (VE) and very platy (VP). A sample of 120 artificial pebbles, each consisting of four samples of 30 per shape-group, were inserted into different positions, in the river bed, such as secondary pool, gravel bars upstream of large blocks, shallow channel in a step, and a gravel bar near the river bank. Results showed that there is no significant shape selectivity in controlling travel length in the small size group, while in the coarser particle classes there is strong shape selectivity. Spheres and in some instances the elongated (rods) particles have the greatest travel length and the highest probability of entrainment, whereas platy pebbles (discs) showed the greatest resistance to entrainment. However, they observed that particle shape selectivity is important for only small and moderate flood events. For large magnitude floods, shape selectivity was not significant.

In terms of the influence of particle weight on transport distance, a considerable amount of scatter was noted in the correlation between weight (size) and travel distance. The small particles were observed to have lower transported distance than that of larger particles due to hiding effects. Small particles were trapped behind large boulders or in the interstices between cobbles and boulders. By using the radio-tracer technique they also obtained some detailed information on the nature of bedload transport in terms of the step-pool system. Particles in the pools were determined to have the highest probability of entrainment and these sites were also determined to be the most favoured locations for deposition.

As a part of a bedload tracing experiments, Stott and Sawyer (1998) investigated travel distances and weight loss of 228 magnetically tagged bedload particles over a two-year period . In terms of travel rates of four shape classes, they found that rod and

spheres-shaped particles had greatest mean travel rates of 0.18±0.09 and 0.18±0.15 m day $^{-1}$ respectively, while discs and blades showed lower mean travel distances 0.11±0.03 and 0.10±0.03 m day $^{-1}$. The difference between the mean travel rate of discs and rods and also blades and rods were statistically significant. The higher mean travel distances of rods and spheres was attributed to the fact that their shape make them more suited to rolling and, once in motion they are less likely to be deposited due to imbrication and bed armouring.

Hassan *et al* (1999) investigated the transport of gravel in an ephemeral sandbed river, the Metsemotlhaba in southern Botswana, over a five year period using magnetic particles of pebble and cobble size. The Tracers were transported in two major flow events of equivalent transported. In the first flow event mean distance of tracers was 837m at a mean burial depth of 0.40m, while in the second events the mean distance of movement was 263m at a mean burial depth of 0.39m. The distribution of distance of movement was determined to be asymmetrical in the first flow event, when the tracer started from a surface location, but was monotonic thereafter. The tracers moved in the low and transitional flow regimes. Burial depth distribution followed the gamma model. In contrast to earlier studies (e.g Bradley *et al.,* 1972; Ashworth and Ferguson, 1989; Schmidt and Gintz (1995) it was found that longitudinal transport of tracers is independent of particle shape and size, and strongly skewed with respect to distance.

2.10 TECHNIQUES FOR MEASURING BEDLOAD TRANSPORT

The movement of bedload is generally accepted to be the most difficult mode of sediment transport to measure. The difficulty arises from the fact that movement occurs at relatively high flow velocities and bedload particles move intermittently. Available measurements are relatively few. Traditionally two basic methods have been used in measuring bedload transport in coarse-bed streams. These are trapping and tracing techniques. Most of bedload measurements have been made by using direct bedload traps. These samplers may be classified into several types according to their underlying principle. Some of these are: box or basket samplers (Ehrenberger, 1932; Mulhofer, 1933; Nesper, 1937; and Swiss Federal Authority, 1939), Pan or Tray samplers (Shamov, 1935), Slot or Pit samplers (Federal Inter-Agency River Basin Committee, 1949; Helley and Smith, 1971; Reid *et al.*, 1980), Pressure-Difference samplers (Federal Inter-Agency River committee, 1940), Vortex-tube (Taconni and Billi, 1987), Pressure-

pad (Reid *et al.*, 1980), Automatic recording of water and coarse sediment discharge (Lenzi *et al.*, 1999), Conveyor-belt traps (Emmet, 1980a). These samplers have been used in order to determine bedload transport rate, yield or obtain continuous measurement of bedload discharge.

2.10.1 Tracer Techniques

In gravel-bed rivers, tracer programs were started in the early 1960s (Takayama, 1965) in attempts to assess bedload transport. Tracer studies have focused on the relation between distance of movement and particle size (e.g. Keller, 1970; Schick and Sharon, 1974; Butler, 1977; Carling, 1987; Ashworth and Ferguson, 1989) or on examining the influence of sedimentological characteristics on the movement of individual particles (Laronne and Carson, 1976; Brayshaw, Frostick and Reid, 1983). In recent years techniques of coarse sediment tracing have advanced remarkable and have been widely used in many areas (e.g. the littoral and fluvial environments) to investigate geomorphological change (Hassan *et al.*, 1991; Schmidt and Ergenzinger, 1992; Hassan and Church, 1992). Sear *et al* (1998) classified the progressive increase in complexity of the scientific objectives of coarse sediment tracing into four main areas of research. These are:

- Estimation of sediment transport rates and volumes
- Analysis of flow competence
- Spatial analysis of sediment transfer processes
- Real time measurements of particle motion.

In terms of bedload transport, experimental studies have shown that using tracers and tagged bed material can provide useful and detailed information on bedload transport processes in coarse-bed streams (Crickmore, 1967; Bunte and Ergenzinger, 1989; Schmidt and Ergenzinger, 1992). To understand the transport mechanisms of coarse-bedload in a upland streams depends on the efficient field monitoring of individual transport distances of discrete particles and of particle populations over a given time period (Nelson and Coakley, 1974; Gomez 1991). Many investigators have proved that tracer methods give valuable information on erosion, mechanisms of transport and deposition. Quantification of the amount of bedload transported and bedload transport rates are also possible. With careful field observations even the path, the velocity and the motion of particle can be detected (Schmidt and Ergenzinger, 1992).

Surface marking – stone painting method

Tracer techniques have commonly consisted of painting pebbles or cobbles. The most common and inexpensive method of labelling has always been the painting or numbering of individual particles (Leopold, Emmet and Myrick, 1966; Laronne and Carson, 1976; Leopold and Emmet, 1981; Thorne and Lewin, 1982; Frostick and Reid, 1982). With careful resurvey, painted particles are able to provide valuable information on the proportion of particles that have or have not been transported. But they provide little data that pinpoint the actual incidence of motion during a flood wave. The major problem encountered using these methods is that particles are relocated by each transporting event not only over large areas of the channel bed, but also throughout the depth of the scour layer, therefore despite the great potential of the method, it is limited to the channel bed surface. Consequently the rate of recovery is generally low and it decreases with particle size and the number of flood events (Table 2.6). Table 2.6 shows that there is a positive relation between particle size and recovery rate. It also shows that the studies using magnetic or iron tracer particles have higher recovery rates than those that used painting stones.

Some of the earliest field experiments with the painted pebbles and cobbles were undertaken by Leopold in the United States and by Takayama in Japan 35 years ago (Hassan *et al* 1984). These studies have been followed by the studies of Leopold *et al.*, (1964); Takayama (some studies) (1965), Leopold *et al* (1966), Ritter (1967), Helley (1969), Schick (1970), Wilcock (1971), Milhous (1972), Laronne and Carson (1976), and Froehlich (1982). In most of these studies data were limited to the surface exposed particles only. Therefore in many of these studies the recovery rate is low and the recovered particles do not represent the entire sample.

Because of the limitation mentioned above there was a growing awareness of the need for more sophisticated measurement techniques. Although radioactive tracers have been used to good effort, these methods do not comply with the present legislation on environmental protection. An alternative, the introduction of the magnetic tracers using both natural magnetic material and cobbles with implanted magnetic cores (Ergenzinger and Conrady, 1982) has offered new possibilities. Studies which used magnetically tagged particles provideinformation on both buried particles and exposed ones, recovery rates are high. Tracers are detected either by a special magnetometer after transport (Arkell *et al* 1983 and Hassan *et al.* 1984) or the transit of the tracered material across a

coil system in the bed. This is measured by means of Faraday principle (Ergenzinger and Custer, 1983; Reid *et al* 1984). Ergenzinger *et al* (1989) pointed out that using this procedure, detailed studies of the time dependency of transport are feasible, and these techniques are especially appropriate at sites containing naturally magnetic pebbles.

Table 2.6 Examples of the field-based bedload tracing experiments carried out with various tracing techniques.

Researcher	Site	Tracing method	Size of particles used (mm)	Recovery rate of particles moved (%)	Number of events	Comments
Nir, 1964	Nahal Zin	iron nails	52-240	4.4	1	
Schick (Per. com)	Nahal Yael	paint	70-201	46.5	1	by (Hassan *et al.*, 1984)
Schick and Sharon 1964	Nahal Yael	paint	pebbles	64	1	
-----	Nahal Yael	paint	pebbles	57	2	
-----	Nahal Yael	paint	pebbles	16	4	
-----	Nahal Yael	paint	32-512	10.5	1	
-----	Nahal Yael	paint	32-512	2.5	10	
-----	Nahal Yael	paint	pebbles and cobbles	52	1	
-----	Nahal Yael	paint	pebbles and cobbles	44	1	
Takayama 1965	Hayakawa	paint	20-150	10	3	
-----	Hayakawa	paint	20-150	23.3	4	
-----	Fukogawa	paint	20-150	21	2	
-----	Fukogawa	paint	20-150	27	4	
-----	Okawa	paint	20-150	39.6	3	
-----	Okawa	paint	20-150	31.9	4	
Leopold *et al.* 1966	Morning Walk Walsh	paint	75-125	38	1	
-----	Morning Walk Walsh	paint	75-125	0	1	
-----	Morning Walk Walsh	paint	75-125	16	5	
-----	Slope Wash tributary	paint	75-150	88	5	
-----	Slope Wash tributary	paint	75-150	78	2	
-----	Gunshot Arroyo	paint	75-150	53	3	
-----	Gunshot Arroyo	paint	75-150	18	4	
-----	Gunshot Arroyo	paint	75-150	15	1	
Keller, 1970	Dry Creek Calif	paint	gravel and pebbles	48.5	-----	
Slaymaker 1972	Nant Calefwr	paint	cobbles	85-100	-----	
Slaymaker 1972	Nant y Grader 9A	paint	cobbles	85-100	-----	

Continued overleaf

Slaymaker 1972	Nant y Grader 9B	paint	cobbles	85-100	-----	
Laronne 1973	Seale's Brook Canada	paint	06-250	05		
Laronne and Carson 1976	Seale's Brook Canada	paint	4-256	5	1	
Butler, 1977	Horse Creek	metal strips	34-116	35	1	
Arkell *et al.* 1983	Plynlimon	paramag netic	5.6-22.4	63	1	
Hassan, 1983	Nahal Hebron	metal and paint	45-180	30.9	2	
Hassan, 1983	Nahal Hebron	metal and paint	45-180	33.8	2	
Ashworth, 1989	Alt Dubhaig	paint	24-147	66	------	
Ashworth 1989	Alt Dubhaig	paint	26-238	68	------	
Ashworth 1989	Alt Dubhaig	paint	24-153	76	------	
Ashworth 1989	Alt Dubhaig	paint	24-170	61	------	
Ashworth 1989	Alt Dubhaig	paint	24-135	89	------	
Ashworth 1989	Feshie	paint	25-171	40	------	
Ashworth 1989	Feshie	paint	24-136	84	------	
Ashworth 1989	Lynsdalselva	paint	90-170	26	------	
Ashworth 1989	Lynsdalselva	paint	35-200	89	------	
Carling, P. (pers. Com)	Carl Beck	paint	15-130	98	------	by (Hassan and Church, 1992)
Carling, P. (pers.Com)	Great Eggleshope	paint	15-130	78	------	by (Hassan and Church, 1992)
Taconni et al., 1990	Virginio Creek	paint	16-128	5-9	------	
Hassan *et al* 1991	Nahal Hebron	Magnet	30-180	80	1	4 sites
-----	Nahal Hebron	Magnet	30-180	93	1	4 sites
-----	Nahal Hebron	Magnet	30-180	93	1	4 sites
-----	Nahal Og	Magnet	30-180	56	1	1 sites
-----	Nahal Og	Magnet	30-180	55	1	1 sites
Schmidt and Ergenzinger 1992	Lainbach	iron tracer	50-170	92	1	
----	Lainbach	iron tracer	50-170	74	2	
----	Lainbach	iron tracer	50-170	17	3	
----	Lainbach	Magnet	950-1000g	93	2	

There have been several different methods and techniques for tracing bedload. These methods may be broadly classified into four groups.

1) Individual natural pebbles are traced in three different ways, such as iron cores, magnetic cores and self emitting radio systems (Hassan *et al.*, 1984; Schimid and Ergenzinger 1992).

2) Individual artificially manufactured pebbles are traced either by adding fine particles of tracers to a matrix of concrete or implanting traceable of self emitting items (radio) into the particles.

3) A bulk sample of natural gravel is artificially traced by magnetic enhancement (Oldfield *et al.*, 1981)

4) Natural gravels traced by high magnetic content and high iron content.

There have also been various methods of detection. These include; the position of the pebble or gravels after a flood event (see Hassan *et al.*, 1984), the passage of pebbles or gravels through the cross-section during a flood event (Reid *et al.*, 1984) and the path, the velocity and motion of pebble during the flood event (Schmidt and Ergenzinger, 1992).

Many investigators have shown that using individual tracer pebbles or cobbles can give important information on bedload transport. Such as; (1) the travel lengths of individual particles, (2) the influence of particle shape, weight and size on travel length and transport probability, (3) selectivity of transport of equal mobility, (4) spatial distribution of particles from point source (5) positions of sedimentation (Hassan *et al.*, 1984; Bunte and Ergenzinger, 1989; Schmidt and Ergenzinger, 1992), (6) particle position within the river morphology (riffle, pool, thalweg, lateral position, bars) (Bunte and Ergenzinger, 1989; Schmidt and Ergenzinger, 1992).

The most common method of tracing individual particles and detecting them after transport event has been to use a sample of pebbles or cobbles. The basic technique is to drill a hole into each individual particle. The tracer (iron or magnet) is then inserted and secured with epoxy. The particle is usually painted to distinguish it from other pebbles on the river channel. Depending on the aim of the experiment, particles are placed into the river channel in different locations. Following an individual flood or flood events tracer particles are relocated in the channel with hand held detectors. Although the particles exposed on the river bottom are easily found, those which are buried at different depth in the river sediment or which are swept far out of reach are

sometime very difficult and time consuming to recover.

Iron Tracer Technique

Many investigators (e.g. Schmidt and Ergenzinger, 1992) have used iron core tracers but the biggest disadvantage in using this method is the low recovery rate of particles after transport (Table 2.6). In highly populated areas the possibility of scrap metals (e.g. wire or bottle cap) in the channel may cause confusion. Bunte and Ergenzinger (1989) pointed out that the vertical range of the metal detector in the river sediment is limited to a depth of some tenths of a meter. Thus to increase the recovery rate the signal made by the metal detector should be as large as possible.

Magnetic tracers

One of the earliest attempts to use magnetic tracer techniques was initiated by Nir, (1964). He coated concrete cobbles with iron oxides, but the low sensitivity of the metal detector used and very small sample size resulted in practically no finds beneath the bed surface. Following Nir, Butler, (1977) marked cobbles with metal strips and relocated them using a metal detector in field. This method significantly improved the recovery rate of cobbles as compared with marked rocks. His method was simply to tag the cobbles by wrapping an aluminium strip around the centre and wiring it in place.

The magnetic tracer technique was first developed by Ergenzinger and Conrady (1982) and used in cobbles for monitoring bedload transport in 1980 at Fiumara Buonamico in Calabria, southern Italy. The aim of the investigation was to determine the initiation of cobble transport. The basic technique was to drill granitic cobbles with an average width of 55 mm, and insert a bar magnet inside them. Using 100 magnetic-tracers the starting conditions of cobbles transport in Buonamico were determined. Ergenzinger and Custer (1982) noted that due to continuous input of magnetic cobbles during the floods, the determination of the transportation rate of cobbles with this technique is quite expensive and time-consuming.

The magnetic tracer technique has been successfully applied by Hassan *et al* (1984). The important advantage of using magnetic tracers in bedload transport investigations is the enhanced recovery rates of magnetised tracers (Table 2.6). Another advantage of using this method is that there are few other magnetic objects that can cause confusion. Using this method also expands the range of detection and even allows

the investigator to find pebbles that have been buried deeply within the riverbed. This method also allows the differentiation between several kinds of magnetic intensities, thus offering scope for a variety of tracers. Hassan *et al* (1984) found that the recovery rate of pebbles tagged with ceramic magnets was 93 %, and 53 % of all the pebbles retrieved were discovered below the channel surface (Table 2.6).

2.10.2 Artificial magnetic enhancement of particle and detection after the flood

Generally no single technique has been developed for tracing the movement of the full size range of stream bedload. Methods used tend to be most successful for the coarsest material (painting pebbles, magnetic tracing, iron tracing, e.t.c). This is because it can be very difficult to dril and insert a magnet into a clast which is smaller than 32 mm in b axis. Preparing tracers and detecting them after floods is very time consuming and limits the number of particles used. Using a strong heat source to magnetise particles may partially overcome these limitations. Magnetic enhancement can be used on the full range of bedload.

Laboratory heat treatment of natural rock alters mineralogical properties and produces a characteristic magnetisation that can be used as a simple and persistent tracer. Oldfield *et al* (1981) first developed artificially magnetic enhancement. They pointed out that the main advantage of the artificially magnetic enhancement method is that a bulk sample containing all grain sizes present in the stream can easily be artificially magnetised, thus being representative for all the material sizes. By comparing the percentage of traced material in the original sample with the sample taken after the transport event the amount of material transported can be quantified.

Oldfield *et al* (1981) pointed out that natural magnetic enhancements occur in soils on a wide range of bedrocks including limestone, granites, shales and sandstones. The artificial magnetic enhancement tracing method may consequently be expected to be applicable to many localities. In their study magnetite and hematite were grown in naturally paramagnetic mudstones and slates by rapid heating in air to 900°C and quenching. They found that the mineralogical changes of the magnetic grains are complex and depend on many interrelated variables. However they developed a very simple but effective heat treatment procedure that optimises the enhancement of magnetic susceptibility and permits practical hydrological field experiments to be performed. They also pointed out that apart from bedload movement studies, the artificial magnetic enhancement method could also be useful in studying other

sedimentological processes such as movement of sand waves and the silting of harbours.

Arkell *et al* (1983) developed an artificial magnetic enhancement technique to investigate sediment transport, from the uplands into the piedmont zone, and from shoal to shoal in upland central Wales. The technique, based on the enhancement of the magnetic susceptibility of the natural bedload, provides an effective tracer, which can be detected in low concentration and in all particle size ranges. They used Optimal laboratory treatment (as explained in Oldfield *et a.,* 1981) to achieve the maximum possible enhancement of the magnetic susceptibility for large amounts of all sizes of material. They noted that from uniformly low values (varying between 0.07 and 0.14 x $10^{-6}m^3kg^{-1}$), heat treatment is capable of producing enhancement in the Plynlimon shales up to a factor of 300. Within the same reach different magnetic signatures could also be actuated in the same material for use as different tracers, by altering the range of magnetic variables used. After floods they traced the magnetic material in the stream using a search coil and compared results with bedload material caught in a trap.

Hassan *et al* (1984) pointed out that the disadvantages of using this method is it is limited by the need to haul particles to an industrial furnace, the high rate of breakages and the requisite of using pebbles with a sufficient iron content.

2.10.3 In-situ determination of bedload transport of natural and tagged tracers

In natural channels the motion of bed particles can not easily be observed due to the turbidity of water and discharge. Existing methods such as labelled (painted) particles (Leopold *et a.,* 1964), or magnetic tracers (Ergenzinger and Condrady, 1982) only provide flood-by-flood or gross seasonal changes in the movement of individual particles and did not provide any indication of the nature of the bedload movement (Reid *et al.,* 1984). Although, some flume studies have been able to examine these parameters, extrapolation of the results to natural rivers is difficult. The importance of tracking particles has led to the development of many different techniques with varying degrees of success and applicability.

This method was first developed by Ergenzinger and Conrady (1982) and used to test the first continuous *in situ* observation of the passage of naturally magnetic coarse material bedload transport (Ergenzinger and Custer, 1982, 1983) in a high energy mountain river Montana, USA. The technical design of this method is as follows:

"According to the Faraday Inductive Principle a voltage peak is induced when a

magnet passes over a coil (copper windings on a iron core). Several sets of coils are inserted into a detector block, which is installed into the bottom of the river reaching from one bank to the other. The signals induced by the magnetic particles passing over the detector block are amplified, filtered, and recorded with spatial electronic devices. This measuring device works automatically and produces a continuous, spatially and temporally high-resolution record. The analysis of this raw data give new insight into the processes influencing coarse-bedload transport, such as bed material supply dependency, time series analysis of the bedload pulses" (Bunte and Ergenzinger, 1989, p 88).

The advantage of using this method is that without any disturbance an unlimited number of real bedload particles can be observed in *situ*. This method can also be applied to any size of river channel without restriction, although the method is expensive and requires considerable electronic expertise. A Further disadvantage of this method is the difficulty of calibrating the signal induced by the magnetic pebbles passing over the detector block. Since the size of the signal may depend on many parameters, such as magnetic content, velocity, magnetic orientation and height above the detector. Thus the calibration of the number of signals registered can only be done by statistical means or by comparison with bedload samples taken simultaneously. Other difficulties are also associated with the tuning of the electronics and the noise-reduction (Bunte and Ergenzinger, 1989).

In order to analyse the practicalities of detecting the transport of naturally magnetic cobbles and pebbles on a stream bed, some observations were carried out by Ergenzinger and Custer (1982) in the region near Bozeman, Montana. To test the method Squaw Creek stream was chosen as the monitoring site, draining the andesitic volcanic terrace of the Gallatin Range, Gallatin County, Montana. The basic idea behind the detector was simple. When a permanent magnet passes over an iron-cored coil of wire, a measurable electrical current is generated. A detector consists of four wire coils wrapped around 1 m long, 2.00 cm diameter iron bar.

The detector was constructed at a log sill in the bed of Squaw Creek, and during a flood in May 1981 the detector recorded the passage of the magnetic particles larger than 32 mm. Extrapolation of the data allowed estimation of total bedload transport. Based on the composition of an unvegateted gravel bar upstream of the detector and on measurement of tributary during the flood, bedload accounted for approximately 66 % of the solid material leaving the drainage basin. Ergenzinger and Custer stressed the

method was widely applicable, because many coarse-bed streams probably contain material at least as magnetic as the andesitic rock in Squaw Creek.

In order to provide clear information about the actual movement of bed particles Reid *et al* (1984) developed an electronic sensing device for permanent installation in the bed of Turkey Brook, Enfield Chase north of London. This device is capable of continuously monitoring the passage of artificial pebbles labelled with a ferruginous material. The sensor provides a continuous record of bedload movement and acts in the same fashion as a conventional metal detector and consists of two elongate unscreened coils. The transmitting coil acts as a search head and is heterodyned with a reference frequency in the receiving coil. Both coils are fully balanced over the entire length of the sensor. During bedload transport the movement of particles labelled with ferruginous material over the sensor distorts the magnetic field and produces a change in the inductance of the coils. The signal is detected, amplified and demodulated to produce a change in DC voltage that can be permanently recorded the strip chart of a suitable potentiometric recorder. The system is designed for automatic operation and is achieved by circuit-closure in a mercury tilt-switch that is attached to a float-controlled arm housed in a stilling well (Reid *et al.*, 1984).

Reid *et al* (1984) stressed the primary reason for developing the "Birkbeck sensor" was an evaluation of the effects of the mutual interference of neighbouring bed particles on initiation motion and transport rates. Particular attention has been given to the small-scale bedform (pebble clusters) which are said to be widespread and occupying about 10 % of the channel floor in stream ranging widely in particle lithology (Brayshaw, 1983).

Reid *et al* (1984) pointed out that the sensor can be made to any length within practical bounds and can be used in conjunction with companion units, providing suitably different output frequencies are chosen. The sensor also functions independently of water depth and can therefore be used on deep flows providing that installation is technically feasible. Another advantage of this system is the automatic detection of the passage of traced particles, as it is compared with other methods. In other words it integrates the possibility of working with individual pebbles, allowing for example, certain position of erosion or deposition to be traced.

Although early discoveries by Ergenzinger and Custer, (1983) and Reid *et al* (1984) have made important advances in the determining the timing and nature of coarse-bedload transport, none of these studies was able to determine the travel length

and travel distances. Furthermore these techniques had several disadvantages. For example installation of these devices is always a problem, and also both methods require the burial of a detector rod in the streambed which limits the application to sites with relatively stable channels and to small streams. Devices are expensive, and transportation of these device is not practical.

Recently Lenzi *et al* (1999) developed a new device which is based on continuous automatic recording of water and coarse sediment transport. The device operates by separating bedload from water discharge and fine sediment and subsequently measuring the two solid components. The separation is obtained by means of an inclined grid: coarse material, exceeding 20 mm, slides over the grid and accumulates in a storage area where its volume is measured by ultrasonic sensor fitted to an overhead travelling crane. Later they modified the recording system by replacing the moving crane by a fixed frame with several ultrasonic sensor which improved the recording of the volume of coarse bedload at closer intervals (less then 10 min). Using this device Lenzi *et al* (1999) could relate bedload transport to particular floods.

2.10.4 Pebble Transmitter system (PETSY)

Edward *et al* (1988) developed and successfully used a radio transmitter to track and locate coarse sediments through a highly mobile, braided river system, the Toklat River, a glacier-fed river located in Denali National Park in central Alaska. They developed radio transmitting equipment that was already used by biologist in tracking fish and game animals. The transmitters are hermetically sealed, including batteries and internal antennas, and transmit a signal pulse at a specified frequency and time interval. They used two type of transmitters for their study, the standard transmitter that emits a signal continuously at a single frequency and time interval, and the motion-sensor-equipped transmitter that also emits a signal at a single frequency but with a time interval that changes depending on whether the particle is in motion or at rest. Frequencies and time intervals of the signal are user specified for both type of transmitters. Transmitter life dependent on the transmitting interval and the size of the battery in the self contained transmitter unit.

A hole was drilled in the selected cobbles with special water lubricated coring bit and transmitters were inserted inside and fixed with epoxy. The cobbles were painted to aid in recovery at the end of field season.

A portable receiver and digital signal processor were used in conjunction with an

"H" pattern directional antenna to locate the radio equipped rocks. By rotating the antenna and observing the signal strength they determined the signal direction. Location of the radio-equipped rock could be determined by moving along an established baseline and determining the point where signal direction was perpendicular to the baseline. During periods of a high flow and turbid water conditions, they were able to successfully track and locate five radio-implanted rocks that travelled greater than 1500 m in 8 days through a highly mobile, braided river system. This technique demonstrated the travel path, travel distance and time of travel of individual particles with a size range of 39 to 64mm. Flood stages and particle burial did not affect the measurements. Edward *et al* (1988) concluded that the technique they used may be applicable during most flow conditions and to all streams types moving large size sediment particles.

A pebble transmitter system was also developed by Ergenzinger *et al* (1989) for studying coarse material erosion, transport, and deposition. This pebble transmitter system was first tested at the Lainbach station in Bavaria (Figure 2.14).

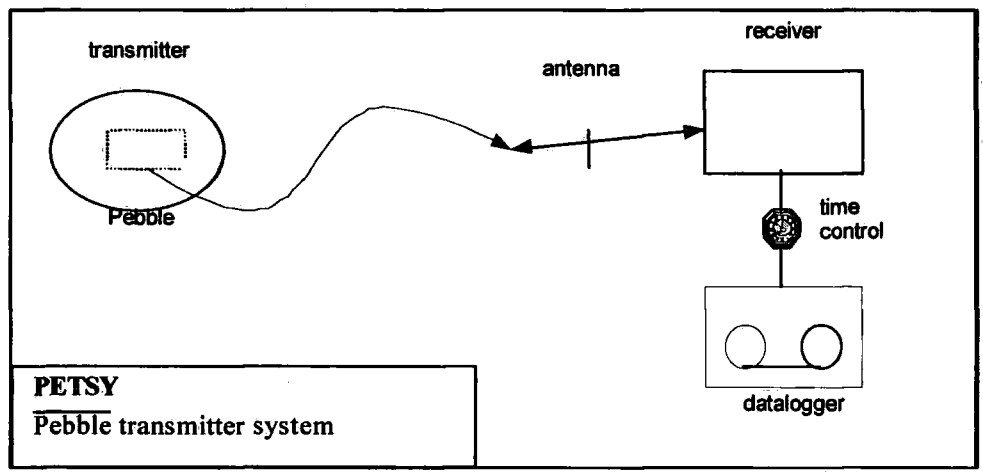

Figure 2.14 Sketch of the Pebble-Transmitter System (PETSY) (After Ergenzinger *et al.*, 1989)

The basic system consists of a transmitter, an antenna, and a data logger. The system operates at a frequency of 150 MHz and the 2 m waves can be received in and outside the water. The system also has three different antennas as stationary, mobile and search detection (Figure 2.14). The stationary antenna system is installed along one bank of the channel to follow movement of the tracer stones. The connections between the antennas and the receiver are changed manually. The mobile antenna is mounted on a tripod and is carried along the river in order to maintain contact with the emitting

cobble. Thus it is possible to trace the position of the radio cobble within a range of about a 100 metres, even below a cover of more than 60 cm of sediment. Using the special search antenna it is possible to determine the point directly above the tracer cobble and to retrieve it quite easily. It is pointed out that this tracing procedure is considerably simpler and more effective than magnetic tracing, but it is very expensive.

First results of pebble transmitter system were obtained at Lainbach Station in Bavaria. The device also gives a precise information on the transition between gliding and rolling and vica versa. The first results demonstrated that, under natural condition, the differentiation of initial entrainment does not primarily depend on primarily difference of the size, form or weight of the material, but much more on the lateral distribution of velocities and shear stresses in the cross-section. Thus Ergenzinger *et al* (1989, 1992), Bunte and Ergenzinger (1989) concluded that PETSY is suitable for detailed investigation of bedload transport of coarse sediment, including: conditions for initial movement, travel velocity and position of deposition of an individual particle and types of movement of particles. The technique is also applicable to material as fine as about 63 mm. When implanted into artificial material the size can be reduced even further. In addition, travel velocities over short time intervals can be measured even more precisely by a stationary antenna system controlled by a computerised logger. Using the result of PETSY it will be easier to test and calibrate bed load functions. Unfortunately, the number of radio pebbles is limited by cost.

Although there have been great advances in the development of new tracer techniques and their successful application to the bedload transport investigations, there is still only limited field data related to coarse material transport.

2.11 CASE STUDIES USING TRACER TECHNIQUES FOR PARTICLES IN GRAVEL BED RIVERS: KEY FINDINGS AND RECOVERY RATES

Table 2.6 summarises some characteristics of the field based studies undertaken using various coarse sediment tracing techniques. Results indicate that over time recovery rate of particles have tended to increase probably due to increasing sophistication of techniques. The Table also shows that studies carried out with magnetic tracer have a greater recovery rate than those using painted pebbles or cobbles. There tends to be an inverse relation between the recovery rate of particles moved and the number of events. Although generalisations are difficult Schick and Sharon (1964), using painted stones had the lowest recovery rate with the greatest number of events,

while Hassan *et al* (1991) and Schmidt and Ergenzinger (1992) using the magnetic tracers had the greater percentage of recovery rate with a smaller number of event.

One of the earliest attempts to use magnetic tracer techniques was initiated by Nir, (1964). The purpose of his investigation was to trace the movement of individual cobbles from selected sites of entrainment to their site of deposition after one flood season in Horse Creek a tributary of the Green River, which flows east out of the Wyoming Range in western Wyoming. It was concluded that this method could be used under water as deep as 1.2 m and tagged cobbles were detected after burial to depths of 20 cm. In this study it was concluded that 35 % of magnetic tagged particles were recovered after one flood season. 61% of stones had been retrieved from burial. The average particle size ranged from 34 to 116 mm (b-axis) (Table 2.6). Almost 95 % of the tagged stones moved and the distance transported was ranged from 0 to 420 m. No clear relationship was found between particle size and distance transported; the distance of transport was related to the position of particles at the time of entrainment. Susceptibility to burial seems to be related to both particle size and position at the time of entrainment.

Laronne and Carson (1976) observed movement of labelled bed material to understand particle mobility and transport processes along a 600 m stretch of Seales Brook a small tributary of the North River Quebec. Several thousand natural bed particles ranging 4-256 mm in diameter were collected from the study river and then classified into four different size groups and painted with various spray-paint colors. The material was reintroduced into the river channel. It was observed that most of the smaller introduced particles immediately disappeared between and underneath cobbles and boulders The percentage remaining on the surface increased with particle size but particle stability decreased. They pointed out that the transportation of the labelled bed material was probably uncharacteristic of the behaviour of the bed material of the surface layer as a whole and that initiation of motion of the labelled particles occurred prior to that of their in situ counterparts. This indicated that the first flood is uncharacteristic of general movements. Because of this, it was concluded that it would not be entirely appropriate to attempt a calculation of actual bed load rates based on the distances of travel of the tagged material. It was also found that the percentage recovery decreased markedly with a decrease in particle size, ranging from 100 % for the coarsest cobble groups to 0.5-1.0 percentage for fine pebbles. This decrease in recovery rate was shown to be the result of selective burial processes. The only strong relationship found

was an inverse logarithmic correlation between distance of transport and weight of particle, which is similar to Leopold *et al.* (1966) and Keller (1970) who found either no relationship. They also found that particle mobility was greatest for material in open-infilled structures and smallest for sediment in tight structural arrangements, and that local bed slope affected both particle entrainment and accumulation.

Use of magnetically enhanced natural bedload as a tracer has significantly improved results, in many areas, especially where forest fires are common and the persistence of fired-induced magnetic minerals are abundant. For example the investigations done by Rummery *et al* (1979) and Rummery (1981) after the major forest fire in the Gwydyr Forest of North Wales in 1976 showed the possibility of the assessment of downstream movement of material derived from the fired areas by carrying out magnetic measurement on sediment samples.

Since 1980, more detailed assessments of the magnetic tracing technique have been carried out, examining sediment transport system in eroding forest ditches and in larger reaches downstream from experimental catchments. Arkell *et al* (1983) used a new magnetic technique to study sediment transport, from the uplands into the piedmont zone, and from shoal to shoal in upland central Wales. The detail of technique is explained in section 2.10.2. The analysis showed that there was a poor relation between bedload transport rates and discharge. They concluded that bedload transport is not solely a function of current hydraulic conditions but also of the channel history, which determines the condition of supply of bedload material and its availability to transport. It was also concluded that in order to distinguish between supply and transport mechanisms the magnetic tracer technique provides a means of tracing the site of erosion and deposition.

The first use of a magnetic device for monitoring bedload transport using artificial magnetic tracers in cobbles was undertaken by Ergenzinger and Conrady (1982) in 1980 at Fiumara Buonamico in Calabria / southern Italy. The aim of the investigation was to determine the initiation of cobble transport. The basic technique was to drill granitic cobbles with an average width of 55 mm, and insert a bar magnet inside them. Using 100 magnetic-tracers the starting conditions of cobbles transport in Buonamico were determined. Ergenzinger and Custer (1982) pointed out that due to continuous input of magnetic cobbles during the floods, the determination of the transportation rate of cobbles with this technique is quite expensive and time-consuming.

Hassan *et al* (1991) used several hundred (450) magnetically tagged cobbles and pebbles to examine distributions of distance of bedload particle movement in natural stream channels with unsteady flow. The study was carried out at two sites: Nahal Hebron in the Negev Desert, and Nahal Og, in the Judean Desert. magnetically tagged particles (the method of tagging particles is explained in Hassan *et al.*, 1984) which ranged between 100-3700g in weight and between 30 and 180 mm in size (b-axis) with a median of 80 mm were placed on the stream bed in Nahal Hebron. The compound poisson model of Einstein-Hubbel-Sayre and a simple gamma function model were compared with observed distribution of moved particles, and of all particles. It was found that both model fit the data reasonably well for small mean displacements, but notably misfits occurred in an event with large mean displacement. They also found that when mean particle travel distance approached the scale of bar spacing, trapping in the bars interrupts particle progress and the dispersion process. The data remain very noisy, so definitive discrimination of suitable models will require trials with more than 10^3 particles.

During flow events the mean burial depth (m) changed between 0.15-0.20 and mean recovery rate changed (percentage) between 80-90 % in Nahal Hebron and 0.15-0.22 m and 55-56 % respectively for Nahal Og (Table 2.6). On the basis of the results, the authors suggest that in gravel-bed streams, the movement of relatively large particles can be described by either model in small event, but the movement becomes more complex in large events either because of a complex hydrography, or particle trapping by major established bed forms. The distributions are, in effect, models only of the local dispersion of sediments.

Hassan and Church (1992) attempted to determine relation between the mean distance of movement observed after a flow event, the event magnitude and the relation between the virtual rate of travel (which is calculated using total time for which the flow is larger than the needed to initiate particle movement) and the magnitude of the sediment mobilising event. The first relation is related to particle entrainment, transportation, and sedimentation.

They pointed out that mean distance of movement, irrespective of grain size, is weakly correlated with stream power, especially near the threshold of movement. The reasons for the weak correlation were attributed the variable effects of bed structure, varying magnitudes of sediment mobilising events, and sampling problems. They found that grain size itself is of marginal significance. They also calculated virtual rate of

travel using total time for which the flow is larger than that needed to initiate particle movement. However, this also bears a weak relation to the excess stream power over the period. They stressed that better results are obtained by relating the virtual rate of travel to the first peak of the flow event only. Thus this indicates that seeding of the tagged particles dominates the observations in the initial flow events.

Schmidt and Ergenzinger (1992) investigated bedload entrainment, travel lengths, step lengths, rest periods using passive (iron, magnetic) and active (radio) tracer techniques in the Lainbach catchment in the Bavarian forealps of Munich-Germany. Particles with iron cores were used as passive tracers and they were to be detected after floods with a metal or magnet detector. They pointed out that these techniques permit the determination of the cumulative travel lengths covered by the stones in the course of a flood and they also provide good information on the spatial distribution of particles.

In order to investigate the influence of weight and grain size on travel length and spatial distribution from point sources after floods events iron tracer (FETT= Ferruginous Tracer Technique) was used. The study period consisted of moderate floods of the summer of 1988 and 1989. The cumulative travel distances of the tracer were recorded after each flood event. 128 cobbles with iron tracer were inserted into the Lainbach channel, along 600 m reach. The iron cobbles also covered all shape categories. During the measuring season of 1988 eight flood events were observed. During searches tracers were identified and their position of each was mapped. It was found that the results from the first effective flood after emplacement were different from those of later floods. This difference was attributed to the uniform starting attitude of tracers. Although the percentage recovery rates found were low for floods 4 and 8 (17 %), it was satisfactory after floods 2 (92 %) and 3 (74 %) as compared for the figures of experiments with painted stones in Hassan *et al* (1984) (Table 2.7).

Table 2.7 Recovery rates and transport lengths of the transported iron tracers (source Schmidt and Ergenzinger., 1992)

Flood number	1 min-max.-mean			2 min-max.-mean			4 – 8 min-max.-mean		
Recovery rate % of total sample	92			74			17		
Travel length (m)	5	141	15	1	204	33	38	670	220
Total travel length (m)	5	141	15	5	343	47	44	763	274

The iron tracer measurements indicated a tendency of size-selective transport of coarse-bedload, although there is also a reasonable amount of scatter in the correlation between size and travel distance. The scatter was attributed to the effect of different position in the channel bed. They also investigated effect of particle shape on transport distance and transport probability which is explained in the previous section. Pebble transmitter system (PETSY) was used (e.g. Ergenzinger *et al.*, 1989; Schmidt and Ergenzinger., 1990) in order to investigate measurement of entrainment, step lengths, and rest periods of transported pebbles and cobbles. A transmitter combined with a battery of 30 mm long, diameter of 16 mm was installed into holes drilled into natural 8 cobbles. With the stationary antenna system along the experimental reach the entrainment and the movements of the pebbles are observed continuously on a high level of temporal and spatial resolution during six floods in summer 1988-1989.

Schimidt and Ergenzinger (1992) concluded that the radio tracer experiments showed a wide range of critical entrainment values for the observed cobbles. Thus the entrainment of pebble or cobble can not be described by a single deterministic approach, since the local velocities, shear stresses, and bed properties are unknown. It was also found that in the step-pool system of the Lainbach River the material lying in the pools has the greatest chance of being entrained and transported. The pools are also the most likely locations of deposition. Thus influence of bed morphology on bedload transport is clearly demonstrated.

Using a radio tracers technique and manual sampling Busskamp and Hasholt (1996) studied coarse-bedload transport in a glacial valley, sermilik, south east Greenland. They found that during the period of investigation the bedload transport was low indicating that glacial valley acts as a sink for coarse particles released by fluvio-glacial erosion. Coarse sediments on the surface of the delta flat seem to be remnants from earlier phases of sedimentation.

Ferguson *et al.* (1998) carried out a series of integrated field, laboratory and modelling studies to investigate downstream fining of river gravels. As a part of their investigation, 1460 magnetic tracer pebbles were used in different section along the Allt Dubhaig, situated in the central part of Scottish Highlands. The main aim of this experiment was to investigate to what extent long-term dispersion of particles of differing size was size selective. Tracer searches were carried out at intervals during 1991-1993. Although it was a long-term experiment and also the large proportion of buried tracers, the recovery rate of magnetic tracers was very high (75%), compared to

paint-only coarse tracers. The results from these experiments showed that there is a clear tendency for travel distances to decrease downstream and coarse tracers to move less distance. Thus, the tracer experiments clearly showed that downstream decrease in bed material size is due primarily to sorting rather than abrasion processes.

2.12 SUMMARY

The present literature review has explained the factors and processes that determine particle shape. These factors are parent rock, chemical and mineralogical composition of the rock, the strength of abrasion processes to which it is exposed during the transport and the post-depositional processes.

Analysis of particle morphology usually involves the description of the two and three-dimensional properties of pebbles. Two-dimensional measurements, generally, involve the determination of roundness, elongation and angularity, while three-dimensional measures are based on determination of form, sphericity and flatness. This literature review also shows the complexities involved in pebble morphology analysis. There are many parameters and indices for describing the shape of a particle and none of these has been universally accepted. Despite being very time consuming direct measurement of pebble shape is recommended because this provides lower operator error, and a choice of statistical analysis. The ultimate choice of methodology depends on the consideration of a number of factors. Pryor (1971) expressed these factors as (a) size of particles to be described, (b) amount of available sample, (c) parameters desired to be used for a particular problem, (d) in duration-state of sample material, (e) parameters obtainable from sample material, (f) desired complexity of parameters, (g) availability of special equipment, (h) expense in time and money. However, comparative studies have proven that the most appropriate measures of shape are Krumbein's (1941) "*Intercept Sphericity*" and Sneed and Folk's "*Maximum Projection Sphericity*" due to their closest correlation to the hydraulic behaviour of particles.

Beside geometric and visual comparison methods, studies have also shown that with the development of automatic image analysers and associated computer software, there has been a great advance in the accuracy and speed of particle shape measurements.

The present review has shown that the number of investigations on the influence of particle shape on bedload transport are relatively few. A limitation with most of these

studies is that they are either concerned with laboratory measurements, flume experiments or field observations. Few of these studies have focused on a combined field and laboratory investigation. Research on the influence of particle shape on bedload transport has recently increased due to the applications of new techniques (e.g. Bunte and Ergenzinger, 1989).

Successful application of new techniques (e.g. Magnetic Tracer Technique (MATT), Pebble Transmitter system (PETSY)) have led to deeper insight into the processes of particle behaviour in various aspects of bedload transport in gravel bed rivers. Existing studies have shown that beside other factors, entrainment and hydraulic behaviour of a particle depends on particle shape, orientation, and its relative projection above the mean bed. Spherical particles have been found to move in a rolling mode and settle much faster than those of particles that are flat which move in a sliding mode and tend to have lower settling velocity. Several studies have demonstrated that the influence of shape on the hydraulic behaviour of particles is affected by variation and complexity of bed roughness. However, despite its importance, the exact mechanisms of how shape influences sediment transport is still not completely understood and there is some conflict among the existing studies. Indeed the literature reviewed here is somewhat confusing on the subject of the significance of particle form on bedload transport behaviour. For example, some studies have shown that, equant particles are entrained more easily than others (Helley, 1969), while some investigators (e.g. Krumbein 1942) noted, once in motion, elongated particles move faster than equant ones. Meland and Norman (1969), on the other hand, suggest there is only a poor correlation between shape and bedload transport. Bradley *et al* (1972) results indicate that disc-like particles are more mobile than the spheroid (compact) ones. However, recent studies carried out with new magnetic tracer techniques (Bunte and Ergenzinger, 1989; Schmidt and Ergenzinger, 1992; Schmidt and Gintz, 1995) and laboratory experiments (e.g. Carling *et al.*, 1992) have shown that spherical and rod shape particles are the least stable and move longer transport distances than flat ones. All these facts clearly highlight the need for a further systematic study to determine the effect of bed material shape on bedload transport in gravel-bed rivers.

CHAPTER 3: RESEARCH DESIGN AND METHODOLOGY

3.1 SCOPE OF CHAPTER

This chapter defines the aims of the present research and describes the methods used to achieve these aims. This includes consideration of the research methods for measuring particle size and shape. The procedures and techniques used in river flow measurements are described. Field methods used to survey the channel, bed material roughness and bed material sampling at the three experimental sites are explained. Methods used in tilting-table experiments are described. The final section explains the photographic visualisation experiments.

3.2 AIMS AND RESEARCH DESIGN

The aim of this study is to investigate the influence of particle shape on bedload transport in coarse-bed rivers. The research design adopted to achieve these aims is shown in Figure 3.1. The main elements of the design are as follows.

1 The methods used to measure particle size and shape are described in detail in Section 3.3.
2 River flows were measured to define discharge during the fieldwork period in order that bedload process results could be related to discharge history (Section 3.4).
3 Transport of different shapes of coarse river gravel and their sorting in two upland gravel rivers were investigated using magnetic tracing experiments (Section 3.5)
4 Boundary conditions of the three experimental reaches were determined by surveying the cross-sectional geometry, bed topography, and measuring the size and shape characteristics of the bed material (Section 3.6).
5 A series of tilting table experiments were carried out to measure the friction angles of particle of different shape and size of particles on various bed roughnesses (Section 3.7).
6 The dynamics of bedload motion were assessed through a series of particle visualisation (photographic) experiments (Section 3.8).

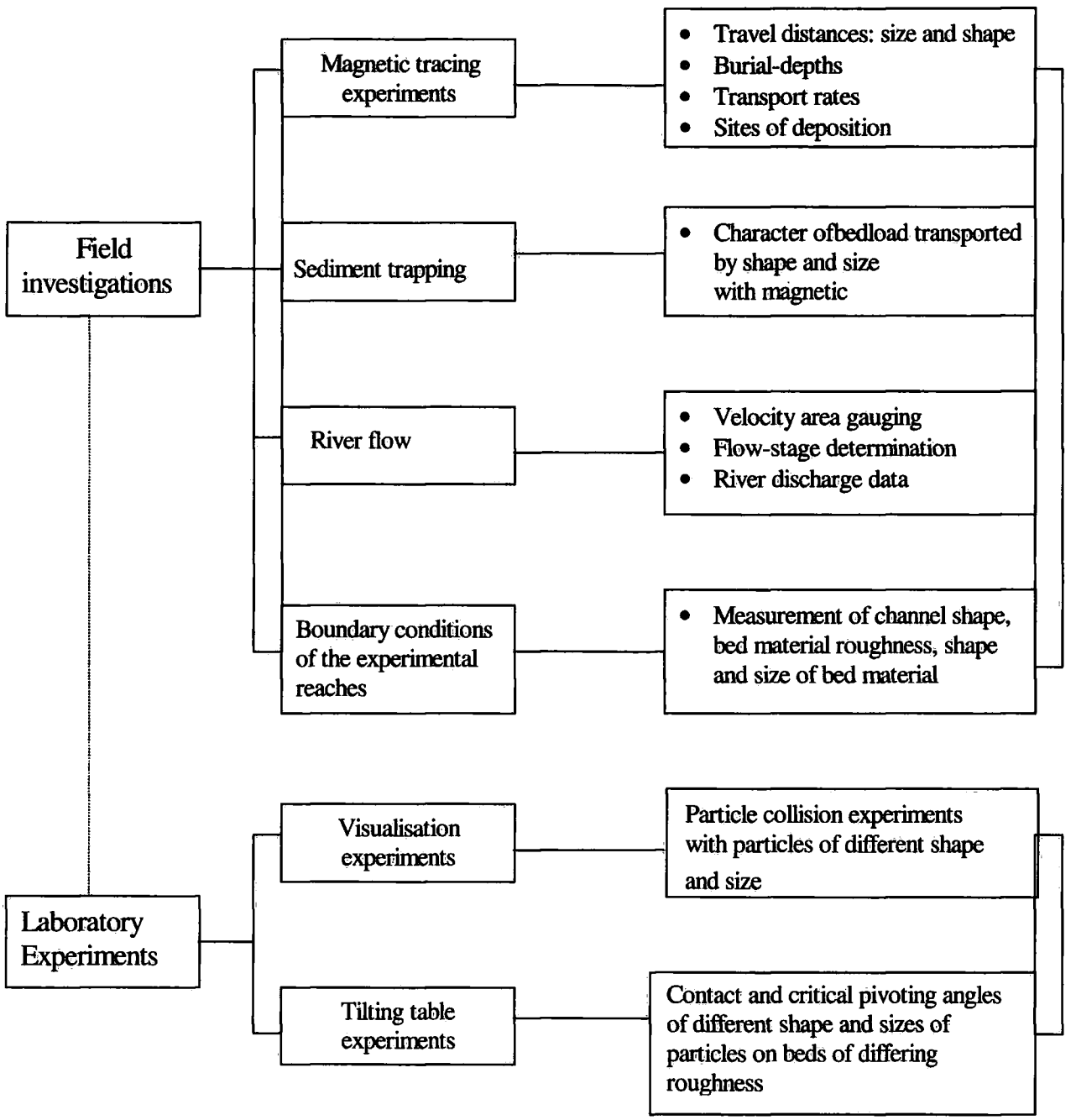

Figure 3.1 Experimental design for the present study

3.3 METHODS OF MEASURING PARTICLE SIZE AND SHAPE

3.3.1 Particle size analysis

In order to describe particle size, direct and indirect measurement techniques were used. Material from the reach-based sampling program was classified using the Wentworth size classification.

Material < 32 mm was sieved into five size classes, while the coarse particles (>32 mm) were classified on the basis of their b (intermediate) axes into seven sizes using a shape box (Shakesby, 1989) and template caliper (Table 3.1).

Table 3.1 Size classes determined by sieving and the direct measurement of the surface and sub-surface bed material

Sieving (mm)	Direct measurement (mm) (Shape box and template calliper)
<2.0	32.0 - 45.3
2.0 - 4.0	45.3 - 64.0
4.0 - 8.0	64.0 - 90.5
8.0 - 16.0	90.5 - 128.0
16.0 - 32.0	128.0 - 181.0
	181 - 256
	>256

For each particle greater than 32 mm, a, b, and c axes were measured using the shape box (Shakesby, 1989), the clast was weighed and the results were recorded.

3.3.2 Particle form

In order to standardise the classification of particle shape the Zingg classification of particle form was used (Figure 3.2). Using the data on a, b and c axes of coarse particle, b/a and c/b ratios were calculated and used to classify particles as spheres, discs, rods and blades (Zingg, 1935). However, In order to produce four distinct shape classes, particles plotting close to the shape boundaries as shown in Figure 3.2 (Standard Zingg limitation) were not used in the experiments, instead, limits

of the ratios of b/a and c/b for the different shape of magnetic tracers were rearranged using the criteria below.

	Zingg standard ratios	**New limited ratios arranged for the present magnetic tracers**
Sphere :	b/a ≥ 0.67 -- c/b ≥ 0.67	Sphere: b/a ≥ 0.70 -- c/b ≥ 0.70
Disc :	b/a ≥ 0.67 -- c/b < 0.67	Disc : b/a ≥ 0.70 -- c/b < 0.60
Rod :	b/a < 0.67 -- c/b ≥ 0.67	Rod: : b/a < 0.60 -- c/b ≥ 0.70
Blade :	b/a < 0.67 -- c/b < 0.67	Blade : b/a < 0.60 -- c/b < 0.60

Where b/a = the ratio of the intermediate axis to long axis and c/b = the ratio of the short axis to the intermediate axis (Figure 3.2, for further detail of the technique see also Chapter 2)

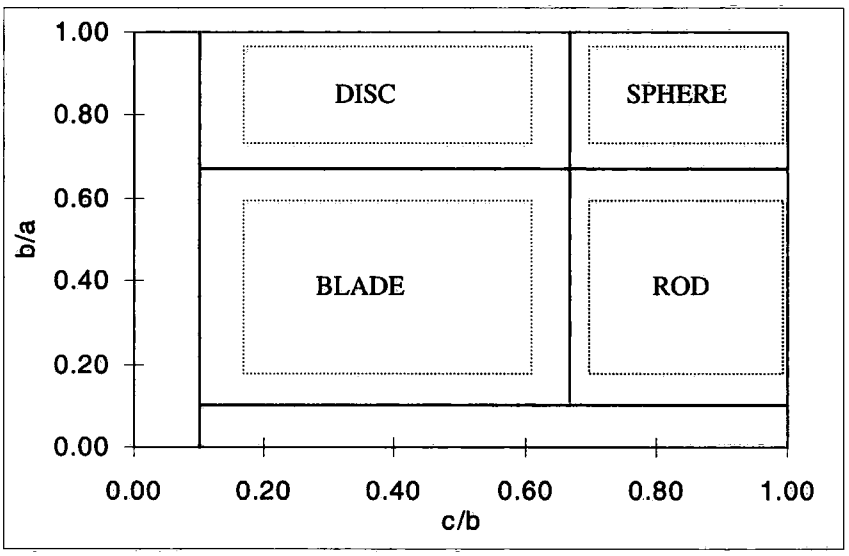

Figure 3.2. The Zingg classification of particle form. (The dashed frames show the shape boundaries arranged for the magnetic tracers).

3.3.3 Roundness

Cailleux's roundness index (Cailleux, 1947) was used to determine the roundness values of the particles. According to this method the radius of the sharpest corner of the particles is measured in the maximum projection plane. The particle is then placed over a series of concentric semicircles of known radius to determine which of the circumferences best matches the curve of the sharpest corner. The radius of this

semicircle is the radius of curvature of the corner (Figure 3.3). The length of the longest axis is then measured, and a value for roundness calculated from the formula:

$$R = (2r/a)\cdot 1000 \tag{3.1}$$

where r is the radius of curvature of the sharpest corner and a is the length of the longest axis. This measure produces values ranging from 0 to 1000, where a perfect disc or sphere-shaped particle has an index of 1000 (Briggs, 1977).

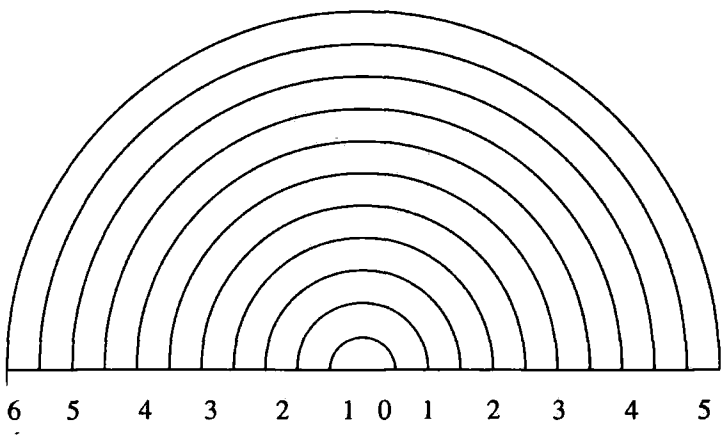

Figure 3.3 Concentric circles used to measure radius curvature in Cailleux's roundness index.

3.3.4 Flatness

Cailleux's flatness index was used to define the flatness values of particles (Cailleux 1947). This index is based on the relationship between the three primary axes of a particle and is determined using the formula:

$$F=((a+b)/2c)\cdot 100 \tag{3.2}$$

where a is the longest axis of the particle, b is the intermediate axis of the particle and c is the shortest axis of the particle. The index ranges from 100 to infinity. The minimum value relates to a perfectly equidimensional particle. The flatter the particle the higher is the flatness index (Briggs 1977).

3.3.5 Sphericity

Krumbein's sphericity index was used to determine the sphericity of particles in each size group (Krumbein, (1941b). Although the Zingg classification of particle form gives an objective and rapid measure of particle form, it does not give a numerical measure of shape. Krumbein's sphericity is given by the following formula:

(3.3)

$$\sqrt[3]{\frac{bc}{a^2}}$$

where a, b and c are the long, intermediate and short particle axes as previously defined. Sphericity values range from a minimum of 0 to a maximum of 1, where 1 indicates a perfect sphere. Krumbein's measure of sphericity produces a single value for each particle.

3.4 STREAMFLOW MEASUREMENTS AND TECHNIQUES

Discharge is gauged on Trout Beck (NY 759 336) approximately 400 m upstream of the confluence with the River Tees (NY 762 338). The site consists of a compound Crump weir, established in 1971 (Figure 3.4). A full flow record is not available due to operating difficulties in the 1980s. Since 1991 the site has been run and maintained by the National Rivers Authority (now the Environment Agency) and the discharge data is recorded at 15 minute intervals. Based on the criteria explained by Herschy (1999), a second site in a straight reach of uniform cross-section was established in November 1997 on the upper Tees (NY 755 339) to provide an estimate of the discharge just upstream of the experimental reach. This consisted of Campbell CR10X data logger connected to a Druck pressure transducer (Figure 3.4). The site is powered by a 12-volt battery connected to a solar panel. Flow stage is recorded every 15 minutes in line with the Environment Agency procedures used at Trout Beck. The river at this second gauging site is relatively straight and for the majority of the stream cross-section flows over bedrock. Using the velocity-area method and following the procedures detailed by Herschy (1999) discharge measurements were made at a range of river flow stages in order to construct a stage-discharge-rating curve.

Gauging of the flow at these two upper sites provided a means of estimating the discharge at the lower Tees site below the confluence (See Figures 4.4 and 4.5 in Chapter 4).

Figure 3.4 Campbell CR1OX data logger connected to a Druck pressure transducer for continuous river stage record on upper Tees (Top), and Compound Crump weir and discharge gauging station on Trout Beck (Bottom).

3.4.1 The Stage-Discharge Curve

Herschey (1999) states the most important part of a velocity-area current meter station is the stage-discharge relation. The rating curve for the Upper Tees station is shown in Figure 3.5. At this site station control is stable over a wide range of stages. Sedimentation is minimal and aquatic vegetation is largely absent. The cross-section varies relatively smoothly and the same boundary roughness conditions apply. Minor problems with icing are encountered in the winter months but over the period of monitoring this has not affected more than a few days of record. Observations over three years confirm that the hydraulics of the site have changed little during this time. Simple stage discharge relationships can be expressed by the equation:

$$Q = C\,h^{n}$$

Where Q is discharge, h is stage and C a constant. If Q is not zero when h = 0, then a stage correction factor (z), the value of the stage at zero flow, must be added

$$Q = C\,(h + z)^{n}$$

This equation can be transformed into logarithms:

$$\log Q = \log C + n \log (h + z)$$

This is the equation for a straight line of the form:

$$y = C + mx$$

where m is the gradient of the line and C is the point of intersection of the line with the y axis. This can be shown graphically by plotting discharge measurements on log-log graph paper. An equation can be fitted to the data using least-squares regression techniques. Normally discharge would be plotted as the dependent variable on the y axis, however tradition dictates that this is plotted on the x axis. However Q is retained as the dependent variable and the regression equation fitted with (h + z) as the independent variable. The value z (stage at zero flow) is derived by trial and error (WMO, 1980). The 'correct' value of z is the value which, makes the stage-discharge relationship plot as a straight line on log-log graph paper. It should be thought of as an 'effective' zero rather than the point at which the channel goes dry (Gordon *et al.*, 1992).

The relationship for the Upper Tees rated section is shown in Figure 3.5. The relation plots as a straight line passing through zero and the rating equation is:

$$Q = 14.328\,h^{1.7287}$$

Because of the difficulties of obtaining velocity measurements at high stages extrapolation of the stage discharge relationship to estimate flood flows is inevitable. In the present case velocity measurements had to be made by wading. Thus the highest gauged flow is approximately 3.6 $m^3 s^{-1}$. This was less than the Bankfull stage for the rated section. Because the rating curve plots as a straight line on log-log paper with minimal scatter (R^2 0.989) it may be extrapolated to higher stages. Shaw (1994) cautions such extrapolations if they exceed 20% of the largest gauged discharge and cannot be checked by other methods. However, Bovee and Milhous (1978) demonstrate that developing a stage-discharge relationship using only three points when extrapolated within the range of 40 to 250% of the calibration flow produced more reliable results than Manning's Equation.

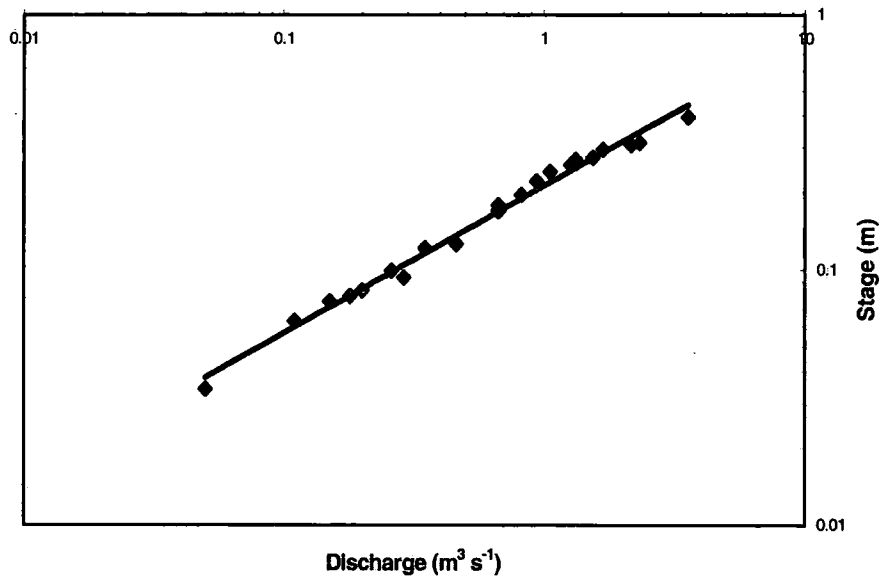

Figure 3.5 Upper Tees rating curve

3.5 MAGNETIC TRACING EXPERIMENTS

The magnetic tracing experiments were carried out on a gravel-bed stream system at the Moor House National Nature Reserve. Three experimental sites were selected, two on the River Tees (lower and upper sites), and one on Trout Beck. Detailed information on the main physical characteristics of the two study catchments is given in Chapter 4.

A total of 900 tracers were prepared for each of the three sites. The size range of the tracers was between 32 mm and approximately 256 mm (b axis). Three size classes

are defined: 32-64 mm, 64-128mm and >128 mm (Table 3.2). The methods used to determine bedload size and shape (form, sphericity, roundness, and flatness) are described in detail in section 3.3 of this chapter. The particles were classified on the basis of their 'b' (intermediate) axis. Particles are restricted to sizes greater than 32 mm because of a combination of practical and experimental considerations. Practical limitations in the use of magnetic tracers require a relatively large particle so that a magnet can be inserted. For each particle, the a, b, and c axes were measured using a particle shape box (Shakesby, 1989). Clasts were weighed and the results recorded. In each of the smaller size classes 400 tracers were prepared. In the larger size class, because of their lower mobility, only 100 tracers were used (Figure 3.6). Within each size class equal proportions of different shaped particles were included. Careful screening of the particles on the basis of the Zingg (1935) shape classification produced four distinct shape classes: spheres, blades rod and discs. Particles plotting close to the shape boundaries shown in Figure 3.2 were not used in the experiment.

Table 3.2 Details of bed material tracers and site characteristics at the three experimental reaches

Site	Colour of tracer	Number of stones in each size class of tracer (mm)			Experiment start date	Mean bankfull channel width	Slope of channel	Bed material size (mm)	
		32-64	64-128	>128				D_{50}	D_{90}
Upper Tees NY 758 339	White	400	400	100	26.11.1997	20.0	0.0006	57.0	99.6
Lower Tees NY 762 338	Orange	400	400	100	10.12.1997	25.0	0.003	80.7	121.6
Trout Beck NY 759 336	Yellow	400	400	100	26.11.1997	12.7	0.0095	97.4	181.0

Particles were drilled and a small RDAL 00029 ferromagnetic magnet was placed inside. The sizes of the magnets inserted into the particles were 20-mm length and 6 mm diameter. Each magnet was sealed in place using silicon gel then the whole particle was painted with masonry paint and labelled with an identification number. All tracer particles were measured (a, b, c axes) in order to provide an identification if the

paint labels were erased. The great advantage of using magnetic tracers is that they can be relocated even if buried; covered in algae, hidden in murky water or the tracer paint is removed by abrasion (Schick *et al.*, 1988). A background and discussion of the methods of the magnetic tracing experiments and bedload transport is given in Chapter Two.

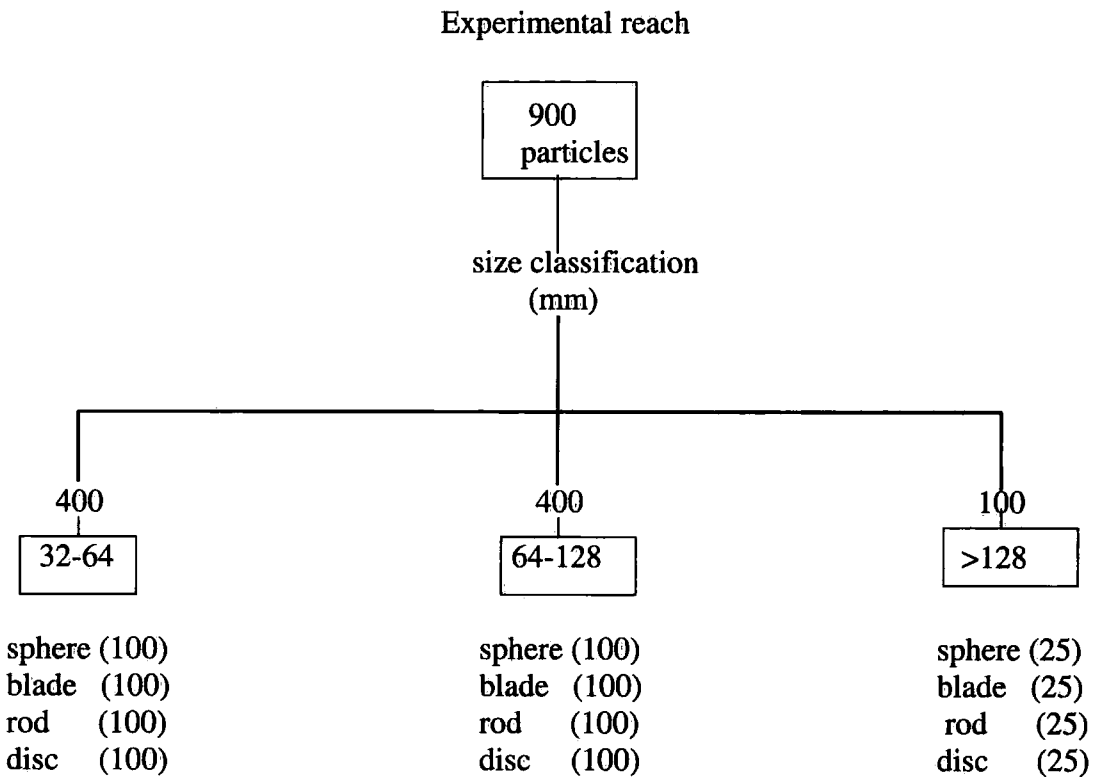

Figure 3.6 Experimental design for magnetic tracing experiments at each experimental reach.

The tracers were placed on the bed in a 3 m wide strip band 2 to 3 m in from the left and right banks across the width of the channel (Figure 3.7). Tracers were 'seeded' randomly into the stream channels in November / December 1997 and allowed to find their own settling position.

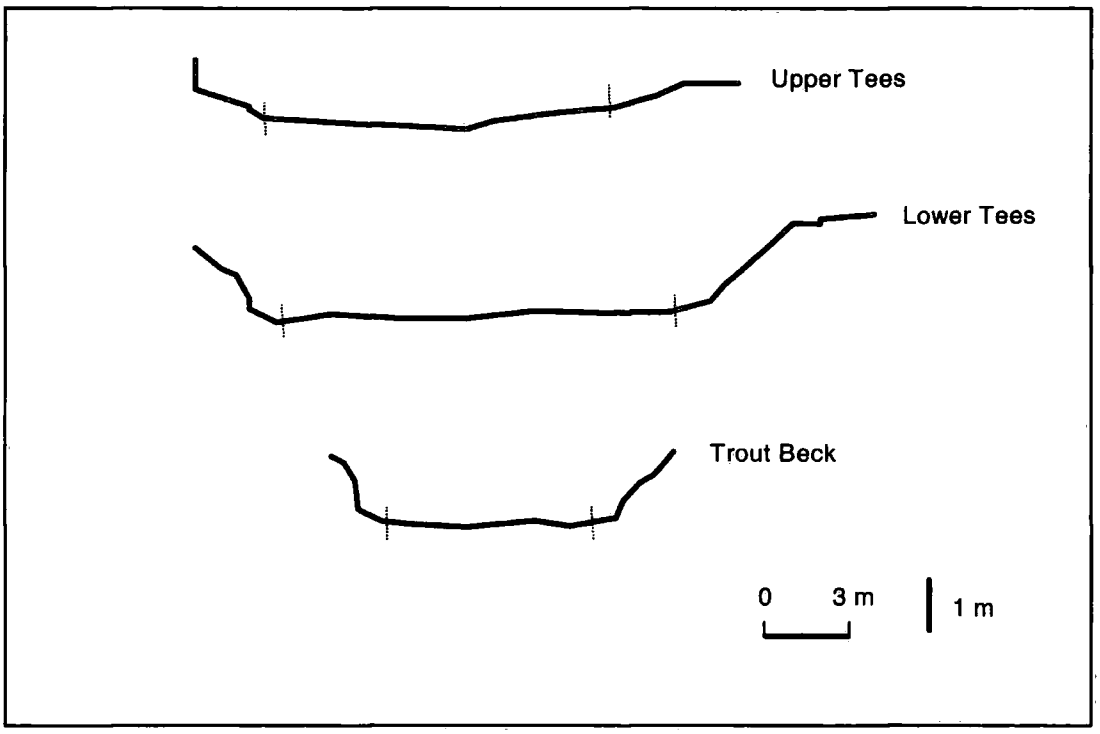

Figure 3.7 The geometry of the cross-sections where magnetic tracers were introduced into the stream channels at three experimental sites. (The sections where tracers were placed are shown between the bands in each cross-section).

Sites were visited weekly to gauge movement and, where noticeable movement had occurred, the sites were resurveyed as soon as discharge conditions permitted (Figure 3.8). The position of each tracer was measured and mapped with reference to a series of monumented pegs set-out along the banks adjacent to the experimental reaches. The position of individual tracer particles was surveyed using two methods: tape survey and EDM survey. Movements less than 3 m from the start line were not included in the analysis. At the outset it was decided that it would not be possible in the initial experiments to visit the sites after every flood, therefore bedload movement events could not be related to individual floods. However as the main interest is the relative movement between different shape classes, this was not seen a major drawback.

The magnetic tracers had a similar lithology to the natural bed material in the three experimental reaches. The range of particle sizes, determined by surface sampling of all particles from 1 m^2 (Wolman, 1954), show that the tracers were similar in size to the resident coarse material. Although there were equal numbers of the tracers in the four shape classes, the natural bed material tended to show a greater number of disc-shaped particles, reflecting the dominance of sandstone lithologies in the natural bed material (Table 3.3).

Figure 3.8 Searching for magnetic tracers at the Upper Tees Site. A magnetic locator was used during all searches.

Table 3.3 Comparison between the proportions (percentages) of different shaped particles in the 'natural' bed material and tracer material at three experimental reaches.

Tracer site	Bed material	Sphere	Blade	Rod	Disc
Upper Tees	Natural	32.2	12.2	12.1	43.4
	Tracer	25.0	25.0	25.0	25.0
Lower Tees	Natural	23.2	16.3	13.6	46.9
	Tracer	25.0	25.0	25.0	25.0
Trout Beck	Natural	22.6	14.9	15.8	46.7
	Tracer	25.0	25.0	25.0	25.0

Comparison of the size and shape characteristics of magnetic tracers used in the field experiments

According to research aims, both shape and size properties of the test particles needed to be replicated at each site. Thus size and shape characteristics of magnetic tracers used at the three experimental sites are compared in Appendix 1 in order to determine similarity between the three sites. The Appendix 1 first examines and compares mean particle size and weight in three size groups and for four shape classes at the three sites (sections A1.2 and A1.3). It considers b/a (the ratio of the intermediate axis of a particle to its longest axis) and c/b (the ratio of the shortest axes of a particle to its intermediate axis) ratios of the test particles (Section A1.4 and section A1.5). The degree of roundness of the tracers are examined and compared (section A1.6). The final two sections (A1.7 and A1.8) summarise sphericity and flatness properties of the tracers in respect to their importance on the hydraulic behavior of a particle during transport. In each section mean values and frequency distributions of the particles are examined and compared statistically to determine whether there is a significant difference between the different sites. Because of the nature of this work this is placed on appendix of the rear of the thesis. A brief summary of the principal findings is given below.

1) In terms of particle size, despite some small differences, the three sites show very similar mean size and also frequency distributions (Figures A1.1 and A1.2) Generally the three sites have very similar mean weight distributions (Figure A1.3), although the Lower Tees site has slightly lower mean weight than the other sites. The greater mean weight of rods and sphere-shaped particles in the medium and large size

groups at almost each site is attributed to the size classification method which, regardless of shape, is based on the diameter of the "b" axes of each particle. In other words, length and thickness of particles were not taken into consideration. Thus for similar sizes, shape of the particles consistently influences the weights and this is more pronounced at larger sizes. In each shape class, mean differences in weight between medium and large size groups at all three sites were found to be significantly greater than that between small and medium size groups (Table A1.4). Mean weights of the particles in all three size groups are lower at the Lower Tees site but increase gradually towards Trout Beck and Upper Tees. Except for disc-shaped particles in the small and medium large group, sphere, blade and rod-shaped-particles have similar frequency distribution in size at the three sites (Figure A1.4).

2) In terms of b/a and c/b ratios of particles, comparisons have shown that the three sites have similar means and frequency distributions within each size group and also for the four shape classes (Tables A1.5 and A1.7). Mean b/a ratios vary between 0.68 (Lower Tees) and 0.67 (Trout Beck and Upper Tees sites).

3) In all three size groups, mean roundness values at the three sites vary between 300 and 400. There is a small difference between the Trout Beck and Upper Tees sites but the difference increase between the Lower Tees, Trout Beck and the Upper Tees site (Table A1.9, Figure A1.9). In each size group, sphere and disc-shaped particles have greater mean roundness values than rods and blades. At the Lower Tees site mean roundness values are, in decreasing order, sphere, disc, blade and rod respectively. At the Trout Beck and Upper Tees sites the orders is sphere, disc, rod and blade. Except in the medium size group, comparisons proved that the three sites have very similar shape distributions and therefore there is no statistically significant difference between them in small and large size groups (Table A1.10)

4) The sphericity of the three sites varies between 0.59 and 0.62 (Table A1.11). Not surprisingly, within each size group sphere-shaped particles always have greatest mean sphericity values (0.84 and 0.86), while blade-shaped have the lowest value (0.30) (Figure A1.11). For all the three size groups at Lower Tees and Trout Beck sites the order of increasing mean sphericity values is blade, rod, discs and sphere. The Upper Tees site also shows a similar trend, except for the medium size group, in which disc-shaped particles have a lower mean value than rod-shaped particles.

5) All the three sites have very uniform mean flatness values, which vary from 265 (Lower Tees) to 267 (Table A1.13, Figure A1.13). Not surprisingly, blade-shaped

particles have the greatest mean flatness values while sphere shaped-particles have lowest values. No statistically significant difference was found between the three sites within each size group in sphere, rod and disc-shaped particles (Table A1.14).

Overall, all three sites in all three size group show very similar size and shape distributions.

3.6 CHARACTERISTICS OF THE THREE EXPERIMENTAL REACHES: RIVER CHANNEL GEOMETRY, BED MATERIAL ROUGHNESS, AND CHARACTERISTICS OF THE BED MATERIAL.

In order to determine the boundary conditions of the experimental sites topographic and bed material size and shape characteristics of the experimental sites were measured.

3.6.1 Topographic methods

The planform geometry of the channels was mapped at each experimental site with reference to a series of pegs set out along the banks adjacent to the experimental reaches (Figure 4.4 In Chapter 4). In addition, at each experimental reach, the cross-sectional geometry of 10 monumented cross sections were surveyed using levelling. Cross-sections were spaced approximately 15 metres apart along the channel. Results of measurement are shown in Chapter 4.

3.6.2 Measuring bed material roughness and sampling of surface and sub-surface bed material

Downstream changes of bed material roughness and surface/sub-surface bed material characteristics were measured in the experimental reaches. At each cross-section, sampling sites were selected to satisfy four conditions:

- lack of evidence of artificial disturbance of bed material
- absence of thick vegetation covering the bed surface which would indicate that bed material had not moved in several years
- bare gravel surfaces were sampled (where possible, upstream parts of bars were selected as sampling site because they contains the coarsest gravel and exhibits little sorting (Kodama, 1992).

Five sampling sections, 30 m apart, were surveyed at each reach. The Wolman (1954) bulk sampling procedure was used. In each section a 1 m^2 quadrat was placed on the selected section of channel bed. Bed material roughness was measured in the downstream and transverse (to the flow) directions using a pin (roughness) frame (Figure 3.9). Pins were spaced at 20 mm intervals and the typical precision in vertical measurements was +/- 2 mm. All exposed bed material within the quadrat was collected, weighed and measured to determine its size and shape characteristics. Bias correction was applied using the method described in Fripp abd Diplas (1993). Two photographs of the sampling sections were taken one before and one after the sampling (See Chapter 4). After removing all surface material, a volumetric sample of the sub-surface bed material was taken. Sampled material was then weighed and sieved to determine the particle size distribution. Enough material was sampled to ensure that the weight of the largest particle was not more than 2 % of the total weight of the sampled material (Kodama, 1992).

Figure 3.9 The pin (roughness) frame used to measure bed material roughness The example shows the frame deployed at the Upper Tees site in a transverse orientation.

3.7 TILTING TABLE EXPERIMENT

Introduction

The critical angle of particle motion has been previously described by several terms: pivoting angle, friction angle and the angle of sliding friction. Some earlier investigators pointed out that both particle pivoting and friction angle varies with the shape, size, and orientation of the individual particles, as well as the shape, size, orientation, and packing arrangement of the particles comprising the local bed (for detail see Chapter 2). The objective of this experiment is to examine the mechanical processes of entrainment, based on the analysis of friction and pivoting angles of particles in various shape and size classes. The lower the friction angles the easier the particle is to entrain. It is assumed that, due to their better rolling capability, sphere and rod shaped particles would entrain at lower friction angles than those that are flat shaped (e.g. disc and blade). The outcome of the tilting table experiments will be related to the field observations to provide some important information in explaining why some tracers have moved longer transport distances than the others in the study reaches.

The test particles used for the present experiments were in various shape and size classes. Two sets of experiments were designed to test this objective: experiments on artificially-formed bed roughness and experiments on naturally formed bed roughness. The experimental design for the tilting table experiments is shown in Figure 3.10.

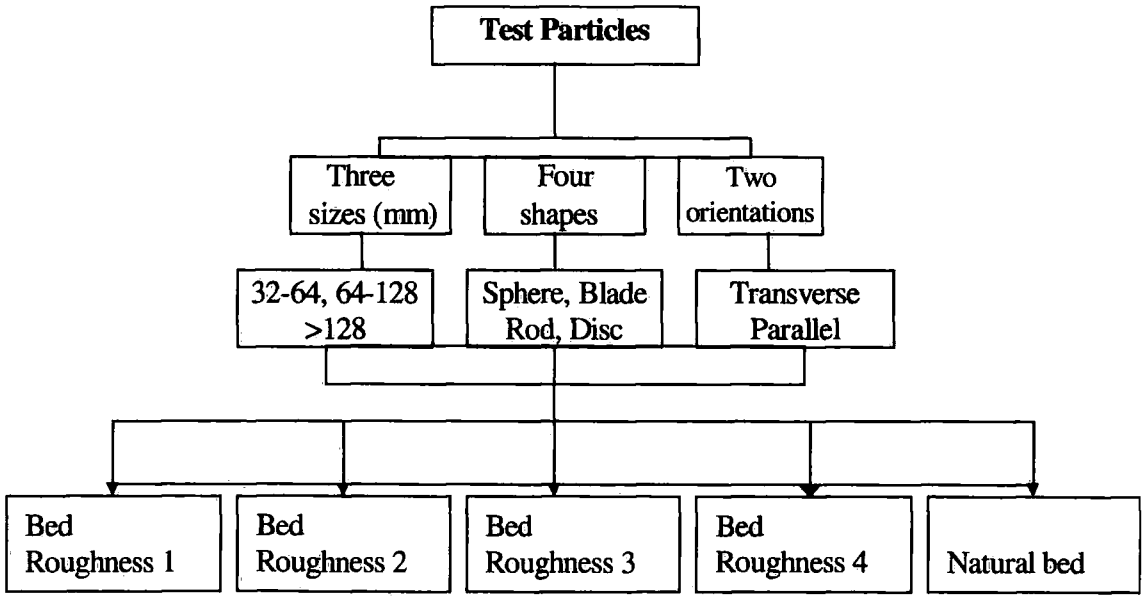

Figure 3.10 Experimental design for the tilting table experiments

3.7.1 Tilting table experiments on artificially formed bed roughness

Sets of experiments were carried out using four artificially-made bed roughness plates. Four metal plates ($1m^2$) were used as base plates for four different bed roughnesses. Figure 3.11 shows one of the artificially formed bed roughness plates (Roughness 4)(for detail see Chapter 6). The roughness was formed using natural coarse gravel of various shape and size. On each base plate the size of the bed particles (base pebbles) was limited to a specific grain size range (Table 3.4). The base pebbles were secured to the base plates with a silicon sealant.

Table 3.4 The grain size characteristics of the four bed roughnesses.

Bed Roughness type	Size of the base grains (b axis)
Roughness 1	8 – 11.2 mm
Roughness 2	16 – 22.4 mm
Roughness 3	32 – 48.0 mm
Roughness 4	64 – 96.0 mm

The test grains used to determine friction angles, on each of the bed roughnesses, included both artificially-moulded particles as well as some naturally-formed pebbles. Three test grain sizes were used: b axes; 24, 48 and 96 mm. The size and shape characteristics of the test particles used for different tilting experiments are given in Chapter 6.

3.7.2 Tilting table experiments on naturally formed undisturbed bed roughness

In order to measure the friction angle on a bed that is composed of naturally formed fluvial gravel, undisturbed samples of the bed surface were obtained from one of the study streams by applying a thin epoxy resin to areas approximately $1m^2$. The hardened rigid surfaces of the bed were excavated and brought into the laboratory and rebedded in a sand tray (See Chapter 6). In order to provide strength, the sample was mounted in a wooded frame. Particular attention was paid to maintain natural grain geometry and texture during the sampling processes. This is why a thin epoxy resin was used to provide a suitably strong, low viscosity adhesive that did not fill the natural pore

surfaces and also alter markedly the natural grain texture of the sampled surfaces. The bed surface was sampled from a site representative of the experimental sites. At the selected experimental site (Trout Beck) the sample was chosen within an area of consistent bed texture. A wire frame was thrown onto the bed while looking away. The frame was placed parallel to flow direction, and sampling of extreme bed topography (bar fronts, etc.) was avoided.

Figure 3.11 One of the artificially-made bed roughness plates. The example shows a tilted metal base plate on which natural coarse gravels (b axes in 64-96 mm size range) were secured.

A random sampling method, which is similar to that of Wolman (1954), was used in order to determine grain shape and size of sampled bed, as explained in Buffington *et al* (1992). Particle size of the excavated bed surface was determined randomly lowering a hand-held needle (while looking away) onto the surface and measuring the selected particle's apparent longest, intermediate and shortest axes with a caliper. Sampling was limited to particles greater than 8 mm. The sampled bed surface was periodically rotated to ensure random particle selection and a total of 100 particles were measured. A tilting apparatus was developed on which the sampled bed was mounted on a tilting board, which was hinged at one end onto a base-board (Figure 3.12). A clinometer was fixed onto the tilting board. The board was tilted by raising it at 1^{o} intervals. Test particles were randomly placed on to the sampled bed. The raising and lowering movement of the tilting board was operated by a sensitive winding mechanism (Figure 3.12).

Following the methodology of Miller & Byrne (1966) and Buffington *et al* (1992), within each size category, particles friction angles were measured by placing selected particles (which had different shapes) on the sampled bed and tilting in the downstream direction until the particles moved out their pockets (Figure 3.11 and Chapter 6). Thus the angle of tilt of the bed at this point was the friction angle for the grain of interest. The test particles used to measure friction angles on each bed were made using art clay and natural stones. Details of the size and shape characteristics of the test particles used in the experiments are given in Chapter six.

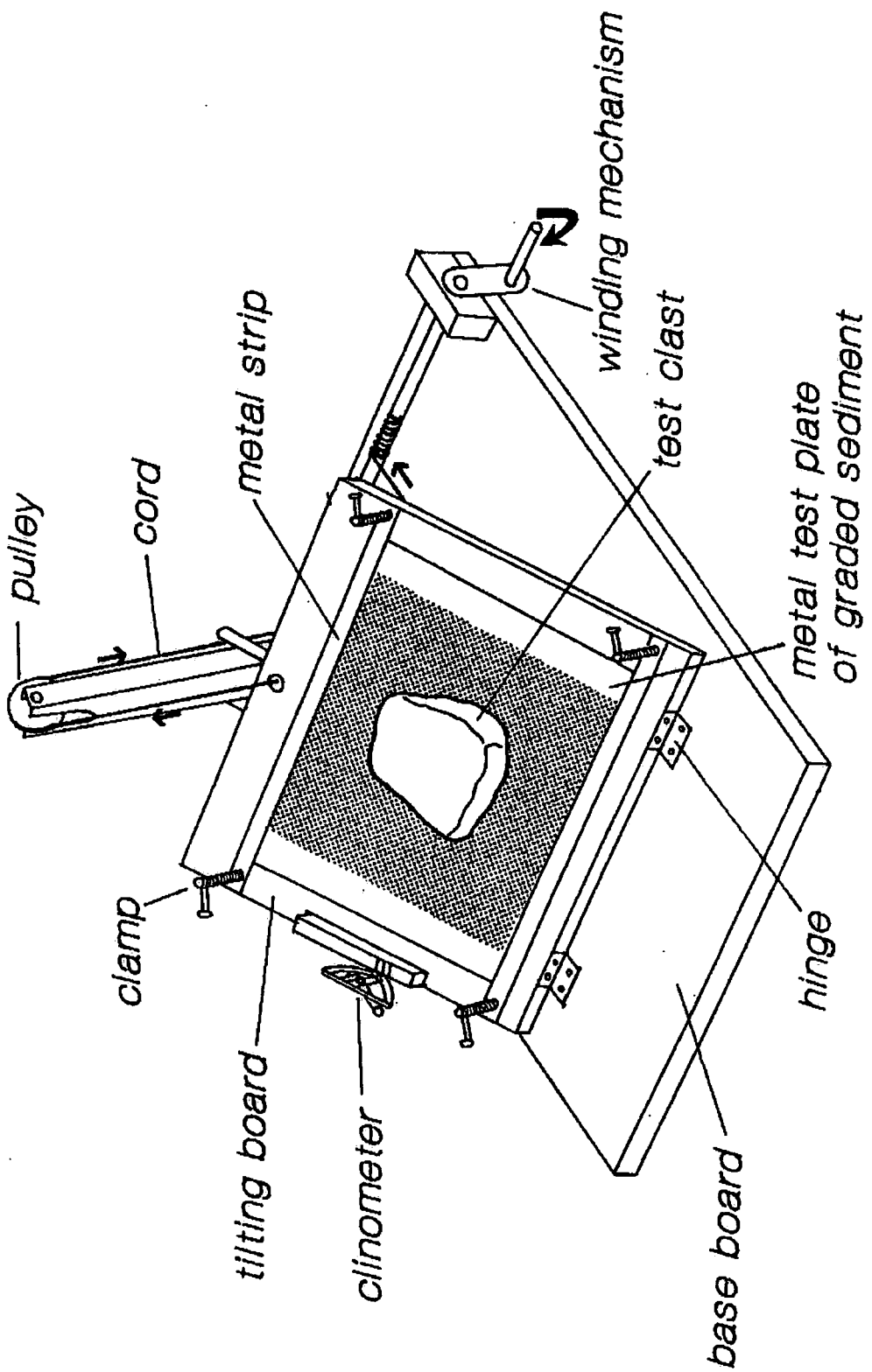

Figure 3.12 Tilting table for measuring friction angle of clast

3.8 VISUALISATION OF PARTICLE MOTION: STROBE PHOTOGRAPHY

Introduction

Shape, size and density are fundamental properties controlling the hydrodynamic behaviour of sediment particles. Grain shape can play a significant role in bedload transport processes by controlling the nature of particle settling and near-bed motion. The aim of these experiments is to investigate the influence of grain shape on settling; grain impact; initial motion and transport of gravel-size particles. These experimental results cannot be directly related to the actual field observation, though they do provide important information on the hydrodynamic behaviour of sediment transport. This may help explain the mechanism of selective sediment transport in gravel bed river.

A series of visualisation experiments were deigned to examine collision and hydraulic behavior of particles of various shape and size in water. The experiments were carried out in a 10 litre rectangular tank. The method follows Schmeeckle (1998). The setup of the experiment is shown in Figure 3.13.

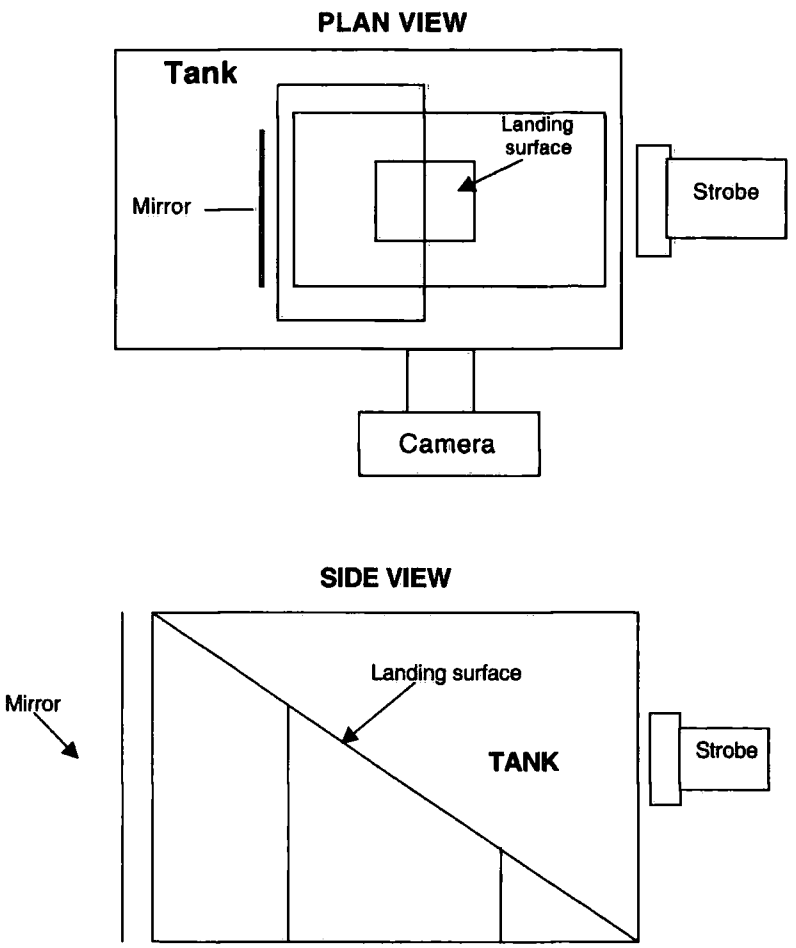

Figure 3.13 Plan and side views of the experimental apparatus used to take strobed photographs of particle collisions with an inclined plane in water.

Particles were dropped onto a 5 mm thick glass plate. The angle of the plate could be inclined. A 35 mm camera with a 35-70 zoom lens (set at 35 mm) was used. A strobe light was directed at the subject at right angles to the camera, and a mirror was placed opposite the strobe with the subject in between. This configuration meant the particles received strobe lighting from two directions. The strobe rate was adjustable with a maximum 250 flashes per second. The back of the tank, opposite the camera, was covered with a piece of black cotton material in order to have clear definition of the particles during movement (Figure 3.13).

The camera shutter was kept open for the duration of each particle drop and collision in order to observe multiple images of the particle before and after impact on a single frame of film. The pattern of each particle were caught on a single frame of film. The film was used was 400 ISO black and white negative film which was uprated to 3200 ISO.

3.9 CONCLUSION

The purpose of the magnetic tracing experiments was to investigate the impact of particle shape and size on the travel lengths of transported sediment. Further to this the influence of bed topography in regard of sediment transported was also considered. These results collectively illustrate the impact different particle size and shape has on transport lengths, though fail to provide an explanation for the observed behaviour. To seek some explanation experimentation with a tilting table and visualisation tank was performed. The tilting table determined the variability in the mechanistic behaviour of particles according to their differing shape, size, and orientation, on different bed roughnesses. The visualisation experiment explained the influence of particle shape, size, and density on the dynamics of bedload motion, i.e. settling velocity; transport velocity; and the collective mode of particle movement.

CHAPTER 4: THE STUDY CATCHMENT AND REGION

4.1 GENERAL DESCRIPTION OF THE STUDY AREA

The main field experiments were undertaken in two coarse-gravel-bed streams in the North Pennines (Figure 4.1). The North Pennines are an area of upland moorland, located at the northern end of the Pennine chain. Most of the area lies above 450 m O.D. with the highest point being the summit of Cross Fell at 893 m O.D. To the North, the area is bounded by the Tyne Gap (Stublick Fault) and to the South by the Staimore Trough (Lunedale Fault). To the West the Pennine Fault produces a large western sloping escarpment. To the East the block is tilted under the Durham Coalfield (Warburton, 1998).

The area is generally characterized by an upland landscape of high, open and exposed plateaux and broad ridges which support moorland and montane habitats with few trees. Large expanses of blanket bog overlie mineral soils that have developed on glacial, solifluction and alluvial materials. Sheep graze the whole area. The North Pennines area is an area of Outstanding Natural Beauty and regarded by many as England's last wilderness (Warburton, 1998).

4.2 GEOLOGY RELIEF AND DRAINAGE

4.2.1 Geology

The solid geology of the Northern Pennines is dominated by rocks of the Carboniferous, consisting mainly of alternating shales, limestones, sandstones, grits and coal. The lithology and structure of the region has been described in detail by Johnson and Dunham (1963), Johnson and Hickling (1970) Taylor *et al* (1971) Burgess and Wadge (1974) and Dunham (1990). The solid rocks range in age from Ordovician, which comprises Borrowdale Volcanics and Skiddaw Slates, to Triassic. The classic Carboniferous stratigraphy of Lower Carboniferous Limestones, Millstone Grit and Coal measures is no longer favoured by modern geologists (Duff and Smith, 1992).

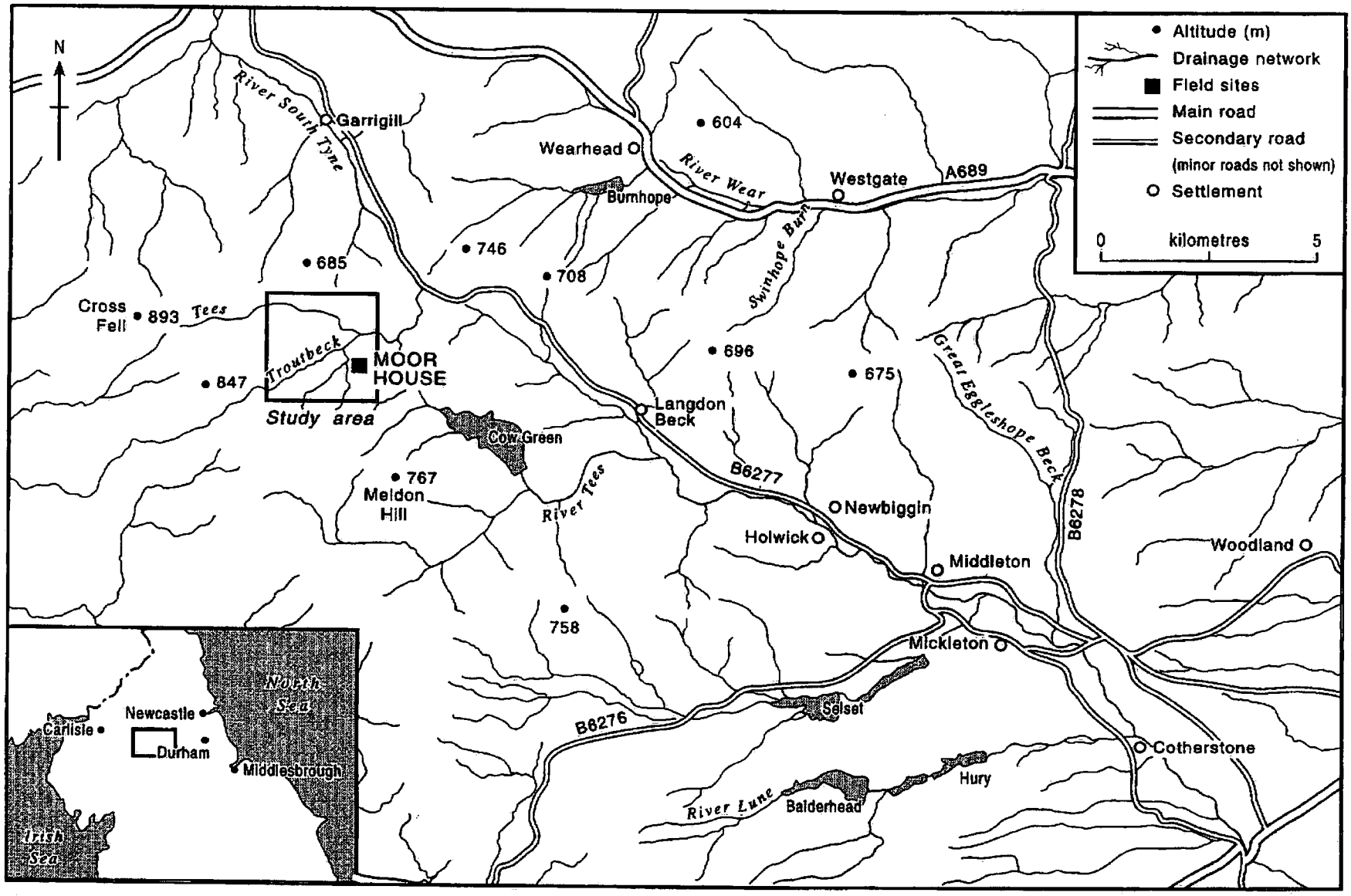

Figure 4.1 Map of the study area (After, Warburton, 1998).

Preferred terms are the Dinantian and Silesian (Figure 4.2). Following the Caledonian orogen, the main geological structures of the region developed in Northern England. These structures are characterized by the 'block and trough system'. The Weardale granite of post Silurian age (400 Ma) occurs as a batholith beneath the area and has been responsible for regional deformation and the gentle eastward dip of the Alston block (Bott, 1967).

During a Permo-Carboniferous intrusive episode the famous dolerites of the Great Whin Sill were deposited. This period was accompained by crustal movement resulting in the development of the Pennine fault scrap at the western edge of the Alston block. Mineralisation of mainly Carboniferous rocks during the early Permian deposited the base metals and minerals (zinc, and iron with smaller quantities of lead copper, silver and cobalt) which have made metal mining in the North Pennines so famous. Although the mining period began in Roman times, until the 17th century mining production was restricted to small-scale operations. However, improved mining techniques in the mid 17th century revolutionised production, leading to a peak in activity in the early 1860s to the 1880s before finally petering out in the early 20th century. The legacy of mining has left an enormous impact on the local landscape (Warburton, 1998).

The most recent solid geology of the area is characterized by the deposition of Permian and Triassic sedimentary rocks. Continued earth movements throughout the Triassic, intra-Jurassic and Teritary resulted in complex regional fault movement in the area. Finally, the youngest extensive sediments are associated with the glaciogenic sediments of the last major glaciation (Late Devensian). Holocene alluvium and colluvium locally mantle the valleys and slopes.

Geomorphological development of the river drainage systems in the region is strongly controlled by the geology and structure. For example, easterly drainage of the region's major river systems is influenced by the eastwards dip of the Alston Block. On a more local scale outcrops of the Great Whin Sill have a strong influence over many surface forms. High Force on the River Tees in Upper Teesdale plunges 22 m over the sill. At this point the Whin Sill is 9 m thick and overlies Carboniferous shale and limestone. Erosion of the shale has resulted in the collapse of the Sill and headwards recession of the waterfall (Goudie and Gardner, 1985).

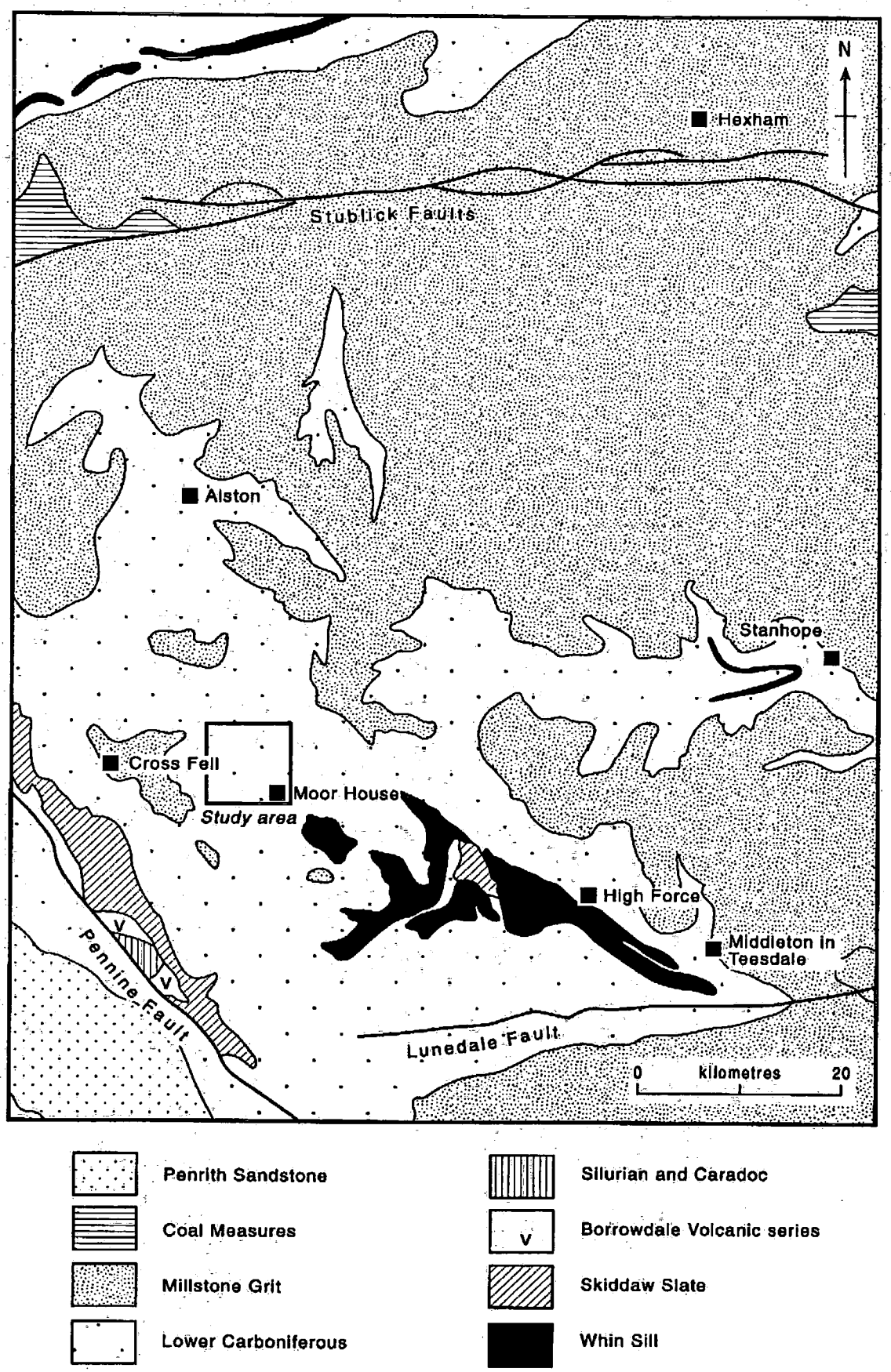

Figure 4.2 Regional geological map showing the location of the study area (After, Warburton, 1998)

4.2.2 Glaciation

The North Pennines have relatively widespread evidence of glacial deposits and erosion. Abundance of meltwater channels and the evidence of glacial plucking on the peaks of the summit ridge of the pennines at Cross Fell and Little Dun Fell shows that even the highest ground in the region was over-ridden by ice at the maximum advance of the Quaternary ice sheets (Peel, 1949; Bradshaw, 1976). During the Late glacial the North Pennines did not support an extensive ice cover but a range of periglacial landforms developed on the summits. Locally small glaciers (e.g. escarpment glaciers) may have developed in localities which favoured northeast orientation and deposition of blown snow (Mitchell, 1991; Wilson and Clark, 1995).

4.3 CLIMATE AND HYDROLOGY

Although there is an extreme paucity of data for upland climates, especially in terms of primary meteorological and climatological data in Britain, the climate at Moor House has been comparatively well documented. Daily meteorological observations, measurements of rainfall rate, continuous river flow and discharge gauging (on the Trout Beck) soil temperature, evaporation, sunshine, radiation and wind speed are available during a greater part of the last three decades.

In general, the North Pennines has an upland maritime climate that is characterized by cool, cloudy and wet conditions, due to the high altitude and proximity to the sea (Manley, 1942, 1943; Simithson, 1985). Rainfall is very high and increases with altitude across the region. High wind, heavy precipitation (2000 mm) and winter snows are the main characteristics of the climate in the area. In winter snow can lie for up to two months and frost action is relatively effective on bare surfaces (Warburton, 1998; Table 4.1).

Table 4.1 Some of the observed climate characteristics in Moor House (NY 757 328, 556 m) (After Warburton, 1998).

Environmental Variables	Value	Note
Annual mean max ^{0}C	8.3	1953-1978
Annual mean min ^{0}C	1.9	1953-1978
Frost days per year	81	
Annual ppt. mm	2010	1941-1970
Precipitation days	247	1956-1979
Daily total max. mm	104.6	January 1977
Snow fall days	61	1953-1978
Fog days	52	Visibility <1 km at 0.900h

In general, the climatic, topography and vegetational factors of the area combine to produce very high runoff. Upland rivers have flashy flow regimes when compared to lowland rivers. This is due to the steeps slopes, high precipitation, impermeable geology and soils and also high drainage densities in upland catchments. In general, the annual cycle follows a typical pattern with higher runoff during the winter months, while lower flows occur in summer months. Figure 4.3 shows rainfall and runoff during the period of October 1994 - October 1999 for the Trout Beck catchment and indicates a highly efficient catchment with very high rainfall : runoff ratios. A main characteristic of Pennine rivers is their flashy nature and the importance of snowmelt in generating runoff (Archer, 1989, 1992). High runoff is generated by connective storms heavy rainfall and / or rapid snowmelt events.

4.4 VEGETATION AND SOILS

The flora and vegetation of upper Teesdale and Moor House are probably more widely known than that of any other area in Britain. The typical present-day mantle of vegetation is made up of ling heather (*Calluna vulgaris*), cotton grass (*Eriophorum* spp) and *Sphagnum* moss together with other bog plants. Currently the main land cover types are extensive blanket and valleys bogs (*Sphagnum* moss), heather and cotton grass moors, with dry heath, acid grassland and bracken on the drier slopes. Sub-alpine

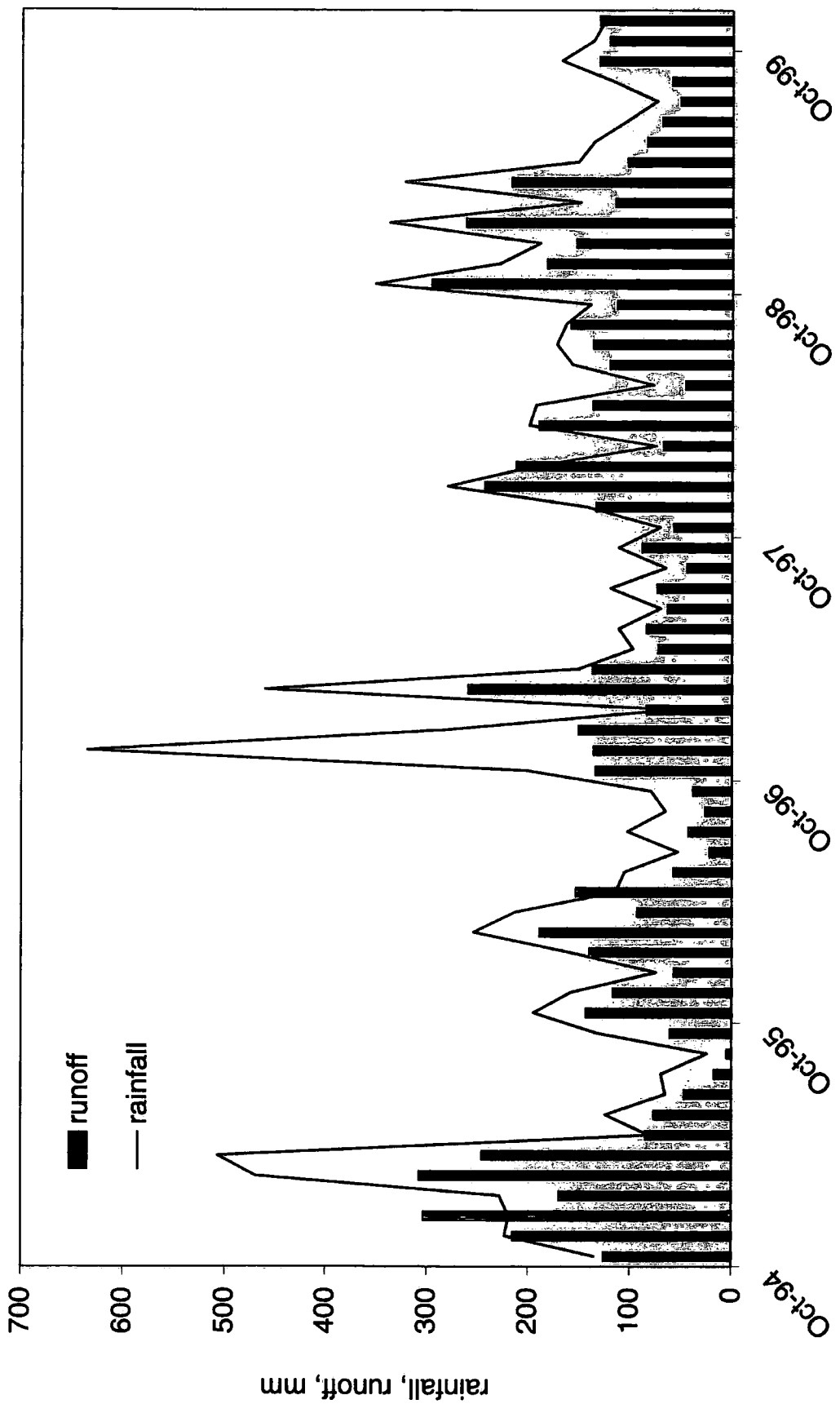

Figure 4.3 Rainfall and runoff during the period of October 1994 - October 1999 in the Trout Beck Catchment.

grasslands occur on the highest summits. Land use is mainly sheep farming with some grouse shooting and beef farming (Warburton, 1998).

During the early and middle Post-glacial (Mesolithic and Neolithic periods) small-scale clearance of the woodland was initiated. Peat started to replace woodland some 3800 years ago in Upper Teesdale. The pace of woodland clearance continued throughout the Bronze Age and Iron Age and by Roman times the majority of the Pennine uplands was probably cleared of forest (Taylor *et al.*, 1971; Pounder, 1989). Climate fluctuations and land-use changes during the Holocene have led to periods of instability.

Mining used to be the main economic activity in the early 19th Century. Although it is difficult to assess fully the effect of mining, it is comparatively easy to see the evidence of such activities in the area. Studies (e.g. Macklin and Rose, 1986; Macklin, 1997) have shown that mining and degradation of the blanket bog by changing land-use practices have had a major influence on the hillslopes, drainage and sediment supply to river systems. The legacy of this period is still very evident in the landscape today. Macklin pointed out that following the last glaciation, Holocene river development has responded to declining sediment supply and isostatic readjustment. Deforestation and metal mining have led to changes in the general trend of alluviation and in places partial valley infilling (Macklin, 1997). Periodic storms cause major changes to upland fluvial environments in terms of both slope and channel sediment systems (Carling, 1986).

Soils of the Pennine uplands are strongly influenced by relief, drainage and parent material. Because of the wet and cool climate, waterlogged soils are widespread and as a result of these the characteristics the peat deposits of the region have formed. Indeed, organic soils, in the form of hill-peat deposits, which strongly influence the hydrology, are dominant in the area. In the past, it was believed that the presence of peat deposits reduces flood intensity and sustains baseflow in streams during periods of low precipitation. However, recent studies have shown that peat is highly productive of runoff and generates little baseflow (Burt *et al.*, 1998). Blanket peat (pH 3.0 to 4.2) is widespread in wet areas (blanket bogs and valley bogs) as are peaty podzols and peaty gley soils (pH 3.5 to 4.5). On better-drained areas and slopes, fell-top podzols and brown earths occur (Johnson and Dunham, 1963). Apart from organic soils, Johnson and Dunham (1963) distinguished six major mineral soil divisions, all derived from carboniferous parent material. These soils are; gleys, podsols, brown earths, red-brown

limestone soils, skeletal soils, soil complexes and solifluxion soil.

4.5 EXPERIMENTAL SITES

The main field experiments were carried out in two coarse gravel-bed streams in the Moor House National Nature Reserve in the Northern Pennines. The experimental sites consisted of two on the River Tees, designated the Lower (NY 762 338), and Upper sites, and one on Trout Beck (NY 759 336) The Trout Beck joins the River Tees between the Upper and Lower Tees sites (Figure 4.4)

These streams were chosen as study sites for six main reasons:

1. Little is known of sediment transport mechanisms in small upland streams. However, upland channels are important, because they constitute a significant part of the total drainage network and are important in erosion and sediment transport processes in upland areas (Klein, 1976). Small headwater streams contribute significant amounts of eroded material to main channels, and are frequently the first parts of the fluvial system to show a response to inadequate land management (Newson 1980; Carling 1983).
2. The analysis of gravel samples, and visual inspection of channel patterns (gravel bedload, high gradients and pool-riffle sequences), suggest that these streams are typical of many other small streams of upland areas.
3. The streams are small enough to allow detailed observations and measurement of the movement of individual bed particles and pebble-sized clasts.
4. The stream channels represent a typical character of wide and shallow upland streams, which become almost dry in the summer months, thus enabling sampling of the surface material. However, flood flows are common.
5. There is no evidence of recent artificial disturbance of bed material.
6. Most of the year there is easy access to the sites (Figure 4.1) and one of the sites (Trout Beck) is gauged by the Environmental Agency.

Table 4.2 shows the main hydrologic and catchment properties of these streams.

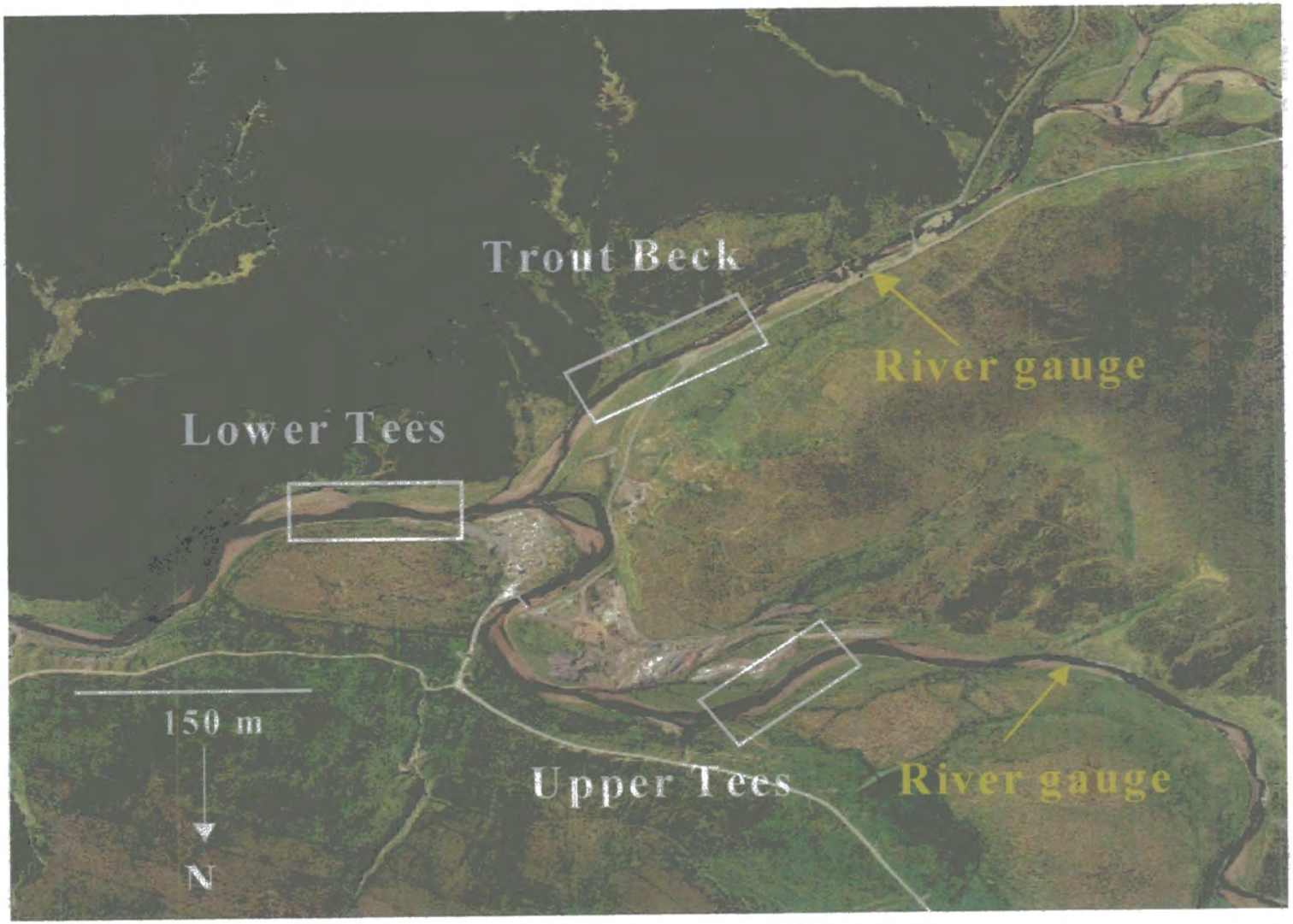

Figure 4.4 A view of the study catchments and the experimental reaches (Reproduced by permission of NERC)

Table 4.2 Main physical characteristics of the study streams.

Name of stream	Catchment area (km^2)	Dominant bedrock lithology	Mean channel width at the experimental sites (m)	Mean channel slope at the experimental sites (m)	Drainage density (km/km^{-2})	Surfacegrain size (mm)	
						(D_{50})	(D_{90})
Trout Beck	11.6	Sandstone limestone Shale	11.30	0.0095	3.57	97.4	181.0
Upper Tees	15.6	Sandstone Limestone	19.40	0.0006	3.15	57.0	99.6
Lower Tees	27.2	Sandstone Limestone	22.10	0.003	3.15	80.7	121.6

4.5.1 Trout Beck

The Trout Beck is a headwater tributary of the River Tees. It drains from the south-west to north-east from the Cross Fell area of the North Pennines (Figure 4.5). The catchment covers an area of 11.6 km^2 and rises to 848m altitude. The Trout Beck catchment lies in Moor House National Nature Reserve, which is managed by English Nature. The south of the catchment is formed by the hills of Dufton Fell (768 m), and Knock Fell (794 m), whilst in the west it is formed by Great Dun Fell (848 m). The northern edge is defined by Milburn Forest and Hard Hill (678 m). The eastern edge runs from the northern slopes of Dufton Fell along the margin of roughsike down to the confluence with the Tees at Trout Beck foot (Figure 4.5).

The Trout Beck catchment is characterized by an upland area dissected by a main valley, which contains a coarse-bed wandering stream. The catchment is about 6 km long and the altitude ranges from 848 m at Great Dun Fell (head of the catchment) to 630 m at the confluence of the River Tees (Figure 4.6). Drainage density is high by British standards and it increases markedly towards the headwater zone, probably due to a combination of high relief, higher rainfall and the impermeability of the rock in the area of superficial till deposits. In addition, the existence of some artificial drainage grips and mining leads also contributes to the higher drainage density. Towards the headwater reach, well-developed gullies have produced particularly high densities. In the lower reaches a large tributary (Moss Burn) joins the main stream from its southern side (Figures 4.5 and 4.6).

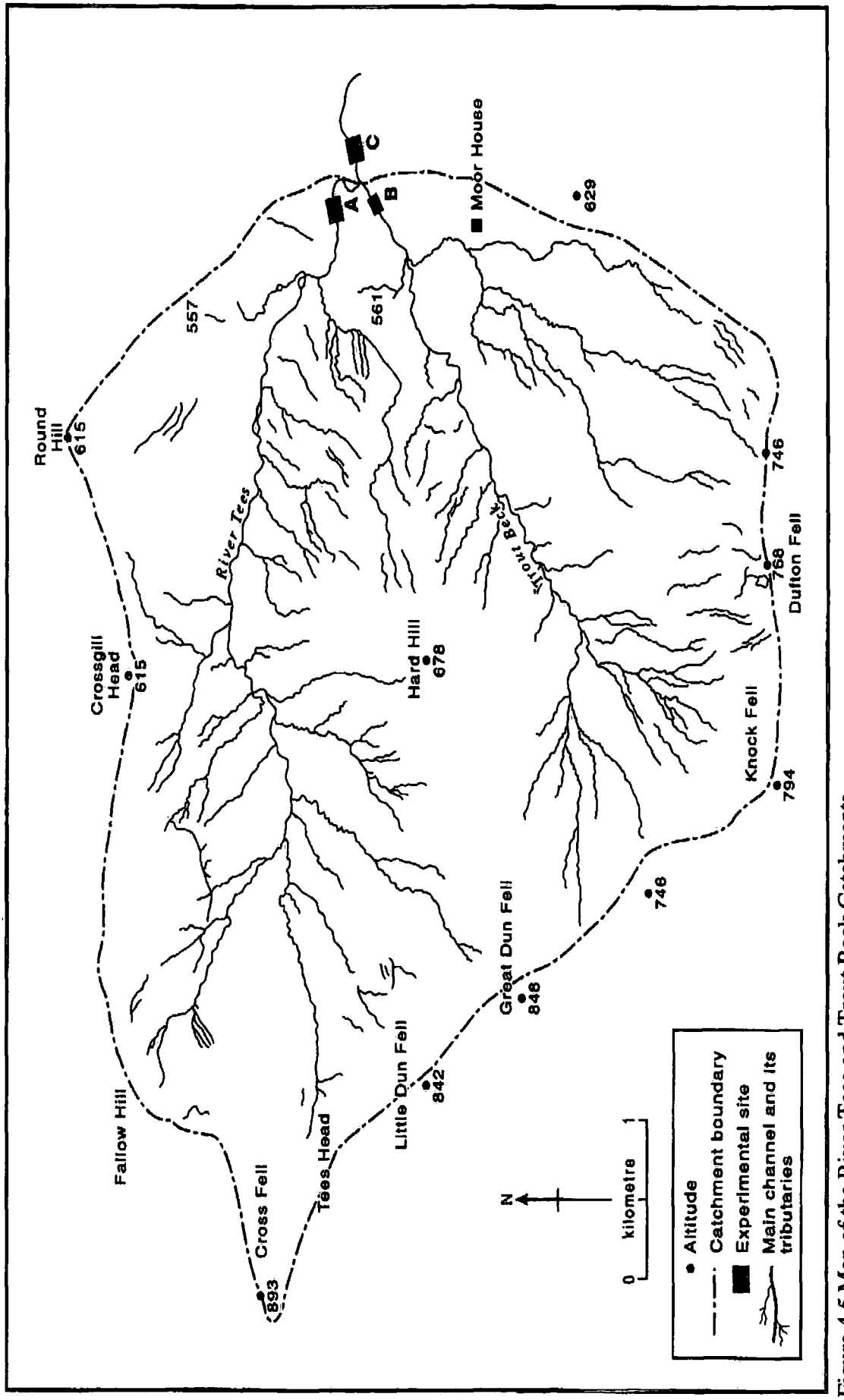

Figure 4.5 Map of the River Tees and Trout Beck Catchments

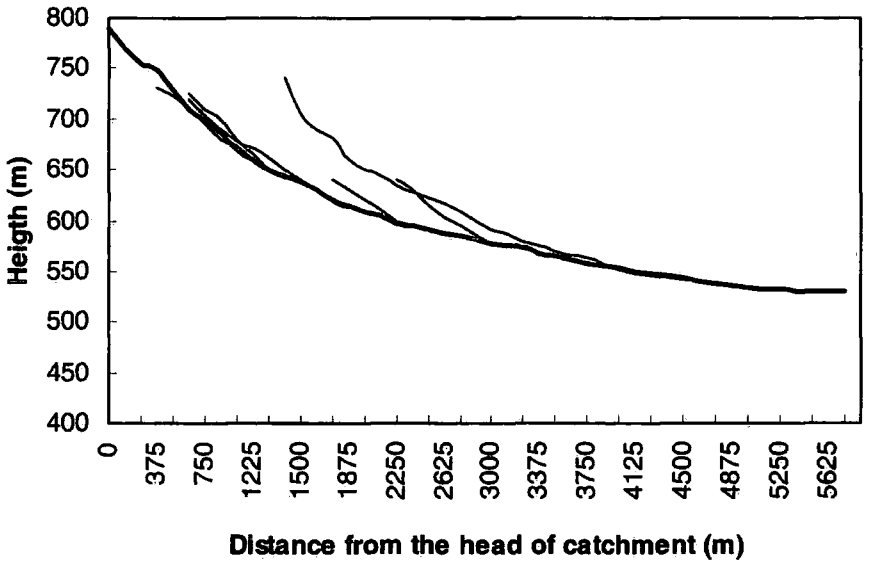

Figure 4.6. Longitudinal profile of the Trout Beck and also its major tributaries (Based on : 1: 25000 Ordnance Survey Map, Outdoor Leisure '31', 1995)

The longitudinal profile of the Trout Beck is concave in shape. (Figure 4.6). The river falls about 200m in its first 2.5 km where the channel is narrow and has steep side slopes. In the lower reaches the channel gradient falls gradually and the channel pattern follows a wandering course. The average channel gradient is 0.0095m at the experimental reach (Figure 4.5).

4.5.2 River Tees

The Tees, which has a total 2400 km^2 catchment area rises in the Cross Fell area but drains to the southeast through Cow Green reservoir out onto the Tees lowland where it diverts east then northeast to join the sea south of Hartlepool.

Two reaches of the Tees were chosen as the experimental sites. One approximately 100 metres below the confluence with Trout Beck and the other approximately 400 upstream of the confluence. The catchment area of the River Tees is 15.6 km^2 (from the upper Tees experimental reach) and it drains Cross Fell, Great Dun Fell, Hard Hill and Knock Fell. The catchment is 7.5 km long and altitude ranges from 893 m at Cross Fell to 630 m at the confluence with Trout Beck (Figure 4.7). The north the catchment is formed by Round Hill (685 m), and Crossgill Head (615 m). In the west it is bounded by Cross Fell (893m), in the south by Little Dun Fell (842 m), Great

Dun Fell (848 m) and Hard Hill (678 m). The eastern boundary runs by the summit of Round Hill (686 m) and the south western slopes of Belbaver Rigg (Figure 4.5). The longitudinal profile of the River Tees is a concave shape. The river falls about 150 m in its first 1.5 km where the channel is narrow and has steep side slopes, and then its gradient decreases slowly (Figure 4.7). The channel pattern contains many bends, separated by straight sections which seldom exceed 200 m in length. The average channel gradient at the experimental sites is very low (0.0006m at the Upper Tees and 0.003m at the Lower Tees). Drainage density of the catchment is high by British standards (3.15 km km^{-2}) and it increases markedly towards the headwater zone, due to high relief, higher rainfall and impermeability of the lithology. On the right bank many tributaries join the channel and the intensity of gullies increase towards the headwater zone (Figure 4.5). In the study reach the river bed material consists of sandstone pebbles and cobbles forming a framework, the interstices of which are filled by a matrix of finer sediments. The overall pattern is of a wandering, coarse-bed stream.

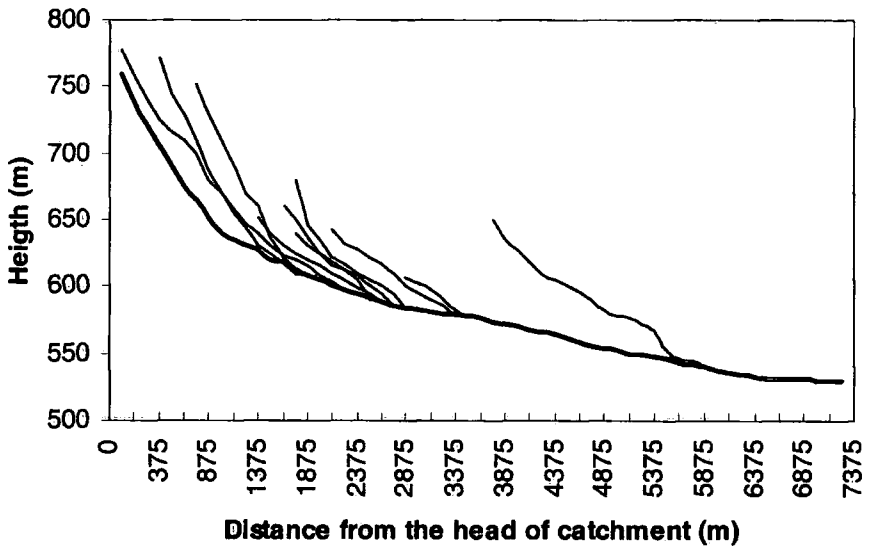

Figure 4.7 Longitudinal profile of the Upper Tees and also its major tributaries (Based on : 1: 25000 Ordnance Survey Map, Outdoor Leisure '31', 1995).

4.6 MAIN PHYSICAL CHARACTERISTICS OF THE STUDY REACHES

The analysis of gravel samples, and visual comparison of channel characteristics (gravel bedload, high gradients in the upstream reaches, wide and shallow channel shapes and crudely developed pool-riffle sequences) suggest that the two study streams are typical of many other small streams of upland areas in the U.K. Comparison of Trout Beck and the Tees shows similar concave longitudinal profiles with average gradients between 0.04 and 0.03 (Table 4.2 and Figures 4.6 and 4.7). Drainage densities are generally high by British standards and vary between 3.15-km km^{-2} for the River Tees and 3.57 km km^{-2} for Trout Beck (Figure 4.5). Sampled bed material in the study reaches consists mainly of sandstone (95 %) and smaller quantities of shale and limestone (5 %).

4.6.1 Channel shape

The velocity of a stream is primarily influenced by cross-sectional form, channel roughness and gradient. In other words, the bedload transport efficiency of a channel depends, in part, on the distribution of shear stress and velocity, both of which vary with channel shape and bed roughness. Several studies have shown that there is a link between channel shape and its transport capability (Hooke, 1995; Park, 1995; Lane and Richards, 1995; Jong and Ergenzinger, 1995). For example, in narrow, deep channels the velocity gradient is highest close to the edges. Thus in such a channel there will be a higher rate of shear near the banks than on the bed. On the other hand, a wide, shallow channel has a higher velocity gradient and a greater rate of shear near the bed than the channel sides, which aids entrainment and transport of bedload (Morisawa, 1968; Pitty, 1971; Gregory, 1977, 1979a and 1979b; Ferguson, 1981).

Measured cross-sections at each site show a wide-shallow channel form which is typical of many upland streams. Figures 4.8, 4.9 and 4.10). The increasing rank of the mean channel widths is 10.3 m, 19.4 m and 22.1 at the Trout Beck, Upper Tees and Lower Tees sites respectively. Lower standard deviation values for the channel widths at Trout Beck (1.33) and Upper Tees (2.00) indicate that the Trout Beck and Upper Tees reaches have a very uniform cross-section changes downstream, while Lower Tees exhibits a relatively wide variation (8.39) (Table 4.3). As significant indicators of channel efficiencies, the lower width-depth ratio and also greater hydraulic radius at

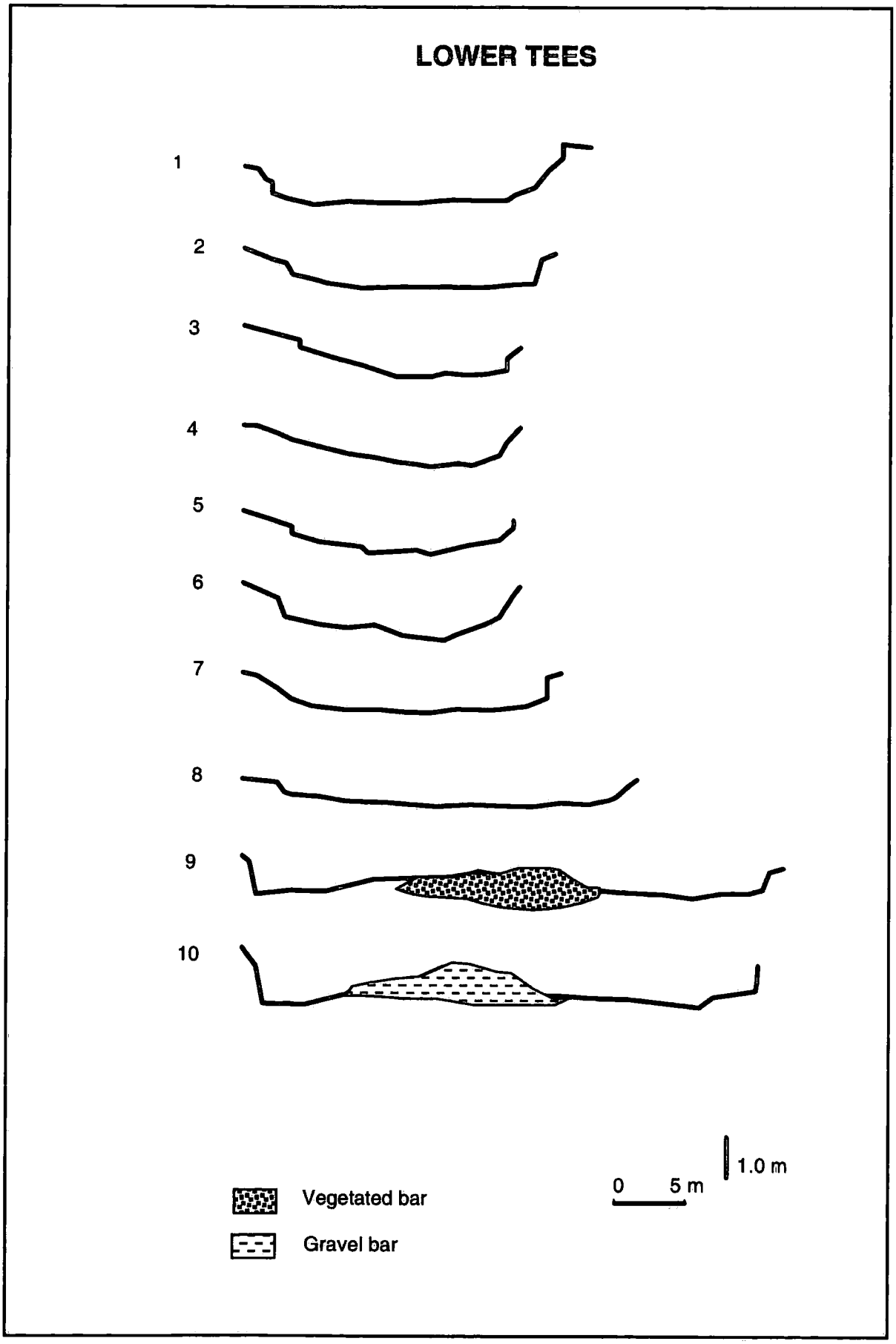

Figure 4.8 Downstream changes in cross-section profiles of the Lower Tees site in August 1998.

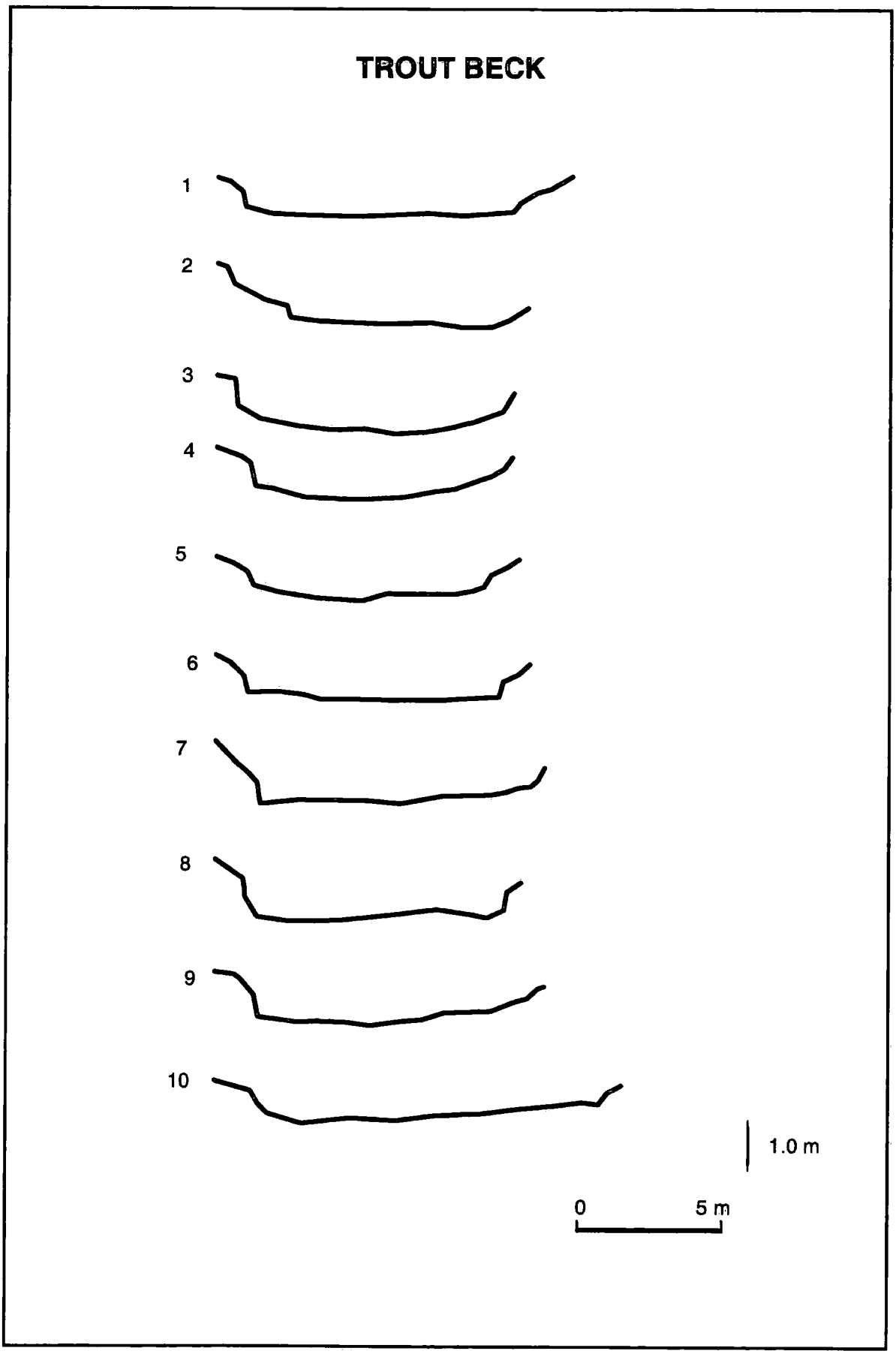

Figure 4.9 Downstream changes in cross-section profiles of Trout Beck, in August 1998.

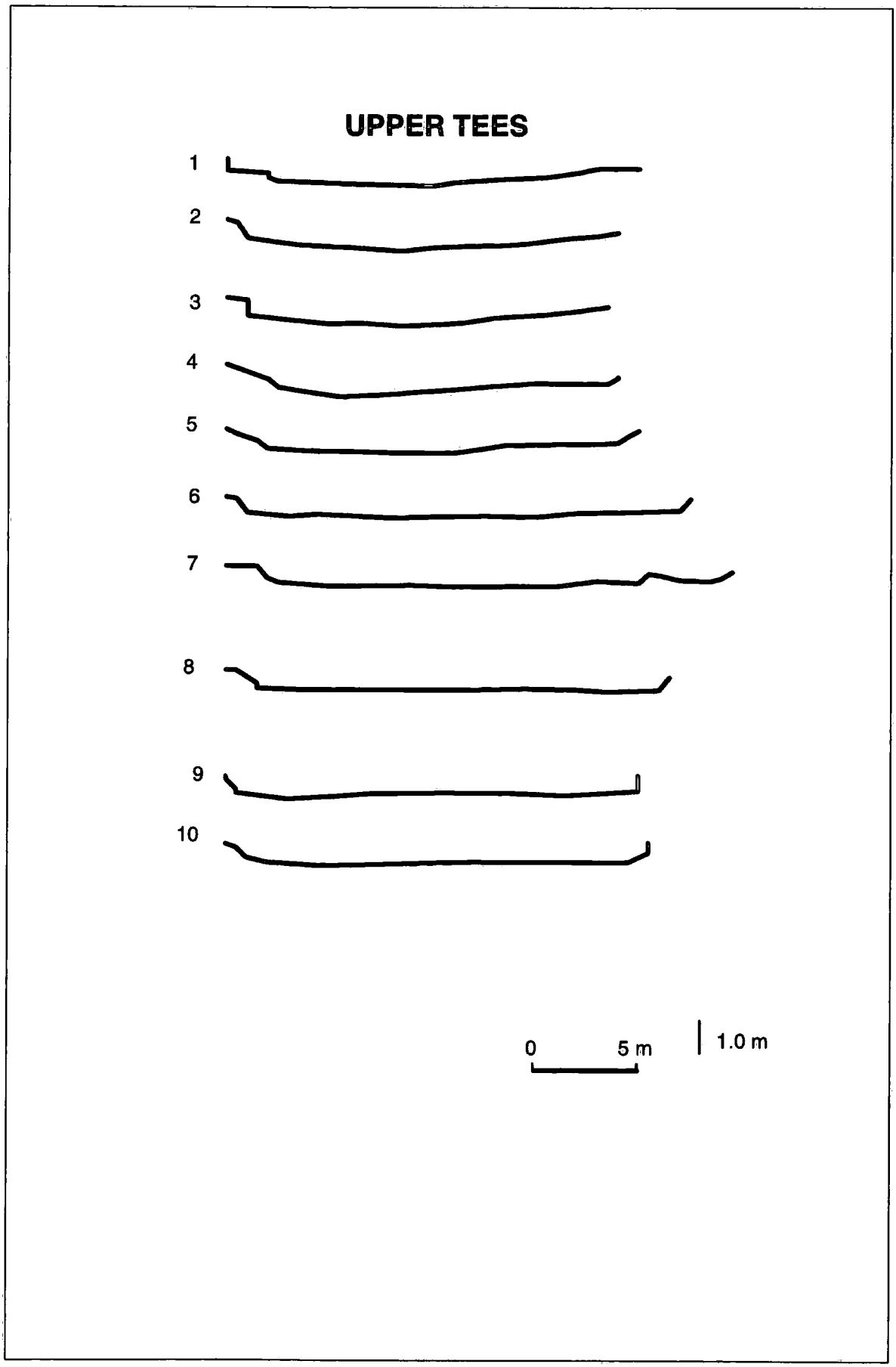

Figure 4.10 Downstream changes in cross-section profiles of Upper Tees, in August 1998.

Table 4.3 Bankfull stream-channel geometry of Lower Tees, Trout Beck and Upper Tees

Upper Tees

Cross sections	Width (m)	Depth (m)	Wetted perimeter (m)	Cross-section area (m^2)	Hydraulic radius	Width-depth ratio	Max depth (m)
1	17	0.25	17	4.3	0.25	68.0	0.76
2	18.5	0.22	14	4.1	0.29	84.1	0.82
3	17.5	0.23	10	4.0	0.40	76.1	0.75
4	17	0.17	16	2.9	0.18	100.0	0.51
5	18	0.22	17	4.0	0.23	81.8	0.4
6	22	0.40	21	8.8	0.42	55.0	0.57
7	22.5	0.39	21.5	8.8	0.41	57.7	0.58
8	21	0.43	19.5	9.0	0.46	48.8	0.59
9	20	0.34	19.5	6.8	0.35	58.8	0.59
10	20	0.37	20	7.4	0.37	54.1	0.53
Mean	**19.4**	**0.30**	**17.6**	**6.0**	**0.34**	**68.4**	**0.61**
Standard Deviation	**2.0**	**0.09**	**3.6**	**2.4**	**0.09**	**16.5**	**0.13**

Lower Tees

Cross sections	Width (m)	Depth (m)	Wetted perimeter (m)	Cross-section area (m^2)	Hydraulic radius	Width-depth ratio	Max depth (m)
1	21.0	0.35	21.0	7.4	0.35	60.0	0.53
2	18.5	0.41	18.0	7.6	0.42	45.1	0.59
3	15.0	0.58	15.0	8.7	0.58	25.9	0.86
4	16.5	0.5	15.5	8.3	0.53	33.0	0.78
5	16.0	0.73	16.0	11.7	0.73	21.9	1.03
6	17.0	0.56	15.5	9.5	0.61	30.4	0.99
7	18.5	0.34	18.5	6.3	0.34	54.4	0.57
8	23.5	0.39	21.5	9.2	0.43	60.3	0.58
9	37.5	0.49	36.5	18.4	0.50	76.5	0.86
10	37.0	0.40	35.0	14.8	0.42	92.5	1.2
Mean	**22.1**	**0.48**	**21.3**	**10.2**	**0.49**	**50.0**	**0.80**
Standard Deviation	**8.39**	**0.12**	**7.98**	**3.77**	**0.12**	**23.11**	**0.23**

Trout Beck

Cross sections	Width (m)	Depth (m)	Wetted perimeter (m)	Cross-section area (m^2)	Hydraulic radius	Width-depth ratio	Max depth (m)
1	12.2	0.46	9.8	5.6	0.57	26.5	0.79
2	10.8	0.82	9.8	8.8	0.90	13.1	1.23
3	10.0	0.79	9.5	7.9	0.83	12.6	1.12
4	9.1	0.45	8.4	4.1	0.48	20.1	0.76
5	8.7	0.36	8.2	3.1	0.38	24.2	0.61
6	9.3	0.35	9.0	3.2	0.36	26.4	0.51
7	10.3	0.2	9.9	2.1	0.21	51.3	0.43
8	9.4	0.59	9.3	5.5	0.60	15.9	0.88
9	10.6	0.64	9.7	6.8	0.70	16.6	0.97
10	12.7	0.39	11.8	5.0	0.42	32.6	0.66
Mean	**10.3**	**0.51**	**9.5**	**5.2**	**0.55**	**23.9**	**0.8**
Standard Deviation	**1.33**	**0.20**	**1.00**	**2.17**	**0.22**	**11.61**	**0.26**

Trout Beck indicate greater stream competence to transport its channel load if other factors are held equal for the three experimental reaches. In other words, greater wetted perimeters, and width-depth ratios and also smaller hydraulic radius values at the Upper and Lower Tees sites may (if discharge is held constant) lead to a decrease of the availability of the streams energy to transport its bedload when compared to Trout Beck (Table 4.3). Indeed comparison of the parameter as shown in Table 4.3 indicates that river channels at the experimental sites of Upper and Lower Tees exhibit relatively shallower channel form, which results in greater friction and a reduced velocity (Figures 4.8 and 4.10). Whereas, the Trout Beck site tends to have a smaller amount of water in its cross-section contact with wetted perimeter, which creates less friction, and allows greater velocity.

At the Trout Beck site almost all cross-sections have greater deeps than the other sites. The increasing order of mean depth is 0.30, 0.48 and 0.51 m for Upper Tees, Lower Tees and Trout Beck. All sites do not show regular downstream changes in depth.

4.6.2 Bed material roughness

Many investigators have shown that surface roughness in gravel-bed channels is one of the important factors controlling bedload transport (Laronne and Carson, 1976; Hassan and Reid, 1990). Indeed, apart from other factors and processes (e.g. size and shape of individual particles, bed armouring, flow characteristics, etc.) the entrainment of individual particles depends also on their relative exposure to the current which is largely controlled by size and shape of the riverbed roughness elements. Thus the character of bed roughness must be examined in order to better understand the mechanisms of bedload transport.

Bed material roughness was measured at five cross-sections in each of the three experimental reaches using a pin frame. Examples of sites where bed material roughness was measured are shown in Figures 4.11, 4.12, and 4.13. Detail of the measurement techniques is also explained in Chapter 3. In terms of downstream changes of the roughness patterns, the Lower and Upper Tees sites have similar bed material roughness, while the Trout Beck has slightly rougher channel bed elements (Figures 4.14, 4.15, 4.16 and Table 4.4). On the other hand there is no regular variation in terms of transverse patterns of roughness distributions between the three sites.

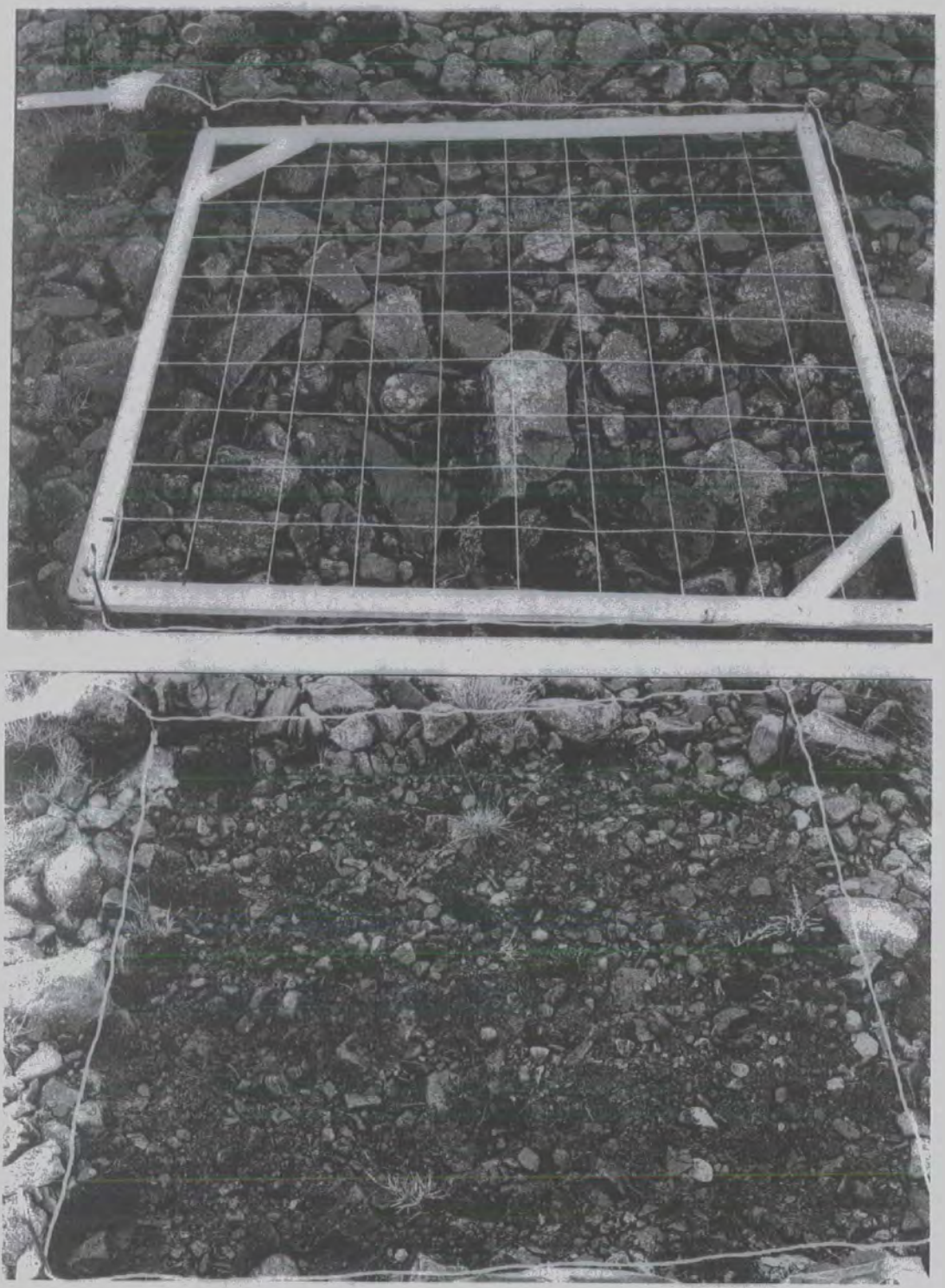

Figure 4.11 Cross-section 10 where bed roughness measurement, surface (above), and sub-surface (below) bed material sampling was carried out at the Lower Tees (Looking downstream).

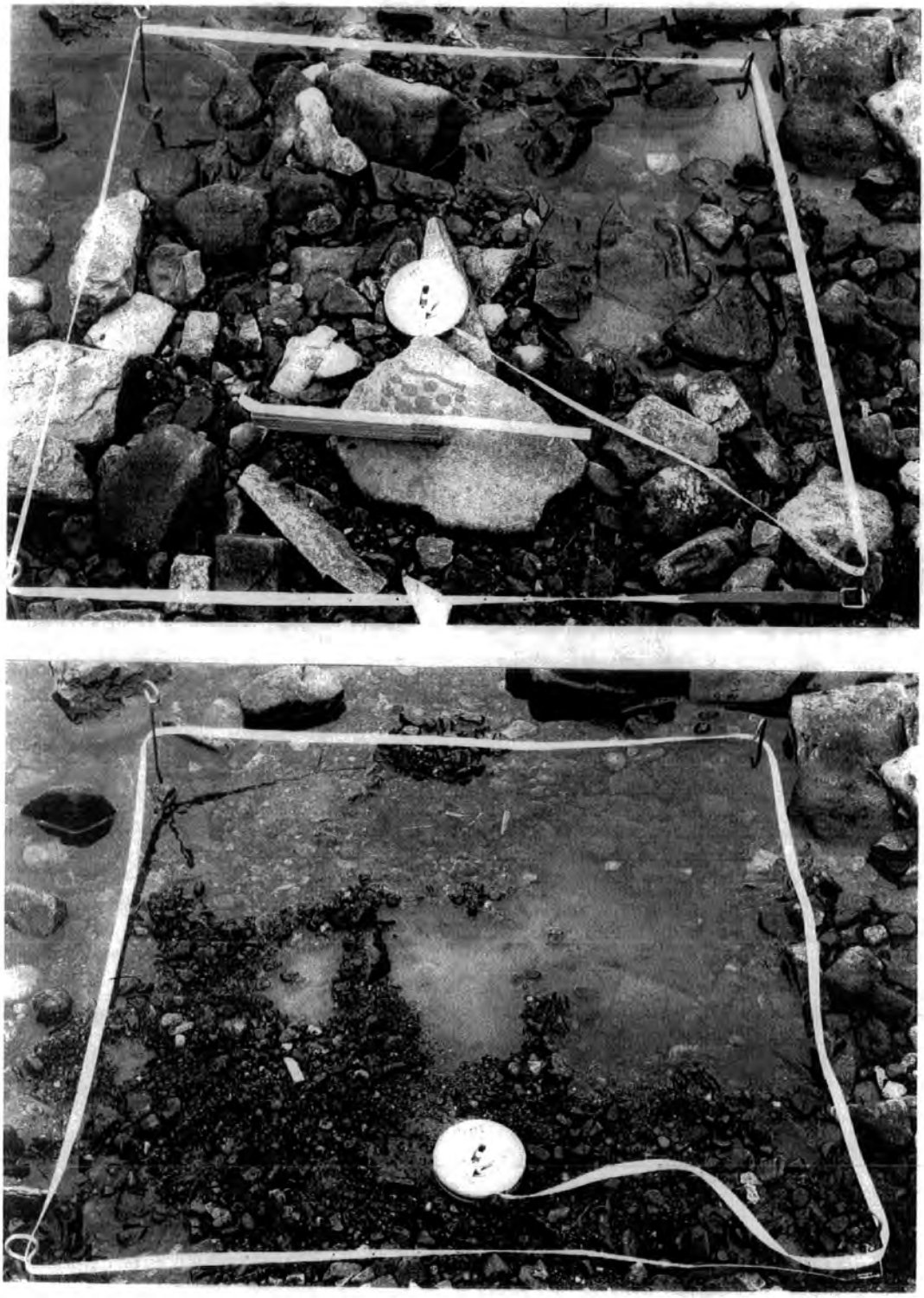

Figure 4.12 Cross-section 3 where bed roughness measurement, surface (above), and sub-surface (below) bed material sampling was carried out at the Trout Beck (Looking downstream).

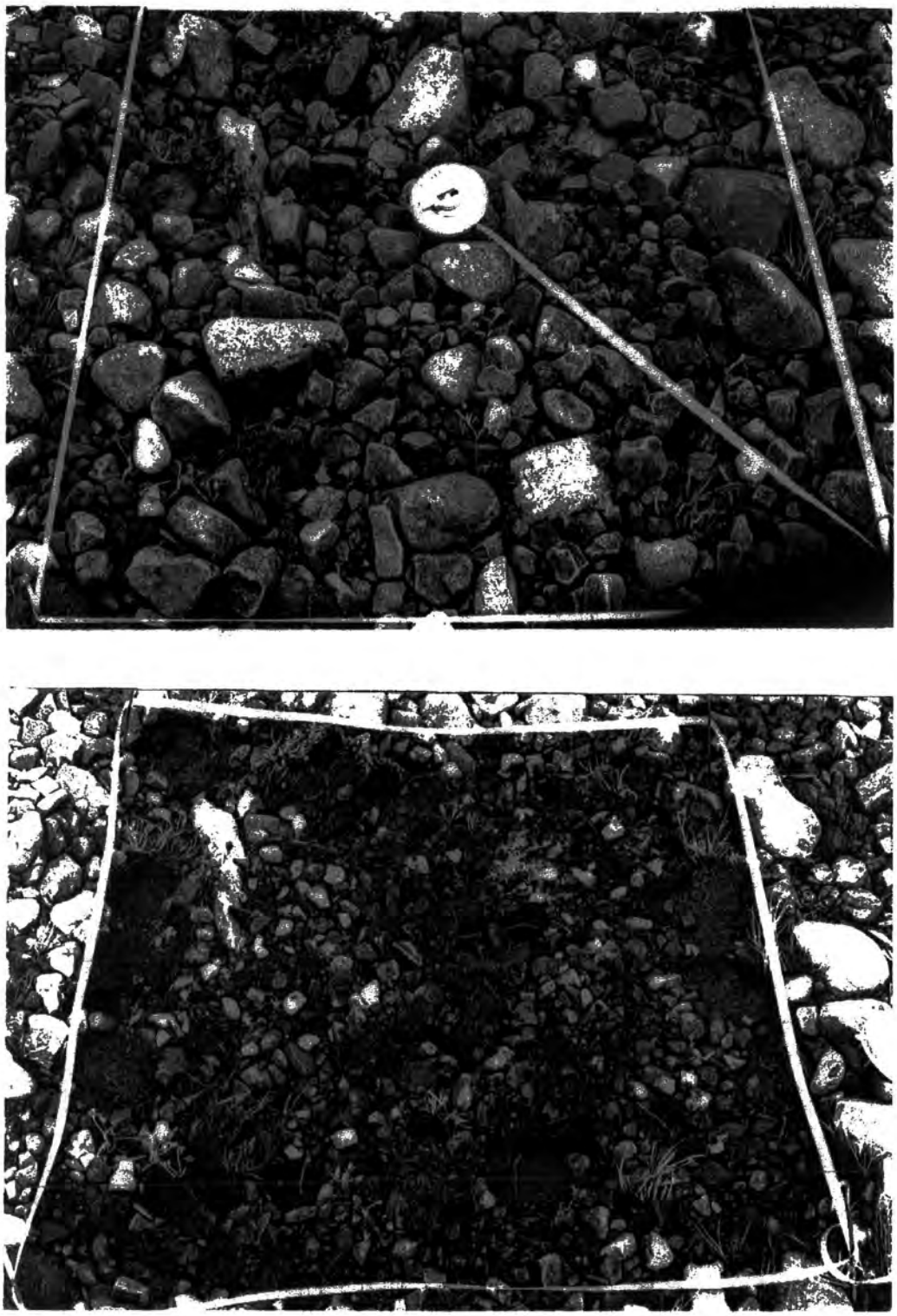

Figure 4.13 Cross-section 7 where bed roughness measurement, surface (above), and sub-surface (below) bed material sampling was carried out at the Upper Tees (Looking downstream).

LOWER TEES

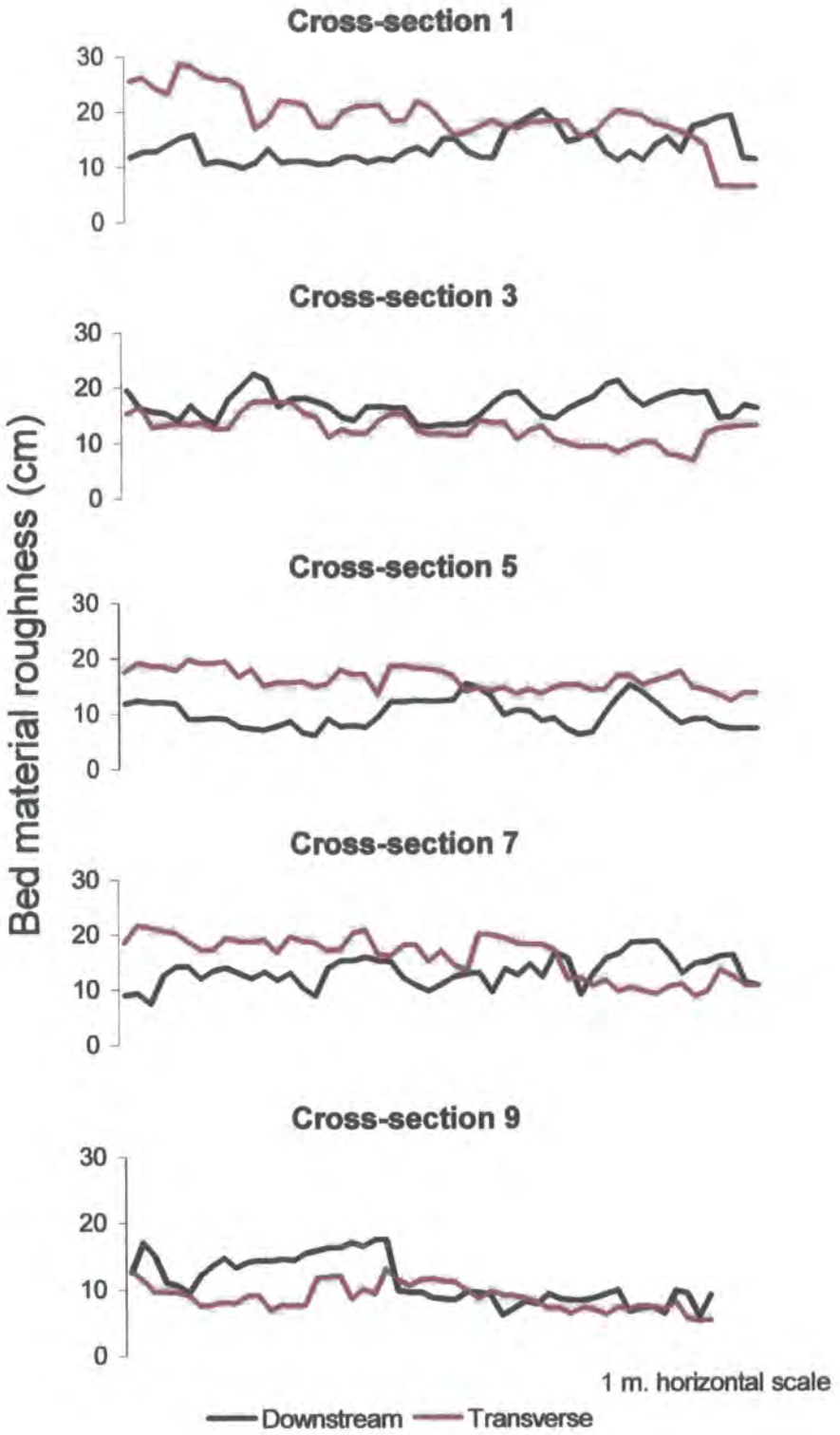

Figure 4.14 Downstream changes of bed material roughness at the Lower Tees site.

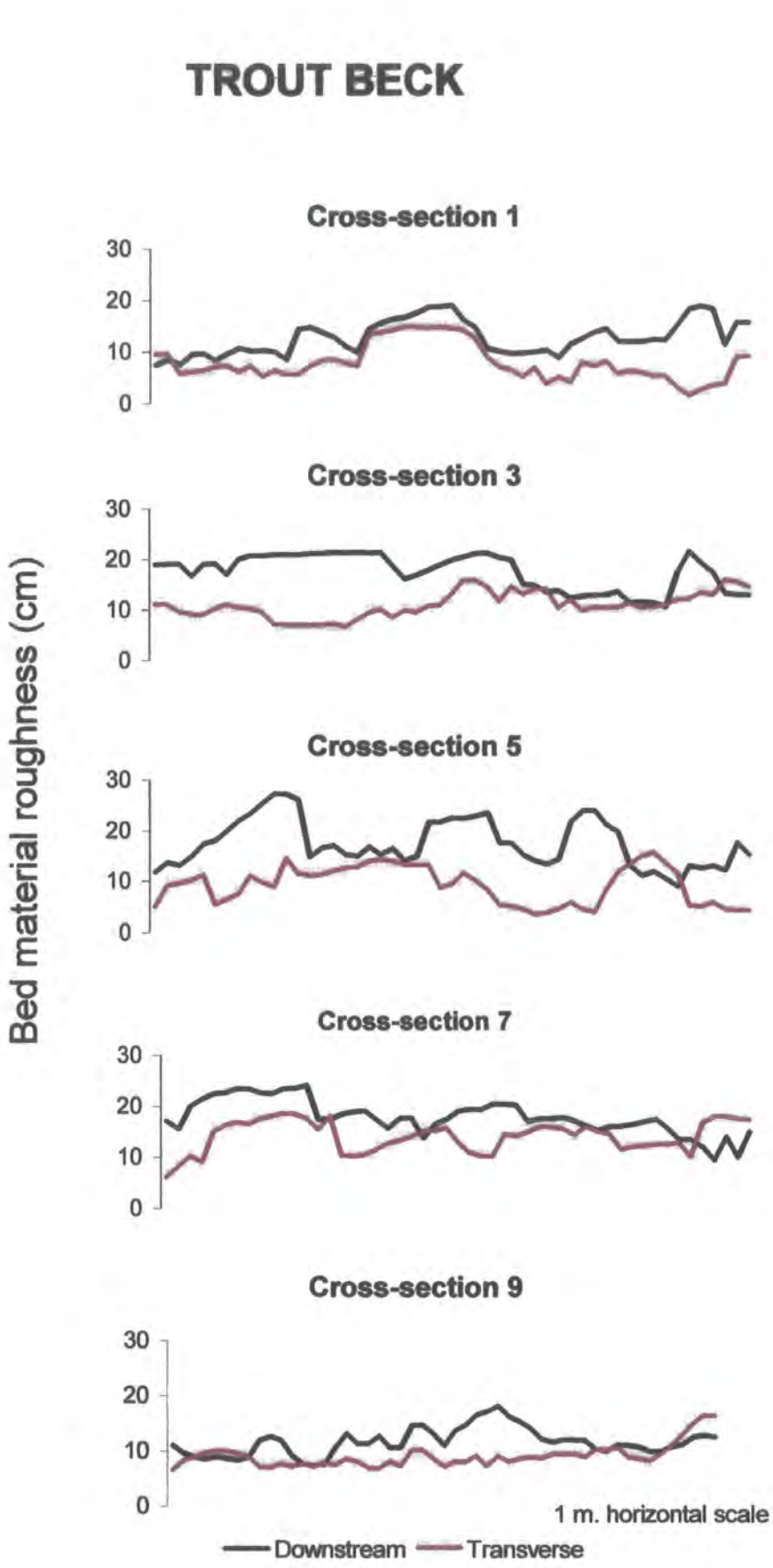

Figure 4.15 Downstream changes of bed material roughness at the Trout Beck site.

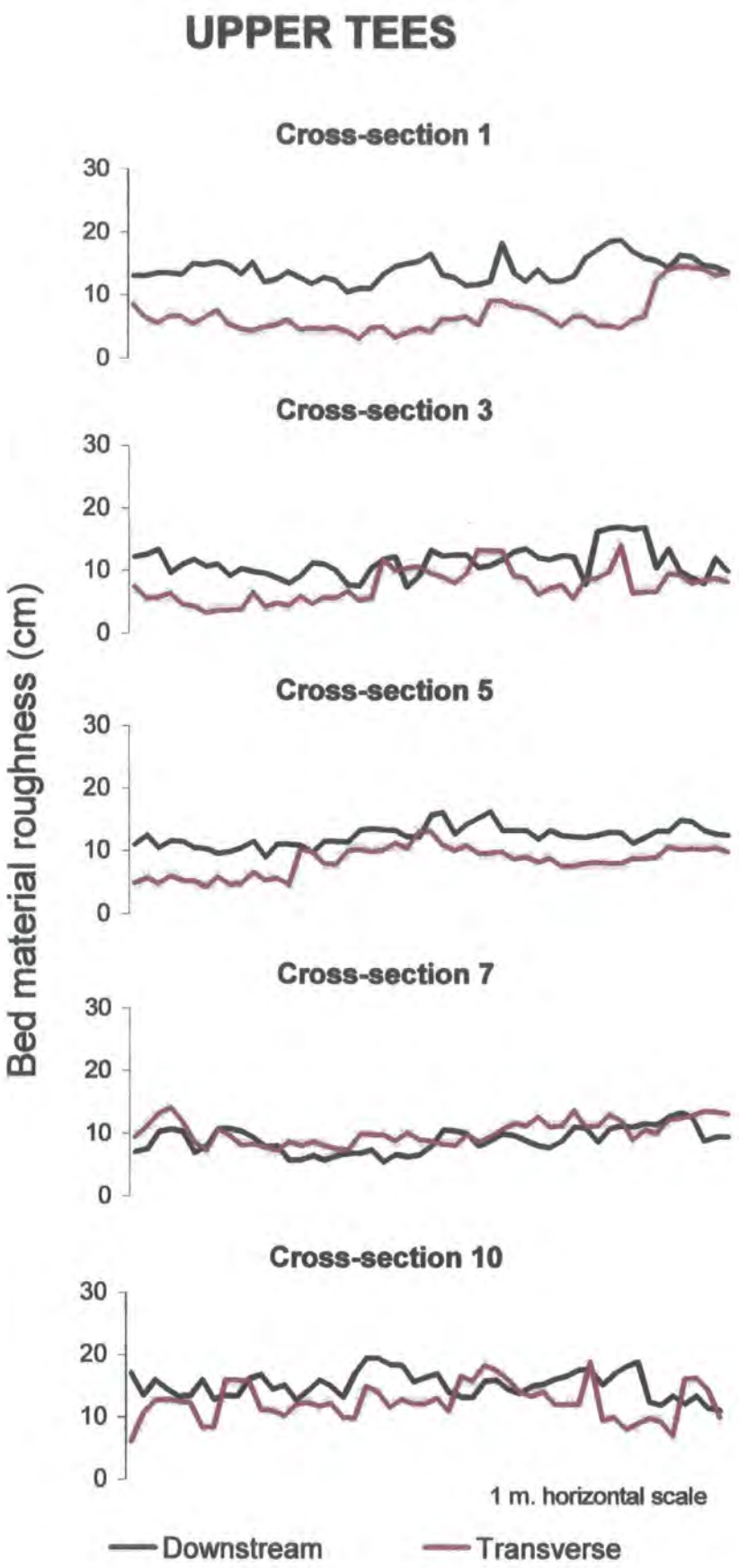

Figure 4.16 Downsream changes of bed roughness at the Upper Tees site.

Statistical comparison of the three sites also implies a statistically significant difference between the patterns of roughness distribution of bed material in the downstream direction, while there are no similar patterns of roughnesses distributions transverse to the channel. The calculated values of F (for an Anova Single test) is 8.77 for downstream patterns, which is greater than critical values (3.88) at the 0.005 of the chosen significance level, while it is only 0.48 for transverse roughness pattern with the same critical value of F. Mean standard deviations, both transverse and downstream directions, vary between 18.2-22.4 mm at the Upper Tees site, and 30.5-26.4 mm at the Trout Beck site.

Among the three sites, in the downstream direction Upper Tees shows the lowest bed roughness patterns (hence low standard deviations) at almost every cross-section, but a similar pattern is not true for the transverse direction (Table 4.4). Table 4.5 shows the mean bed material size (D_{50} and D_{90}) and mean standard deviation values of both transverse and downstream patterns of roughness distributions for the three experimental sites and indicates that there tends to be a positive relation between downstream pattern of bed roughness (hence high standard deviation) and D_{50}, and even more noticeably, D_{90}. There is no similar relation for the transverse patterns of bed roughness and D_{50} and D_{90}.

Table 4.4 Standard deviations of the elevation of bed roughness (mm) in downstream and transverse directions at Lower Tees, Trout Beck and Upper Tees.

	Lower Tees		**Trout Beck**		**Upper Tees**	
Cross-section	Down-stream	Trans-verse	Down-stream	Trans-verse	Down-stream	Trans-verse
1	20.8	50.2	30.4	30.6	20.0	30.1
3	20.3	20.7	30.5	20.6	20.4	20.7
5	20.5	20.0	40.7	30.7	10.6	20.3
7	20.6	40.0	30.4	30.1	20.0	20.0
9	30.5	20.0	20.5	20.2	20.1	20.9
Mean	**22.5**	**30.2**	**30.5**	**26.4**	**18.2**	**22.4**

Tables 4.5 Relationship between bed material size (D_{50} and D_{90}) and standard deviations of the elevation of bed roughness in downstream and transverse directions at the three experimental reaches.

	Downstream		Transverse	
	D_{50} (mm)		D_{90} (mm)	
	Size	St. Dev.	Size	St. Dev.
Lower Tees	80.7	20.8	121.6	30.2
Trout Beck	97.7	30.5	181.0	30.0
Upper Tees	57.0	20.0	99.6	20.6

4.6.3 Bed material size

Surface and fine sub-surface sediment were sampled and analyzed at five locations for each of the three experimental sites in order to measure downstream changes in surface and sub-surface bed material size (Figure 4.11, 4.12 and 4.13). The Wolman (1954) bulk sampling procedure, outlined in Chapter 3, was used. Sampled surface bed material was classified into seven size categories and both cumulative frequency distributions as well as D_{50} and D_{90} were determined for each sample together with overall mean values for each reach.

Figure 4.17 shows particle size frequency distributions of surface and sub-surface bed material (in weight) for five samples at the three experimental reaches. Figure 4.18 shows the cumulative percentage of surface bed material particle size distributions for the same sites. Figures 4.17 and 4.18 indicate that, overall, the three sites have similar percentage weight of surface and sub-surface bed material size distribution patterns. In fact all cross-sections demonstrate the most typical features of a gravel river bed which is a relatively coarse surface cover in comparison with the gravel/sand mixture beneath (Church *et al*, 1987). This greater percentage of coarse size bed material in the surface material and abundance of finer in the subsurface material at almost each experimental site may indicate the existence of a typical bed armouring structure developed by coarse material (Figures, 4.11, 4.12, 4.13, and Figure 4.17). Indeed, Figure 4.17 indicates that the greater percentage of surface bed material (in weight) is coarser than the 45.3-64 mm size range and the majority is distributed with the 64 to 181 mm size range, while for the sub-surface material the greater percentage of the particles is distributed below the 45.5-64 mm size range. On the other hand, frequency distributions of the number of particles

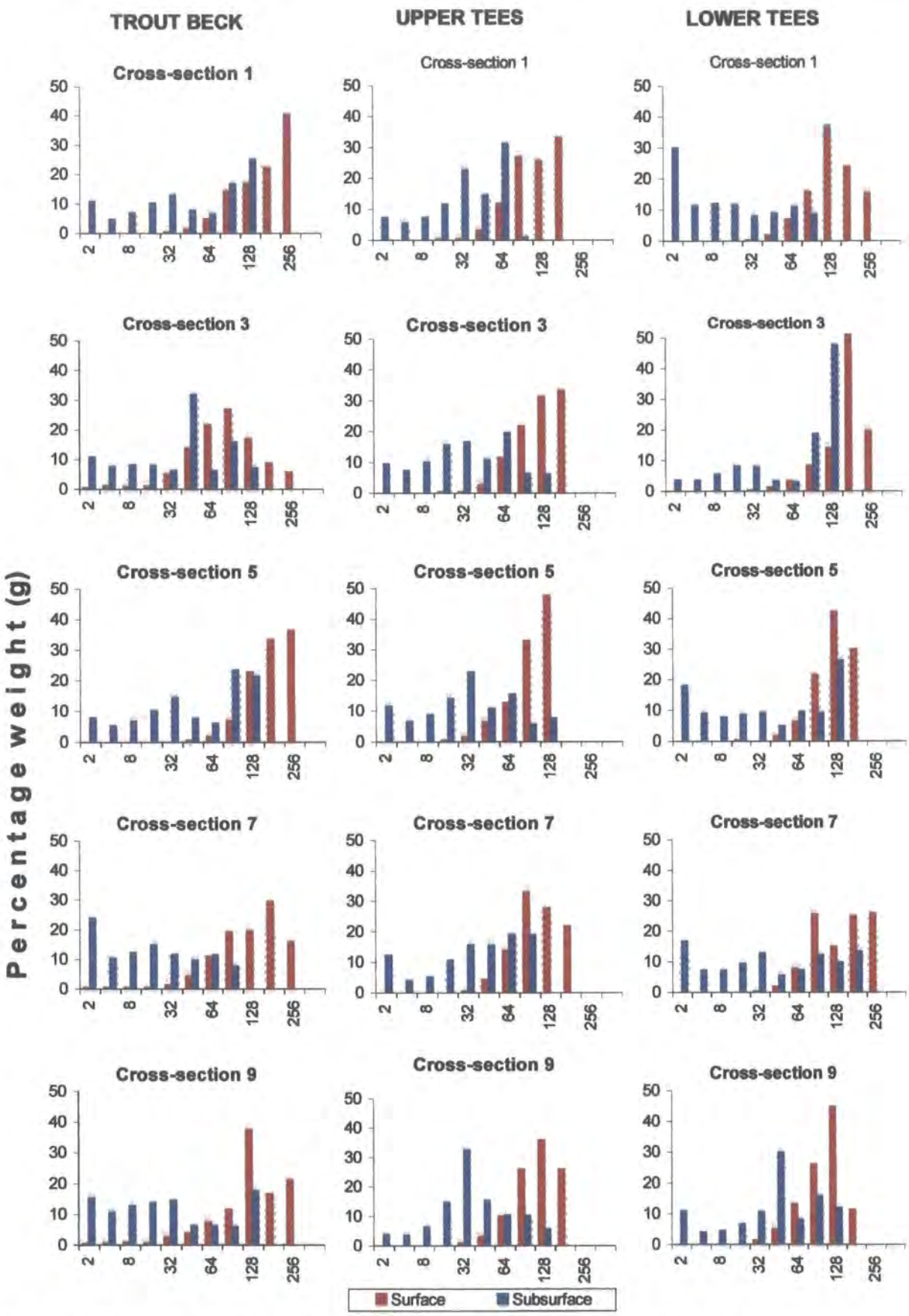

Figure 4.17 Size distributions of surface and sub-surface bed material for five samples at the three experimental sites on the River Tees and Trout Beck (size indicated: upper limit of category; e.g. 32 indicates 16-32 mm class).

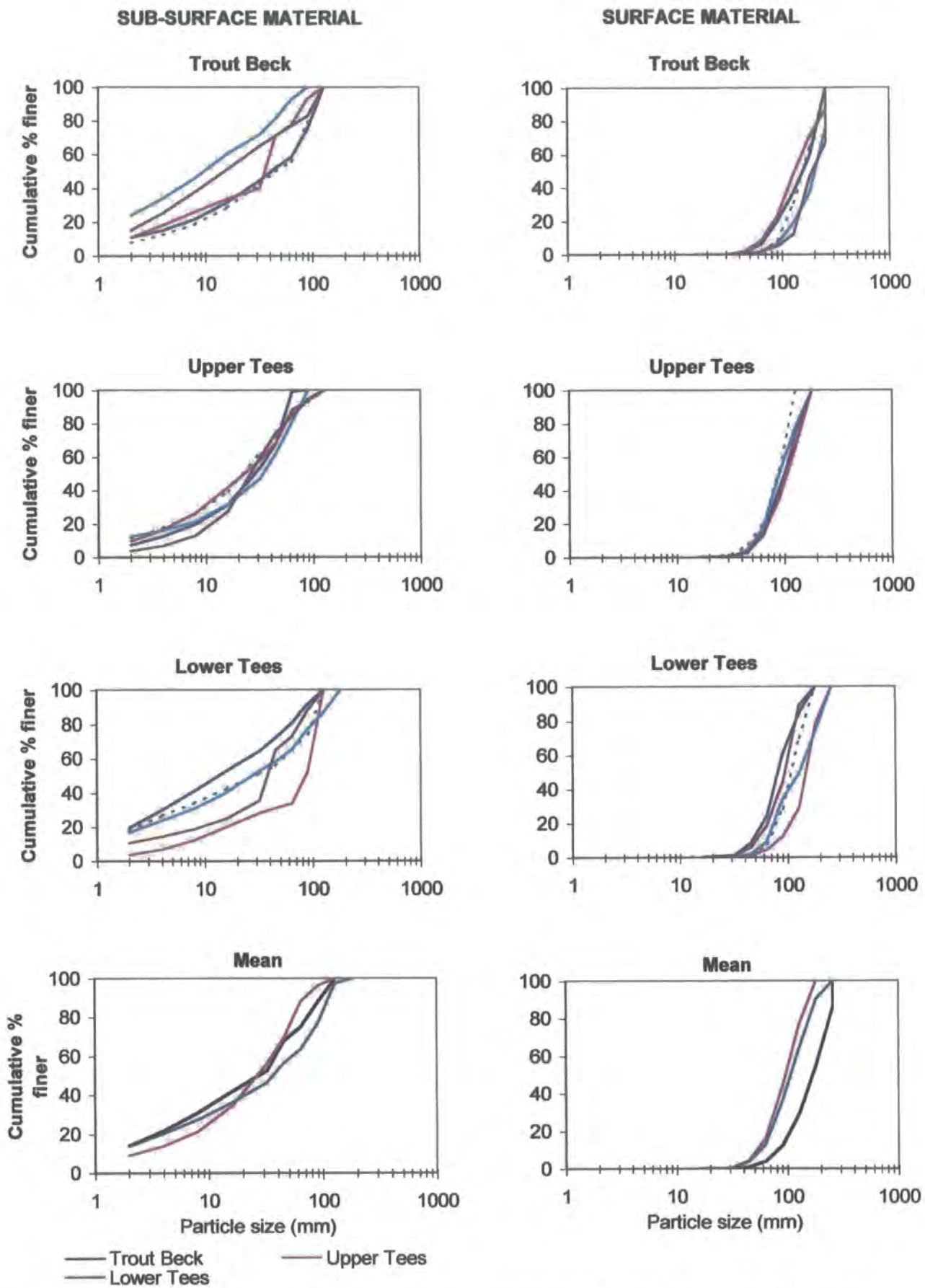

Figure 4.18 Cumulative percentage of particle size distributions for surface and sub-surface bed material at the three experimental sites. Note: Five lines in the upper 6 graphs show five sites (cross-sections) for each site.

of surface bed material are different than that of distributed in weight. Figure 4.19 shows that the number of particles increases noticeably between 45.3 and 90.5 mm for almost each cross-section at the three experimental reaches and the frequencies tend to decrease above and below this size range. It also shows that, except two crossections at the Upper Tees site, at each experimental reach the greatest number of particles is distributed between 45.3 and 64 mm.

Table 4.6 shows the results of the particle size analysis of the bed material at the three experimental reaches and indicates that there is no consistent difference between the cross-sections at each site. However, comparison of the three sites indicates that sampled surface bed material size in the Trout Beck reach is greater than at the other sites. There is a lack of coarse size material >181 mm size at the Upper and also the Lower Tees sites, while it was recorded in many crossections of the Trout Beck. The decreasing order of particle size (both D_{50} and D_{90}) is Trout Beck (57.0 and 181.0), Lower Tees (80.7 and 121.6) and Upper Tees (57.0 and 99.6) respectively (Table 4.6). Figures 4.17 and Figure 4.18 show that in the Trout Beck, there is a wide range of size distribution of surface bed material, which indicates a slightly poorer sorted bed material. This probably reflects inputs of freshly eroded bedrock from the local channel perimeter.

Table 4.6. Downstream changes in particle size distributions of the surface bed material sampled in three experimental reaches (Cs. indicates the cross-sections where bed material was sampled).

	Cs. 1		Cs. 3		Cs. 5		Cs. 7		Cs. 9		Mean	
	D_{50}	D_{90}	D_{50}	D_{90}	D_{50}	D_{90}	D_{50}	D_{90}	D_{50}	D_{90}	D_{50}	D_{90}
Upper Tees	58	110	60	110	53	80	54	98	60	100	57.0	99.6
Lower Tees	70	120	95	140	69	110	60	150	55	88	80.7	121.6
Trout Beck	78	165	70	160	94	160	125	200	120	220	97.4	181.0

In terms of sub-surface bed material size, Figures 4.17 and 4.18 indicate that sub-surface bed material at almost every experimental site tends to have a relatively wide size range and also even distributions in comparison with surface material. Much of the sub-surface bed material is distributed below 90.5 mm size. Table 4.7 shows that

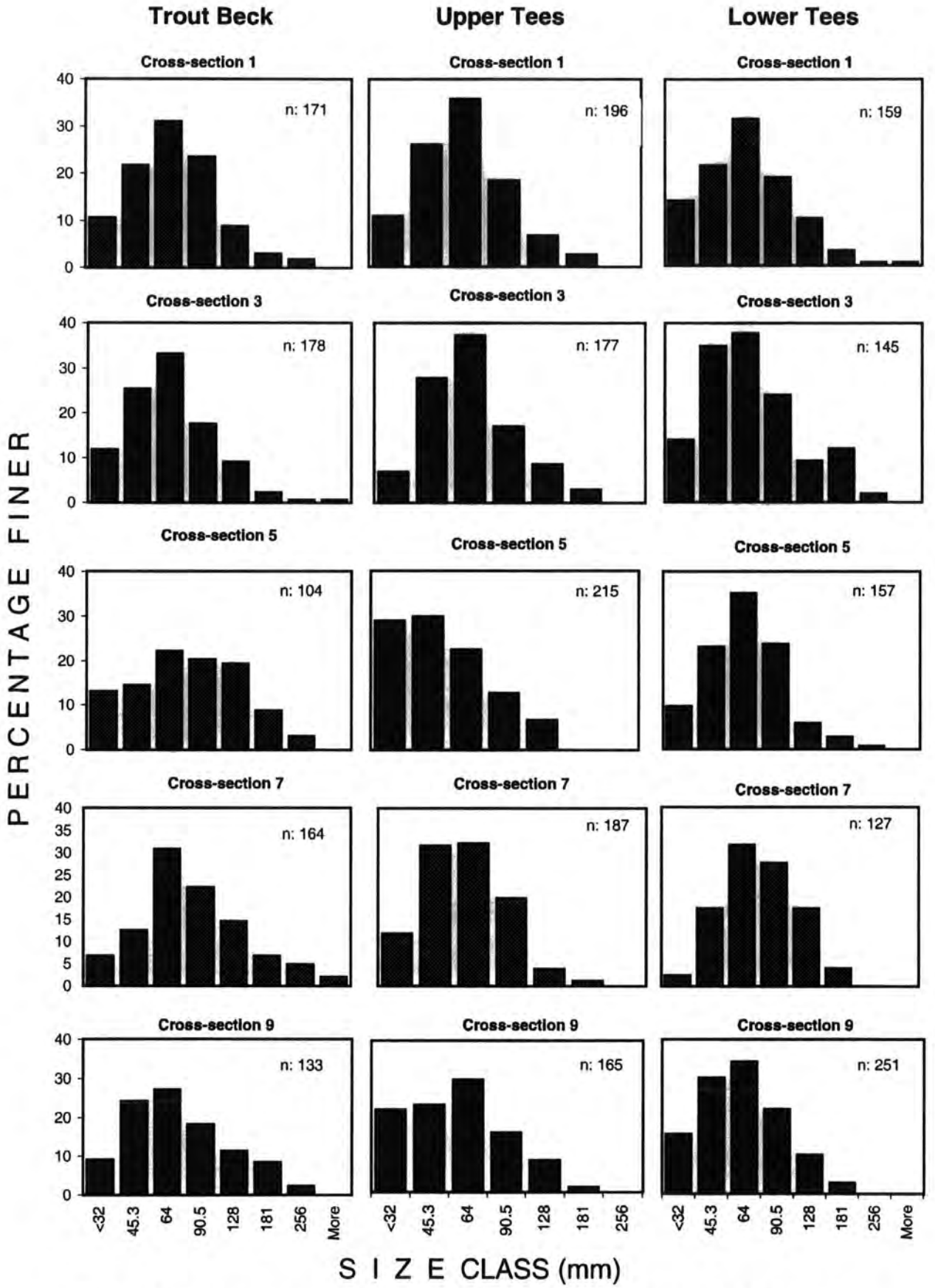

Figure 4.19 Size distributions of surface-bed material for five samples at the three experimental sites on the River Tees and Trout Beck. (size indicated = upper limit of category; e.g. 64 indicates 45.3-64 mm class)

D_{50} varies between 14 and 88 mm at the Lower Tees site, 10 and 48 mm at the Trout Beck site and 23-43 mm at the Upper Tees site. Despite considerable variation in D_{50} between the cross-sections at each site, D_{90} shows relatively small ranges (Table 4.7). At the Lower Tees site D_{90} varies between 80 and 95 mm, at Trout Beck 45-115 and at the Upper Tees site 52-78 mm. However, Mean D_{50} varies between 28 at the Upper Tees /Trout Beck and 38 mm at the Lower Tees sites, while mean D_{90} varies between 68 mm (Upper Tees) and 120 (Lower Tees). Figure 4.17 also show that at each site there is a noticeably sharp increase in the percentage weight of particles > 32 mm, while other size ranges have lower percentages.

Table 4.7 Downstream changes in particle size distributions of the sub-surface bed material sampled in three experimental reaches (Cs. indicates the cross-sections where bed material was sampled).

	Cs. 1		Cs. 3		Cs. 5		Cs. 7		Cs. 9		Mean	
	D50	D90	D50	D90	D50	D90	D50	D90	D50	D90	D50	D90
Lower Tees	14	90	88	90	28	80	28	88	38	95	38	120
Trout Beck	41	115	28	82	48	115	10	45	17	100	28	110
Upper Tees	28	58	23	72	23	72	43	78	27	52	28	68

4.6.4 Bed material shape

The main lithology of the two catchments is well-bedded (flaggy) sandstone, which results in a dominance of platy, discoidal particles. Figures 4.20, 4.21and Table 4.8 clearly show that the natural bed material (>32 mm size group) at each of the experimental sites tends to show a greater number of disc-shaped particles, reflecting the sedimentary nature of many of the local lithologies. The decreasing order of frequency for shapes, overall, is disc, sphere, rod and blade (Table 4.8). Figure 4.21 also shows that, in the natural particles, there are greater number of particles close to the shape boundaries. This contrasts with the magnetic tracers where there are very distinct gaps between the shape boundaries. Details of the methods of determination of particle shape (form, roundness, sphericity, and flatness) are explained in Chapter 3.

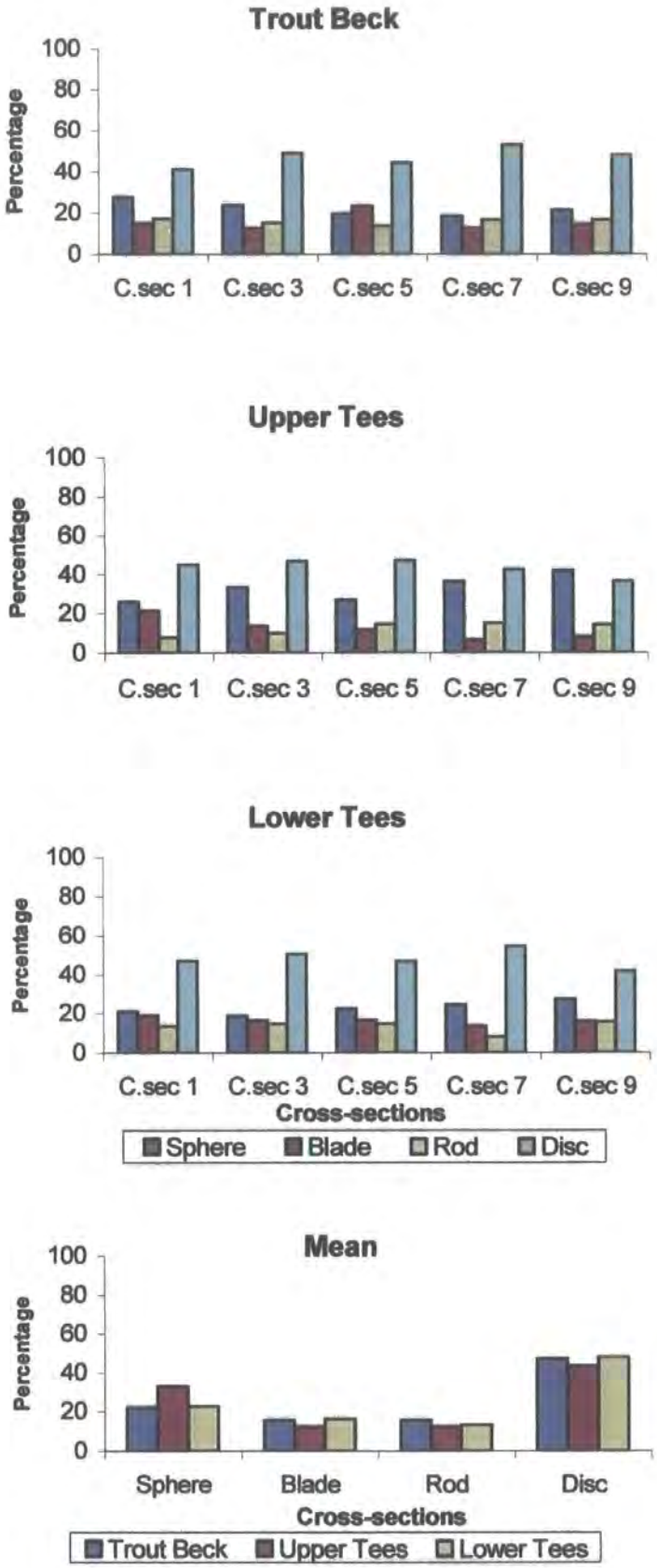

Figure 4.20 Percentage of sampled bed material shape distributions at the three experimental sites.

Table 4.8 Percentage bed material shapes in the surface bed material of >32 mm size at the three experimental sites

	Lower Tees	Trout Beck	Upper Tees
Total sample	940	690	838
	%	%	%
Sphere	32.2	22.6	23.2
Blade	12.2	14.9	16.3
Rod	12.8	15.8	13.6
Disc	43.4	46.7	46.9

Table 4.9 gives details of the percentage of spheres, blades, rods and discs of >32 mm size group at the five cross-sections along each of the experimental sites. Figure 4.21 shows the percentage of the four shape classes for each of the sites and indicates that, overall; the three sites have very similar shape distributions. Discs are the most common shapes in each cross-section at each site. Disc frequencies at most of the cross-sections (except Cross-section 9 at Upper Tees) exceed 40 % of the total particles (Table 4.8). The frequencies of discs are 41-47 %, 41-53 % and 36-47 % for the Lower Tees, Trout Beck and the Upper Tees sites respectively. After discs, spheres are the second most frequent shape: 19-27 % (Lower Tees), 18-27 % (Trout Beck) and 26-42 % (Upper Tees). Both blades and rods are of lower frequency but very similar in proportion at almost every cross-section along the reaches (Figure 4.21).

Table 4.9 Mean particle roundness, sphericity, flatness and weight for the three experimental sites. (S: sphere, B: blade, R: rod, D: disc, M: mean)

	Upper Tees					**Lower Tees**					**Trout Beck**				
	S	B	R	D	M	S	B	R	D	M	S	B	R	D	M
Round-ness	260	163	183	212	**243**	238	106	147	204	**211**	196	115	145	188	**191**
Spheri-city	0.79	0.59	0.66	0.68	**0.71**	0.81	0.53	0.65	0.68	**0.68**	0.78	0.55	0.63	0.68	**0.67**
Flat ness	194	292	170	254	**203**	148	267	173	267	**232**	150	317	176	276	**234**
Weight (g)	258	254	216	238	**241**	452	356	379	419	**401**	747	628	494	546	**604**

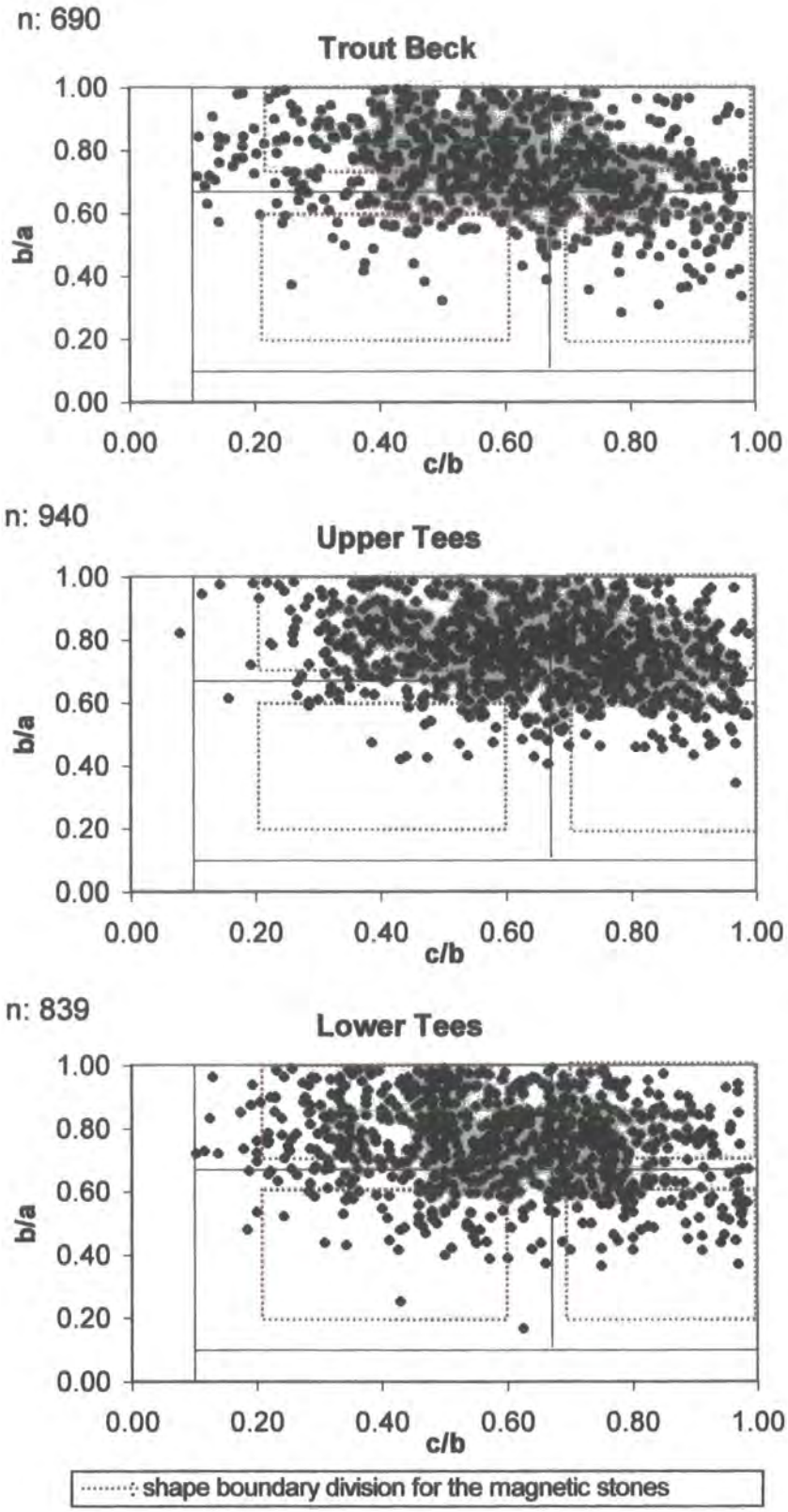

Figure 4.21 Classification of particle shape of sampled bed material at the three experimental sites (based on Zingg 1935).
Note: The frames with red dashes show the shape boundaries of the magnetic stones.

Table 4.9 shows the mean roundness, sphericity and flatness of the sampled bed material at the three experimental sites for the four shape classes and all particles collectively. It indicates that mean roundness of the four shape classes at theUpper Tees site tends to be greater than at the other sites. The decreasing order of mean roundness is 205, 174 and 161 at the Upper Tees, Lower Tees and Trout Beck sites respectively. At the Upper Tees site, particles in each shape class have greater mean roundness values than at the other sites. Statistical comparisons show that there is significant differences in mean roundness of spheres, blade and disc-shaped particles between the three sites, while there is no significant difference between the rods from the three sites (Table 4.10). In terms of sphericity and flatness distributions, Table 4.10 shows that there is no statistically significant differences between mean sphericity of the sphere-shaped particles between the three sites, although differences are significant for blade, rod and disc-shaped particles. In terms of their mean flatness, sphere and rod-shaped particles show no significant difference between the three sites, while differences are significant for blade and discs.

Table 4.9 indicates that despite a similarity in bed material mean weights between the Upper and Lower Tees, bed material at the Trout Beck site tends to be much heavier than at the other sites in almost each shape group. Table 4.10 also indicates that there are some statistical differences between the three sites for the distributions of all shapes, but the extent of differences increases for sphere and disc shaped particles. The increasing order of rank is rod, blade, sphere and disc.

Table 4.10 Statistical comparison (F – test) of the three sites in terms of natural bed material roundness, sphericity, flatness and weight. (The critical value of F at the 0.05 level for roundness, sphericity, flatness and weight is 3.01).

	Roundness	Sphericity	Flatness	Weight
Sphere	**6.31**	1.70	1.13	**12.41**
Blade	**11.89**	**5.68**	**4.08**	**7.34**
Rod	2.39	**4.41**	1.99	**4.46**
Disc	**15.38**	**3.06**	**4.76**	**14.21**

Comparison of natural bed material sampled at the three sites and the magnetic tracers used for the experiments shows that there are some differences in mean roundness, sphericity, flatness and weight of particles. At almost every experimental site and within each shape group (except small sized blade-shaped bed material at the Upper Tees site, and medium sized rods at the Lower Tees site, which have slightly greater mean roundness values) the magnetic tracers have greater mean roundness than that of natural bed material and the differences become almost double in both sphere and disc-shape particles (Tables 4.11, 4.12 and 4.13). At each site, the differences between the mean roundness of natural bed material and the magnetic tracers for each of the size groups in sphere and disc-shaped particles are greater than for the other shapes. These differences also tend to increase from the Lower Tees to the Upper Tees and the Trout Beck sites respectively. For the rod and blade-shaped particles, however, the differences in roundness diminish noticeably both in the small and medium size groups and also in the mean of the three sized groups.

For sphericity and flatness, sphere-shaped magnetic tracers have greater sphericity and hence lower flatness values than the natural bed material for all three size groups. Higher sphericity and roundness of sphere-shaped magnetic tracers may promote greater rolling capability than the natural bed material. The lower sphericity and higher flatness values of the blade and disc-shaped magnetic particles also indicates that they have a relatively flatter and more discoidal shape than the natural particles (Tables 4.11, 4.12 and 4.13). These flat particles may then be less prone to rolling than natural material.

In terms of weight, Tables 4.11, 4.12 and 4.13 show that there are smaller differences between the mean weight of natural bed material sampled and the magnetic tracers in the small and medium size groups and there is also a lack of larger size particles in natural bed material at the three sites. Overall, in magnetic tracers there tends to be an increase in mean particle weight as compared with the natural bed material within all shape classes and in small and medium size groups at all the sites. For example, at the Upper and Lower Tees sites, differences between the mean weights of magnetic tracers and bed material are less in disc-shaped particles in the small and medium size groups, while the greatest values are in rod-shaped class. The increasing order of difference between the mean weight of magnetic tracers and natural bed material is disc, blade, sphere and rod for the small and medium size group, whereas in the large size, it is disc, sphere, rod and blade respectively. However, a similar

distribution is not true for the Trout Beck (Table 4.13), where the mean weights of natural bed material are greater than the magnetic tracers in the medium and large size groups of the sphere-shaped class, in the medium size of blades and also in the large size of disc-shaped particles. In the small size group, on the other hand, disc, sphere, blade, and rod-shaped magnetic tracers have greater mean weights than that of natural ones and the increasing rank of the differences is disc, sphere, blade, and rod for the small size group. For the Trout Beck, however, in the large size group, spheres and discs in the natural material have greater mean weight than that of magnetic tracers, while the mean weight of blade-shaped magnetic tracers is greater than natural blades. There are not enough rods among the natural particles for comparison to be made for this shape class.

In general, at all the sites rod-shaped particles, in both the magnetic tracers and natural bed material, tend to be heavier than the other sites shape classes. The possible reason is that, despite their similar *b* axes, within each size group, the rod-shaped particles have thicker *c* axes and also the *a* axes of rods tend to be longer than for other shapes.

Despite their similar size range at all the sites, within almost each size group, mean weights of magnetic tracers tend to be greater than that of the natural particles. The possible reason might be attributed to the fact that, within each size range, b axes of the magnetic tracer are slightly greater than that of natural ones. Another reason is that rod and blade-shaped magnetic tracers are of well-defined shape and therefore they have longer a axes, while in the natural particles this is not always the case (see Appendix 1).

Table 4.11 Comparison of mean roundness, sphericity, flatness and weight of bed material and tracer material at Upper Tees. (**: Indicates the amount of particles less than 5 that are not included for the calculation of the mean values).

Upper Tees											
		Sphere					Blade				
		small	medium	large	All			small	medium	large	All
Roundness	Natural	282	238	**	270	Roundness	Natural	199	126	**	176
	Tracer	553	550	435	538		Tracer	173	189	248	188
Sphericity	Natural	0.80	0.79	**	0.79	Sphericity	Natural	0.58	0.57	**	0.57
	Tracer	0.86	0.86	0.85	0.86		Tracer	0.41	0.35	0.3	0.37
Flatness	Natural	145	287	**	146	Flatness	Natural	264	287	**	270
	Tracer	127	128	127	127		Tracer	480	453	359	455
Weight (g)	Natural	118	337	**	258	Weight (g)	Natural	104	326	**	254
	Tracer	215	708	4656	927		Tracer	265	687	4158	885
		Rod					Disc				
		Small	medium	large	All			small	medium	large	All
Roundness	Natural	201	164	**	168	Roundness	Natural	263	243	131	253
	Tracer	212	293	282	256		Tracer	568	478	435	563
Sphericity	Natural	0.66	0.65	**	0.66	Sphericity	Natural	0.70	0.68	0.65	0.69
	Tracer	0.55	0.57	0.61	0.56		Tracer	0.65	0.48	0.62	0.57
Flatness	Natural	167	173	**	168	Flatness	Natural	236	260	264	244
	Tracer	197	197	180	195		Tracer	287	328	338	310
Weight (g)	Natural	152	346	**	216	Weight (g)	Natural	87.1	322	1684	238
	Tracer	402	1773	7175	1764		Tracer	147	418	1734	444

Table 4.12 Comparison of mean roundness, sphericity, flatness and weight of bed material and tracer material at Lower Tees (**: Indicates the amount of particles less than 5 that are not included for the calculation of the mean values).

Lower Tees											
		Sphere						Blade			
		small	medium	large	All			small	medium	large	All
Roundness	Natural	281	215	217	257	Roundness	Natural	153	102	64	133
	Tracer	537	439	468	486		Tracer	238	158	260	205
Sphericity	Natural	0.79	0.82	0.81	0.80	Sphericity	Natural	0.55	0.54	0.51	0.54
	Tracer	0.84	0.85	0.86	0.85		Tracer	0.46	0.36	0.48	0.42
Flatness	Natural	153	144	147	150	Flatness	Natural	292	329	179	310
	Tracer	131	129	132	130		Tracer	396	522	365	449
Weight (g)	Natural	123	791	3059	452	Weight (g)	Natural	112	654	2221	356
	Tracer	207	968	3555	917		Tracer	191	798	3365	813
		Rod						Disc			
		Small	medium	large	All			small	medium	large	All
Roundness	Natural	163	131.2	**	154	Roundness	Natural	258	202	153	202
	Tracer	214	127	279	183		Tracer	554	239	453	403
Sphericity	Natural	0.65	0.64	**	0.65	Sphericity	Natural	0.68	0.67	0.68	0.68
	Tracer	0.55	0.54	0.59	0.55		Tracer	0.66	0.65	0.65	0.65
Flatness	Natural	170	176	**	171	Flatness	Natural	260	269	273	264
	Tracer	198	205	191	200		Tracer	288	313	313	302
Weight (g)	Natural	163	908	**	379	Weight (g)	Natural	91	526	2492	419
	Tracer	387	1275	5522	1352		Tracer	110	669	2007	569

Table 4.13 Comparison of mean roundness, sphericity, flatness and weight of bed material and tracer material at Trout Beck (**: Indicates the amount of particles less than 5 that are not included for the calculation of the mean values).

Trout Beck											
		Sphere						Blade			
		small	medium	large	All			small	medium	large	All
Roundness	Natural	235	200	153	215	Roundness	Natural	148	123	75	132
	Tracer	626	601	465	597		Tracer	211	211	254	216
Sphericity	Natural	0.78	0.79	0.78	0.78	Sphericity	Natural	0.55	0.54	0.56	0.55
	Tracer	0.85	0.85	0.84	0.85		Tracer	0.44	0.46	0.47	0.45
Flatness	Natural	151	153	147	151	Flatness	Natural	299	350	301	320
	Tracer	130	130	131	130		Tracer	441	427	370	427
Weight (g)	Natural	124	780	6162	747	Weight (g)	Natural	117	786	3657	628
	Tracer	209	764	4108	889		Tracer	233	657	3939	833
		Rod						Disc			
		Small	medium	large	All			small	medium	large	All
Roundness	Natural	163	127	**	137	Roundness	Natural	214	188	163	200
	Tracer	252	273	265	263		Tracer	531	481	531	509
Sphericity	Natural	0.63	0.63	**	0.63	Sphericity	Natural	0.67	0.68	0.68	0.68
	Tracer	0.52	0.56	0.60	0.55		Tracer	0.65	0.61	0.63	0.63
Flatness	Natural	175	176	**	176	Flatness	Natural	266	267	294	270
	Tracer	212	195	182	201		Tracer	301	350	334	327
Weight (g)	Natural	194	1342	**	494	Weight (g)	Natural	90	483	3015	546
	Tracer	400	1391	7145	1590		Tracer	140	794	1855	621

CHAPTER 5: MAGNETIC TRACING EXPERIMENTS: RESULTS FROM THE THREE EXPERIMENTAL SITES.

5.1 INTRODUCTION

This chapter presents the results of an experiment designed to investigate the influence of bed material shape on bedload transport in two gravel-bed rivers, (River Tees and Trout Beck). As described in Chapter 3, river flow and bedload movements were monitored from 24 November 1997 to 24 September 1999. This chapter firstly analyses river flow and discharge and relates it to magnetic tracer movement during the fieldwork period (Section 5.2). Section 5.3 presents the results collected from five field surveys. General downstream patterns of tracer movements are discussed in Section 5.4. The influence of shape (sphericity, roundness) and size (a, b, c axes and weight) parameters of the magnetic tracers on transport distance is tested statistically in Section 5.5. Section 5.6 discusses missing and buried tracers at the three experimental sites for the different survey periods and also for the entire period of study. The spatial distribution of magnetic tracers in river channels at the three experimental sites is summarised in section 5.7. Section 5.8 examines the size and shape characteristics of trapped bedload collected in the Trout Beck sediment trap and sampled river bed material and compares these results with the magnetic tracing experiments. Finally, the key points raised by the experiment are discussed and summarised in section 5.9.

5.2 RIVER FLOW DURING THE MONITORING PERIOD

Figures 5.1 shows 15 minute time series estimates for the monitoring period (November 1997 to September 1999) at the Trout Beck, the Upper Tees and Lower Tees sites. As explained in Chapter 3, gauging of the flow at these two sites provides a means of estimating the discharge at the Lower Tees site just below the confluence. The sum of the two upstream discharges provided a reasonable estimate of the discharge at the Lower Tees site (Figure 5.1). In general, for most of the period, mean discharge values for the Upper Tees appear to be greater than Trout Beck due to its larger catchment area (15.6 km^2) when compared with the Trout Beck (11.4 km^2).

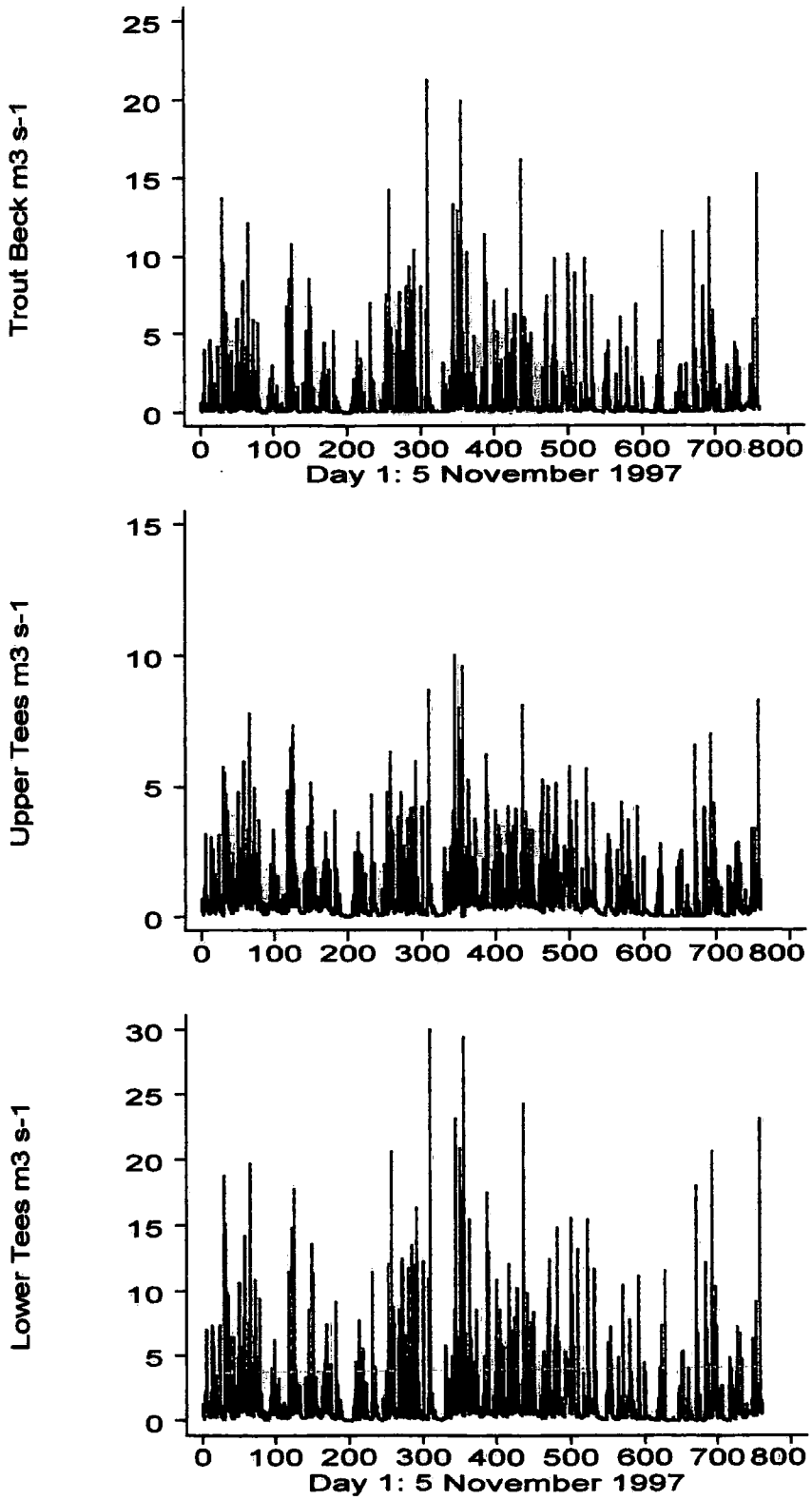
Trout Beck m3 s-1
25
20
15
10
5
0
0 100 200 300 400 500 600 700 800
Day 1: 5 November 1997
Upper Tees m3 s-1
15
10
5
0
0 100 200 300 400 500 600 700 800
Lower Tees m3 s-1
30
25
20
15
10
5
0
0 100 200 300 400 500 600 700 800
Day 1: 5 November 1997

Discharge in the Trout Beck and River Tees catchments is of a flashy nature, typical of upland river regimes. High runoff is generated by both convective storms and heavy rainfall / rapid snowmelt events which tend to responsible for the major floods in the area (Newson, 1989). Figure 5.2 shows the mean monthly discharge distributions for 1998 and 1999 periods and it indicates that annual cycle of discharge for the two catchments follows a typical pattern with higher runoff during the winter months and lower flows in the summer months. Indeed, the contrast between discharge in the very rainy months of December through March and the drier months of May and August is very clear.

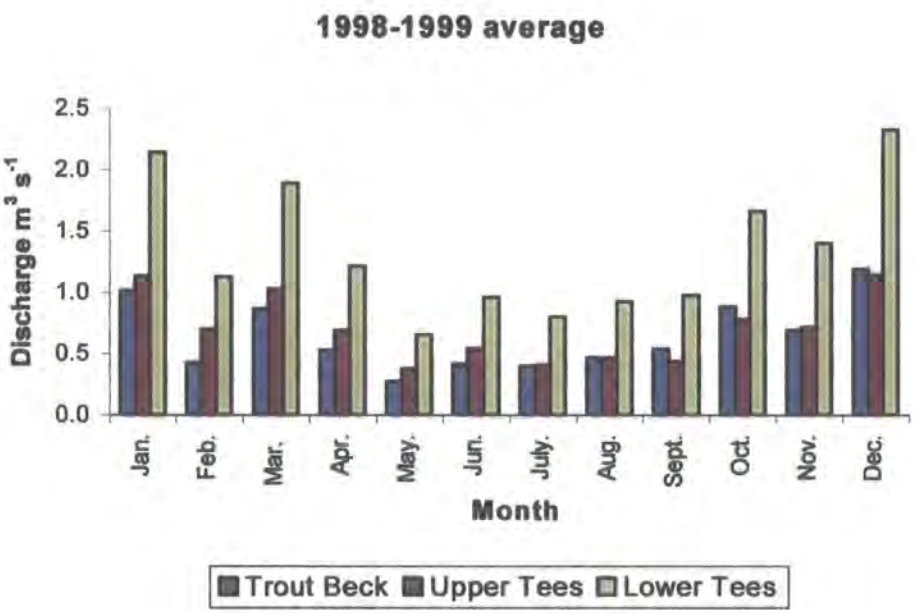

Figure 5.2 Monthly mean discharge for the average of 1998 and 1999 years at the Upper Tees, Trout Beck and Lower Tees Catchments.

Figure 5.3 summarises river flow between the tracer surveys and further demonstrates the rivers are very flashy and that there were numerous storm peaks and high flow periods. Figure 5.3 also shows that, in general, despite its smaller catchment area (11.4 km^2) the size of peak flows at Trout Beck are noticeable greater than the Upper Tees site (15.6 km^2). Thus, during the period November 26th 1997 to July 6th 1999 at Trout Beck there were 44 storm peaks exceeding 5 $m^3 s^{-1}$, 11 exceeding 10 $m^3 s^{-1}$, and 3 exceeding 15 $m^3 s^{-1}$, while at the Upper Tees catchment there were only 21 storm peaks exceeding 5 $m^3 s^{-1}$ and there was no flow greater than 10 $m^3 s^{-1}$ (Table 5.1). At the Lower Tees site, however, the number of storm peaks increased significantly due to the combined discharge of the two tributaries, such as 59 storm peaks exceeding

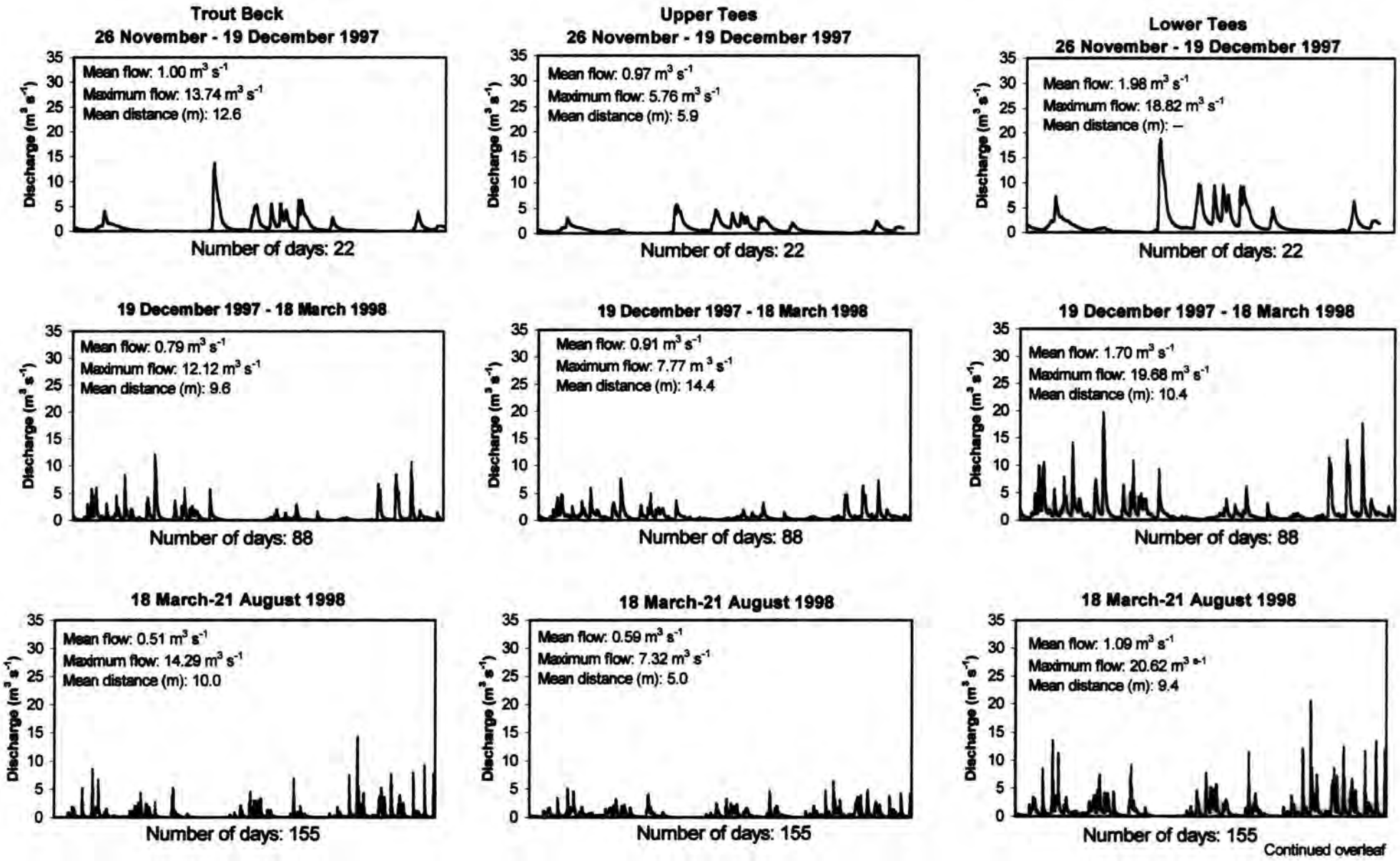

Continued overleaf

Figure 5.3 Flow discharge during the magnetic tracer monitoring period at the three experimental reaches.

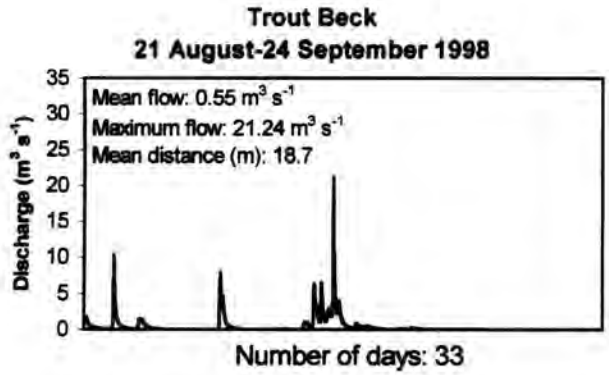
Trout Beck
21 August-24 September 1998
Mean flow: 0.55 m3 s-1
Maximum flow: 21.24 m3 s-1
Mean distance (m): 18.7
Discharge (m3 s-1)
Number of days: 33

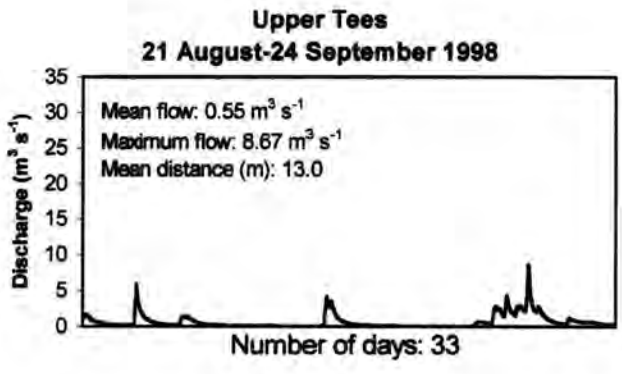
Upper Tees
21 August-24 September 1998
Mean flow: 0.55 m3 s-1
Maximum flow: 8.67 m3 s-1
Mean distance (m): 13.0
Discharge (m3 s-1)
Number of days: 33

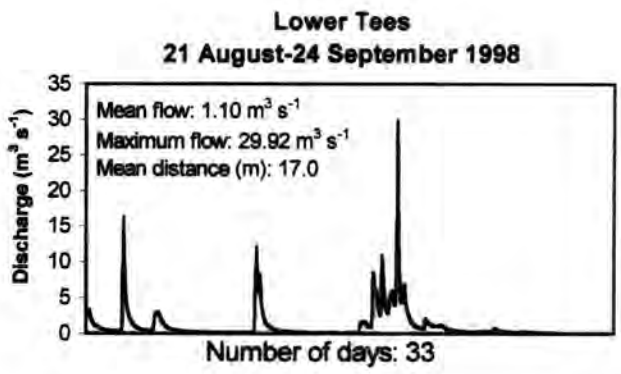
Lower Tees
21 August-24 September 1998
Mean flow: 1.10 m3 s-1
Maximum flow: 29.92 m3 s-1
Mean distance (m): 17.0
Discharge (m3 s-1)
Number of days: 33

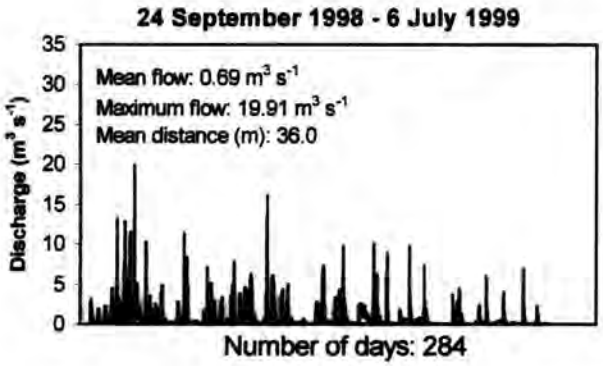
24 September 1998 - 6 July 1999
Mean flow: 0.69 m3 s-1
Maximum flow: 19.91 m3 s-1
Mean distance (m): 36.0
Discharge (m3 s-1)
Number of days: 284

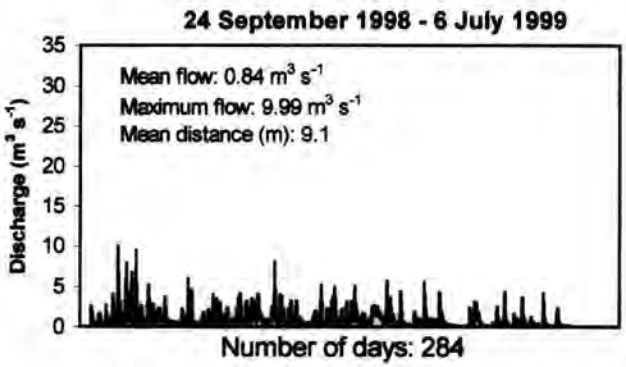
24 September 1998 - 6 July 1999
Mean flow: 0.84 m3 s-1
Maximum flow: 9.99 m3 s-1
Mean distance (m): 9.1
Discharge (m3 s-1)
Number of days: 284

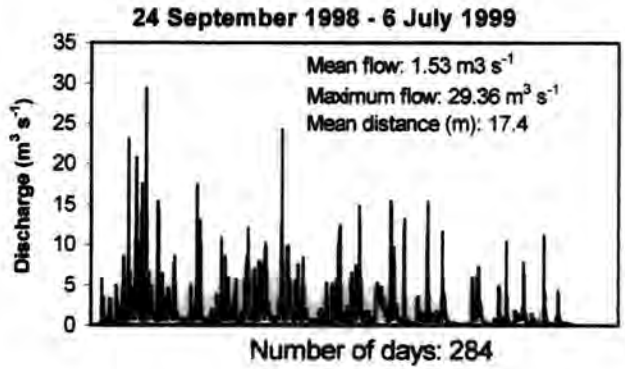
24 September 1998 - 6 July 1999
Mean flow: 1.53 m3 s-1
Maximum flow: 29.36 m3 s-1
Mean distance (m): 17.4
Discharge (m3 s-1)
Number of days: 284

5 $m^3 s^{-1}$, 29 exceeding 10 $m^3 s^{-1}$, and 16 exceeding 15 $m^3 s^{-1}$. The highest three recorded flows at Trout Beck site were 21.4 $m^3 s^{-1}$, 19.90 $m^3 s^{-1}$, and 14.29 $m^3 s^{-1}$, while at Upper Tees the rank is 9.99 $m^3 s^{-1}$, 8.67 $m^3 s^{-1}$ and 7.77 $m^3 s^{-1}$ (Table 5.1 and Figure 5.3).
The timing of flood peaks is broadly synchronous between the two catchments and travel times from the two gauging sites to the confluence were approximately equal.

Table 5.1 Storm peaks during the magnetic tracer monitoring. Periods between individual survey at Trout Beck, the Upper Tees and the Lower Tees are shown. (T.B. Trout Beck, U.T. Upper Tees, L.T. Lower Tees)

26 November-19 December 1997				19 December 1997-18 March 1998			
Discharge $m^3 s^{-1}$	T.B.	U.T.	L.T.	Discharge $m^3 s^{-1}$	T.B.	U.T.	L.T.
5-10	5	1	7	5-10	4	1	3
10-15	1	0	0	10-15	1	0	3
>15	0	0	1	>15	0	0	1
18 March-21 August 1998				21 August-24 September			
Discharge $m^3 s^{-1}$	T.B	U.T	L.T	Discharge $m^3 s^{-1}$	T.B	U.T	L.T
5-10	14	3	10	5-10	4	3	6
10-15	2	0	10	10-15	1	0	3
>15	0	0	2	>15	1	0	2
24 September 1998-6 July 1999				All periods			
Discharge $m^3 s^{-1}$	T.B	U.T	L.T	Discharge $m^3 s^{-1}$	T.B	U.T	L.T
5-10	17	13	33	5-10	44	21	59
10-15	6	0	13	10-15	11	0	29
>15	2	0	10	>15	3	0	16

5.2.1 Initiation of bedload transport

The initial movement of a clast on a coarse bed river is a complex phenomena which is controlled by many factors. These factors depend on particle physical properties (e.g. particle size, shape, density and structure arrangement); sedimentological characteristics of the bed (e.g. texture, packing, armouring, bed forms) and local hydraulic conditions of the flow (e.g. discharge, velocity, duration) (Naden,

1988; Hoey, 1989; Gomez and Church, 1989). Knighton (1998) identified two sets factors that are largely responsible for the observed large variations in the threshold of initial motion of coarse particles (Table 5.2).

Table 5.2 Factors producing scatter about threshold of the initiation of particle movement (after Knighton, 1998 and Naden, 1988)

Flow conditions	**Bed-material characteristics**
Definition of the entrainment threshold	Degree of exposure or relative protrusion of grains
Use of average shear stress or velocity	Pivoting angles
Spatial variability of shear stress or velocity over the bed	Imbrication or clustering of particles
Irregularity of turbulent eddying	Degree of packing
	Grain shape
Channel size	Grain size distribution or relative size
	Microtopography

The initiation of transport is very difficult to predict. The flow intensity controlling initial particle movement and eventual transport is measured by shear stress, velocity or stream power (Richards, 1982). Given the variations explained above, even within a uniformly rough portion of a stream bed, there are point-to-point variations in the factors that control the critical shear stress of each individual grain (Kirchner, 1990). Carson and Griffiths (1987) stated that spatial variation in particle size together with effects of bed forms on local flow conditions, render mean channel parameters for predicting bedload transport somewhat meaningless in many rivers.

Particles are entrained in reaches in which bed shear stress and velocity vary over very short distances due to local variations in channel slope, size and shape characteristics of bed material and also bed packing arrangements. Thus it is difficult to determine a critical discharge which represents initial transport of the bed material for the whole stream. In the present study, there is no local hydraulic information available at the three sites. Reach-based estimates of mean and peak discharge, shear stress and stream power for the three sites are shown in Table 5.3.

Table 5.3 Reach-based estimates of discharge (Q), shear stress (τ = e.*g*.R.S) and stream power (Ω = e.*g*.Q.S) values for the three experimental reaches.

Sites	Unit mean Q $m^2 s^{-1}$	Unit peak Q $m^2 s^{-1}$	Stream power for mean Q (Ω)	Stream power for max. Q (Ω)	Shear Stress (τ)
Upper Tees	0.058	0.970	0.0045	0.0588	0.0020
Lower Tees	0.103	2.851	0.0421	0.8804	0.0144
Trout Beck	0.064	2.062	0.0614	1.9797	0.0512

Flow characteristics at the three experimental reaches vary considerably. Discharge is highest at the Lower Tees site, while means are relatively similar at the Trout Beck and Upper Tees sites. Peak discharges are much greater at Trout Beck than the Upper Tees. Stream power and shear stress also show marked variations. The lowest values are for the Lower Tees site which has a virtually flat (reach) long profile. Trout Beck has the highest values. This mainly reflects differences in stream channel slope of the three reaches.

There are several bedload discharge equations which are appropriate to mountain rivers with coarse sediment (e.g. Shields, 1936; Meyer-Peter and Muller, 1948; Schoklitsch, 1969; Ackers and White, 1973; Mizuyama, 1977; Bagnold, 1980 and Smart, 1984). Although Shields, (1936) equation is considered the most common approach to prediction of the critical conditions for bedload movement, it was found to be less suitable because of practical difficulties associated with the dependency on depth. This is because, depth is a variable that it is difficult to measure accurately in steep rough flows. An alternative to the Shields equation is a discharge-based equation (critical water discharge), such as the Schoklitsch (1962) equation. Bathurst *et al* (1987) stated that initiation of bedload transport could be best predicted by the Schoklitsch approach modified to allow for the effect of non-uniform sediment size distribution. However, for sediments with a wide size distribution, the initiation of transport may not involve movement of all available sediment sizes. Nevertheless in a test of several bedload transport equations, Bathurst *et al* (1987) and later Agostino and Lenzi (1999) demonstrated that the Schoklitsch approach was most suited to mountain rivers of the type similar to the present study sites.

In order to predict initiation of bedload transport for each of the experimental sites, water discharges were converted into unit discharges and a critical discharge calculated using the Schoklitsch (1962) equation (Bathurst *et al*, 1987).

$$q_c = 0.26\left(\frac{\rho_s}{\rho} - 1\right)^{5/3} \frac{D_{40}^{3/2}}{S^{7/6}} \quad (5.1)$$

where q_c is the critical unit water discharge ($m^2\ s^{-1}$) at which bedload transport begins; p_s is the density of sediment (2.65); p density of water (1.0); D_{40} is size of particle median axis for which 40 percent of the sediment is finer (m); S is channel slope.

This equation was used because; discharge data are readily available for the study sites and it has been shown to be appropriate for coarse-bed, mountain streams (Bathurst *et al*, 1987).

The critical unit water discharge determined for the Upper Tees, Lower Tees and Trout Beck sites are 40.77 $m^2\ s^{-1}$, 6.32 $m^2\ s^{-1}$ and 3.34 $m^2\ s^{-1}$ respectively.

Table 5.4 The greatest unit discharges recorded ($m^2\ s^{-1}$) during the monitoring period at the three experimental reaches

Survey period	Trout Beck	Upper Tees	Lower Tees
1	1.335 (0.00)	0.297 (0.01)	0.851 (0.13)
2	1.176 (0.35)	0.401 (0.01)	0.891 (0.14)
3	1.387 (0.42)	0.377 (0.01)	0.933 (0.15)
4	2.062 (0.62)	0.447 (0.01)	1.354 (0.21)
5	1.933 0.58)	0.970 (0.02)	2.851 (0.45)

(The values in bracket show unit discharges as a ratio of the critical discharge for each site).

Comparison of the peak unit discharges (Table 5.4) and the critical discharge values for each of the experimental sites shows that, despite observed tracer movements at all three sites, in none of the survey periods do unit discharges exceed the critical discharge values. This suggests that either the Schoklitsch approach is a poor predictor of bedload transport or sporadic bedload transport is occurring below the critical value

for 'whole-bed' disturbance. Observations suggest that the situation over the monitoring period is best described by low transport rates over a fairly static bed. Transport of particles at discharges less than the critical value are to be expected because locally the flow will be sufficient to entrain some bed material due to higher than average flow strength or bed material configurations are suited to local entrainment.

The inherent imprecision of bedload transport equations to predict threshold of gravel transport steams from a number of factors (Naden, 1988). These include:

- Flume data used to evaluate the performance of the Schoklitsch's equation. These may not reflect actual conditions of entrainment in coarse-bed river channels.
- Average reach slopes used for the calculation critical discharge do not reflect local conditions.
- Tracers used for the experiments sit on a static bed and do not integrate well with natural bed material. This is not the situation for which Schoklitsch's equation was developed, e.g. grain exposure is greater for tracer clasts than the general bed material.
- The critical discharge figures determined here represent bulk transport rates rather than single particle movements.

5.2.2 Relation between discharge and the mean transport distance of the magnetic tracers

The mean transport distances of the magnetic tracers in relation to discharge during each of the survey periods are shown in Figure 5.4. Figure 5.4 suggests that, at the three experimental sites the relation between mean discharge and the mean transport distance of the magnetic tracers for each survey period is weak. For example, although mean discharge values at the three experimental sites were the highest between the period of 26 November-19 December, the mean transport distances were less. On the other hand Figure 5.4 clearly shows that at each of the experimental sites, there is a much stronger positive relation between peak flow and mean transport distances.

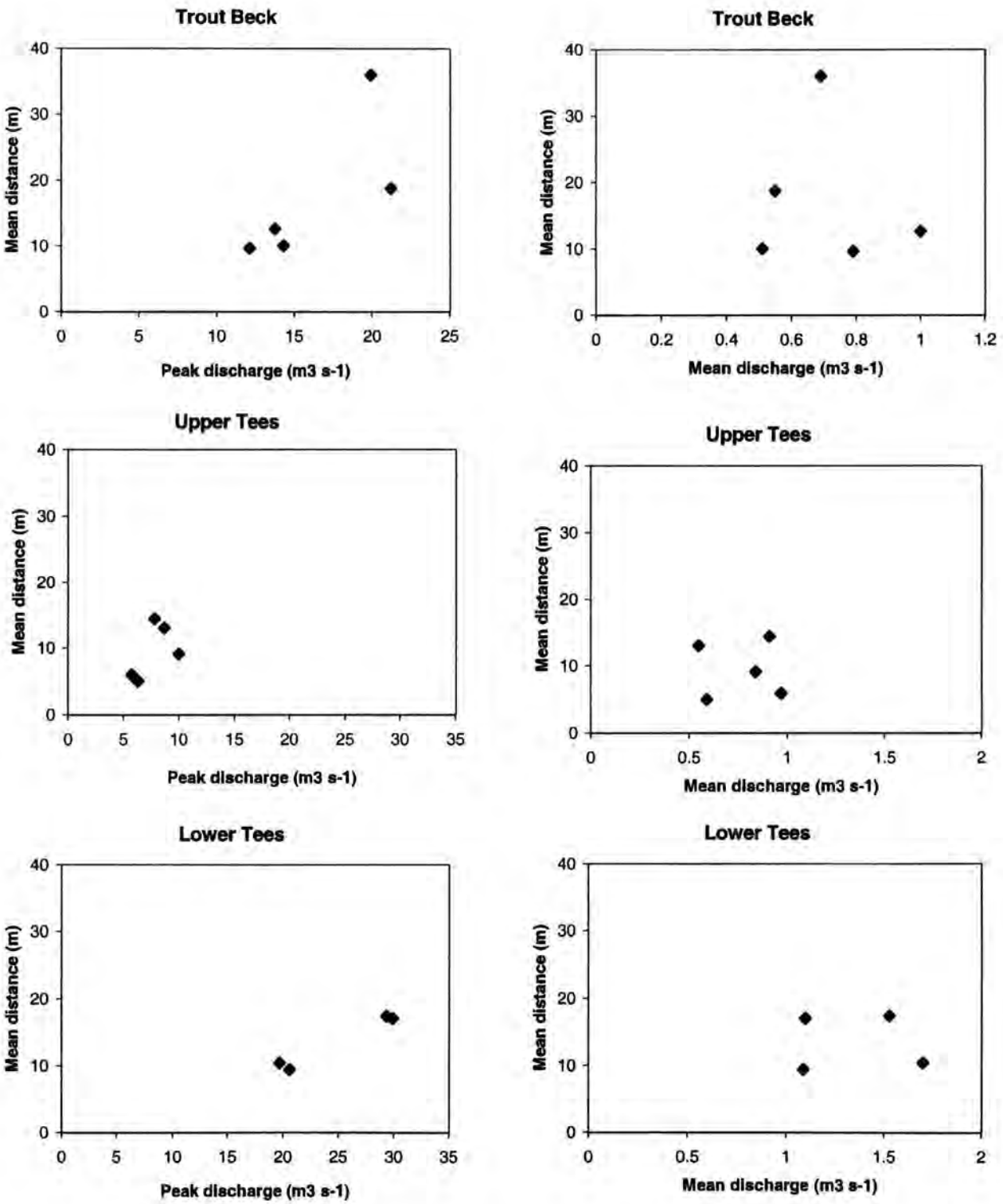

Figure 5.4 Relationship between peak and mean flow and mean transport distances of tracers for individual survery period at the three experimental sites.

5.3 RESULTS AND ANALYSIS OF MAGNETIC TRACING EXPERIMENTS AT THE THREE EXPERIMENTAL SITES

To assess the influence of bed material shape and size on transport of coarse river gravels a series of magnetic tracing experiments were set-up at three experimental reaches at the Moor House National Reserve. 2700 magnetic (coloured) stones of differing shape, size and weight were introduced at three stream cross-sections in three experimental reaches. (Figures 5.5 and 5.6). The size and shape characteristics (e.g. sphericity, flatness, and roundness) of the magnetic particles are given in Appendix 1. The experimental design and site characteristics of the three experimental reaches have been explained in detail in Chapters 3 and 4.

Table 5.5 Dates of magnetic stone surveys and the history of movement at the three sites.

Survey Date	Upper Tees	Lower Tees	Trout Beck
1. December 1997	+	No tracers	+
1. March 1998		+	+
2. August 1998	+	+	+
4. September 1998	+	+	+
5. July 1999	+	+	+

+: Movement ---: No movement

During the monitoring period (November 1997 to September 1999), tracers were resurveyed when noticeable movement had occurred. During resurvey particles were mapped in place. Only when identification was difficult particles were removed from the bed. These 'disturbed' particles were placed back in their pockets after measurement. The transport distances and the new locations of the tracers at the three sites were documented on five occasions between 18th December 1997 and 6st July 1999. Movement of the tracers during the whole monitoring period and the survey dates at the three experimental sites are shown in Table 5.5. Tracers were introduced at the

Figure 5.5 Cross-sections at Trout Beck (above) and Lower Tees (below) where yellow (a) Trout Beck and orange (b) Lower Tees magnetic tracers were placed respectively. Flow is from left to right for both sites. Grid references are: NY 759 336 and NY 762 338 for Trout Beck and Lower Tees respectively.

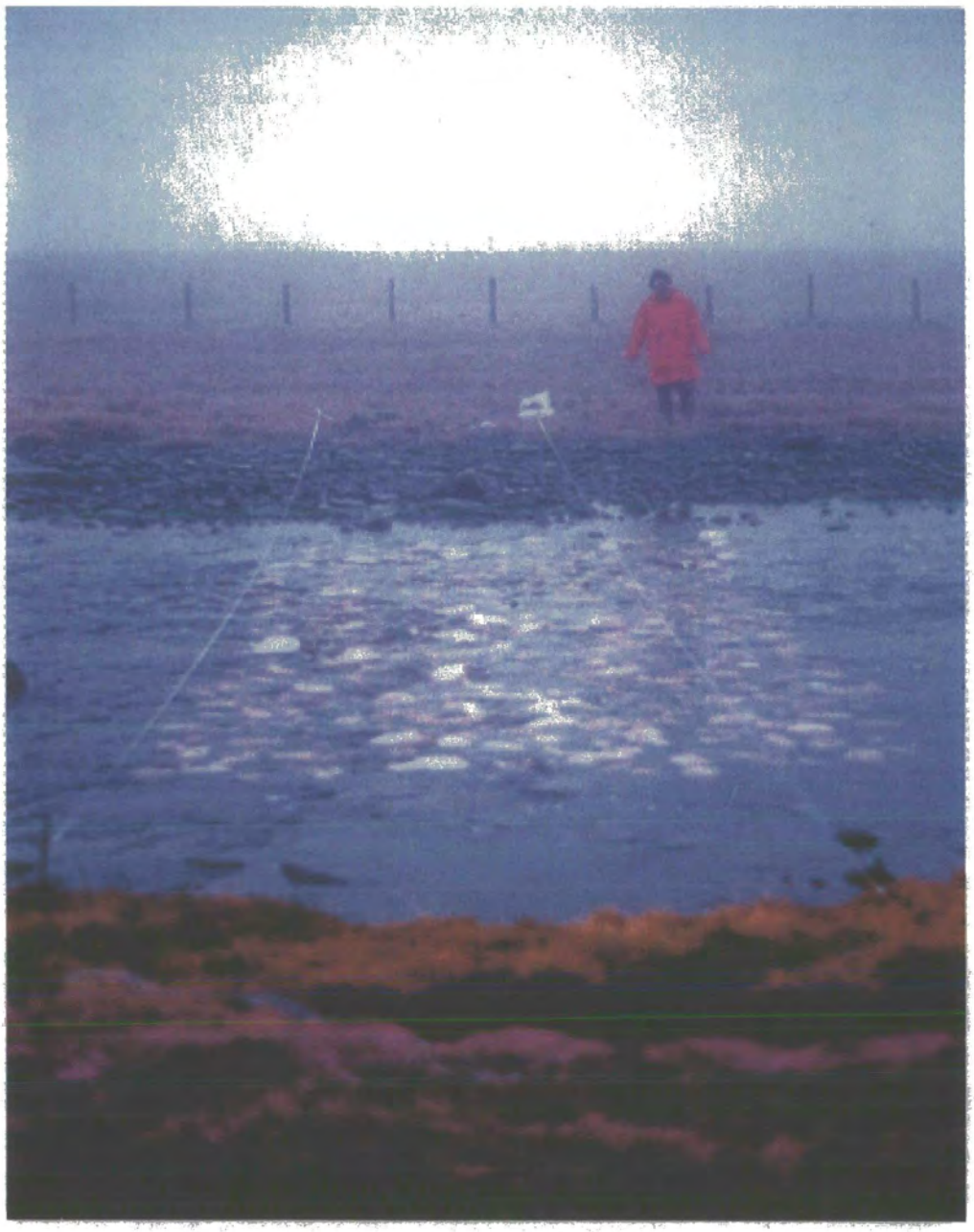

Figure 5.6 Cross-section at Upper Tees (NY 758 339) where white magnetic tracers were placed. Flow is from left to right.

Lower Tees site 10 December 1997. Discharge over the survey period is shown for each of the experimental sites in Figure 5.3.

In the following sections transport distances of tracers are presented as 'mean transport distance' which is the mean transport distance of all tracers moved up to that date, and 'period mean transport distance' which indicates the mean transport distances for all mobile tracers in a given period. Although some of the earlier studies (e.g. Hassan and Church, 1992) also worked out 'virtual rate of travel distances' which is based on using total time for which flow is larger than that needed to initiate clasts movement, in the present study this is not calculated. This is because, due to lack of information on local flow conditions at any of the sites a single critical discharge value could not be determined.

5.3.1 First survey (Period of record: 26th November–19th December 1997)

During this period, the mean flows were 1.00 $m^3 s^{-1}$ at Trout Beck and 0.98 $m^3 s^{-1}$ at Upper Tees. The peak flow was 13.74 $m^3 s^{-1}$ at Trout Beck, while at Upper Tees it was 5.76 $m^3 s^{-1}$.

Upper Tees

Of the total sample of 900 magnetic tracers, only 15 individual stones were recorded to have moved at the Upper Tees site (Table A2.1 and Figure 5.7). This constitutes less than 2 % of the total sample at the site. Most of the transported particles remained close to the starting point. The mean distance moved for all particles was 5.9 m. None of the particles were buried or disappeared during this period. The majority of the mobile tracers were in the medium size group (6 small, 8 medium and 1 large size group). In the sphere shaped group, a total of 8 stones moved (2 small, 5 medium, and 1 large) with a mean distance of 6.5 m. In the rod shaped class a total of 5 stones moved, (2 small and 3 medium), with a mean distance of 4.5m, while there was no movement for the large sized rods. There was no significant difference between the mean transport distances of small and medium size rods. In the disc group, only two stones moved, one small sized disc moved 7.8 m, and one medium sized disc moved 5.8 m (Table A2.1 and Figure 5.7).

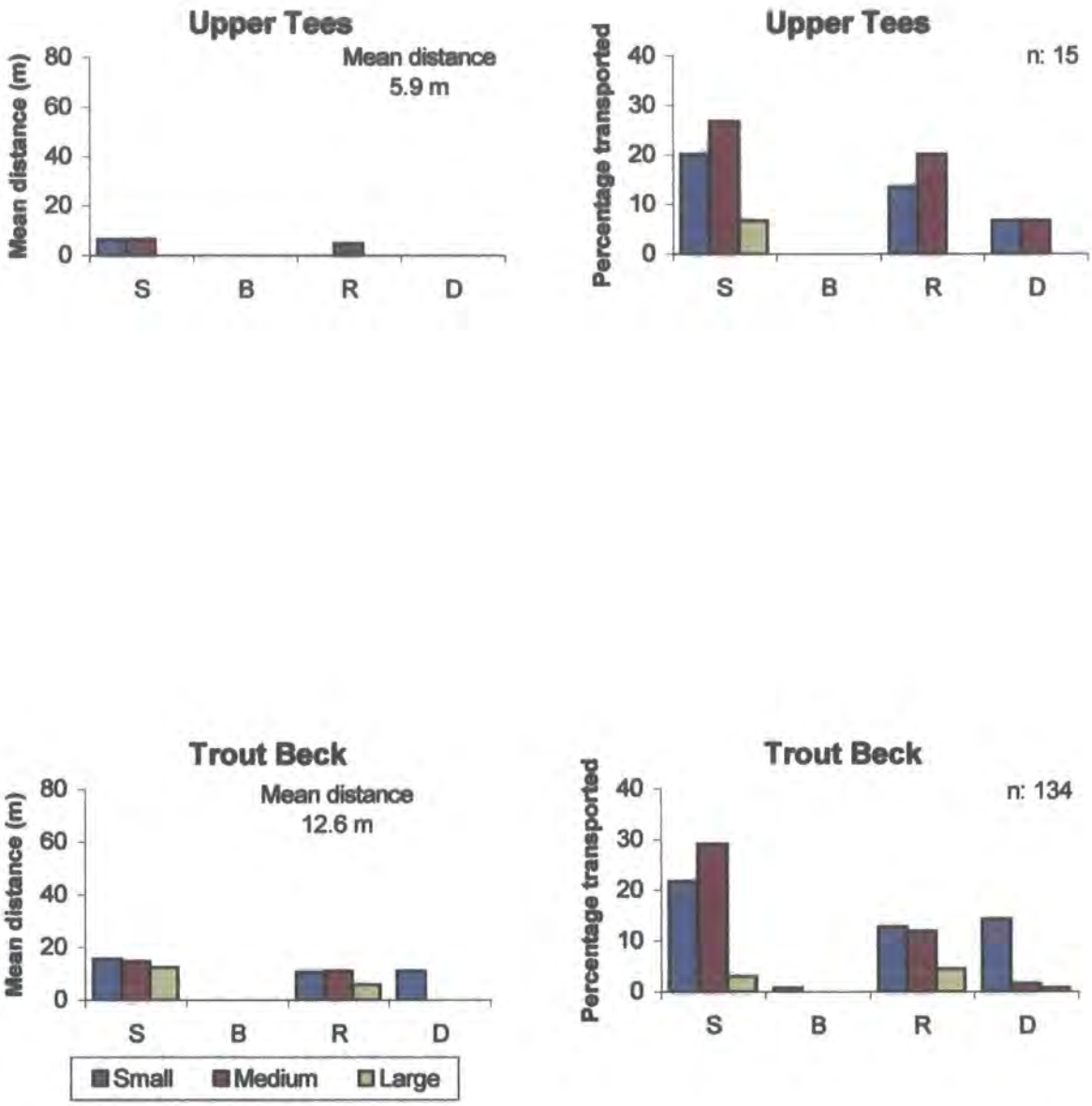

Figure 5.7 Percentage and mean distances of transported particles for the period of 26th November-19th December 1997 at Upper Tees, Lower Tees and Trout Beck (S: sphere, B: blade, R: rod, D: disc).

Trout Beck

At Trout Beck a total of 134 stones moved during the period (66 small, 57 medium and 11 large), representing 15% of the 900 magnetic stones (Table A2.1 and Figure 5.7). The mean distance moved for all the moved particles was 12.6m. Small sized particles constitute the greatest number of tracers moved. Overall, sphere-shaped particles constituted the largest group of stones moved, and had the greatest transport distances. There was no movement for blade-shaped particles (Table A2.1). The greatest observed movement was 62.4m by a medium sphere. In the sphere-shaped group, a total of 72 stones moved (53.7 % of the total stones moved) with a mean distance of 14.8m (Table A2.1). 29 of the mobile particles were in the small group and 39 in the medium size groups while only 4 large stones moved. Rod-shaped clasts represented the second longest mean transport distance. A total of 39 (29.1% of the total) moved with a mean transport distance of 9.8 m. Although there was no great difference between the number of particles moved and mean distances moved by the small and medium rods, both the number of particles transported and the mean transport distance decrease noticeably with the large sized rods (Table A2.1 and Figure 5.7). In the disc-shaped class a total of 22 stones (16.4 %) moved with a mean transport distance of 10.2m. Table A2.1 indicates that 19 (86.4 %) of the transported stones were small-sized discs, which moved the longest mean transport distance (10.9m).

5.3.2 Second survey (Period of record: 19th December 1997–18th March 1998)

Upper Tees

During this period the mean flow was 0.91m^3 s^{-1} and peak flow was 7.78 m^3 s^{-1}. A total of 43 magnetic tracers representing 4.8 % of the total number were mapped. The mean distance moved for all particles was 15.6 m. The greatest observed movement was 93.5m by a medium sphere. Table A2.2 and Figure 5.8 show what appears to be a decrease in both the number of particles transported and also their mean transport distance as particle size increases. An exception are the medium size sphere-shaped particles in which both the number of particles and their mean transport distances are greater than that of the small size group.

In terms of shape, there is a similar distribution to the previous period. Sphere-shaped particles show a greater increase both in the number of tracers transported and also their mean transport distances, while there is no movement in the blade-shaped

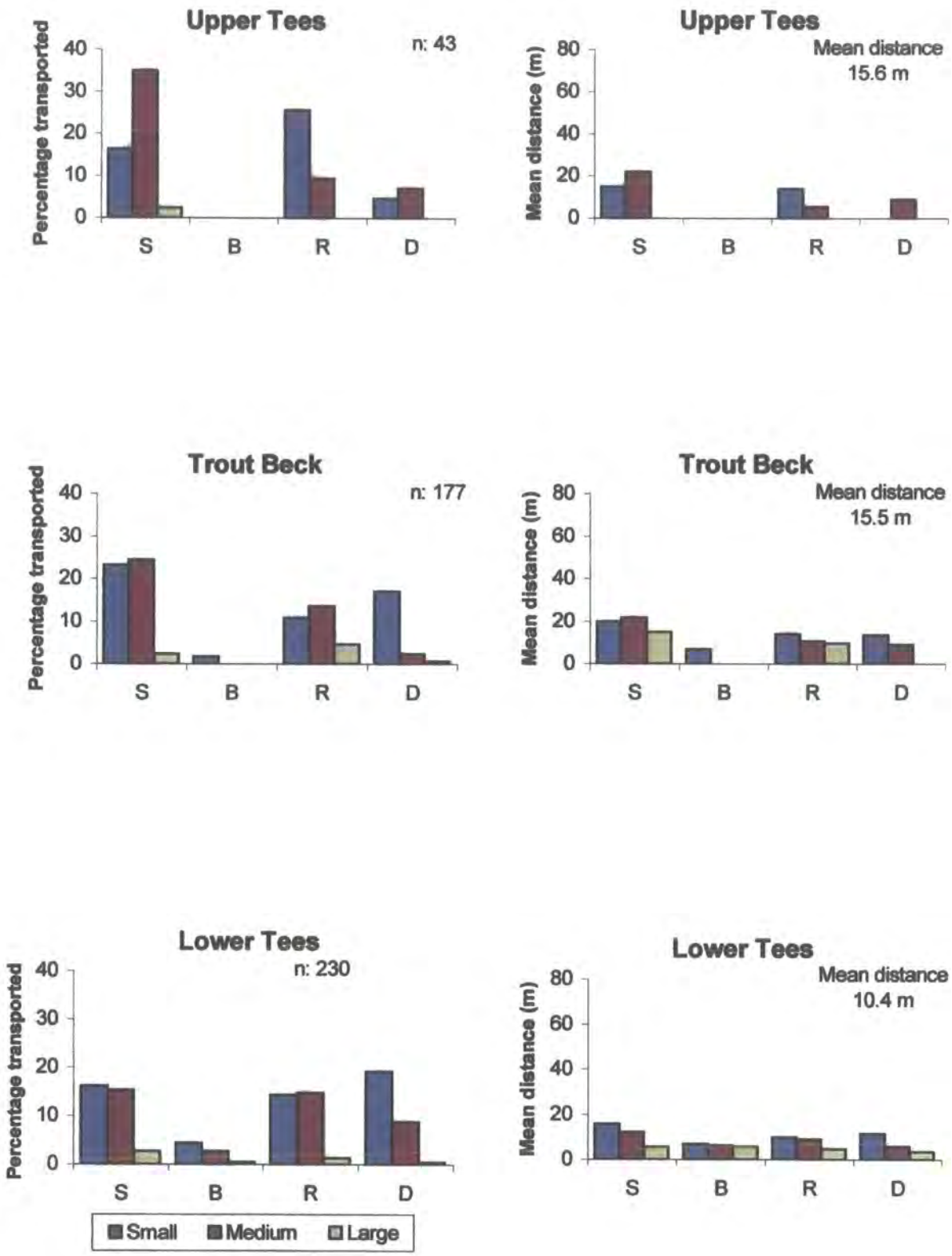

Figure 5.8 Percentage and mean distances of transported particles for the period of 19 December 1997-18 March 1998 at Upper Tees, Lower Tees and Trout Beck (S: sphere, B: blade, R: rod, D: disc).

class and less movement of the disc-shaped particles (Table A2.2). Overall, regardless of size, the mean distances moved by all spheres, rods and discs for this period were 19.4m, 11.5m and 10.6m respectively.

Trout Beck

During this period (between first and second surveys) mean and peak flows were 0.79 $m^3 s^{-1}$ and 12.12 $m^3 s^{-1}$ respectively. However Table 5.1 shows that there were also 5 peak flows vary between 5$m^3 s^{-1}$ and 10$m^3 s^{-1}$. Up to the present survey, 177 tracers moved and the mean distance transported was 15.5m. The longest distance moved was 127 m by a medium sphere. In terms of size, there is a noticeable decrease both in the number of the tracers transported and also their mean transport distances in the large size group. In terms of shape, sphere-shaped particles constitute the greatest percentage of particles transported and show the longest mean distance. Blade-shaped particles show the least (Table A2.2). Within each shape class most of the particles moved were in the small and medium size group and there is a noticeable decrease in the mean transport distances in the large size group. In the disc shaped class, however, many of the particles moved were in the small size group and there is a noticeable decrease in numbers moved as particle size increases. In the blade shaped class only three particles moved all the small size group, with a mean transport distance of only 6.8m (Figure 5.8).

Lower Tees

The Period mean and peak flows were 1.70 $m^3 s^{-1}$ and peak 19.68 $m^3 s^{-1}$ respectively. Other recorded number peak flows during the period were; three between 5 and 10$m^3 s^{-1}$, and three between 10 and 15 $m^3 s^{-1}$.

During this period a total of 230 (25.5 %) out of the 900 tracers were recorded to have moved. The mean distance moved for the particles was 10.4 m. The maximum distance moved was 74.1m by a small rod. Both the number of tracers transported and their mean transport distance tends to increase in the small and medium size groups, while it is noticeably less in the large size group (Table A2.2).

Sphere and rod-shaped tracers have the longest mean transport distance and also the greatest number of transported particles (Table A2.2 and Figure 5.8). In the sphere-shaped class a total of 78 tracers moved with a mean transport distance of 13.1m. The numbers of tracers moved and also their mean transport distances are very similar for

both the small and medium size of spheres, but in the large sized group spheres have lower values. There is a similar pattern for rod-shaped particles. For example the number of rods moved are almost equal (33 and 34) in small and medium sized groups, while, it becomes less in the large rods (Table A2.2). The total number of discs moved was 65 with a mean transport distance of 9.4m. The small sized group dominates these moved. This is different from spheres and rods where the number of small and medium sized particles moved is similar. The small sized discs also have the greatest mean transport distances than that of the medium and large sizes (Table A2.2). A total of 17 particles moved in the blade-shaped group with mean transport distance of 3.37 m, which is the smallest numbers of particles moved and shortest movement when compared to the other shapes.

5.3.3 Third survey (Period of record: 18 March – 21 August 1998)

Upper Tees

During this period (between surveys 2 and 3) the mean flow was 0.59 $m^3 s^{-1}$ and only three peak flows were recorded greater than 5$m^3 s^{-1}$ with a highest level of 6.33 $m^3 s^{-1}$ (Table 5.1). Little movement was recorded for this period and none of the stones were lost or buried.

The number of particles moved up to the present survey was 51, which constitute 5.6 % of the total number of tracers at the site. There were no great differences between the mean distance transported (15.6m) or the longest distance moved (medium sphere, 93.7 m) between this and the previous survey.

In terms of shape, Table A2.3 and Figure 5.9 show that in common with earlier surveys, sphere-shaped particles demonstrate the greatest frequency of transport and mean transport distances. In decreasing order of importance the percentage of tracers transported and their mean transport distance are 54.9 % /18.3m for spheres, 29.4 % /12.9m for rods, and 13.7 % /9.0m for discs. In the blade class only 1 small particle moved 25.8m.

Trout Beck

During this period mean flow was 0.51$m^3 s^{-1}$. A total of 16 storm peaks, 14 were greater than 5 $m^3 s^{-1}$ and two were between 10m and 15 $m^3 s^{-1}$ were recorded with a peak flow of 14.29 $m^3 s^{-1}$ which is slightly greater than that of previous period (Table 5.1).

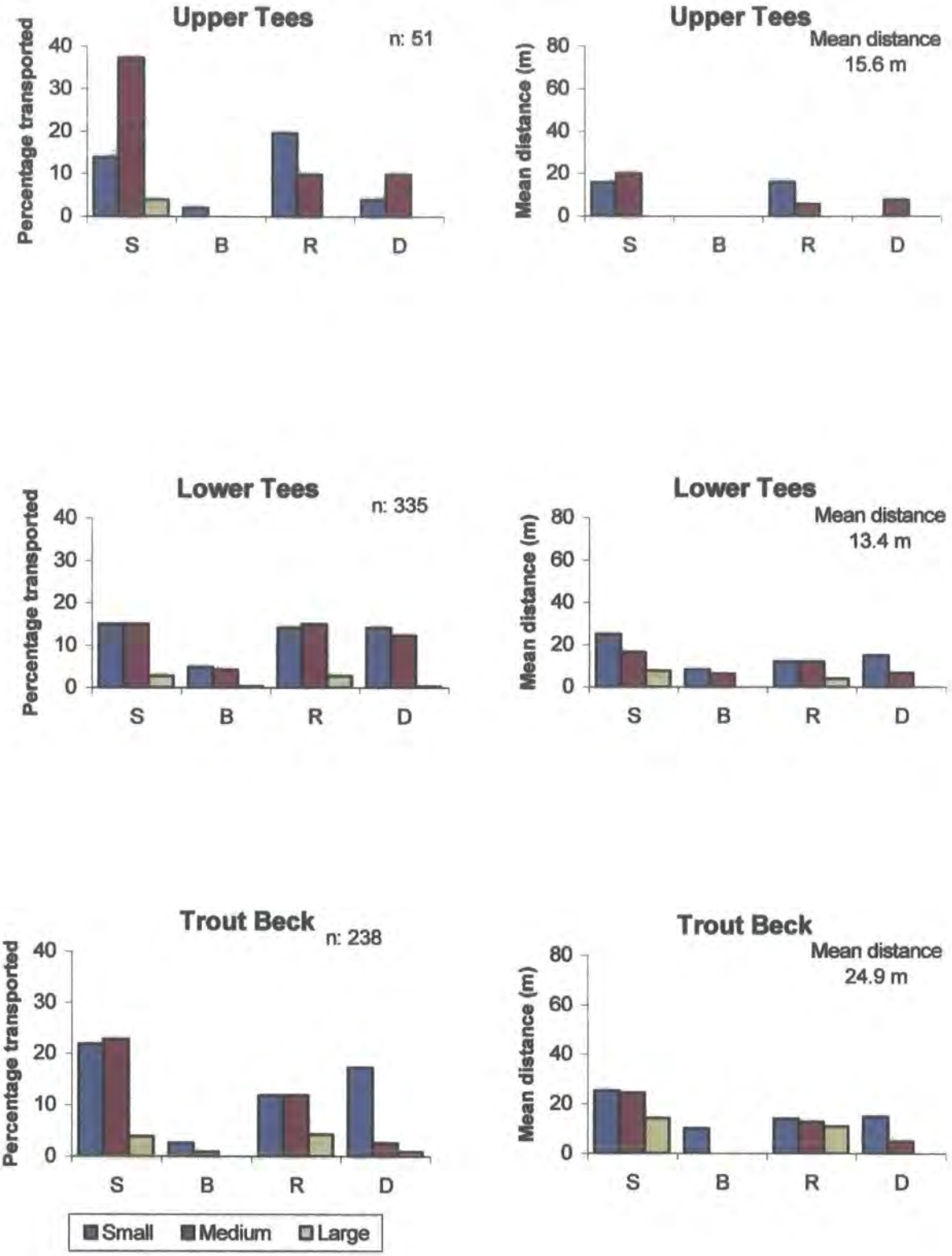

Figure 5.9 Percentage and mean distances of transported particles for the period of 18 March-21 August 1998 at Upper Tees, Lower Tees and Trout Beck (S: sphere, B: blade, R: rod, D: disc).

Up to this survey, the total numbers of magnetic tracers moved were 238, which is 26.4% of the total tracers at the site. The mean distance moved for all the particles was 24.9m. The greatest observed movement was 116.5 m by a medium sphere. The numbers of tracers transported are 127, 90 and 21 for the small, medium and large size groups respectively. The mean transport distances for the small and medium size groups are almost the same (18.6m and 18.8m), while it is only 11.7m for the large size group (Table A2.3).

In terms of shape, the pattern is similar to that observed in the previous surveys, that is the numbers are greater for the sphere, rod and disc-shaped classes than for the blade class (Table A2.3). In decreasing order of importance is sphere, rod, disc and blade shapes. Similar to the other sites, sphere-shaped particles show the greatest mean transport distances than the other shapes (Figure 5.9).

Lower Tees

During this period, mean flow was 1.09 $m^3 s^{-1}$ and in total 22 storm peaks were recorded with the highest value being 20.62 $m^3 s^{-1}$ (Table 5.1).

Up to the present survey the cumulative number of particles moved was 335 (37 %) of the total at the site. The mean distance moved for all particles was 13.4 m. The maximum distance moved was 106 m by a small sphere. Similar to earlier surveys, both the number of transported tracers and their mean transport distance tends to increase in the small and medium size group, while it is noticeably less in the large size group (Figure 5.9, Table A2.3).

In terms of shape, sphere and rod-shaped tracers appear to have the longest mean transport distance and also the greatest number of stones transported (Figure 5.9). The percentage of the number of tracers and also their mean transport distances in the four shape classes during this period are 32.5% (19.9 m), 31.6% (11.2 m), 26.6% (10.8 m), and 9.3% (6.9 m) for the spheres, rods, discs and blades respectively (Table A2.3).

5.3.4 Fourth survey (21st August 1998 – 24th September 1998

Despite lower mean flow discharges, the highest peak discharges were recorded at the Trout Beck and Lower Tees sites. It was the most important period for tracers movement and tracer loss.

Upper Tees

During this period the mean flow was 0.55m^3 s^{-1} and three storm peaks were recorded with a maximum of 8.67m^3 s^{-1} (Table 5.1 and Figure 5.3).

In the present survey, 190 (21.1%) out of the 900 tracers were recorded to have moved (Table A2.4). The mean distance transported by all the relocated particles was 15.9 m. The longest distance moved was 120 m by a medium size sphere. In terms of size, there is an increase in both the number of tracers transported and also their mean transport distance in the small and medium size group, while there are only a few movements in the large size group.

In general, there is a similar distribution to the previous survey. Sphere-shaped particles show the greatest number of tracers transported (81) and the largest mean transport distance (19 m). In common with the earlier surveys, rod-shaped particles show the second most important movements both in the number of tracers moved (60) and mean transport distance (14.4m), while disc and blade-shaped particles are 38-13.9m and 11-8.7m respectively. During this period the maximum mean transport distance (22 m) and greatest number of tracers moved (41) were in the medium size sphere group, while the least number and the shortest transport distances were recorded in the large blade group (1 stone moved 8.4m) and the large disc group (1 stone moved 4.5m). Sphere-shaped tracers showed the longest maximum transport distance compared to the other shapes in the medium and large size groups, whereas in the small size group small rods had the longest transport distances (Figure 5.10, Table A2.4).

Over the period, 86 particles, many of which were in small size group (small 65, 21 medium), could not be relocated. The percentage distribution of the missing stones in four shape classes is %33.2, %30.2, %29.1 and %2.3 for disc, blade, sphere and rod respectively. Only 4 stones were found to be buried, with a mean depth of 7.5 cm.

Trout Beck

During this period mean flow was 0.55 m^3 s^{-1} and six peak storms were recorded with a maximum of 21.24m^3 s^{-1} (Table 5.1 and Figure 5.3).

In the present survey, the total number of tracers moved was 413 (45.9%) The distributions are similar to the patterns recorded at other sites. The mean distance transported for all the tracers was 24.9m. The longest distance moved was 159.9 m by a medium sized sphere. In terms of size, there is a noticeable increase both in the number of tracers transported and their mean transport distance in almost every size group

(Table A2.4). The decreasing order of the mean transport distances is 28.2m, 24.1m and 15.1m for the small, medium and large size groups respectively (Table A2.4).

Regardless of size, sphere-shaped particles show an overall increase both in the number of tracers transported (154) and also their mean transport distances (38 m). Rod-shaped particles show the second greatest movements both in terms of the number of tracers (125) moved and their mean transport distances (21.3m), while the distribution for the disc and blade-shaped particles is 86 moved/16.6m and 51/6.7m respectively (Table A2.4, Figure 5.10). During this period the maximum mean transport distance (45.2m) and the greatest number of tracers moved (154) were from the small sphere group, while large blades represented the least number of tracers moved (6), and the shortest transport distances were shown in the medium blade class (6.0m) and large disc class (6.9m). Sphere-shaped tracers have the longest mean maximum transport distances in each of the size groups (Figure 5.10). For this period the decreasing order of the mean transport distances of particles of different shapes in the small size group is 45.2m, 25.5m, 20.5m, and 7.4m for spheres, rods, discs, and blades respectively. For the medium and large size groups, despite a decrease in the mean distance, the order is similar, while for largest sizes the rank order is 24.2m for spheres, 14.6m for rods, 7.4m for blades, and 6.9m for the discs.

Lower Tees

During this period mean flow was 1.10 $m^3 s^{-1}$ and 11 peak storms were recorded with a maximum discharge of 29.37$m^3 s^{-1}$ which was the largest discharge recorded during the monitoring period (Table 5.1 and Figure 5.3).

In the present survey a total of 506 (56.2%) out of the 900 tracers were recorded to have moved. 141 tracers disappeared, many of which were in small size group (115 small, 25 medium and 1 in large size group), could not be located. The mean distance moved for all the particles was 21.9 m. The maximum distance moved was 131.8m for a small sphere. In contrast to the previous survey, medium sized tracers constitute the greatest percentage of tracers moved (small 40.1%, medium 51.6%, and large 8.3%). However, despite having the greater number of particles transported, the mean transport distance of the medium sized group was less than that for the smaller sizes e.g. for the small, medium and large size particles transport distances is 25.5m, 20.3m, and 13.8m respectively (Figure 5.10, Table A2.4).

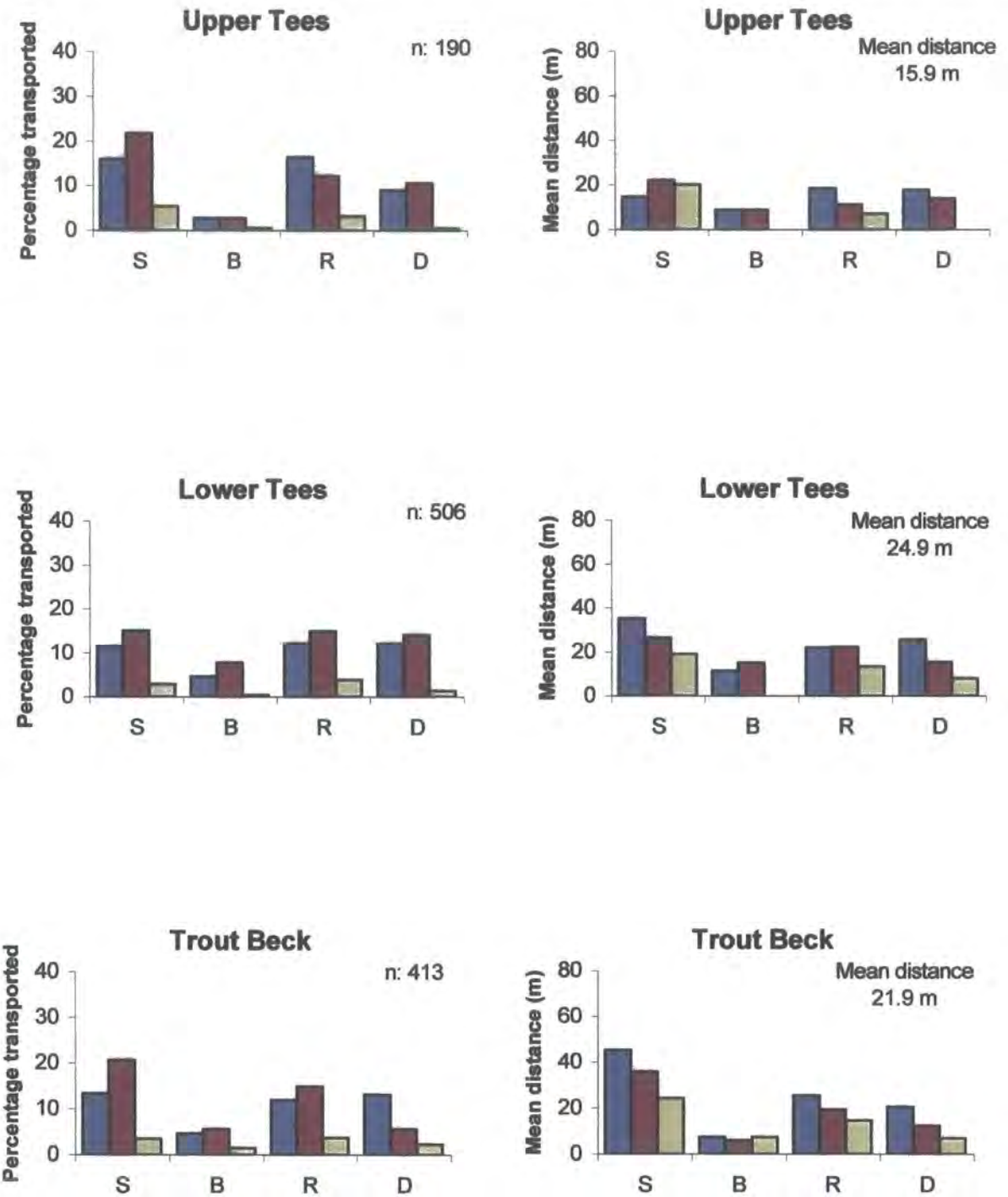

Figure 5.10 Percentage and mean distances of transported particles for the period of 21 August-24 September 1998 at Upper Tees, Lower Tees and Trout Beck (S: sphere, B: blade, R: rod, D: disc).

In terms of shape, the sphere, rod and disc-shaped tracers show noticeably longer mean transport distances and greater number of transported particles than the blade-shaped particles (Figure 5.10). Mean transport distances for spheres, rods, discs and blades are 29.0m, 20.9m, 19.3m, and 13.3m respectively. Similar to earlier surveys in each size group, sphere-shaped particles show the greatest mean transport distances, while blades show the least (Figure 5.10). In the small and large size groups, the decreasing order of the mean transport distances is spheres, discs, rods and blades, while in the medium size group the rank is sphere, rod, disc and blade (Table A2.4).

5.3.5 Final survey (24 September 1998 – 11 July.1999)

During this period, overall 1221 tracers moved at the three experimental reaches. It was the longest and second most important period for tracer movement. In general, little transport was observed at Upper Tees, while at Trout Beck and Lower Tees noticeable movements were recorded (Table A2.5 and Figure 5.11).

Upper Tees

Mean flow for the final survey was 0.84 $m^3 s^{-1}$ with a peak value of 9.99$m^3 s^{-1}$. Total number of tracers moved up to date is 203 and 97 tracers disappeared. The mean distance transported by all relocated particles was 17.2 m. The longest distance moved was 146 m by a small rod. The number of medium sized particles transported was slightly greater than the small ones, while it decreases significantly in the large size groups.

In terms of shape, spheres comprise the greatest percentage of number of transported particles and the longest mean transport distance, while blade-shape particles show the least transport (Figure 5.11). The rank order for the number of particles transported and also their mean transport distances is 82 (20.7 m) for spheres, 68 (16.4 m) for rods, 40 (14.2 m) for discs, and 13 (9.0 m) for blade (Table A2.5). In each shape class, most of the particles moved were in the medium and small size groups (Table A2.5). However, despite less number of movements, the mean transport distance of spheres in the medium size group is slightly greater than that of the small sizes. In the disc shaped class, however, many of the particles moved were in the medium size group and there was only one particle in the large size group. The total number of discs moved and mean transport distances for the medium and small size discs are 24/13.8m and

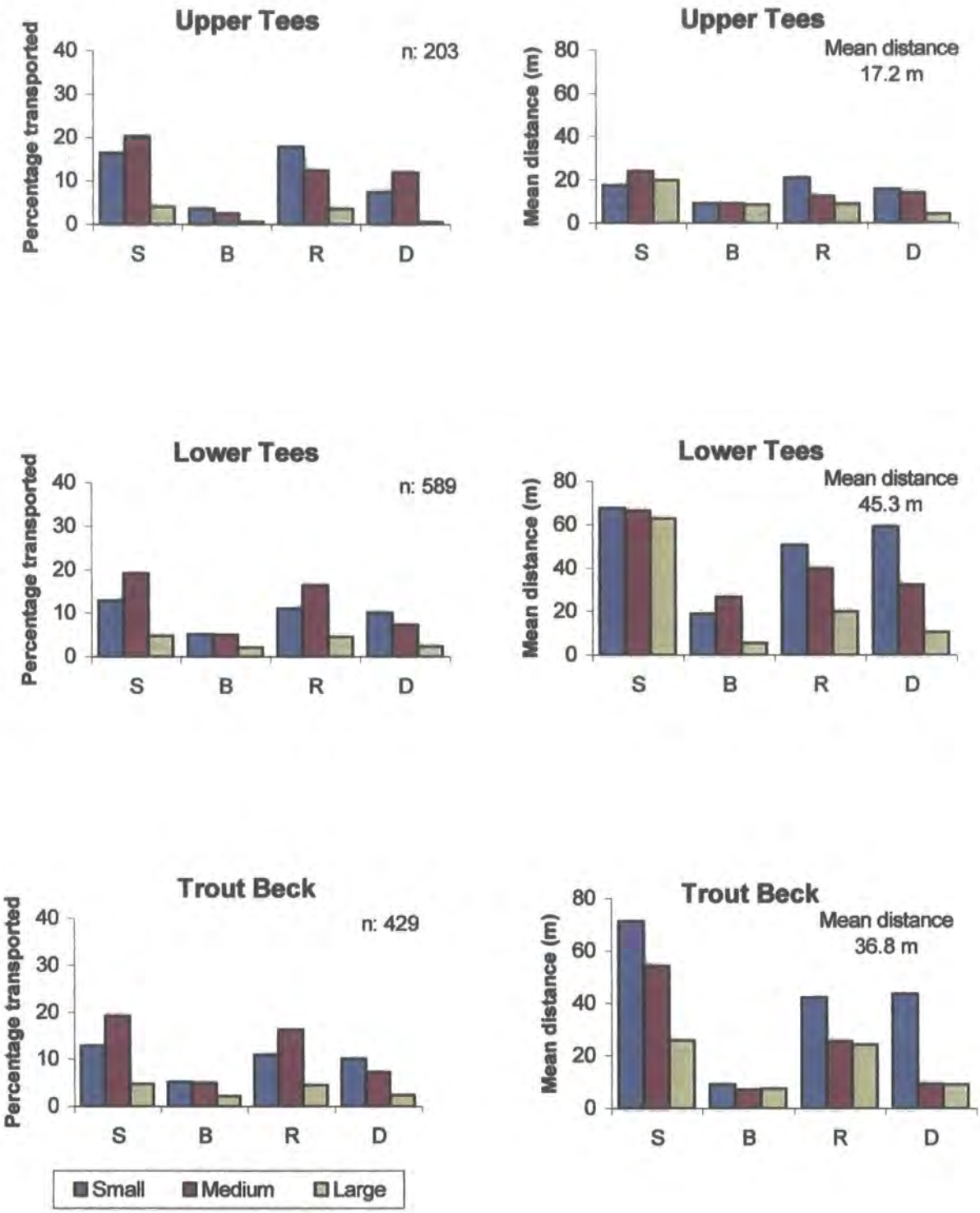

Figure 5.11 Percentage and mean distances of transported particles for the period of 24 September 1998 -6 July 1999 at Upper Tees, Lower Tees and Trout Beck (S: sphere, B: blade, R: rod, D: disc).

15/15.6m respectively (Table A2.5). In the blade shaped class, a total of 13 tracers moved, 7/9.0m small, 5/8.9m medium size and 1/8.5m large.

Trout Beck

During this period mean flow was 0.69 $m^3 s^{-1}$ which a total 25 storm peaks (17 between 5 and 10 $m^3 s^{-1}$, 6 between 10-15 $m^3 s^{-1}$ and 2 greater than 15 $m^3 s^{-1}$) were recorded. The maximum flow was 19.91$m^3 s^{-1}$ (Table 5.1 and Figure 5.3).

In the whole 429 (48%) out of the 900 tracers were recorded to have moved up to date. Altogether, 206 particles could not be found and 110 particles were buried. Most of the particles disappeared (73.7%) and buried (63.6%) were in small size group. Mean depth of burial was 7.3 cm.

The mean distance moved for the particles was 36.8m compared with 17.2m at Upper Tees and 45.3m at Lower Tees. The greatest observed movement was 399m by a small rod. The number of particles moved in the medium size group is greater than that of small and large size group (small size: 167, medium size: 204 and large size: 58). However, particles in the small sized tracers moved further downstream. The mean transport distances for the small and medium size groups were 47.8m and 32.6m respectively, while it is only 19.6m for the large size group.

In terms of shape, the patterns are generally similar to those observed in the previous surveys. In other words, both the numbers of tracers moved and also measured mean transport distances tend to be greater in the sphere, rod and to some extent in disc-shaped classes than the blade-shaped class (Table A2.5 and Figure 5.11). For the period, sphere-shaped particles show greater mean transport distances than the other shapes. The mean transport distance for spheres is 56.6m, while it is 31.1m for rods, 20.8m for discs, and 7.9m for blades. In the sphere and rod shape classes most of the particles transported are in the small and medium size groups. Comparison of the four shapes clearly indicates that spheres within all size groups move in greater numbers and the longest mean transport distances.

Lower Tees

During this period mean flow was 1.53 $m^3 s^{-1}$. In total 56 storm peaks were recorded. Of the 56 storms peaks, 33 were between 5-10 $m^3 s^{-1}$ 13 were between 10-15 $m^3 s^{-1}$ and 10 of them were >15 $m^3 s^{-1}$. The highest peak flow was 29.37 $m^3 s^{-1}$ which was similar to the peak flow recorded in previous period (Table 5.1 and Figure 5.3).

In the present survey, the total number of tracers moved was 589 (65.4%) out of the 900 and 140 have not moved at all. In total 171 particles disappeared and 121 particles were buried. Many of the particles which disappeared (71.3%) and buried (48.7%) were in the small sized group. In general the burial depths were shallow. The mean of burial was 8.5 cm. The cumulative mean distance moved for all the particles was 45.3m which is the greatest distance at the three sites. The maximum distance moved was 361 m was by a medium rod (the longest movement recorded during the monitoring period). Similar patterns of movement still persist. In other words, the number of transported tracers and their mean transport distance tends to increase in the small and medium size group of particles, while it is noticeably less in the large size group (Figure 5.11, Table A2.5).

5.4 GENERAL PATTERNS OF MOVEMENT

5.4.1 Size-shape and distance of travel of magnetic tracers at the three sites

For the entire monitoring period, the cumulative mean transport distance and the survey period mean transport distances are shown in Figure 5.12. The greatest total mean transport distance are in the Lower Tees, while the Upper Tees has the smallest. Total mean transport distance of the tracers at Lower Tees site is almost three times greater than the Upper Tees. There is little variation in mean transport values between the different surveys at Upper Tees. For example, there is virtually no change between survey periods of 2, 3, 4 (15.6 m:15.6 m:15.9 m) and little change between surveys 4 and 5 (16m:17m) at Upper Tees. Indeed, the total difference in mean transport distance between Surveys 2 and final survey is only 1.6 m at Upper Tees, while it is 21.3 m at Trout Beck and 34.9 m at Lower Tees. Lower total mean transport at Upper Tees might be attributed to lower bankfull discharges (See Chapter 4). In contrast transport distances at Trout Beck and Lower Tees are much greater. There is a gradual increase in the total mean transport distance from one survey to another with an exception between surveys 3 and 4 where there is little variation. The ratio of reach based shear stress to the critical shear stress (τ/τ_{50}) at the Upper Tees, Lower Tees and the Trout Beck sites are 0.042, 0.214 and 0.640 respectively. The lower value of τ/τ_{50} ratios at the Upper and Lower Tees sites indicate a relatively stable bed conditions, when compared to the Trout Beck reach.

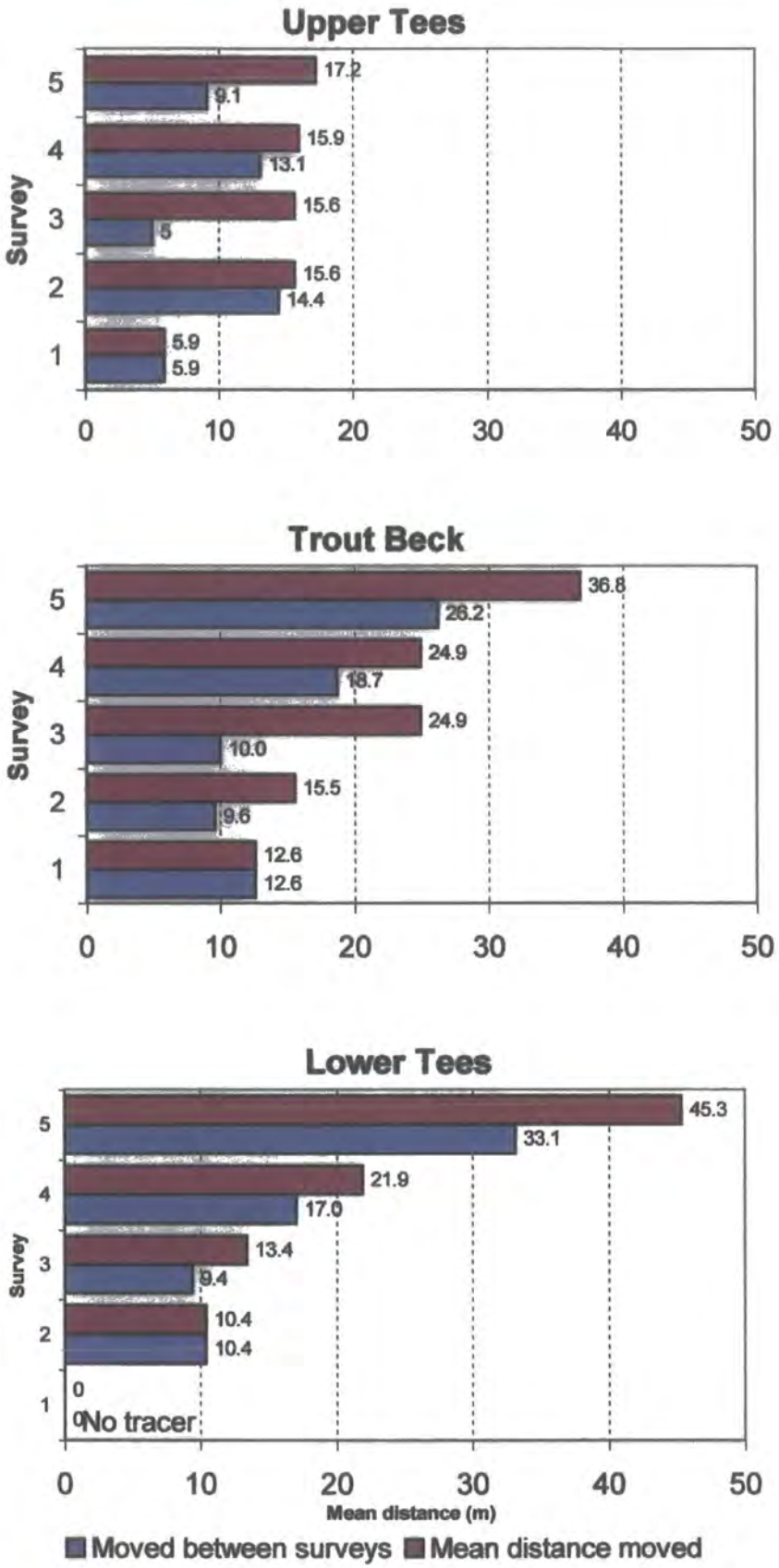

Figure 5.12 Cumulative and survey period mean transport distances of tracers during the fieldwork period at the Upper Tees, Trout Beck and the Lower Tees sites.

Table 5.6 Number of particles moved and mean transport distances for the five surveys at the three experimental reaches.

Survey	Mean Distance (m)	Standard deviation	Max Distance (m)	Total moved	Sphere n m	Blade n m	Rod n m	Disc n m
UPPER TEES								
1	5.9	2.2	10	15	53 - 6.5	0.0	33 - 4.8	13 - 6.8
2	14.4	17.7	93.4	40	55 - 12.8	0.0	35 - 14.9	10 - 9.8
3	5	5.0	93.8	30	52 - 6.3	0.0	35 - 4.0	14 - 2.9
4	13.1	13.0	70.3	170	41 - 14.8	6 - 8.7	33 - 11.6	37 - 13.0
5	9.1	10.2	101	107	29 - 9.2	5 - 6.1	29 - 12.6	21 - 5.6
TROUT BECK								
1	12.6	10.7	62.4	134	54 - 14.8	2 - 3.3	29 - 14.1	16 - 10.2
2	9.6	11.8	70.4	154	5 - 12.4	2 - 5.7	27 - 6.8	21 - 6.9
3	10.0	11.5	90	201	51 - 12.4	4 - 5.9	24 - 7.5	21 - 8.0
4	18.7	22.7	145	390	37 - 27.7	12 - 6.4	30 - 16.1	21 - 13.7
5	26.2	35.8	181	360	39 - 40.0	12 - 7.5	29 - 18.9	20 - 21.7
LOWER TEES								
1	--	--	--	--	--	--	--	--
2	10.4	9.2	74.1	230	34 - 33.9	10 - 7.4	33 - 7.9	26 - 6.8
3	9.4	13.6	106	290	31 - 14.9	10 - 4.3	29 - 7.9	28 - 6.8
4	17.0	16.2	106	464	29 - 20.7	12 -12.4	31 - 16.8	28 - 15.4
5	33.1	40.9	362	544	29 - 46.5	14 -16.8	29 - 29.0	27 - 32.5

In terms of mean transport distances for tracers moving in the period between surveys, Figure 5.12 and Table 5.6 indicate that at the Upper Tees site there is considerable small variation in movement between the period of surveys. At Trout Beck and the Lower Tees sites period mean transport distances with the exception of the first survey tend to increase from one survey to another

At all sites, of the 1221 tracers which were transported 74.4% moved between 3-50 m, 15.8% between 50-100m, 8.6% between 100-200 m, 1.1% between 200-300, 0.1% in excess of 300 m.

5.4.2 Comparison plots of tracer distributions based on Sneed and Folk Shape classification

Magnetic tracer classes were originally selected on the basis of a Zingg plot but it is now more widely recognised that the Sneed and Folk ternary diagram should be adopted as a standard because variations in particle shape can be shown less bias (Benn and Ballantyne 1993). Plotting follows a modified Sneed and Folk method as described prepared by Hockey (1970). This involves a simple revision of the original co-ordinate system with the right axis plotted as an inverse (1 – (b/a)).

Figure 5.13 shows comparison plots of tracer clasts distributions of the whole tracer set and those recorded "as moved" after the 5th survey. The density of points illustrates the intensity of transport at the three sites. Upper plots show the four classes of tracers used in the experiments at each site. In Sneed and Folk terms they are equivalent to the Zingg classes as follows.

Sphere	-	Compact
Disc	-	Platy, very platy
Rod	-	Elongates
Blade	-	Very bladed

The pattern of transport portrayed in the density of points is very clear: compacts > elongates > platy > blades.

Figures 14.a, b and c show the relation between scaled particle size and scaled transport distance. The scaling procedures follow the method and rationale outlined by Hassan and Church (1992) and Church and Hassan (1992). Briefly, particle size was scaled by

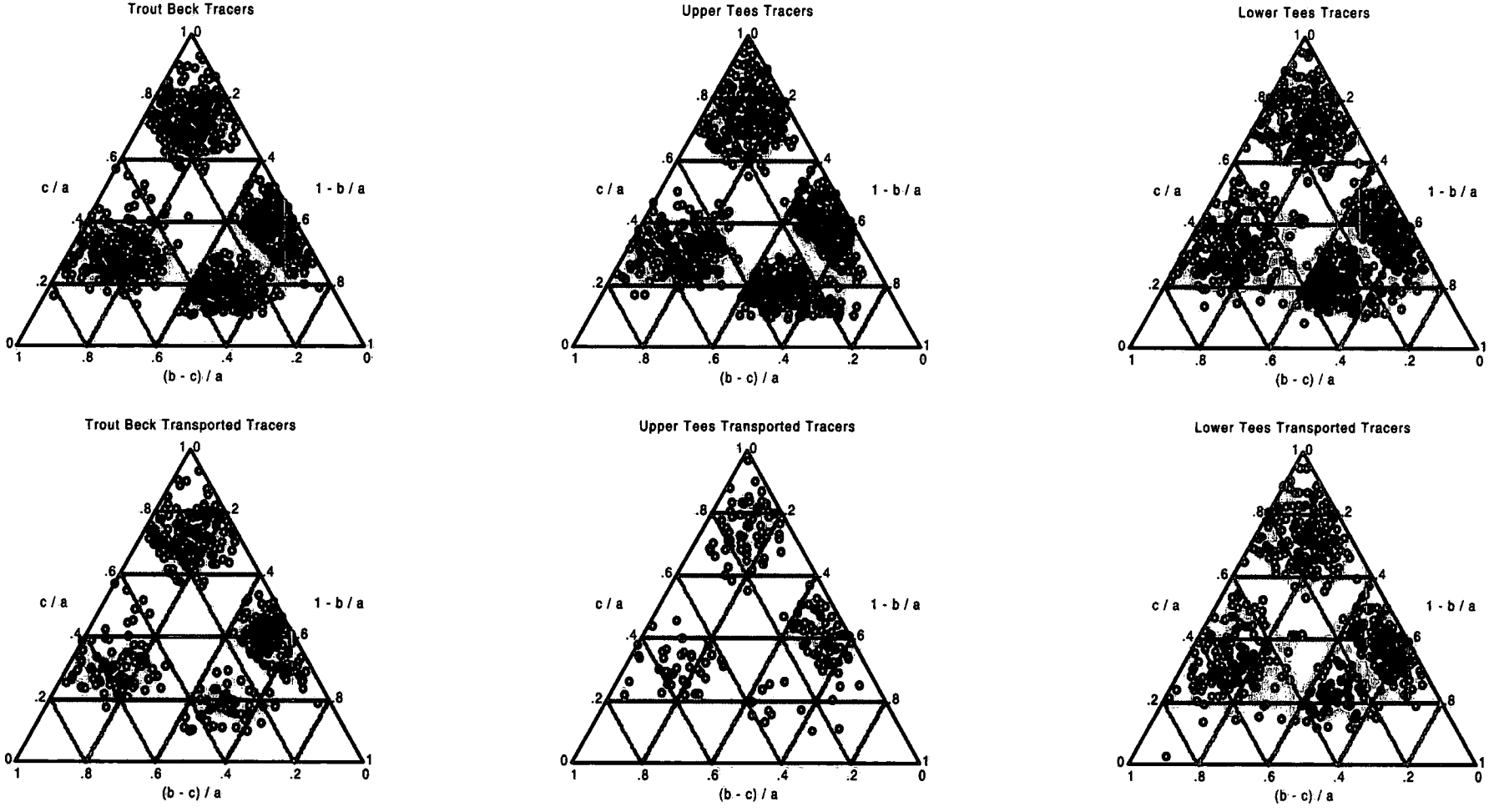

Figure 5.13 Sneed and Folk graphs, showing plots of tracer clast distributions of the whole tracer set and those moved after the 5th survey at the three experimental reaches.

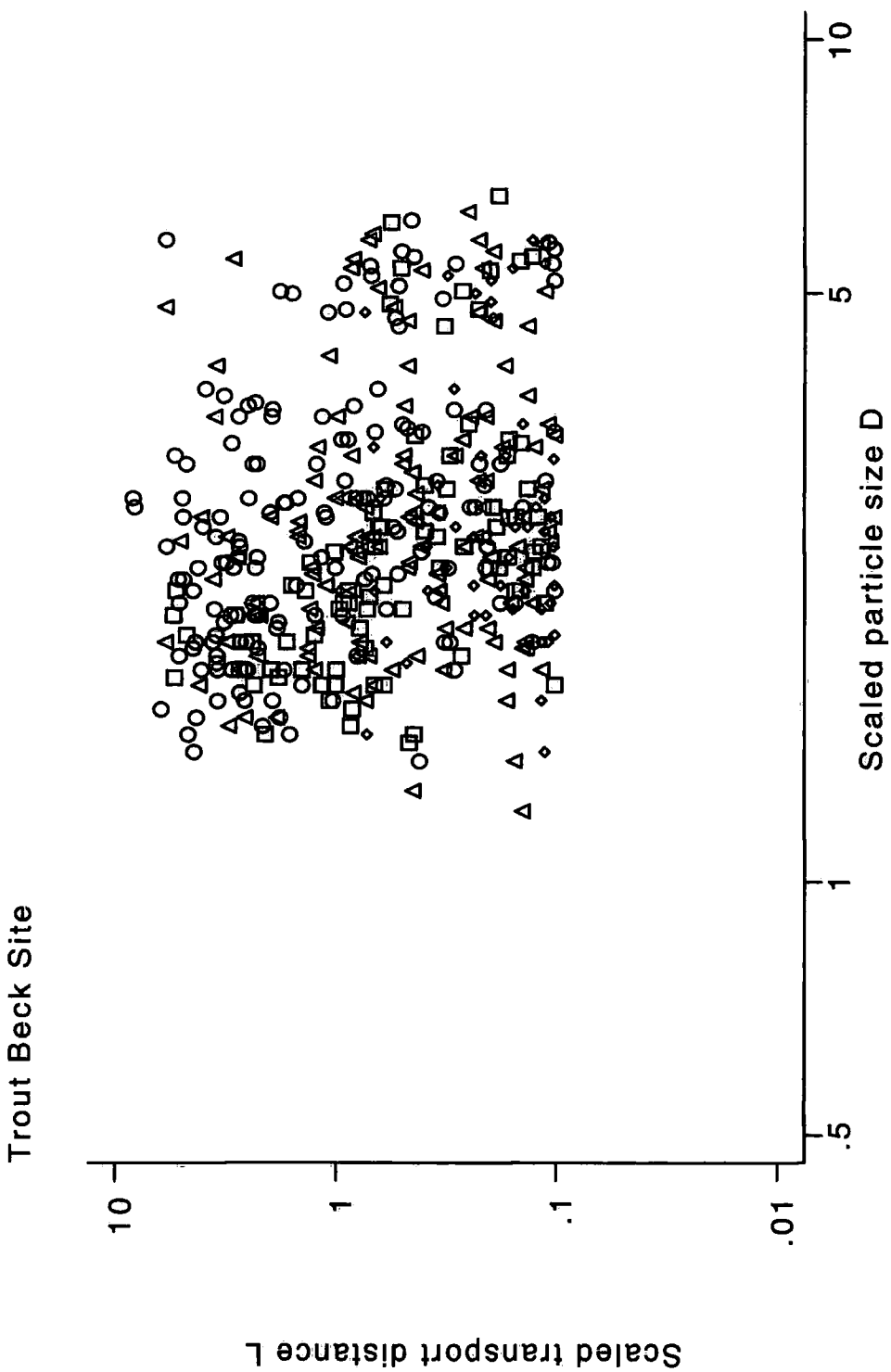

Figure 5. 14a Relationship between scaled transport distance and scaled particle size for sphere, blade, rod and disc shaped tracers for the final survey, at the Trout Beck site (O: Sphere, ◇: Blade, △: Rod, □: Disc).

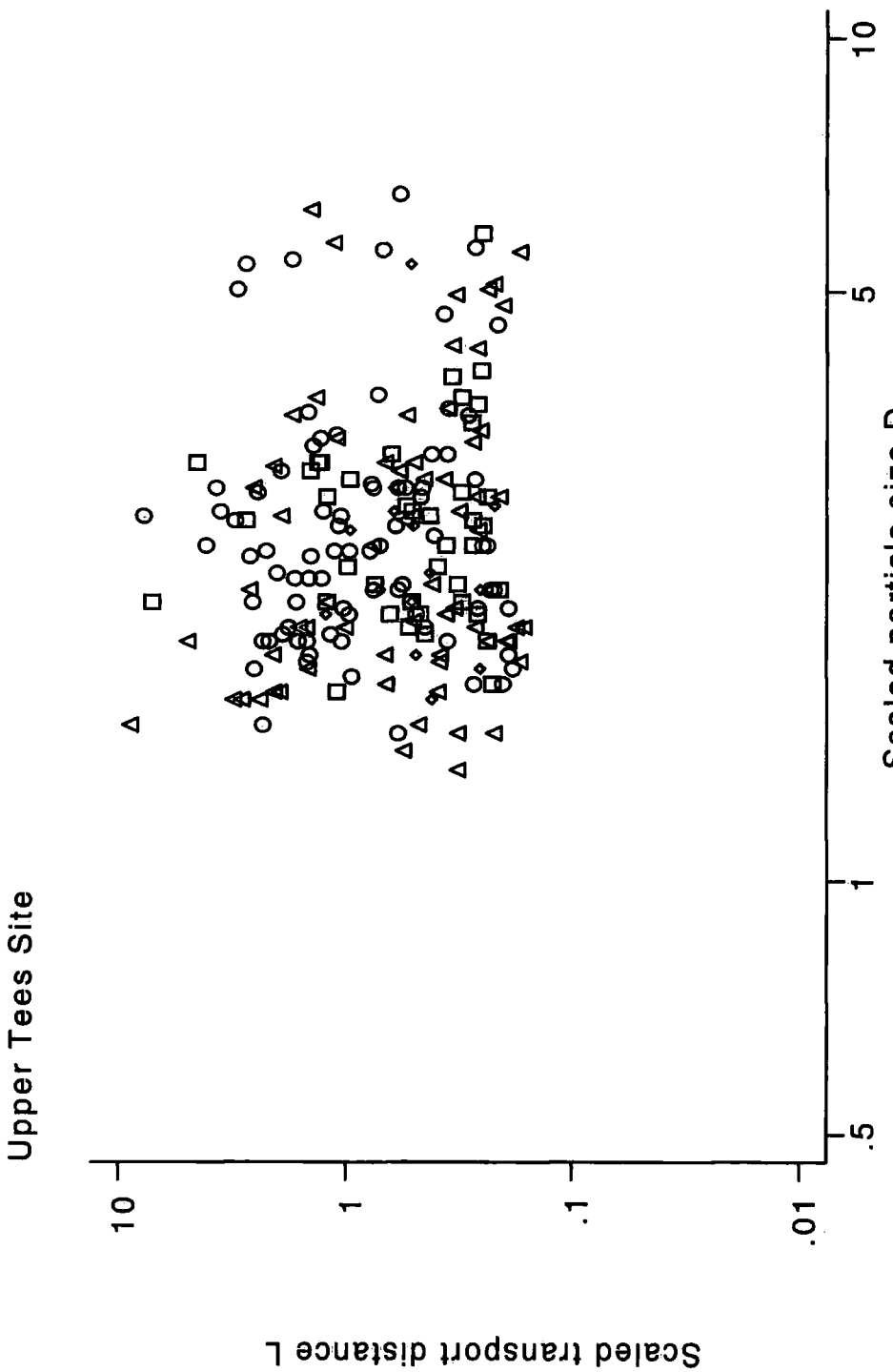

Figure 5.14.b Relationship between scaled transport distance and scaled particle size for sphere, blade, rod and disc-shaped tracers for the final survey, at the Upper Tees site (O: Sphere, ◇: Blade, △: Rod, □: Disc).

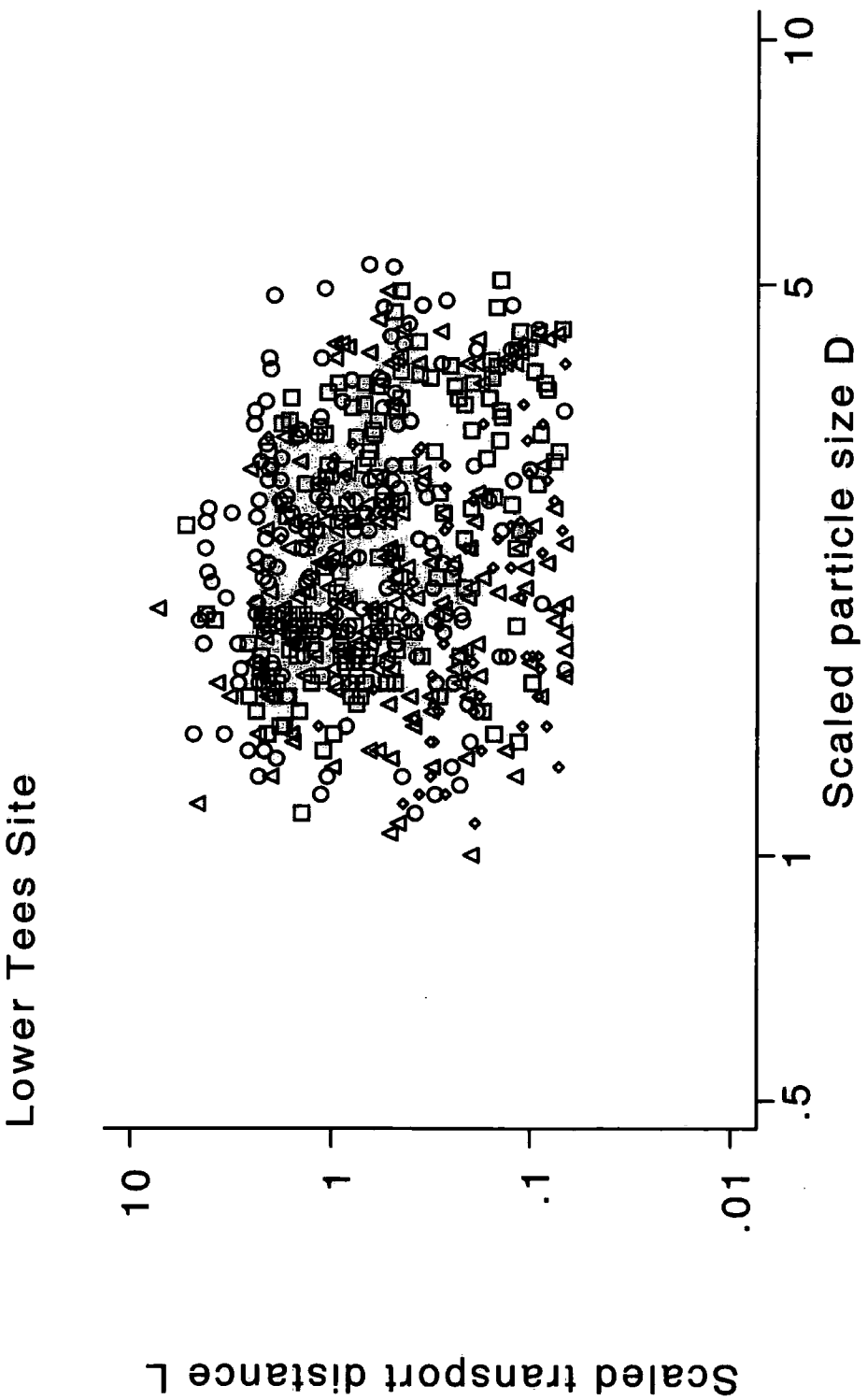

Figure 5.14c. Relationship between scaled transport distance and scaled particle size for sphere, blade, rod and disc shaped tracers for the final survey, at the Lower Tees site (O: Sphere, ◊: Blade, △: Rod, □: Disc).

dividing size by the median b axis diameter of the subsurface bed material. Distance was scaled using the mean distance of the median size group of the surface material. For instance, tracer movement data were grouped into half phi 1/2 (Ø) classes. The mean transport distance was then calculated for the half phi class containing the D_{50} surface grain-size (Table 5.7). Data plotted for the three sites, and divided into shape classes, are shown in Figure 5.14a, b and c.

Table 5. 7. Scaled distance values [D_{50} surface values]
For the three experimental sites (Church and Hassan, 1992).
Values are in (m).

Survey No:	Upper Tees	Trout Beck	Lower Tees
1	5.9	14.9	-
2	11.1	20	9.8
3	12.1	22.7	13.5
4	15	23.3	22.7
5	16.4	29.3	48.9

In general, the plots show a tremendous scatter of points. Careful examination show that particles can be differentiated by shape corresponding to different plotting zones. Spheres and rods plot towards the top right of the diagram and blades towards the bottom. Although, there is no distinct trend in the data and there is very little evidence of size-selective displacements, few clasts plot in the top right hand of the scatter suggesting larger particles are less frequently transported. This conclusion does not fully support the general relation proposed by Church and Hassan (1992). Analysis of transport distance by size show a slight tendency for size selective transport (Tables A2.1-A2.5). However, it should be remembered that the data used by Church and Hassan (1992) was highly averaged and therefore much more "collapsed".

5.4.3 Shape distribution of the total number of tracers moved and mean transport distances during the monitoring period

Figure 5.15 shows the variation in the total number of tracers moved and also their total mean transport distances for four shape classes. This generally indicates that the number of sphere and rod-shaped particles transported are greater than blade and disc-shaped particles. Furthermore the numbers tend to increase noticeably from one

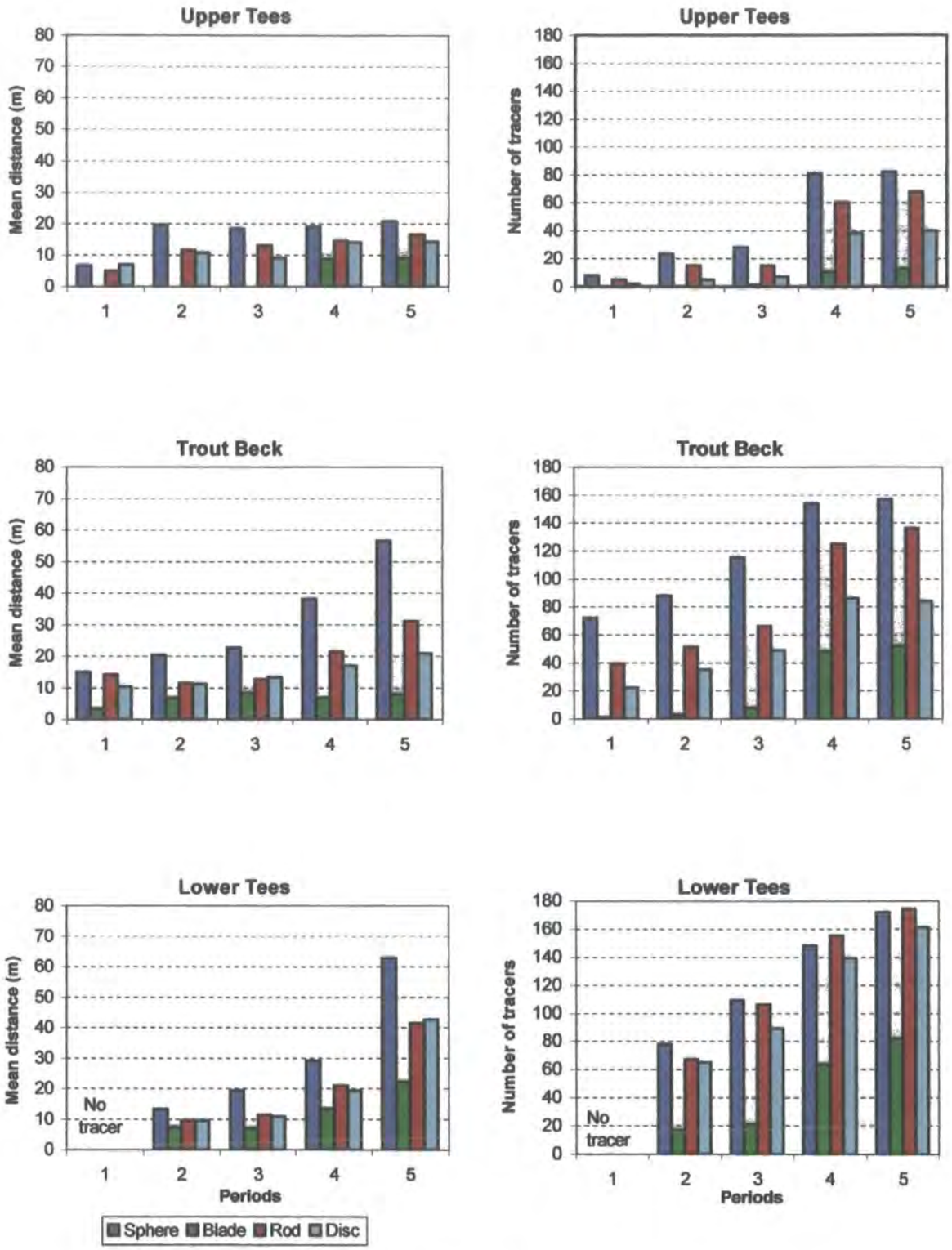

Figure 5.15 Total number of tracers moved through five survey periods and mean transport distances of four shape classes during the monitoring period at the three experimental sites.

survey to another. At the Upper Tees site and Trout Beck for each survey in decreasing order of importance the number of tracers transported in various shapes is sphere, rod, disc and blade. At Lower Tees the order is same for the surveys 1, 2 and 3 but for the surveys 4 and 5 the number of rods is slightly greater than spheres.

At each site, the number of blade-shaped particles transported are much less. In terms of total mean transport distances, Figure 5.15 shows spheres represent the greatest total mean transport distances, while blades show the least distances, except the final survey at Lower Tees where disc-shaped particles have slightly longer total mean transport distance (Figure 5.15). The total mean transport distances for the sphere, rod and disc-shaped particles tend to increase from one survey period to another at the three sites but this is not always true for blades (e.g. Upper Tees and Trout Beck). The increase in mean transport distance between surveys is noticeable greater for sphere-shaped particles than other shapes. At the Upper Tees for the first three surveys there is no movement.

5.4.4 Shape distributions of the number of tracers moved and mean transport distances for the tracers moved in period between surveys.

Figure 5.16 and Table 5.6 show variations in the total number and mean transport distances of tracers of differing shapes moved in the period between surveys (period mean transport distances) during the monitoring period and results indicate a similar pattern to the total mean transport distances. In general, there tends to be a gradual increase in both the number of particles moved and also the mean transport distances from one survey to another. At each site the majority of particles moved and the longest mean transport distances measured were in surveys 4 and 5 respectively (Figure 5.16 and Table 5.6). Figure 5.16 also shows that at the Upper Tees, differences between the mean transport distances of various shapes are smaller than at the other sites.

5.4.5 Frequency of movement of tracer clasts at the three experimental sites

Figure 5.17 shows the frequency of movement for the tracers at the three experimental reaches. A value of zero indicates no movement during the monitoring period a value of 5 indicates the tracer was recorded "as moved" after each survey. In general, tracers at Upper Tees show rather lower frequency of movement (in both different sizes and shape groups), while the Lower Tees shows the greatest frequency of

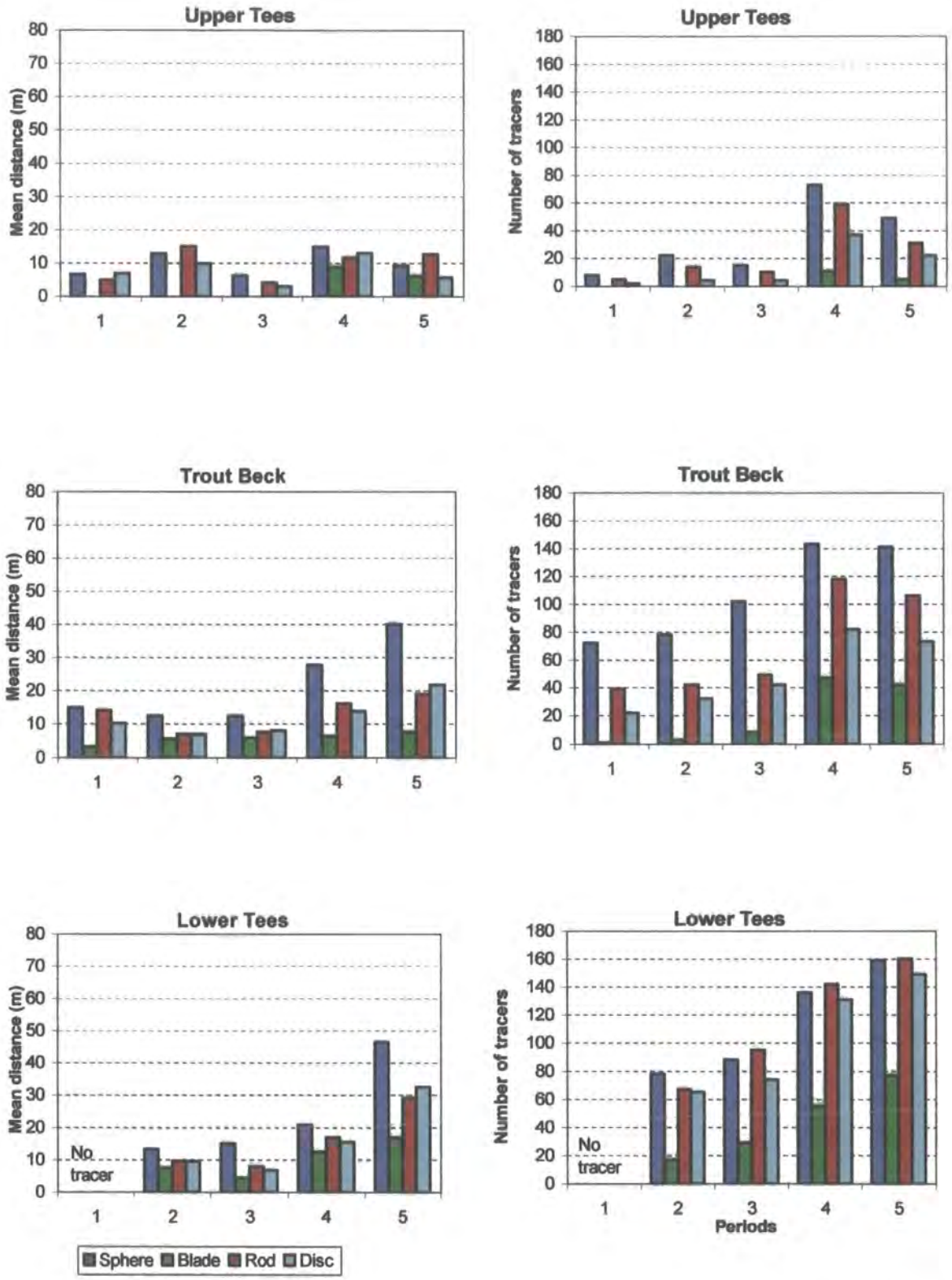

Figure 5.16 Variation in the number of tracers moved between individual periods and mean transport distances of four shape classes during the monitoring period at the three experimental sites.

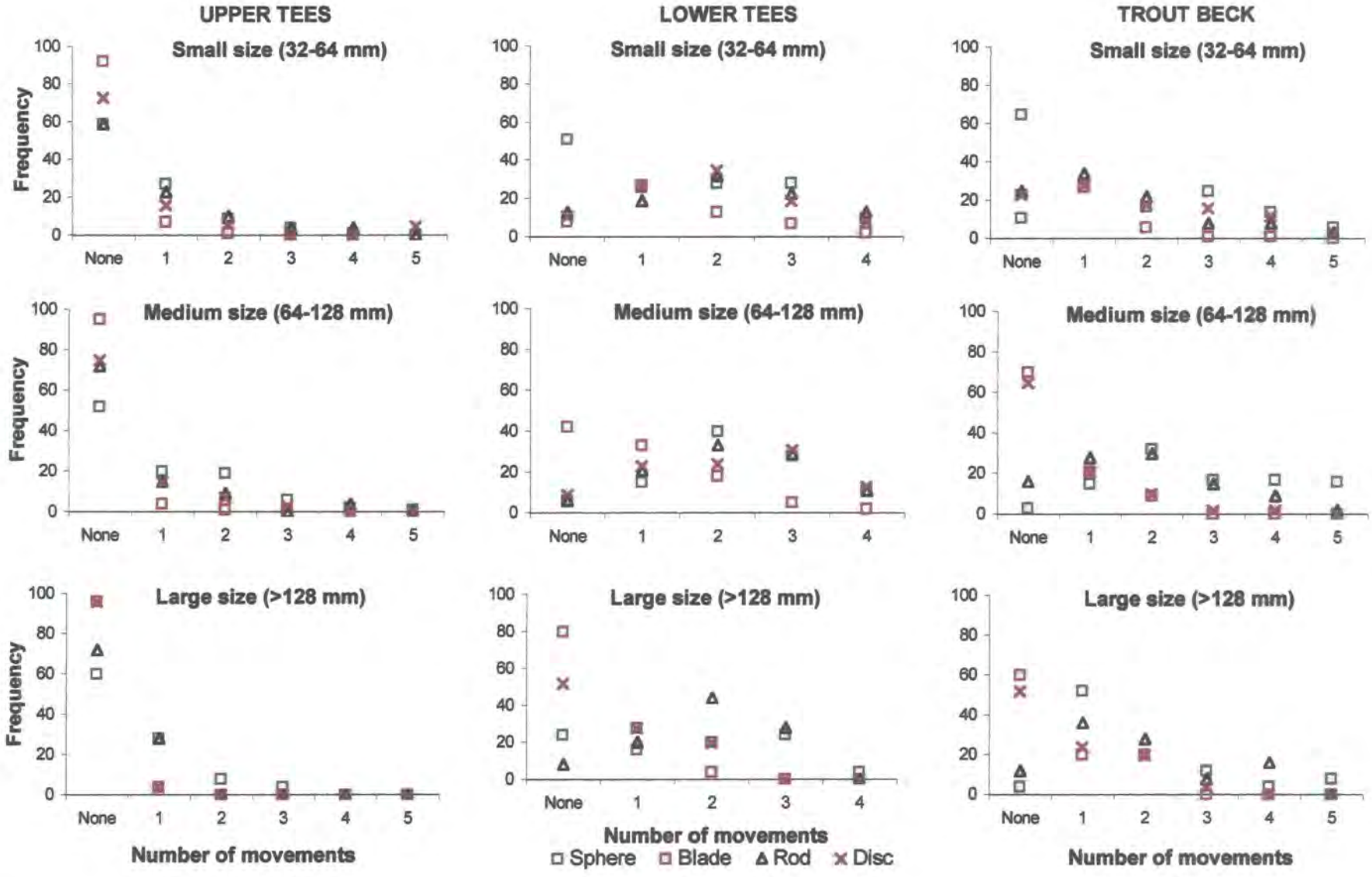

Figure 5.17 Frequency of movement for the magnetic tracers in four shapes classes and three size groups at the three experimental reaches.

movement. In terms of frequency of the number of movement for the particles of various size, Figure 5.17 indicates that, within each size group, there is a noticeable decline in total numbers as the frequency of movement increases at each site. The proportion of unmoved particles is greatest at Upper Tees.

In term of shape, Figure 5.17 indicates that there is a considerable variation in the frequency of movement in the different shape classes. Difference in particle shape appears to have greater influence on frequency of movement than particle size. Among the unmoved tracers blade and disc-shaped particles represent the greatest percentage compared to spheres and discs. In general, sphere and rod-shaped particles tend to have the greatest frequency of movement, while blades and discs constitute the least. At Upper Tees, spheres represent the greatest percentage of the particles that moved 1, 2 and 3 times. At Trout Beck for each survey number of movement for sphere and rod-shaped particles is greater than disc and blades, while blades represent the less percentage. At the Lower Tees, however, percentage of the number of discs and blades is greater for particles that have move once, while spheres and rods represent the greatest percentage in the particles that moved 2, 3, and 4 times.

5.5 STATISTICAL ANALYSES

5.5.1 Multiple regression analysis: factors affecting travel distance of tracers.

The results of regression and multiple regression analyses are presented in Tables 5.9 and 5.10. Data were analysed for each of the experimental sites separately. Table A1.15 summarises shape and size characteristics of the data used in the analysis. Some variables were Log10 transformed so that their distributions were normalised. For each of the experimental sites, correlations between tracers shape, size parameters and transport distances were calculated (Table 5.9). Several regression models were developed using the parameters, listed in Table 5.8. Model parameters were selected so that they were independent and problems of intercorrelation were avoided.

Table 5.8 Variables of size and shape used in the analyses.

Variable	Units	Formula
a-axis	mm	--
b-axis	mm	--
c-axis	mm	--
Weight	(g)	
Krumbein Roundness	--	R = (2r/a)x1000
Sphericity	--	$\sqrt[3]{bc/a^2}$

5.5.2 Correlation of distance traveled with size and shape variables

Correlation of distance travelled with size and shape variables at the three sites for each survey are presented in Table 5.9. The data were log10 transformed before each coefficient was calculated. Data from each site were analysed separately.

In general the results of regression and multiple regression analysis show similar patterns at the Lower Tees and Trout Beck sites. At the Upper Tees site correlations between the independent variables and transport distance are relatively weak due to lower transport rates (Tables 5.9). Correlation values for each of the individual parameters show that both particle a-axis and Krumbein sphericity are the most useful predictors of transport distance. The *c*-axis measurements at Lower Tees and Trout Beck sites showed no significant correlation with distance (Table 5.9).

Table 5.9 also shows that, in general, correlation between individual predictors and transport distance tends to become stronger over time. At the Upper Tees there is no statistical significant correlation between any of the variables and tracer transport distances for the first three surveys. However for the surveys 4 and 5 both sphericity and flatness show significant correlations with distance. Correlations between the independent variables and transport distance are consistently more significant at the Lower Tees and Trout Beck sites. This suggests that the influence of the predictors tend to become stronger with distance at these sites.

At each site there tends to be a negative correlation between transport distance and particle weight, flatness, *a* and *b* axes, while other parameters such as sphericity and roundness ratios show positive correlations with distance.

Tables 5.9 Correlation of distance travelled (Log transformed) with size and shape (log transformed) variables for the three experimental sites. Bold values indicate significance of 0.05 level.

	A axis	B axis	C axis	b/a ratio	c/b ratio	Cailleux Roundness	Krumbein Sphericity	Cailleux Flatness	Weight	Significant value
Upper Tees										
Survey 1	-0.183	-0.044	-0.175	0.218	-0.234	0.380	0.093	0.082	-0.118	*0.575*
Survey 2	-0.109	0.009	0.042	0.117	0.044	0.099	0.150	-0.131	-0.080	*0.376*
Survey 3	-0.240	-0.216	-0.045	0.049	0.155	0.101	0.178	-0.179	-0.249	*0.348*
Survey 4	-0.118	-0.051	0.104	0.092	0.177	0.066	**0.205**	**-0.215**	-0.042	*0.185*
Survey 5	-0.173	0.088	0.077	0.133	0.172	0.058	**0.221**	**-0.225**	-0.091	*0.181*
Lower Tees										
Survey 1	---	---	---	---	---	---	---	---	---	---
Survey 2	**-0.338**	**-0.240**	-0.076	**0.215**	0.097	**0.225**	**0.278**	**-0.221**	**-0.250**	*0.181*
Survey 3	**-0.370**	**-0.288**	-0.125	**0.208**	0.091	**0.214**	**0.226**	**-0.218**	**-0.298**	*0.148*
Survey 4	**-0.202**	**-0.176**	0.013	**0.122**	**0.182**	**0.223**	**0.223**	**-0.233**	**-0.128**	*0.115*
Survey 5	**-0.299**	**-0.180**	0.021	**0.202**	**0.180**	0.107	**0.230**	**-0.280**	**-0.176**	*0.115*
Trout Beck										
Survey 1	-0.147	-0.015	0.089	0.179	0.156	0.112	**0.257**	**-0.253**	0.055	*0.219*
Survey 2	-0.160	-0.023	0.140	**0.203**	**0.222**	0.186	**0.326**	**-0.336**	-0.044	*0.19*
Survey 3	**-0.207**	-0.087	0.110	**0.187**	**0.236**	0.149	**0.319**	**-0.336**	-0.097	*0.181*
Survey 4	**-0.360**	**-0.203**	**0.149**	**0.256**	**0.356**	**0.246**	**0.441**	**-0.464**	**-0.169**	*0.128*
Survey 5	**-0.413**	**-0.282**	0.066	**0.246**	**0.281**	**0.306**	**0.433**	**-0.379**	**-0.256**	*0.128*

These trends are expected given our knowledge of transport processes. This is because, these parameters influence particle rolling. The greater the sphericity, roundness, and c/b ratio the more particles move in a rolling mode. Flatness, weight, a and b axes of particles show significant but negative correlations with transport distance. A particle with a long axis, greater size/weight and platy-shape is expected to have greater resistance to movement. Therefore they tend to be more stable compared to particle which are light, more equant and round, or flat but light.

5.5.3 Multiple regression results

Multiple regression analyses are based on total distances transported by all moved tracers during the all monitoring period. Only moved tracers were considered for the analyses. Results (Multiple R) at Trout Beck show a greater percentage of the variation in transport distance is explained by the regression models (Table 5.10). The combination of the three independent variables that represent the greatest explanation of the variance at Trout Beck and Upper Tees are c-axis, roundness and weight with a 50.3% and 27.5% respectively. An alternative model involving *a*-axis, roundness and weight provides a similar level of explanation at the Lower Tees site (33.4%).

Overall, the results of the multiple regression analysis clearly indicate that, together with roundness and weight, particle c-axis, and sphericity (at Trout Beck and Upper Tees) have the greatest correlation with transport distance. A-axis is also in some cases well correlated with distance but b-axis showed poor correlation with distance at the three sites (Table 5.10). Although the correlation between the *c*-axis and transport distance is low, the multiple regression model shows that the *c*-axis is important along with other parameters. Although particle *c* and *a* -axes are related to particle size and are statistically independent, in terms of sediment transport, axial dimensions and shape parameters can not be isolated. As it is explained in Chapter two and also demonstrated with the Tilting table experiments, the mode of particles movement is strongly controlled by the c/b ratio of a particles, the greater the c/b ratio the more likely particle rolls. Particles with greater c/b ratio are considered either sphere or rod-shaped depending on a-axis. As a result, except for the influence of weight, which is related to size, axial dimensions (*a, b* and *c*-axes) should also be considered as part of shape parameters. In general, the level of explanation involving these models is generally low. Several others significant factors such as local flow conditions and bed roughness are not included in the models.

Table 5.10 Multiple regression analysis: factors affecting transport distance (Log 10 distance) of magnetic tracers at Lower Tees.

Parameters (Model structure)	Multiple R	F ratio	F significance	Standard Deviation	N
		Lower Tees			
Model 1: Distance: a-axis, roundness, weight	33.4	24.6	5.24E-14	0.437	590
Model 2: Distance: b-axis, roundness, weight	23.9	11.8	1.53E-07	0.450	590
Model 3: Distance: c-axis, roundness, weight	33.1	24.1	9.96E-15	0.437	590
Model 4: Distance: sphericity, roundness, weight	29.1	18.1	3.12E-11	0.444	590
		Trout Beck			
Model 1: Distance: a-axis, roundness, weight	44.6	35.1	2.48E-20	0.464	429
Model 2: Distance: b-axis, roundness, weight	42.4	31.3	3.27E-18	0.469	429
Model 3: Distance: c-axis, roundness, weight	50.3	48.0	9.87E-27	0.447	429
Model 4: Distance: sphericity, roundness, weight	49.9	44.7	3.78E-25	0.451	429
		Upper Tees			
Model 1: Distance: a-axis, roundness, weight	21.4	3.2	0.025	0.892	203
Model 2: Distance: b-axis, roundness, weight	11.5	0.9	0.442	0.907	203
Model 3: Distance: c-axis, roundness, weight	27.5	5.4	0.001	0.878	203
Model 4: Distance: sphericity, roundness, weight	25.0	4.4	0.005	0.885	203

5.6 MISSING AND BURIED TRACERS

There were no tracers recorded as missing during survey periods 1 and 2 at the three experimental sites due to low movement rates. Most of the particles moved remained close to the starting lines and on the surface of the bed.

5.6.1 Third and fourth surveys

Up to survey 3, a total of, 133 particles could not be located (Lower Tees, 98 and Trout Beck, 35). No particles were observed to be missing at Upper Tees site. Considering the two sites, there tends to be a noticeable increase in the numbers missing with decreasing particle size: small size group (99), medium size (34) but there are no missing stones in the large sizes.

Up to survey 3, a total of, 97 particles were found to be buried at the Trout Beck site (54) and Lower Tees (43) with a mean depth of burial the same at both sites (8.2 cm). At each site, there tends to be an inverse relation between the particle size and the number of buried stones. The majority of the buried particles are in the small size group (53%) which tends to decrease in the medium (35.7%) and large size groups (11.2%).

Up to survey 4, the total number of tracers that could not be relocated has risen to 328 at the three sites, 86 at Upper Tees, 101 Trout Beck and 141 Lower Tees. The greatest percentage of the missing particles and the greatest numbers of buried particles were in small size group and there tends to be a noticeable decrease with size. In terms of shape, the number of missing particles in the rod-shaped class is always less than the other shapes.

Altogether 120 particles were found to have been buried at various depths at the three experimental sites. In decreasing order the number of burial particles is 83 at Lower Tees, 33 at Trout Beck and 4 at Upper Tees. The mean burial depths for the Upper Tees, Trout Beck and the Lower Tees sites were 7.5, 5.2 and 6.4 cm respectively. At the Lower Tees site and at Trout Beck the number of buried particles tend to be greatest in the small and medium size groups, while at the Upper Tees there were only 4 buried particles (three of medium size and one of large size).

5.6.2 Final Survey

Altogether 474 magnetic tracers, which represent 17.5 % of the total tracers (2700) at the three sites, had disappeared during the monitoring period. The percentage of the missing stones was 10.8% at the Upper Tees, 22.9% at Trout Beck and 19.0% at the Lower Tees. The small disappearance rate at Upper Tees may be the result of the low number and shorter distances of tracer movement. On the other hand, the greater loss at Trout Beck and the Lower Tees may be the result of deeper-burial and greater and longer transport distances. Over the entire period and for the three sites combined, the percentage of missing particles in the small size group, is much greater than the medium and large size groups (73.2%). A similar distribution is also true for each experimental site; %75.3 at Upper Tees, %70.5 at Lower Tees and %73.8 (Table 5.11).

In terms of shape, the number of missing particles is greatest in the blade and disc-shaped categories than for spheres and rods (150 blade, 132 in discs, 121 in sphere and 70 in rods). Decreasing order of loss at the Trout Beck site is 67 blades, 59 discs, 48 spheres and 32 rods, while the order at the Lower Tees is 55 blades, 43 spheres, 37 discs and 36 rods. At the Upper Tees site, rods represent the smallest number of missing (3), while the distribution is 28, 30 and 36 for blade, sphere and disc-shaped tracers respectively. (Table 5.11).

In total, 241 magnetic tracers were found to have been buried (10 Trout Beck, 110 Trout Beck and 121 Lower Tees). There is a similar pattern of distribution to the previous surveys in terms of the number of buried particles and also their mean depth. The maximum burial depths are 22cm, 20cm and 10cm at the Trout Beck, Lower Tees and the Upper Tees sites respectively. The number of buried tracer increases with decreasing size at each site (Table 5.12 and Figure 5.18). In general numbers buried tend to increase in the finer sized tracers (133 small, 100 medium and 10 large size). During the whole monitoring period, the Lower Tees shows the greatest number of particles buried (121), while there were 110 buried particles at Trout Beck and only 10 at the Upper Tees. Table 5.12 also shows that there tends to be a slight increase in the mean depth of particles with particle size. In increasing rank, at the Lower Tees, is 6.3 cm, 6.4 cm and 8.1 cm for small, medium and large size group respectively. There is a similar pattern at the Trout Beck (5.2 cm small, 6.5 cm medium and 8.3 cm large size groups). A slight positive relation exist between depth of burial and particle sphericity at the Lower Tees and the Trout Beck sites (Figure 5.18).

Table 5.11 Number of missing particles during the entire period of 24 September 1998 to 6 July 1999 at Upper Tees, Lower Tees and Trout Beck and the three sites combined.

	Upper Tees				Lower Tees				Trout Beck				All Sites		
	S	**M**	**L**	**All**	**S**	**M**	**L**	**All**	**S**	**M**	**L**	**All**	**S**	**M**	**L**
Sphere	21	9	0	30	33	10	0	43	37	11	0	48	91	30	0
Blade	19	9	0	28	38	16	1	55	38	25	4	67	95	50	5
Rod	3	0	0	3	23	13	0	36	27	5	0	32	53	18	0
Disc	30	6	0	36	28	7	2	37	50	8	1	59	108	21	3
Total	73	24	0	97	122	46	3	171	152	49	5	206	347	119	8

Table 5.12 Number of buried particles and mean depth of burial (cm) at the three experimental reaches during the period of 24 September 1998 to July 1999. Note: First values in each column represent the number of buried particles and the second values represent the mean burial depth.

	Trout Beck				Lower Tees				Trout Beck				All sites			
	S	**M**	**L**	**All**	**S**	**M**	**L**	**All**	**S**	**M**	**L**	**All**	**S**	**M**	**L**	**All**
Sphere	3-5.0	2-7.5	1-5.0	6-6.0	18-8.6	23-8.4	1-10	42-8.6	29-8.7	18-6.9	2-10	49-8.1	50-8.4	44-7.7	4-8.8	98-8.1
Blade	0	0	0	0	8-7.3	13-8.1	0	21-7.8	12-5.8	2-4.5	0	14-5.6	18-6.4	15-7.6	0-0.0	33-6.9
Rod	1-5.0	2-5.0	0	3-5.0	11-7.8	12-8.6	1-6.0	24-8.1	11-6.2	10-9.1	1-5.0	22-7.4	22-7.0	24-8.5	2-5.5	48-7.7
Disc	0	1-10	0	1-10	22-8.9	11-10	1-10.0	34-9.3	18-6.5	6-5.5	1-10	25-6.4	39-7.8	18-8.5	2-10	59-8.1
Total/ average	4-5.0	5-7.5	1-5.0	10-7.0	59-6.3	59-6.4	3-8.1	121-8.2	70-5.2	36-6.5	4-8.3	110-6.9	129-7.7	101-8.0	8-8.3	238-7.8

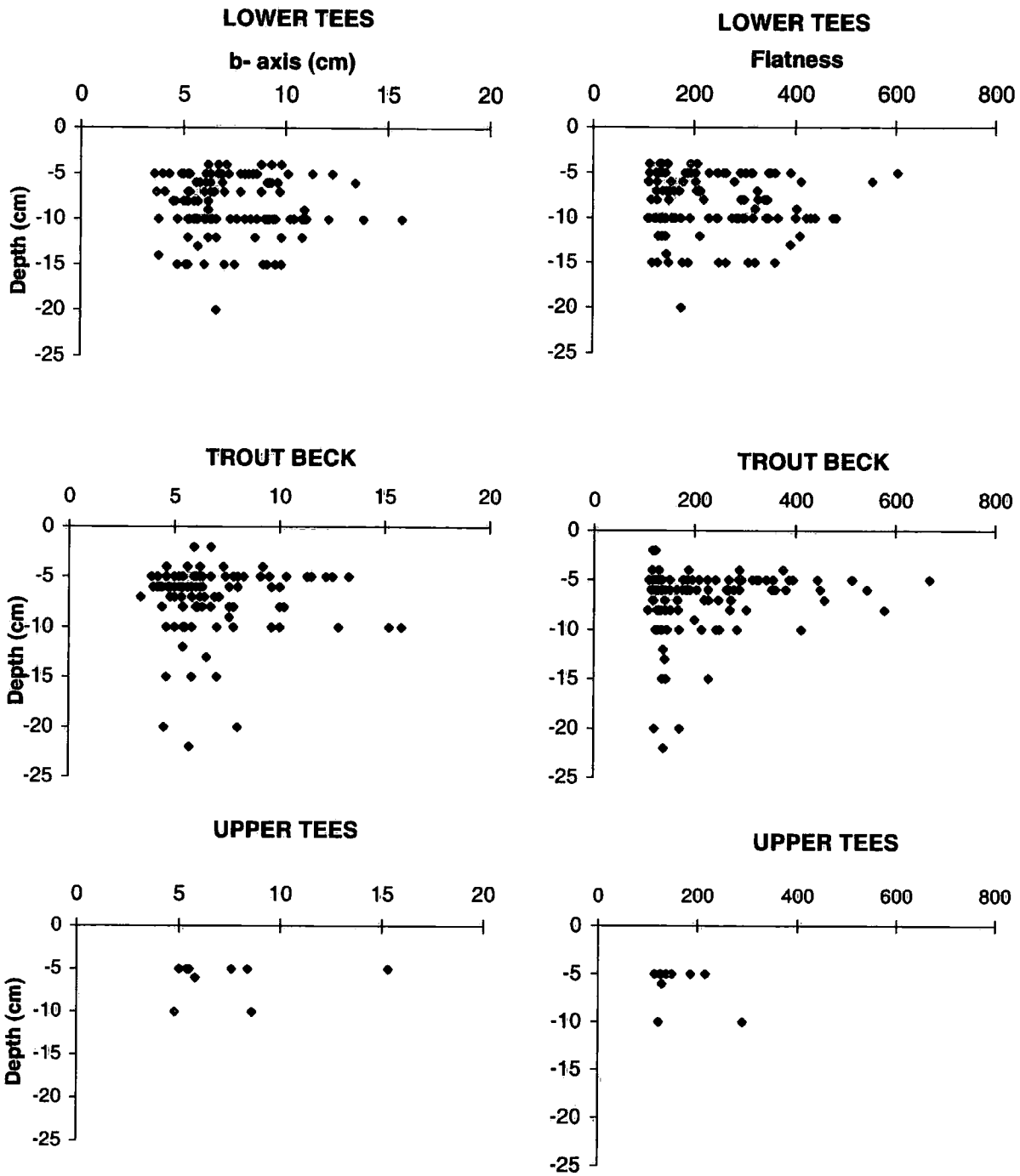

Figure 5.18 Relationship between tracer flatness, b-axis and burial depths, at the three experimental sites for the final survey.

5.7 SPATIAL DISTRIBUTION OF MAGNETIC TRACERS IN RIVER CHANNELS AT THE TROUT BECK, UPPER TEES AND LOWER TEES SITES

Figures 5.19, 5.20 and 5.21 show the spatial distribution of magnetic tracers for different survey periods at the three experimental reaches. These surveys have been selected to show the general patterns of the tracers. Full details of survey dates and travel distances can be found in the previous sections of this chapter. Results are plotted in terms of shape class of the tracer particles and size. Only particles, which have moved greater than 3 meters beyond the start line, are considered. This corresponds to approximately 23% of Upper Tees tracers, 65% of Lower Tees tracers and 48% of the Trout Beck tracers. Originally 900 tracers were introduced at each site. The large numbers of tracers involved allow detailed appreciation of the movement patterns. Previous studies (e.g. Laronne and Duncan, 1992; Hassan *et al.*, 1999) often do not include enough tracers for such patterns to be clearly described.

Comparison of the general spatial patterns of tracer distribution at the three experimental sites shows tracers at the Trout Beck and the Lower Tees sites are distributed more extensively than at the Upper Tees site. However, tracer densities tend to decrease with distance transported at the Trout Beck and the Lower Tees sites, while at the Upper Tees site the distribution is more patchy.

Between the start line and section 3 the majority of the tracers are distributed fairly evenly across the channels both at the Trout Beck and Lower Tees sites. Beyond Section 3 the tracers become concentrated along the line of the main thalweg which is close to the right bank at both sites. Comparison with the channel cross-section geometry (Figure 4.9) shows that the dispersion of the tracers at the Trout Beck is clearly concentrated in the deeper channel sections (Figure 5.19, between Sections 3 and 8). At the Lower Tees site tracers are concentrated towards the right bank (Figure 5.20). However, the cause of this spatial distribution is rather different than for Trout Beck. This is because, during higher flows the main current between sections 2 and 3 is diverted from left bank towards the right bank. Tracer distributions beyond section 9 at Trout Beck and beyond section 7 at the Lower Tees site tend to be more dispersed due to shallower depths as the channel widths increase (Figure 5.19 and 5.20). A closer examination shows that, for the final survey, widths of the tracers distribution across the channel at the Trout Beck site are approximately 7m between sections 2 and 3, less than

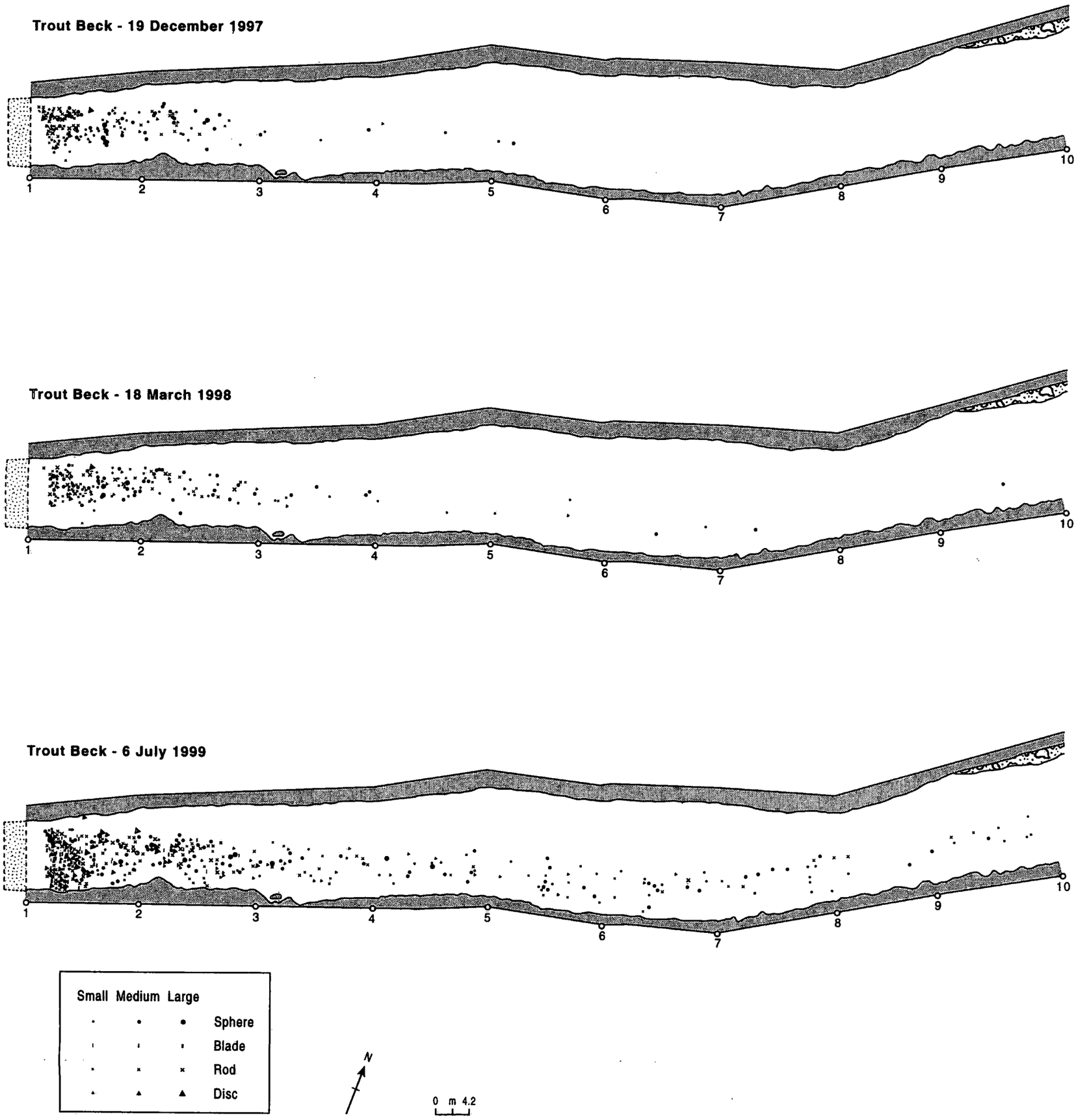

Figure 5.19 Spatial distribution of magnetic tracers at the Trout Beck site (The shadow box is the "seeded" zone where tracers were introduced. Symbols show the size and shape of individual tracer clasts).

Lower Tees - 1 August 1998

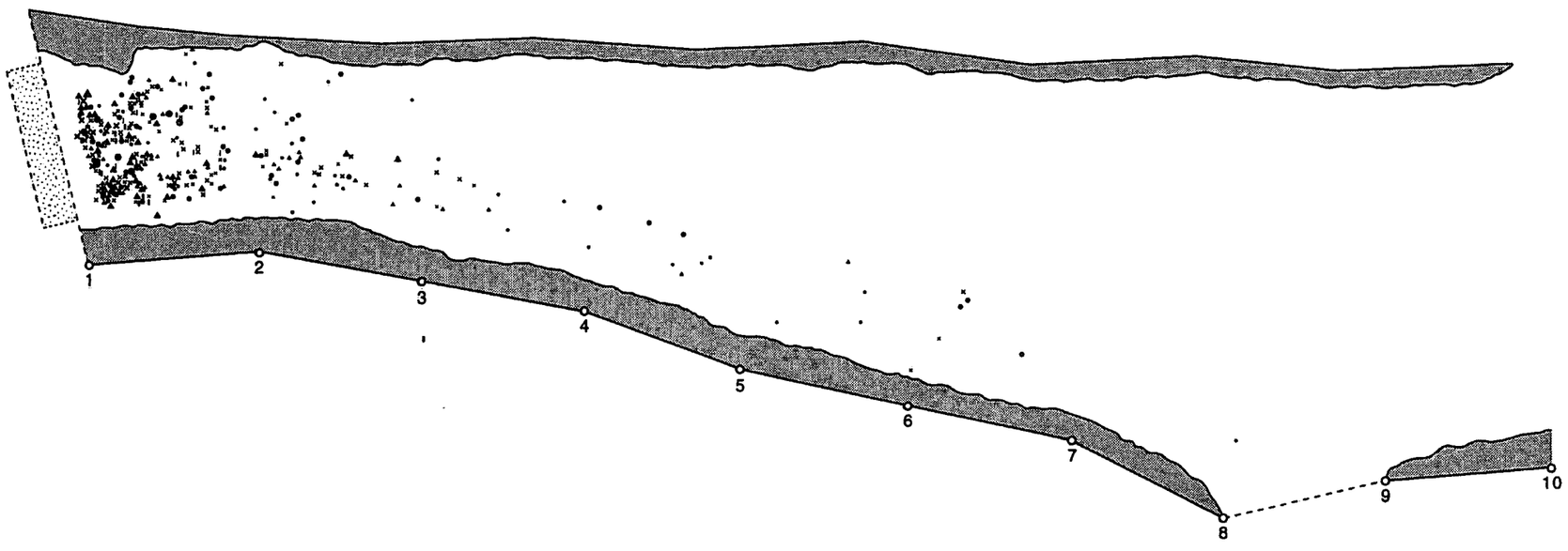

Lower Tees - 6 July 1999

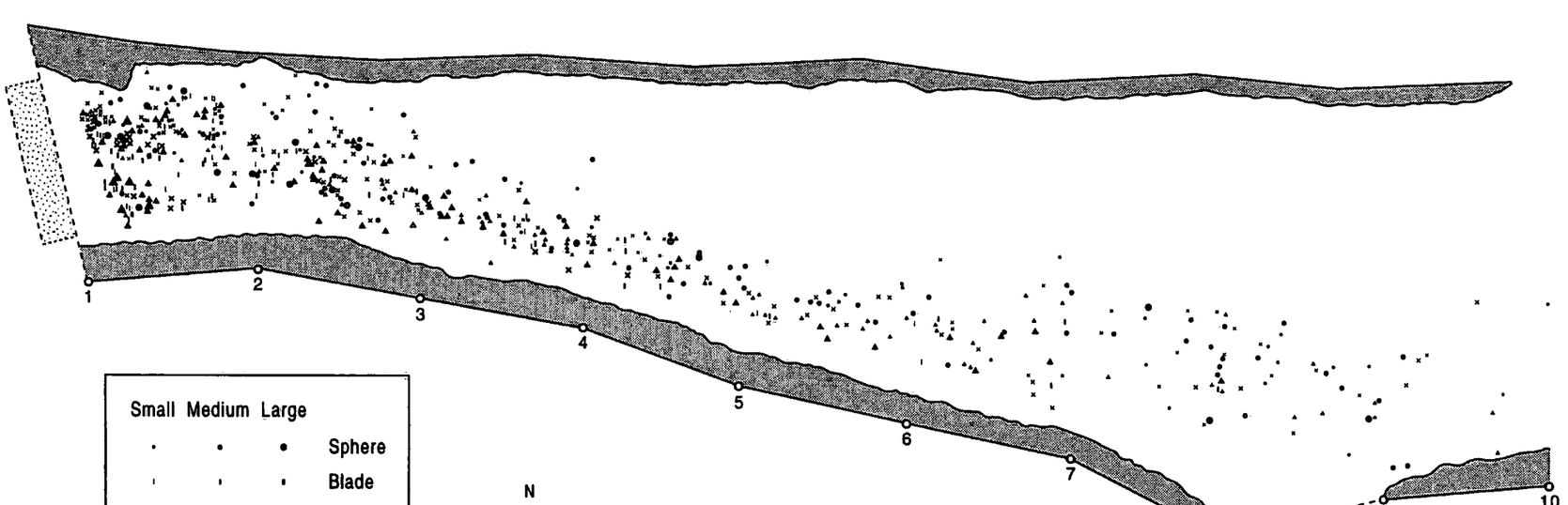

Figure 5.20 Spatial distribution of magnetic tracers at the Lower Tees site (The shadow box is the "seeded" zone where tracers were introduced. Symbols show the size and shape of individual tracer clasts).

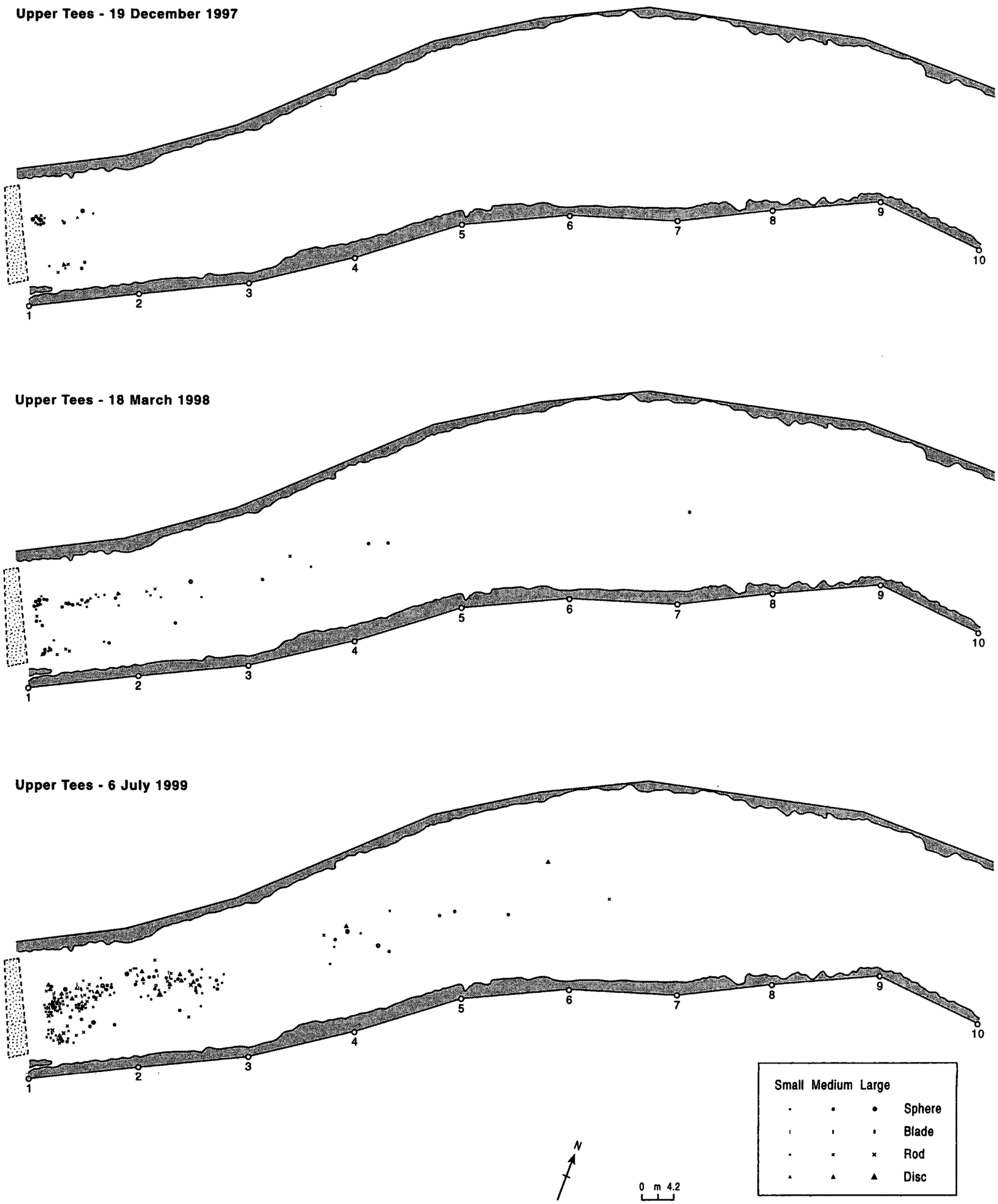

Figure 5.21 Spatial distribution of magnetic tracers at the Upper Tees site (The shadow box is the "seeded" zone where tracers were introduced. Symbols show the size and shape of individual tracer clasts).

4 m at section 4, 5m between sections 5 and 6, around 3m between sections 6 and 7, and 6m at section 8. Lower Tees tracers reflect a similar pattern to Trout Beck but the distribution at each section is noticeable wider. For example, in common with Trout Beck, the distribution is even across the channel between sections 2 and 3, but beyond section 3, it tend to be thinner and more sparse. Beyond section 3, there are hardly any tracers along the left bank. Between sections 3 and 4, average tracers width is approximately 8m, between sections 4 and 5 it is 6.5m, at section 6 it reaches 9m and between sections 7, 8 and 9 distribution is relatively sparse and average width for the distribution increases up to 12m.

Compared to the other sites, the tracer distribution is more patchy at the Upper Tees site. However, Figure 5.19 shows that for the first survey period (26 November-19 December 1997) there were only 16 tracer movements and all of them were distributed between three meters of the starting line and section 1. For the second survey period (19-December 1997-18 March 1998), although the maximum extent of distribution increased up to section 5, the majority of tracers were concentrated below section 2. The final survey shows two main groups of tracer deposition, one between starting line and section 2 and the other is between sections 2 and 3. There are no tracers between sites 3 and 4. Although there are some tracers beyond Section 3 the density of tracers declines noticeably and there are no tracers beyond section 7. In contrast to the other sites the main thalweg at the Upper Tees is close to the centre of the channel.

In general, the uneven distributions of the tracers across the channel suggest that bedload transport at the three experimental sites is rather intermittent and the whole bed is quite stable. In other words, tracers are moving over a fairly 'static' bed.

In terms of size, it is clear that there is preferential movement of the small and medium size classes. Although some large particles moved, the majority of the transport is confined to the first 30 metres downstream (Figures 5.19, 5.20 and 5.21). The general pattern, at the three experimental sites, shows a decrease in the frequency of movement with distance down the channel. In terms of shape Figures 5.19, 5.20 and 5.21 clearly show that spheres-and rods-shaped particles are transported by far the greatest distance. Discs show a lesser degree of transport compared to spheres and rods and blade-shaped particles appear to have moved the shortest distances and in the least numbers. Indeed, Figure 5.19, 5.20 and 5.21 clearly show that there is a significant decrease in the number of disc and blade-shaped tracers with distance downstream at each of the experimental sites.

5.7.1 The distribution of tracer displacement at the Upper Tees, Lower Tees and Trout Beck sites.

Figure 5.22 shows tracer displacements for each site after each survey. Data are scaled by dividing the distance moved by each individual particle in each event by the mean distance of each event. Histogram classes correspond to 0.25 intervals of the mean. Total frequencies are shown to convey the different magnitude of tracer movements between surveys. This method of plotting is similar to Hassan and Church's (1992). Figure 5.22 clearly shows the data are highly skewed. Event distributions are fairly irregular with some secondary peaks and very long tails with some particles moving up to 8 times the mean.

The form of these distributions has prompted some workers (e.g. Hassan and Church, 1992) to fit Gamma or Einstein-Hubbell-Sayre models to the observed data. Generally such models fit the distribution reasonably well for small displacements. However for larger displacements, where morphological elements in the channel (bars, bends, etc.) start to influence sedimentation patterns, the models tend to become unstable.

Figure 5.23 shows three graphs that demonstrate the goodness of fit a simple Gamma model to the observed displacement data. These Gamma quartile-quartile plots have been used previously to demonstrate the applicability of this type of model to observed data (Cox, 1992). All three plots show some correspondence with gamma model. However beyond a certain distance the model fit is poor. The explanation of this is that over greater distances towards the tail of the distribution, where tracers are fewer, spatial sorting exerts a stronger influence. For example at the Upper Tees site beyond 60 m the model fit is poor at the Lower Tees site, the model fit is better over a larger range of displacements but eventually at around 120m the pattern starts to breaks down.

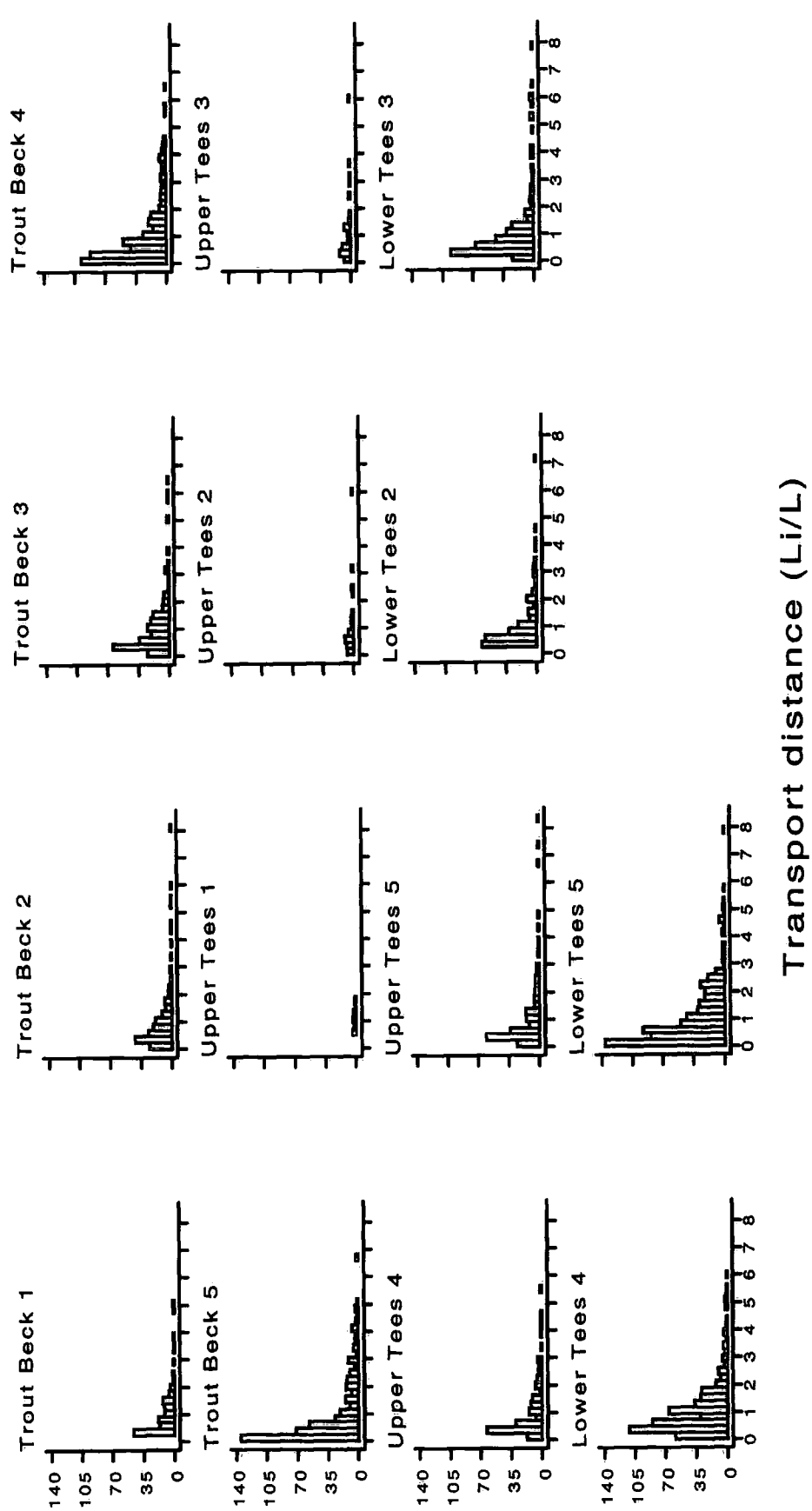

Figure 5.22 Distributions of tracer displacement for the five survey periods at the Upper Tees, Lower Tees and the Trout Beck sites.

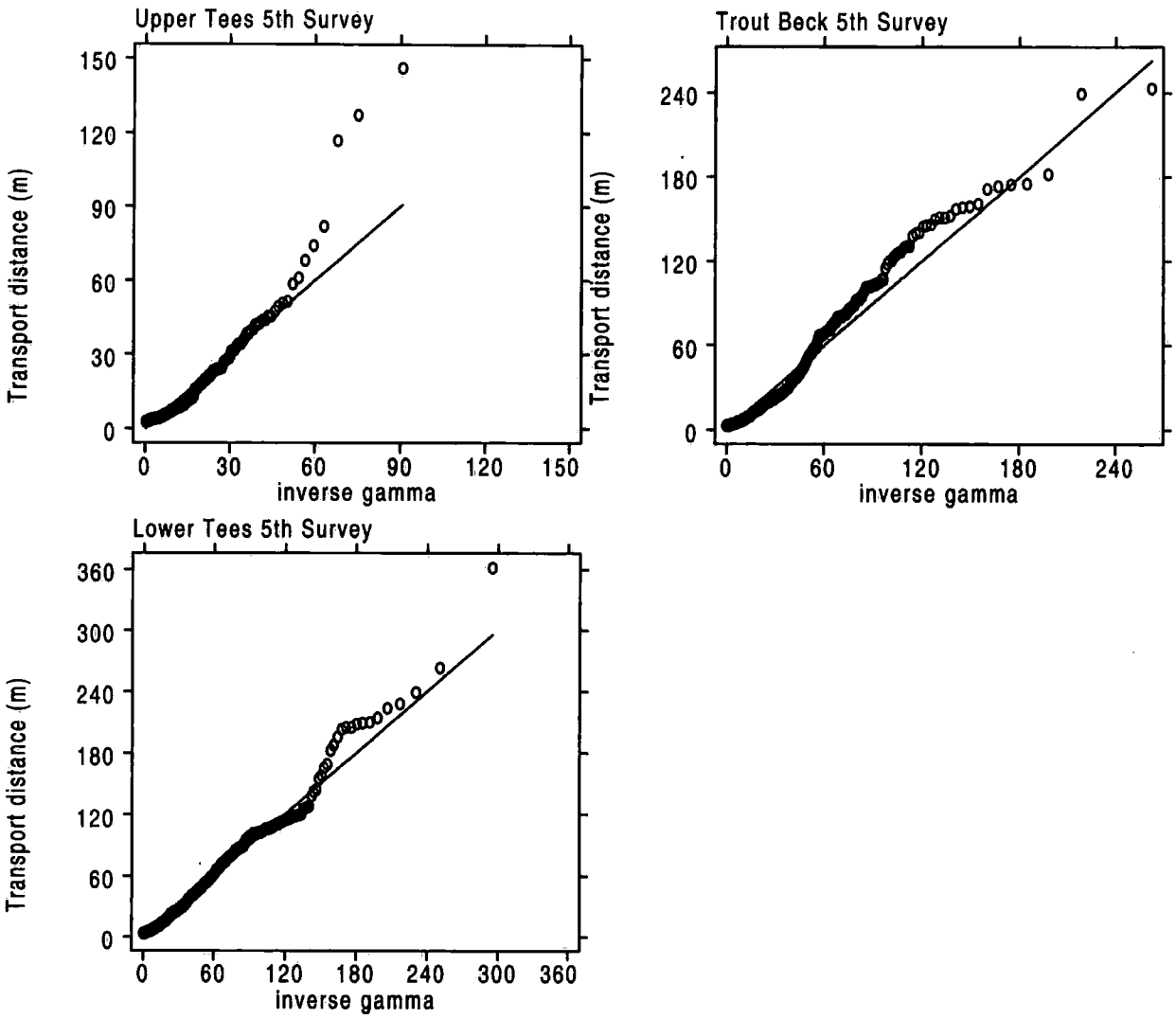

Figure 5.23 Goodness of fit of a simple Gamma model to the observed displacement data for the Upper Tees, Lower Tees and the Trout Beck sites. Final survey results.

5.8 COMPARISON OF THE SIZE AND SHAPE CHARACTERISTICS OF TROUT BECK TRAPPED (TRANSPORTED) BEDLOAD AND RIVER SAMPLED BED MATERIAL

In the experimental reaches bed material is coarse and poorly sorted in size and shape. Therefore, shape characteristics of the natural bed material are assumed to be somehow different than the magnetic tracers used for the field experiments. In terms of size, small size bedload is expected to be transported selectively compared to larger size coarse material. Spheres and rod-like particles are also assumed to be transported more easily. In order to test these hypotheses the nature of trapped bedload was compared with surface bed material sampled in the Trout Beck reach. The bed material is generally similar upstream and downstream of the Trout Beck weir which acts as a partial bedload trap (Warburton and Evans, 1998). However, the trap is not 100 % efficient so some finer components of the bedload are assumed to pass through. Thus, because of this limitation grain-size distributions are biased. Bedload was sampled twice, on two different occasions, 20 December 1997 and 30 August 1999, from behind the weir. Bulk samples of 97.6 kg and 90.4 kg were collected from the centre of the stilling pond.

Table 5.13 Mean size and shape properties of Trout Beck trapped bedload and sampled (five samples) surface bed material.

	A axis	B axis	C axis	Radius of curvature	b/a	c/b	Cailleux Round Ness	Krumbein Sphericity	Cailleux Flatness	Mean weight (g)
Bed material	9.6	7.0	4.0	0.8	0.74	0.60	188.6	0.67	237.3	640.5
Trap sample 1	7.1	5.3	3.3	0.8	0.77	0.64	221.8	0.71	202.3	218.0
Trap sample 2	7.0	5.3	3.2	0.8	0.77	0.62	242.4	0.70	230.2	267.2

Table 5.13 compares the mean size and shape characteristics of trapped bedload and bed material sampled (5 samples) from the Trout Beck reach. Results show the sampled bed material is greater in size, and more angular than the trapped bedload. The mean values of a, b and c axes, weight of the bed material are greater than the trapped-bedload. On the other hand, compared to sampled bed material, roundness and sphericity of the trapped-bedload tend to be greater (Table 5.13). Figure 5.24 shows

normal and cumulative percentage distributions of bed material and trapped bedload. In the transported material most of the particles are in the smaller size range. For example, 73.8 % of material is greater than 64 mm in the bed material, while it is only 56.3 % for Trap sample 1, 57.3 % for Trap sample 2. However, D_{50} sizes are very similar.

Statistical comparison of size and shape characteristics of bed material and trapped bedload are shown in Table 5.14. This clearly demonstrates that, within each shape class, there are statistical significant differences between weight and the a, b, and c axes of particles between the trapped bedload and sampled bed material. Indeed, in all shape class, particles in the trapped-bedload are lighter in weight and also smaller in size (a, b, and c axes) than the sampled bed material (Table 5.13).

Table 5.14 Statistical comparison of mean size and shape characteristics of bed material of Trout Beck with bedload trapped at the same site.

Parameters	Sphere	Blade	Rod	Disc
a-axis	**-4.00**	**-6.00**	-1.65	**-6.01**
b-axis	**-3.59**	**-6.27**	-2.02	**-5.89**
c-axis	**-3.16**	**-4.39**	**-2.30**	**-4.31**
Radius	-0.81	-0.94	0.01	-0.77
b/a ratio	**2.80**	-0.65	0.29	1.70
c/b ratio	1.75	0.90	-0.30	1.56
Roundness	1.53	1.48	0.28	**3.88**
Sphericity	**3.37**	0.39	0.13	**2.38**
Flatness	**-2.67**	-1.10	0.77	-1.62
Weight	**-3.12**	**-4.61**	**-2.98**	**-4.45**

(The critical values of 'T' at the 0.05 significant level is 1.97.The values shown in bold indicate a statistical significant difference between the compared parameters)

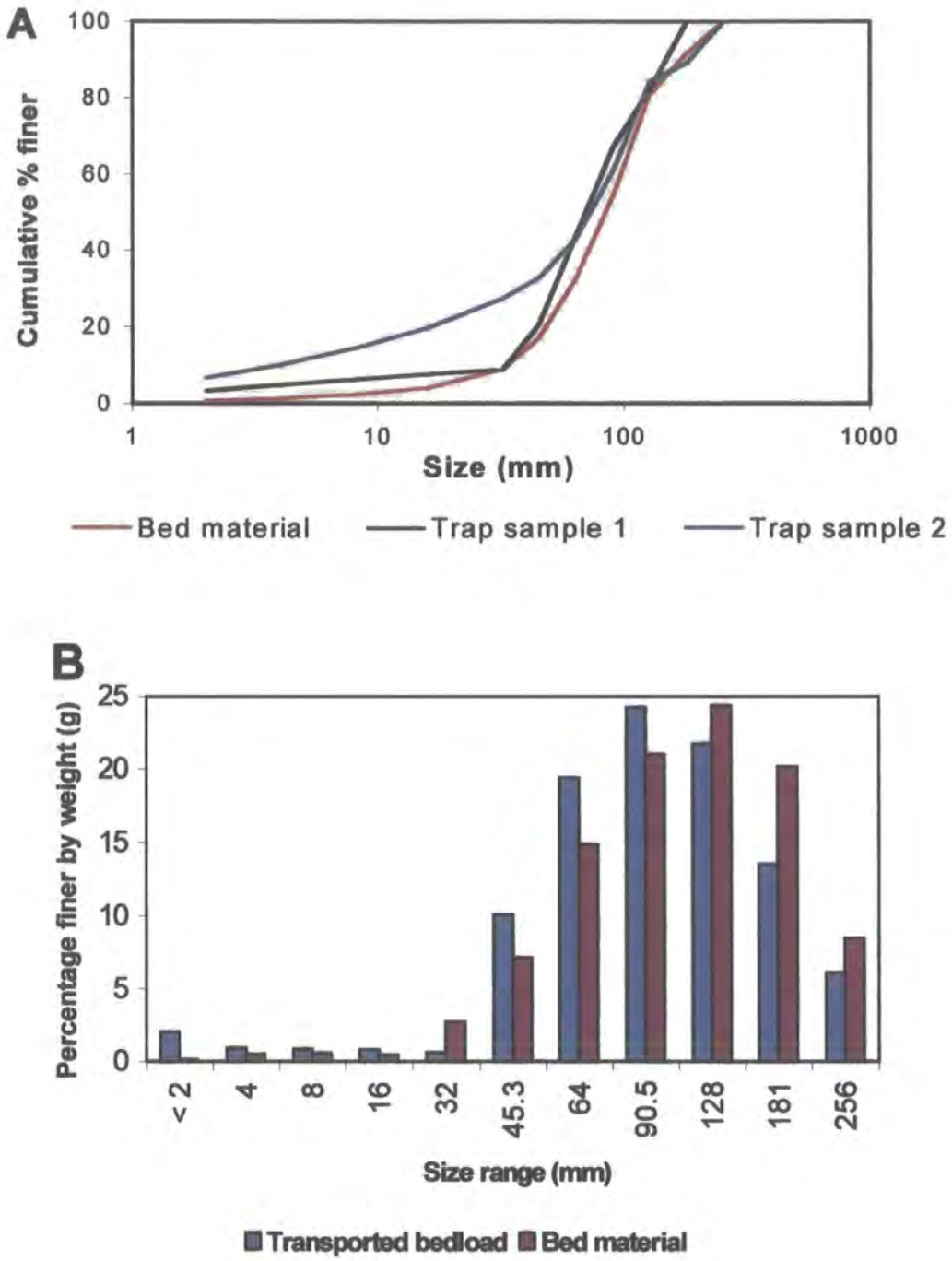

Figure 5.24 Cumulative percentage (A) and normal size distributions (*by weight*) of sampled-bed material and trapped-bedload (B) at Trout Beck (size indicated = upper limit of class; e.g. 4 indicates 2-4 mm size range).

5.8.1 Shape

Figure 5.25 and Table 5.15 show particle shape distributions of trapped bedload and sampled bed material in the monitoring reach. Although discs-shaped particles dominate the shape distribution both in the bed material and trapped-bedload, the frequency of sphere-shaped particles in the trapped material is noticeable greater than the bed material. Table 5.15 and Figure 5.25 C also suggest that regardless of size, blade and rod-shaped particles are under-represented in the trapped material. A similar, but less marked, tendency is also evident for discs.

Table 5.15 Shape distributions of the trapped-bedload and sampled bed material at Trout Beck

Shape classes	Bed material	Trap 1	Trap 2
Sphere	21.9	31.2	32.1
Blade	15.4	9.8	10.4
Rod	15.7	13.9	11.6
Disc	47.0	45.1	45.8

Table 5.16 compares the shape of transported particles and reach material by size category and indicates that disc-shaped particles are most important in each size group and become increasingly dominant with greater size. It also shows that rods, spheres and blades are more frequent than discs in the small and medium size categories. As particle size increases, the number of particles in each shapes class decrease both in the bed material and also in transported material. Comparison of bed material and trapped material indicates that spheres are over-represented in the small and medium size group. Disc-shaped particles, on the other hand, tend to be over-represented in the larger, and to some extend, in the medium size groups, while they are under-represented in the smaller size ranges (Table 5.15).

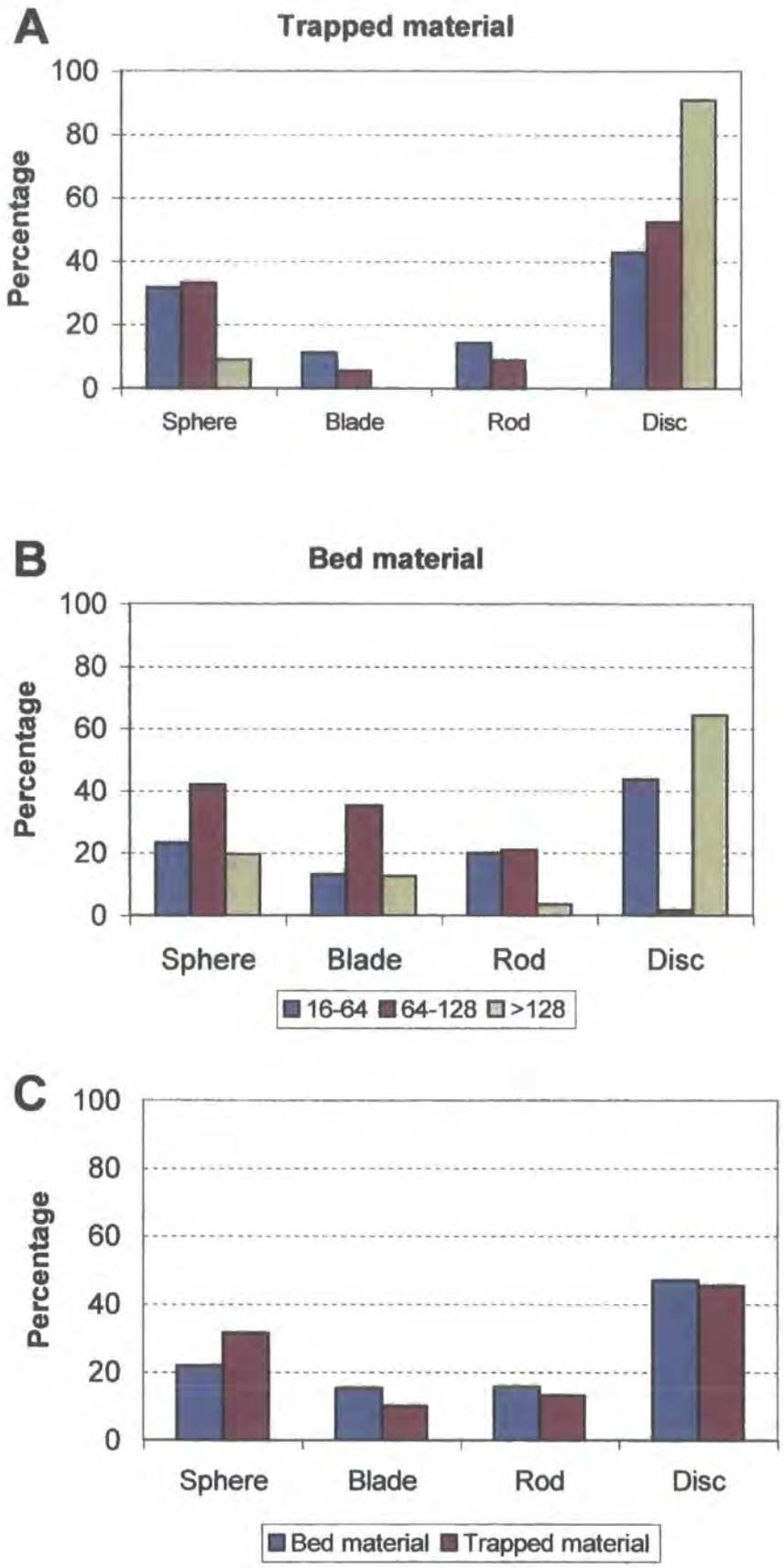

Figure 5.25 Shape distributions of sampled bed material and trapped bedload in three size groups and the three size groups combined at the Trout Beck site.

Table 5.16 Size-frequency distributions of trapped material and bed material in three size groups and four shape classes at Trout Beck

Trapped- material					Bed material				
Size (mm)	16-64	64-128	>128	Total	Size (mm)	16-64	64-128	>128	Total
Sphere	166 (31.6)	41 (33.1)	1 (9.1)	208	Sphere	95 (23.2	50 (22.3)	11 (19.6)	156
Blade	59 (11.2)	7 (5.6)	0 (0.0)	66	Blade	54 (13.2)	42 (18.8)	7 (12.5)	103
Rod	75 (14.3)	11 (8.9)	0 (0.0)	86	Rod	82 (20.0)	25 (11.2)	2 (3.6)	109
Disc	225 (42.9)	65 (52.4)	10 (90.9)	300	Disc	179 (43.7)	107 (47.8)	36 (64.3)	322
Total	525	124	11	660	Total	410	224	56	690

Note: Values in brackets show percentage of distribution

Table 5.17 Mean roundness, sphericity, and flatness in different size class of trapped material and bed material at Trout Beck.

	Trapped material			Bed material		
Size (mm)	16-64	64-128	>128	16-64	64-128	>128
Roundness	235	211	170	207	171	147
Sphericity	0.70	0.72	0.68	0.67	0.67	0.68
Flatness	212	208	321	224	247	261

Table 5.17 summarises mean roundness, sphericity and flatness of transported and bed material in 16-64, 64-128 and >128 mm size groups at Trout Beck. Mean roundness values of trapped-material in each size group tend to be higher than the bed material. There tends to be a decrease in roundness with size both in the transported material and bed material. Mean sphericity values for all size categories are low for both transported material bed material as compared to magnetic tracers. However, Table 5.17 shows that mean sphericities of transported particles within in each size group tend to be greater than those of the bed material. Table 5.17 shows that, except for the large size group, mean flatness of trapped particles in the small and medium size groups is slightly lower

than the bed material. There is no consistent variation of flatness with size in the transported material, while in the bed material particle flatness increases slightly with size.

Table 5.14 shows that there is no statistical significant difference in the roundness of sphere, blade and rod-like particles between the trapped bedload and the sampled bed material. Disc-like particles in the trapped bedload are more round and spherical than bed material. Sphere-like particles in the trapped bedload are more spherical compared to the bed material, while there is no statistical significant differences between sphericity of blade and rod-like-particles of the trapped bedload and the sampled bedload. Overall comparison of trapped bedload and sampled bed material suggests that particles in the trapped bedload are more spherical, and rounded (sphere and disc-like particles), lower in weight and smaller in size (for each shape class) when compared to the bed material (Table 5.14).

5.8.2 Comparison of trapped transported material, resident material and magnetic tracers

Table 5.18 shows that, in the trapped material the majority of particles (almost 80%) fell in less than 64mm size category, while in the bed material the distribution is more even.

In terms of shape, the number of transported magnetic tracers are greater in number and moved the longest mean transport distances in the sphere class. In the trapped-material, spheres are also over-represented compared to the sampled bed material.

In general, natural bed material in Trout Beck is for less uniform in shape than the magnetic tracers. Figure 5.26 shows Zingg diagrams of the shape of all trapped material, sampled bed material and magnetic tracers used for the experiment at Trout Beck. It can be seen that very few particles in both the bed material and also the trapped material tracers are "true" spheres, blades, rods and discs (which would plot in the extreme corners of the Zingg diagrams). Many of the spheres and discs were blocky in nature due to their sandstone lithology. Although, magnetic tracers are naturally formed in shape, geometrically they are closer to perfect sphere, blade, rod and discs compared to natural bed material. This is because, particles plotting close to the shape boundaries were not used for the experiments (in order to make four distinct shape classes on the basis of Zingg (1935) shape classification).

Table 5.19 Number and percentage of bed material, trapped particles and magnetic tracers moved in Trout Beck during the monitoring period.

	Bed material				**Trapped-material**				**Magnetic tracers moved**			
Size (mm)	16-64	64-128	>128	Total	16-64	64-128	>128	Total	32-64	64-128	>128	Total
Sphere	95 (23.2	50 (22.3)	11 (19.6)	156 (22.6)	166 (31.6)	41 (33.1)	1 (9.1)	208 (31.5)	55 (32.9)	82 (40.2)	20 (34.5)	157 (36.5)
Blade	54 (13.2)	42 (18.8)	7 (12.5)	103 (14.9)	59 (11.2)	7 (5.6)	0 (0.0)	66 (10.0)	22 (13.2)	21 (10.3)	9 (15.5)	52 (12.1)
Rod	82 (20.0)	25 (11.2)	2 (3.6)	109 (15.8)	75 (14.3)	11 (8.9)	0 (0.0)	86 (13.0)	47 (28.1)	70 (34.3)	19 (32.8)	136 (31.7)
Disc	179 (43.7)	107 (47.8)	36 (64.3)	322 (46.7)	225 (42.9)	65 (52.4)	10 (90.9)	300 (45.4)	43 (25.7)	31 (15.2)	10 (17.2)	84 (18.6)
Total	410	224	56	690	525	124	11	660	167	204	58	429

Figure 5.27 compares the natural bed and tracer material at Trout Beck using the alternative Sneed and Folk plots. Shape distributions of the bed material, tracer population, transported bed material (collected in a sediment trap) and the transported tracers.

In terms of Trout Beck bed material, all tracers fall at the extremes of the natural bed material shape distribution. The greatest frequencies of natural bed material are compact blades and bladed classes. The focus is in the centre of the ternary diagram. Therefore natural shapes tend to be underestimated in the tracers used. Nevertheless there are some examples of all tracers shapes in the natural bed material. In the Trout Beck trapped material, the range of shapes is very similar to the bed material shapes, although there is a slight tendency for more compact shapes to be more frequent in the transported material.

In terms of transported tracers, differences in the density of points between various shapes are very clear. The majority of transported tracers are in the compact and rod shapes. Conversely platy (disc) and blades are poorly represented. The numbers of rods in the transported tracers are greater but these are not well-represented in the natural bed material (Figure 5.27).

Table 5.19 shows shape characteristics of bed material, trapped bedload and the magnetic tracers used in the experiment. Higher b/a and c/b axes ratios and also greater roundness and sphericity values indicate that, particles in the sphere-shaped group of the magnetic tracers are more spherical and round than the bed material and trapped material. Blade shaped-particles, in trapped and bed material have greater c/b axis ratio than magnetic tracers used for the experiments. This suggests that blades in both bed and trapped material are more marginal to rod shape, compared to magnetic tracers. Likewise, many of the rods and blades in bed material and trapped material are "marginal" characterised by high b/a axes tending towards sphere and disc respectively (Table 5.19). The higher c/b ratios in disc-shaped particles in bed and trapped material also indicates that they are marginal to sphere shape, while discs in magnetic tracers tend to be flat.

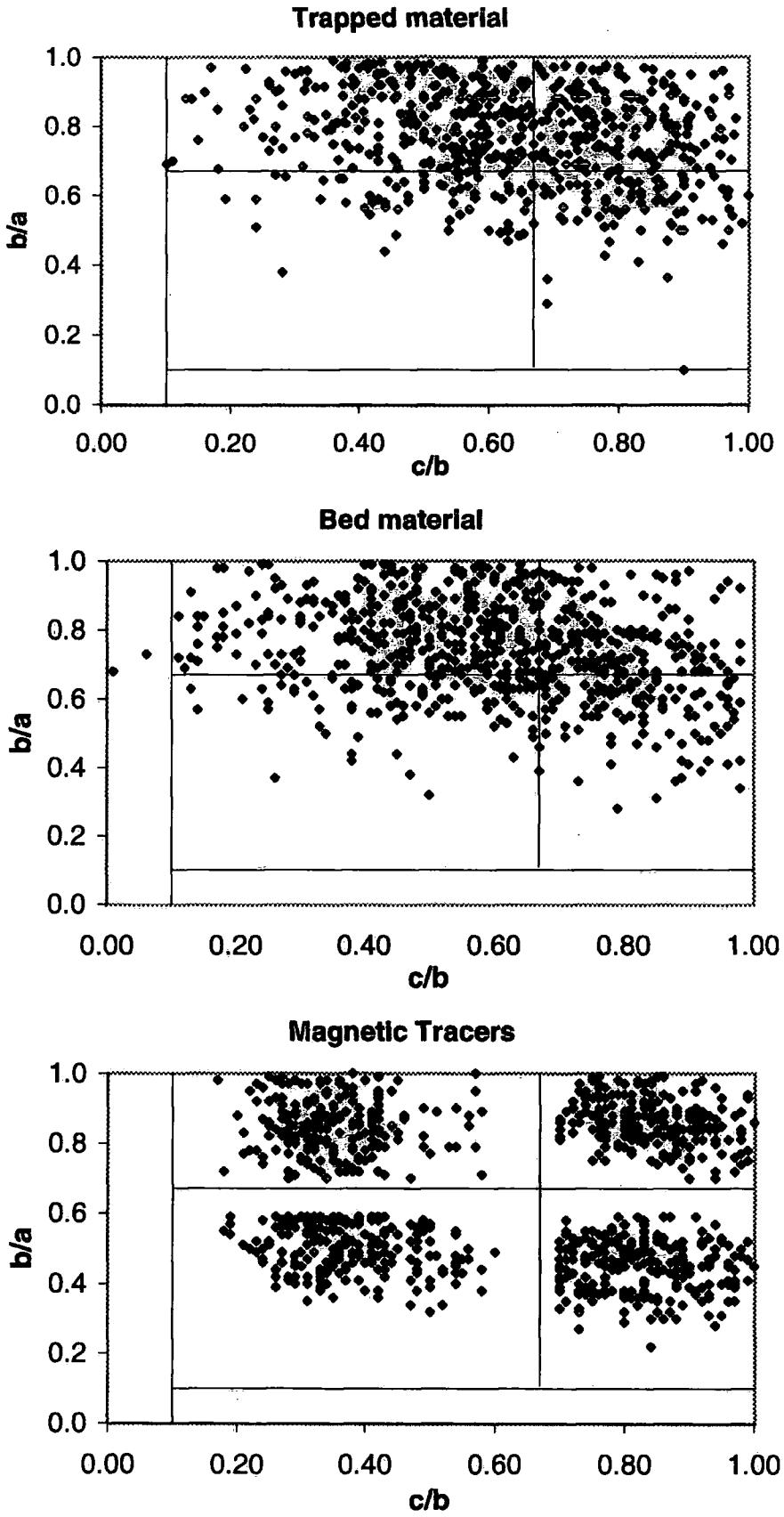

Figure 5.26 Shape distributions of the trapped-bedload, sampled bed material and magnetic tracers in the monitoring site of Trout Beck. (Distributions based on Zingg classification of particle form).

Table 5.19 Sphericity, roundness and flatness characteristics of trapped material, sampled bed material and magnetic tracers at Trout Beck

	Sphere					Blade					Rod					Disc				
	b/a	c/b	Roundness	Sphericity	Flatness	b/a	c/b	Roundness	Sphericity	Flatness	b/a	c/b	Roundness	Sphericity	Flatness	b/a	c/b	Roundness	Sphericity	Flatness
Trap sample 1	0.81	0.80	321	0.81	142	0.58	0.53	152	0.64	275	0.52	0.82	193	0.70	177	0.84	0.50	235	0.7	232
Trap sample 2	0.81	0.79	268	0.8	144	0.58	0.47	168	0.54	327	0.56	0.81	141	0.63	182	0.83	0.47	267	0.68	281
Bed Material	0.78	0.78	223	0.78	151	0.59	0.49	135	0.55	319	0.56	0.82	170	0.63	174	0.83	0.48	200	0.68	268
Magnetic tracers	0.86	0.84	597	0.85	129	0.50	0.37	216	0.45	427	0.45	0.83	263	0.55	201	0.85	0.35	509	0.63	327

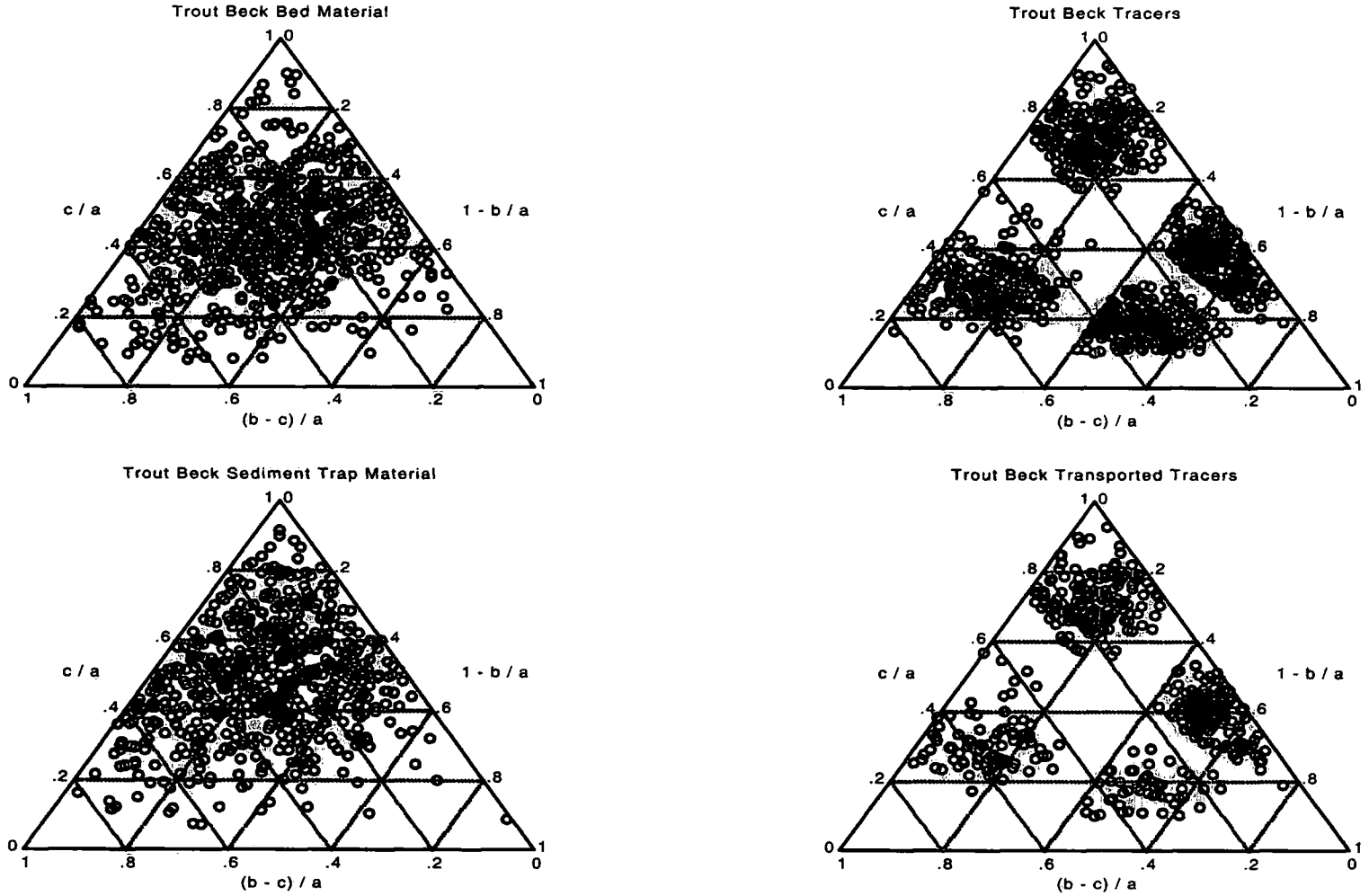

Figure 5.27 Sneed and Folk plots showing the shape characteristics of the natural bed material and magnetic tracers at Trout Beck.

Table 5.20 Statistical comparison of mean shape parameters of Trout Beck bed material /trapped bedload and the magnetic tracers used for the field experiments at the Trout Beck site.

	Sphere	Blade	Rod	Disc
Radius	**-21.33**	**12.07**	**-18.08**	**-19.16**
b/a ratio	**-9.79**	**12.34**	**14.1**	**-10.41**
c/b ratio	**-6.98**	**9.66**	-0.51	**18.68**
Roundness	**-24.74**	**-6.98**	**-8.68**	**-20.42**
Sphericity	**-12.96**	**15.27**	**13.05**	**4.84**
Flatness	**9.86**	**-8.88**	**-6.51**	**-7.77**

(The critical values of 'T' at the 0.05 significant level is 1.97. The values shown in bold indicate a statistical significant difference between the compared parameters)

Table 5.20 compares mean shape characteristics of bed material /trapped bedload and the magnetic tracers used for the field experiments at the Trout Beck site and indicates that, within each shape class, the natural bed material is significantly different than the magnetic tracers. For example, compared to the magnetic tracers, sphere-like particles in natural bed material are relatively angular (low roundness) and less spherical. Blade-rod-and disc-like particles are less rounded but more spherical than those in magnetic tracers. This indicates that blade and rod-like particles in the bed material are "marginal" tending towards sphere and disc shapes respectively.

5.9 DISCUSSION AND CONCLUSION

5.9.1 River flow and magnetic tracer transport distances

This sub-section examines the relationship between the magnetic tracers transport distances and river flow during the monitoring period.

River flow was only competent to transport magnetic tracers in the Trout Beck, and the River Tees during winter storm peaks. The river flow in the two catchments is very flashy and numerous storm peaks were recorded during the monitoring period

(Figures 5.1 and 5.3). The flashy nature of the river reflects the relative impermeability of the rocks, and superficial till deposits and soils, which, together with high relief, lead to high and quick responses of streamflow to heavy rainfall. Compared to the Upper Tees catchment, the greater size of peak flows at Trout Beck is due to its larger catchment area and also channel shape (Table 5.1 and also see Chapter 4). The fact that tracers were transported for only very short periods at the two rivers is a typical characteristics of gravel bed rivers and it is also in accordance with previous bedload studies in similar environments (e.g. Newson, 1981; Gintz, *et al.*, 1996).

It was found that peak flow discharge and also its duration has an important influence on both the number of tracers and also their transport distances. Both the numbers of tracers and also their transport distances increased with peak flow discharge rather than mean flow at the three experimental reaches

Flow characteristics show considerable variation between the three sites. However, because of lack of local hydraulic information available at the three experimental sites, reach-based estimates of mean and peak discharge, shear stress and stream power could only be estimated. Results showed a big variation in flow characteristics between the three sites (Table 5.3). As expected the highest discharge values were recorded at the Lower Tees site. Although, mean discharge values are similar at the Trout Beck and Upper Tees, peak discharges are much greater at Trout Beck than the Upper Tees. Stream power and shear stress also show marked variations (Table 5.3). The lowest values were at the Lower Tees site due to its relatively flat long profile (Table 5.3).

The Schoklitsch (1962) equation was used to predict critical discharges for initiation of bedload transport at the three sites due to its applicability to coarse-bed rivers. However, results showed that, despite observed tracer movements, for none of the survey periods unit discharges exceed the critical discharge values at all three sites (Table 5.4). This suggests that Schoklitsch approach, to predict the critical discharge for bedload transport is either not applicable to the present river or sporadic bedload transport is occurring below the critical value for 'whole-bed' disturbance. The situation over the monitoring period is best described by "low transport rates over a fairly static bed". Transport of particles at discharges less than the critical value are to be expected because locally the flow will be sufficient to entrain some bed material due to higher than average flow strength or bed material configurations suited to entrainment.

These results indicate that in coarse-bed rivers prediction of critical discharges

for bedload transport is difficult. This is because in such rivers, flow resistance is complex and generally controlled by many factors (e.g. spatial variation in large and small scale bed roughness elements, and local characteristics of the bed material characteristics; shape, size and density). Some investigators (e.g Naden, 1988; Carling, 1989; Hoey, 1989, Ferguson and Ashworth, 1992 and Knighton, 1998) also found a strong interrelationship amongst form, flow and bedload transport in gravel bed rivers and adressed some factors that lead to scatter and uncertainties in the initiation of bedload movement.

5.9.2 Tracer movement

In terms of tracer movement at the three sites, a gradual increase was determined in the total mean transport distances from one survey period to another at the Lower Tees and Trout Beck, while there was no great variation at the Upper Tees (Figure 5.12 and Table 5.6). Overall, tracers at the Lower Tees and Trout Beck were transported further (mean transport distances 45.3m and 36.8 m respectively) and also moved more frequently (Figure 5.17) than the Upper Tees site (17.2 m). Despite their similar mean discharge values (Figure 5.3), tracers at the Trout Beck site moved more in number and also further downstream compared to the Upper Tees site due to very different peak discharge values (Figure 5.3). This is because channel at the Trout Beck site is relatively narrow and deep (hence higher bankfull discharge), while it is wide and shallow at the Upper Tees site (see Chapter 4).

Results of magnetic tracing experiments showed that both size and shape selectivity occurs at the three experimental reaches. In terms of size, preferential movement occurred in the finer particle size classes with tracers located along the channel thalweg moving the greatest distance (Figures 5.19, 5.20, 5.21). The smaller particles were transported farthest, compared with medium and large size clasts (Table 5.6, Figures 5.28a, b and c and Figure 5.29). However, the relation between scaled particles size and scaled transport distances showed only a slight evidence of size-selectivity, compared to the influence of shape (Figure 5.14a, b and c).

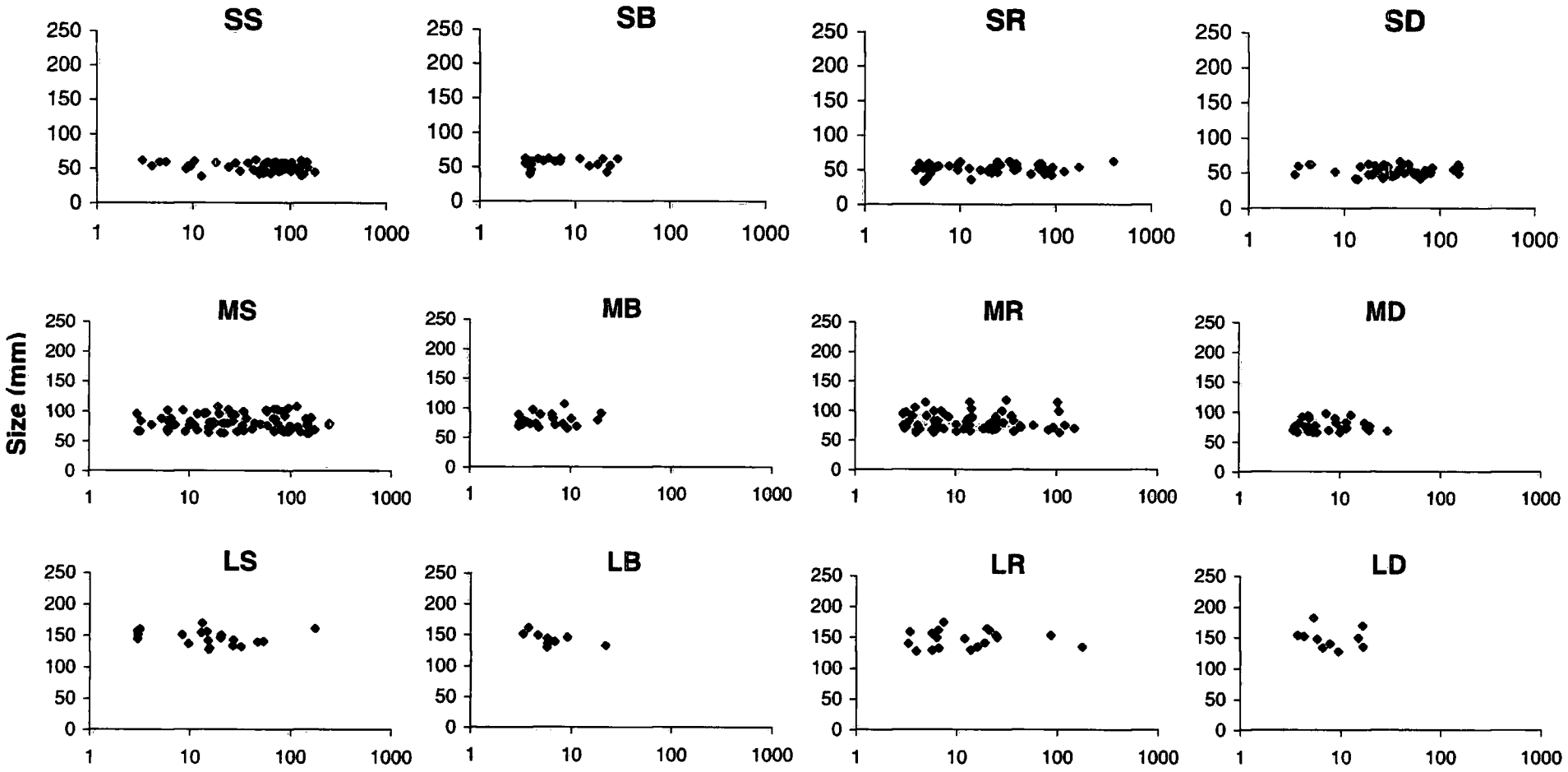

SS: Small sphere, MS: Medium sphere, LS: Large sphere
SB: Small blade, MB: Medium blade, LB: Large blade
SR: Small rod, MR: Medium rod LR: Large rod
SD: Small disc, MD: Medium disc, LD: Large disc

Figure 5.28a Tracer sizes and transport distances for the final survey at the Trout Beck site.

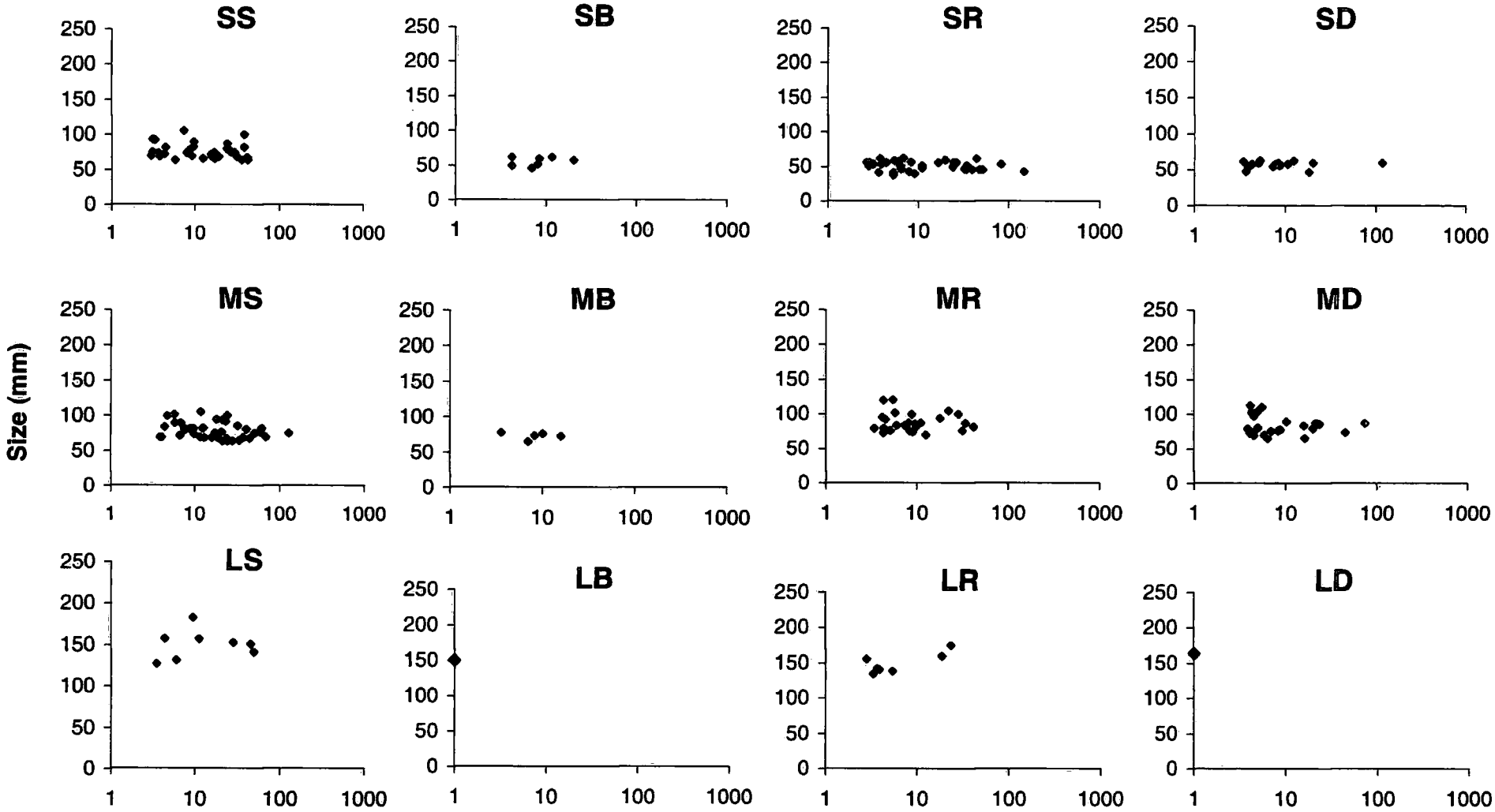

Figure 5.28b Tracer sizes and transport distances for the final survey at the Upper Tees site.

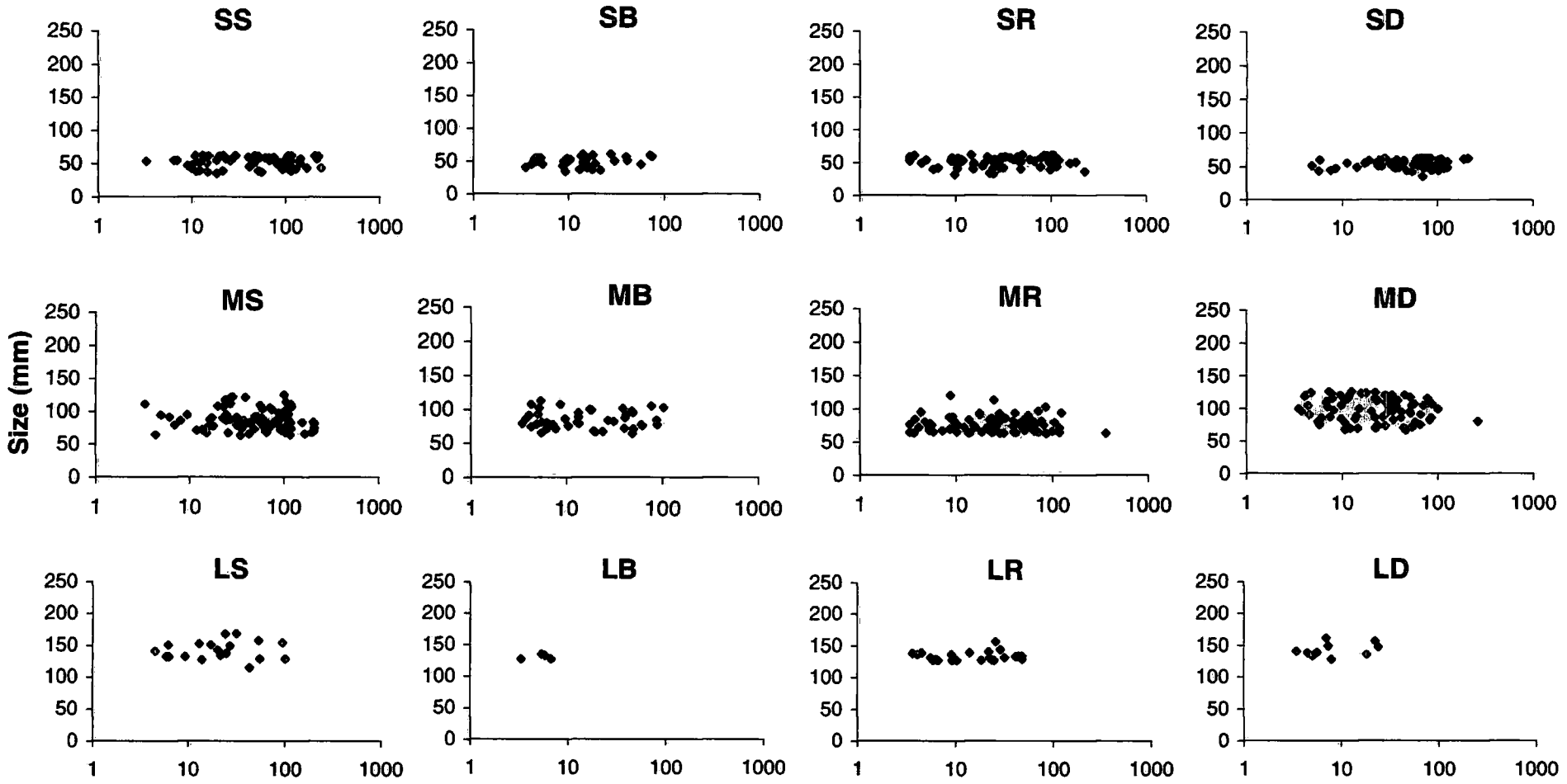

SS: Small sphere, MS: Medium sphere, LS: Large sphere
SB: Small blade, MB: Medium blade, LB: Large blade
SR: Small rod, MR: Medium rod LR: Large rod
SD: Small disc, MD: Medium disc, LD: Large disc

Figure 5.28c Tracer sizes and transport distances for the final survey at the Lower Tees site.

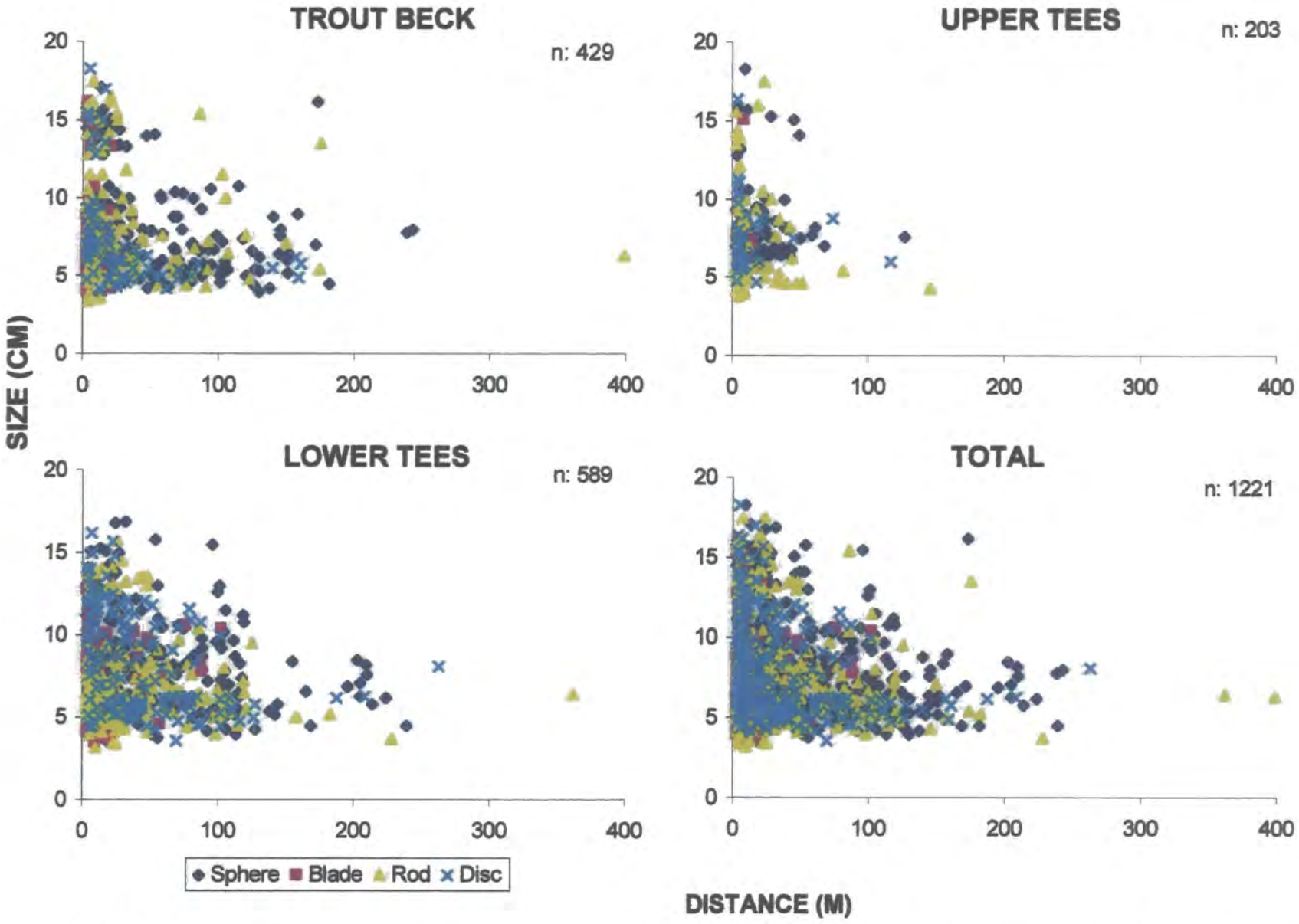

Figure 5.29 Magnetic tracer sizes and transport distances for the final survey, at the Upper Tees, Lower Tees and Trout Beck sites and the three sites combined.

As with size, a similar consistent relation was observed between tracer weight and transport distances in each shape class. Although there were some differences between the three sites, the similar patterns of weight and transport distance occur for all three experimental reaches (Figure 5.30).

Statistical comparisons showed that along with the other factors, size has a significant influence on particle transport distance (Tables 5.9 and 5.10). The findings of Ashworth and Ferguson (1989), Schmidt & Ergenzinger (1995) and also Ferguson *et al* (1998) are somewhat similar to those of the present study. Schmidt & Ergenzinger (1995) investigated bedload transport with active (radio) and passive (iron, magnetic) tracers in a step-pool mountain river and found that among coarse pebbles transport lengths of the 500g tracers are significantly longer than those of the 2000g tracers. However, they also found that the trend does not remain for the much smaller particles. For example, the small 100g particles had much lower maximum transport lengths because they were trapped behind large boulders or interstices between cobbles and boulders. The field experiments of Ferguson *et al* (1998), carried out with 1460 tracer pebbles in the Allt Dubhaig, also proved that smaller size tracers moved far greater distances downstream than coarser tracers.

Although small size tracers moved longer mean transport distances than the medium and large size groups, percentage of the number of tracers moved by size showed that number of tracers moved in the medium size group are greater (49.8%) than the small (41.5%) and large (32.5%). This suggests that bedload entrainment in the study reach may be to some extent conforming to the 'equal mobility' pattern proposed by Parker *et al* (1982) and Andrews (1983) for streams with mixed calibre beds. The possible explanation for this distribution might be that, compared to larger size particles, entrainment of small size particles in a rough bed is more difficult due to hiding effect by larger size bed material roughness elements (Carson and Griffiths 1987). However, once they are entrained, due to their lower weights, they might be picked up into a temporary suspension and transported further downstream, while the larger ones may move close to the channel bed either in a rolling or sliding mode depending of their shape and also the character of bed roughness elements. Results of tilting table experiments also demonstrated that, on a rough bed, regardless of their shape, small size test particles moved at relatively greater friction angles than those of larger ones (Chapter 6). In addition, some studies (e.g. Komar and Li, 1986; Naden, 1987; Wiberg and Smith, 1987) also pointed out that the particle which are coarser than

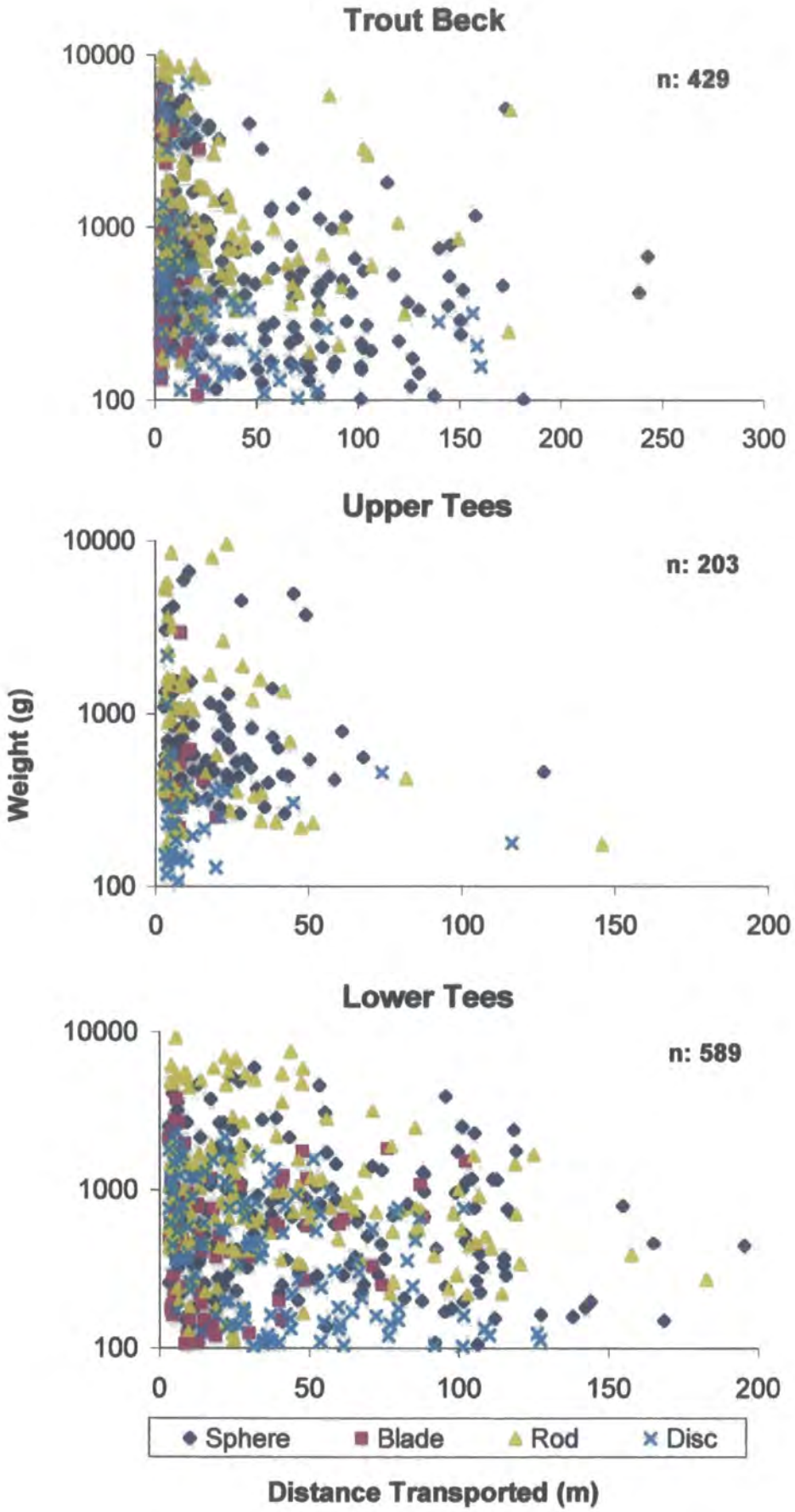

Figure 5.30 Magnetic tracer weights and transport distances for the final survey the three sites combined.

average particles size of bed material tend to move easier, while entrainment is more difficult for those that are finer than average size of bed material due to the protrusion and hiding effects of bed roughness elements and also bed packing arrangements and pivoting angles. However, when the comparison is made between medium and large, it was found that, in both percentage of the number of tracers and also frequency of movement decrease in large size group at each of the experimental site (Figure 5.17). This is probably large size particles (>128mm) are very heavy to entrain at most of the time, though they protrude into the flow compared to surrounding small size particles. Indeed, there is no greater difference between the small and medium size groups in both weight and also size, while difference increases for size group tracers.

In terms of shape, in general, all shapes showed a decrease in distance and frequency of transport as size increases (Figure 5.28a, b, c). It was found that, regardless of size, sphere, rod and to some extend disc-shaped tracers have been transported by far the greater distances and also more in number, while blades moved least (Tables A2.1-A2.5). Results have clearly shown that within each size group spheres and to some extent rods travelled much longer distances than similar-sized disc and blades (Figure 5.28a, b, c). The reason why the spheres and to some extend rods have longer mean transport distances but discs and blades do not, may be that, because spheres and rods are largely rolled rather than lifted, the rate at which spheres are moved by rolling is more directly related to the flow.

Correlation and multiple regression have been partially successful in explaining influence of the shape and shape parameters on particle transport distances (Tables 5.9, 5.10). Multiple regression has shown that level of explanation of the influence of shape and size factors on transport distances was generally low. This indicates that several other factors such as local flow conditions, variations in channel gradient, local bed structures bed material roughness should be included in the models. Indeed, multiple regression was able to explain the influence of the existing shape and size parameters, by a maximum of 27.5%, 33.4% and 49.9% of the variation in transport distances at Upper Tees, Lower Tees and Trout Beck respectively.

In correlation analyses the least useful predictor was particle c axis which was not statistically significant in either experimental site, whereas particle a axis and Krumbein sphericity were both found to be the most significant predictors affecting transport distances (Table 5.9). Based on the results of the multiple regression analysis it was found that, together with roundness and weight, particle c-axis, and sphericity have the

greatest correlation with transport distance. A-axis also is, to some extent, well correlated with distance but b-axis showed poor correlation with distance at the three sites (Table 5.9).

Although the correlation between the c-axis and transport distance is low, multiple regression models showed that the c-axis is important along with other parameters sites. Although particle c and a -axes are related to particle size and they are considered to be statistically independent, in terms of sediment transport, axial dimensions and shape parameters can not be isolated as it is explained in Chapter 2 and also demonstrated with friction angle measurements (Chapter 6).

5.9.3 Missing and buried tracers

Based on the results, a positive relation was found between the number of missing particles and the frequency of particles moved. Altogether 474 magnetic tracers, which represent 17.5 % of the total tracers (2700) at the three sites, have disappeared during the whole monitoring period. In general the number of the missing stones is the least (97) at the Upper Tees and greater at Trout Beck (206) and the Lower Tees (171) (Table 5.11).

The low disappearance rate at Upper Tees may be the result of the low number and shorter distances of tracer movement. On the other hand, the greater loss at Trout Beck and Lower Tees may be the result of deeper-burial, by mixture of coarse and fine material, and greater rate and longer transport distances (Table 5.12). As expected, the rate of missing and burial increased with length of period, during which tracers was not surveyed (e.g. between surveys 3 and 4) and also sizes of event occurred (e.g. between surveys 4 and 5) (Table 5.21).

Table 5.21 Number of missing tracers during the monitoring period at the three experimental reaches.

Surveys	Upper Tees	Lower Tees	Trout Beck	Total
Up to Survey 3	0	133	35	168
3 - 4	86	8	66	160
4 - 5	11	30	105	146
Total	97	171	206	474

Over the entire monitoring period, more small sized tracers were lost. Indeed, at each of the experimental site, the percentage of missing particles in the small size group, is much greater than the medium and large size groups (75.3%at Upper Tees, 70.5% at Lower Tees and 73.8% at Trout Beck (Table 5.11). The greater percentage of missing stones in the small size tracers might be attributed to their easy transportable capability and also greater rate of burial compared to larger tracers.

In terms of shape, the number of missing particles is greater in the blade and disc-shaped categories than for spheres and rods. The decreasing order for the missing particles are in 150 blade, 132 in discs, 121 in sphere and 70 in rods -shaped particles (Table 5.11). The possible reason why the flat shaped tracers had the greatest missing rate is probably that because of their less transport rate they might have been buried by the more active bed material.

Burial depths of tracers may provide some vital information to predict the evidence of the depth of active layer in a coarse-bed river. Combined with the three sites, in total, 238 magnetic tracers were found to have been buried with a mean depth of 7.8cm (Table 5.12). The maximum burial depths were –22cm (Lower Tees), -20cm Trout Beck) and, 10cm (Upper Tees). These values are relatively small compared to other studies (e.g. Ferguson et al, 1998 found 45cm). As similar to the missing tracers and probably for similar reasons, an inverse relation exists between the numbers of buried tracers and particle size (133 small, 100 medium and 10 large) (Table 5.12 and Figure 5.18). An inverse relation found between flatness and tracer burial depth. The more flatter the particles the lower the burial depth (Figure 5.18).

The greateer number of burial tracers at Lower Tees (121) and to some extent at the Trout Beck site (110) might be the result of high rate of bed bedload transport at these sites, or abundance of loose, mixed calibre material that might have buried the magnetic tracers.

5.9.4 Size and shape of trapped bedload compared with resident reach material in the monitoring reach

Size: Assuming that the trapped-bedload is reasonably indicative of the size characteristics of bedload transport in Trout Beck River, size composition of trapped-bedload particles at the monitoring reach appeared to be smaller than the bed material. In the trapped-bedload the majority of the particles are in the smaller size ranges (Table 5.13 and Figure 5.24). This may indicate a degree of size selectivity, as found by other

coarse bedload studies (Li and Komar, 1986; Ashworth and Ferguson, 1989; Komar and Shih, 1992 and Ferguson *et al*, 1998). Another possible reason might be that smaller particles might be transported on average greater distances than larger particles leading to their greater representation in the trapped bedload.

Shape: To some extent shape composition of the trapped bedload and how it varies between the different size fractions simply reflects lithological control. The dominant sandstone lithology in the Trout Beck catchment tends to produce large tabular, flat slabs, which result in the dominance of flat particles in the cobble fraction of the reach material.

Disc-like particles are more common in both sampled bed material and also in the trapped bedload, while blade-and rod-like particles represent the lower percentages respectively (Figure 5.25 and Tables 5.15 and 5.16). Although sphere-like particles have the second in importance both in the trapped bedload and in the sampled bed material, the ratio is much smaller when compared to discs. It is also clear that as clast size increases the percentage of disc-like particles increases markedly which is similar with the size distribution of sampled material in the experimental reach (Table 5.16). The reason for the greater frequency of discs in the larger size clasts might be attributed to the effect of bedrock structure on clast shape. Comparison of trapped-bedload and bed material clearly shows that, except in the small size group where disc-like particles are under-represented, within all size groups of the trapped-bedload, sphere-and disc-like particles are more common, while blade-and rod-like particles are-under represented. A possible explanation for the over-representation of disc-and sphere-like particles in the trapped-bedload might be the higher rolling capability of sphere-shaped clasts due to their greater sphericity. Comparison indicated that disc-like particles in the trapped bedload are more spherical, more rounded in shape and also are lighter in weight and as well as smaller in size (a, b, and c axes) than those in the sampled bed material (Table 5.17). Indeed Table 5.14 clearly shows that, in contrast to other shapes, there is a statistical significant difference in the degrees of roundness, sphericity size and weight of discs-like particles between the trapped-bedload and sampled bed material. Thus, compared to the sampled bed material, greater sphericity and roundness of discs in the trapped material and also their smaller size/weight suggests that, these particles might have been rolled due to their marginal shapes (sphere-like particle forms) (Sneed *et al.*, 1958; Ashworth & Ferguson., 1989; Schmidt & Gintz., 1995). In terms of blade-and

rod-like particles, Table 5.14 shows that although blade-and rod-like particles (as similar to disc-like particles) are significantly smaller in size and also light in weight than those of in the sampled bed material (Table 5.14), they are still under-represented in the trapped bedload. The reason might be attributed to their lower sphericity and roundness degree. In other words, despite their small size and less weight, blade-and rod-like particles were not as mobile as disc-like particles due to their angularity. This highlights the importance of sphericity and to some extent roundness on particle transport. Statistical comparisons also suggested that there is no statistical difference in the sphericty and roundness degrees of blade-and rod-like particles between the trapped-bedload and sampled bed material.

Comparison of magnetic tracers and trapped-bedload suggested that, although sphere-and disc-like particles in the natural bed material are transported preferentially, influence of size selectivity in the trapped material is stronger than shape selectivity when compared to the magnetic tracers. There are several reasons that might be attributed to this difference. First of all, the natural particles in the experimental reach deviate from an ideal shape which will reduce the influence of shape on transport. As it was demonstrated in Chapter 7, small differences in shape produce fairly large differences in hydrodynamic behaviour. Secondly, natural bed material in Trout Beck is a less uniform in shape (Figure 5.26). In both the bed material and trapped material, few particles are "true" spheres, blades, rods or discs. Many of the sphere-and disc-like particles were blocky. Although, magnetic tracers are naturally formed in shape, geometrically they are closer to a perfect sphere, blade, rod and disc compared to natural bed material.

Comparison indicates that in the Trout Beck bed material, clasts fall at the extremes of the natural bed material shape distribution. Natural bed material shapes are dominated by compact blades – bladed forms. Therefore some natural shapes are underestimated in the tracers used (Figure 5.27). Nevertheless there are some examples of all tracers shapes in the natural bed material. Comparison also clearly suggests that within each shape class, most of the trapped-bedload and sampled bed material have relatively low roundness values than the magnetic tracers. The possible reasons for this might include; the short course of travel by the bedload material in the Trout Beck catchment as compared with other rivers and the discontinuous inputs of fresh angular material along the channel. Sphericity of sphere-like particles in the Trout Beck is relatively low and less rounded compared to the magnetic tracers, suggesting that the

upland position of the Trout Beck is not sufficient to result in spherical clasts through abrasion. Another reason for the low sphericity values of the bed material is the sandstone lithology, which leads to flat clasts that are also resistant to abrasion compared with many other lithologies (e.g. limestone, shale). (Table 5.19 in trapped section). Blade-like particles in trapped bedload and bed material have greater c/b axis ratio, suggesting blades in both bed and trapped material are more marginal to rod-like shape. Likewise, many of the rods and blades in bed material and trapped material are "marginal" characterized by high b/a axes tending towards sphere and disc respectively (Table 5.19). The disc-like particles in bed and trapped material were also found to be more marginal to sphere shape due to their higher c/b ratios.

These differences are assumed to be important factors in bedload transport studies because, in gravel bed rivers, natural bed material shape deviates considerably from the ideal shapes and hence may not conform to models established for sphere, blade, rod and disc settling and transport. In other words, these variations in shape may lead to fairly large differences in hydrodynamic behaviour of particles. This is because, as it is shown in chapter 7, there is a direct relationship between sphericity and the velocity at which a particle of a particular volume will settle in a fluid or roll along a bed. Settling and transport velocities of irregular-shaped natural particles were found to be significantly different from artificial and natural particles with ideal shapes. Thus, no simple pattern of settling and transport velocities was found between particles of irregular shapes and to some extent size (Figures 7.23, 7.24 and 7.25). The experiments carried out with magnetic tracers of ideal shapes do not directly represent actual particle motion in a natural channel. Nevertheless they are a useful starting point for the systematic investigation of this general problem.

CHAPTER 6: VARIABILITY IN FRICTION ANGLES AND THE MECHANISTIC BEHAVIOUR OF PARTICLES OF DIFFERING SIZE AND SHAPE, ON BEDS OF VARYING GRAVEL ROUGHNESS.

6.1 SCOPE OF CHAPTER

This chapter presents the results of the tilting table experiments designed to investigate the variability in friction angles and the mechanistic behaviour of particles of differing size and shape, on beds of varying gravel roughness. An introduction outlining the importance of selective entrainment of grains of differing size and shape from a natural sedimentary deposit is given. Some common terms associated with the experiments and a broad objective of the chapter are described. Sections 6.3 and 6.4 describe variability of friction angle in relation to particle size, shape and orientation on four different bed roughness types. Variability in friction angles measured with particles of equal weight but different shapes and also with natural particles of different shapes and orientations is discussed in Sections 6.5 and 6.6 respectively. Sections 6.7 and 6.8 discuss the friction angles measured on a naturally formed river bed with particles of differing size, shape and orientation. Variability in friction angles measured with the particles of equal weight but varying shape on a naturally formed river bed is discussed in Section 6.9. Section 6.10 examines friction angles of natural particles of varying shape measured on the natural bed. The effect of particle roundness on friction angle is examined in Section 6.11. Finally, the key points raised by the experiments are discussed and summarised in Section 6.12

6.2 INTRODUCTION

In bedload transport selective entrainment of grains of differing size and shape from a natural sedimentary deposit is an important process (Sneed and Folk, 1958; Meland and Normand, 1969; Li and Komar, 1986; Carling *et al.*, 1992; Hassan and Church, 1992). However, despite much research, the mechanisms of selective entrainment are still incompletely understood (White and Day, 1982, Komar, 1987;

Naden, 1988; Gomez and Church, 1989; Schmidt and Ergenzinger, 1992; Schmidt and Gintz, 1995). Many bedload transport studies have shown that there are complex interactions which occur between channel sediments and streamflow (Hoey, 1992; Ferguson and Ashworth, 1992). These complexities suggest observations of flow dynamics and sediment transport must be, at least partly, based on either laboratory experiments or flume studies (Kirchner *et al.*, 1990; Carling *et al.*, 1992). Several investigations have been based on grain friction and pivoting analysis as functions of grain size, shape (rollability and angularity), and factors such as imbrication (White, 1940; Miller and Byrne, 1966; Komar and Wang, 1984; Li and Komar, 1986; Kirchner *et al.*, 1990; Buffington *et al.*, 1992; Dietrich and Kirchner, 1992).

Before considering the objectives of this chapter it is worthwhile briefly outlining some common terms associated with this kind of study. The Friction angle is the angle of repose, which expresses the resistance of a grain to removal by the interlocking friction in a sediment between individual grains and the flow. There is a relationship between critical boundary shear stress of a particle, its friction angle and the relative protrusion of grains on bed surfaces (Kirchner, *et al.*, 1990). Generally, friction angle distributions are expressed as a function of test grain size, median bed grain size, and a bed sorting parameter. Friction angles decrease with increasing grain size relative to the median bed grain size, and are a systematic function of sorting, with lower friction angles associated with poorer sorting (Buffington *et al.*, 1992). In contrast, the pivoting angle relates to the contact point of a particle with an underlying grain. The first movement occurring when the moment of force exerted by the flowing fluid exceeds the moment of the particle's weight force. Particle pivoting angles have an important effect on the threshold of movement. Pivoting angles of a specific particle depend on size, shape and imbrication. With uniform grain sizes, the pivoting angle and thus entrainment depend on grain shape, grain 'rollability' (as determined by the c/b axial diameter ratio) and angularity, which produces grain interlocking. Measurements have shown that there is an inverse relationship between pivoting angle and entrainment threshold. Because of interlocking of the particles which inhibits movement, angular particles have greater pivoting angles than rounded sphere-shaped particles (Komar and Li. 1986).

The broad objective of this chapter is to examine the processes of selective particle entrainment, based on an analysis of particle friction angles. Results of friction angle measurements are presented for particles of various shapes, size and orientation

on a variety of artificially and naturally formed bed roughnesses. The experimental design and measurement techniques for the tilting table experiments are briefly explained here and in Chapter 3.

Briefly, four metal plates ($1m^2$) were used as base plates for four different bed roughnesses. The roughness was formed using naturally formed coarse gravel of various shape and size. On each base plate the size of the bed particles (base pebbles) was limited to a specific grain size range (Table 6.1). The base pebbles were secured to the base plates with silicon cement (Figure 6.1).

Table 6.1 Grain size distributions of the four bed roughnesses.

Bed Roughness type	Size of the base grains (b axis)
Roughness 1	8 – 11.2 mm
Roughness 2	16 – 22.4 mm
Roughness 3	32 – 48 mm
Roughness 4	64 – 96 mm

The test grains used in the friction angle experiments were either artificially-formed using artificial or naturally formed coarse gravel. Three test grain sizes were classified in terms of their b (intermediate) axes; 24, 48 and 96 mm (Table 6.2). The test particles were of the following shapes: sphere, blade, rod, and disc. For each test particle, measurements were repeated 50 times on each of the four bed roughness types. For example on roughness 1: 50 measurements was made for the sphere, 50 for the blade in a transverse orientation, and another 50 in a parallel orientation blade. Similarly, 50 parallel for rod, and another 50 for transverse rod and 50 for disc-shaped particles.

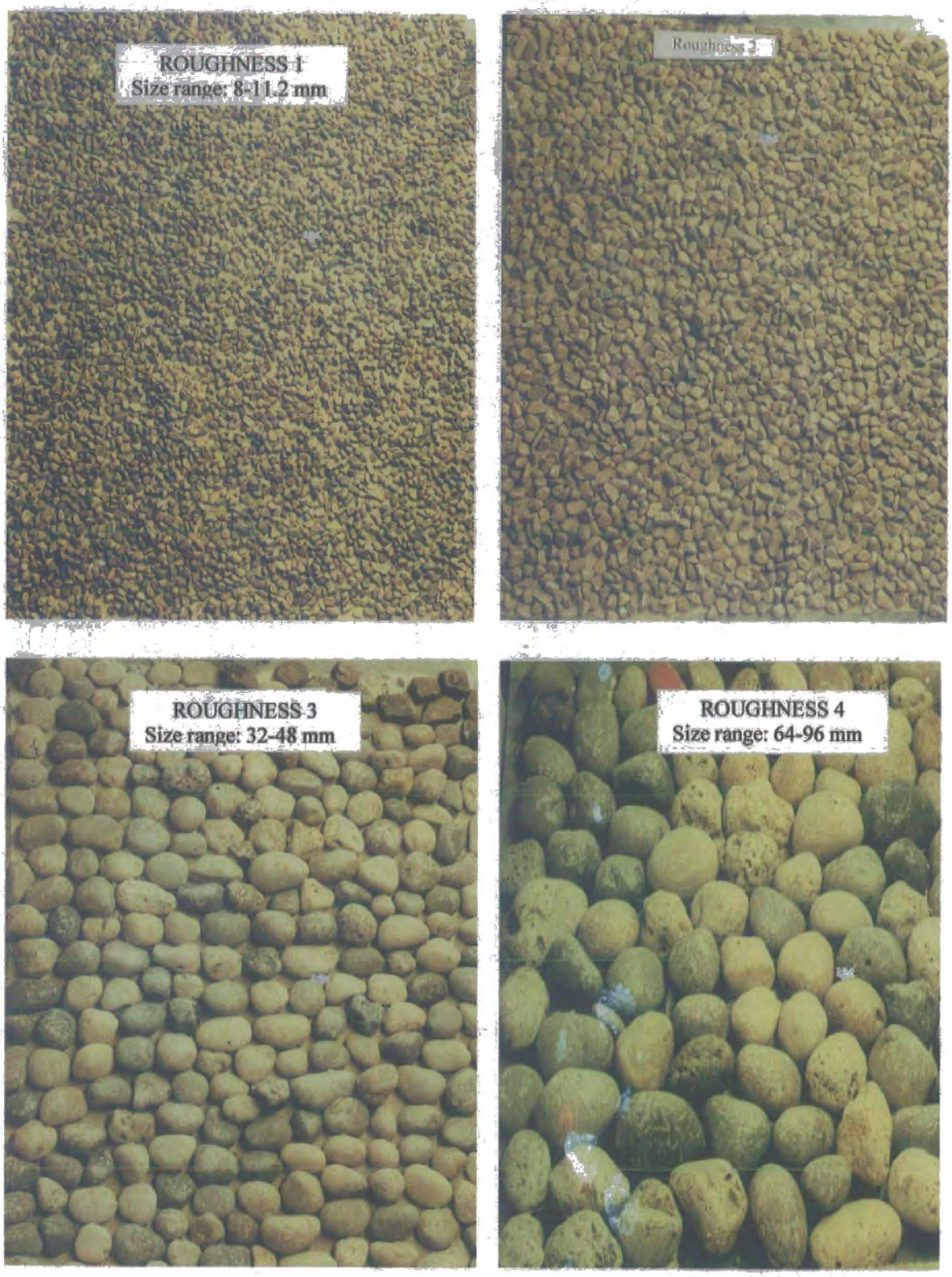

Figure 6.1. The bed roughness types used in the friction angle experiments. Particle form varies with the size of the roughness elements.

6.3 VARIABILITY OF FRICTION ANGLE IN RELATION TO PARTICLE SIZE AND BED ROUGHNESS.

Table 6.2 Mean friction angles and standard deviations measured for three size groups on four bed roughness.

Bed	Test grain size (b-axis)		
Roughness type	24 mm	48 mm	96 mm
Roughness 1	49 (0.2)	39 (8.9)	33 (7.4)
Roughness 2	50 (11.0)	44 (9.8)	34 (8.6)
Roughness 3	55 (12.0)	44 (10.5)	37 (9.9)
Roughness 4	70 (11.6)	54 (10.0)	44 (9.3)

Note: The first figure in each row is the friction angle (degrees) and the second is standard deviation (brackets).

The size of the test particles and the results of the measurements for the tilting table experiments are shown in Table 6.2. Mean friction angles for each test size group were calculated by summing all the measurements regardless of any shape and orientation differences, then dividing by the number of measurements. Table 6.2 and Figure 6.2 indicate that, in general, there is an inverse relation between mean friction angle and test particle size. For the smallest test particles on almost each bed roughness type the measured mean friction angles are much greater than those of the medium and large sized particles. (Figure 6.2 and Table 6.2). Friction angles increase as bed roughness increases for all test particles but the increase is more noticeable for the small sizes.

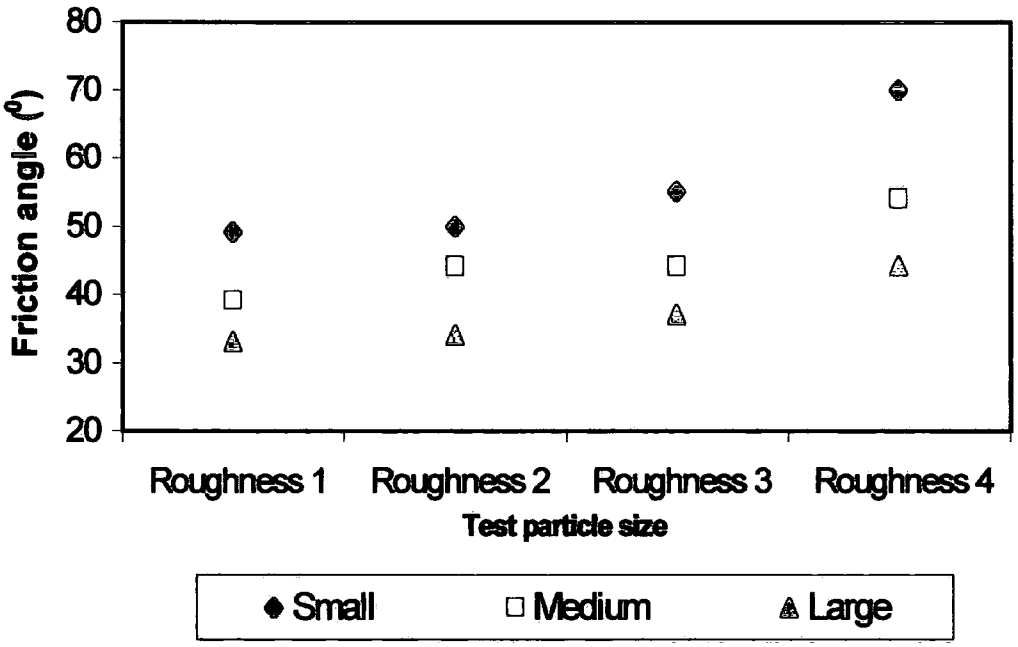

Figure 6.2 Mean friction angles measured for the three test clast sizes on four bed roughness types

Although there are consistent differences in friction angles between the different sizes and roughness types, the size of these differences varies in magnitude. Table 6.2 shows that differences between roughnesses 1 and 2 and also between roughnesses 2 and 3 are only 1° and 5° for small size test particles, 5° and 0° for medium size test particles and 1° and 3° for the large size test particles, but differences increases noticeably up to 15° for small, 10° for medium and 7° for large size test particles between the roughnesses 3 and 4. These differences must result in both a greater increase in bed material roughness and also a variation in particle packing geometry of Roughness 4. Indeed, visual inspection of the roughness surfaces (Figure 6.1) shows that because of increasing bed grain size and better sorting there are many pockets that are large enough to trap small and medium test particles. Given the large grain size of bed roughness 4 there is a marked decrease in the ratio of test grain size to bed grain size.

On each bed roughness type, measurements have shown that there is a noticeable relation between friction angle and d/D ratio. In other words, regardless of test particle shape, friction angle depends on the ratio of test grain size (d) to those over

which it is pivoting (D). The smaller the ratio of d/D, the greater friction angles at which test particles move. Figure 6.3 also shows that on each bed roughness type, friction angles increase as the ratio of test grain size to bed mean particle size decreases. The greatest friction angles tend to correspond with the lowest ratios of d/D.

Figure 6.3 indicates that, over all the bed roughness types, there tends to be a slight decrease in standard deviation values with increased d/D ratios. This indicates that smaller grains have a large range of friction angle distributions. As test particle size increases (hence increased d/D ratio) the standard deviation value decreases (Table 6.2) The small-size test particles show no great difference in standard deviation values between various bed roughnesses. The range varies between 10.2 and 12. Measurements with medium-and large-size test particles, however, show that standard deviation tends to decrease as the test particle size increases on lower roughness beds. Standard deviation ranges between 8.9 (on Roughness 1) and 10.5 (on Roughness 4) for medium-size test particles and the ratio is 7.4 (on Roughness 1) and 9.9 (on Roughness 4) for the large size test particles (Table 6.2). This indicates that, due to their greater d/D ratios, the larger grains move easily at a small range of low friction angles on less rough beds.

Table 6.3 Mean friction angles and the d/D ratios measured for three test size groups on four bed roughness.

Bed Roughness type	**Test grain size (b-axis)**		
	24 mm	**48 mm**	**96 mm**
Roughness 1	2.5 (49)	5.0 (39)	10.0 (33)
Roughness 2	1.25 (50)	2.5 (44)	5.0 (34)
Roughness 3	0.6 (55)	1.2 (44)	2.4 (37)
Roughness 4	0.3 (70)	0.6 (54)	1.2 (44)

Note: The first values in each row represent the d/D ratio and the second is friction angle (degrees).

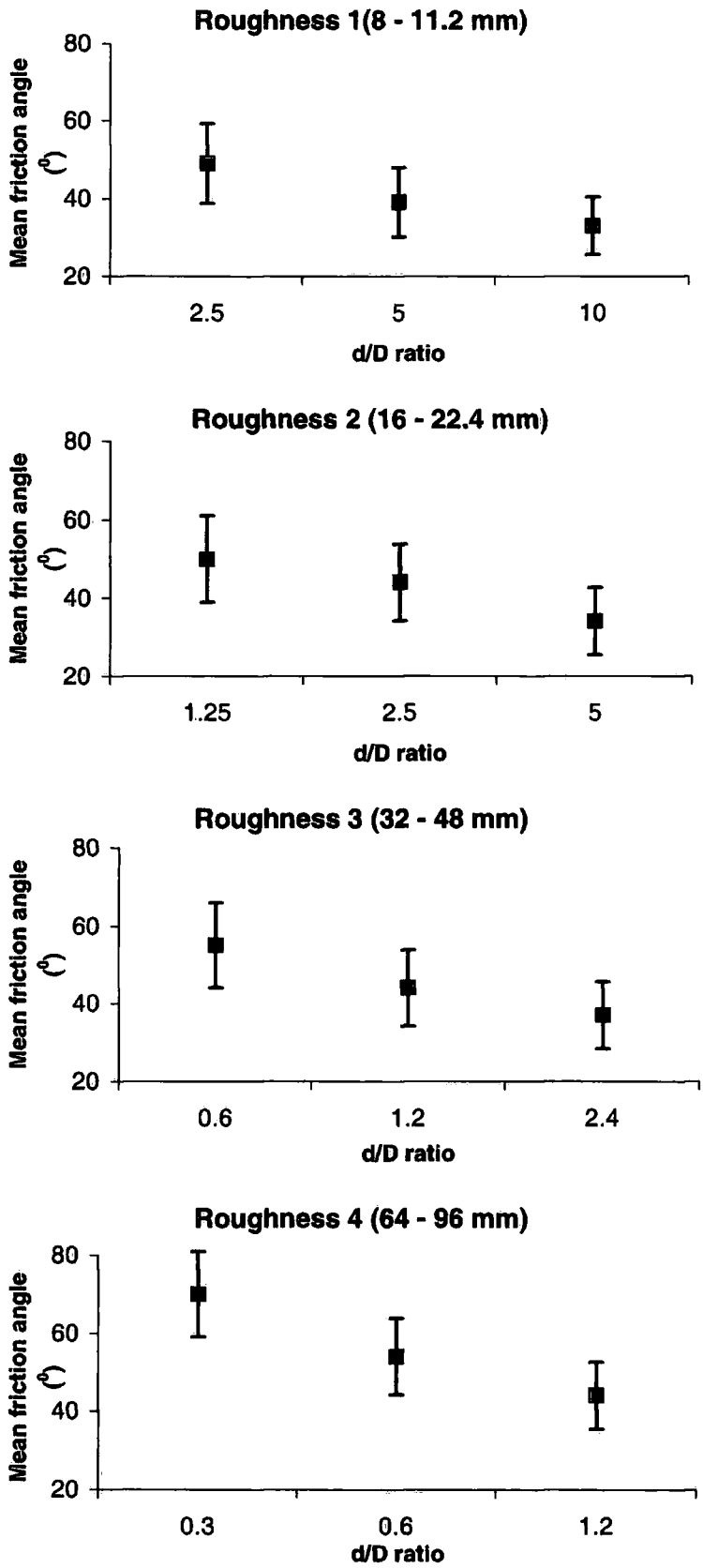

Figure 6.3 Friction angles for particles of different size as a function of the d/D ratio, d being the diameter (b axis) of the pivoting (test) particles and D the mean diameter of the base particles.

6.4 VARIABILITY OF FRICTION ANGLE IN RELATION TO PARTICLE SIZE, SHAPE AND ORIENTATION ON FOUR DIFFERENT BED ROUGHNESS TYPES

Table 6.4 generally shows that, regardless of shape, there tends to be an inverse relationship between particle size and friction angle. Mean friction angles decrease with particle size and the differences tend to be greater for spheres and rods with a transverse orientation than for blades any orientation.

In terms of shape, for all test sizes, sphere-and rod-shaped particles with transverse orientations have lower mean friction angles on all bed roughness types. Discs, blades (regardless of orientation) and rods with a parallel orientation have greater friction angles. This indicates that apart from particle size, shape and orientation also have very significant influences on friction angles (Table 6.4). Spheres and discs have no preferred orientation and hence no significant difference in friction angles in different positions; however rods and blades can move at very different friction angles when placed in parallel or transverse orientations (Figure 6.4 and Table 6.4).

Table 6.5 shows the statistical significance of friction angles measured with various shape/orientations of test particles in three size groups on four bed roughness types. Generally there is no significant differences in measured friction angles between blades (regardless of orientation), discs and parallel rods. A similar relation is also true between spheres and transverse-rods on virtually all bed roughnesses. However, differences are significant between blades, discs, parallel-rods, spheres, and transverse-rods. Particles with low c/b ratios tend to move at similar friction angles. Differences in friction angles tend to be important between the particles that have different ratios of c/b axes, such as between spheres and blades or between transverse-rods and discs or blades. Table 6.4 also shows that differences in friction angles between various shapes are less significant for small-sized particles on the roughest bed. This tends to be more important as bed roughness decreases or test particle-size increases.

On the smoothest bed and with the smallest test particles, the test particles moving at the lowest friction angles were spheres and rods positioned transverse to the slope, while the most stable particles were blades (regardless orientation), parallel rods and discs. For the smallest test particles the differences in mean friction angles between

Table 6.4 Mean friction angles for four shape classes in three size groups on four different bed roughnesses.

Bed roughness type	Small test grain (b: 24 mm)						Medium test grain (b: 48 mm)						Large test grain (b: 96 mm)					
	S	B.T	B.P	R.T	R.P	D	S	B.T	B.P	R.T	R.P	D	S	B.T	B.P	R.T	R.P	D
Roughness 1	39	51	58	33	55	55	27	43	44	25	42	52	22	37	35	19	41	44
Roughness 2	45	50	58	38	53	57	30	50	58	27	46	55	20	41	42	20	39	41
Roughness 3	51	59	59	44	55	60	35	48	50	33	46	52	27	39	37	30	40	46
Roughness 4	69	72	75	58	63	81	46	58	58	41	57	63	34	48	47	33	48	52

B.T : Blade with transverse orientation
B.P: Blade with long axis parallel to the flow
R.T: Rod with transverse orientation
R.P: Rod with long axis parallel to the flow
S: Sphere
D: Disc

Table 6.5 Statistical significance of friction angles measured with various shape/orientation of test particles in three size groups on four bed roughness types.
(critical value of "t" at the 0.05 significance level is 1.98 for each of the experiments. S: sphere, B: blade, R: rod, D: disc, P: parallel orientation, T: transverse orientation.). Bold type shows significant values

ROUGHNESS 1

	Small size						Medium size						Large size				
	PB	TB	PR	TR	D		PB	TB	PR	TR	D		PB	TB	PR	TR	D
S	**9.10**	**5.60**	**7.80**	**3.40**	**8.20**	S	**9.94**	**9.15**	**9.14**	1.62	**15.40**	S	**11.04**	**10.73**	**13.23**	**2.60**	**12.65**
PB	----	**3.20**	1.40	**12.90**	1.50	PB	----	0.68	1.15	**10.69**	**3.37**	PB	----	1.44	**4.10**	**14.44**	**4.96**
TB	----	----	1.96	**9.12**	1.96	TB	----	----	0.43	**9.91**	**4.12**	TB	----	----	**2.38**	**13.38**	**3.44**
PR	----	----	----	**11.54**	0.05	PR	----	----	----	**9.94**	**4.75**	PR	----	----	----	**15.98**	1.34
TR	----	----	----	----	**12.20**	TR	----	----	----	----	**16.10**	TR	----	----	----	----	**14.77**

ROUGHNESS 2

	Small size						Medium size						Large size				
	PB	TB	PR	TR	D		PB	TB	PR	TR	D		PB	TB	PR	TR	D
S	**6.05**	1.98	**3.40**	**2.91**	**4.68**	S	**13.3**	**10.1**	**8.20**	**2.13**	**14.59**	S	**12.72**	**10.88**	**12.51**	0.34	**11.71**
PB	----	**4.66**	**2.74**	**9.62**	0.80	PB	----	**3.22**	**5.38**	**14.66**	1.37	PB	----	0.54	1.44	**13.75**	0.21
TB	----	----	1.72	**5.21**	**3.24**	TB	----	----	**2.09**	**11.53**	**2.32**	TB	----	----	0.74	**11.64**	0.32
PR	----	----	----	**6.68**	1.66	PR	----	----	----	**9.81**	**4.84**	PR	----	----	----	**13.80**	1.14
TR	----	----	----	----	**7.79**	TR	----	----	----	----	**16.03**	TR	----	----	----	----	**12.57**

ROUGHNESS 3

	Small size						Medium size						Large size				
	PB	TB	PR	TR	D		PB	TB	PR	TR	D		PB	TB	PR	TR	D
S	**3.31**	**2.81**	1.94	**2.57**	**3.44**	S	**6.07**	**5.70**	**5.26**	0.98	**7.72**	S	**4.85**	**6.24**	**6.52**	1.55	**8.30**
PB	----	0.20	1.94	**6.37**	0.58	PB	----	0.60	1.51	**8.03**	0.77	PB	----	1.15	1.51	**3.82**	**4.10**
TB	----	----	1.41	**5.53**	0.70	TB	----	----	0.90	**7.76**	1.50	TB	----	----	0.40	**5.32**	**3.24**
PR	----	----	----	**5.14**	**2.21**	PR	----	----	----	**7.59**	**2.65**	PR	----	----	----	**5.64**	**2.87**
TR	----	----	----	----	**6.15**	TR	----	----	----	----	**10.72**	TR	----	----	----	----	**7.62**

ROUGHNESS 4

	Small size						Medium size						Large size				
	PB	TB	PR	TR	D		PB	TB	PR	TR	D		PB	TB	PR	TR	D
S	**2.17**	0.88	**2.38**	**4.14**	**4.26**	S	**5.93**	**6.91**	**5.76**	**3.20**	**7.46**	S	**6.28**	**7.24**	**8.61**	1.22	**10.5**
PB	----	1.45	**5.66**	**7.17**	**2.77**	PB	----	0.10	0.37	**8.72**	**2.07**	PB	----	0.47	0.61	**7.13**	**2.14**
TB	----	----	**4.00**	**5.74**	**4.14**	TB	----	----	0.53	**10.07**	**2.17**	TB	----	----	0.10	**8.14**	1.71
PR	----	----	----	**2.46**	**8.39**	PR	----	----	----	**8.67**	**2.47**	PR	----	----	----	**9.68**	1.83
TR	----	----	----	----	**9.50**	TR	----	----	----	----	**9.93**	TR	----	----	----	----	**11.52**

spheres, rods (with transverse orientation) and blades (with every orientation) and discs are greater on the smoothest bed. For example, the mean friction angles (on Roughness 1) for transverse rods and spheres are scarcely more than half those for blades (in any orientation), parallel rods and discs. However, as bed roughness increases, there is a general increase in the mean friction angle for all shapes, but the difference in mean friction angles between the various shapes decreases (Table 6.4). In other words, increasing the roughness provides an increasingly stable base for all test grains. This is because an increase in bed roughness results in a greater spacing of pivot points, which creates a more stable resting position for the test particles. Although there is always a greater difference in friction angle between the parallel and transverse orientation in rod shapes, the relative difference decreases as bed roughness increases. For the small test particles on the smoothest bed (Roughness 1), parallel blades have the greatest friction angle (58^0), and in decreasing order the other shapes are: 55° for both parallel rods and discs, 51° for transverse blades, 39° for spheres and 33° for the transverse rods (Table 6.4). On Roughness type 4, however, discs have the greatest friction angle (81°) and the decreasing order is 75° and 72° for parallel and transverse blades respectively, 69° spheres, 63° parallel rods and 58° transverse rods.

For the medium size test grains, Tables 6.4, 6.6 and Figure 6.4 show that for most shapes, friction angles are lower than those for the smaller-sized test grains on each of the bed roughness types. On almost all the bed roughnesses discs are the most stable, with the highest friction angles, whereas transverse rods and spheres are the least stable shapes. As with the small test grains, the medium-sized particles show only small differences between blades (parallel and transverse orientation), parallel rods and discs. Friction angles for these shapes are always greater than for spheres and transverse rods, but differences diminish as bed roughness increases. Transverse rods tend to have the lowest friction angles on each bed roughness, while spheres are a close second.

Measurements with large-sized test particles show that friction angles for all particles are smaller than those measured with small and medium-sized test particles (Table 6.4 and Figure 6.4). In other words, particles in all shape classes on every bed roughness start to move at lower friction angles. Measurements with spheres and rods show very low friction angles, which are very different from the other shapes on roughnesses 1 and 2. However, as Figure 6.4 and Table 6.4 show, the difference in friction angle between particles of different shape and orientation decreases as the bed roughens. On the smoothest bed (roughness 1), rods with transverse orientation (19°)

and spheres (22°) have the lowest friction angles and the increasing rank order for parallel blades, transverse blades parallel rods and discs is 35°, 37°, 41° and 44° respectively. Measured friction angles are not very different between roughness 1 and roughness 2 for spheres and transverse rods but differences increase for parallel and transverse blades, as well as for parallel rods (Tables 6.4, 6.5 and Figure 6.4). On roughness 3 and roughness 4 spheres and transverse rods have the lowest mean friction angles but differences between other shapes decrease in comparison the roughnesses 1 and 2.

Friction angle distributions for the various test particles at different orientations on different bed roughnesses are shown in Table A3.1. The results confirm that spheres and transverse rod-shaped particles tend to move at the lowest friction angles. Especially on the smoothest bed (roughness 1), cumulative friction angle distributions systematically steepen with increasing particle size for transverse rods and spheres (Figure 6.5). Figure 6.6 shows the friction angle distributions for particles with different shapes and orientations on various bed roughnesses. Both Figures 6.5 and 6.6 indicate that differences in friction angle distributions between various shapes (especially in the small size group) tend to decrease as bed roughness increases. Figure 6.6 also indicates that transverse rod and sphere-shaped particles predominantly move over a smaller range of friction angles, while blade and disc-shaped particles have much wider distributions.

The standard deviations for the friction angles measured for different shapes averaged on four bed roughnesses are shown in Table 6.6. For the small-size test particles on roughness 1, there is no significant difference in the standard deviations between the different shapes. Standard deviations vary from 7.9 (transverse rod) to 11.3 (parallel blade). On all the other bed roughnesses small-sized spheres and transverse-rods have the greatest standard deviations and this increases as bed roughness increases. In rank order for spheres the standard deviation is 13, 14 and 15 for roughnesses 2, 3 and 4, while for transverse rods the order is 12, 12.7 and 13.5 for roughnesses 2, 4 and 3 respectively. These results indicate that, for the smallest test particles, spheres and rods with transverse orientations have a relatively large range of friction angles as bed roughness increases. On the other hand, there is no similar systematic variation in standard deviation for parallel and transverse blades or parallel rods and discs on the same bed roughnesses. Thus spheres have the highest standard deviations while parallel rod have the lowest. Large standard deviations in the spheres and transverse-rods arise

Table 6.6 Standard deviations for friction angle measurements with test grains from six shape/orientation classes on four different bed roughnesses. B.T: Blade with transverse orientation, B.P: Blade with parallel orientation, R.T: Rod with transverse orientation, R.P: Rod with parallel orientation, S: Sphere, D: Disc

Bed roughness type	Small test size (24 mm)							Medium test size (48 mm)							Large test size (96 mm)						
	S	B.T	B.P	R.T	R.P	D	Mean	S	B.T	B.P	R.T	R.P	D	Mean	S	B.T	B.P	R.T	R.P	D	Mean
Roughness 1	9.7	11.0	11.3	7.9	11.1	9.9	10.2	5.2	11.1	11.0	5.9	10.0	10.0	8.9	5.3	8.3	6.1	4.9	8.5	11.0	7.4
Roughness 2	13.0	10.0	9.0	12.0	10.0	12.0	11.0	8.2	11.0	11.7	9.0	10.2	8.4	9.8	6.0	11.0	10.0	5.1	8.4	11.0	8.6
Roughness 3	14.0	12.9	9.9	13.5	8.4	13.3	12.0	11.7	11.7	12.7	7.4	9.9	9.7	10.5	9.6	9.2	10.0	7.7	9.6	13.2	9.9
Roughness 4	15.0	10.9	10.5	12.7	9.3	11.0	11.6	8.8	8.3	10.7	9.1	10.0	13.0	10.0	6.9	11.4	12.3	6.8	9.0	9.3	9.3
Mean	12.9	11.2	10.2	11.5	9.7	11.6	11.2	8.5	10.5	11.5	7.9	10.0	10.3	9.8	7.0	10.0	9.6	6.1	8.9	11.1	8.8

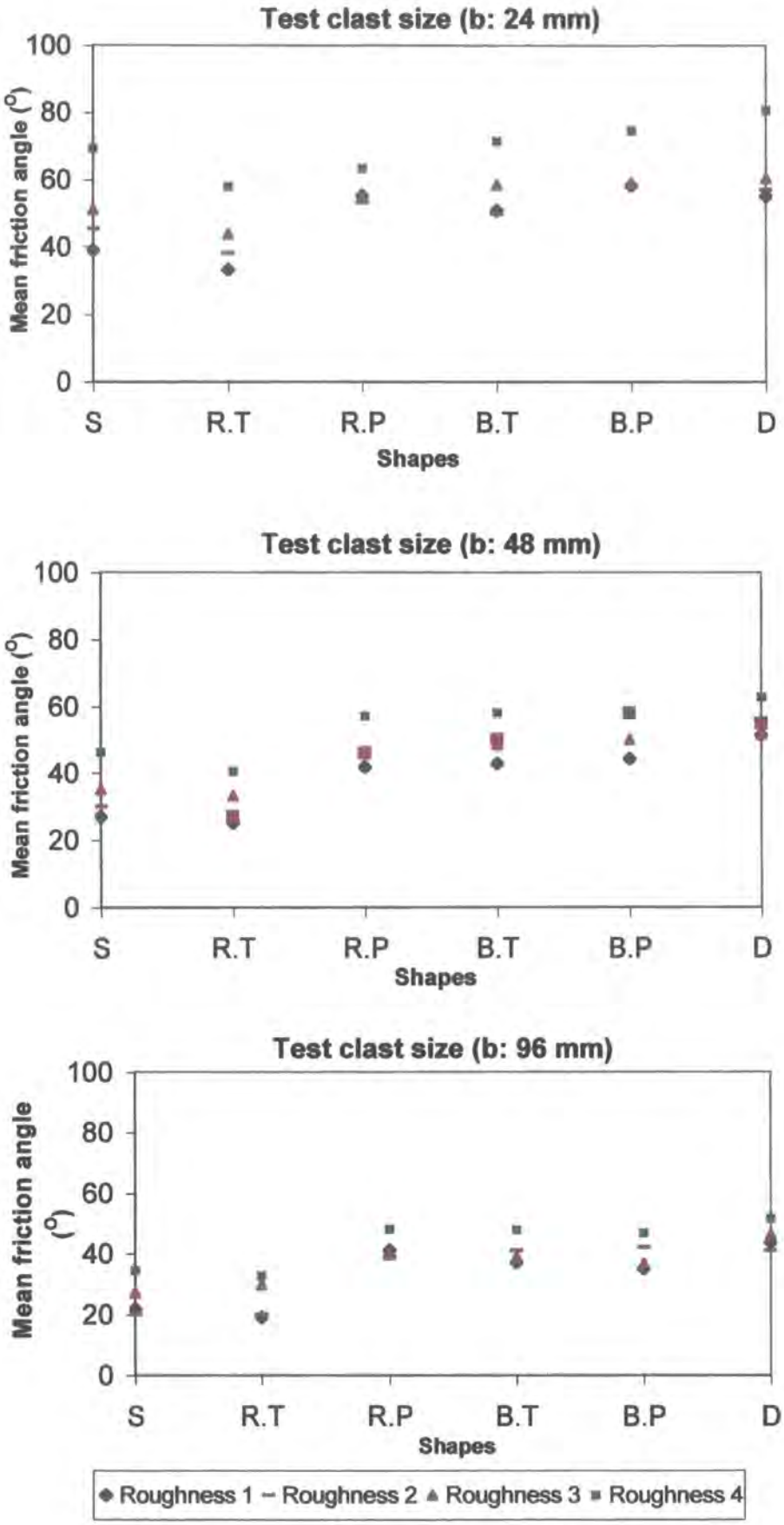

Figure 6.4 Mean friction angles measured for different shape/orientation of particles in three test size groups on four bed roughnesses. (S: sphere, B: blade, R: rod, D: disc, P: parallel orientation, T: transverse orientation.).

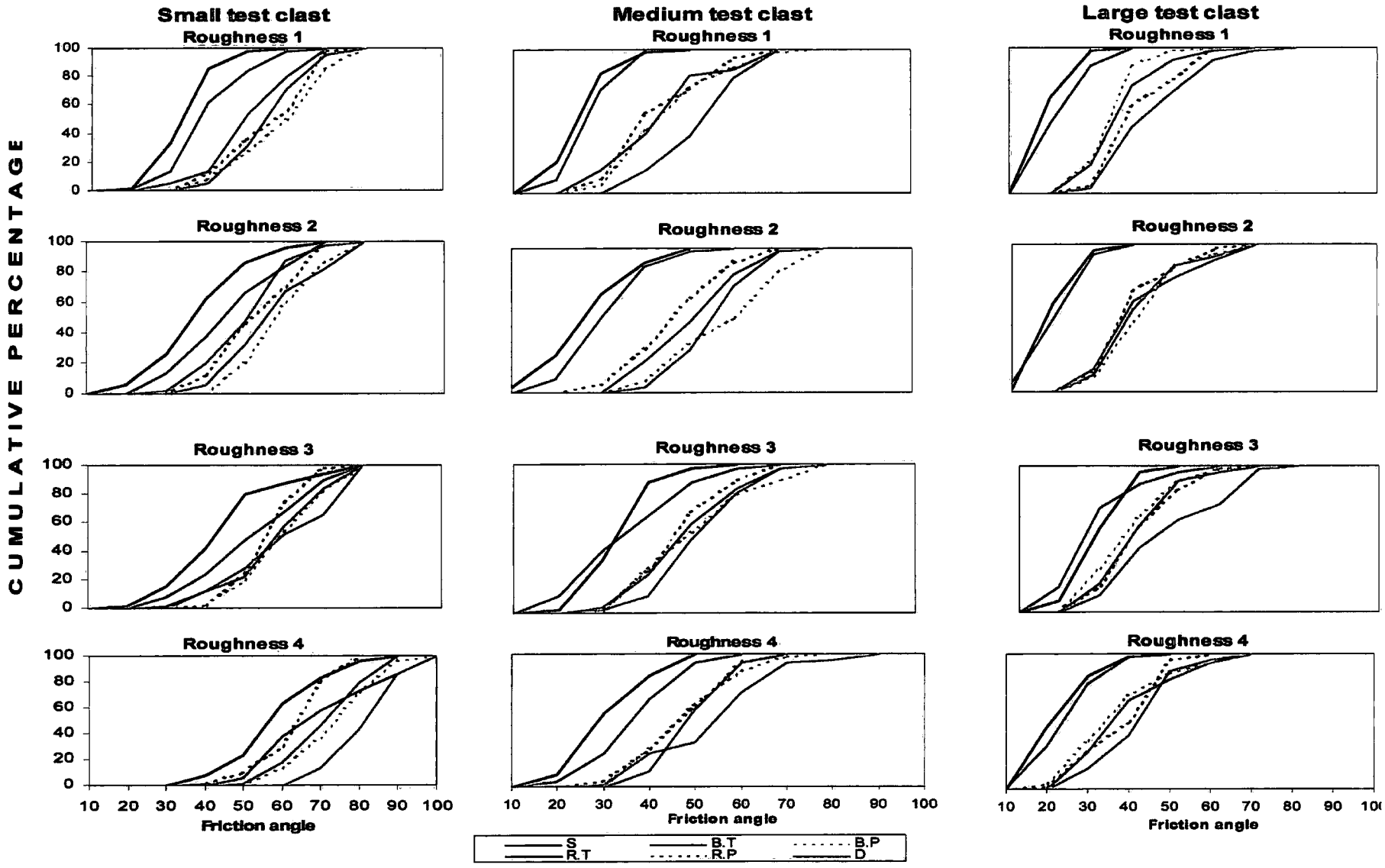

Figure 6.5 Cumulative friction angle distributions for the test particles with different shape and orientation in three size categories and on four bed roughnesses.

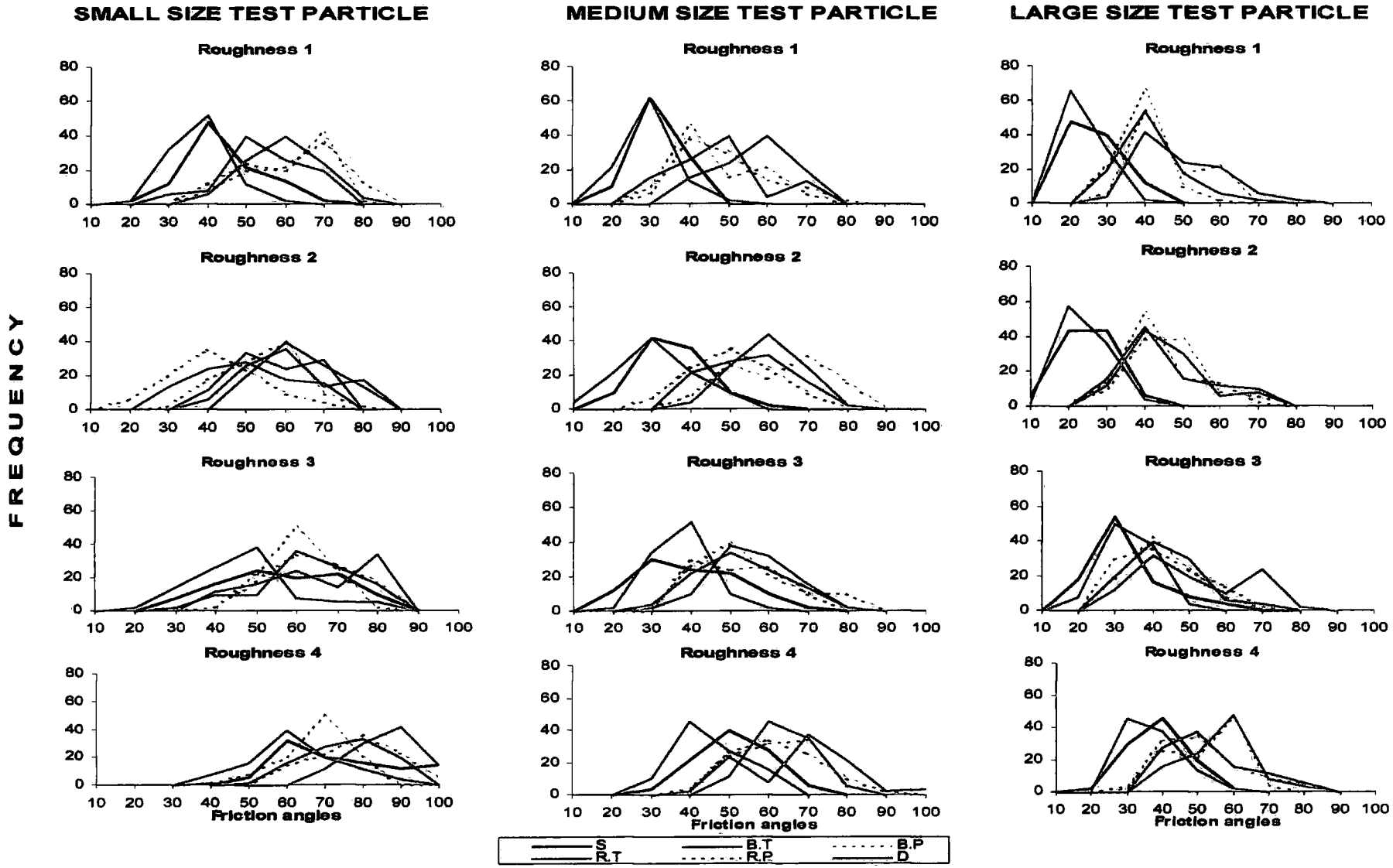

Figure 6.6 Friction angle distributions for the test particles of diffrent shapes and size on four bed roughnesses.

because spheres and transverse particles sit easily into the cols between the bed base particles. The depth of these cols varies spatially on the base depending mainly on the sorting of the bed material. If the bed is formed with artificial large-scale unsorted grains, rather than being highly sorted (uniform size bed grains), the cols between the base particles would probably be deeper. Thus because of poor sorting of the bed material, small-sized sphere-shaped particles may sit in large and deep cols which requires a relatively high friction angle for entrainment. In other places, if the sphere is large enough to bridge the cols, a low friction angle results. On the other hand both transverse and parallel rods, as well as discs cannot easily sit in the cols between the particles, and largely bridge across the gap (because of their large projection surface) and hence sit on top of the bed particles. Thus friction angle measurements with flat particles (low c/b ratio) lead to a lower range of standard deviation values but greater friction angles.

For medium-sized test particles, spheres and transverse rods have lower standard deviations on every bed roughness types when compared with the small test particles (Table 6.6). On almost all roughness types, except for discs on roughness 2 and 4, there is no significant variation between blades (with every orientation), parallel rods and discs (Figure 6.6).

In general, large-sized test particles show lower standard deviation values on bed roughness 1 than those of small and medium size test particles. Transverse-rods and spheres have the lowest standard deviations. As with small and medium test particles there is an increase in standard deviation as bed roughness increases (except roughness 3). These measurements also demonstrate that, on small bed roughnesses, large transverse rods and spheres have very steep and uniform friction angle distributions, but the uniformity of the distribution decreases with increasing bed roughness (Figures 6.5, 6.6.and Table A3.1). Blades in both orientations, parallel rods and disc-shaped particles, on the other hand, have generally larger standard deviations and there is also no systematic variation between different bed roughnesses. (Figure 6.6 and Table 6.6). For large size test particles, transverse rods have the lowest standard deviation on Roughness 1 (4.9), which is also the lowest value among the three size ranges of test particles, while discs have the greatest (13.2).

6.5 VARIABILITY IN FRICTION ANGLES OF PARTICLES OF EQUAL WEIGHT BUT VARYING SHAPE AND ORIENTATIONS ON BEDS OF DIFFERENT ROUGHNESS.

Many earlier experiments on friction angles concentrated mainly on the importance of particle size in relation to different bed roughnesses (Kirchner *et al.*, 1990; Buffington *et al.*, 1992). Although it was found that friction angles decrease with increasing relative grain size, it was also discovered that there was a large scatter in the results. In the measurements undertaken here the effect of particle weight is standardised and the investigation focused on how particles of equal mass but different shape affect friction angles. Although the weight of a particle has no bearing on its mechanistic behaviour in tilting table experiments, it is important in fluvial environments. Standardising the mass of a particle reduces the degree of freedom when forming differing shaped particles.

For the experiment, four artificially made particles of similar weight (750 g) were compared. These were of sphere, blade, rod and disc shapes. Dimensions of the test particles are given in Table 6.7. Each particle was placed randomly on the bed. Two particle orientations were considered; long axis parallel to and transverse to the slope. As similar to the previous experiments, measurements were repeated 50 times for each of the test particles on each of the four bed roughness types.

Table 6.7 The tri-axial dimensions (cm) and weights (g) of the test particles (equal weight in four shape classes) used for the experiment.

Shape	a-axis	b-axis	c-axis	Weight
Sphere	8.6	8.6	8.6	750 g
Blade	16.0	6.8	3.0	750 g
Rod	11.4	6.0	6.0	750 g
Disc	10.0	10.0	3.4	750 g

The results show that, in general, spheres and transverse rod-shaped particles have the lowest mean friction angles on almost every bed roughness (Table 6.8). Mean friction angles tend to increase towards the roughest bed for each particle shape. On bed roughness 1 the mean friction angle for parallel-rods is almost double that for transverse rods. This difference decreases slightly as the bed roughens (Table 6.8 and Figure 6.7). On the other hand, parallel and transverse blades do not show a similar difference.

Table 6.8 Mean friction angle distributions of test particles with equal weight but six shape/orientation classes on the four different bed roughnesses

Bed roughness	SHAPE AND ORIENTATION					
	S	B.T	B.P	R.T	R.P	D
Roughness 1	19.4	40.3	34.6	19.9	40.6	38.7
Roughness 2	22.3	37.9	41.7	25.2	42.8	39.9
Roughness 3	27.8	42.3	40.2	28.2	47.6	43.4
Roughness 4	33.2	52.9	48.0	34.9	54.4	51.2
Mean	**25.7**	**43.4**	**41.1**	**27.1**	**46.4**	**43.3**

B.T : Blade with transverse orientation
B.P: Blade with parallel orientation
R.T: Rod with transverse orientation
R.P: Rod with parallel orientation
S: Sphere
D: Disc

Table 6.9 shows the results of statistical comparisons of friction angles measured with the test particles. Results indicate that, on almost all bed roughness types, statistical differences in mean friction angles are less between blades with parallel and transverse orientations, parallel-rods and discs. However, differences tend to become more significant between spheres, transverse-rods and blades (regardless of orientation) parallel rods, and discs.

Table 6.9 Statistical comparison of friction angles measured with test particles that have equal weight but various shape/orientation on four bed roughness types. (critical value of "t" at the 0.05 is 1.98 for each measurements. The values shown in bold indicate a statistically significant difference between the compared shapes/orientations).

Roughness 1

	PB	TB	PR	TR	D
S	**15.58**	**14.24**	**21.00**	0.57	**12.83**
PB	----	**3.69**	**5.38**	**14.76**	**2.60**
TB	----	----	0.20	**13.77**	0.82
PR	----	----	----	**20.12**	1.19
TR	----	----	----	----	**12.39**

Roughness 2

	PB	TB	PR	TR	D
S	**8.96**	**13.36**	**11.44**	**2.36**	**9.31**
PB	----	**2.11**	**2.32**	**7.74**	0.93
TB	----	----	0.54	**12.03**	0.91
PR	----	----	----	**10.19**	1.26
TR	----	----	----	----	**8.03**

Roughness 3

	PB	TB	PR	TR	D
S	**6.53**	**8.57**	**12.09**	0.37	8.25
PB	----	0.97	**3.49**	**6.59**	1.38
TB	----	----	**2.75**	**8.81**	0.51
PR	----	----	----	**12.60**	**2.00**
TR	----	----	----	----	**8.40**

Roughness 4

	PB	TB	PR	TR	D
S	**9.42**	**13.50**	**15.00**	1.34	**11.00**
PB	----	**2.79**	**3.71**	**7.94**	1.69
TB	----	----	0.92	**11.70**	0.91
PR	----	----	----	**13.05**	1.77
TR	----	----	----	----	**9.53**

Figure 6.7 and Table 6.9 show that there are no major difference in mean friction angles between transverse-blades, parallel-rods and discs on roughness 1. On roughnesses 2, 3 and 4 (with the exception of transverse blades), mean friction angles increase for all shapes and orientations (Figure 6.7 and Tables 6.8 and 6.9).

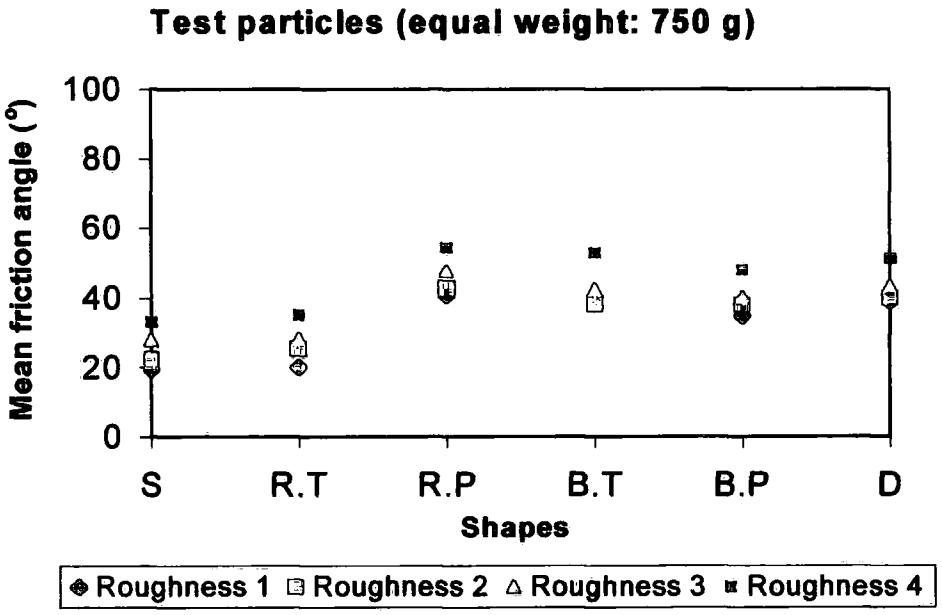

Figure 6.7 Mean friction angles for particles of various shapes but equal weights.
(S: sphere, B.T: Blade in transverse orientation, B.P: blade with parallel orientation, R.T: rod with transverse orientation, R.P: rod with parallel orientation, D: disc)

There are no major differences between mean friction angles on bed roughnesses 1 and 2 for discs, parallel rods and spheres, but differences increase for parallel-blades and transverse-rods. The increasing order of the average friction angle over all the bed roughnesses is 25.7° for spheres, 27.1° for transverse rods, 41.1° for parallel blades, 43.3° for discs, 43.4° for transverse blades and 46.4° for transverse rods. These results indicate that spheres and transverse rods have relatively low mean friction angles on most bed roughnesses. As a controlling factor, orientation has a significant influence on mean friction angle for rod-shaped particles. Rods with transverse orientation have noticeably lower mean friction angles. However, a similar relationship does not exist between transverse and parallel blades. The effect of orientation on mean friction angle decreases as bed roughness increases for blade-shaped particles, but this is not true for

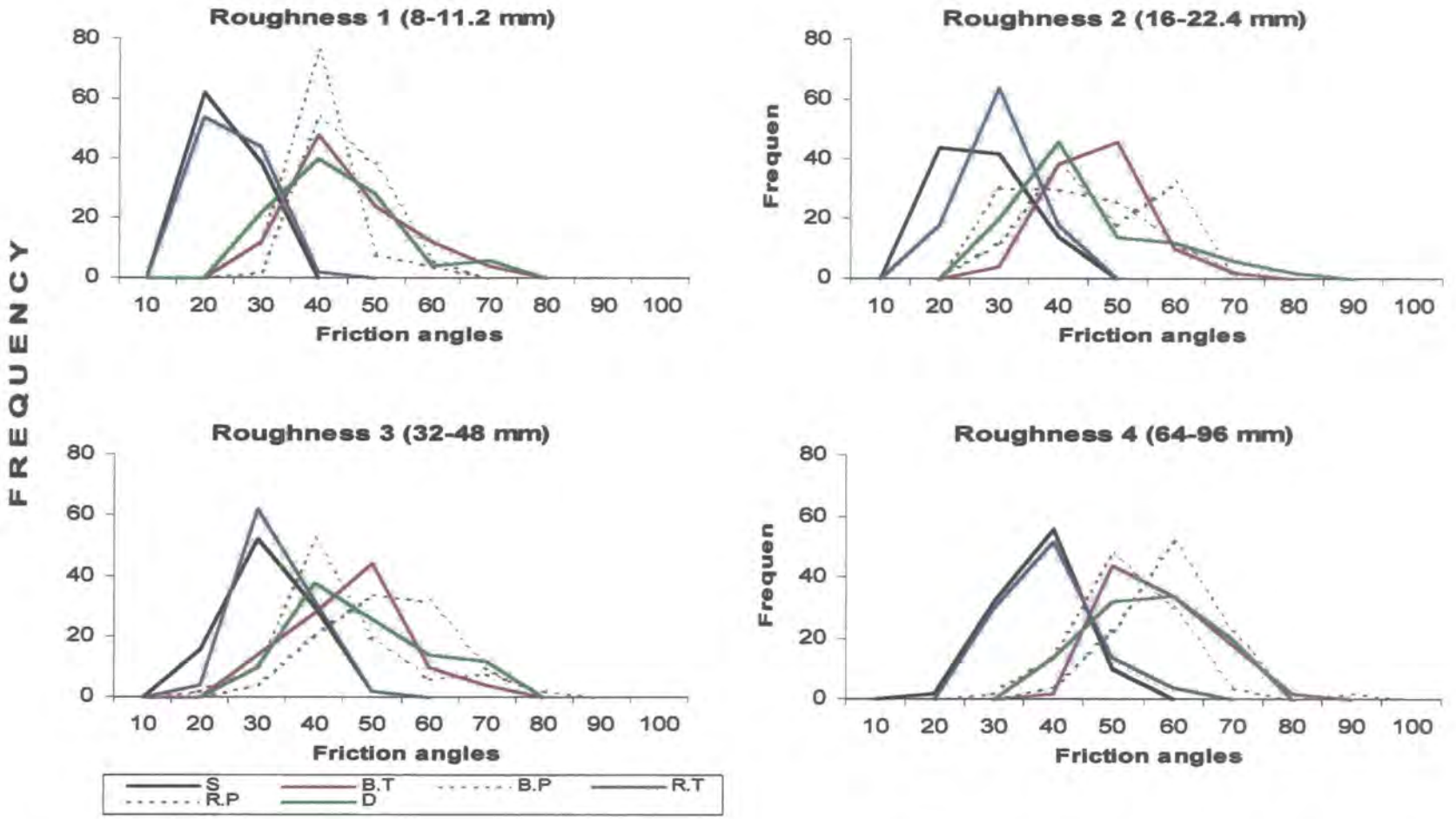

Figure 6.8 Friction angle distributions of the test particles with equal weight but different shapes and orientation on four bed roughnesses. (S: sphere, B.T: blade with transverse orientation, B.P: blade with long axis parallel to slope, R.T: rod with transverse orientation, R.P: rod with long axis parallel to slope, D: disc).

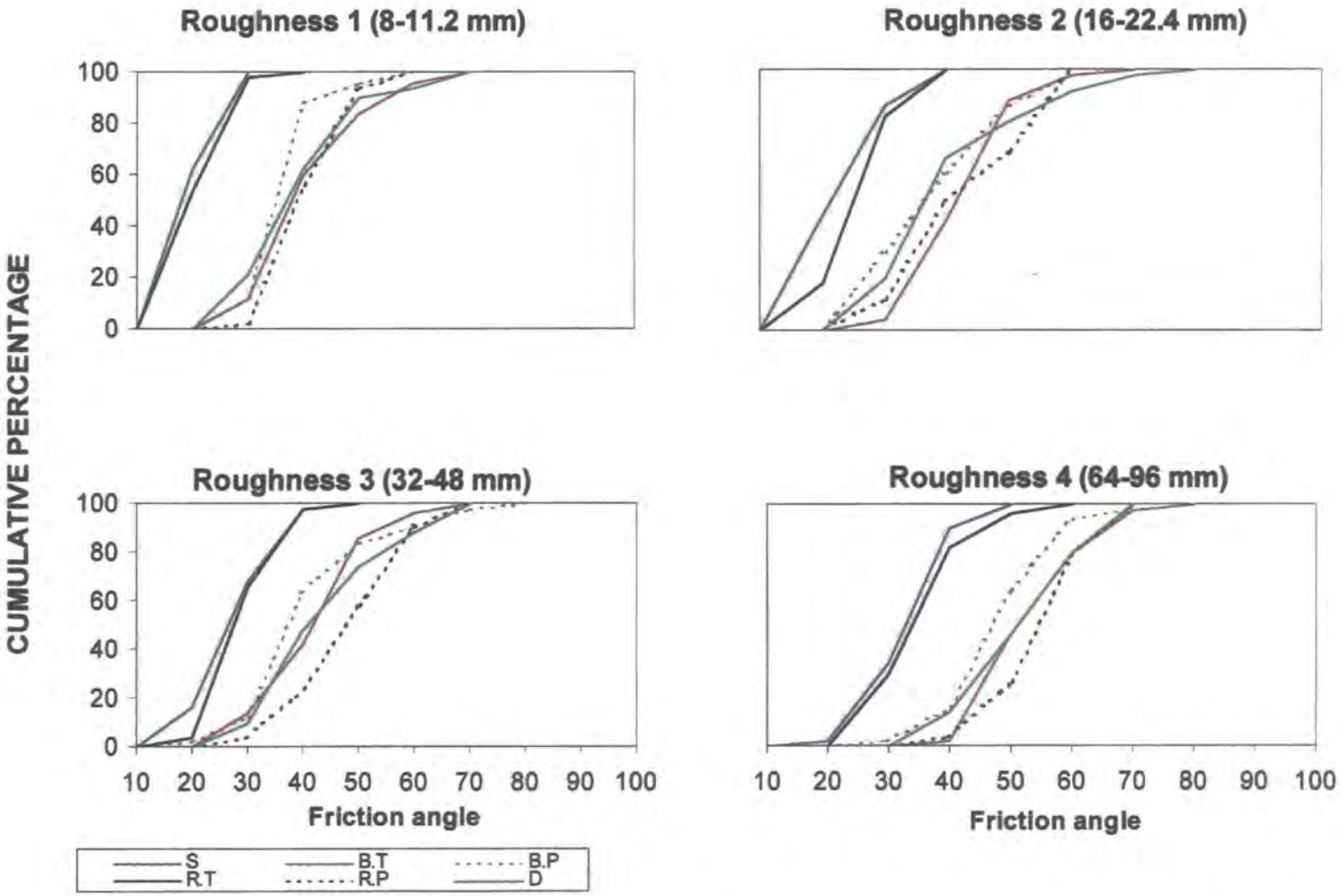

Figure 6.9 Cumulative percentage distributions of friction angles for test particles with equal weight but different shapes on four bed roughnesses.

rod-shapes. The distributions of the friction angle of the tilting table tests for particles of equal weight but different shapes and orientations on various bed roughnesses are shown in Figures 6.7, 6.8 and also in Table A3.2.

Particles of all shapes and orientations placed on Roughness 1 tend to have a relatively low range of friction angles and low standard deviations (Appendix 8 and Table 6.10). Spheres and rod-shaped particles tend to have lower friction angles and distributions are clustered around the mean (Figure 6.8). Figures 6.8, 6.9 and Table A3.2 show that there is an inverse relation between the friction angle of spheres and transverse-rods and bed roughness. On Roughness 1, spheres and transverse-rods have noticeably lower friction angles and have more uniform friction angle distributions. They have lower standard deviation values than the other shapes and, hence, their cumulative friction angle distributions are relatively steep. However, on rougher beds (especially on the roughest bed) there tends to be a decrease in the uniformity of friction angle distributions (Table 6.10 and Figure 6.9). Figure 6.8 shows that despite a very similar distribution between spheres and transverse rods on almost every bed roughness, distributions are not similar for other shapes of test particle with various orientations. These differences in friction angle distribution between parallel and transverse blades, parallel rods and disc-shaped particles lead to an irregular variation in standard deviation values from one roughness to another.

Table 6.10. The standard deviations of the friction angle distributions of the test particles with equal weight, six various shapes/orientations on four different bed roughnesses.

Bed Roughness	**SHAPES WITH VARIOUS ORIENTATIONS**					
	S	**B.T**	**B.P**	**R.T**	**R.P**	**D**
Roughness 1	4.3	9.5	5.4	4.5	5.7	9.8
Roughness 2	6.6	10.1	7.9	5.6	10.8	11.6
Roughness 3	6.7	11.7	9.92	5.4	9.5	11.6
Roughness 4	5.9	9.3	8.4	6.9	8.0	9.9
Mean	**5.9**	**7.9**	**10.1**	**5.6**	**8.5**	**10.7**

B.T : Blade with transverse orientation
B.P: Blade with parallel orientation
R.T: Rod with transverse orientation
R.P: Rod with parallel orientation
S: Sphere
D: Disc

6.6 VARIABILITY OF FRICTION ANGLES WITH NATURAL PARTICLES OF DIFFERENT SHAPES AND ORIENTATIONS ON DIFFERENT BED ROUGHNESSES.

In the previous section friction angles were measured using artificially-formed test-particles that had symmetrical shapes. In general, it was found that friction angles were strongly dependent on particle shape, particle orientation, size and also roughness characteristics of the bed. In this section natural pebble-sized particles are used to determine the friction angles for the same experiments just undertaken. The aim of using natural pebbles is to determine whether they would give results similar to those obtained from the earlier experiments with artificially-formed test particles. However, it is important to note that shapes of the natural test particles used in these experiments are not similar to those that are transported in the study rivers. In other words, natural gravel carried by the Trout Beck is less uniform in shape (See Chapters 4 and 5). Therefore very little of the natural bed material is in the form of "true" spheres, blades, rods and discs. Thus most of the blades and rods are "marginal", tending towards spheres and disc, respectively. Many of the spheres and discs are also blocky in nature. Although the particles used in these experiments are naturally formed, geometrically they are much closer to perfect spheres, blades, rods and discs than is usual in natural bed material. Therefore, their hydraulic behaviour and friction angles are assumed to be different from the natural bed material at the three study sites.

Four natural sandstone pebbles (b-axis 72-84 mm) were used for the measurements. These particles had shapes approximating to a sphere, a blade, a rod and a disc. The dimensions of the particles are given in Table 6.11.

Table 6.11. The tri-axial dimensions (cm) and weights (g) of the natural test particles used for the experiment.

Shape	a-axis	b-axis	c-axis	Weight (g)
Sphere	8.4	8.0	7.7	736.0
Blade	28.7	7.2	3.6	727.0
Rod	26.0	7.2	7.0	1175.0
Disc	10.0	8.4	2.8	378.0

Table 6.12 and Figure 6.10 shows the mean friction angles of the natural test particles for the four bed roughness types. In general, all shapes have lower mean friction angles on bed Roughness 1. Friction angles increase as bed roughness increases which is similar to the previous experiments.

Table 6.12. Mean friction angles (in degrees) of the natural test particles in various shape classes on four different bed roughnesses.

Bed	SHAPES AND ORIENTATIONS					
roughness	S	B.T	B.P	R.T	R.P	D
Roughness 1	20	40	35	24	39	39
Roughness 2	27	46	40	30	39	44
Roughness 3	28	53	43	35	46	47
Roughness 4	34	55	50	36	54	58
Mean	**27.3**	**48.5**	**42**	**31.3**	**44.5**	**47.0**

The difference in mean friction angles between the Roughness 1 and the roughest bed (Roughness 4) are 14° for the sphere, 15° both for the blade in parallel and transverse orientation and for the parallel-oriented rod, 17° for the transverse rod and 19° for the disc-shaped particle. Comparison of the mean friction angles measured with artificial particles of equal weight but different shapes and natural particles of different shapes and weight indicate that, except for the naturally formed rod in a parallel orientation, mean friction angles of the natural test particles were greater than the artificial. Except on bed Roughness 1, the mean friction angles recorded with natural particles were slightly greater than those with artificial particles of equal weight (Table 6.8 and Table 6.12).

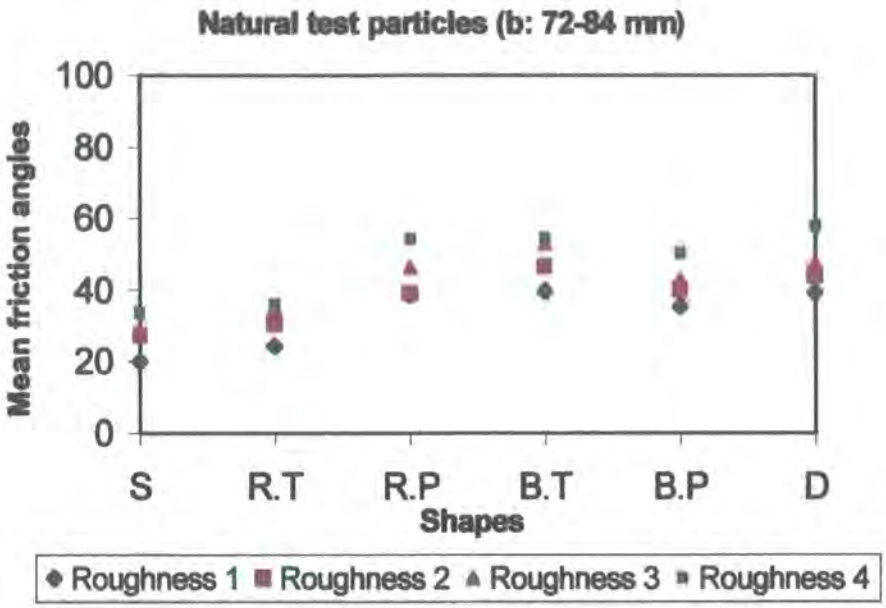

Figure 6.10. Mean friction angles of natural particles of various shapes.

(S: sphere, B.T: Blade in transverse orientation, B.P: blade in parallel orientation, R.T: blade in transverse orientation, R.P: rod in parallel orientation, D: disc).

As with the earlier measurements, spheres and transverse rods have the lowest mean friction angles on almost every bed roughness. In terms of the effect of orientation on mean friction angle, Table 6.12 and Figure 6.10 show that particle orientation is as important as particle shape and size. There is always a large and therefore statistically significant difference between parallel and transverse orientations of rods on every bed roughness (Table 6.13).

The results of the tilting tests are listed in Table A3.3. Figure 6.11 indicates that on Roughness 1 all particles move over a small range of friction angles and therefore have lower standard deviations (Table 6.14). Hence, the cumulative friction angle distributions are relatively steep (Figure 6.12). The range of friction angles increases as bed roughness increases (Figure 6.11 and Table A3.3).

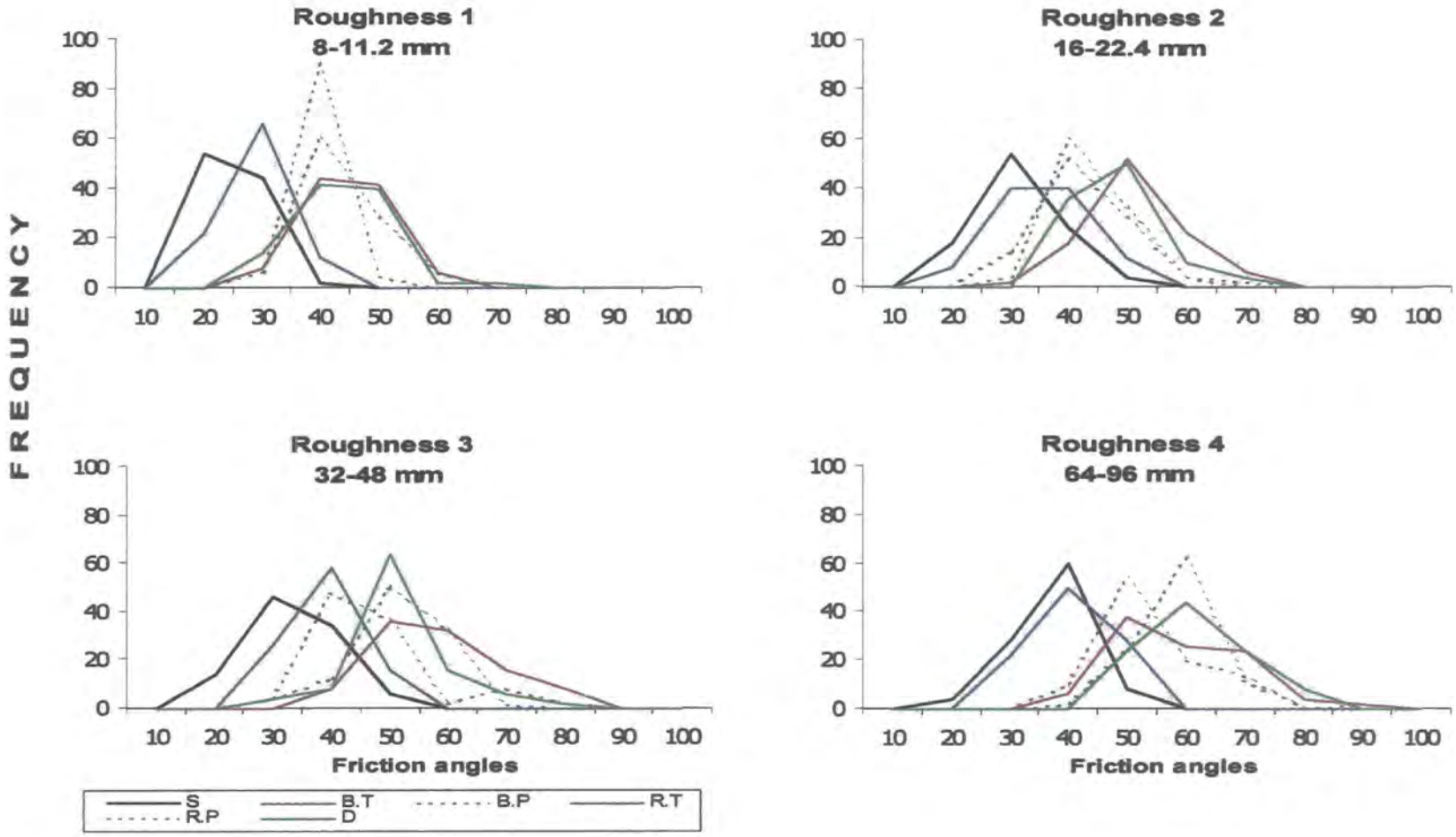

Figure 6.11 Friction angle distributions of the natural test particles with different shpes and orientation on four bed roughnesses.

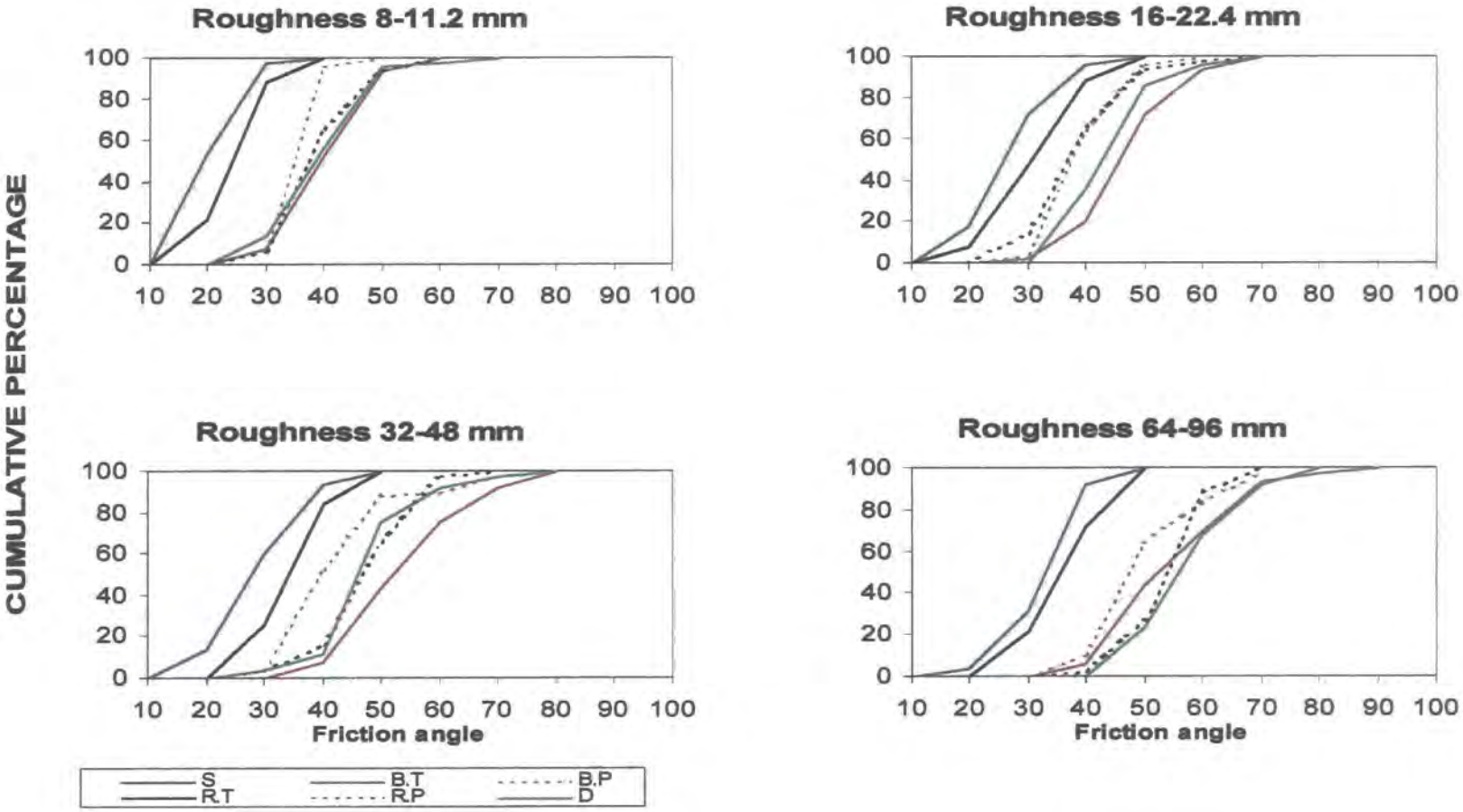

Figure 6.12 Cumulative friction angle distributions for natural test particles in different shapes and orientation on four bed roughnesses (S: sphere, B.T: transverse blade, B.P: parallel blade, R.T: transverse rod, P.R: parallel rod, D: disc).

Table 6.13 Statistical comparison of friction angles measured with natural test particles of various shapes and orientations on four bed roughness types. Critical value of "t" at the 0.05 level is 1.98 for each measurement. (The values shown in bold indicate a statistically significant difference between the compared shapes/orientations).

	Roughness 1						Roughness 2				
	PB	TB	PR	TR	D		PB	TB	PR	TR	D
S	**18.54**	**17.21**	**15.42**	**4.60**	**15.56**	S	**10.44**	**14.07**	**8.03**	**2.62**	**12.26**
PB	----	**3.92**	**2.82**	**12.62**	**3.32**	PB	----	**4.62**	0.88	**6.48**	**2.77**
TB	----	----	0.71	**13.02**	0.20	TB	----	----	**4.84**	**10.66**	1.71
PR	----	----	----	**11.52**	0.47	PR	----	----	----	**5.23**	**3.23**
TR	----	----	----	----	**11.77**	TR	----	----	----	----	**8.96**

	Roughness 3						Roughness 4				
	PB	TB	PR	TR	D		PB	TB	PR	TR	D
S	**7.91**	**13.43**	**11.36**	**4.27**	**11.21**	S	**10.46**	**12.38**	**16.10**	1.77	**15.40**
PB	----	**5.00**	1.83	**4.79**	**2.41**	PB	----	**2.10**	**2.28**	**8.48**	**4.01**
TB	----	----	**3.66**	**10.65**	**2.87**	TB	----	----	0.25	**10.42**	1.72
PR	----	----	----	**8.03**	0.79	PR	----	----	----	**13.06**	**2.38**
TR	----	----	----	----	**8.10**	TR	----	----	----	----	**13.11**

(S: sphere, B.T: Blade in transverse orientation, B.P: blade in parallel orientation, R.T: blade in transverse orientation, R.P: rod in parallel orientation, D: disc).

In common with the previous experiments, Table 6.14 shows that there are statistically significant differences between blades (regardless of orientation), parallel-rods, discs and spheres and also transverse rods but these differences decrease noticeably among blades (with both orientations), parallel rods and discs and a similar pattern is also true between transverse-rods and spheres. Table 6.16 also shows that, although, there is no significant difference between transverse and parallel rods, differences are relatively constant and significant between transverse rod and parallel rod on almost every bed roughness.

Table 6.14 The standard deviations of the friction angle distributions of the natural test particles in four shape classes on four different bed roughnesses

Bed roughness	SHAPES WITH VARIOUS ORIENTATIONS					
	S	B.T	B.P	R.T	R.P	D
Roughness 1	4.5	6.7	3.8	4.9	7.3	7.6
Roughness 2	6.5	7.4	6.2	7.5	8.3	7.4
Roughness 3	7.7	10.3	10.1	6.5	7.7	9.1
Roughness 4	6.3	10.2	9.5	7.4	6.4	9.2
Mean	**6.3**	**8.7**	**7.4**	**6.6**	**7.4**	**8.3**

(S: sphere, B.T: Blade in transverse orientation, B.P: blade in parallel orientation,R.T: blade in transverse orientation, R.P: rod in parallel orientation, D: disc).

6.7 VARIABILITY OF FRICTION ANGLES IN RELATION TO PARTICLE SIZE AND SHAPE ON A NATURALLY FORMED RIVER BED

Many early friction angle measurements were carried out on artificially-formed bed roughnesses, which differ from natural river beds. For example, Kirchner *et al* (1990) found that the surface topography of a water-worked bed is complex and therefore friction angle and particle protrusion vary widely among individual grains, even for a single grain size on a single bed. Comparison of unworked and water-worked surfaces clearly showed that the friction angle distributions of the two surfaces are very different. Friction angles measured on the unworked bed were found to be significantly greater than those for the water-worked bed. These differences increased with decreasing test grain size due mainly to the variations in grain packing geometry, local variability in the pocket geometry and grain protrusion (Kirchner *et al.*, 1990).

Following the use by Kirchner *et al* (1990) of flume-made surfaces, Dietrich and Kirchner (1992) presented the first friction angle data from the naturally-formed gravel surfaces of a streambed (For further details see Chapter 2). Although these earlier studies have done much to advance the understanding of the relationship between friction angle and particle size on natural bed surfaces, it is surprising that the effect of different particle shape on friction angle has not been investigated. In other words, the results obtained from these studies did not fully characterise the nature of the particle motion. This is because variations in friction angle distributions were expressed only as a function of test grain size, median bed grain size, and a bed sorting parameter. This

suggests that, in order to understand better the mechanisms of the particle motion, apart from other factors, the relationship between different grain shape and friction angles also needs to be investigated on a naturally-formed bed.

Thus the aim of this section is to measure the variability in friction angles in relation to particle shape and size on a bed that is composed of naturally-formed fluvial gravels. In order to achieve this an undisturbed sample of the bed surface (approximately $1m^2$) was collected from the Trout Beck experimental site. In common with Buffington *et al* (1992) method, the sampled bed was rebedded in a pebble and resin mixture, which was then mounted securely on a tilting table. The detail of the sampling method is explained in Chapter 3. The surface particle size of the bed surface was determined by applying Wolman's (1954) sampling method (See Chapter 3). Sampling was limited to particles greater than 8 mm. Figure 6.13 shows the grain size distribution of the sampled bed and Figure 6.14 is a photograph of the bed. The median particle size of the bed is 63 mm (D_{50}), while D_{90} is 103 mm, indicating a relatively poorly sorted gravel. The photograph shows that the surface of the bed is different from the artificially-formed bed roughnesses in terms of packing and the degree of infilling of grain pockets by fines (Figure 6.14). Packing of grains tends to vary noticeably due to spatial differences in grain-size distribution. Using this natural bed the same series of friction angles experiments as described in section 6.1 were carried out. The same set of test particles (both artificial and natural) were used. Due to the heavy weight of the natural bed sample and the nature of the tilting table, angles greater than 70° could not be measured on this test surface.

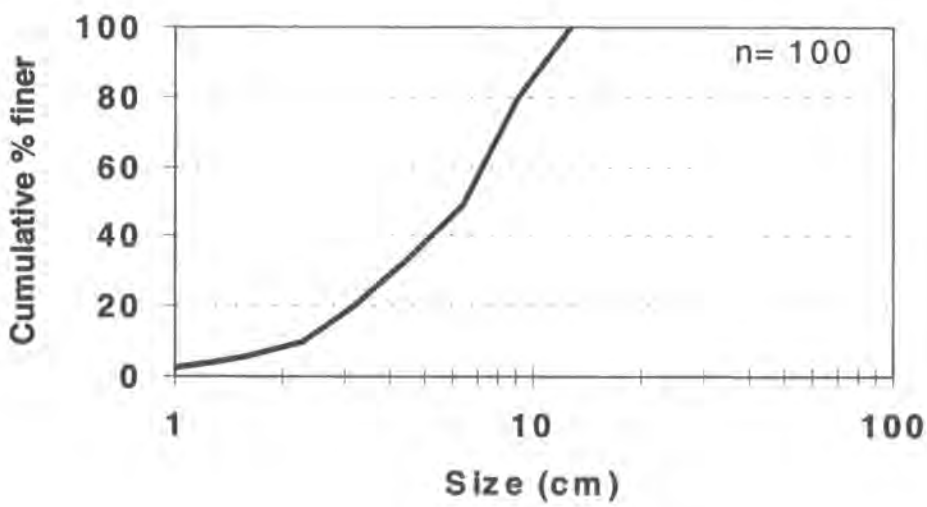

Figure 6.13 Cumulative percentage size distribution of the sampled natural bed.

Figure 6.14 The undisturbed natural channel bed used to determine friction angles for particles of various shape, orientation, size and weight Several of which are illustrated). Flow direction is from top to bottom of the picture. The field of view is approximately 65 cm across. From left to right axis of the large rod in the right of the photo is 96 mm.

6.8 VARIABILITY OF FRICTION ANGLE IN RELATION TO PARTICLE SIZE AND SHAPE ON A NATURALLY-FORMED BED

Table 6.15 Mean friction angle and standard deviation distributions for particles of various shapes and orientation in the three size groups for experiments with the natural bed. Note: values in brackets represent standard deviations for each shape.

Test Particles (b-axis)	Shape and orientation						
	S	B.T	B.P	R.T	R.P	D	Mean
24 mm	66 (9.2)	64 (8.2)	65 (7.2)	54 (7.6)	56 (7.2)	68 (3.7)	62.1 (7.2)
48 mm	51 (11.0)	57 (7.5)	56 (9.3)	49 (10.9)	58 (6.4)	59 (10.0)	55.0 (9.1)
96 mm	35 (7.5)	58 (8.9)	59 (7.2)	39 (10.0)	54 (7.4)	58 (8.5)	51.0 (8.3)
Mean	**50.6**	**59.7**	**60**	**47.3**	**56**	**61.7**	

(S: sphere, B.T: blade in transverse orientation, B.P: blade in parallel orientation, R.T: rod in transverse orientation, R.P: rod in parallel orientation, D: disc)

The results of the tilting tests are summarised in Table 6.15. In general there is a similar trend between the results of mean friction angle distributions measured on artificially-formed bed roughnesses and those from the natural bed.

In terms of size, Table 6.15 and Figure 6.15 indicate that, regardless of shape, there is the expected inverse relation between the mean friction angle and the test particle size. These results indicate that, in general, the mean friction angles measured on the natural bed are similar to those measured on artificially-formed bed roughnesses. However, measurements on roughnesses 1, 2 and 3 exhibit smaller mean values for most of the test particles (see Table 6.2). As with the previous experiments carried out on artificially-formed bed roughnesses, there is a greater difference between the mean friction angles of small and large spheres and also small and large transverse-rods in comparison with other shapes. In all size groups, spheres and rods with transverse orientation are the least stable particles (Table 6.15 and Figure 6.15). Table 6.16 shows a statistical comparison of the mean friction angles of particles of various shapes and size on the natural bed and indicates a relatively similar pattern of distribution to the previous friction angle measurements carried out on artificially-formed bed roughnesses.

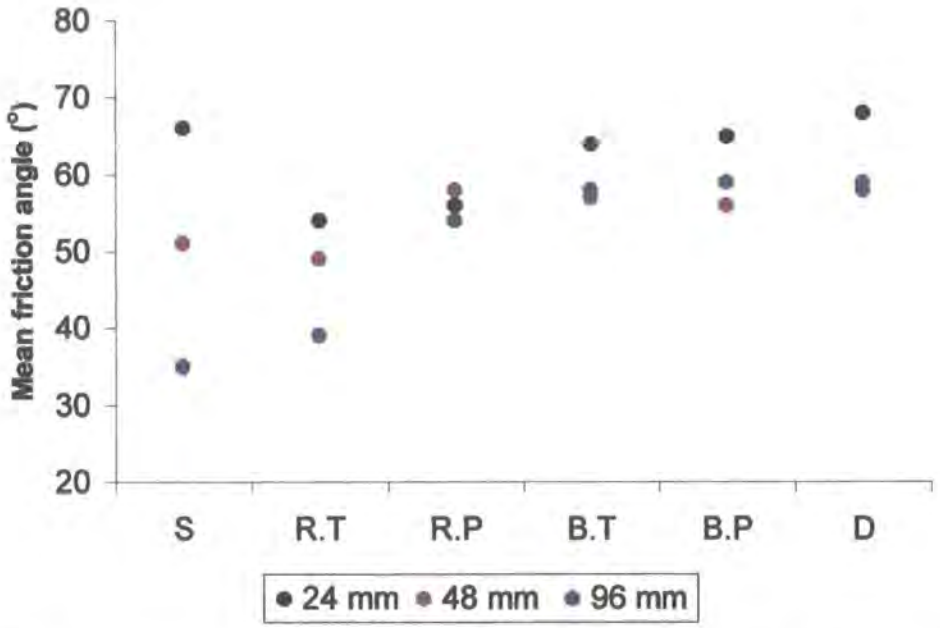

Figure 6.15 Mean friction angles for the different shapes and orientations of particles in the three size groups on the naturally formed bed (S: sphere, T.B: transverse blade, P.B: parallel blade, T.R: transverse rod, P.R: parallel rod, D: disc).

Table 6.16 Statistical significance of friction angles measured with various shapes and orientations of test particles of the three size groups on the natural bed. Note: The values shown in bold indicate a statistically significant difference between the compared shapes/orientations. (critical value of "t" at the 0.05 significance level is 1.98 for each measurements).

NATURAL BED

	Small size (24 mm)					Medium size (48 mm)					Large size (96 mm)				
	PB	**TB**	**PR**	**TR**	**D**	**PB**	**TB**	**PR**	**TR**	**D**	**PB**	**TB**	**PR**	**TR**	**D**
S	0.90	1.27	**6.3**	**7.10**	1.70	**2.30**	**3.20**	3.90	1.10	**3.40**	**15.90**	**13.90**	**12.90**	**2.30**	**14.10**
PB	----	0.50	**6.10**	**7.10**	**3.40**	----	0.80	1.50	**3.50**	1.30	----	0.20	**2.80**	**10.80**	0.50
TB	----	----	**5.30**	**6.20**	**3.60**	----	----	0.70	**4.50**	0.60	----	----	2.30	**9.80**	0.20
PR	----	----	----	1.10	**11.10**	----	----	----	**5.30**	0.10	----	----	----	**8.50**	**2.10**
TR	----	----	----	----	**12.0**	----	----	----	----	**4.50**	----	----	----	----	**9.80**

Comparisons of the mean friction angles measured on the natural bed and on artificially-formed bed roughnesses indicate some significant differences. Mean friction angles measured with small, medium and large test particles on the natural bed tend to be greater than those measured on artificially-formed roughnesses 1, 2 and 3 and the differences increase with decreasing bed roughness. However, differences between the mean friction angles on the natural bed and on roughness 4 and also, to some extent, on roughness 3 decline noticeably for each test particle compared to the other roughness types (Figure 6.16). Table 6.17 compares (statistically) mean friction angles measured on the natural bed and on artificially-formed beds and indicates that for almost every size group, differences for spheres and rods (with transverse orientation) are not statistically significant between the natural bed and roughness 4, but it tends to increase significantly as bed roughness decreases. However, there is no similar consistent variation for the other shapes. For example, for the small-sized test particles there is no significant difference in mean friction angles measured with parallel rods between the natural bed and roughnesses 1, 2 and 3, while it become significant on roughness 4. There is also some degree of irregular variation for transverse and parallel blades, and for discs. With medium-and large-sized test particles, differences in mean friction angles measured on the natural and artificial bed roughnesses tend to decrease as bed roughness increases for each shape of test particles.

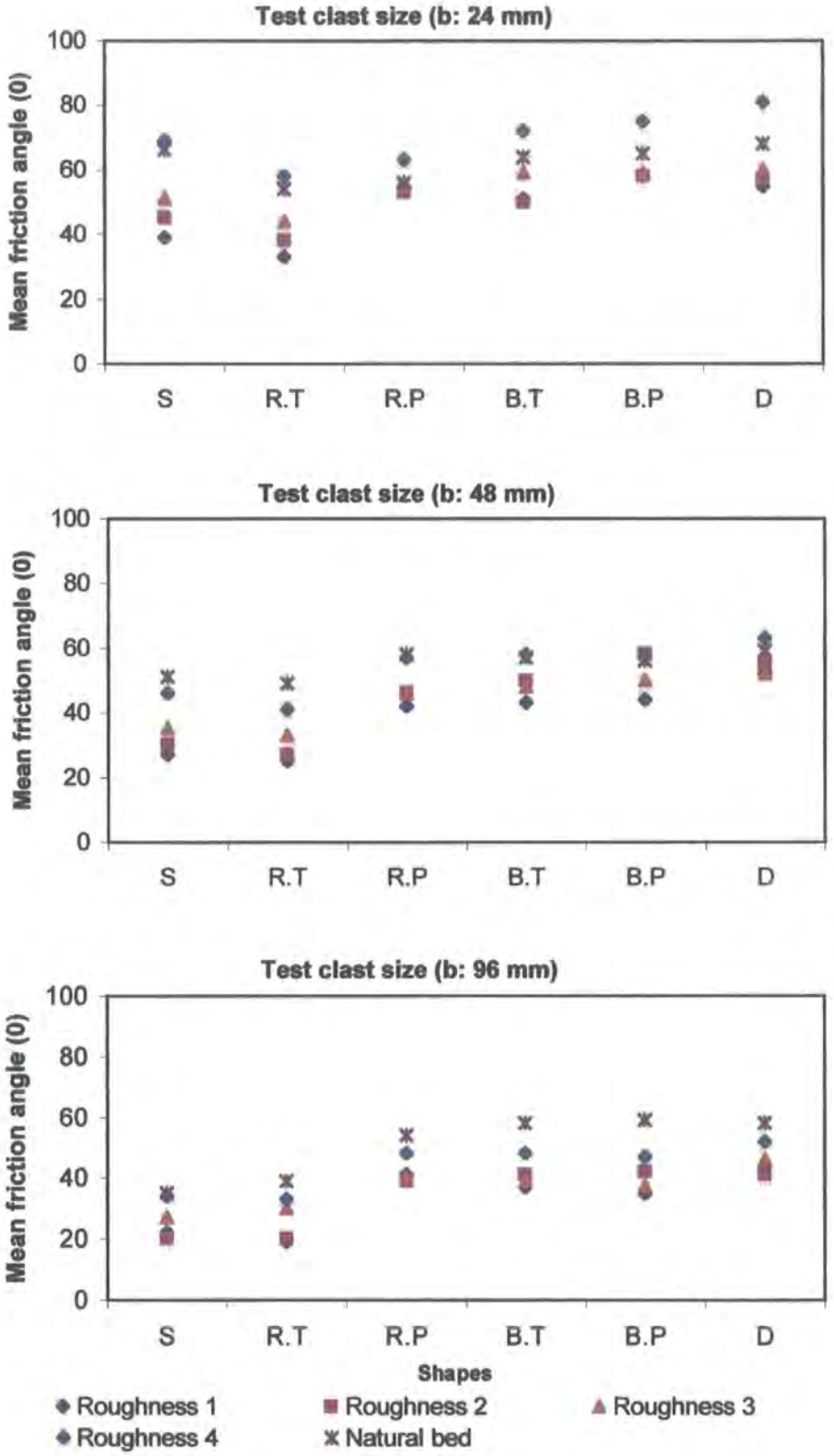

Figure 6.16 Mean friction angle distribution for the test particles of different shapes and sizes on natural and artificially-formed bed roughnesses.

Table 6.17 Statistical comparison of mean friction angles measured on the natural bed and on artificially-formed bed roughnesses 1, 2, 3 and 4 for test particles of various shape/orientation classes and the three size group.

Small size (24 mm)					Medium size (48 mm)					Large size (96 mm)				
	R.1	R.2	R.3	R.4		R.1	R.2	R.3	R.4		R.1	R.2	R.3	R.4
S	**14.2**	**9.45**	**6.33**	1.36	S	**14.30**	**10.68**	**7.21**	**2.62**	S	**9.98**	**10.58**	**4.69**	0.59
TB	**6.5**	**7.77**	**2.40**	**4.03**	TB	**7.70**	**3.70**	**4.57**	0.36	TB	**12.2**	**8.53**	**10.59**	**4.97**
PB	**3.20**	**3.70**	**3.14**	**5.66**	PB	**5.67**	0.81	**2.76**	0.87	PB	**17.51**	**9.63**	**12.51**	**5.80**
TR	**13.3**	**7.91**	**4.55**	1.92	TR	**13.54**	**10.94**	**8.46**	**4.24**	TR	**12.69**	**11.97**	**5.26**	**3.85**
PR	0.81	1.40	0.08	**4.69**	PR	**9.66**	**7.35**	**7.20**	0.83	PR	**8.32**	**9.68**	**8.62**	**3.79**
D	**8.85**	**6.58**	**4.11**	**7.35**	D	**3.50**	1.92	**3.50**	1.81	D	**7.24**	**8.45**	**5.21**	**3.52**

(S: sphere, B.T: transverse blade, B.P: parallel blade, R.T: transverse rod, P.R: parallel rod, D: disc, R: roughness)

Figures 6.17, 6.18 and Table A3.4 show normal and cumulative friction angle distributions for the three test grain sizes and six shapes/orientations. Comparison of Figures 6.17 and 6.6 indicates that for the small-sized test particles, the range of the friction angle distributions measured on artificially-formed bed roughnesses tends to be greater than for those measured on the natural bed and differences increasing with increase bed roughnesses. The ranges of distributions tend to be smaller with increasingly large test particles for the artificially-formed bed roughnesses. On the natural bed, however, mean friction angles measured with medium-and large-sized test particles show a wider range of distributions for almost all shapes (Table A3.4). Indeed, comparison of Tables 6.6 and 6.15 clearly shows that on artificially-formed bed roughnesses standard deviation values of all shapes in the small size group are much greater than those measured on the natural bed and the differences tend to increase with increasing in bed roughness. Sphere-and to some extent transverse rod-shaped test particles on both natural (for small and medium test particles) and artificial (for small test particles) beds show the greatest standard deviation values and hence the largest range of distributions. For the medium-sized test particles distributions for spheres, parallel blades, transverse rods and discs tend to be wider on the natural bed, while on artificially-formed beds the mean standard deviation values for small- and medium-sized test particles tend to decrease.

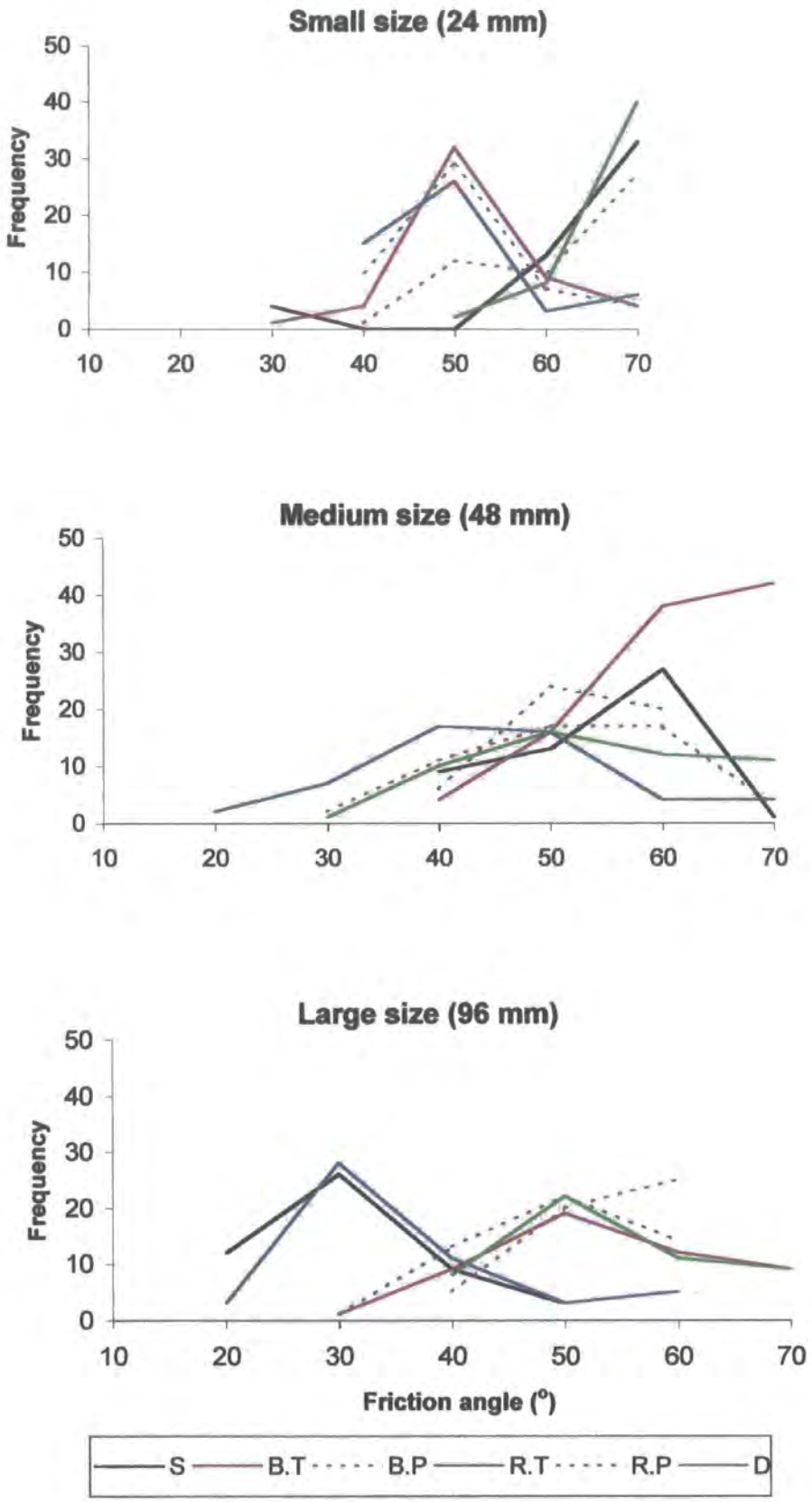

Figure 6.17 Friction angle distributions for the test particles of different shapes and size on natural bed roughness (Note: The frequency value at 70° represents the proportion of immobile particles).

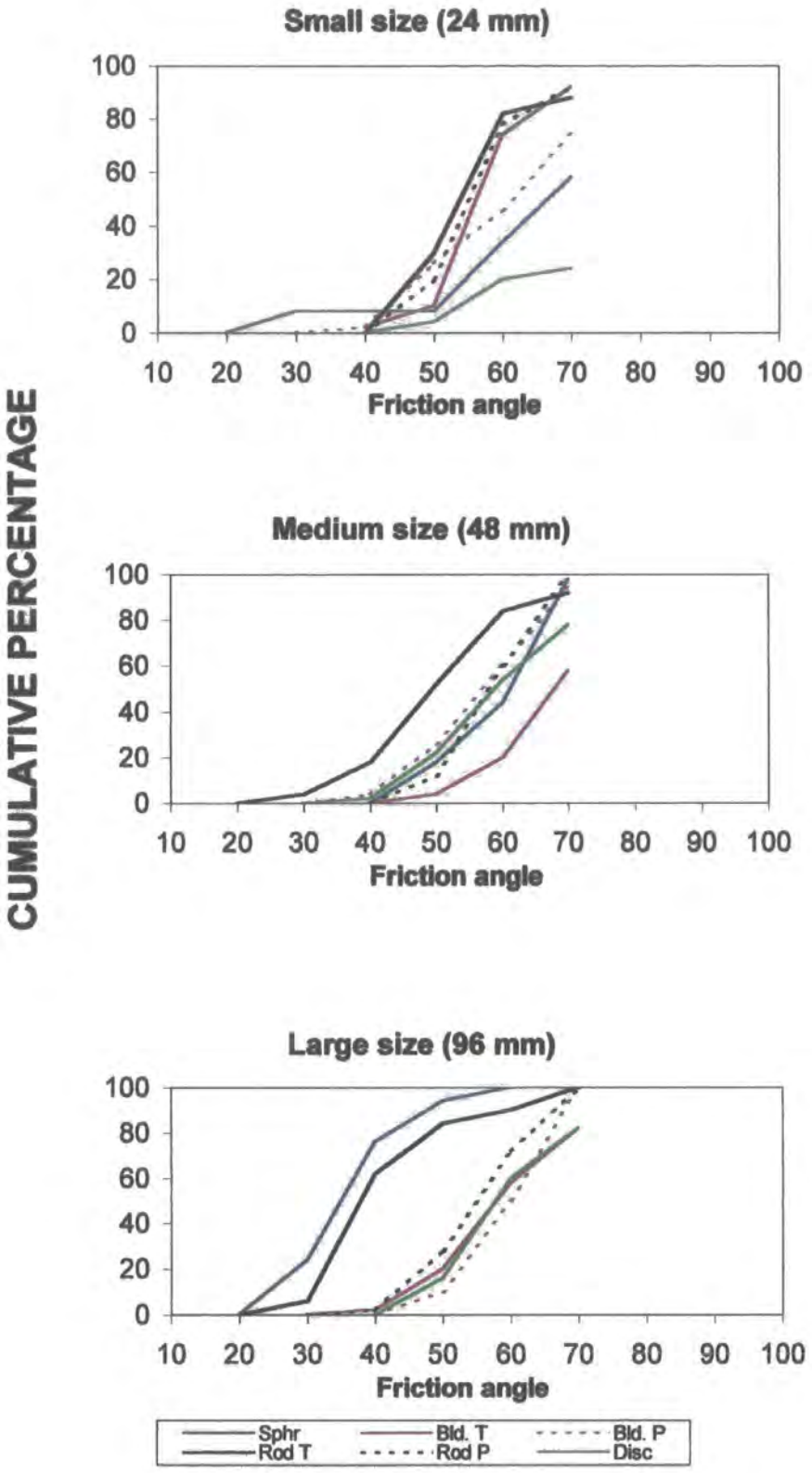

Figure 6.18 Cumulative friction angle distributions for test particles bed of different shape and orientation in three size groups on the natural bed. (Note: Where the cumulative frequency curves fail to reach 100 % at a tilting angle of 70°, the percentage remaining represents that of the immobile particle).

Comparison of Figure 6.5 and 6.18 suggest that on both natural and artificially-formed bed roughnesses, for the small size group, differences between the cumulative friction angle distributions for the particles of various shapes are smaller than for those measured with medium-and large-sized test particles. As the size of test particles increases and becomes greater than the size of bed roughness elements, spheres and transverse rod shows relatively lower range of friction angle distributions compared to other shapes /orientations. This suggests that the influence of shape on friction angle tends to increase with increasing d/D ratio.

6.9 VARIABILITY IN FRICTION ANGLES OF ARTIFICIAL PARTICLES OF EQUAL WEIGHT BUT VARYING SHAPE AND ORIENTATIONS ON A NATURALLY FORMED (RIVER) BED.

This sub-section summarises the results of measurements that aimed to investigate how particles of equal mass but different shape affect friction angles on a natural river bed. The measurements are also compared with previous findings to determine whether there is any difference between friction angles measured on artificial bed roughnesses and those measured on natural river bed. The same set of test particles, as used on the artificially formed bed roughness, were used. Thus, four test particles with similar weight (750 g) were compared for the experiments. Dimensions of the test particles (sphere, blade, rod and disc shapes) are given in Table 6.7. As with previous experiments, two particle orientations were considered; long axis parallel to and transverse to the slope. Measurements were repeated 50 times for each of the test particles on natural river bed.

Table 6.18 Mean friction angles and standard deviations for particles of equal weight in six shape/orientation classes on the natural bed.

	Shape and orientation						
Test particles	**S**	**B.T**	**B.P**	**R.T**	**R.P**	**D**	**Mean**
Friction angle (°)	44	55	57	47	59	62	54.0
Standard deviation	10	8	11	11	8	8	9.3

(S: sphere, B.T: blade in transverse orientation, B.P: blade in parallel orientation, R.T: rod in transverse orientation, R.P: rod in parallel orientation, D: disc)

The friction angles show a strong dependence on particle shape and orientation. As previously, spheres and transverse rods show similar but lower mean friction angles than the other shapes, while discs exhibit the most stable behaviour with the greatest friction angles (Table 6.18). Spheres, transverse rods and parallel blades also represent greater standard deviation values, indicating a wider range of distribution compared to the other shapes (Table A3.5). Comparison of Tables 6.8 and 6.18 shows that mean friction angles measured on the natural bed show greater values than those of measured on artificially-formed bed roughnesses and the extent of difference increases with decreasing test particle size (hence decreasing d/D ratio). Comparison of Figures 6.8 and 6.19 also suggests that mean friction angles on the natural bed have a greater range of distributions and are also more irregular compared to those measured on artificially-formed beds roughnesses. Although the natural test particles (especially the disc and the rod) were of different in weight, unlike the test particle with equal weights, there is a noticeable similarity between the mean friction angle distributions of the two groups of particles. Mean friction angles measured with particles of equal weight, except transverse blades and discs, are slightly greater than those measured with natural test particles (Table 6.18 and 6.20).

Table 6.19 Statistical comparison of friction angles measured with particles of equal weight in various shape/orientation classes on the natural bed (critical value of "t" at the 0.05 is 1.98 for each measurements).

	PB	TB	PR	TR	D
S	**5.90**	**5.40**	**8.00**	1.40	**7.48**
PB	----	1.10	1.17	**4.23**	**2.82**
TB	----	----	**2.62**	**3.59**	**4.58**
PR	----	----	----	**5.92**	1.99
TR	----	----	----	----	**7.48**

Table 6.19 exhibits statistical comparison of friction angles measured with particles of equal weight in various shape/orientation classes on the natural bed. In general there is a similar pattern of distribution to the previous experiments; there is no significant difference between sphere and transverse rods. There is also no difference between parallel rods and discs or between parallel blades and parallel rods, while there

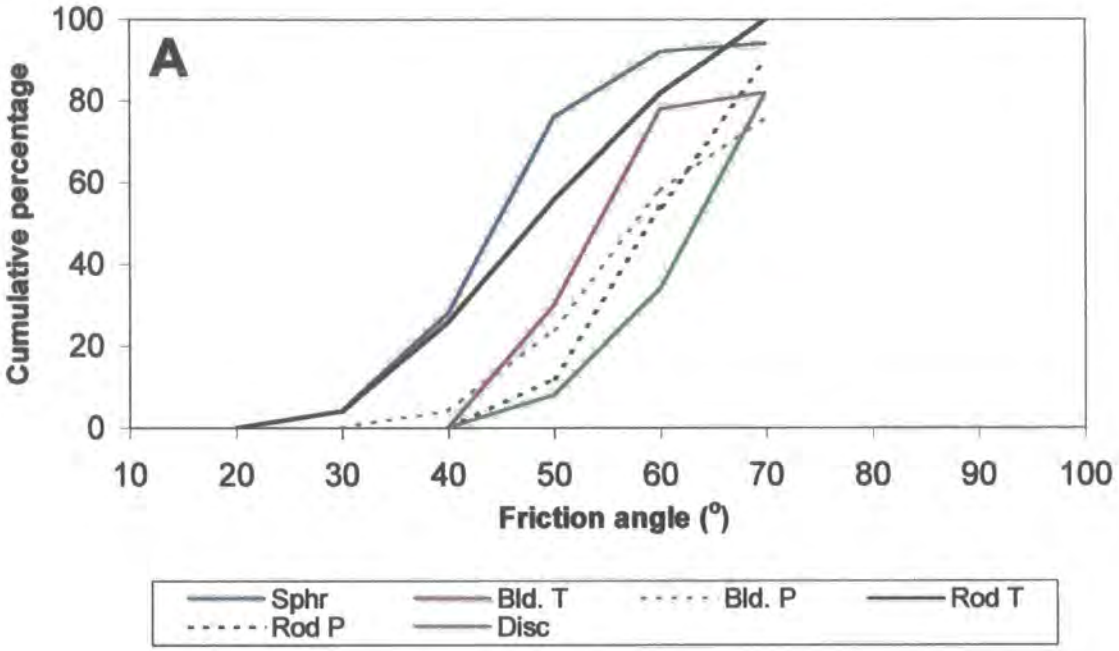

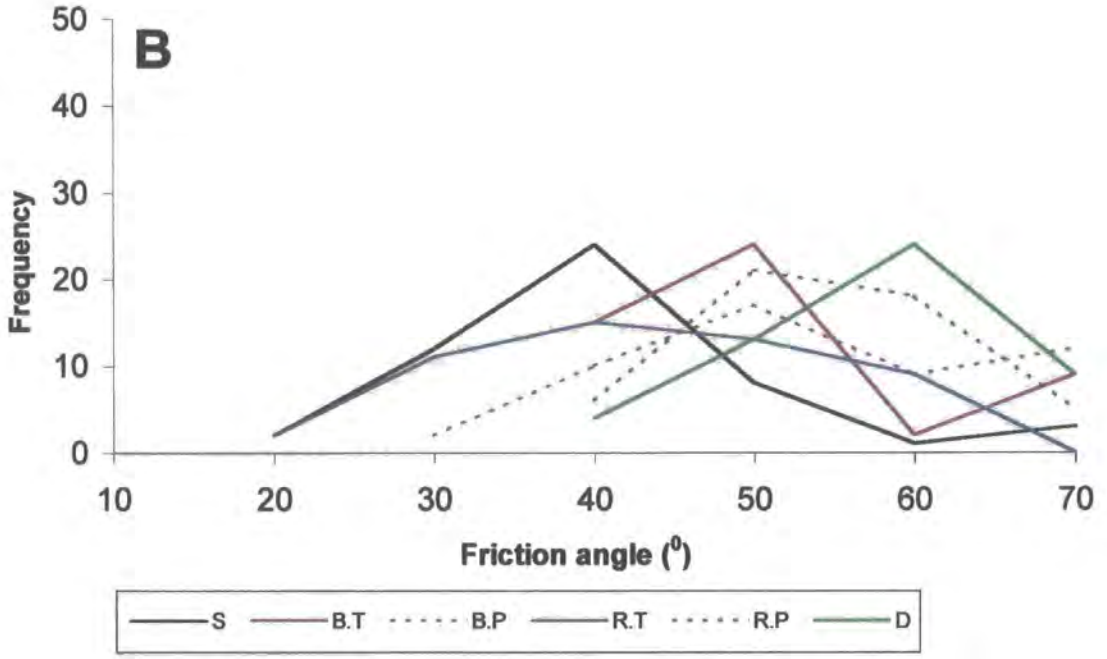

Figure 6.19 Normal (A) and Cumulative (B) frequency distributions of friction angles measured with test particles of equal weight in various shapes on the natural test bed.
(Note: Where the cumulative frequency curves fail to reach 100 % at a tilting angle of 70°, the percentage remaining represents that of the immobile particles).

is some degree of statistical difference for the other shapes. However, comparison of Table 6.9 and 6.19 suggests that the extent of the difference tends to be smaller than those measured on artificially-formed bed roughnesses.

6.10 VARIABILITY IN FRICTION ANGLES OF NATURAL PARTICLES OF VARYING SHAPE AND ORIENTATIONS ON THE NATURAL BED

In this section, variability of friction angles for naturally formed test particles of different shapes is examined based on measurements on the sampled natural bed. In common with previous measurements, results reveal a strong dependence of mean friction angle on particle shape and orientation. The results of mean friction angles for each shape are shown in Table 6.20. Table 6.20 and Figure 6.20 demonstrate a strong tendency for spheres and transverse rods to have lower mean friction angles than the other shapes and orientations. Table 6.21 shows that there is no statistically significant difference between spheres and transverse rods, parallel blades and parallel rods, and also parallel blades and transverse rods. Table 6.21 also shows that the extent of the significance varies noticeably between the particles of various shapes and orientations. Comparisons of Table 6.20 and Table 6.12 indicate that the mean friction angles for the naturally-shaped test particles measured on the natural bed are relatively greater than those measured on artificially-formed bed roughnesses and that the differences increase with decreasing bed roughness.

Table 6.20 Mean friction angles and standard deviations for naturally-formed test particles of various shapes and orientations on the natural bed.

	Shape and orientation						
Test particles	S	B.T	B.P	R.T	R.P	D	Mean
Friction angle (°)	42	56	49	45	52	64	51.3
Standard deviation	12	7	7	12	12	8	9.7

(S: sphere, B.T: blade in transverse orientation, B.P: blade in parallel orientation, R.T: rod in transverse orientation, R.P: rod in parallel orientation, D: disc)

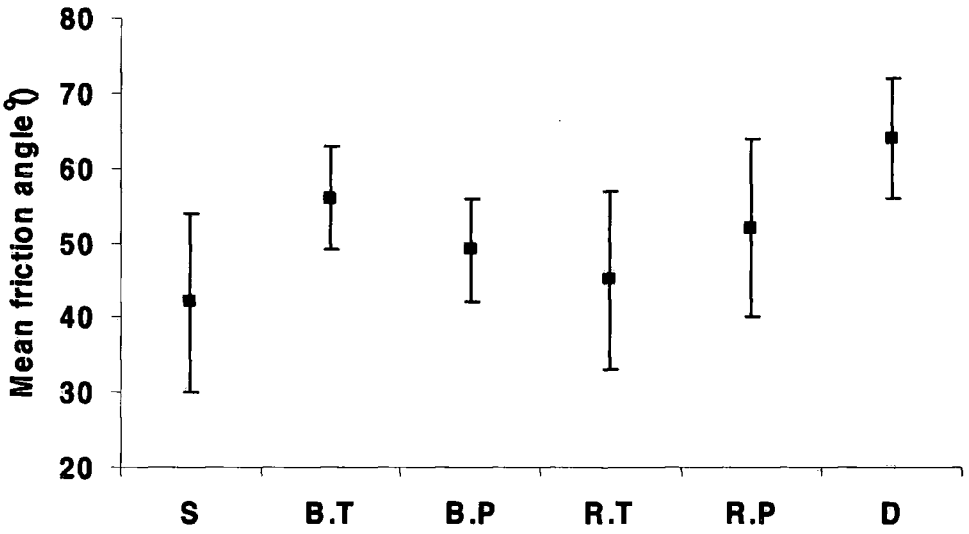

Figure 6.20 Mean friction angles for natural test particles of different shape and orientation on the naturally formed bed. Error bars show the extent of standard deviations for the test particles. (S: sphere, B.T: transverse blade, B.P: parallel blade, R.T: transverse rod, P.R: parallel rod, D: disc).

Table 6.21 Statistical comparison of friction angles measured with natural stones in various shape/orientation classes on the natural bed.

	PB	TB	PR	TR	D
S	**3.09**	**6.80**	**3.89**	0.89	**10.78**
PB	----	**5.11**	1.58	1.99	**10.55**
TB	----	----	**2.24**	**5.67**	**5.53**
PR	----	----	----	**2.96**	**6.40**
TR	----	----	----	----	**9.62**

Note: The values shown in bold indicate a statistically significant difference between the compared shapes/orientations. (critical value of "t" at the 0.05 level is 1.98 for each measurements).

Despite their lower mean values, sphere and rod shapes show a wider range of distributions compared to other shapes (Figure 6.21 and Table A3.6). The range of friction angles varies between 30° and >70° for spheres and transverse rods, while it is between 40° and >70° for blades with either orientation, parallel rods and discs. Spheres and rods, therefore, show rather greater standard deviations than on the artificially-

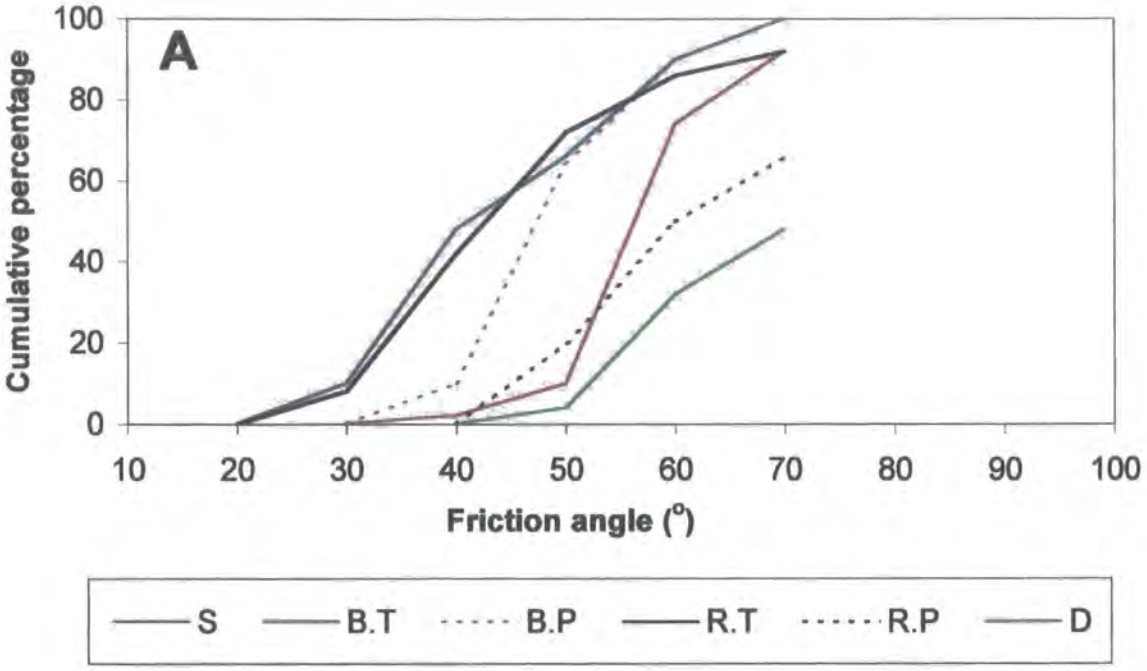

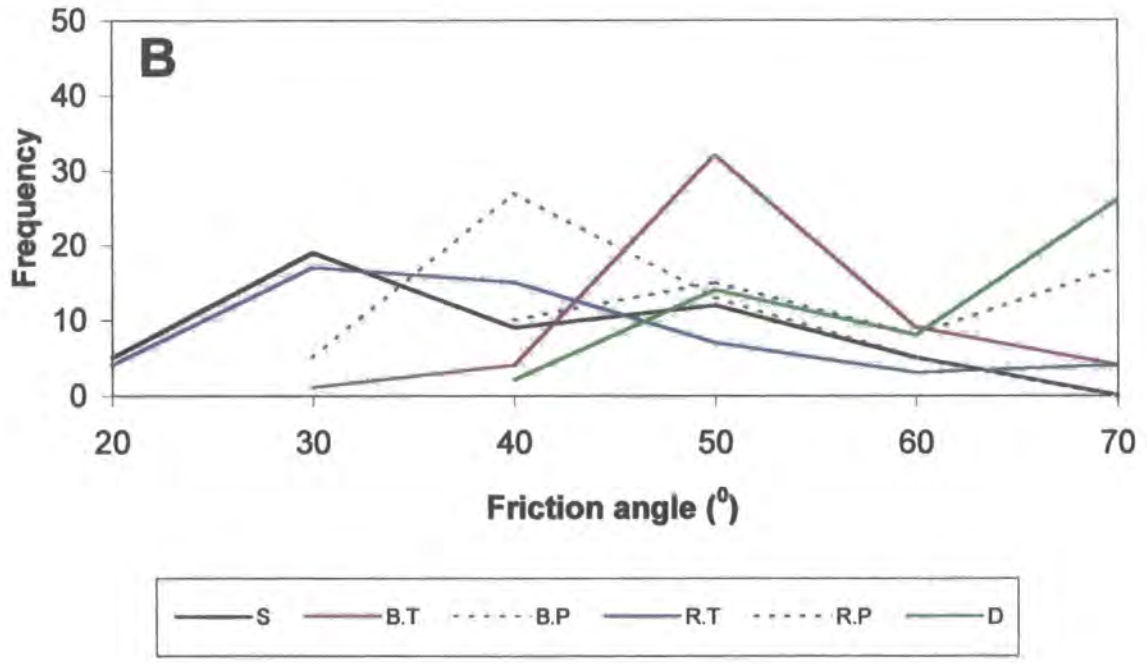

Figure 6.21 Normal (A) and Cumulative (B) frequency distributions of friction angles measured with the naturally formed test particles in various shapes on the natural bed. (Note: Where the cumulative frequency curves fail to reach 100 % at a tilting angle of 70°, the percentage remaining represents that of the immobile particles).

formed bed roughnesses, probably due to the greater variability of surface packing arrangement (poor sorting) of the natural bed, which may strongly influence friction angle distributions (Table 6.14 and 6.20)

6.11 EFFECT OF PARTICLE ROUNDNESS ON FRICTION ANGLE

The effect of particle roundness on friction angle on various bed rougnesses was evaluated with particles of equal size (b-axis) but different roundness values. The size, shape and roundness characteristics of the test particles are given in Table 6.22. Five experiments were carried out on five different bed roughnesses. For each experiment, ten artificial concrete particles with various roundness values in two shape classes were compared. These were a well-rounded sphere, a rounded sphere, a sub-angular sphere, an angular sphere and a cube. In the rod-shaped class the test particles were a well-rounded rod, a rounded rod, a sub-angular rod an angular rod, and a very angular rod (Table 6.22). Each particle was placed randomly on the bed. Two particle orientations were considered for the rod; long axis parallel to slope, and long axis transverse. The experiments were repeated 50 times for each of the four bed roughnesses and on the natural bed.

Table 6.22 The tri-axial dimensions (cm), shape and roundness characteristics of the artificial test particles used for the experiment.

Shape and angularity	a-axis	b-axis	c-axis	Radius	Cailleux roundness	Krumbein sphericity
Sphere (very rounded)	4.8	4.8	4.8	2.4	1000	1.00
Sphere (round)	4.8	4.8	4.8	1.8	750	1.00
Sphere (sub- angular)	4.8	4.8	4.8	1.2	500	1.00
Sphere (angular)	4.8	4.8	4.8	0.6	250	1.00
Sphere (cube)	4.8	4.8	4.8	0.1	42	1.00
Rod (very round)	9.6	4.8	4.8	4.8	1000	0.63
Rod (round)	9.6	4.8	4.8	3.6	750	0.63
Rod (sub-angular)	9.6	4.8	4.8	2.4	500	0.63
Rod (angular)	9.6	4.8	4.8	0.1	250	0.63
Rod (very angular)	9.6	4.8	4.8	0.1	21	0.63

Observations on Bed Roughness 1 show that rolling was the dominant mode of movement for the well-rounded sphere-and rod-shaped particles placed in transverse positions. The cube sometimes slid or rolled. On the other hand, rod-shaped particles placed in parallel orientations moved by sliding regardless of their roundness values. Well-rounded spheres and rods in transverse orientations tended to move at very low friction angles. Table 6.23 and Figure 6.22 show that, in general, there is a positive relation between the mean friction angles of test particles (regardless of their degree of roundness) and increasing the bed roughness for spheres and transverse rods. When bed roughness increases, particles tend to move at higher friction angles regardless of their roundness. Although there are clear differences in the mean friction angles between the well-rounded sphere and the cube and also between the well-rounded transverse-rod and the angular rod on Rougnesses 1 and 2, these differences tend to decrease as bed roughness increases (Table 6.23 and Figure 6.22). This indicates that the effect of particle roundness on friction angle diminishes as bed roughness increases.

On Bed Roughness 1 there is a noticeable difference in friction angles between the test particles of various roundness. The rank order of the differences for sphere-shaped particles is 22.8° for the very round sphere, 25° for the round sphere, 26.6° for the sub-angular sphere, 31.6° for the angular sphere and 34.6° for the cube. For the rod-shaped particles the order is also 19.5° for the well rounded-rod, 22.2° for the rounded rod, 24.9° for the sub-rounded rod, 28.3° for the angular rod and 34.2° for very angular rod. Although there is a similar ranking in friction angles on the bed roughness 2, differences between particles of different roundness diminishes on roughnesses 3 and 4 and there tends to be no systematic variation between different roundness types (Tables 6.23 and Figure 6.22). There is also a similar pattern for rod-shaped particles of various roundness values with transverse orientation. Indeed, although there is a great difference between the lowest and highest friction angle values on Roughness 1, it decreases distinctly towards Roughness 4.

Despite its poor size sorting and complex bed packing geometry, the natural bed shows some relation between test particle roundness and mean friction angle. Table 6.23 indicates that, despite its greater roughness (similar to bed roughness 4) there tends to be an inverse relation between mean friction angles and particle roundness for spheres and transverse rods. This is contrary to the results measured on artificially-formed beds where differences between test particles of various roughness decrease with increasing

Table 6.23. Mean friction angles of sphere and rod-shaped particles with various roundness values and orientations on five different bed roughnesses. (R: round VR: very round A: angular SA: sub angular VA: very angular)

Bed roughness	SPHERE					ROD (Transverse orientation)					Rod (Parallel orientation)				
	VR	R	SA	A	Cube	VR	R	SA	A	VA	VR	R	SA	A	VA
Roundness 1	22.8	25.0	26.6	31.6	34.6	19.5	22.2	24.9	28.3	34.2	41.6	45.2	38.2	44.2	40.7
Roundness 2	33.3	30.4	34.2	35.7	37.1	28.4	25.5	30.5	31.3	34.7	46.7	45.6	47.2	48.0	46.8
Roundness 3	34.4	34.7	35.0	36.8	37.1	33.4	34.5	36.1	36.3	36.4	46.8	47.6	48.4	49.4	49.1
Roundness 4	43.0	43.1	46.1	45.1	45.5	41.8	39.8	42.1	39.8	45.1	53.8	50.0	52.6	52.1	53.8
Natural bed	37.8	42.8	43.2	44.3	47.5	36.7	44.1	43.6	48.9	46.7	54.1	51.2	54.5	55.9	54.3
Mean	**34.3**	**35.2**	**37.0**	**38.7**	**40.4**	**32.0**	**33.2**	**35.4**	**36.9**	**39.4**	**48.6**	**47.9**	**48.2**	**49.9**	**48.9**

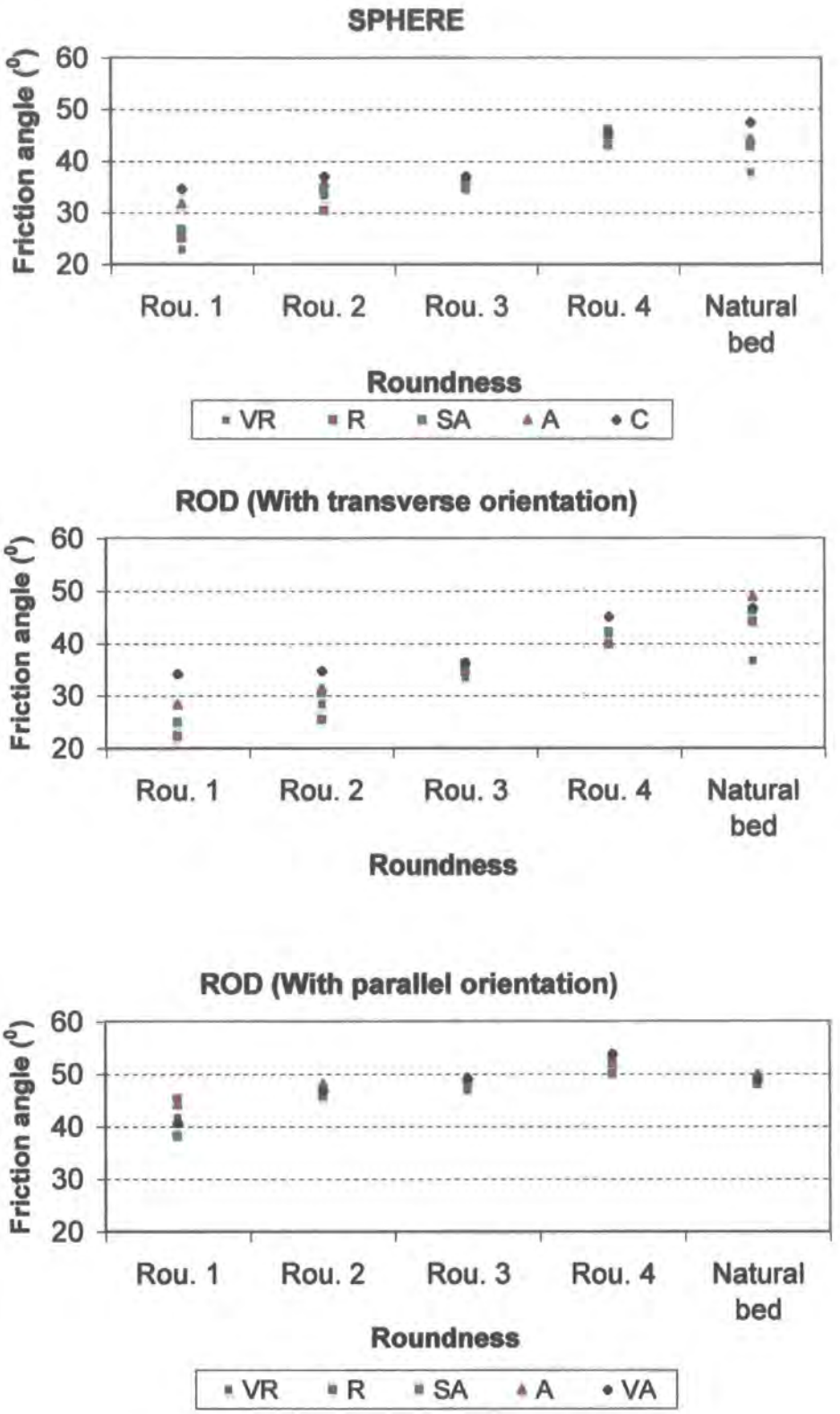

Figure 6.22 The distribution of mean friction angles in five ranges of roundness of sphere and rod-shaped particles on five bed roughnesses.
(VR: very round, R: round, SA: sub-angular, A: angular, VA: ,very angular, C: cube, Rou: bed roughness).

bed roughness. Very rounded sphere-and rod-shaped test particles exhibit the lowest mean friction values (sphere: 37.8° and rod: 36.7°) but it tends to increase with decreasing particle roundness (sphere 47° and transverse rod: 48.9°). However, there is no similar pattern for rod-shaped test particles with parallel orientation for any of the bed roughness types.

Friction angles of the test spheres and rods as percentiles on different bed roughness types are shown in Table A3.7. Figure 6.23 also demonstrates the cumulative frequency of the mean friction angles of spheres and rods (both transverse and parallel orientation) with different roundness values on various bed roughness types. They indicate that on roughnesses 1 and 2, sphere-and transverse rod-shaped test particles with greater roundness move over a small range of friction angles and there tends to be an increase in the range of friction angles with a decrease in test particle roundness. On the other hand, on roughnesses 3, 4 and also on the natural bed, there is a general increase in the range of the distribution of friction angles. Differences between the friction angles of test particles of various shapes diminish with increasing bed roughness for the artificially-formed bed roughnesses (Table A3.7). However, there is still a decrease in friction angles for particles that have greater roundness.

Indeed, Table 6.24 indicates that the extent of statistical differences between particles of various roundness tends to decrease with increasing roughness of artificially-formed beds. On the natural bed, however, there are still statistically significant differences between the particles of various roundness value in the case of both spheres and transverse rods.

Comparison of rod-shaped particles (rounded, sub-angular and angular rods) in transverse and parallel orientations on the four artificial bed roughnesses indicates that there is no statistically significant variation between the five roundness types on most bed roughnesses with particles of parallel orientation (Table 6.24). However, for the transverse rods (as explained above) there is some degree of statistical difference between the five roundness types on roughnesses 1 and 2, on the natural bed and also, to a lesser degree, roughnesses 3 and 4.

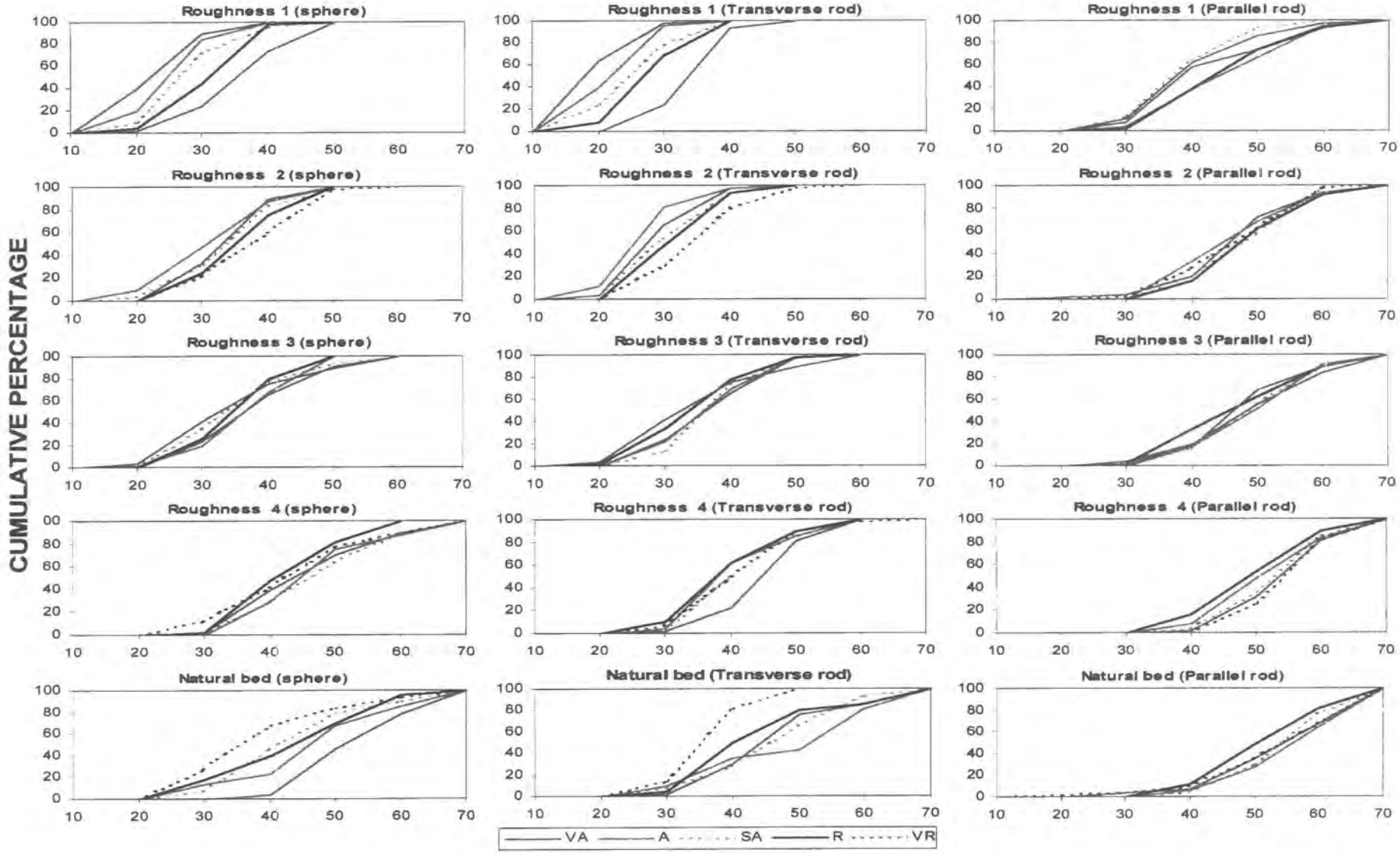

Figure 6.23 Cumulative friction angle distributions for sphere and rod-shaped particles of equal size but different roundness values on four artificia formed bed roughness types and natural bed. (R: round, VR: very round A: angular SA: sub angular VA: very angular)

Table 6.24. Statistical comparison of friction angles measured with sphere-and rod-shaped particles of equal size but different roundness values on four bed roughness types (critical value of "F" (Anova) at the 0.05 level is 2.40 for each measurement).

Bed Roughness	Sphere (very round/round/sub-round/angular/cube)	Transverse -rod (very round/round/sub-round/angular/very angular)	Parallel-rod (very round/round/sub-round/angular/very angular)
Roughness 1	**55.812**	**83.424**	1.789
Roughness 2	**4.012**	**13.038**	0.041
Roughness 3	0.709	**2.684**	0.765
Roughness 4	1.366	**2.998**	0.573
Natural bed	**4.390**	**7.941**	1.757

The frequencies of the friction angles for spheres and transverse rods of various roundnesses tend to increase with bed roughnesses. The differences are greatest on the natural bed. Table 6.25 shows that there tends to be a similar increase in the standard deviations of test particles as bed roughness increases with differences becoming greatest on the natural bed.

6.12 DISCUSSION AND CONCLUSION

The entrainment of a particle by a flowing fluid mainly depends on the balance of the forces acting on the particle and on its pivoting or friction angle. This friction angle strictly depends on the particles contact point with the underlying grains. As several studies have shown, the degree of contact of a particle is controlled by many factors, such as grain size and bed sorting parameter, test grain shape and orientation, as well as the size, shape, orientation and packing arrangement of the grains constituting the local bed surface (Komar and Li. 1986; Kirchner *et al.*, 1990; Carling *et al.*, 1992).

As briefly explained in the introduction to this chapter and also in the review in Chapter 2, many earlier studies expressed friction angle mainly as a function of test grain size, median bed grain-size or bed sorting parameters. Only a few investigations (e.g. Komar and Li, 1986; Kirchner *et al.*, 1990) have pointed out the importance of particle shape (form, roundness) on its friction angle.

Table 6.25 The standard deviations of friction angle distributions of sphere and rod-shaped particles with various roundness values and orientations on artificial and natural bed roughnesses (R: round VR: very round A: angular SA: sub angular VA: very angular).

Bed rougness	SPHERE					ROD (Transverse orientation)					Rod (Parallel orientation)				
	VR	R	SA	A	Cube	VR	R	SA	A	VA	VR	R	SA	A	VA
Roundness 1	5.3	4.9	5.5	5.5	6.4	5.1	5.6	6.0	5.2	6.1	10.2	8.9	8.4	8.7	9.2
Roundness 2	6.1	8.0	7.6	6.0	7.3	5.7	5.8	6.2	5.3	6.9	9.6	9.7	8.3	7.3	8.7
Roundness 3	9.9	6.9	8.2	7.3	8.6	8.1	7.6	6.5	7.3	7.1	8.9	9.3	9.1	8.6	10.2
Roundness 4	10.0	7.4	9.5	9.2	10.1	7.7	7.5	7.2	6.9	7.4	5.9	8.0	7.1	7.6	6.6
Natural bed	12.1	11.9	10.4	11.9	13.1	9.5	11.3	10.5	13.8	13.4	10.7	8.7	8	9.3	9.5

In terms of size, friction angle measurements showed reasonable agreement with previous experiments. Figure 6.24 and Table 6.26 summarise results of all the friction angle measurements carried out with particles of various sizes, weight and shapes (natural and artificial) on various bed roughnesses and indicate that the friction angle for any shape class depends on the ratio of test grain size (d) to the size of those over which it is pivoting (D). The smaller the ratio of d/D, the greater the friction angles at which test particles moved. Friction angles decreased with increasing particle size (hence greater d/D ratio) relative to the median bed particle size. With increasing bed roughness, small-size test particles tended to have a larger standard deviations, whereas as the size of test particles increased or bed roughnesses decreased, test particle started to move in a smaller range of friction angles, hence yielding lower standard deviations. These findings, in general, show reasonable agreement with previous experiments (e.g. Miller and Byrne, 1966; Li and Komar, 1986). Using sphere-shaped test particles (steel ball bearings and glass marbles ranging in diameter from 0.23 to 3.77 cm), Li and Komar also found that pivoting angles is a function of d/D ratio, the greater the d/D ratio with the lesser the pivoting angle (See Figure 2 in Li and Komar 1986).

In terms of shape, it was found that on a given bed roughness and for a constant size, the friction depends on particle shape and orientation. For all measurements, non-spherical test particles showed greater friction angles than spherical ones. For almost all the measurements, a very clear difference was found in both mean friction angle and also friction angle distributions between spheres-and transverse rods-and all other flat-shaped particles, namely, blades with parallel and transverse orientations, discs, and rods with parallel orientations (Figures 6.24, 6.25 and Table 6.26). Measurements undertaken in three size groups of artificially-formed particles, natural particles, and particles with equal weight but various shapes, all clearly showed that spheres and transverse rod-shaped particles tend to have lower friction angles than blades (with parallel and transverse orientation), rods (with parallel orientation) and discs. Results showed that, across the range of particles tested, spherical particles tended to have lower critical friction angles. Departure from a spherical form leads to an increase in grain stability (Figure 6.23, 24 and Table 6.26). These findings are similar to Li and Komar's (1986) results. Li and Komar (1986) measured pivoting angles for uniform sizes of spheres, ellipsoids and angular particles and found that pivoting angles measured with ellipsoid and angular particles are significantly greater than for spheres.

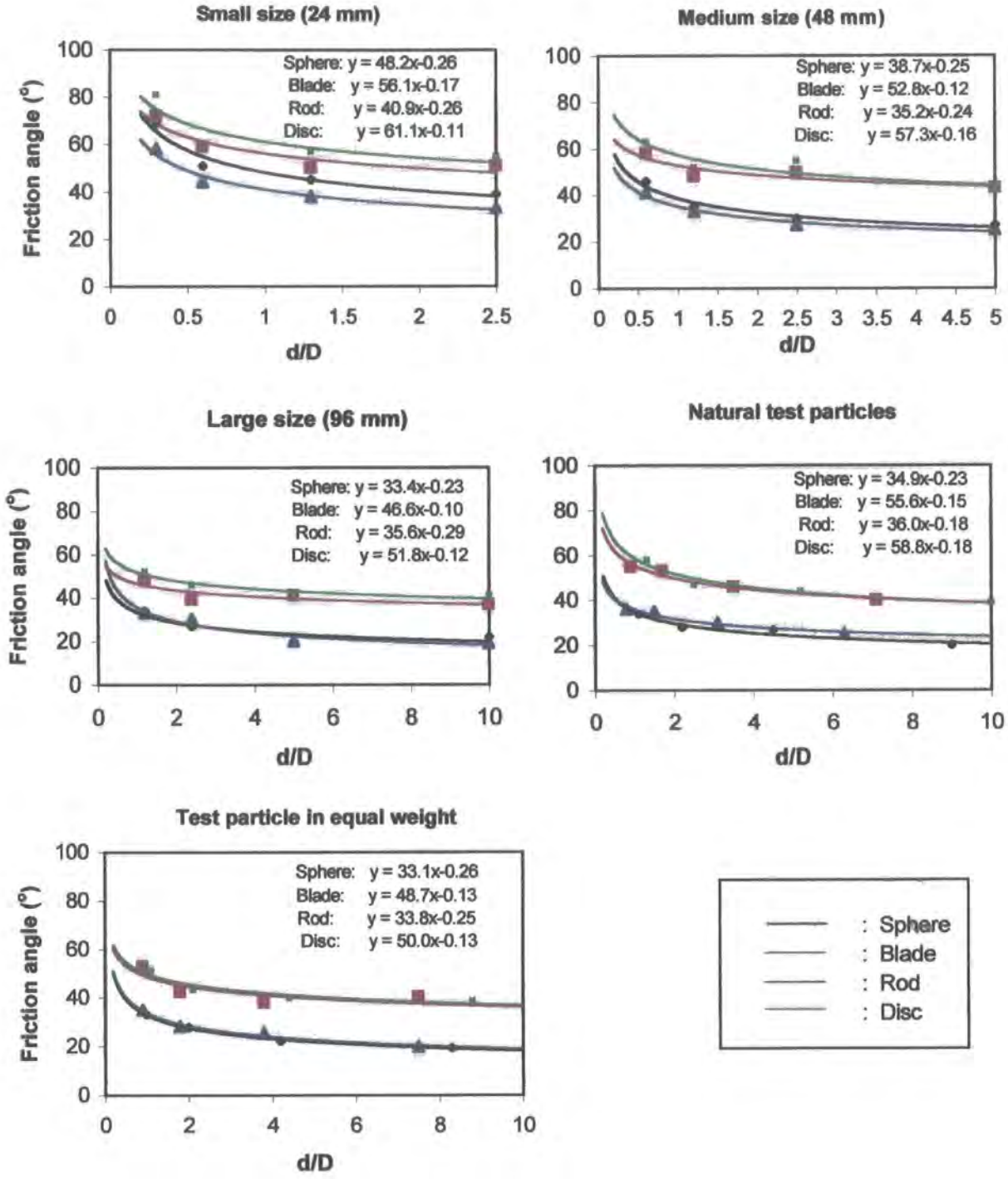

Figure 6.24 Summary of all the friction angle measurements carried out with particles of various sizes, weights and shapes (natural and artificial) on various bed roughnesses. The curves fitted follow the general emprical relationship discussed by Li and Komar (1986). The form of the equation is as follows:

$$\Phi = e\left(d/D\right)^{-f}$$

where Φ is the friction angle, d being the diameter of the pivoting test particle and D is the diameter of the base grains and e and f are coefficients.

Thus they also found that, apart from size, pivoting angles depend on grain shape, particularly on the ratio of the shortest to the intermediate axis (c/b ratio). (See Figures 3, 4 and 5 in Li and Komar, 1986).

The reason why spheres and transverse rod-shaped particles always have lower friction angles is attributed to the fact that spherical particles (with a higher degree of roundness) always have greater rolling capability, while other shaped-particles are more likely to slide. This is expected given the '*c/b* ratio', the ratio of the smallest to the intermediate axial diameters. Flatter particles move by sliding rather than by pivoting and rolling. Thus sliding particles, in most instances, tended to show higher friction angles, while rolling grains have lower values. As some investigators have already illustrated (Komar and Li, 1986; Carling *et al.*, 1992), these variations in particle behaviour are thought to relate to critical shear stress, relative mobility and selective entertainment in a flowing fluid.

All measurements showed that particle orientation has a significant influence on friction angle. Rods placed in a parallel position tend to have friction angles, that were almost double than for transverse-rods (Figure 6.25 and Table 6.26). A similar relation was not observed between parallel and transverse blades. Transversely orientated rods always roll out of place at low friction angles, while blades in every orientation, rods in parallel orientations and discs tend to slide at relatively high friction angles. This indicates that the c/b ratio of a particle also has an important effect on its movement. Particles with a high c/b, ratio, well-rounded and in a transverse orientation tend to have lower friction angles than in parallel orientations with a lower c/b ratios. It was also observed that the effect of particle orientation on friction angle tends to decreases as bed roughness increases. Although there is no very clear and regular difference in mean friction angle values between parallel and transverse blades, measurements undertaken with natural particles and particles of equal weight showed that parallel blades on most bed roughnesses tend to have lower friction angles than those of transverse blades (Figure 6.25 and Table 6.26). The reason might be that, on an inclined surface, blades with a parallel orientation may have fewer obstructions with the underlying bed material and hence lower friction, while in a transverse orientation the contact area of the particle across the bed may prevent it from being entrained. In other words, the parallel blade has less contact area across the inclined bed and this results in easier sliding.

Measurements show that as bed roughness increases the difference between various shapes tends to diminish (Figure 6.25 and Table 6.27). This is especially

Table 6.26 Summary of the friction angles measurements carried out with particles of various shapes and sizes on artificial and naturally formed bed roughnesses.

On artificially formed bed roughnesses

	S	B.T	B.P	R.T	R.P	D
Small size test particle (b: 24 mm)						
Roughness 1	39	51	58	33	55	55
Roughness 2	45	50	58	38	53	57
Roughness 3	51	59	59	44	55	60
Roughness 4	69	72	75	58	63	81
Medium size test particle (b: 48 mm)						
Roughness 1	27	43	44	25	42	52
Roughness 2	30	50	58	27	46	55
Roughness 3	35	48	50	33	46	52
Roughness 4	46	58	58	41	57	63
Large size test particle (b: 96 mm)						
Roughness 1	22	37	35	19	41	44
Roughness 2	20	41	42	20	39	41
Roughness 3	27	39	37	30	40	46
Roughness 4	34	48	47	33	48	52
Test Particles with equal weight						
Roughness 1	19.4	40.3	34.6	19.9	40.6	38.7
Roughness 2	22.3	37.9	41.7	25.2	42.8	39.9
Roughness 3	27.8	42.3	40.2	28.2	47.6	43.4
Roughness 4	33.2	52.9	48	34.9	54.4	51.2
Natural test particles						
Roughness 1	20	40	35	24	39	39
Roughness 2	27	46	40	30	39	44
Roughness 3	28	53	43	35	46	47
Roughness 4	34	55	50	36	54	58

On a natural bed

Test particle size (b axis)	S	B.T	B.P	R.T	R.P	D
Small (24 mm)	66	64	65	54	56	68
Medium (48mm)	51	57	56	49	58	59
Large (96mm)	35	58	59	39	54	58
Natural test particles	42	56	49	45	52	64
Particles with equal weight	44	55	57	47	59	62

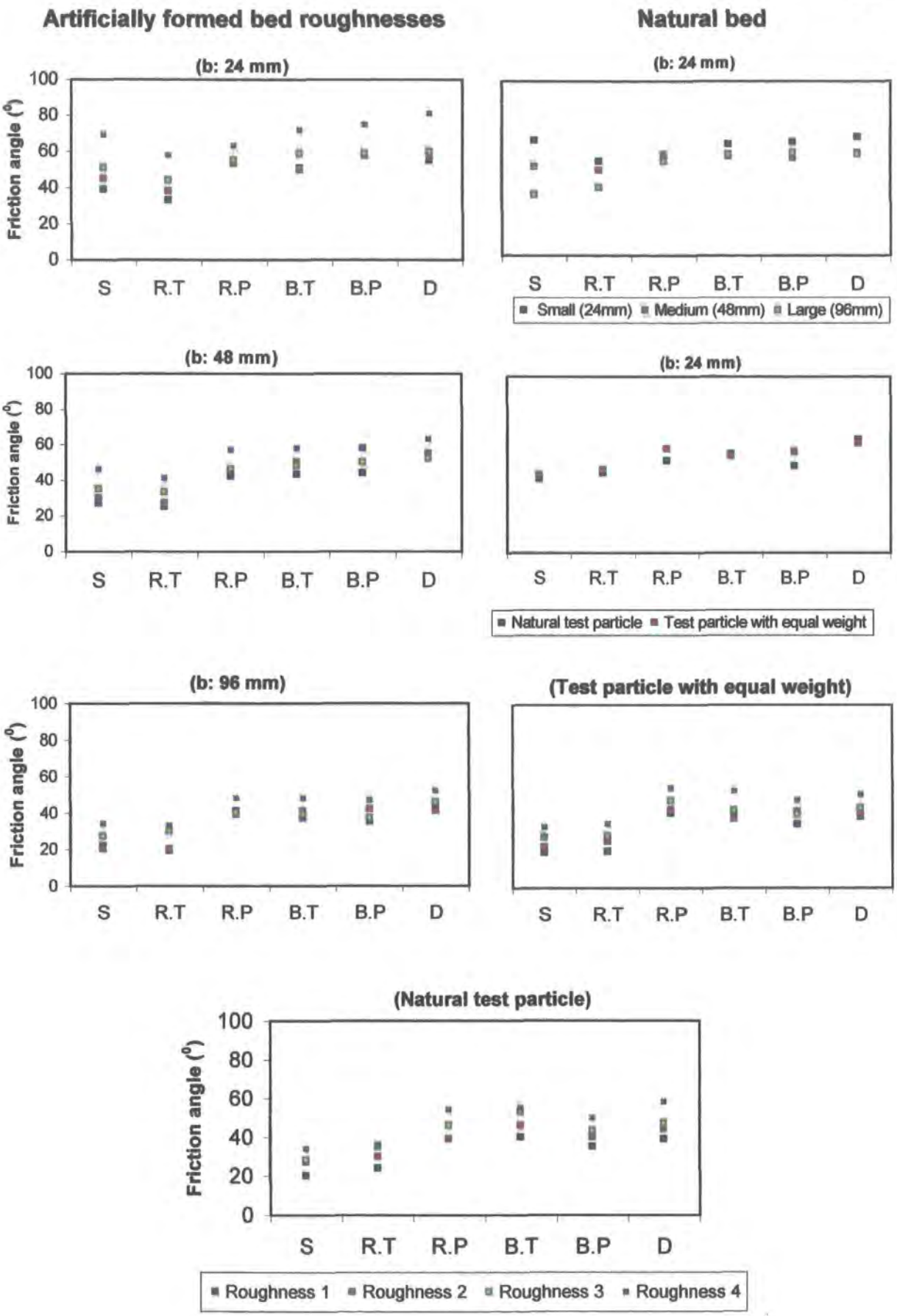

Figure 6.25 Summary of the friction angles measurements carried out with particles of various shape and size on artificial and naturally formed bed roughnesses.

obvious for spheres and transverse rods. On the smoothest bed, spheres and transverse rods tends to move at relatively lower friction angles, but as roughness increases they entrain at higher friction angles. There is no similar relationship for flat particles. The reason might be the fact that the sphere and transverse rods tend to sit more easily in the pockets between the adjacent particles as bed roughness increases. Flat-shaped particles bridge the grains and do not sit in a stable position.

In terms of particle roundness, the experiments showed that on the smoother artificial beds, highly rounded particles tended to have lower friction angles than those of more angular particles. Measurements also showed that, on artificially-formed beds, as bed roughness increases the effect of particle roundness on friction angle becomes less important. However, measurements carried out on a natural bed indicate that, despite its heterogeneous mixture of particle sizes and shapes (which leads to a varying grain packing geometry, and also complex bed roughness elements), there is still an inverse relation between test particle roundness and mean friction angle. This result does not support the above suggestion that the effect of particle roundness on mean friction angle diminishes with increasing bed roughness. The possible reason for this difference might be attributed to the fact that artificial and naturally formed beds have relatively different structures in terms of grain packing geometry, size, shape and sorting etc (Komar & Li, 1986; Kirchner *et al.*, 1990 and Dietrich & Kirchner, 1992). Artificially-formed beds (such as Roundnesses 3 and 4) have looser packing arrangements with many pore spaces (Compare Figures 6.1 and 6.14). This is because they were made with very uniform particles in size and shape (Figure 6.1). For the naturally formed bed, on the other hand, during normal sediment transport events such large pores between the large size particles of the bed is filled with smaller sized sediment which results in a smooth surface on which particles with greater roundness may move more easily.

Consequently, it has been found that particle friction angle depends on (and varies with) many factors. These are shape, size, orientation and roundness of test particles, degree of bed roughness and its packing arrangement. It was also found that, although the measurements showed some degree of similarity in mean friction angles on artificial and naturally formed beds, large variations in size, shape, bed packing arrangements of the natural bed (which exhibit a point to point spatial variation) have rather different control on the distribution friction angles.

The main findings for the friction angle measurements are as follow:

1. In terms of size, the friction angle for any shape class depends on the ratio of the test grain size (d) to the size of those over which it pivots. The greater the ratio the lower the friction angles at which particle start to move.
2. In terms of shape, on a given bed roughness and for a constant size, the friction angle depends on sediment shape and orientation. Sphere and rods with a transverse orientation moved at lower friction angles relative to flat-shaped particles, (blades in any orientation, parallel-rods and discs). Departure from a spherical form leads to an increase in grain stability.
3. Measurements taken with rod-shaped particles showed that orientation has a significant influence on friction angle. Rods in a parallel orientation to the slope tend to be much more stable than those placed in a transverse orientation.
4. An inverse relation was observed between bed roughness and test particle shape. As bed roughness increases differences between various shapes as well as various orientations tends to diminish.
5. Observations showed that on smoother bed roughnesses, particles with greater roundness tend to move at relatively lower friction angles. However, as bed roughness increase the influence of particle roundness on initial movement decreases.

CHAPTER 7: THE INFLUENCE OF PARTICLE SHAPE ON BEDLOAD TRANSPORT DYNAMICS – VISUALISATION EXPERIMENTS

7.1 SCOPE OF CHAPTER

This chapter presents the results of the visualisation experiments designed to investigate the influence of particle shape on bedload transport. First, it begins with an introduction outlying the importance of shape, size and weight on the hydraulic (dynamic) behaviour of sediment during transport. This includes; particle settling velocity, the angle of repose, the importance of shape and experimental investigations of particle motions. Section 7.3 describes settling and transport velocities of particles of various shapes. Influence of artificial particles of differing shape and size on settling and transport velocities are presented in section 7.4. Section 7.5 examines changes in settling and transport velocities of particles of different shape in relation to weight. Settling velocities of the natural particles is discussed in section 7.6. Settling and transport velocities of irregular shaped natural particles are presented in section 7.7. Initial motion and movement of particles of varying shape on bed of varying roughness is discusses in section 7.8. Finally, the key points raised by the experiments are discussed and summarised in section 7.9.

7.2 INTRODUCTION

Several studies have shown that particle shape, size and weight are important properties affecting the hydraulic behaviour of sediment during transport and deposition (e.g. Lane, 1938; McNown and Malaika, 1950; Allen, 1969; Carrigy, 1970; Komar and Reimers, 1978; Hallermeier, 1981; Willetts and Rice, 1983; Li and Komar, 1992a, b). Particles entrained from a bed are transported by the flow in a variety of ways, depending on their shape, size and density, as well as the viscosity and velocity of the transporting fluid. Generally three modes of transport have been described for coarse gravel particles in water. These are sliding, rolling and saltation. During sliding,

particles remain in continuous contact with the bed, although they may tip-up or down slightly during travel. A rolling particle turns continuously about a flow-transverse axis, while remaining essentially in contact with the bed. Saltation involves the progressive forward movement of a particle in a series of short intermittent jumps along the channel bed. Saltation continues as long as the flow is turbulent enough to lift particles and carry them downstream. However, as Abbot and Francis (1977) pointed out there is no sharp division between the three modes of particle motion. In stronger flows the three modes will occur simultaneously.

The purpose of this chapter is to examine the influence of shape on settling, grain impact and motion of gravel-size particles.

7.3 PARTICLE SETTLING VELOCITY AND ANGLE OF REPOSE: THE IMPORTANCE OF SHAPE

The hydraulic behaviour of a particle is significantly influenced by its settling or fall velocity. The settling velocity of a particle depends on the shape, size, and density of the individual particle; on the concentration of particles in the fluid; on the fluid viscosity; and on the turbulence intensity. For a particle to settle at all, it must have a higher mean density than the fluid in which it is immersed (Pye, 1994a).

Studies have shown that, with particles of constant density, apart from size, which is considered the most important factor, shape is significant in controlling the settling velocity. Settling velocity of low sphericity sand-size particles has been found to be much lower than those of spheres. In general, the greater the departure of a particle from a spherical shape, the greater is the reduction in its settling velocity and the more irregular its motion during settling (Wadell, 1934; Komar and Reimers, 1978; Baba and Komar, 1981a, 1981b; Hallermeier, 1981; Cui *et al.*, 1983; Pye, 1994b). Although settling is not a highly significant aspect of transport of coarse size particles in gravel-bed rivers, since most of the time, movement occurs by sliding or rolling, such material may intermittently lose contact with the bed and may be temporarily suspended. In high flow events sliding and rolling are disturbed by vertical particle movements. Under these circumstances, flat-shaped particles may easily be lifted up as a result of increasing velocity and turbulence, and may spend a longer time away from the bed (*saltation*) and, as a result, be transported further downstream. Spherical particles would (if lifted) settle more easily and move downstream in a rolling mode. Therefore for

coarse-size material differences in the settling velocities of individual particles may be controlled by shape. Particles of similar size but different shape or the same shape but different size may show quite different settling behaviour (Komar and Reimers, 1978; Allen, 1985). Experimental studies have shown that the effect of shape on settling velocities diminishes with decreasing particle size. Pye (1994b) attributed this relationship to the fact that at large Reynolds numbers (equation 7.1), the greater relative magnitude of surface irregularities causes the particles to spin, tumble, and rock to a greater degree, shedding turbulent eddies, that deflect the trajectory of the grain and reduce its overall terminal settling velocity.

(7.1)

$$Rp \equiv \frac{v_f dp}{\mu}$$

Where Rp is particle Reynolds number, v_f: fall velocity, d: diameter of the particle, p: density of the water, μ: dynamic viscosity (Dingman, 1984) .

Experimental studies have shown that variations in particle form have a greater influence than particle surface texture or roundness on settling rates in both air and water. Of particular significance appears to be the degree of particle flatness. Flatness is an important shape characteristics that has an influence across a wide particle-size range, although the effect is greater for larger grains (Wilde, 1952; Alger, 1964; Romanovskij, 1966; Komar and Reimers, 1978; Baba and Komar, 1981; Halllermeier, 1981; Hottovy and Sylvester, 1979). These studies generally demonstrate that, when compared with a sphere of the same volume and density, the flatter the particle, the slower the settling. This can be explained partly by the large cross sectional area (measured perpendicular to the flow direction) of a strongly flattened particle to its volume, and hence higher flow resistance. Another reason is that the highly curved edges of such particles result in flow separation at much lower Reynolds numbers than in the case of more spherical particles. As a result, strong flattening may induce instabilities in the settling of a particle, which will cause rotation, tumbling and oscillation so that the settling velocity of the particle will decrease (Stringham and Guy, 1969; Allen, 1985). Middleton and Southard (1978) pointed out that the same kinds of flow regimes as developed around spheres, can be developed around many shapes, but the details of motion and the exact values of drag coefficients and of the Reynolds numbers for the transition from one regime to another differ between shapes. At high

Reynolds numbers, values for drag coefficients (C_D) vary from less than 0.1 for well streamlined shapes to more than 1.0 for flat discs transverse to the flow. They also noted that settling of non-spherical particles is quite complicated and therefore it cannot be represented by a single diagram of the drag coefficient and Reynolds number. In other words, for particles of irregular shape, there is no simple relationship between the laws of resistance and laws of settling due to the following factors (Middleton and Southard, 1978):

1. Differences in orientation of the particle may results in variation in resistance relative to the flow.
2. A varying sequence of orientations may be assumed by a settling particle, with the pattern of fall determined not only by the Reynolds number but also by the moment of inertia of the particle.
3. Non-spherical particles are unlikely to settle along a straight vertical path, instead, they tend to adopt a side-to-side oscillating type of motion. A particle does not usually show a steady motion and its drag coefficient continually changes with changes in orientation. Thus a simple equation of drag and gravity forces is not possible.

The response of a disc-shaped particle to the force moment produced by form drag is attributed to the moment of inertia (Middleton and Southard (1978) and four different responses were identified by Willmarth *et al* (1964) and Stringham *et al* (1969). These are;

1. ***Steady flat fall***; with the disc oriented normal to the flow. This takes place at Reynolds numbers less than 100, when the viscous forces are large enough to damp out the oscillations that tend to be produced by the pressure moment.
2. ***Regular oscillation fall***: about a position normal to the flow, with little deviation of the settling disc from a straight vertical line of fall.
3. ***Glide-tumble***: this is a pattern of fall in which the disc swings from side to side as is falls, and assumes a high angle to the vertical, or actually tumbles over, at the end of each swing.
4. ***Tumble fall***: during the falling stage, the disc continuously tumbles end-over-end, and moves along a path that is almost straight but oblique to the vertical.

Figure 7.1 shows examples of the last three of these fall patterns.

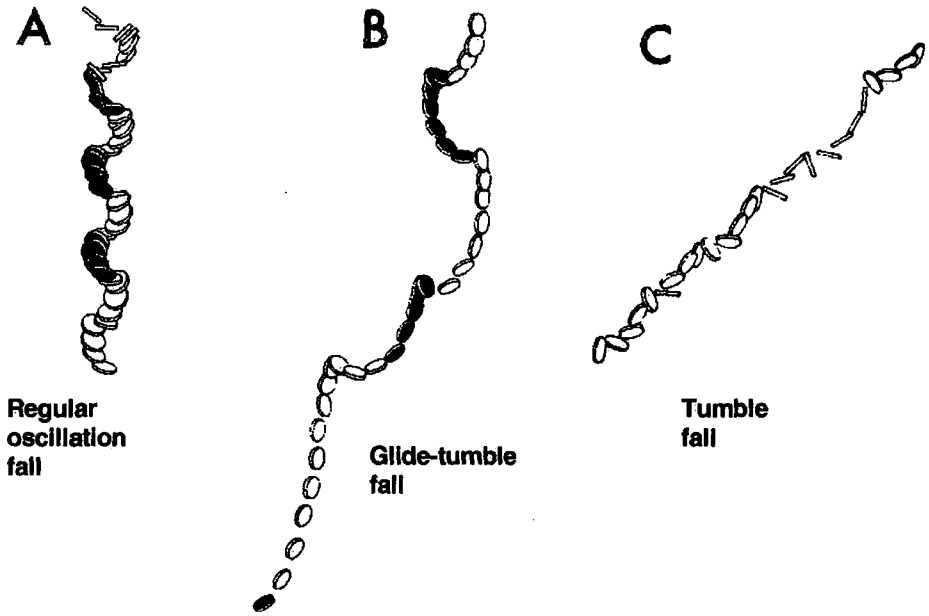

Figure 7.1 Settling patterns of a disc (Middleton and Southard, 1978, pp 4.9). (A) Requlor oscillation pattern; (B) Glide-tumble pattern; (C) Tumble pattern.

The influence of particle roundness on settling velocity has not been thoroughly investigated, probably due to the difficulty in defining an adequate rounding coefficient (Goossens, 1987). However, it has been demonstrated that roundness and surface texture variations have less effect on settling velocity than does overall grain form (Goldbery and Richardson, 1989). The most important effect of roundness on settling is that the flow will separate easily at sharp protuberances on the particle surface, so that the flow around same particles will become turbulent even at relatively low velocities. This induces a high fluid resistance and consequently a lower settling velocity of the particle. (eg. Wilson and Huang (1979)).

In order to determine any changes in rate of settling due to particle roundness and particle surface texture, a series of settling velocity measurements were carried out by Garnett (1966). The effect of particle roundness was found to be substantial and variations in particle roundness have the greatest influence on settling velocity. Sharp-edged discs had fall velocities 8-28 % lower than well-rounded discs, with the partly rounded discs falling at an intermediate rate. For particles having a high shape value (e.g. cylinders), the presence of sharp edges reduced the settling velocity by 12-21 % of

the rate of fall of well-rounded cylinders. With the other particle properties held constant, three different surface textures for both discs and spheres had only a minor influence on settling velocity.

Goossens (1987) investigated the combined effect of particle flattening and rounding on the terminal fall velocity. His investigation was based mainly on Dietrich's (1982) compilation of the experimental data obtained by 18 previous authors who characterised their particles using the Corey shape factor and the Folk-Powers roundness index. It was found that the combined effect of flattening and roundness is greater than that of either characteristic in isolation, and that the nature of the effects is broadly similar in both air and water. For larger sized particles, however, it was found that the effect of rounding is of greater significance, although it was still secondary to the importance of particle flattening.

7.4 EXPERIMENTAL INVESTIGATIONS OF PARTICLE MOTIONS

Particle motion on a natural bed is dependent on many factors. The factors include size, shape and to some extent surface characteristics of particles, as well as size, shape and roughness characteristics of the channel bed. These factors have been shown to have significant effects on test particles friction or pivoting angles. Indeed, the friction angle of a particle depends on its size, median bed grain size, and the degree of bed sorting. Earlier studies (eg. Komar and Li. 1986; Buffington *et al.*, 1992) have shown that friction angles decrease with increasing grain size relative to the median bed grain size, and are a systematic function of sorting, with lower friction angles associated with poorer sorting (See Chapter 6). Pivoting angle, on the other hand, is related to the contact point of a particle with an underlying grain, which is also dependent on the shape and size of test particles and also size, shape and imbrication of underlying bed material. Particle pivoting angles have an important effect on the threshold of movement (more detail see Chapters 2 and 6).

As well as settling velocity, when other parameters are held constant (similar size, form and density), the roundness of particles has been found to be significant in controlling their entrainment and transport. For example, a single perfectly rounded sphere on a flat surface is much more easily entrained and kept in motion by a fluid than a highly angular particle of equivalent weight. Li and Komar (1986) and Komar and Li (1988) clearly showed (for uniform-sized particles) that angular particles of crushed

gravel have larger pivoting angles than either spherical particles or ellipsoids of the same size (See Chapter 2). The difference in pivoting angle between the angular and more rounded particles was found to greater with increasing grain size (Pye, 1994b).

As part of the present study a series of visulatisation experiments were carried out with natural and artificially moulded gravel-size particles. Two sets of experiments were undertaken in a 10 litre, water-filled rectangular tank. Figure 7.2 shows the experimental design.

For the first set of experiments, particles were dropped, through water, onto a 30° inclined, smooth glass plate, which is adopted as standard from the literature (Schmeeckle, 1988) . A camera mounted outside the tank, normal to the sloping glass, recorded the fall and movement of each particle. A strobe light (strobe rate 25 flashes / second) was mounted orthogonal to the camera. By keeping the camera shutter open for the duration of each particle drop multiple images of the particle could be recorded on the same frame of film (for detail of the technique see Chapter 3). Settling velocities, rebound angles and trajectory paths were measured from the photographs by plotting successive centres of mass of the particle. Figure 7.3 illustrates the schematic settling and transport paths of a particle from the point of release to the point of transport cessation. Despite some irregularities due to variations in particles shapes, settling velocity of a particle tends to be vertical, while transport velocity is parallel to the plane.

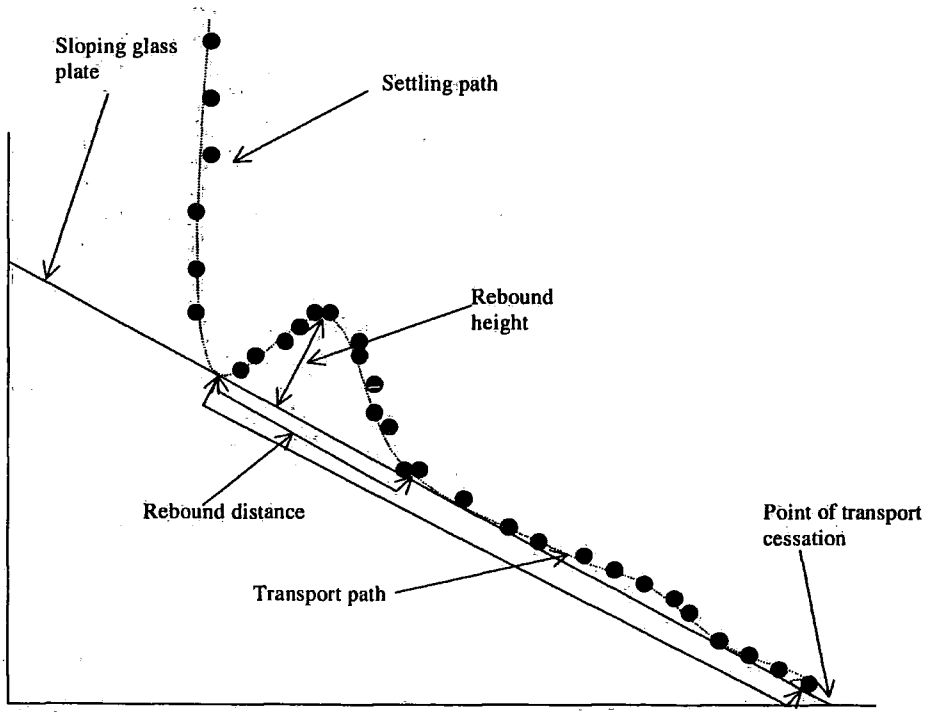

Figure 7.3 A typical settling and transport path of a particle

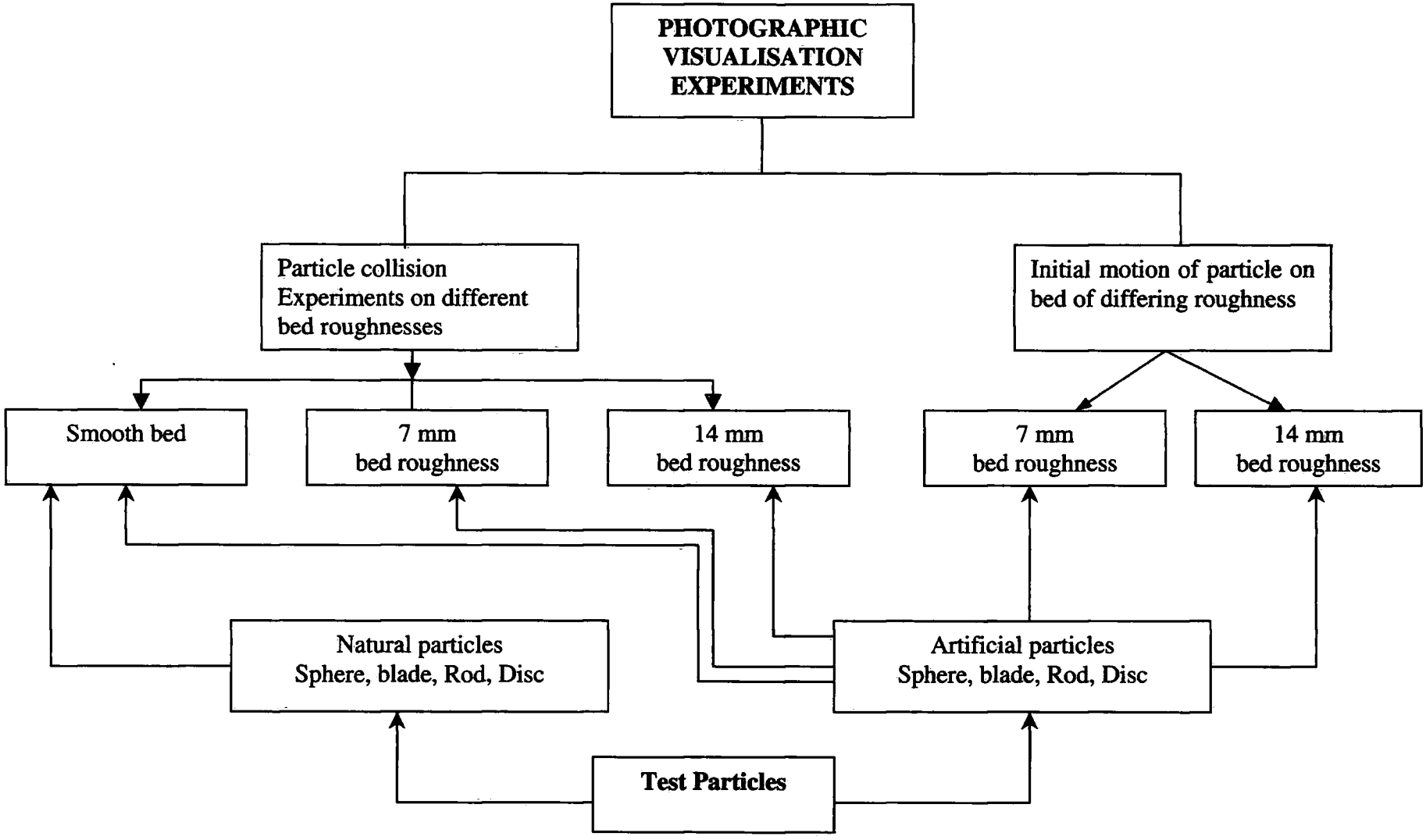

Figure 7.2 Experimental design for the visualisation experiments

The aim of the experiment as: To determine settling and transport velocities of artificial and natural particles of differing shapes and size; and to determine the changes in settling and transport velocities of artificial particles of different shape in relation to weight.

A second set of experiments, using the same set-up as the first but this time investigating the initial motion of particles of various shapes and sizes, was undertaken on two beds of differing roughness. Each bed was tilted until the test particle moved from its pocket of origin. Strobe-light photographs were taken at the initiation of motion. This method was developed from work undertaken by Schmeeckle, (1998).

7.5 SETTLING AND TRANSPORT VELOCITIES OF PARTICLE OF VARIOUS SHAPE.

Settling velocities of four particle shapes were measured for artificially-moulded and natural particles.

Table 7.1 The tri-axial dimensions (mm) and weights (g) of artificial particles used for the settling velocity experiments.

Shape class	A axis	B axis	C axis	Roundness	Sphericity	Corey Shape Factor (CSF)	Weight (g)
Sphere	10.0	10.0	10.0	1000	1.00	1.0	0.85
Blade	20.0	10.0	2.0	100	0.37	0.1	0.69
Rod	20.0	10.0	10.0	200	0.63	0.7	2.41
Disc	10.0	10.0	2.0	600	0.58	0.2	0.27

$$Corey\ Shape\ Factor = \frac{D_c}{\sqrt{D_a D_b}}$$

H Note: D_a, D_b and D_c show long, intermediate and short axes of a particle respectively.

Settling and transport velocities of artificial particles of similar b-axis size but varying shapes (sphere, blade, rod, disc) were measured. The three axes and weights of each of these particles are given in Table 7.1. The density of the artificial particles was approximately 1.48. For each shape 10 measurements of settling velocity and transport velocities were taken to determine a mean and standard deviation. Figure 7.4 summarises the settling and transport paths of four artificial grain shapes and the paths overlaid using the point of impact of the particles with the glass plate as a common reference position. Characteristics movement patterns can be observed:

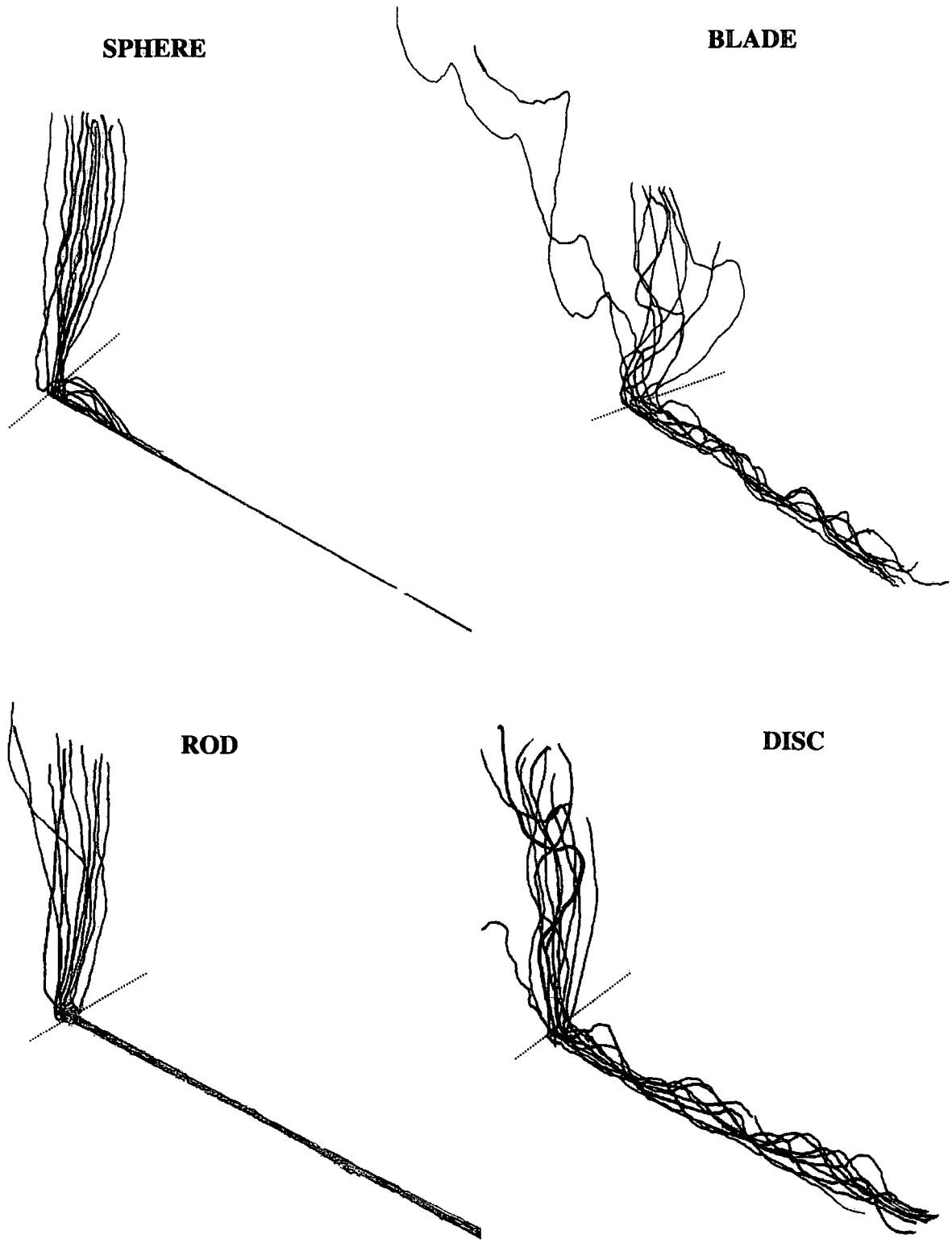

Figure 7.4 Summary of particle settling and transport paths for four particle shapes in water striking a glass surface inclined at 30° degrees. The same experiment was replicated ten times for each particle. The dotted line shows the division between settling and transport paths.

Sphere - Falls steadily during settling. Because of high speed of impact sphere shows a large rebound followed by a smooth rolling motion.

Rod - Shows a steady fall with some rotation. Rebound is minimal and transport is by relatively smooth rolling with the long axis transverse to the slope.

Blade - Settling paths are highly variable, often showing a glide and tumble motion. Although impact angles are highly variable rebound is negligible. Transport is variable but usually follows an oscillatory sequence of 'collapse,-slide-lift-stall-collapse-slide' with the long axis transverse to the slope.

Disc - Disc tend to follow either a regular oscillatory settling path or a glide and tumble motion. There is little rebound on impact and transport follows a similar pattern to the blade with occasional 'on edge' rolling.

Figures 7.5, 7.6, 7.7, and 7.8 are typical strobe-light photographs of sphere, blade, rod, and disc-shaped particles. Four replicate runs are shown for each shape class. Spheres and rod-shaped particles generally tend to settle in a more uniform fashion, despite a slight initial increase in rate of settling (Figures 7.5). All the tests in Figure 7.5 showed almost the same settling velocity and uniform settling trajectories. After the initial impact on the base plate the sphere tends to rebound slightly and then rolls downslope. However, the velocities of rolling slightly increase as the particle rolls further. Figure 7.6 shows that, except for experiment 4, which shows a slightly greater settling velocity, the rod also showed very uniform settling. In each image the rod tends to settle with its a axis transverse to the slope and to roll with the same orientation. There is little rebound after the initial impact and the rod tends to roll and accelerate with downslope distance.

Blade and disc shapes, however, showed a more complex and irregular hydraulic behaviour depending on their orientation. In general, for blade and disc-shaped particles (Figures 7.4, 7.7 and 7.8) the settling paths tended to be much longer and irregular than for the rod and sphere shapes. Settling velocities are greatest when the test particle falls in a vertical orientation, whereas in a horizontal orientation, particles tend to move laterally, leading to a slower settling velocity. In Figure 7.7 the paths made by the movements of the four blades show some degree of irregular settling. For example, in the initial part of the settling path (Photograph 1), the blade tends to fall in a horizontal plane and then stall. It then began to fall in a vertical plane with an increased settling rate. Before hitting the slope it again turns in a horizontal plane.

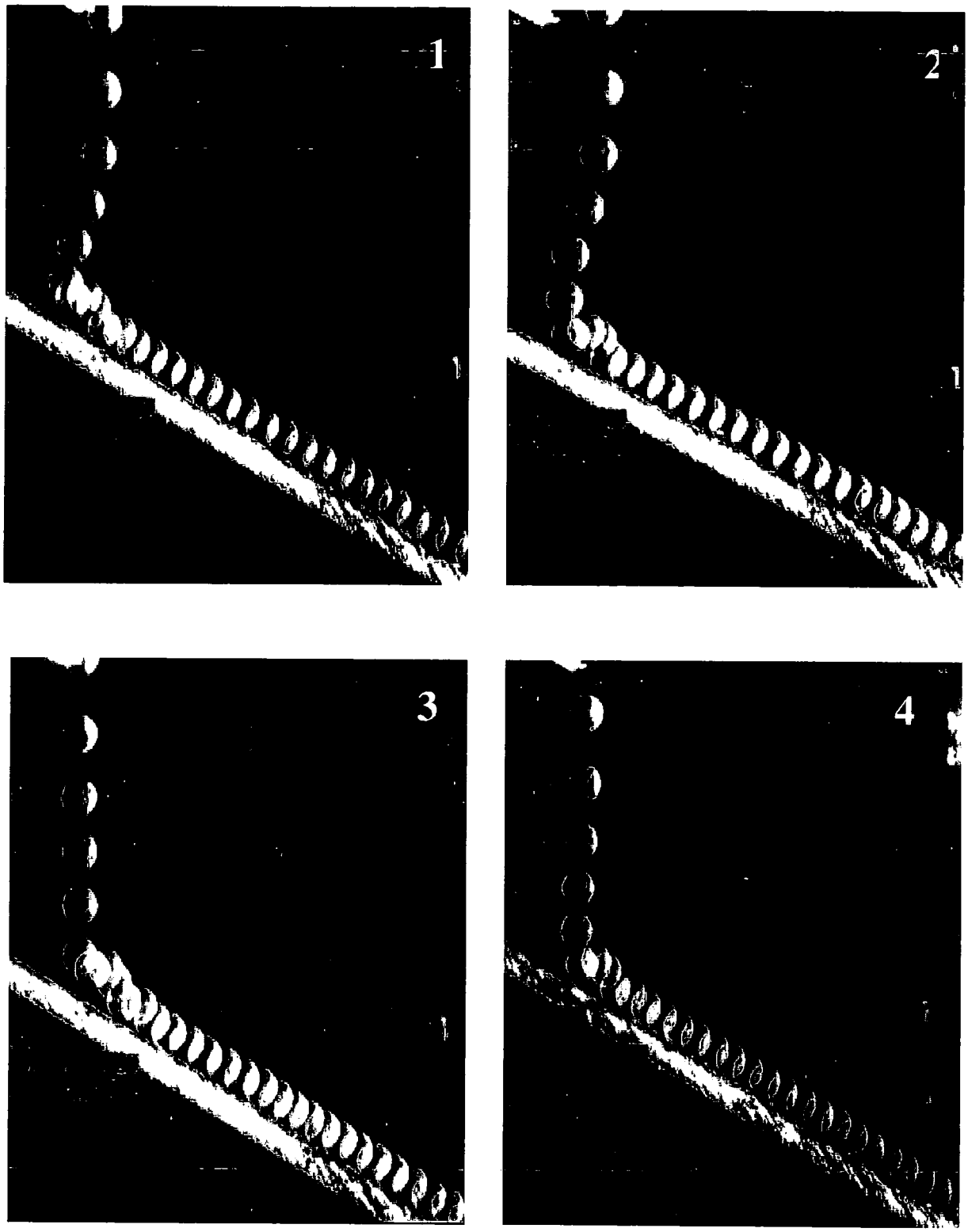

Figure 7.5 Strobe-light photographs of sphere particle striking a glass surface inclined at 30^0 degrees in water. The same experiment was replicated 10 times. These photographs show four examples. The strobe rate was set at 25 flashes per second.

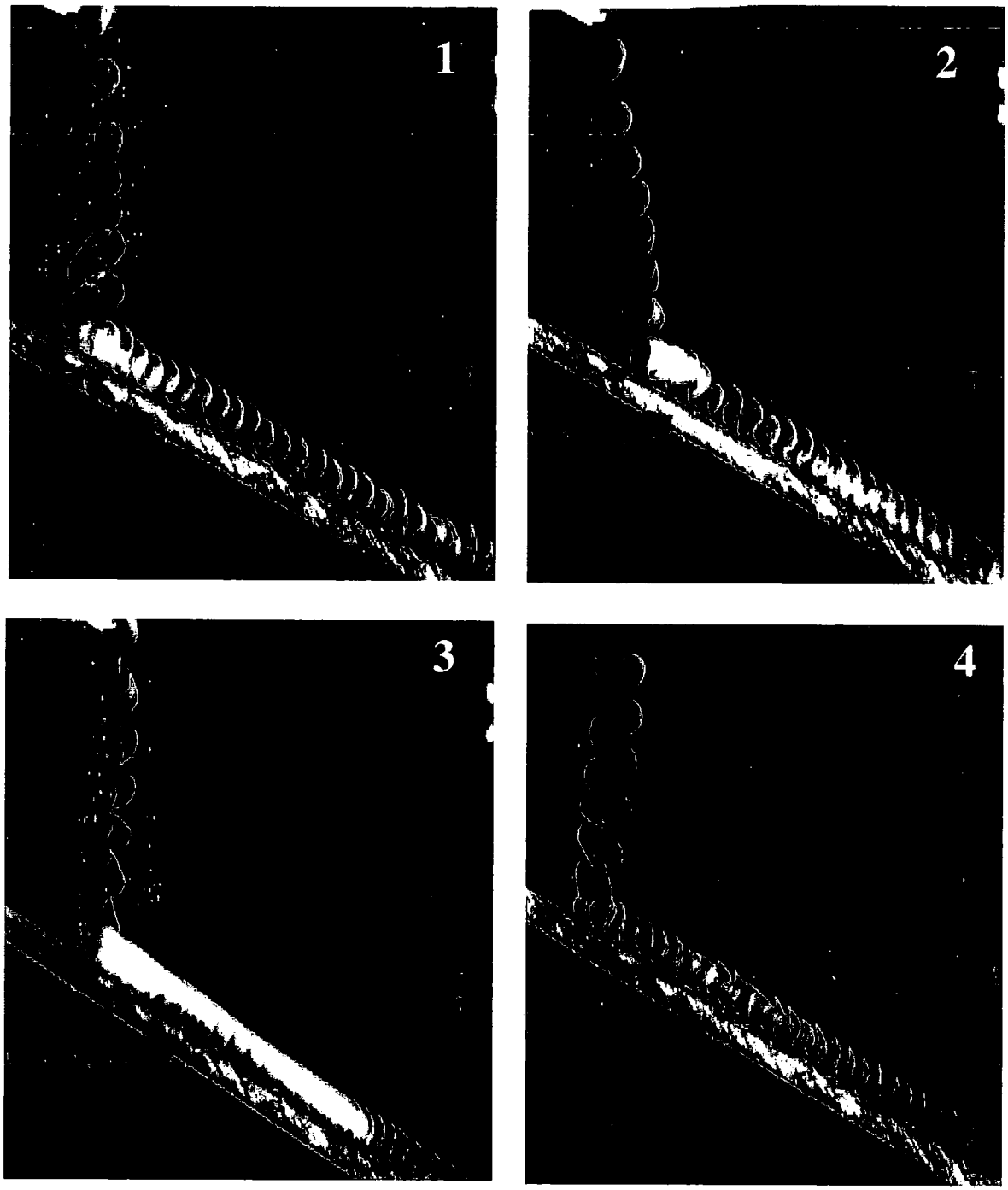

Figure 7.6 Strobe-light photographs of rod particle striking a glass surface inclined at 30^0 degrees in water. The same experiment was replicated 10 times. These photographs show four examples. The strobe rate was set at 25 flashes per second.

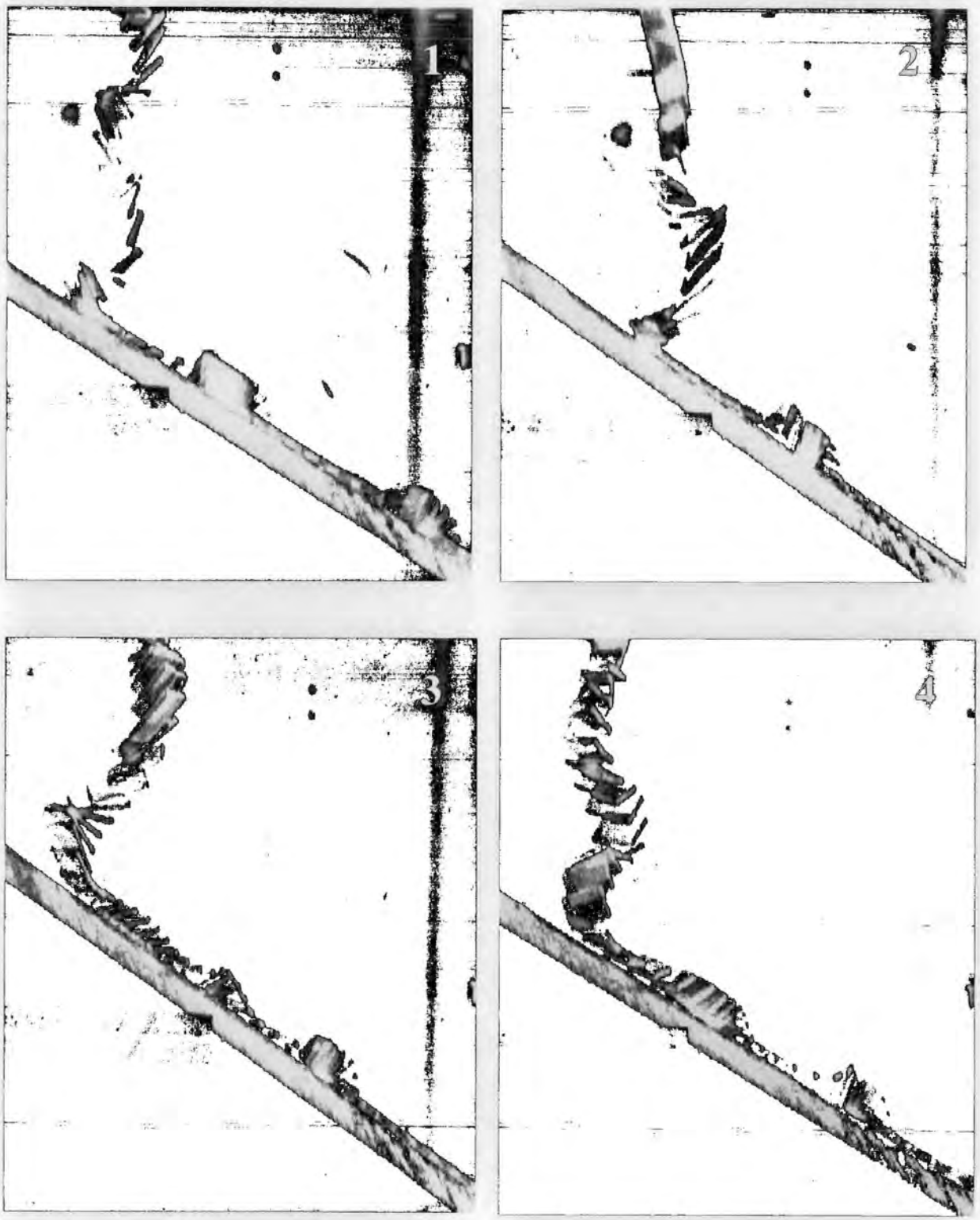

Figure 7.7. Strobe-light photographs of blade particle striking a glass surface inclined at 30^0 degrees in water. The same experiment was replicated 10 times. These photographs show four examples. The strobe rate was set at 25 flashes per second.

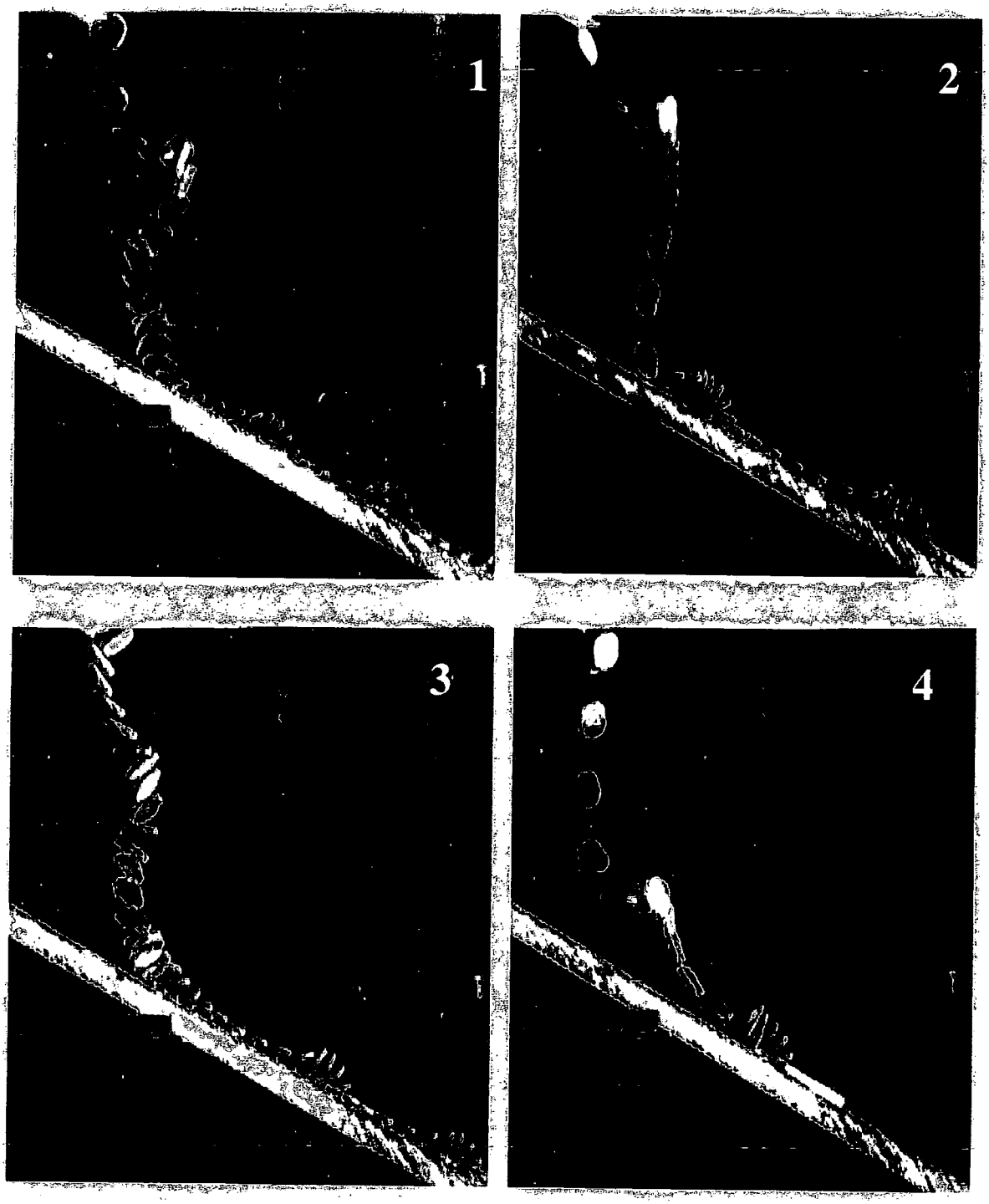

Figure 7.8 Strobe-light photographs of disc particle striking a glass surface inclined at 30^0 degrees in water. The same experiment was replicated 10 times. These photographs show four examples. The strobe rate was set at 25 flashes per second.

After the initial impact with the glass plate it tends to accelerate in a sliding mode and then stall by standing on its vertical plane with its long axis transverse to the slope. Following a short movement in a vertical plane the particle collapsed on its horizontal plane and accelerated again, which result in a second vertical motion in the lower part of slope, after which it collapses again. Photograph 2 on the other hand reflects an initial increase in settling velocity due to a fall in a vertical plane. In the middle of the settling path, the particle reorientates itself in a horizontal plane, which results in a momentary stop, and then it turns on a vertical plane leading to increased settling velocity. Before its impact with the glass plate, the particle reorientates itself and hits the base slope at a low angle. This gentle impact on the slope initially caused a slow downslope sliding but then the particle accelerated until lift in a vertical plane was generated, resulting in a momentarily stall, then collapse again on the horizontal plane and acceleration downslope in a sliding mode. Photographs 3 and 4 in Figure 7.7 also show similar settling and transport velocity patterns to photographs 1 and 2.

Discs show similar hydraulic settling behaviour to blades. Discs tend to change orientation from a vertical position to horizontal or from horizontal to vertical, which results in differential settling rates (Figure 7.8). As the larger surface area of a particle turns to a horizontal position, the contact area of the water column with the particle surface increases and this leads to a greater resistance which results in lower settling velocity. Whereas a fall with vertical plane minimises the resistance which leads to an increase in settling velocity. For instance, comparison of photographs 1 and 3 and 2 and 4 in Figure 7.8 reveal very different settling velocities due to differences in particle orientation. In photographs 1 and 3, the particle was falling in a horizontal plane over most of its settling path, resulting in rather slow settling, while in photographs 2 and 4 movement was generally in the vertical plane, resulting in faster settling. In terms of the settling trajectories, Figures7.7 and 7.8 also show that sinuous settling paths occur if a particle is in a horizontal position, whereas in a vertical downward movement, particle settling paths seem to be relatively straight.

Detailed analysis of Figures 7.7 and 7.8 indicates variability in settling rate. For example, in Figure 7.7, photograph 1 in the upper section of the settling path, there are only three images where particle orientation is vertical and settling is rapid, while for the middle section of the path, the number of images increases to six (revealing lower settling velocity) where the particle tends to twist in a horizontal plane. In the lower section, the settling velocity decreases again and the number of images increases to

seven because of the horizontal settling orientation. Similar settling patterns also exist for photographs 2 and 4. Subsequent to an initial increase in settling, the disc twisted to a horizontal position and thus stopped momentarily. In the latest stage of settling, the disc again twisted to a vertical position, which resulted in an increase in settling velocity.

In terms of mode of movement and the observed transporting velocities on the smooth base plate, the experiments show that sphere and rod-shaped particles move in a rolling mode. After the initial impact, the sphere tended to rebound slightly and then move down in a uniform rolling mode. For rod there was little rebound and it tends to roll with the long axis transverse to the base plate (Figures 7.4, 7.5 and 7.6). Discs and blades showed little rebound after, regardless of the orientation of strike. However, discs and blades move in an irregular sliding mode. Figures 7.7 and 7.8 show that after initial contact with the sloping plate, particles accelerated down the slope and then became elevated from the plate, finally resettling on to the plate again. This cycle of slide and lift appeares to be repeated along the slope (Figure 7.4).

Table A4.1 shows the settling and transport velocities of individual particles for each shape class and also their mean and standard deviation values. Figure 7.9 shows the mean settling velocities of particles of different shapes. Both Figure 7.9 and Table A4.1 indicate that particle flatness has an important influence on the settling velocity. The more the particles are flattened, the slower they will settle compared with spheres and rods of the same size and density. Indeed, sphere-and rod-shaped particles tend to have greater mean settling velocities than blades and discs, which have relatively similar mean values. The increasing order of the rank is 14.6 cm s^{-1} for discs, 16.8 cm s^{-1} for blades, 29.4 cm s^{-1} for rods, and 37.0 cm s^{-1} for spheres. Table A4.1 indicates that sphere-and rod-shaped particles tend to settle faster and also have fairly uniform settling velocities. Blades and discs settle more slowly and show relatively large scatter around their mean values.

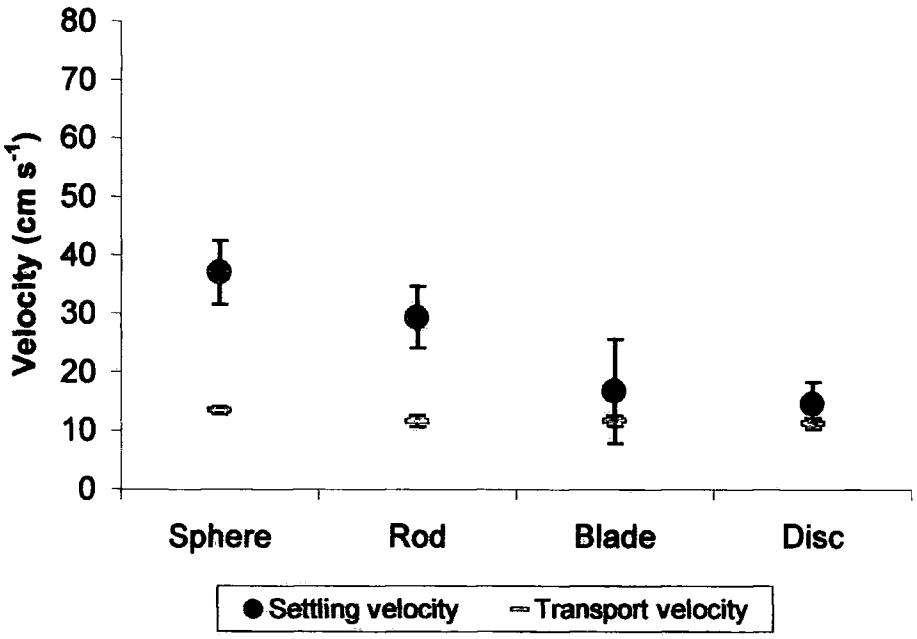

Figure 7.9 Settling and transport velocities of artificial particles of sphere, blade rod and disc shapes with b-axes 10 mm.

In terms of particle transport velocity, Table A4.1 and Figure 7.9 show that, despite faster mean settling velocity for spheres and rods than for blade-and disc-shaped test particles, a similar pattern in the mean transport velocities does not emerge. Mean transporting velocities are much lower than the settling velocities of spheres, blades, and rods (Table A4.1 and Figure 7.9). For sphere-shaped particles, transport velocities vary between 13.3 cm s^{-1} and 14.3 cm s^{-1} with a standard deviation value of 0.6. For rods the velocity varies between 10 cm s^{-1} and 13.3 cm s^{-1} with a standard deviation value of 0.9. Differences between the individual transport velocities varied between 10 and 12.5 for blade and disc with a standard deviation value of 0.9. After the collision with the base plate, blade-shaped particles did not move for two measurements. For the disc shapes in four out of the 10 experiments test particles did not move after impact.

7.6 SETTLING AND TRANSPORT VELOCITIES OF ARTIFICIAL PARTICLES OF DIFFERING SHAPE AND SIZE

In order to investigate the influence of particle shape and size on settling velocity, form of movement (rolling or sliding) and trajectory paths a series of experiments were carried out with artificially-moulded gravel-size particles. The test particles were arranged in three size groups in terms of their intermediate axes (b-axis):

5 mm small, 10 mm medium and 15mm. The tri-axial dimensions (mm), weights (g) and shape properties of the particles are summarised in Table 7.2. Individual particles were dropped twice, through water, onto an 30° inclined smooth glass plate.

Table 7.2 Summary of the tri-axial dimensions (mm), weights (g) and shape properties of test particles in three size groups

	A	B	C	Radius	Roundness	Sphericity	Flatness	Weight
Small size								
Sphere	5	5	5	2.5	1000	1.00	100	0.14
Blade	10	5	1	2.5	500	0.37	750	0.14
Rod	10	5	5	2.5	500	0.63	150	0.29
Disc	5	5	1	2.5	1000	0.58	500	0.09
Medium size								
Sphere	10	10	10	5	1000	1.00	100	0.85
Blade	20	10	2	2.5	250	0.37	750	0.69
Rod	20	10	10	2.5	250	0.63	150	2.41
Disc	10	10	2	5	1000	0.58	500	0.27
Large size								
Sphere	10.5	15	10.5	5	952	1.00	100	2.50
Blade	30.4	15	3	2.5	164	0.32	682	2.19
Rod	30	15	10.5	2.5	167	0.50	193	6.60
Disc	10.5	15	2	5	952	0.58	525	0.71

Figures 7.10, 7.11 and 7.12 are typical strobe-light photographs of the particles in the different shape classes and in the three size groups. After the initial collision with the glass plate there was no substantial rebound except for a small degree of rebound for spheres. Blade and disc-shaped particles showed the most complex settling modes, while spheres and rods show more consistent patterns. Table 7.3 contains the relevant settling and transport velocity information taken from each photograph. Table 7.3 and Figure 7.13 show that, in common with previous experiments, in each size group, sphere-and rod-shaped particles tend to have faster mean settling velocities than discs and blades. In the small size group, the average settling velocities are 28.6 cm s^{-1}, 22.5 cm s^{-1}, 12.2 cm s^{-1} and 11.9 cm s^{-1} for sphere rod, disc, and blade respectively. In the medium size group again rods and spheres show faster mean settling velocites; 30.6 cm s^{-1} for spheres, 34.3 cm s^{-1} for rods, 12.6 cm s^{-1} for blades, and 11.8 cm s^{-1} for discs,

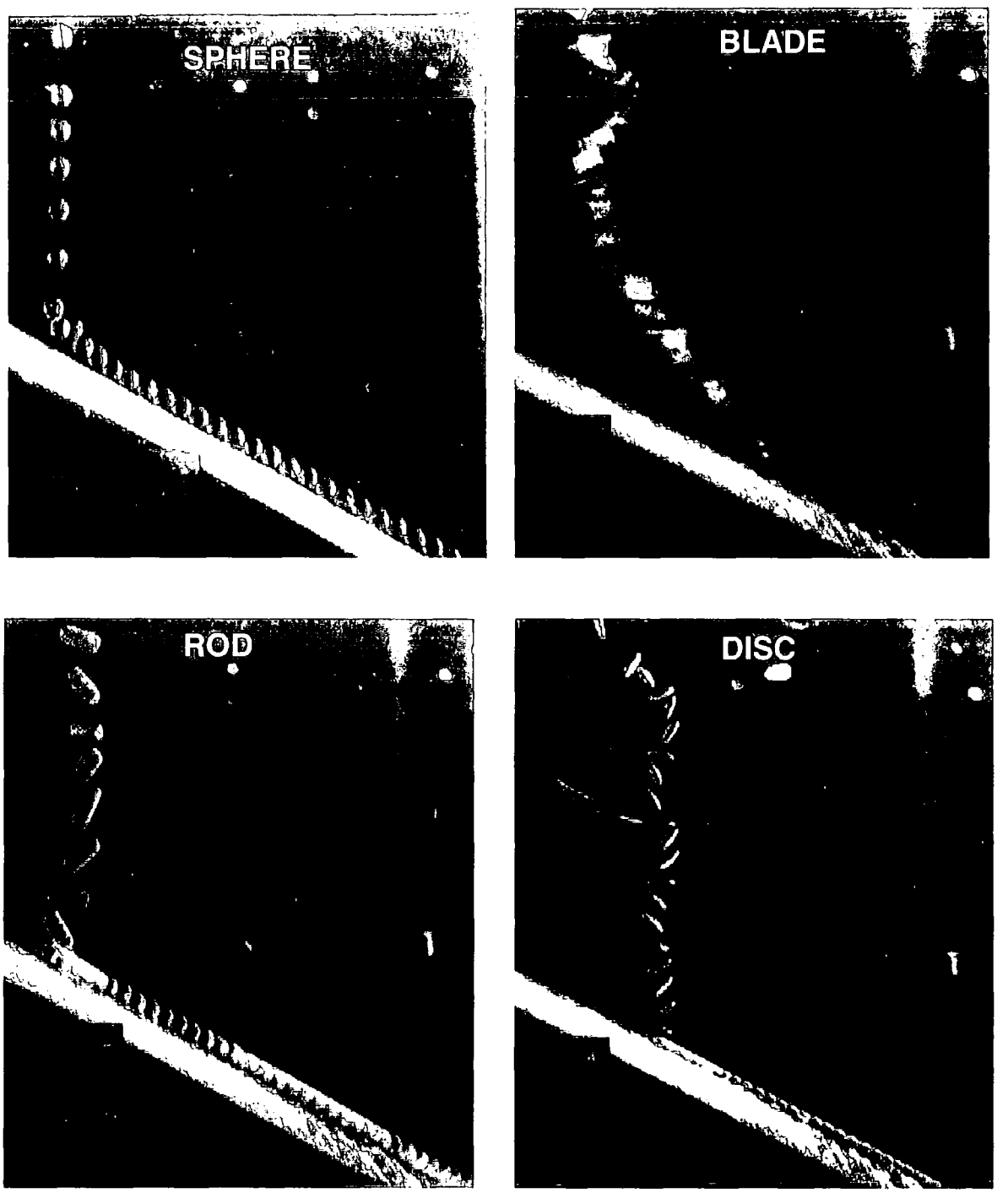

Figure 7.10 Strobe-light photographs of small sized sphere, blade, rod and disc particles striking a glass surface inclined at 30^0 degrees in water. The same experiment was replicated twice for each particle. These photographs show four examples. The strobe rate was set at 25 flashes per second.

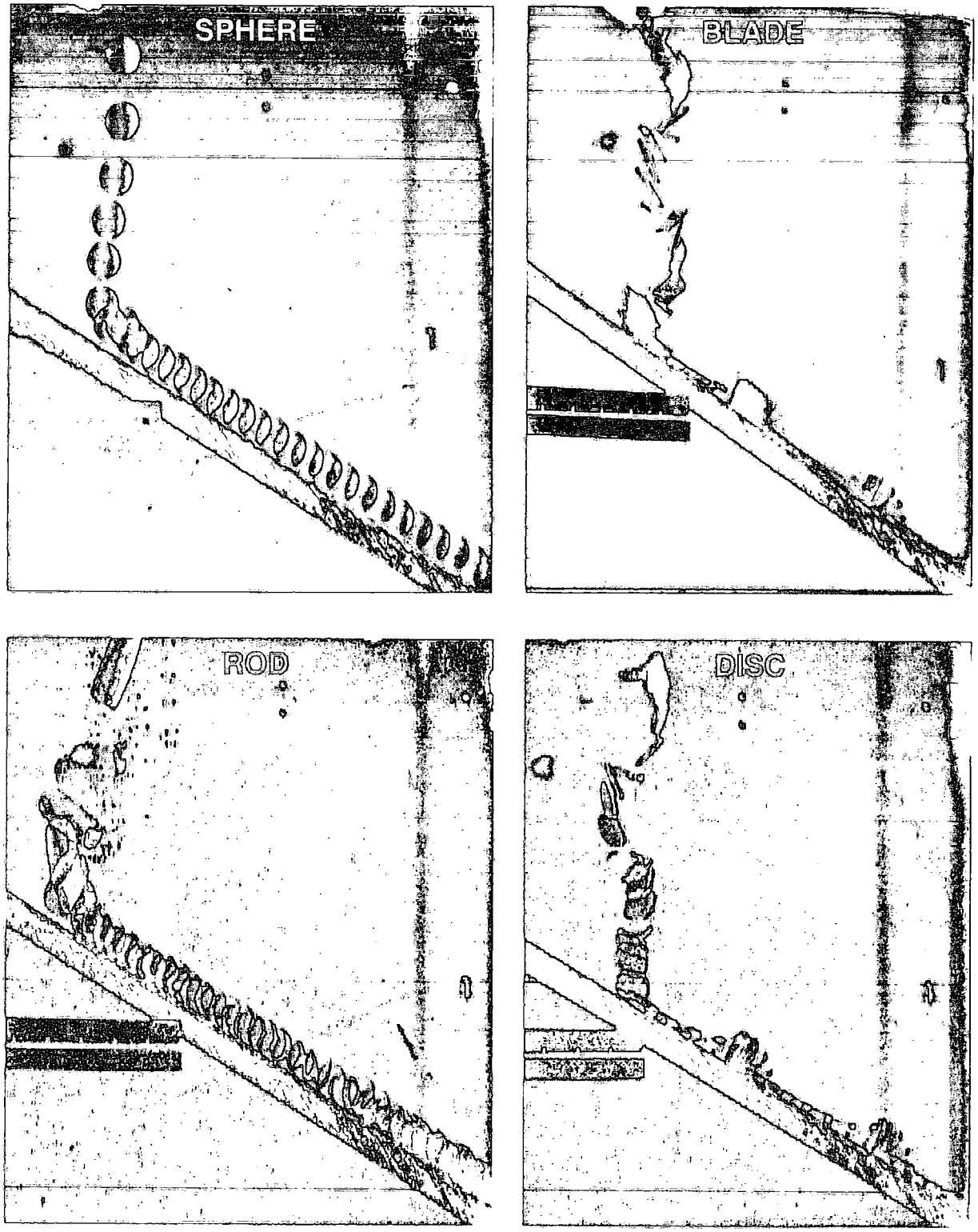

Figure 7.11 Strobe-light photographs of medium sized sphere, blade, rod and disc particles striking a glass surface inclined at 30^0 degrees in water. The same experiment was replicated twice for each particle. These photographs show four examples. The strobe rate was set at 25 flashes per second.

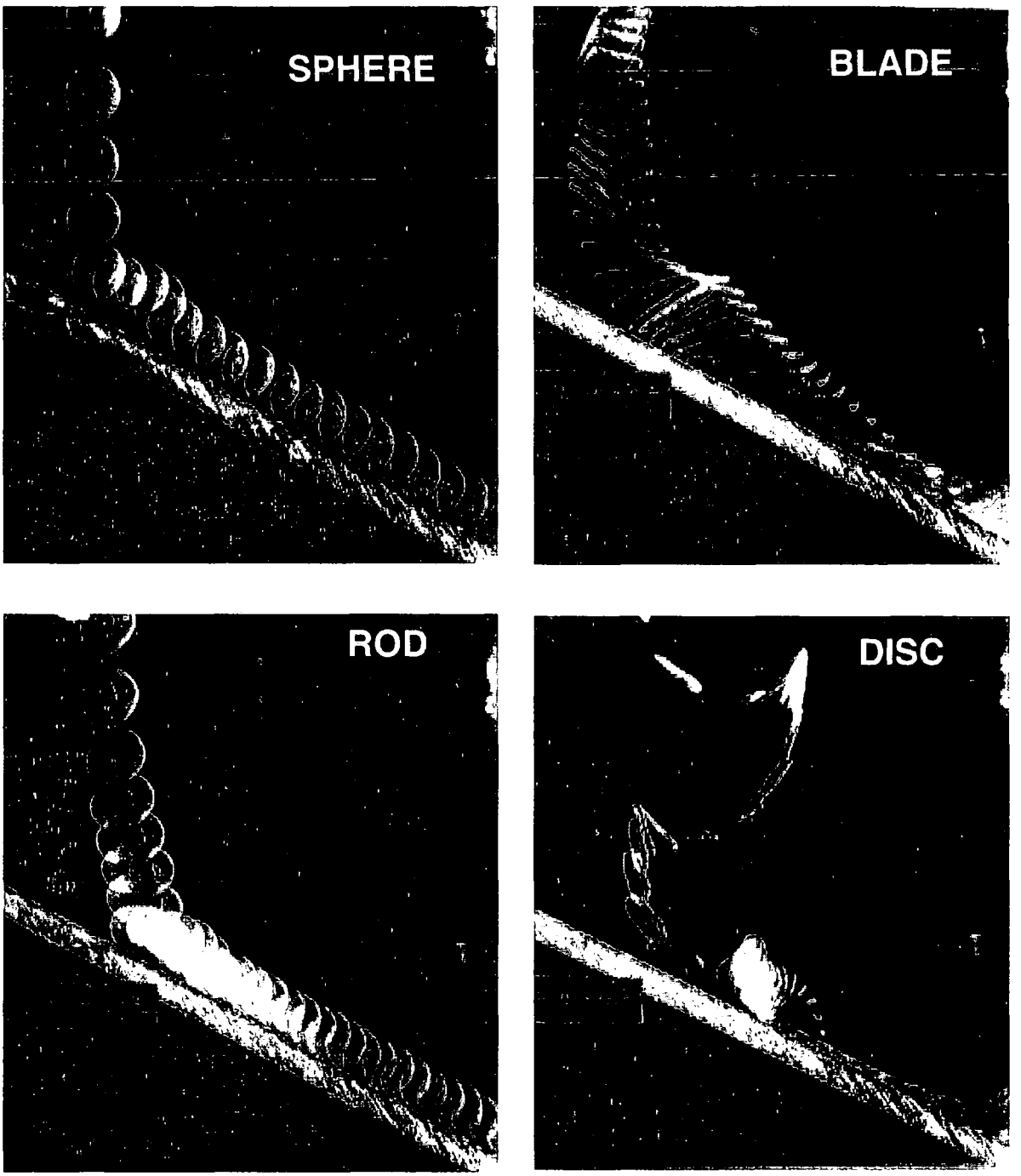

Figure 7.12 Strobe-light photographs of large sized sphere, blade, rod and disc particles striking a glass surface inclined at 30^0 degrees in water. The same experiment was replicated twice for each particle. These photographs show four examples. The strobe rate was set at 25 flashes per second.

while in the large size group the rank is also 34.3 cm s^{-1} for both spheres and rods, 14.4 cm s^{-1} for blades and 12.6 cm s^{-1} for discs. For almost all shape classes (Table 7.3) there is an increase in the settling velocity with particle size. The increasing rate of mean settling velocity for sphere-shaped particles is greater than blade and disc. In the small medium and large size groups it varies between 28.6, 30.6 and 34.3 respectively for spheres, while for rods the variation is between 22.5 (small size) and 34.3 (large size). There is a similar trend for blades, 11.9-14.4, and discs, 12.2-12.6.

Table 7.3 Summary of mean settling and transport velocities of test particles in three size groups. (S:sliding, R:rolling)

Shape	Settling velocity cm s^{-1}	Transport velocity cm s^{-1}	(Settling velocity/ transport velocity)	Mode of transport
		Small		
Sphere	28.6	11.8	2.42	R
Sphere	28.6	12.5	2.29	R
Blade	13.3	10.0	1.33	S
Blade	10.5	No movement		S
Rod	20.0	10.5	1.90	R
Rod	25.0	9.1	2.75	R
Disc	12.5	10.5	1.19	S
Disc	11.8	7.1	1.66	S
Mean	**18.8**	**10.2**	**1.84**	
		Medium		
Sphere	28.6	15.4	1.86	R
Sphere	33.3	14.3	2.33	R
Blade	11.8	10.5	1.12	S
Blade	13.3	15.4	0.86	S
Rod	28.6	11.8	2.42	R
Rod	40.0	9.5	4.21	R
Disc	11.8	9.5	1.24	S
Disc	11.8	10.5	1.12	S
Mean	**22.4**	**12.1**	**1.85**	
		Large		
Sphere	28.6	15.4	1.86	R
Sphere	40.0	16.7	2.40	R
Blade	13.3	14.3	0.93	S
Blade	15.4	13.3	1.16	S
Rod	40.0	12.5	3.20	R
Rod	28.6	11.8	2.42	R
Disc	11.8	12.5	0.94	S
Disc	13.3	11.1	1.20	S
Mean	**23.9**	**13.4**	**1.78**	

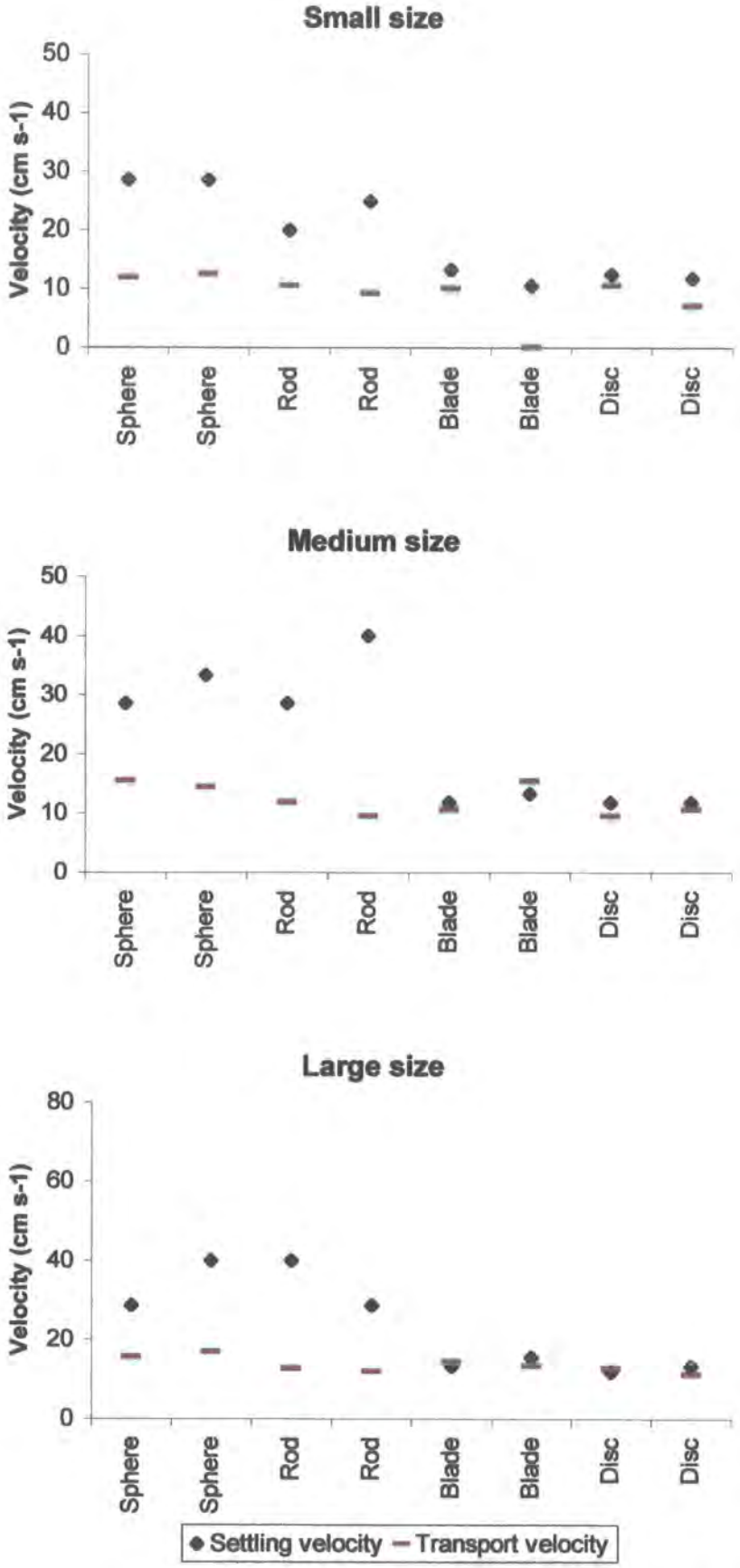

Figure 7.13 Settling and transport velocities of particles of the four shape classes in three size groups.

In terms of transport velocities, it appears that, regardless of shape, velocities tend to increase slightly with size (Table 7.3). Figure 7.13 shows small differences between settling and transport velocities of blade-and disc-shaped particles, with greater differences for rod-and sphere-shaped particles in each size group. The ratio of settling velocities to transport velocities indicates the importance of settling to transport. Within almost every size group settling velocities for sphere and rod-shaped particles are noticeable greater than that of blades and discs. The reason might be attributed to two factors. Sphere-and rod-shaped in each size group tend to be of greater weight, which leads to faster settling, and have smaller projection areas compared to discs and blades.

Ratios of settling velocities to transport velocities are greater in sphere-and rod-shaped particles in each size group (Table 7.3). The greater rates indicate greater settling velocities compared to transport velocities. Table 7.3 shows that, within each size group, blade-and disc-shaped particles tend to have rather lower ratios than the sphere and rod-shaped particles. This indicates that differences between settling and transport velocities for blades and disc-shaped particles are smaller compared to the sphere-and rod-shaped particles. However, there is no indication that ratios of settling velocity to transport velocities vary regularly with size.

7.7 CHANGES IN SETTLING AND TRANSPORT VELOCITIES OF PARTICLES OF DIFFERENT SHAPE IN RELATION TO WEIGHT

In the previous section test particles within each size group differed in weight (Table 7.2). Sphere-and rod-shaped particles tend to be heavier than blades and discs due to their greater c axes. In this section, a series of experiments were carried out with artificially-moulded gravel-size particles in order to determine changes in settling and transport velocities of different particle shapes in relation to weight. The dependence of settling velocity is clearly demonstrated in settling equations such as Stokes Low. Particles were classified into three weight classes. In each class particles were prepared using wet clay of equal weight. However, on drying resultant weights showed some slight differences. Therefore, in each group test particles were of approximately equal weight but differed in shape. The tri-axial dimensions (mm), weights (g) and shape properties of each particle are summarised in Table 7.4. Methods followed those of the previous experiments.

Table 7.4 Summary of the tri-axial dimensions (mm), weights (g) and shape properties of test particles in three weight groups.

	A axis	B axis	C axis	Radius	Round-ness	Spheri-city	Flatness	Weight
Small group								
Sphere	10	10	10	5.0	1000	1.00	100	0.94
Blade	28	10	2	2.5	179	0.29	950	1.00
Rod	17	7	7	5.0	588	0.55	171	0.98
Disc	16	16	3	2.5	313	0.57	533	0.99
Medium group								
Sphere	13	13	13	5.0	769	1.00	100	2.38
Blade	41	12	3	2.5	122	0.28	883	2.73
Rod	26	9	9	5.0	385	0.49	194	2.58
Disc	25	25	3	2.5	200	0.49	833	2.66
Large group								
Sphere	17	17	17	8.0	941	1.00	100	3.91
Blade	54	16	3	2.5	93	0.25	1167	4.38
Rod	29	11	11	6.0	414	0.52	182	4.18
Disc	32	32	3	2.5	156	0.45	1067	4.10

Figures 7.14, 7.15 and 7.16 show the typical strobe-light photographs taken of the particles in different shape classes in three weight groups and indicate a similar pattern of settling and transport velocities determined with particles in the three size groups. Table 7.5 and Figure 7.17 shows that, despite their similar weights, mean settling velocities of the sphere-and rod-shaped particles are noticeable greater than discs and blades in almost each weight group. Regardless of shape, mean settling velocities tend to slightly increase with weight. The increasing rank of the mean settling velocities is 29.5 cm s^{-1}, 31.7 cm s^{-1} and 33.3 cm s^{-1} for small, large and medium size groups respectively (Table 7.5). Within each weight group, spheres tend to show the fastest settling velocities, while discs, except in the small group, show the slowest rates. The decreasing order of settling velocities in the small group is sphere, rod, disc and blade, while for the medium and large size groups the ranks are sphere, rod, blade and disc (Table 7.5). Within each weight group spheres have relatively uniform vertical settling trajectories, while rods show similar settling velocities but with slightly more rotation about their long axis. Discs and blades on the other hand exhibit slower, more irregular modes of settling depending on their orientation.

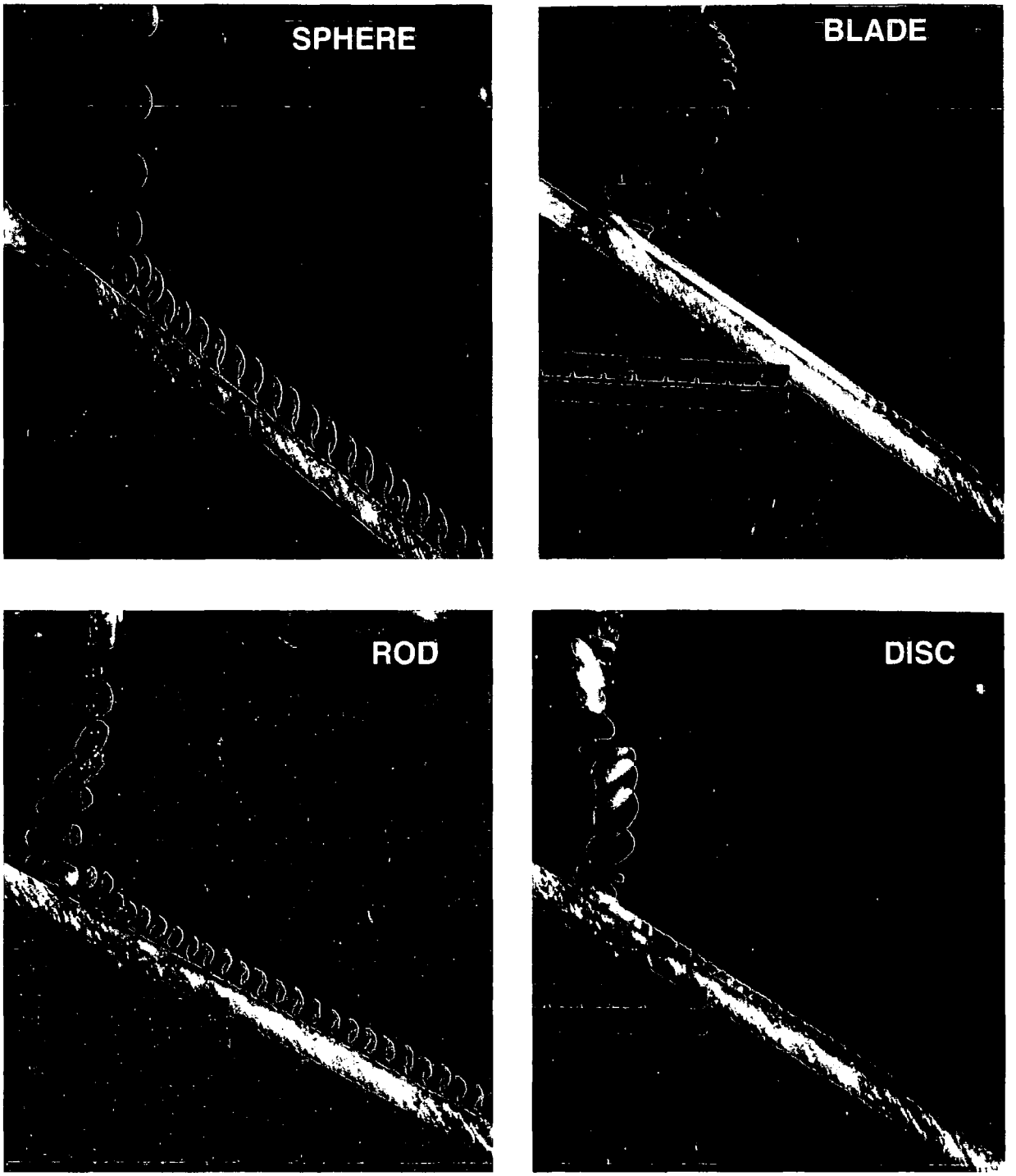

Figure 7.14 Strobe-light photographs of smallest weight of sphere, blade, rod and disc particles striking a glass surface inclined at 30^0 degrees in water. The same experiment was replicated two times for each particle. These photographs show four examples. The strobe rate was set at 25 flashes per second.

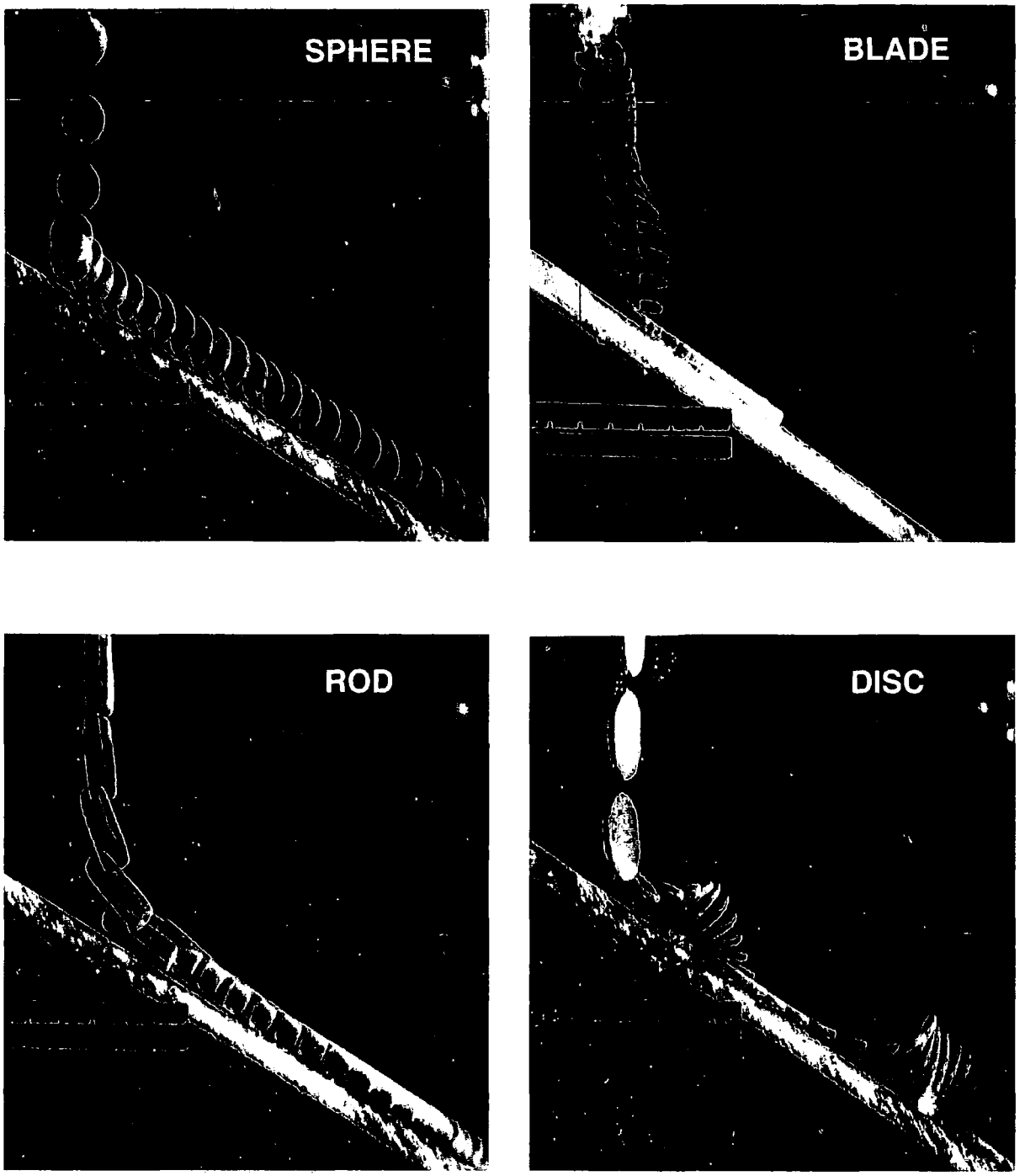

Figure 7.15 Strobe-light photographs of the medium weight class of sphere, blade, rod and disc particles striking a glass surface inclined at 30^0 degrees in water. The same experiment was replicated two times for each particle. These photographs show four examples. The strobe rate was set at 25 flashes per second.

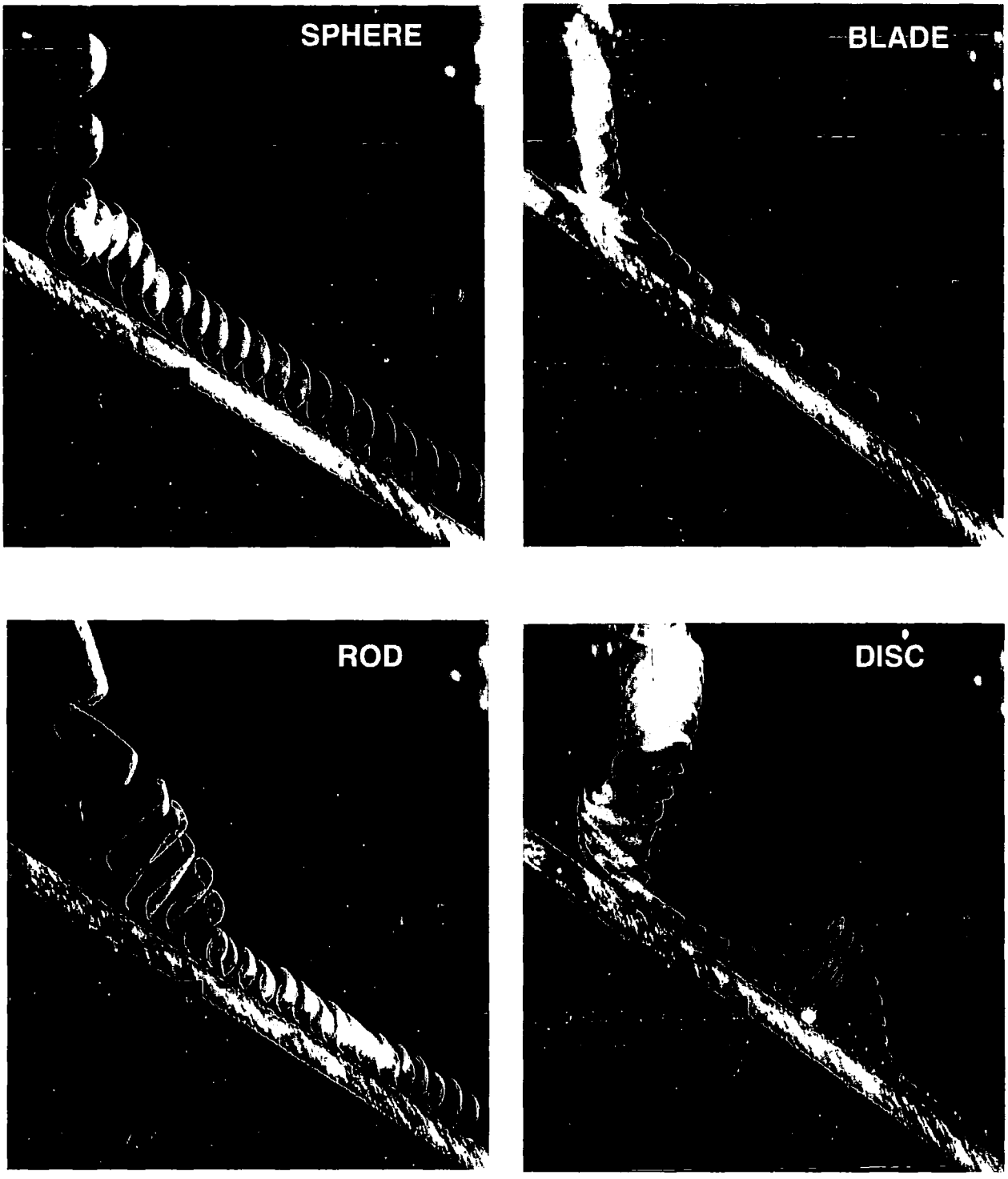

Figure 7.16 Strobe-light photographs of the heaviest weight of sphere, blade, rod and disc particles striking a glass surface inclined at 30^0 degrees in water. The same experiment was replicated two times for each particle. These photographs show four examples. The strobe rate was set at 25 flashes per second.

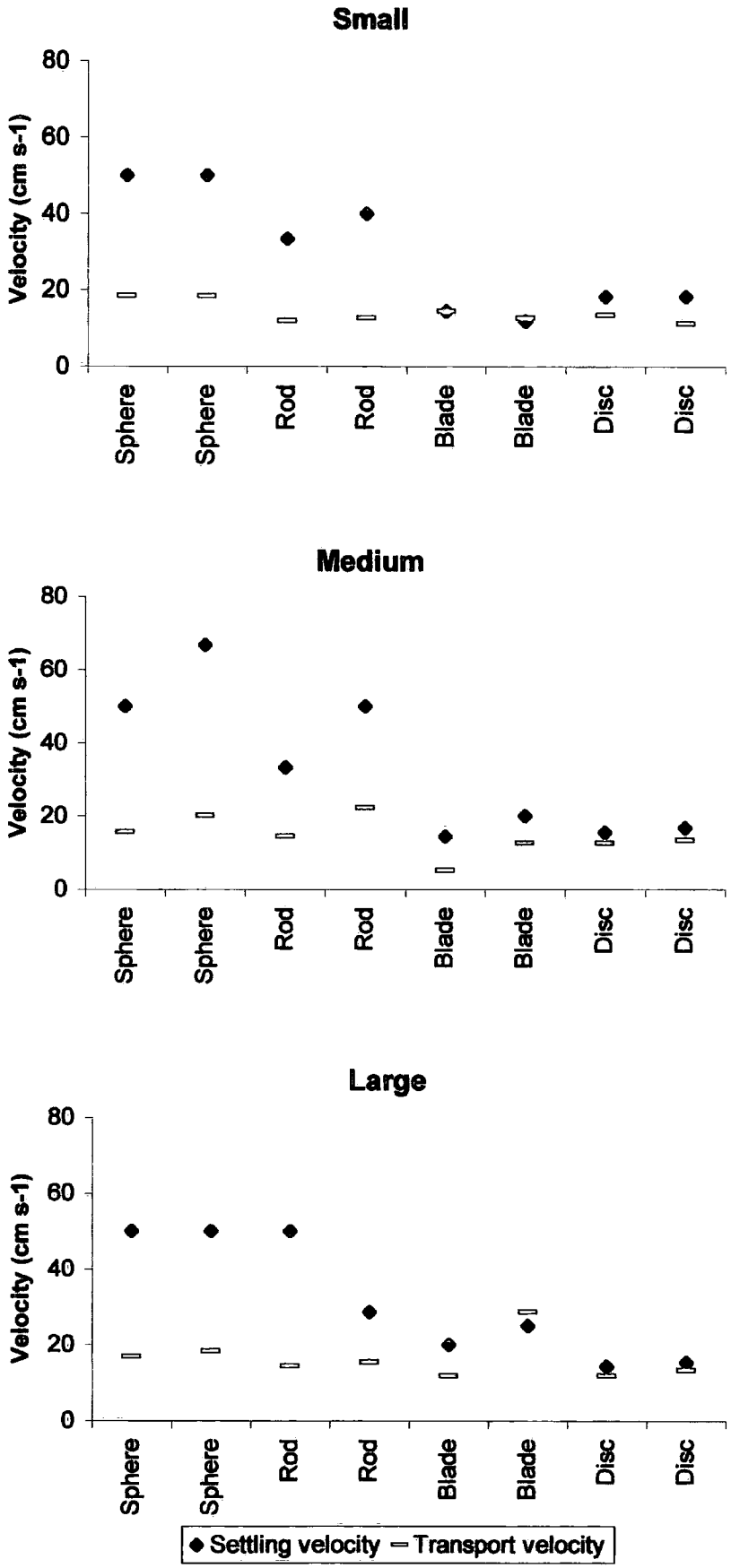

Figure 7.17 Settling and transport velocities of particles of the four shape classes in three weight groups.

Table 7.5 Summary of the mean settling and transport velocities of test particles in three weight groups (R: rolling, S: sliding mode).

Shape	Settling velocity cm s^{-1}	Transport Velocity cm s^{-1}	(Settling vel./ transport vel.)	Mode of transport
		Small		
Sphere	50.0	18.2	2.74	R
Sphere	50.0	18.2	2.74	R
Blade	14.3	14.3	1.00	S
Blade	11.8	12.5	0.94	S
Rod	33.3	11.8	2.82	R
Rod	40.0	12.5	3.20	R
Disc	18.2	13.3	1.36	S
Disc	18.2	11.1	1.63	S
Mean	**29.5**	**14.0**	**2.10**	
		Medium		
Sphere	50.0	15.4	3.25	R
Sphere	66.7	20.0	3.34	R
Blade	14.3	5.0	2.86	S
Blade	20.0	12.5	1.60	S
Rod	33.3	14.3	2.33	R
Rod	50.0	22.2	2.25	R
Disc	15.4	12.5	1.23	S
Disc	16.7	13.3	1.26	S
Mean	**33.3**	**14.4**	**2.31**	
		Large		
Sphere	50.0	16.7	2.99	R
Sphere	50.0	18.2	2.75	R
Blade	20.0	11.8	1.69	S
Blade	25.0	28.6	0.87	S
Rod	50.0	14.3	3.50	R
Rod	28.6	15.4	1.86	R
Disc	14.3	11.8	1.21	S
Disc	15.4	13.3	1.16	S
Mean	**31.7**	**16.2**	**1.96**	

7.8 SETTLING VELOCITIES OF THE NATURAL PARTICLES

Settling velocities of four particle shapes (sphere, blade, rod, disc) were measured for natural particles. The three axes and weights of each of these particles are given in Table 7.6. Density for the natural (sandstone) particles is 2.41. The same set of experiments as those described in Section 8.4 were repeated for the natural particles. Behaviour between the two sets of experiments cannot be compared directly due to difference in particle density.

Table 7.6 The tri-axial dimensions (mm) and weights (g) of natural particles used for the settling velocity experiments.

Size (mm)	A axis	B axis	C axis	Roundness	Sphericity	Corey Shape Factor (CSF)	Weight (g)
Sphere	10.5	10.3	10.3	952	0.99	1.0	3.34
Blade	20.9	9.0	3.5	96	0.42	0.3	1.64
Rod	20.4	10.0	10.0	196	0.62	0.7	3.83
Disc	10.2	10.2	3.0	392	0.67	0.3	0.67

In general, sphere-and rod-shaped particles produced a similar pattern of settling and transport velocities (rolling) to the artificial particles. Blade-and disc-shaped particles, on the other hand, exhibited more uniform and relatively shorter settling paths as compared to those measured with artificially formed particle shapes. Figures 7.18, 7.19, 7.20, and 7.21 are typical strobe-light photographs of natural gravel sphere, blade, rod, and disc-shaped particles. Figure 7.18 shows that sphere-shaped particles have a relatively consistent pattern of settling. After the initial impact with the glass plate both the rebound height and also damping distances of the natural sphere tended to be greater than for artificial ones probably due to the greater density of natural the particles. Photograph 1 in Figure 7.18 shows the settling velocity of a natural sphere that is slightly greater than photographs 2, 3 and 4, which show higher rebound and longer damping distance. The Rod showed a similar pattern of settling to the sphere but for the rod there was little rebound and a shorter damping distance (Figure 7.20). In Figure 7.20, (photographs 1 and 2) the rod hit the base plate with its long axis in a vertical plane which caused a small rebound, and then it reoriented itself with the long axis transverse to the slope. In Photograph 3, however, damping distance seems to be much longer than the others, while there is no rebound for photograph 4. In each experiment, the rolling velocity of the rod tended to increase slightly downslope.

With few exceptions (photograph 2 in Figure 7.19 and photograph 4 in Figure 7.21), natural blade and disc-shaped particles settle in relatively straight, vertical paths that are more constant than with the artificial particles. However, in relation to transport velocity, similar patterns of motion between artificial and natural particles were observed. The blade in Figure 7.19 (photographs 1and 4), shows a straight vertical line of fall with its long axis in a vertical plane. Photograph 3 also exhibits a straight line of

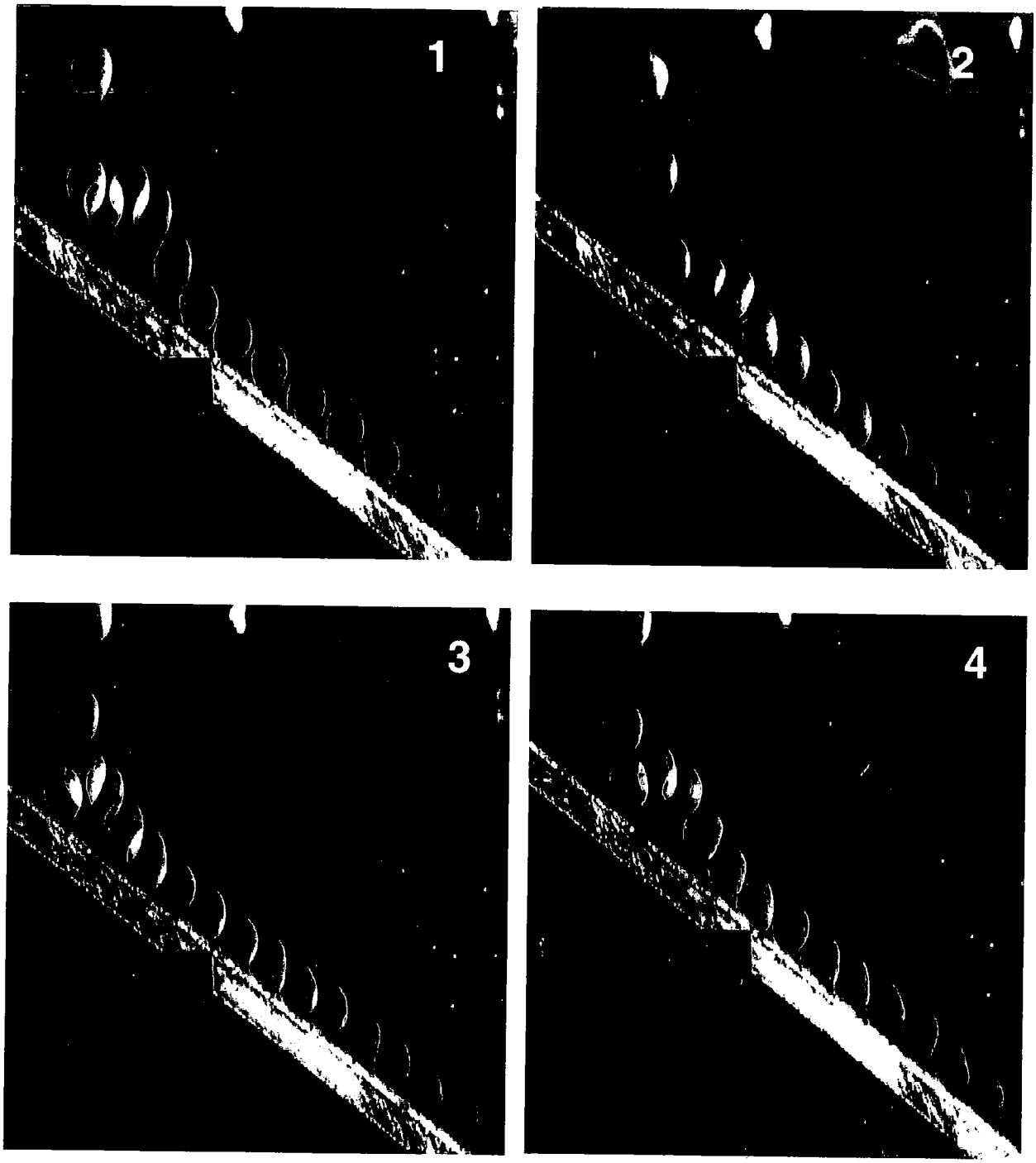

Figure 7.18 Strobe-light photographs of a natural sphere striking a glass surface inclined at 30^0 degrees. The same experiment was replicated 10 times in water. These photographs show four examples. The strobe rate was set at 25 flashes per second.

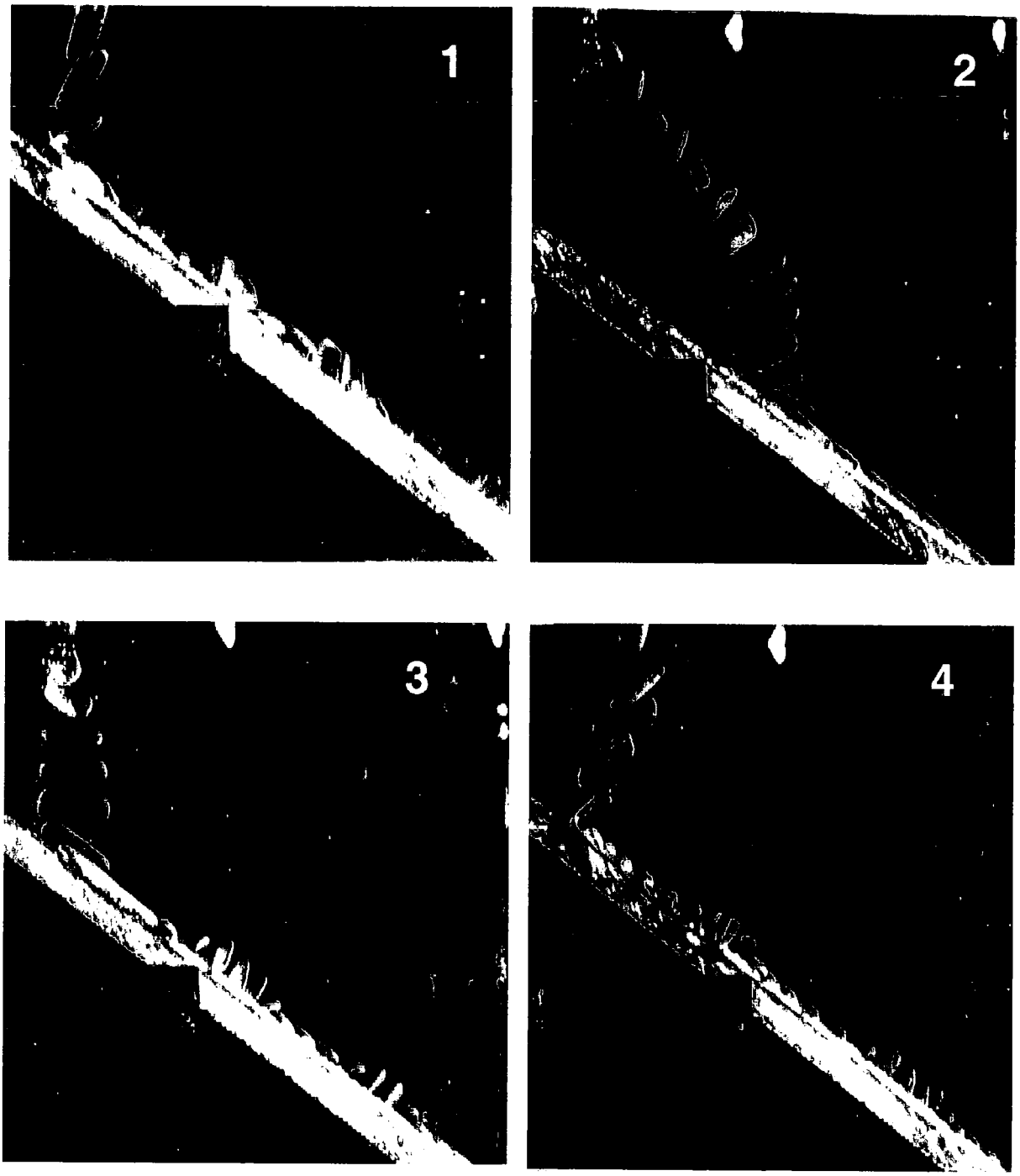

Figure 7.19 Strobe-light photographs of a natural blade striking a glass surface inclined at 30^0 degrees. The same experiment was replicated 10 times in water. These photographs show four examples. The strobe rate was set at 25 flashes per second.

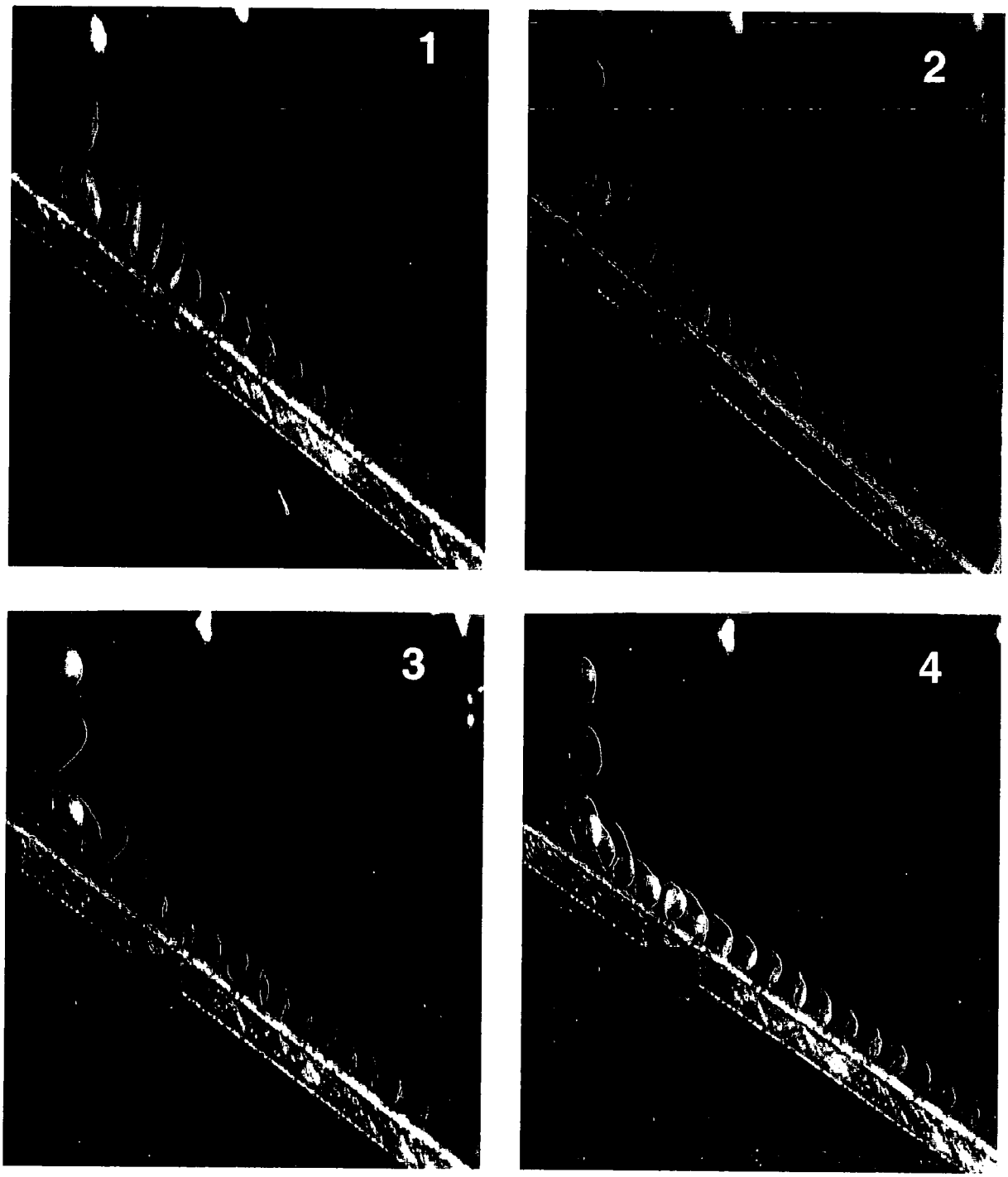

Figure 7.20 Strobe-light photographs of a natural rod striking a glass surface inclined at 30^0 degrees. The same experiment was replicated 10 times in water. These photographs show four examples. The strobe rate was set at 25 flashes per second.

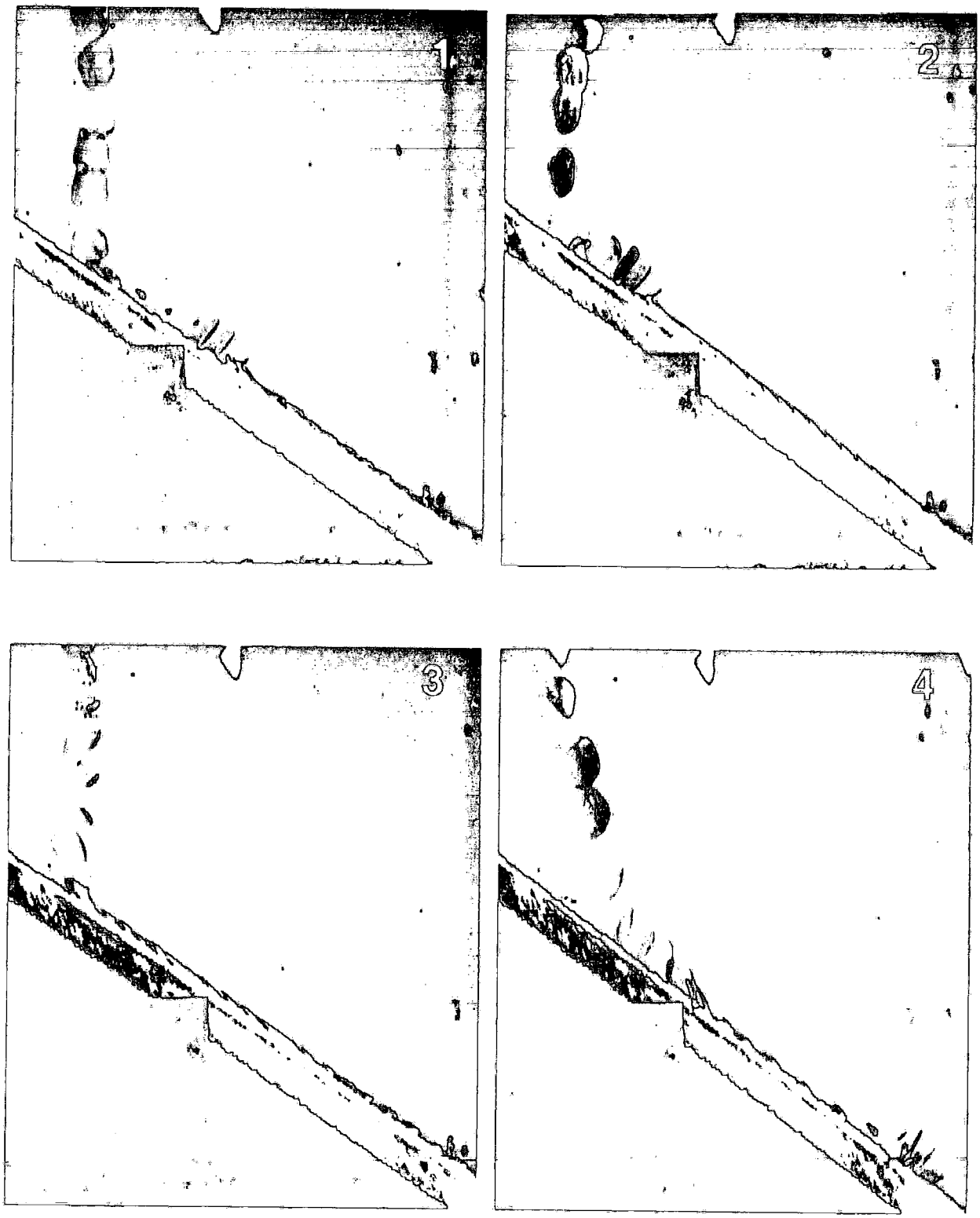

Figure 7.21 Strobe-light photographs of a natural disc striking a glass surface inclined at 30° degrees. The same experiment was replicated 10 times in water. These photographs show four examples. The strobe rate was set at 25 flashes per second.

fall but its maximum projection area parallel to the slope, which caused a relatively slow settling rate. Photograph 2, on the other hand, exhibits a different pattern of settling in which the bladed continuously tumbled end-over-end and moves along a path that was almost straight but oblique to the vertical. In terms of transport, except for photograph 2, each image shows similar pattern of movement. Following the initial impact the blade with its long axis transverse to the slope, accelerates with a sliding mode, which then leads to an elevation of the particle in a vertical plane (which result in a decrease in transport velocity). It then collapses onto a horizontal plane and slides again. This irregular pattern of movement with varying sequence of orientation is repeated downslope. The blade in Photograph 2, on the other hand, slid at an almost constant velocity with its long axis parallel to the slope. This indicates that blades sliding downslope with long axes transverse to slope tend to accelerate. This acceleration forces the blade to elevate and changes its orientation from the horizontal to the vertical plane or from vertical to a horizontal plane which leads to irregularity in transport. On the other hand, a blade moving downslope with its long axis parallel to slope shows a relatively consistent sliding mode of movement along the slope. (Photograph 2 in Figure 7.19).

The natural disc (except in Photograph 1 in Figure 7.21) shows a relatively straight and vertical pattern of fall that is noticeably different from the artificial particles. However, comparison of the four images in Figure 7.21 indicates that, despite their straight settling path, the difference between the four settling velocities is mainly due to variation in particle orientation. For example, in Photograph 1 reveals that there was an initial increase in settling velocity of the disc falling in a vertical plane. It then turned in a horizontal plane, which caused a decrease in settling velocity. Finally it began its vertical fall again with an increase in settling velocity. After the first impact on the glass plate, it accelerated with a sliding motion until it lifted and then collapsed again in a horizontal plane. It then accelerated again in a sliding mode and a second elevation took place. Photograph 2 reveals the disc falling in a vertical plane along the whole settling path, resulting in a rather greater settling velocity than the other images, while in Photograph 3 its falling in its maximum projection plane horizontal to flow along the whole settling path that led to a rather slow settling velocity. Photograph 4 represent a pattern of fall in which the disc settled in a vertical plane and moved along a straight path that was oblique to the vertical. Both photographs 3 and 4 show a consistent sliding mode of movement in which the disc tended to accelerate with

downslope distance. A close examination of the four images indicates that if the particle impacted on the base plate with a vertical plane it tended to jump (photograph 2) or accelerate immediately after the landing, which then led to an elevation in the upper slope (photograph 1). On the other hand, if the landing took place in a horizontal plane, the particle tended to slide along most of the slope and accelerate towards the bottom of the slope.

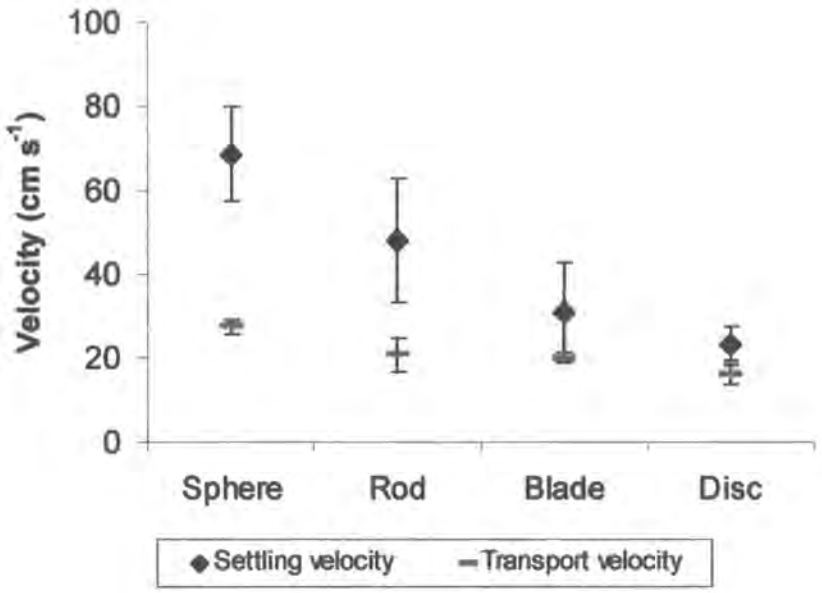

Figure 7.22 Settling and transport velocities of natural particles of sphere, blade, rod and disc with b-axes varying between 9.0 and 10.2mm.

Settling and transport velocities for the natural sphere-blade-rod-and disc-shaped particles are shown in Table A4.2. In general, the settling velocity of natural particles is similar to those measured for artificial ones, e.g. higher settling velocities for sphere- and rod-shaped particles, lower values for disc-and blade-shaped particles. However, natural particles tend to settle much faster due to their greater density (2.41) than the artificial particles used (1.48). Mean settling velocities vary between 68.8 cm s^{-1} (sphere) and 23.4 cm s^{-1} (disc). Again, sphere-and rod-shaped particles show greater settling velocities. The increasing order of the mean velocities are 23.4, 31.4, 48.1 and 68.8 cm s^{-1} for disc-blade-rod-and sphere-shaped particles respectively (Figure 7.22 and Table A4.2).

The settling and transport velocities of individual particles within each shape class and their mean and standard deviation values (Table A4.2) indicate that settling velocities, for individual sphere-and rod-shaped particles tend to be greater, and more

consistent than for blade-and disc-shaped particles. For sphere-shaped particles, settling velocity is very uniform (68.8 cm s^{-1}) with a standard deviation of 11. It changes between 34.4 cm s^{-1} and 68.8 cm s^{-1} for rod-shaped particles with a standard deviation of 48.1. For blades, however, settling velocities are much greater and vary between 15.3 cm s^{-1} and 68.6 cm s^{-1} with a standard deviations of 14.6. Discs, on the other hand, shows less variation between the individual measurement (19.6-22.9 cm s^{-1}) with a small standard deviation of 4.1 (Table A4.2).

In terms of particle transport velocity, the pattern is similar to the artificial particles, with is no great variation between different shapes. Table A4.2 and Figure 7.22 show that, on a 30° inclined smooth base plate, mean transport velocities tend to decrease from sphere (27.5 cm s^{-1}) to rod (20.9 cm s^{-1}), blade (20.2 cm s^{-1}) and disc (16.1 cm s^{-1}) respectively. However, for a given distance, mean transporting velocities are much lower than that of settling velocities for all shape classes and the difference becomes greatest for sphere-shaped particles, while it is smallest for discs (Table A4.2 and Figure 7.22). For spheres, rolling velocities vary between 25.0 cm s^{-1} and 28.6 cm s^{-1} (standard deviation 1.7), while for rods it varies between 20.0 cm s^{-1} and 22.2 cm s^{-1} with a standard deviation value of 1.1. On the other hand, as with artificial particles, the differences between the individual measurements tend to increase for the blade (16.7-28.6 cm s^{-1}) and disc, (12.5-20.0 cm s^{-1}). Greater standard deviation in transport velocities of blade and disc-shaped particles (both from the tilting table experiments and the photograph visualisation evidence) result because variations in particle orientation have a significant effect on settling rate and the nature of the particle transport velocity. Comparison of artificial and natural particles within the same size range and same shape class showed that density has an important influence on particle settling velocity and hence Reynolds number. Natural particles are greater in density than artificial particles. This leads to higher settling rates and hence greater Reynolds number values for natural particles, while artificial particles settle have small Reynolds number (Table A4.1 and Table A4.2). Mean Reynolds number for the settling velocity of natural particles is almost twice (6188) that of the artificial particles (3700).

7.9 SETTLING AND TRANSPORT VELOCITIES OF IRREGULAR SHAPED NATURAL PARTICLES

Although it is well known that the settling velocity of a particle is strongly dependent on its shape (McNown and Malaika, 1950; Graf, 1971; Komar and Remiers, 1978; Baba and Komar, 1981; Dietrich, 1982) there have been few studies investigating the settling velocities of natural particles with irregular shapes. These are appreciably different from ideal shapes such as spheres, ellipsoids and cubes (Goossens, 1987). Indeed, most natural particles do not have regular geometrical shapes. The purpose of this section is to examine the settling and transport velocity of irregular shape natural particles in the 4-8 mm and 8-16 mm size groups.

Natural (irregularly shaped) particles were selected in two two size ranges 4-8 mm and 8-16 mm. The test particles were taken from Trout Beck (Chapter 3). In each size group 10 particles were randomly selected from a total sample of 100. The reasons for choosing these size ranges were ease of measurement (measuring the three axial diameters of a pebble is much easier and accurate than on a sand grain) and also these ranges were most commonly transported in floods at the experimental sites. It was also assumed that much smaller size ranges would reduce the effect of particle shape on settling and transport velocities. Sandstone particles with an average density of 2.41g cm^{-3} were used. The tri-axial dimensions (mm), weights (g) and shape properties of each particle are summarised in Table 7.7 and Figure 7.23. Each particle within the two size groups was dropped twice through water, onto a 30° inclined, smooth glass plate. Settling velocity, form of movement (rolling or sliding) and trajectory paths were measured from the photographs.

Figures 7.24 and 7.25 are typical strobe-light photographs of the two size groups settling in water. In terms of settling velocities, the experiments show that there is no simple pattern of settling and transport velocities between the particles of various shapes and size. However, in common with the earlier experiments Table 7.8 and Figure 7.26 show that sphere and rod-like particles tend to settle slightly faster than blade-like and disc-like particles. Mean settling velocity of the large particles (42.2 cm s^{-1}) is noticeable greater than the small size group (30.7 cm s^{-1}). High standard deviation values for the large size particles indicate that differences between the settling velocities of various shapes is greater than in the small size group. This may also imply a positive relation between the particle size and the influence of shape on settling velocity. In other words, as particle size increases, differences between the settling velocity of

Table 7.7 Summary of the tri-axial dimensions (mm), weights (g) and shape characteristics of irregular-shaped natural test particles in two size groups.

Stone No	A axis	B axis	C axis	Radius of curvature	Roundness	b/a ratio	c/b ratio	Sphericity	CSF	Shape	Flatness	Weight (g)
					(4-8 mm)							
1	12.0	8.0	6.0	2	333	0.67	0.75	0.72	0.6	Sphere	167	0.86
2	13.0	7.0	4.0	1	154	0.58	0.57	0.56	0.4	Blade	250	0.49
3	13.0	7.0	4.0	2	308	0.54	0.57	0.56	0.4	Blade	250	0.64
4	10.0	8.0	4.0	2	400	0.80	0.50	0.58	0.4	Disc	225	0.39
5	13.5	8.5	4.0	1	148	0.63	0.47	0.52	0.4	Blade	275	0.57
6	7.0	7.0	6.0	1	286	0.98	0.86	0.90	0.9	Sphere	117	0.43
7	5.5	3.8	2.1	2	342	0.69	0.55	0.59	0.5	Disc	105	0.21
8	9.5	5.5	5.0	2	421	0.58	0.91	0.78	0.7	Rod	150	0.45
9	12.0	6.5	4.0	1	167	0.54	0.62	0.59	0.5	Blade	231	0.68
10	7.0	5.0	4.5	1	286	0.71	0.90	0.83	0.8	Sphere	133	0.23
					(8-16 mm)							
1	27.0	14.0	5.0	4	296	0.52	0.36	0.40	0.3	Blade	410	2.60
2	20.0	13.0	13.0	2	200	0.65	1.00	0.87	0.8	Rod	127	4.04
3	13.0	12.0	6.0	4	615	0.92	0.50	0.61	0.5	Disc	208	2.04
4	17.0	13.0	3.0	3	353	0.76	0.23	0.34	0.2	Disc	500	1.20
5	13.0	12.0	5.5	2	308	0.92	0.46	0.58	0.4	Disc	227	1.34
6	20.0	12.0	10.5	2	200	0.60	0.88	0.77	0.7	Rod	152	2.74
7	18.0	13.0	11.0	5	556	0.72	0.85	0.80	0.7	Sphere	141	3.06
8	27.0	15.5	5.0	2	148	0.57	0.32	0.39	0.2	Blade	425	3.33
9	16.0	13.0	6.0	2	250	0.81	0.46	0.56	0.4	Disc	242	1.45
10	25.5	11.0	7.0	2	157	0.43	0.64	0.56	0.4	Blade	261	2.14

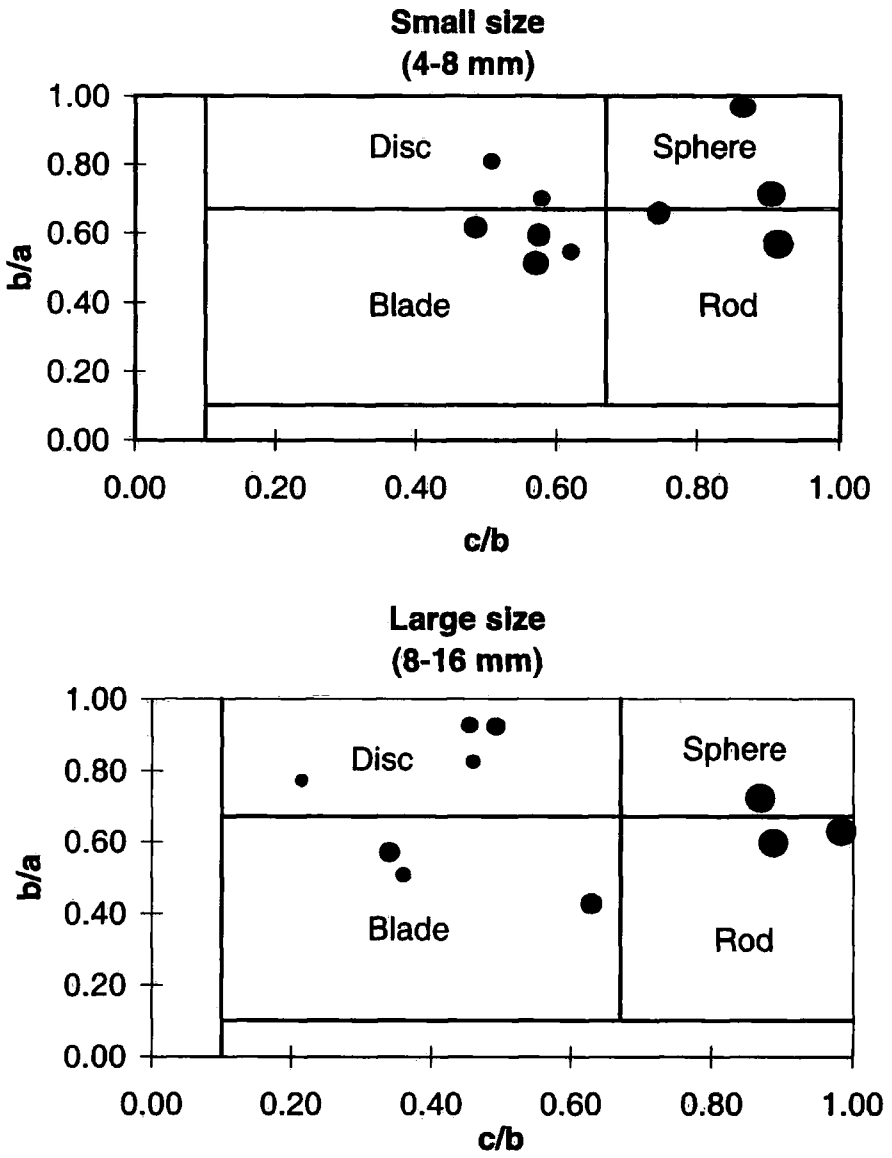

Figure 7.23 Shape distribution of naturally formed irregular particles, based on Zingg (1932) classification of particle form. Note: Size of symbols indicates relative settling velocities.

Table 7.8 Summary of settling and transport velocity experiments carried out with natural test particles in two size groups. (Values in italics indicate the particles settling in vertical plane. S: sliding mode, R: rolling mode).

Stone No:	Settling velocity (cm s^{-1})	Transport velocity (cm s^{-1})	Mode of transport	Shape
		Small size group (4-8 mm)		
1	27.5	18.2	S	Sphere
1	34.4	8.0	S	Sphere
2	22.9	11.1	S	Blade
2	22.9	9.1	S	Blade
3	22.9	22.2	S	Blade
3	45.8	15.4	S	Blade
4	22.9	15.4	S	Disc
4	22.9	11.8	S	Disc
5	22.9	15.4	S	Blade
5	22.9	11.1	S	Blade
6	34.4	16.7	R/S	Sphere
6	34.4	15.4	R/S	Sphere
7	27.5	9.5	S	Disc
7	34.4	14.3	S	Disc
8	34.4	12.5	R/S	Rod
8	*45.8*	*14.3*	*R/S*	*Rod*
9	34.4	18.2	S	Blade
9	27.5	15.4	S	Blade
10	27.5	13.3	R	Sphere
10	45.8	11.8	R	Sphere
Mean	30.7	13.9		
Standard D.	8.1	3.5		
		Medium size group (8-16 mm)		
1	27.5	22.2	S	Blade
1	27.5	20.0	S	Blade
2	68.8	22.2	R/S	Rod
2	45.8	22.2	R/S	Rod
3	34.4	25.0	S	Disc
3	34.4	20.0	S	Disc
4	19.6	16.7	S	Disc
4	22.9	16.7	S	Disc
5	27.5	20.0	S	Disc
5	34.4	16.7	S	Disc
6	45.8	18.2	R/S	Rod
6	*68.8*	*20.0*	*R/S*	*Rod*
7	45.8	20.0	R	Sphere
7	68.8	20.0	R	Sphere
8	*68.8*	*18.2*	*S*	*Blade*
8	*68.8*	*22.2*	*S*	*Blade*
9	27.5	22.2	S	Disc
9	27.5	4.8	S	Disc
10	34.4	16.7	S	Blade
10	45.8	18.2	S	Blade
Mean	**42.2**	**19.1**		
Standard D.	**17.4**	**4.1**		

various shapes tends to be greater. In the small size group, mean settling velocities vary between 40.1 and 34.0 cm s^{-1} for rods and spheres respectively, while for disc-like and blade-like particles it is 26.9 and 27.8 cm s^{-1}. In the large size group, there tends to be an increase in mean settling velocities for almost all shapes. Mean settling velocities are 57.3 for sphere and rod-like, 43.3 for blade-like and 28.8 cm s^{-1} for disc-like particles. Table 7.8 also indicates that particles falling in a vertical plane have relatively greater settling velocities than those falling in a horizontal plane. Differences in the mean settling velocities between spheres, blades and discs, tend to be smaller in the 4-8 mm size than the 8-16 mm size.

In common with earlier findings, sphere-and rod-like particles followed more vertical settling paths and had greater settling velocities than blade-and disc-like particles, which tended to settle in the horizontal plane (Figure 7.26). In the small size group, disc (photograph 1) and blade particles (photograph 2) have lower settling velocities than spheres (photographs 3, 5 and 6) and rods (photograph 4). Despite the difference between their weights, discs (0.39g) and blades (0.64g) had similar settling velocities. However, the greater projection area of the blade and horizontal settling plane increase the drag force and thus prevent it from settling rapidly. A similar relation may also be found between spheres of different weights. The weights of the spheres in photographs 5 and 6 are 0.23g and 0.86g respectively, although they have the same settling velocity. The reason is probably that the sphere weighing 0.23g had a greater sphericity value (0.77) than the sphere weighing 0.86g (0.69). The particle with greater sphericity is expected to settle faster due to less drag. Although sphere-like particles in Photograph 5 and 6 (in Figure 7.24) have the same settling velocity values (27.5 cm s^{-1}), the rod-like particle in photograph 4 has a noticeable greater settling velocity. The reason might be attributed to the fact that this rod-like particle, for much of its settling path, fell in a vertical plane, thus reducing drag.

In the large size group (Figure 7.25), rod-like particles show greater settling velocity and more vertical settling paths. However, comparison of blade and disc-like particles indicates that these particles (photographs 1 and 4) settled much faster and have straighter paths than well-formed blades (in photograph 2) and discs (in photograph 5). The reason is that maximum projection areas of the blade in photograph 2 and the disc in photograph 5 are greater than the blade in photograph 1 and the disc in Photograph 4.

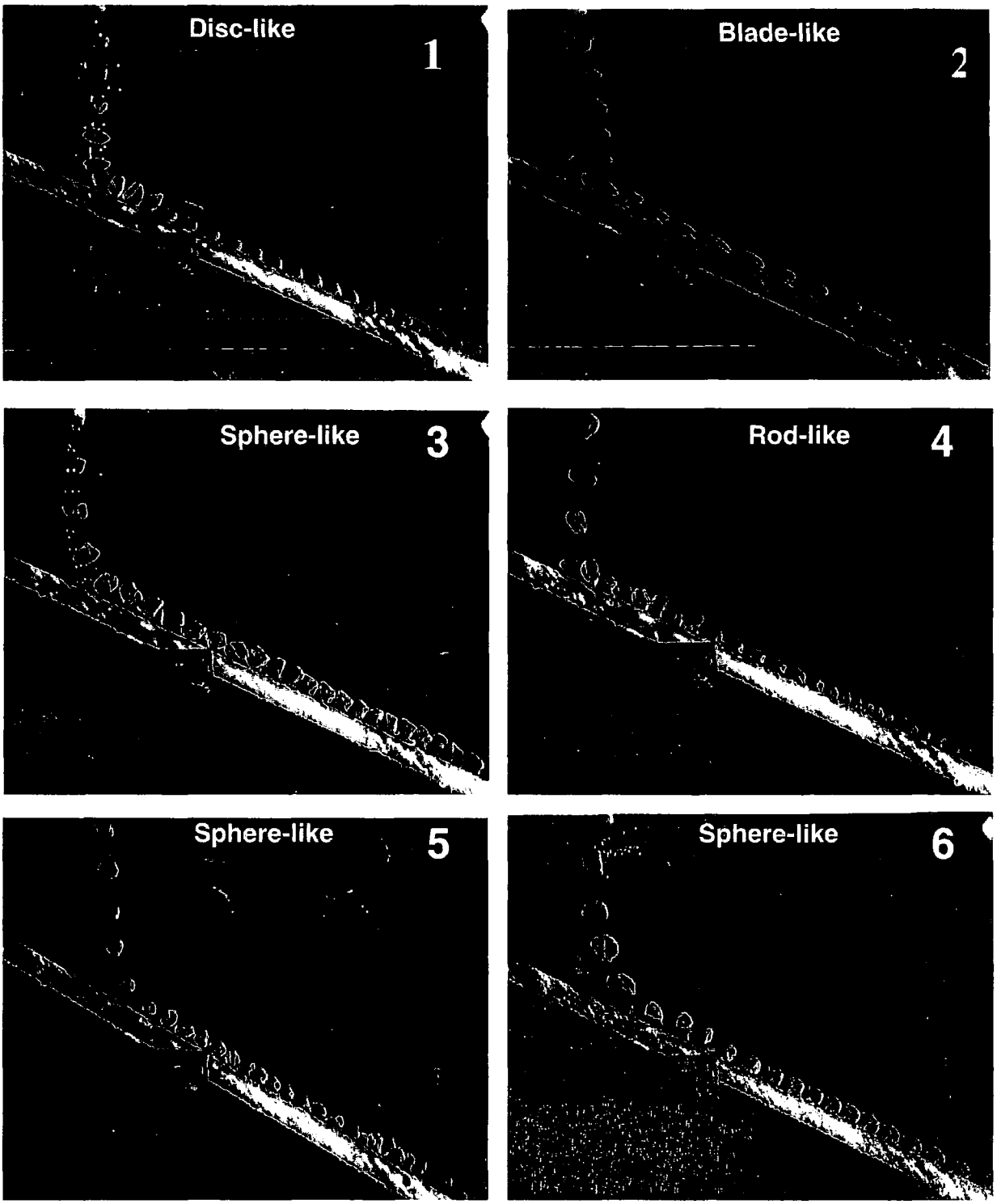

Figure 7 24 Strobe-light photographs of 4-8 mm size natural particles striking a glass surface inclined at 30° degrees. The same experiment was replicated twice for each particle. These photographs show six examples. The strobe rate was set at 25 flashes per second.

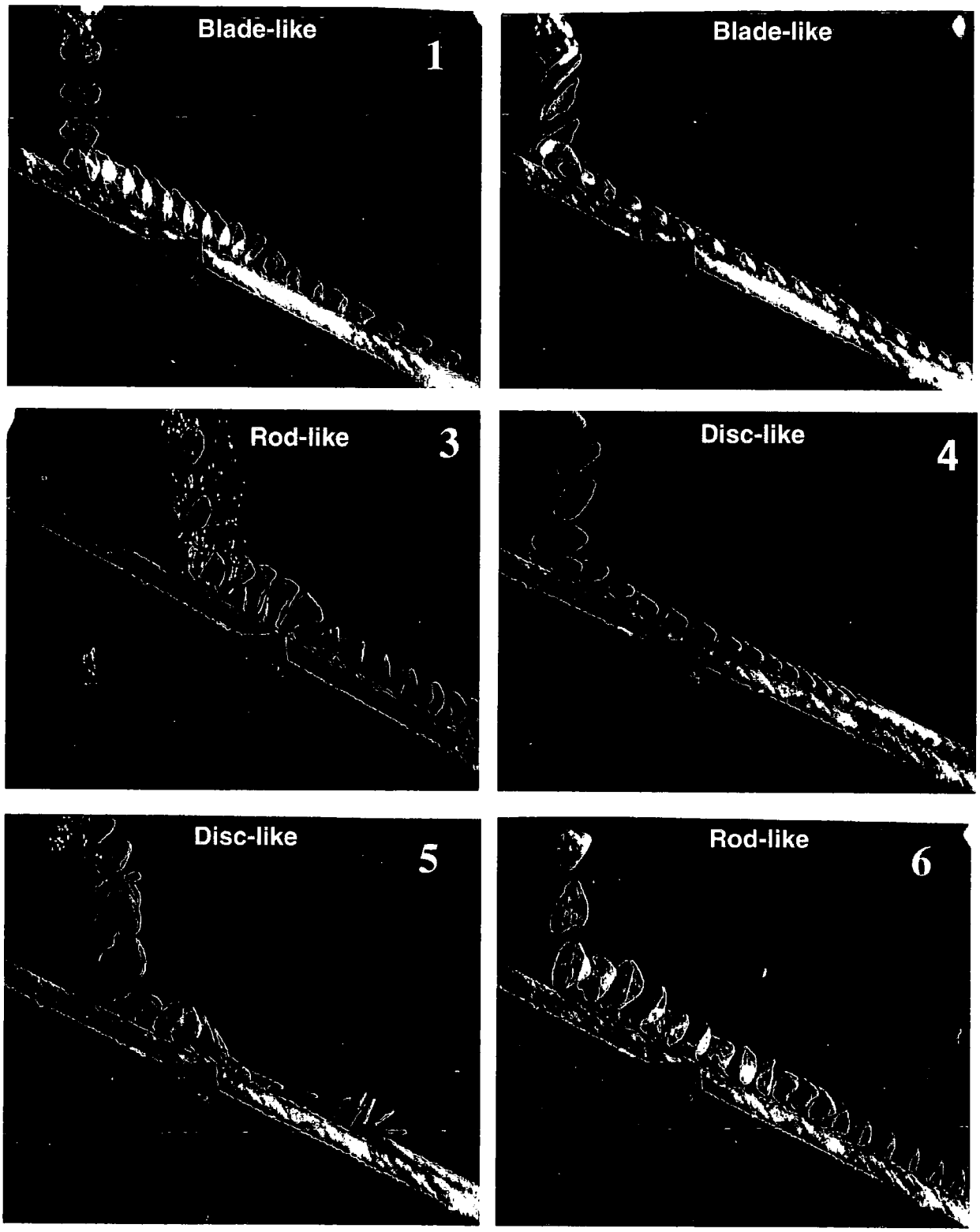

Figure 7.25 Strobe-light photographs of 8-16 mm size natural particles striking a glass surface inclined at 30° degrees. The same experiment was replicated two times in water. These photographs show six examples The strobe rate was set at 25 flashes per second.

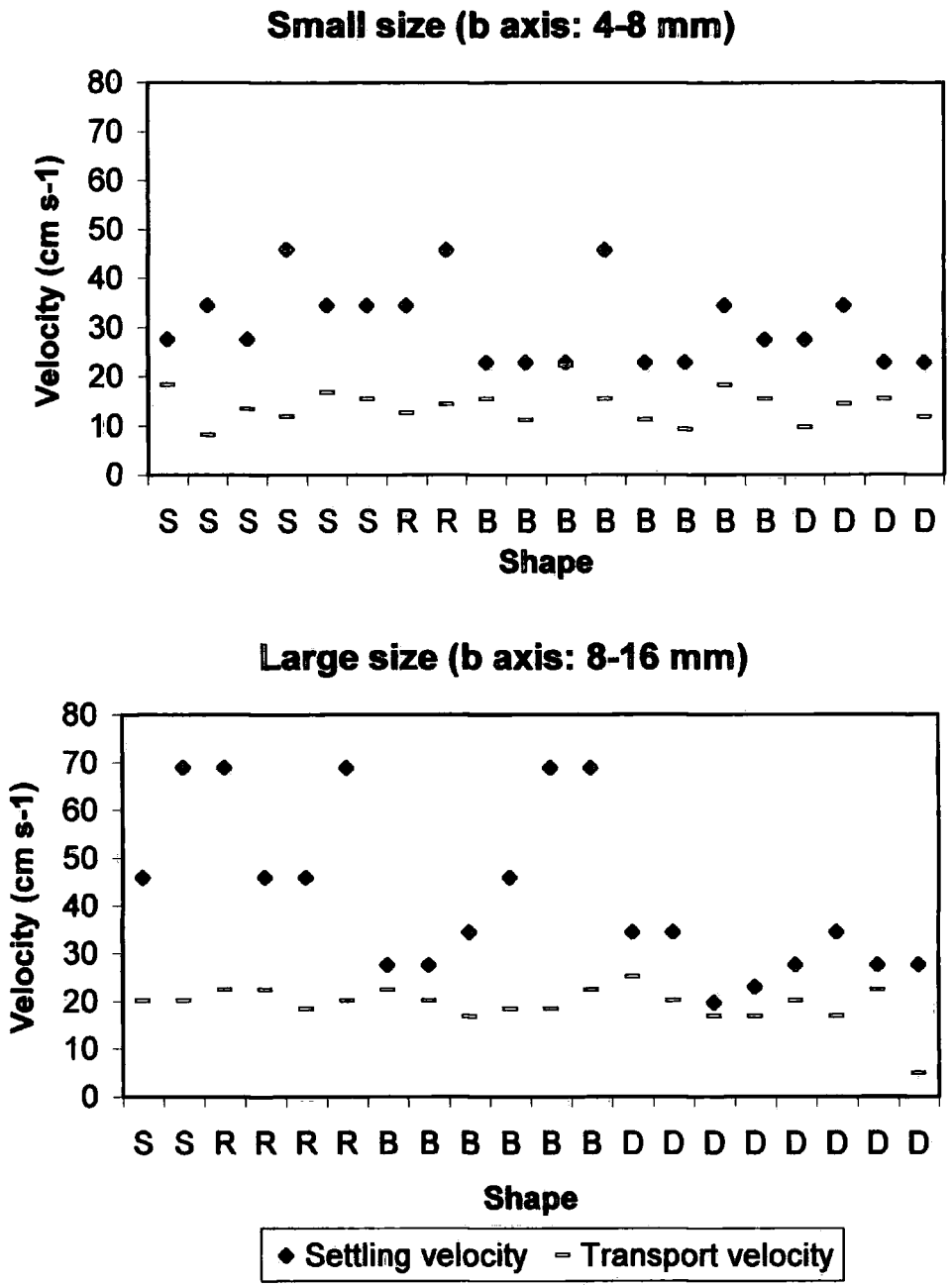

Figure 7.26 Settling and transport velocities of irregular shaped natural particles in two size groups. (S: sphere-like, B: blade-like, R: rod-like, D: disc-like)

In terms of the mode of movement and the transport velocities, Table 7.8 shows that mean transport velocity for large size particles (regardless of shape) is much greater than the mean small size group (13.9 cm s^{-1} small and 19.1 cm s^{-1} large size groups). However, lower standard deviations in each size group indicate that there is no greater variation between the transport velocities of different shapes. In contrast to the previous experiments carried out with uniform-shaped particles, in which rod-and sphere-shaped particles moved in rolling modes, most of the irregularly-shaped natural test particles exhibited a sliding mode of movement rather that rolling. For example, although they are expected to roll, in Figure 7.24 (photographs 4, and 6) and Figure 7.25 of (photographs 3 and 6), sphere-and rod-like particles moved in a sliding mode. The reason might be attributed to their rather lower sphericty and roundness values. For example the spheres in Figure 7.24 (Photographs 3 and 5) move in a rolling mode because of their greater roundness and sphericity degrees and hence lower flatness, while in Figure 7.25 the rod (Photograph 4) and sphere (Photograph 6) tend to move in a sliding mode, but occasionally change to rolling mode, probably due to their lower sphericity and roundness values (Table 7.7). This highlights the fact that apart from particle form (eg. sphere, rod, blade and disc), other shape properties (eg. degree of sphericity, roundness, flatness etc.) have also significant influence on the hydraulic behaviour of particles. Even small variations in these shape parameters result in significant differences in transport mechanisms.

7.10 INITIAL MOTION AND MOVEMENT OF PARTICLESS OF VARIOUS SHAPE ON BED OF VARYING ROUGHNESS.

A series of experiments were undertaken using four test grain shapes to investigate (a) how critical friction angle depends on grain shape and the relative size of the pivoting grain relative to the underlying roughness and (b) the mode of movement of artificial particles of various shape on two different bed roughnesses.

Four artificial particles with different shapes but the same size range (b-axis) were placed on beds with different forms of roughness elements. Size, shape and weight characteristics of each particle are given in Table 7.1. Two bed roughnesses were formed by attaching glass rods of different diameters (7 and 14 mm) across the sloping glass plate. With the test particle in place, the beds were tilted until the test particle

moved from its pocket of origin. For each of the test particles five measurements were taken. For blade-and rod-shaped test particles, five measurements with transverse orientation and five with parallel orientation were collected. Table 7.9 summarises the results of these experiments.

Table 7.9 Critical pivoting angles (in degrees) measured with artificial test particles in four shape classes on two bed roughnesses (T: transverse orientation, P: parallel orientation).

	Roughness 1 (7 mm)						**Roughness 2 (14 mm)**					
Measu-rement No:	Sphere	Blade T	Blade P	Rod T	Rod P	Disc	Sphere	Blade T	Blade P	Rod T	Rod P	Disc
1	29	35	39	28	29	34	37	60	46	44	42	51
2	28	43	36	30	27	36	34	60	38	45	41	58
3	29	39	38	29	32	36	38	57	47	45	43	57
4	27	32	38	34	33	35	39	53	46	44	36	61
5	27	42	41	32	32	41	38	64	40	43	52	60
Mean	28	38.2	38.4	30.6	30.6	36.4	37.2	58.8	43.4	44.2	42.8	57.4
St.Dev.	1.00	4.66	1.82	2.41	2.51	2.70	1.92	4.09	4.10	0.84	5.81	3.91

The results of the measurements are shown in Figures 7.27, 7.28, 7.29 and in Table 7.9. In general, on all bed roughnesses, sphere-and rod-shaped particles showed a lower pivoting angle and thus a low threshold value for entrainment. Table 7.9 shows that as bed roughness increases the critical friction angle also increases for particle of all shapes. The differences in the mean friction angles between the two roughnesses (Roughness 1 to Roughness 2) are 9.2 for spheres, 12.8 for blades, 12.9 for rods and 21.0 for disc-shaped particles (Table 7.9).

The mode of movement for the artificial particles of various shapes on two different bed roughnesses (7 and 14 mm) are shown in Figures 7.30 and 7.31. Settling and transport paths for the sphere and rod were very similar on both roughnesses. Rebound after initial impact was negligible and the particles moved by rolling. However, on the 14 mm roughness surface, movement was a little more irregular with fluctuations in velocity as the particles passed over the underlying pockets. The disc and blade, on the other hand, showed a very different pattern of movement (Figures 7.30 and 7.31). They settled along a regular oscillatory path. On the 7 mm roughness surface the disc and blade impacted at an angle of approximately 45°, then they collapsed and began to slide. The particles accelerated until there was sufficient lift to allow them to climb from the bed. The particles then 'stalled', collapsed and began sliding again (Figure 7.31). On the 14 mm roughness, these particles impacted on their edges rotated

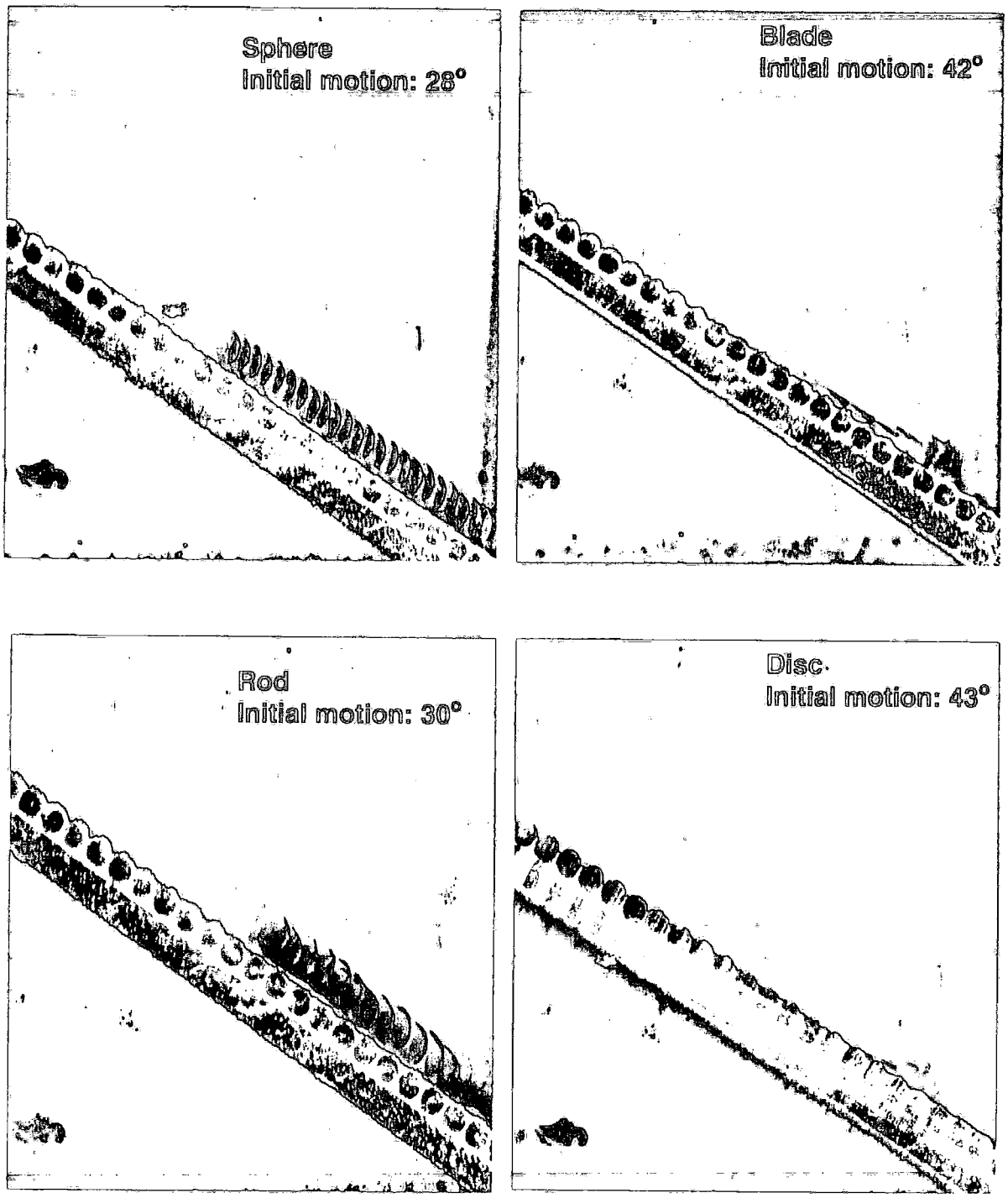

Figure 7.27 Initial motion of sphere, blade, rod and disc particles on 7 mm roughness elements inclined at different degrees. The same experiment was replicated five times in water. These photographs show four examples. The strobe rate was 25 flashes per second.

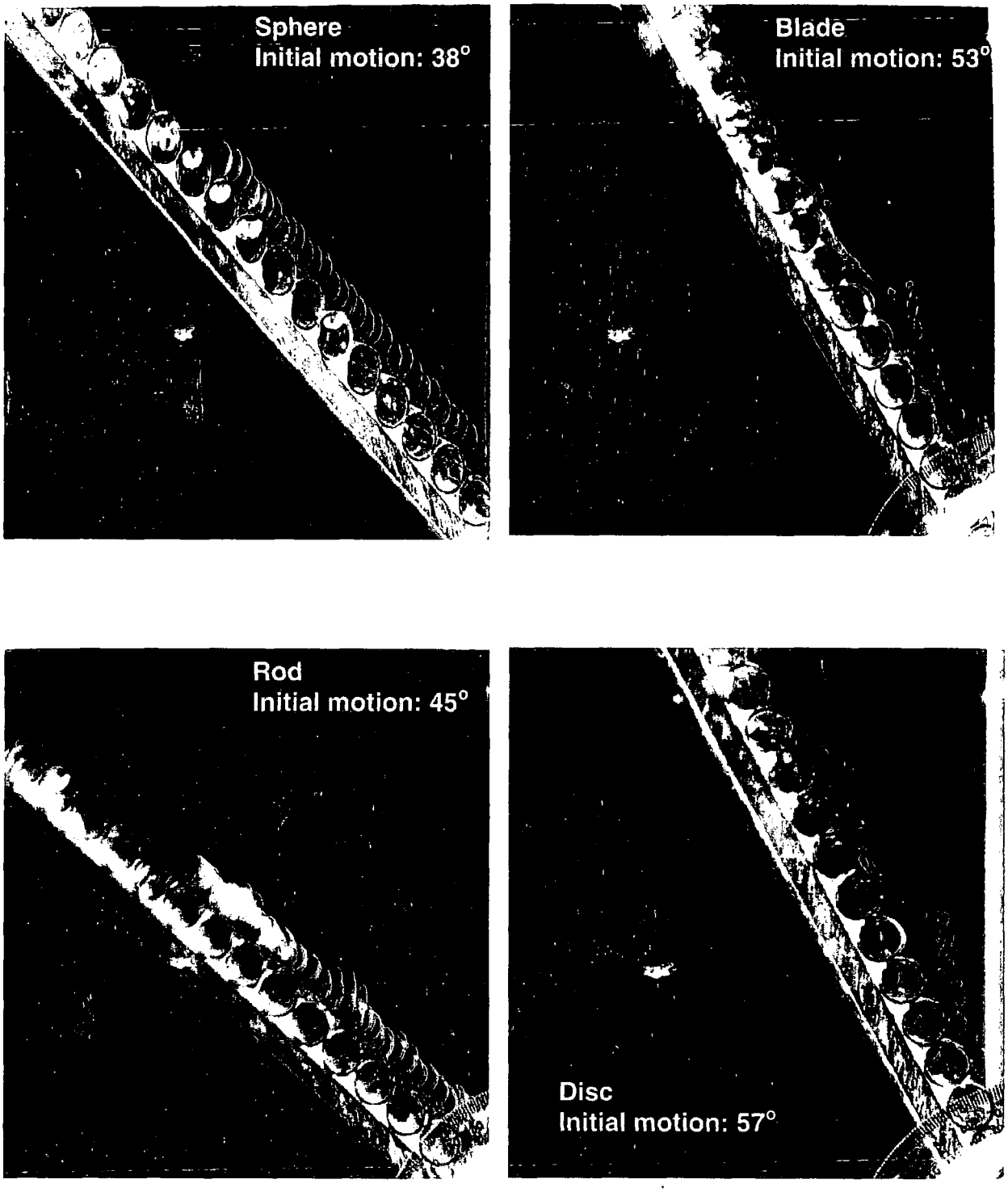

Figure 7.28 Initial motion of sphere, blade, rod and disc particles on 14 mm roughness elements inclined at different degrees. The same experiment was replicated five times in water. These photographs show four examples. The strobe rate was 25 flashes per second.

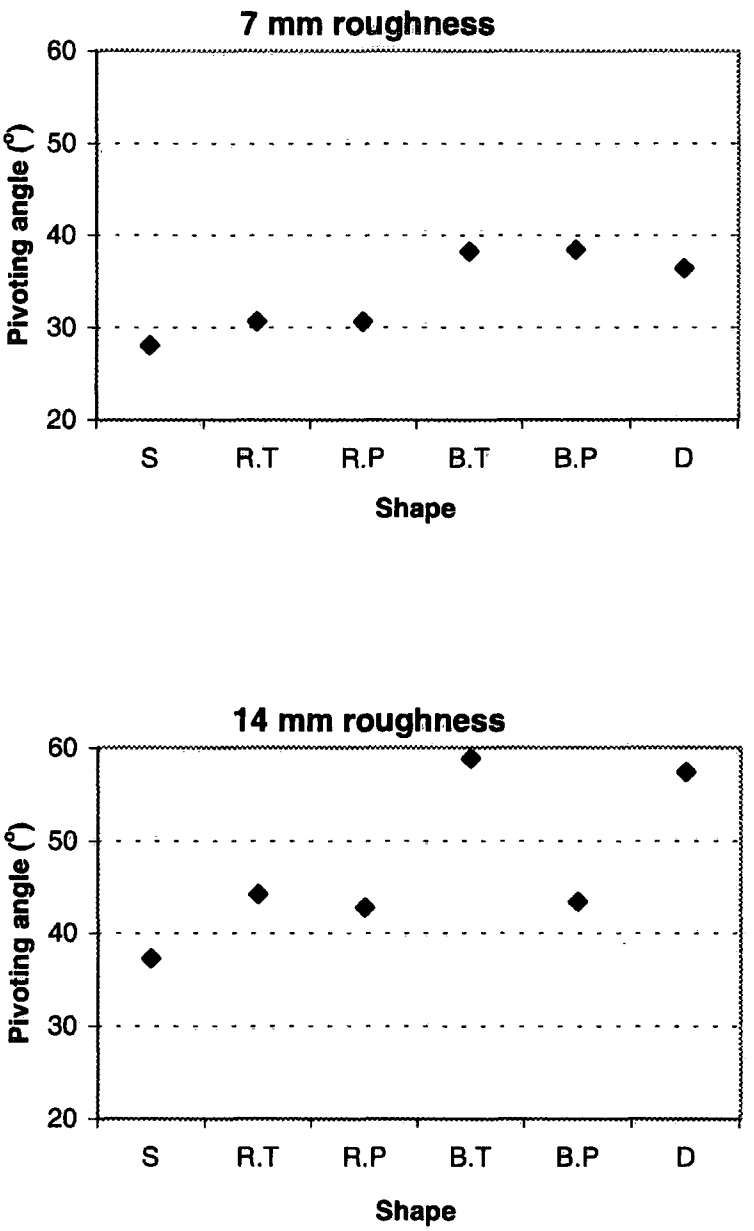

Figure 7.29 Angles of initial motion for particles of various shapes and orientation on two diffrent bed roughness. (T: transverse, P: parallel orientation)

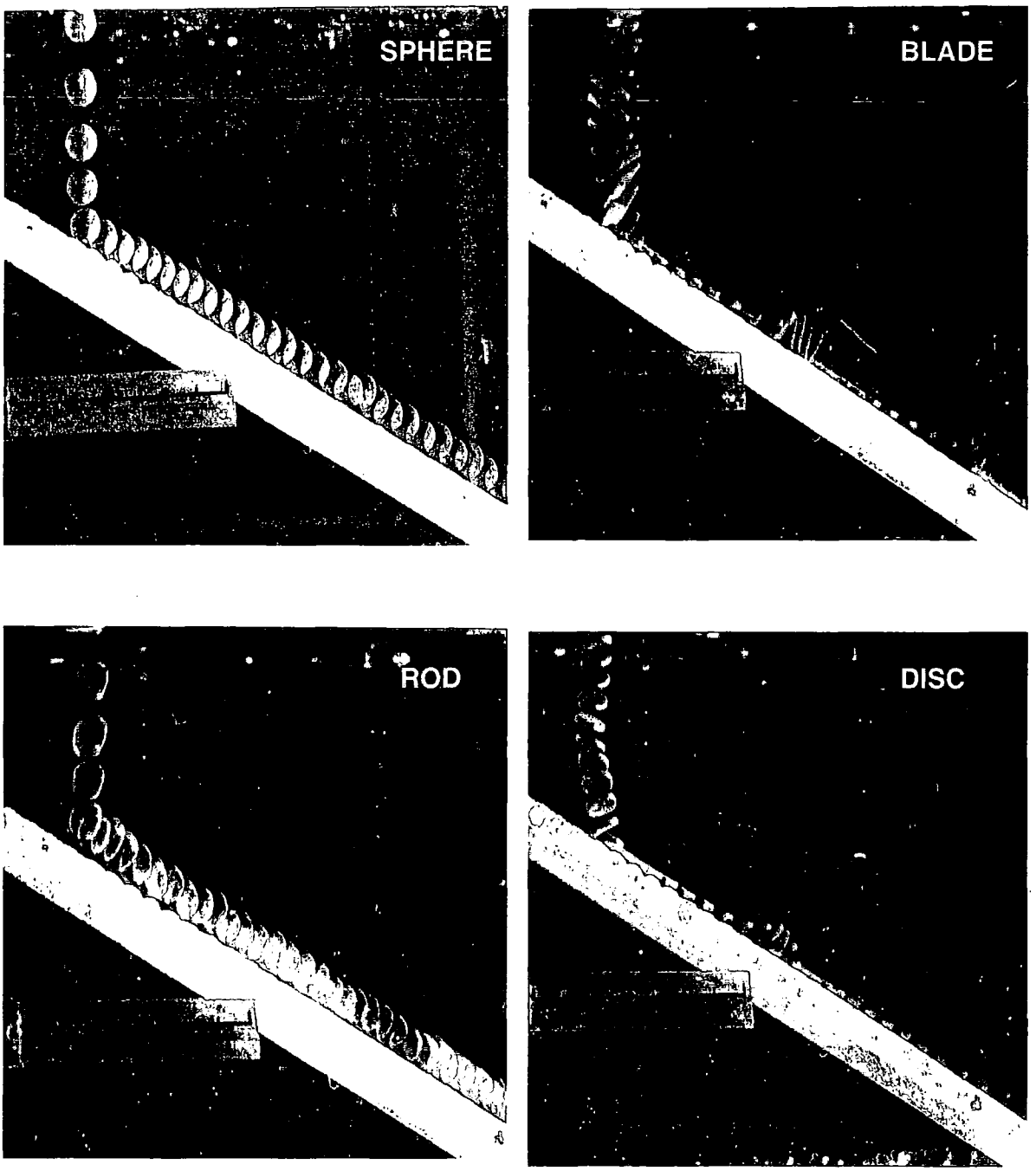

Figure 7.30 Strobe-light photographs of sphere, blade, rod and disc particles striking a 7 mm roughness element inclined at 30° degrees in water. The same experiment was replicated five times for each particle. These photographs show four examples. The strobe rate was at 25 flashes per second.

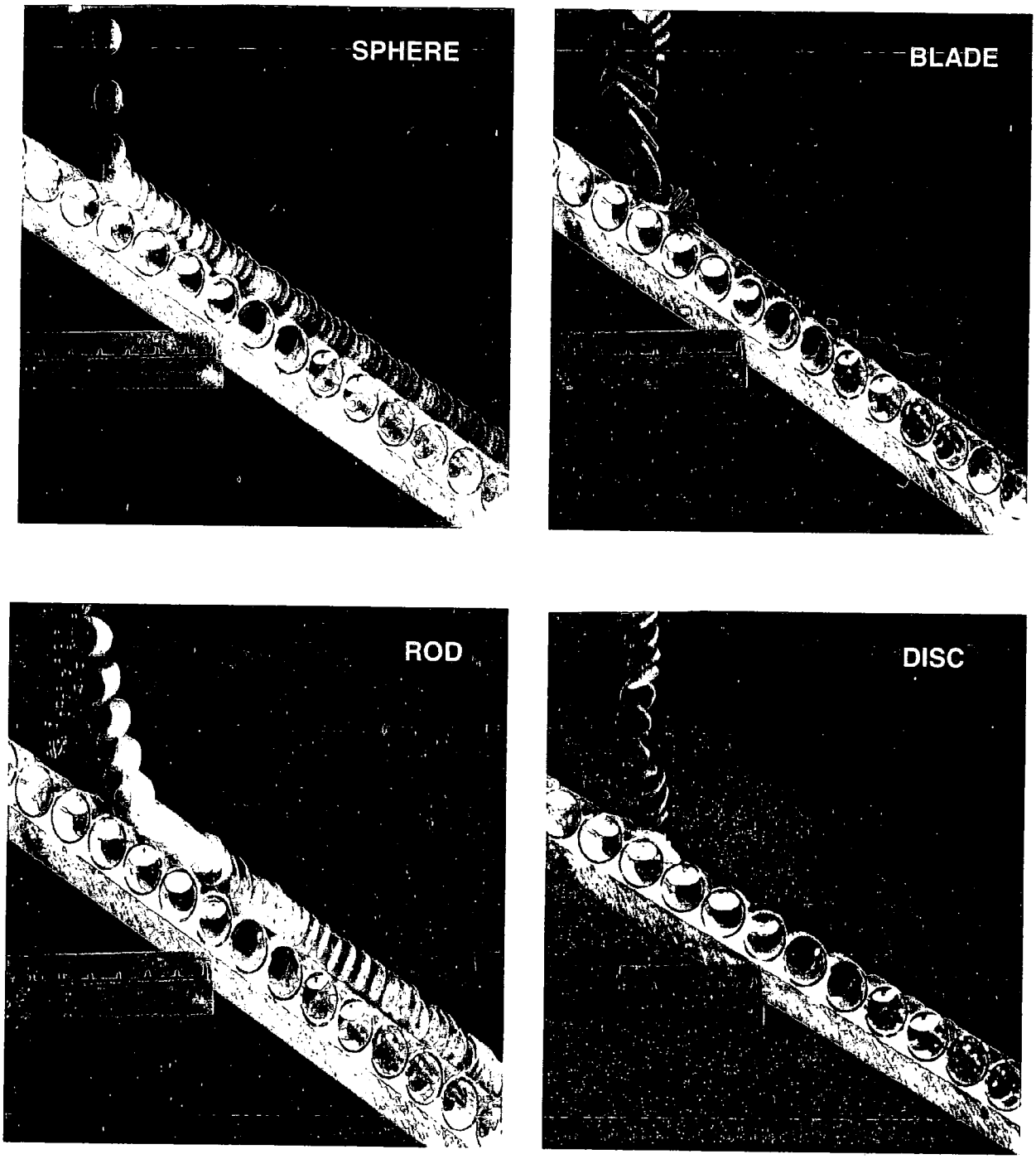

Figure 7.31 Strobe-light photographs of sphere, blade, rod and disc particles striking a 14 mm roughness element inclined at 30° degrees in water. The same experiment was replicated five times for each particle. These photographs show four examples. The strobe rate was at 25 flashes per second.

and began to slide. However, the first pocket the disc encountered immediately stopped it. The leading edge of the grain abutted against the upstream face of the roughness element and motion ceased (Figures 7.30 and 7.31). At 30° the slope is well below the critical friction angle for this particle and roughness (57°). The blades exhibited a similar movement pattern to that on the 7 mm roughness surface. It accelerated in a sliding mode, stalled, collapsed and began sliding again.

Comparison of these results to the findings of friction table experiments (Chapter 6) indicate some similarities. Both experiments show that particles transverse to the slope tend to entrain at lower slope angles than those of parallel orientation. There is an inverse relation between bed roughness and initial motion of particles and this relation tend to be stronger for sphere-shaped particles. Both experiments have showed that sphere-and rod-shaped particles tend to entrain at lower pivoting angle than discs and blades and the most frequent mode of movement is rolling for spheres and rods (transverse to the slope), whereas for discs and blades it is sliding

7.11 DISCUSSION AND CONCLUSION

This investigation has focussed on the influence of the particle shape, size and orientation on the mode of motion and threshold entrainment conditions, based on visualisation experiments.

The nature of settling is a function of particle mass, size, shape and orientation. Experiments have shown that there are some fundamental differences in settling velocities and the pattern of settling trajectories between particles of various shape classes (Figure 7.4 and Figure 7.32). First of all, spheres and rods exhibited more uniform settling patterns and modes of movement. Spheres settled vertically in a very uniform fashion, whereas rods also showed similar settling with slightly more rotation about their axes (Figure 7.4). Blade and disc shapes, however, showed a more complex and irregular hydraulic behaviour. For blade- and disc-shaped particles the settling paths are much longer and irregular (sinuous) than for the rod and sphere shapes. (Figure 7.4).

An important control upon settling behaviour is particle settling orientation. A particle with its maximum projection area horizontal to the water tends to settle more slowly than a particle with its long axis inclined at a 90° to the flow. This differential settling velocity reflects differences in resistance to settling. Discs showed similar hydraulic settling behaviour to blades. For most of the observations, blade-and disc-

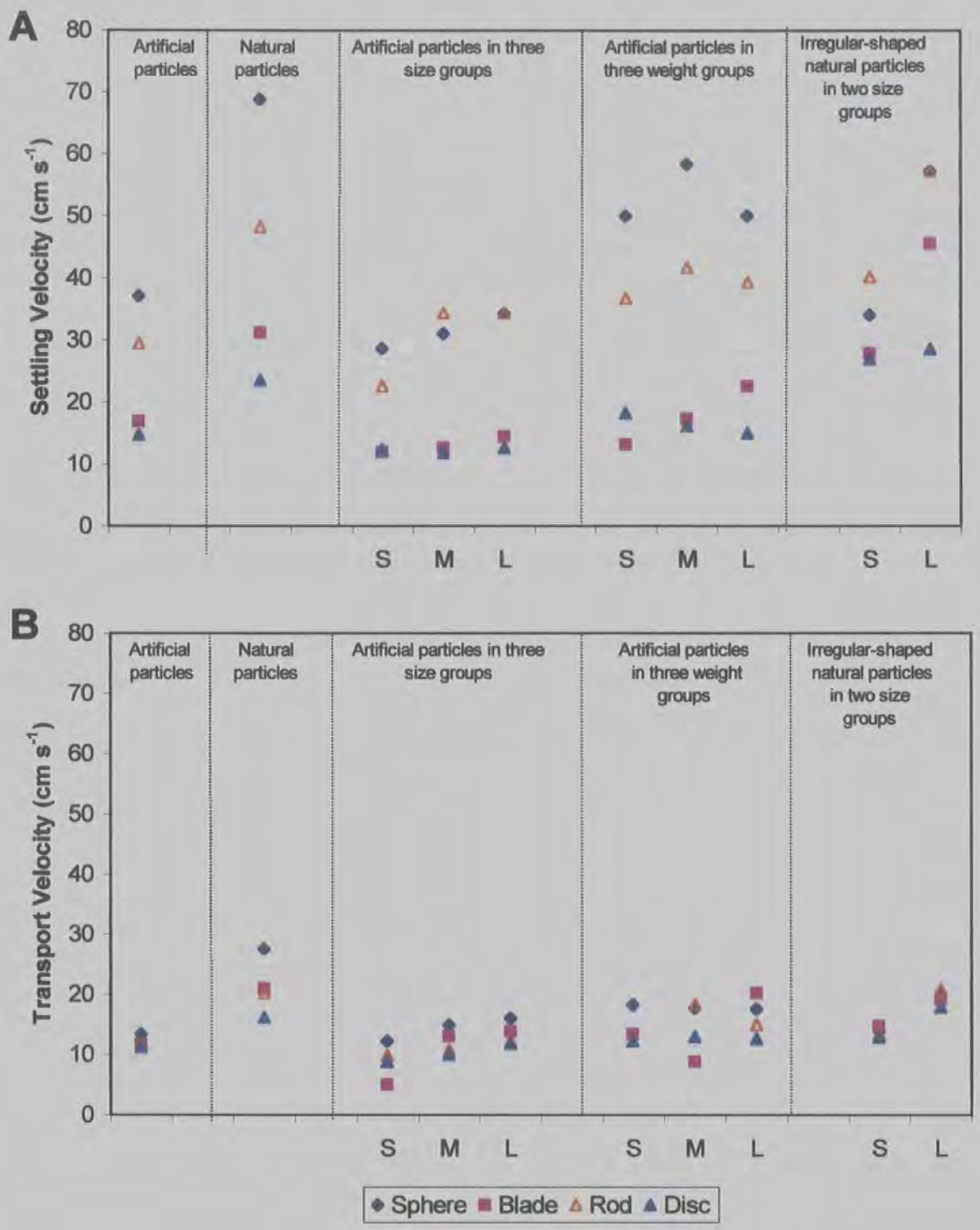

Figure 7.32 Mean settling (A) and transport (B) velocities for particles of various shapes, size and weight groups of natural and artificial particles (S, M, and L indicate small, medium and large size groups respectively).

shaped test particles tended to change their orientation from a vertical position to horizontal or from horizontal to vertical, which resulted in different settling rates. As the larger surface area of a particle turns to a horizontal position, the contact area of the water column with the particle surface increase and this leads to a greater resistance which results in lower settling velocity. Whereas a downward movement with a vertical orientation was found to minimise resistance, leading to an increase in settling velocity. Settling tended to be slower when disc and blade particle were in a horizontal orientation, whereas in a vertical downward movement, particle settling paths seemed to be relatively straight and settling velocity greater. It has been shown that as a particle settles and changes orientation, the rate of settling will also vary. Settling in a vertical orientation tended to be faster than settling with the maximum projection area parallel to the base. Spheres and rods settle along more uniform paths.

In terms of the settling paths, it has been demonstrated that, in common with the findings of Willmarth *et al* (1964) and Stringham *et al* (1969) some disc-and blade-shaped particles showed an irregular oscillation during settling. Disc and blade-shaped particles exhibited a glide-tumble-like settling pattern in which they swung from side to side as they settled (Figure 7.4, 7.7 and 7.8). Tumble settling was also observed as flat-shaped particles continuously tumbled end over end, and moved along a path that was straight but oblique to the vertical.

In terms of mean transport velocity and the mode of transport, experiments showed that show that, in general, mean transporting velocities are much lower than the settling velocities of spheres, blades, and rods (Tables A4.1, A4.2 and Figure 7.32). Despite faster mean settling velocity for spheres and rods than for blade-and disc-shaped test particles, a similar clear difference in the mean transport velocities between various shapes does not exist. In relation to the mode of transport, it was observed that the initial impact of a particle with the sloping plate (inclined at 30° from horizontal) produces two distinct sets of behaviours. First spheres impact the plate and bounce off, whereas, discs and blades hit the slope plate in a more gentle way and then begin to slide down the slope. Spheres always rebound and rods sometimes rebound, but blades and discs do not. This might be attributed to the fact that spheres and rods offer less resistance during settling because of their smaller surface areas therefore impact the plate at a greater velocity. Following the initial impact the velocity of movement along the sloping plate was almost constant for rods and spheres, whereas discs and blades tended to accelerate.

The mode of movement down the slope is again a function of particle shape. For most of the experiments, spheres exhibited a uniform rolling mode with close contact with the bed. Similarly rods rolled down the slope with their long axes transverse to the slope. Discs and blades moved mostly in a sliding but more complex movement during their transport.

7.11.1 Comparison of artificial and natural particles with various shapes

It has been found that general patterns of motion for natural particles are similar to those identified earlier with artificial particles. There is little difference between the movement of spheres and rods, while blades and discs show greater differences, particularly in settling. The motion of natural grains appeared to be more complex and less hydrodynamically predictable. Small differences in shape produce fairly large differences in hydrodynamic behaviour. Comparison of the settling and transport velocities of natural particles indicated that spheres settle faster, followed by rods, blades and discs (Figure 7.22 and Table A4.2). Although there are much smaller differences, transport velocities follow a similar pattern. It was found that the transport velocity of a particular grain is always less than its settling velocity, often by a factor of two or three. The implications for sediment transport are interesting. Lower transport velocities mean slower movement at the bed. Rolling is faster than sliding. However, slower settling velocities do not equate directly with lower transport rate as a particle once entrained may remain in the upper flow profile longer and as a consequence step length may be greater.

In terms of settling and transport velocities of irregular-shaped natural particles, experiments have shown some significant differences between artificial and natural particles with ideal shapes. In general, no simple pattern of settling and transport velocities was found between particles of irregular shapes and to some extent size (Figures 7.24, 7.25 and 7.26). Particles with angular shapes are observed to show a greater variability in settling behaviour and irregular patterns of motion. This is an important factor in bedload transport studies because, in gravel bed rivers, natural bed material shape deviates considerably from the ideal shape type and hence may not conform to models established for sphere, blade, rod and disc settling and transport (Figure 7.23). This suggests that, despite some indications about the settling and transport mechanisms of particles of various shape and size, the experiments carried out

here with artificial and natural particles of ideal shapes do not directly represent actual particle motion in a natural channel. However, some general trends appear to be valid. The more spherical the shape the faster it settles. Departure from a spherical form leads to a decrease in settling velocity. The sphere and rod-like particles tend to settle faster and move by rolling, while disc and blade-like particles tend to show slower settling rates and, in most instances, move by sliding mode.

7.11.2 Friction (Pivot) Angle Measurements

Generally, sphere-and rod-shaped particles were found to have noticeably lower friction angles than blade and disc shapes. The orientation of elongate particles (rods and blades) has an influence on the friction angle. As bed roughness increases the critical friction angle also increases. Differences in friction angles between the two roughness types are greatest for blades (transverse orientation) and discs (Table 7.9). This is because the intermediate axes (10 mm) of these grains tends to lodge in the pockets of the 14 mm roughness elements and the small a axis inhibits pivoting out of the pocket. However, a blade moving in parallel orientation (long axis 20 mm) 'bridges' the roughness elements and has a friction angle similar to the 7 mm roughness type. In both cases movement is by sliding. Thus, it was found that, overall, the initial motion of a particle is controlled by its dimensions, relative grain-size and the mechanism of movement (pivoting or sliding). Spherical particles have a more irregular movement pattern on the coarser bed. On the 14 mm roughness, after initial movement, the grain tends to 'pivot and drop' from pocket to pocket.

7.11.3 Settling and Transport on Rough Beds

In terms of settling and transport on different bed roughnesses, comparisons of the behaviour of the particles of various shapes showed some distinct differences. Spheres and rods showed very similar settling and transport paths on both roughnesses (7 and 14 mm), although on the 14 mm roughness transport was a little more irregular with fluctuations in velocity as the particle passed over the underlying pockets. The discs and blades showed a very different pattern of movement by settling along a regular oscillatory path. Subsequent to the initial impact on the 7 and 14 mm roughnesses, discs and blades tended to collapse and begin to slide. The particles accelerated until there was sufficient lift to allow them to climb from the bed (Figure 7.30, 7.31).

These experiments have clarified some aspects of the hydraulic behaviour of particles (in different shape and size characteristics) that cannot be observed directly in the field. However, these observations cannot directly be related to bedload transport mechanisms in a stream for the following reasons:

Firstly, in a coarse-gravel channel, flow resistance is more complex and generally controlled by large-scale roughness elements and the local characteristics of the bed material. Even under a steady flow there is a wide scatter in the relationship between hydraulic variables and bedload transport. The roughness elements also have very complex arrangements depending on the size and shape characteristics of bed material, local bed gradient and flow conditions. Thus particles moving over these beds may have relatively complex hydraulic behaviour compared with those on a relatively smooth bed with constant gradient. The present experiments was carried out on a relatively constant slope (30^0) with no roughness. Although two settling and transport experiments were also carried out on rough beds, they cannot directly represent natural gravel bed roughnesses, since they were made up with uniform sized (7 mm and 14 mm) roughness elements. When the test particles were released onto inclined plates (either smooth or with roughened slopes) they tended to roll or slide continuously depending on particle shape, due to the constant and high gradient of slope. Spheres and rods generally tended to move in a smooth rolling motion, while transport for the blades and discs usually varied with an oscillatory sequence of collapse-slide-lift-stall-collapse-slide with long axis transverse to the slope. As earlier studies (e.g. Hassan and Church, 1992) have demonstrated, the movement of coarse particles in a gravel bed is not continuous, but instead consists of a series of step and rest periods due to complex bed roughness elements, local flow condition and variation in channel gradient.

Secondly, in terms of shape and size characteristics of test particles, it was clear there were some clear differences between the test particles used for the present experiments and natural particles moving in a natural river channel. Most of the test particles used (both artificial and natural) for the present experiments were geometrically 'ideal' shapes, whereas in a gravel-bed river, bed material (in most cases) will not include 'true' spheres, blades, rods and discs (which would plot in the extreme corners of the Zingg diagram). In other words, in a natural gravel bed river many of the spheres and rods are very blocky with rather lower roundness values, while blades and discs are rather thicker with high c/b axis ratios and tending towards equant diameters. Thus, as it was shown in the experiments carried out with irregular shaped natural

particles, particles with irregular shapes (typical of a natural stream channel) probably do not have similar hydraulic behaviour to those demonstrated here with ideal shapes. Finally, a major control on the settling behaviour is particle density. The experiments carried out with artificial test particles may not truly represent actual settling rates. This is because, as shown with natural particles, natural particles tend to settle much faster than the artificial particles due to their greater density.

7.11.4 Implications for bedload transport

Although the results of these experiments cannot be directly related to the actual stream channels, they may shed light into some problems encountered in sediment transport mechanisms in gravel bed rivers.

One of the findings of the present study is that particle shape has an important influence on its hydraulic behaviour. Experiments have proved that settling and transport velocities are predominantly controlled by particle shape, orientation, size and to some extent density. Sphere-and rod-shaped particles tend to settle faster than the other shapes (Figure 7.32). It was also found that, apart from shape, the velocity of settling increases with size and density. Within the same size-and shape-ranges particles with greater density tend to settle much faster than those of with lower density.

In a gravel-bed river channel the majority of particles are irregular in shape rather than geometrically ideal shapes. The present study clearly showed that particles with irregular shape have very complicated hydraulic behaviour. In other words they do not settle or move in a way in which an ideal shaped particle of natural or artificial form behaves. However, although irregular shaped particles in a natural channel do not have similar hydraulic behaves to those with ideal shape, their proximity to any ideal shape (either spherical or flat) indicates their type of hydraulic behaviour. In other word, a sphere-like particle tends to have a hydraulic motion similar to a well-formed sphere. Along with the high roundness degree, the more spherical the particles the faster it settles or rolls on a surface. Similarly, depending on its proximity to perfect flat-shaped particles, blade and disc-like particles tend to settle rather more slowly and move in a sliding mode.

The present study also showed that increased irregularity of particle shape, such as blocky sphere and rod-like particles with low roundness, or disc and blade-like particles with greater c/b ratio, may diminish the influence of shape on hydraulic behaviour. In this case the effect of size becomes the dominant factor on particle

transport phenomena. It was also found that the influence of particle shape on both settling and transport mode increases with increasing size.

The experiments here demonstrated that the degree of bed roughness and channel gradient has a significant influence on the initial motion of a particle and also its hydraulic behaviour. For a given size, shape and density, the entrainment of a particle sitting on a bed depends on the degree of bed roughness and also local channel bed gradient. In the light of the present experiments it is likely that, on a rougher river bed, the initial motion of all particle and also their movement will be retarded by the bed roughness elements. It has been shown that as the bed is roughened, particles begin to move at relatively greater friction angles.

Finally, the proportion of time a particle spends in settling or transport mode is critical in determining the transport rate. Size and shape are crucial in governing this. In the field natural particles will tend (dependent in size) to spend a greater proportion of their transport history in "transport mode" rather than in "settling" or indeed "lift" modes. Therefore, differences in transport velocities are probably more important than settling velocities. Furthermore in natural bedload transport, when multiple particles are in motion, the whole process is completed by inter-particle collisions and local near-bed turbulence (Schmeeckle, 1988). However, following the dispersion of particles in the channel, the shape and size selectivity (sorting) becomes importance factors.

CHAPTER 8: SUMMARY AND CONCLUSIONS

8.1 INTRODUCTION

The aim of this study was to investigate the influence of bed material shape on bedload transport in coarse-bed rivers. A combined field and laboratory approach was adopted. A series of magnetic tracing experiments were undertaken in three experimental reaches on River Tees and Trout Beck, North Pennines, U.K. In the laboratory pebble friction angle measurements and particle visualisation experiments were carried out. The empirical results of this work form the main body of this thesis. The following main objectives were investigated:

1. To determine experimentally, the influence of particle shape on the dynamics of bedload motion.
2. To determine the travel lengths of particles in different shape and size classes after particular flow periods.
3. To examine the influence of bed topography on travel lengths and transport of different shape and size classes.
4. To determine variability in friction angle and mechanistic behaviour of particles of different size, shape, orientation and roundness on beds of varying gravel roughness.

This chapter summarises the main findings of this thesis and makes links between the different methods of investigation. A synthesis of the main findings is presented, followed by discussion of the limitations of this work. A final section outlines suggestions for further study.

8.2 INFLUENCE OF PARTICLE SHAPE ON THE DYNAMICS OF BEDLOAD MOTION.

Experiments have clearly shown that the hydrodynamic behaviour of a particle is strongly related to its shape. Visualisation experiments demonstrate that shape is an important particle characteristic which has a fundamental influence on settling rates and the mode of near-bed transport. Settling patterns and modes of movement of sphere- and rod-shaped particles are relatively simple. Sphere-shaped particles have a steady fall during settling, a large rebound on impact with the bed, followed by a relatively smooth rolling motion. Rods also exhibited a steady fall with some rotation. However, rebound is minimal and near-bed movement is dominated by a rolling mode (with long axis transverse to the slope). Discs and blades, on the other hand, show much greater variability often showing 'glide and tumble motion'. Following impact on the bed both types of particle show negligible rebound (section 7.5). Mode of transport for blades is variable but follows an oscillatory sequence of 'collapse-slide-lift-stall-collapse-slide' with the long axis transverse to the slope. Discs showed either a regular oscillatory settling path or a glide and tumble motion. Although occasionally, discs move by edge rolling, the mode of transport is generally similar to the blade (section 7.5, Figure 7.4).

Apart from shape, particle orientation produced variation in settling behaviour. Experiments demonstrate that settling tends to be slower when disc and blade particles were in a horizontal orientation, whereas in a vertical position, particle settling paths seemed to be relatively straight and settling velocity was greater (Figures 7.7, 7.8, 7.10 and 7.12). This differential settling velocity reflects different resistance to settling. Blade- and disc-shaped test particles tend to change their orientation from a vertical position to horizontal or from horizontal to vertical, which results in different settling rates. It has been shown that as a particle settles and changes orientation, the rate of settling also varies.

In general, settling and transport velocities of natural particles show a similar pattern of settling to those of artificial particles (spheres settle fastest, followed by rods, blades and discs) (Figures 7.18-7.22 and Table A4.2) but particle density was found to be an important factor influencing settling rate. Natural particles in all shapes always showed greater settling velocities than the artificial particles (section 7.8).

Compared to the very distinct settling velocities, differences in near-bed transport velocities of the four shapes were found to be much smaller although velocities variations follow a similar pattern. The transport velocity of a particular grain is always less than its settling velocity, often by a factor of two or three (section 7.9). On a smooth bed, particles moving in rolling mode (e.g sphere and rod) tended to have a faster transport velocity than those sliding (Figures 7.30 and 7.31). However, slower settling velocities do not equate directly with lower transport rate as a particle once entrained may remain in the upper flow profile longer and as a consequence the step length may be greater. On a rougher bed, on the other hand, spherical particles tend to move around bed roughness elements (section 7.9).

Although, similar patterns of settling and transport motion were determined between the geometrically-perfect artificial shapes and natural particles, experiments carried out with irregular-shaped natural particles showed more complex and less hydrodynamically predictable settling and transport motions (section 7.8). In other words, no simple pattern of settling and transport velocities were found between particles of irregular shapes and to some extent size (Figures 7.24, 7.25 and 7.26). Particles with angular shapes showed a greater variability in settling behaviour and irregular patterns of motion. This is an important factor in bedload transport studies because, as it is mentioned above, in gravel-bed rivers, natural bed material shape deviates considerably from ideal shape types hence may not conform to simple models established for sphere, blade, rod and disc (Figure 7.2). This finding suggests that, despite some indications about the settling and transport mechanisms of particles of various shape and size, the experiments carried out here with artificial and natural particles of ideal shapes do not directly represent actual particle motion in a natural channel (e.g. particle collisions have not been considered as part of the transport mechanics). However, some general trends appear to be valid. The more spherical the shape the faster it settles. Departure from a spherical form leads to a decrease in settling velocity. The sphere and rod-like particles tend to settle faster and move by rolling, while disc and blade-like particles tend to show slower settling rates and, in most instances, move by sliding mode.

8.3 MAGNETIC TRACING FIELD EXPERIMENTS – TRAVEL LENGTHS

The field experiments provided the opportunity to test the influence of particle shape and size on transport distance on two coarse-bed rivers. Results of the magnetic tracing experiments showed evidence of both size and shape selectivity. Preferential movement occurred in the finer (32-64 mm) particle size classes with tracers located along the channel thalweg moving the greatest distance (Figures, 5.19, 5.21). The majority of the large particles (>128 mm) moved only shorter distances. Generally, all shapes showed a decrease in distance and frequency of transport as size increased (Figures, 5.17 and 5.28a, b, c). Results indicate that although there were some differences in transport distances between the three experimental reaches due to the local bed topography and variations in flow, similar patterns of size and transport distance occurred for all three reaches (Figure 5.29 and Tables A2.1-A2.5). Differentiating between weight, size and shape revealed some consistent patterns in transport (Figures 5.30). It was also found that differences between the mean transport distances of tracers tend to become smaller, as size decreases. This indicates that influence of shape on particle transport distance tend to less importance in the finer size (32-64 mm) particles, while in the coarser particle classes (64-128 mm and >128 mm) clast transport distances were more strongly shape-selective. These finding are similar to those of Schmidt and Gintz (1995).

In terms of shape, during virtually all survey periods, sphere-shaped particles were transported the greatest distance and in greatest numbers. Rods and discs also moved preferentially but blades moved only short transport distances (Figures 5.28a, b, c and Table 5.6). These patterns were consistent over the monitoring period. Similar experiments by Schmidt and Ergenzinger (1992), Carling *et al* (1992), Schmidt and Gintz (1995) and Stott and Sawyer (1998) also concur with present results, although particle shapes do not correspond exactly between experiments.

The relationship between the scaled tracer size and scaled transport distance indicates that, despite a large scatter in the results at the three experimental sites, sphere and rod-shaped tracers had longer transport distances compared to discs and blades. In terms of size, only slight evidence of size-selective displacements were observed. Small size tracers moved slightly longer transport distances than the medium sized groups (Figure 5.14a, b and c).

Although the present magnetic tracing experiments have yielded valuable information on shape and size selectivity, the shapes of the tracers were deliberately selected. However, in coarse-bed rivers, natural bed material shape deviate considerably from ideal shapes and does not comply exactly to sphere, blade, rod and disc-shaped particles. In many natural settings variability in particle form is less pronounced and patterns of downstream changes in particle shapes are not apparent (Huddart, 1994).

Analysis of trapped-bedload and sampled bed material gave some important insights into the transport of natural bedload at Trout Beck experimental reach. In general, compared to the results of magnetic tracers, much stronger size selectivity was apparent and, to some extent, shape selective transport. Small particles in the trapped bedload were over-represented compared to bed material (Table 5.16). Disc- and, to some extent, sphere-like particles were found to be more common in both sampled bed material and also in the trapped bedload. Blade- and rod-like particles were found in the smallest proportions (Figure 5.25 and Table 5.16). It is also clear that as clast size increases the percentage of disc-like particles also increase. The reason for the greater frequency of discs in the larger size clasts was attributed to the influence of bedrock structure (sandstone) on initial clast shape. Compared to the sampled bed material, sphere- and disc-like particles were over-represented, while blade- and rod-like particles were under-represented in the trapped-bedload (Table 5.16). Statistical comparisons also showed that sphere and disc-like particles in the trapped bedload are significantly more spherical, rounder and smaller in size when compared to sampled bed material (Table 5.14). This suggested that, due to their greater sphericity and roundness, as well as their smaller size/weight, sphere- and disc-like particles in the trapped-bedload were potentially more mobile. Indeed, discs found in the trapped bedload tended to be more spherical. Although blade- and rod-like particles in the trapped bedload are smaller in size (thus lighter in weight) than those in the sampled bed material, they are still under-represented when compared to this material (Table 5.14). This suggests, apart from size, other characteristics of particles such as sphericity and roundness should also be taken into account. In other words, the lower transport capability of blade- and rod-like particles in the trapped bedload is attributed to their lower sphericity and roundness. This highlights the importance of sphericity and to some extent roundness on particle transport. Indeed comparisons also showed that blade- and rod-like particles have relatively lower sphericity and roundness values than sphere and disc-like particles both in the sampled bed material and also in the trapped bedload (Table 5.19). It was also

found that there is no statistical difference in the sphericty and roundness of blade- and rod-like particles between the trapped-bedload and sampled bed material (Table 5.14).

Results of correlation and multiple regression analyses have been partially successful in explaining the influence of shape on particle transport (Tables 5.9, 5.10). Multiple regression, incorporation shape and size parameters, explained a maximum of 27.5%, 33.4% and 49.9% of the variance in transport distance at Upper Tees, Lower Tees and Trout Beck sites respectively. Results of the multiple regression analysis showed that at each experimental site, roundness, weight, particle c-axis and sphericity were most highly correlated with transport distance. A-axis is also well correlated with distance but b-axis showed poor correlation with distance at the three sites (Table 5.9). Results of the correlation versus distance analysis showed that particle a-axis and sphericity also were the most significant predictors affecting transport distances, while the least useful predictor was particle c-axis (Table 5.9).

In general, although sphere- and disc-like particles in the natural bed material are transported preferentially, the influence of size selectivity in the trapped material was found to be stronger than shape when compared to the magnetic tracing results. The reason for this difference is that the natural particles in the experimental reach deviate from ideal shapes and show much less shape variability than the tracer material. Both in Sneed and Folk plots and Zingg graphs distinct differences between shape distributions of natural bed material and the magnetic tracers are seen. On a Sneed and Folk graph, the majority of the natural bed material clusters in the centre of ternary diagram (Figures 5.26 and 5.27). Conversely these are the exact shapes which are underestimated in the tracers.

Because tracer roundness differed from natural bed material, tilting table experiments, carried out with particles of various sizes on different bed roughnesses were used to investigate this influence on particle initial motion. Experiments showed a slightly lower friction angle with increasing roundness (Table 6.23, Figures 6.22 and 6.23). However, the influence of particle roundness tends to decrease with increasing bed roughness relative to test particles (Table 6.23).

8.4 INFLUENCE OF BED TOPOGRAPHY ON TRAVEL LENGTHS AND TRANSPORT OF DIFFERENT SHAPE AND SIZE CLASSES.

Spatial patterns of tracer distribution at the three experimental sites showed a strong relation between the channel geometry and paths of tracer movement. At Trout Beck and the Lower Tees sites the majority of tracers movement was concentrated along the line of the main thalweg where the channel is deeper and velocity highest (Figur 5.19, 20 and 21). Although a general pattern of movement could be observed, the distribution also reflected several random variations. Thus, apart from shape, size and density of particle, the exact location in the channel is also thought to be an important factor in determining transport. In other words, the location of particles (e.g. how close to thalweg, imbricated or buried) before or after particular flow events has an important influence on whether or not particles move and over what distance. This is highlighted by the fact that, apart from longitudinal distribution, the importance of lateral sorting of tracers should also be considered. Hoey (1992) has pointed out the necessity of spatial sorting in studying of the movement of single grains, and stated that in addition to longitudinal and vertical sorting, planimetric sorting should also to be considered. He suggests that planimetric sorting (cross-channel sorting) may result in some particles being transferred into areas of the bed that are relatively more or less active than the mean during the course of an event.

Scaled tracer displacements, which were determined by dividing the distance moved by each individual particle in each event by the mean distance of each event, showed that event distributions are highly skewed with some secondary peaks. It has been shown previously that both Einstein-Hubbell-Syre and Gamma model fit the distributions reasonably well for small displacements but for larger displacements the models tend to become unstable due to the possible effects of morphological elements (spatial sorting) in the channel (Figures 5.22 and 5.23). This is shown at all three experimental sites (See also section 5.7).

The relation between the scaled mean particle size and scaled distance for the means of the data demonstrates shape selectivity at each of the sites. Particle size was scaled by dividing mean size of whole the tracers by the median (b axis) diameter of the surface bed material (D/D_{50}). Mean travel distance was scaled by dividing mean distance of each shape class by the mean distance of all tracers which is equal to median diameter of the surface bed material ($L_{D50\ surface}$). Spheres always plot on top (greatest

transport distances) followed by rods and discs and finally blades. Sizes of transported material differ at the three sites (Figure 8.1). At the Lower Tees site D and D_{50} are very similar, at Upper Tees $D > D_{50}$, while at the Trout Beck $D < D_{50}$. This suggests an interesting hypothesis: where tracer size is greater than the bed material size, shape effects are less pronounced. Where tracer size is less than bed material size shape is more important. This suggests that differentiation between shape would be greatest at the Trout Beck site and least at the Upper Tees. These results somewhat contradict the findings from the friction angle measurements in which the influence of particle shape on friction angle decreased with increase of test particle size relative to the bed roughness elements (d/D ratio). In other words, on less rough surfaces, differences between the friction angles of various shapes tended to be much clearer than those measured on rather rough surfaces (See Chapter six). Results from tracing experiments also showed that differences between the transport distances of various shapes tends to increase with increasing tracer sizes. This also suggests that shape selectivity becomes stronger with increasing particle size. This apparent contradiction may be resolved because the magnitude of the differences between d/D or D/D_{50} differ for the different experimental datasets.

Particles of various size and shape showed different movements on various bed roughnesses. Both in the tilting table experiments and also the visualisation experiments it was demonstrated that, on a smooth bed, following the initial movements, test particles tended to roll or slide (depending on their shape) continuously, following a relatively straight path. On the smooth bed sphere- and rod-shaped particles move faster (rolling) than blade-and disc shaped (sliding) particles. On rougher beds, the motion of spheres is retarded by the bed roughness elements. Spheres tend to follow irregular paths, meandering around obstacles, which leads to lengthening of transport paths. Discs-and blade-shaped particles moved by a sliding over the roughness elements. These findings are similar to those of Carling *et al.,* (1992). Experiments, on the two roughness types (Figures 7.27 and 7.28) show that the spherical particle have more irregular movement patterns on coarser beds. On the 14 mm roughness, after initial movement, the grain tends to 'pivot and drop' from pocket to pocket (See section 7.10).

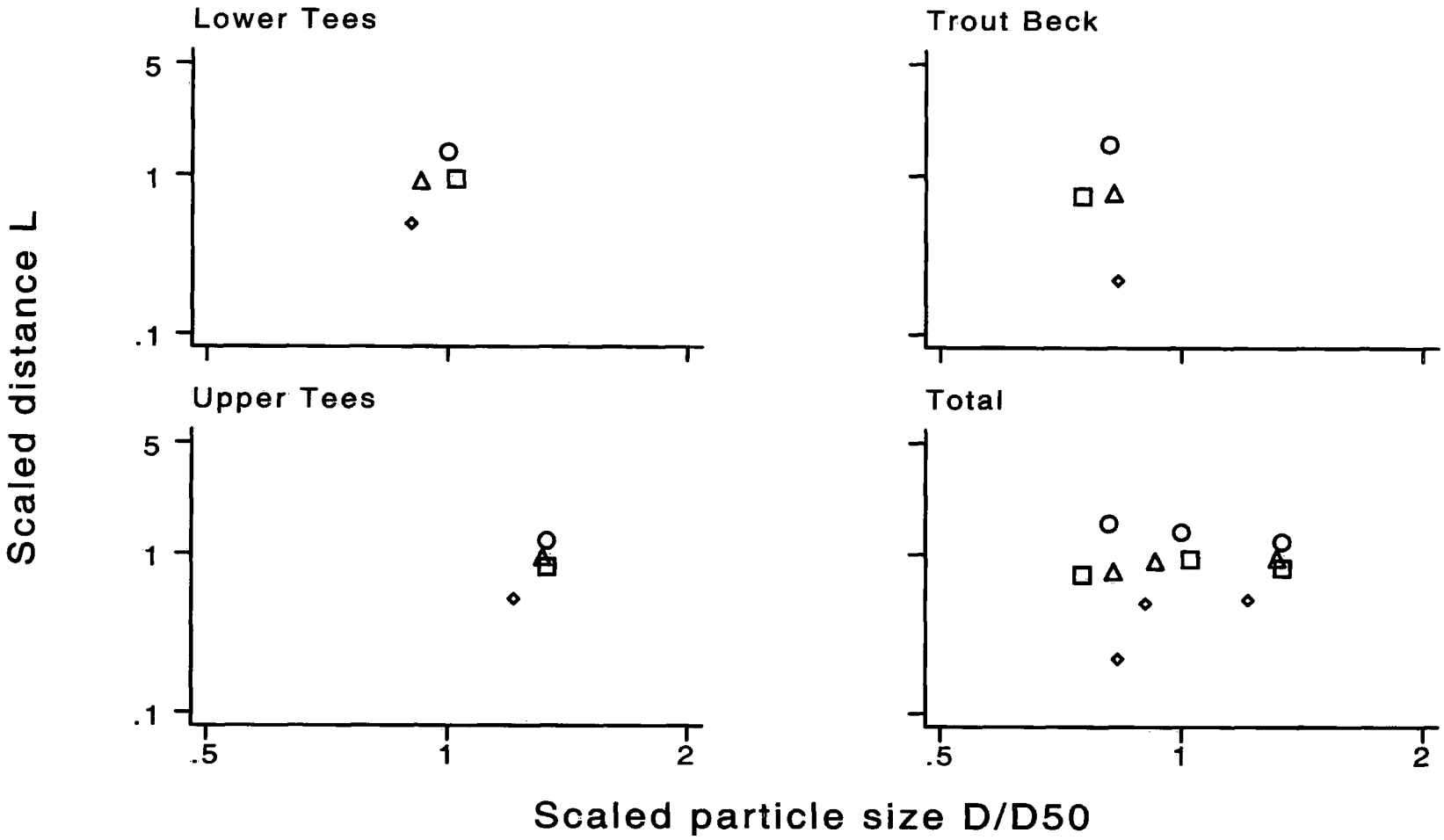

Figure 8.1 The relation between the scaled mean particle size and scaled transport distance for means of all data for the three experimental sites and the three sites combined (?: Sphere, Δ: Rod, Y: Disc. ◊: Blade).

8.5 VARIABILITY IN FRICTION ANGLES AND THE MECHANISTIC BEHAVIOUR OF PARTICLES OF DIFFERENT SIZE, SHAPE, ORIENTATION AND ROUNDNESS ON BEDS OF VARYING GRAVEL ROUGHNESS.

Based on the measured friction angles, it was clearly demonstrated that particle mobility depends on interaction between the test grain size, shape (form and roundness) and character of bed roughness elements (size, shape, sorting) over which it moves. Regardless of shape, results showed that friction angle depends on the ratio of test grain size (d) to the size of those over which it is pivoting (D). The smaller the ratio of d/D, the greater the friction angles at which test particles moved. Friction angles decreased with increasing particle size (hence greater d/D ratio) relative to the median bed particle size (Table 6.3 and Figures 6.3 and 6.24). The dependence of friction angle on the ratio of test particle size to those it rests is important in an assessment of selective entrainment of grains from a bed of mixed sizes, which is typical of coarse bed rivers. These findings, in general, show reasonable agreement with previous experiments (e.g. Miller and Byrne, 1966 Komar and Li, 1986; Kirchner *et al.*, 1990).

In terms of shape, both the tilting table experiments and visualisation experiments show that shape, orientation and to some extent, particle roundness has a significant influence on particle friction angles. An inverse relation was found between particle sphericity and friction angle. For almost all the measurements, statistically significant differences were found between friction angle of spheres, transverse rods and all other flat-shaped particles, namely, blades with parallel and transverse orientations, discs, and rods with parallel orientations (Chapter six). Departure from a spherical form led to an increase in grain stability (Figure 25 and Table 6.26). Across the full range of test particle sizes, spheres and transverse rod-shaped particles tended to move at relatively lower friction angles due to their easy rolling capability. Sliding particles such as blades, rods (with parallel orientation) and discs, in most instances, tended to show higher friction angles.

These results clearly indicate that rollability of a particle is an important factor on its hydrodynamic behaviour. Spherical particles (with a higher degree of roundness) always have greater rolling capability, which is primarily related to the '*c/b* ratio', (the ratio of the smallest to the intermediate axial diameters). The greater the *c/b* ratio, the smaller the value of the friction angle and the more easily the particle can be pivoted out of position during entrainment. Flatter particles, on the other hand, moved by sliding

rather than pivoting and rolling due to a lower *c/b* ratio. Such variations in particle behaviour have been shown to relate to critical shear stress, relative mobility and selective entertainment in a coarse bed rivers (Komar and Li, 1986; Carling *et al.*, 1992).

As with shape, particle orientation showed a significant influence on the observed friction angle. Rods (with a high c/b ratio and well-rounded) placed in a parallel position (long axis parallel to slope) always moved at relatively higher friction angles than that of placed in transverse orientation (long axis transverse to slope) (Figure 6.25 and Table 6.26). A similar relation was not observed between parallel and transverse blades because of its lower c/b ratio. However, the influence of particle orientation on friction angle tends to decrease as bed roughness increases. Although a slight difference was still observed between the parallel and transverse blades orientation, in which parallel blades on most bed roughnesses tend to have lower friction angles than those of transverse blades (Figure 6.25 and Table 6.26), it was not consistent in all measurements.

Results also indicate that on less rough beds, sphere and transverse-rods moved at relatively lower friction angles compared to blade-and disc-shaped particles, the differences between spheres, transverse-rods and blades and discs tend to decrease on rougher beds (Figure 6.25 and Table 6.26). A similar relation is not true for flat particles. This is because, sphere and transverse rods tend to sit more easily in the pockets between the adjacent particles as bed roughness increases. Flat-shaped particles bridge the grains and do not sit in a stable position (Komar and Li, 1986; Carling *et al.*, 1992).

For sphere and rod-shaped particles, the degree of particle roundness has been found to be important factor influencing initial motion of a particle. On smoother beds, highly rounded particles tended to be more mobile than those of more angular particles, while the influence of particle roundness on initial movement tended to be less important with increasing bed roughness. Surprisingly, on the natural bed, which is relatively rough, more rounded test particles still tended to move at lower friction angles. Results, measured on the natural bed, do not conform with the findings above. The effect of particle roundness on initial motion does not diminish with increasing bed roughness. The most likely reason for this difference is attributed to the fact that artificial and naturally formed beds have different structures (e.g. grain packing

geometry, size, shape and sorting etc) (see Figures 6.1 and 6.14 and section 6.8) (Komar & Li, 1986; Kirchner *et al.*, 1990 and Dietrich & Kirchner, 1992).

8.6 AN OVERALL SUMMARY

Tables 8.1, 8.2 and 8.3 compile the results from the separate field and laboratory experiments. An attempt is made to standardise the results by reporting 'relative' values. In each case results are reported relative to those of the sphere. For example, in terms of the field tracer experiments, relative values of mean and maximum transport distance of the blade, rod and disc-shaped tracers are compared to spheres. Smaller values indicate lower mean and maximum transport distances relative to the sphere, while greater values indicate longer transport distances. Blade and disc-shaped tracers show relatively low values, while rods have very similar values to spheres with some values are even greater than spheres. Compared to Upper Tees, relative differences in the mean transport distances between the four shapes (especially between blade and the other shapes) are greater at the Trout Beck and Lower Tees (Table 8.1). This indicates that selective transportation between four shapes tends to be greater with increasing mean transport distance. In general, relative differences between the four shapes are greater at Trout Beck site, while it tends to be smaller at Lower Tees and Upper Tees respectively (Table 8.1). The possible reasons are probably lesser transport distances at the Upper Tees and influence of bed morphological elements (wide and shallow channel, pool, bars etc.) at the Lower Tees site. In terms of maximum transport distances, rod-shaped particles show the greatest values, while blades are least at the Upper and the lower Tees site. Discs also show larger values than spheres and blades at Lower Tees (Table 8.1).

Comparison of transported bedload and sampled bed material using the enrichment factor, indicates that sphere-shaped particles are over-represented in the trapped bedload, while discs, rods and blades are consequently under-represented in decreasing proportions (Table 8.1).

Table 8.1 Overall summary of the results from the field experiments

Magnetic tracing experiments		Sphere	Blade	Rod	Disc
Mean transport distances	Upper Tees	20.7 m	0.43	0.79	0.68
	Lower Tees	62.7 m	0.35	0.66	0.68
	Trout Beck	56.6 m	0.14	0.55	0.37
Maximum transport distances	Upper Tees	127.1m	0.16	1.15	0.91
	Lower Tees	239.4m	0.43	1.51	1.10
	Trout Beck	243m	0.12	0.72	0.66
Transported bedload enrichment factor compared to sampled bedload	Trout Beck	1.31	0.64	0.79	0.93

In terms of tilting table experiments, differences between the measured friction angles of test particles of various shapes are calculated relative to the spheres. The smaller values indicate lower friction angles at which particles move (Table 8.2). Most of the measurements indicate that, relative to sphere-shaped test particles, disc, blades (both transverse and parallel orientation) and parallel rods show noticeable greater values, while values for transverse-rods tend to be lower. However, Table 8.2 also show that differences between relative values of various shapes tend to decrease with increasing bed roughness.

Results of the visualisation experiments carried out with all test particles (both artificial and natural) and in each size group showed that relative to sphere, blade and disc-shaped particles have lower values (hence lower settling velocity), while values for rods for most of the measurements are similar to sphere or slightly greater (Table 8.3). Despite clear differences in settling values of various shapes and orientations, relative values between the transport velocities are highly similar.

Results (from both field and laboratory experiments) demonstrated that spherical or rod-shaped particles are more mobile and transported longer transport distances than flat shaped particles, namely, blades and to some extent discs. Table 8.4 summarises mobility of particles of different shapes based on field and laboratory experiments and

Table 8.2 Overall summary of the results from the tilting table experiments.

		Tilting table experiments					
		Sphere	Blade		Rod		Disc
		(degrees °)	T	P	T	P	
Artificial test particles In small size	Roundness 1	39	1.31	*1.49*	0.84	*1.41*	1.41
	Roundness 2	45	1.11	*1.29*	0.84	*1.18*	1.27
	Roundness 3	51	1.16	*1.16*	0.86	*1.10*	1.18
	Roundness 4	69	1.10	*1.10*	0.84	*0.91*	1.17
	Natural bed	66	0.96	*0.98*	0.81	*0.84*	1.03
Artificial test particles In medium size	Roundness 1	27	1.59	*1.63*	0.92	*1.56*	1.93
	Roundness 2	30	1.67	*1.93*	0.90	*1.53*	1.83
	Roundness 3	35	1.37	*1.43*	0.94	*1.31*	1.49
	Roundness 4	46	1.26	*1.26*	0.89	1.24	1.37
	Natural bed	51	1.12	*1.10*	0.96	*1.14*	1.16
Artificial test particles in large size	Roundness 1	22	1.69	*1.59*	0.86	*1.86*	2.00
	Roundness 2	20	2.05	*2.10*	1.00	*1.95*	2.05
	Roundness 3	27	1.44	*1.37*	1.11	*1.48*	1.70
	Roundness 4	34	1.41	*1.38*	0.97	*1.41*	1.52
	Natural bed	35	1.66	*1.69*	1.11	*1.54*	1.71
Test particles in equal weight but different shape classes	Roundness 1	19	2.11	*1.84*	1.10	*2.16*	2.10
	Roundness 2	22	1.73	*1.91*	1.14	*1.95*	1.82
	Roundness 3	28	1.50	*1.43*	1.00	*1.71*	1.54
	Roundness 4	33	1.61	*1.45*	1.10	*1.64*	1.55
	Natural bed	44	1.25	*1.30*	1.10	*1.34*	1.41
Natural test particles	Roundness 1	20	2.00	1.75	1.20	1.95	1.95
	Roundness 2	27	1.70	1.48	1.48	1.44	1.62
	Roundness 3	28	1.89	*1.54*	1.25	*1.64*	1.69
	Roundness 4	34	1.62	*1.47*	1.10	*1.59*	1.71
	Natural bed	42	1.33	*1.17*	1.10	*1.24*	1.53

(T: transverse, P: parallel orientations. Values in italics indicate a parallel orientation)

Table 8.3 Overall summary of the results from the visualisation experiments. Values shown in the 'sphere' column are velocities in cm s^{-1}. All other row values are relative to this.

Test particles		VISUALISATION EXPERIMENTS	Sphere	Blade	Rod	Disc
Artificial test particles		Settling	37.0	0.45	0.79	0.39
		transport	13.4	0.87	0.87	0.84
Natural test particles		Settling	61.9	0.51	0.78	0.39
		transport	27.5	0.73	0.76	0.59
Test particles in three size group	Small	Settling	28.6	0.42	0.79	0.43
		transport	12.0	0.42	1.22	0.72
	Medium	Settling	31.0	0.42	1.10	0.38
		transport	14.9	0.87	0.72	0.67
	Large	Settling	34.3	0.42	1.00	0.38
		transport	16.1	0.86	0.76	0.73
Test particles in three weight groups	Small	Settling	50.0	0.28	0.73	0.36
		transport	18.2	0.74	0.67	0.67
	Medium	Settling	58.4	0.29	0.71	0.28
		transport	17.7	0.49	1.03	0.73
	Large	Settling	50.0	0.45	0.79	0.30
		transport	17.5	1.15	0.85	0.72
			Sphere-like	**Blade-like**	**Rod-like**	**Disc-like**
Irregular-shaped natural particles	Small	Settling	34.3	0.81	1.17	0.83
		transport	13.9	1.05	0.96	0.91
	Large	Settling	57.0	0.80	1.00	0.50
		transport	20.0	0.98	1.04	0.89

clearly indicates that for almost each experiment, sphere and rod-shaped particles are less stable than discs and blades. Overall, results from both field and laboratory experiments showed that shape is one of the fundamental properties controlling hydrodynamic behaviour of sediment particles. Thus, particle shape can play a significant role in bedload transport processes by controlling the nature of near-bed motion.

Table 8.4 Mobility of particles of different shapes determined from field and laboratory experiments. Note: The sizes of circles represent the rank order of particle mobility not the magnitude or significance of the differences. The greater the size the more easily a particle is moved, transported or settles.

Experiments		Sphere	Rod	Disc	Blade
Magnetic Tracing experiment	Mean transport distance	○	○	○	○
	Maximum transport distance	○	○	○	○
Transported bedload	Enrichment factor compared to sampled bedload	○	○	○	○
Tilting table experiments	Friction angle measurements	○	○	○	○
Visualisation experiments	Settling velocity	○	○	○	○
	Transport velocity	○	○	○	○

○ : Most easily moved ○ ○ ○: Least easily moved

8.7 LIMITATIONS OF THE STUDY

1. An important limitation of the present experimental design relates to the division of the tracers into arbitrary shape classes. Natural bed material generally shows a continuous range of size and shapes. However, by categorising bed particles into sphere, blade, rod and disc shapes, a lot of information on the precise size and shape of the tracer distribution is lost. Restricting tracers to discrete shape classes has meant that some of the shapes in the natural bed material have not been represented. Nevertheless categorisation of shape is inevitable given the problems of assigning a single class to describe particle form.

2. In the present study, the separation between the small and medium size groups was not as great as between the medium and the larger size group. For example, the means of the small and medium size groups of tracers at the Lower Tees site are 52mm, 87mm respectively, while it is 147mm for the large size group. A similar division is also true for the other sites. This is one of the reasons that differences between the small and medium size groups are smaller in both number of tracers transported and also mean transport distance at the experimental sites. This is important because as Schmidt and Gintz (1995) also found, the influence of weight on lengths of magnetic tracers becomes statistically significant only when classes of major differences in weight are compared.

3. Despite their similar lithology and density, the roundness values of tracers used for the field experiments were significantly greater than the natural bed material at the three experimental sites (Chapter 4, Table 5.19, 5.20). As some of the earlier investigators demonstrated (e.g. Li and Komar, 1986; Komar and Li, 1986; Carling *et al.*, 1992) particles with greater roundness are more mobile than those with lower roundness values (see Chapter 6).

4. Variations in sediment transport dynamics could not easily be related to discharge due to lack of detailed local hydraulic information and limited direct observations. Although, the Schoklitsch (1962) equation was used to predict critical discharges for initiation of bedload transport, the results were far from a satisfactory. The large errors in this method probably reflect to the effects of wide sediment size range, bed armouring, variations in local channel slope, etc. These factors can result in bedload discharge varying over an order of magnitude or more for a given set of estimates of flow conditions (Klingeman and Emmett, 1982; O'Leary, and Beschta, 1981; Swanson, *et al.*, 1982; Hoey, 1989).

5. As the experiment progressed, identification numbers of some tracers were partly or completely washed away. This led to some difficulty in identifying individual tracers despite having information about the three axes of each.

6. In each survey period the position of tracers were measured using tape measures with reference to a series of monumented section set out along the banks adjacent to the experimental sites (Chapter 3). During windy conditions the accuracy of the measurements was reduced due to difficulties with the tape. Typical accuracies were +/- 3 cm over 5 m, +/- 5 to 8 cm over 10 m and +/- 10-15 cm over 15 m.

7. Despite some important limitations, the visualisation experiments clearly demonstrated significant differences in the hydrodynamic behaviour of particles due to variance in shape, size and density. However, these experiments do not represent the exact mechanisms by which particles settle or move in a gravel-bed channel. This is because, all the experiments were carried out in a water-filled rectangular tank in which the water was static. The angle of the sloping glass plate was kept constant (30°) for most of the experiments and sloping surface was smooth. In a two-dimensional experiment particle behaviour, is visualised in X, Y space. The third dimension Z was largely ignored. This introduces some variability in the results. Although two different bed surfaces were formed using two types of glass rod oriented across the sloping glass, these roughness types do not exactly represent an actual river bed. This is because in coarse-bed mountain rivers flow is relatively turbulent and flow velocity varies spatially due to local variation of bed roughness elements, channel slope, and cross-section geometry. Therefore in a coarse-bed river, settling and transport mechanisms of a particle of any shape, are assumed to be much more complex than those observed in visualisation experiments.

8. In terms of the friction table experiments, the range of d/D values was too restricted. The majority of the measurements were carried out with coarse size test particles. In a natural stream bed, however, there is a large range in the particle size distribution which is a typical characteristic of many gravel-bed rivers. The lower range of d/D may lead to an overestimate the importance of hiding factors which is thought to have significant influence on equal mobility of transport in gravel bed rivers (Parker and Klingeman, 1982; Parker *et al.*, 1982).

9. Another important limitation for the present study is that the majority of the friction angle measurements were carried out on artificial bed roughness sheets which were formed with uniform, well-sorted particle sizes. However the surfaces of natural river

bed are very different from the artificially-formed bed roughnesses in terms of their packing and the degree of infilling of grain pockets by fines. Packing of grains and also the roughnesses of a stream bed tend to vary noticeably due to spatial differences in grain-size distribution (Hoey, 1989, 1992; Kirchner, 1990; 1992; Buffington *et al.*, 1992; Carling *et al.*, 1992). These differences between the artificial and naturally formed beds are thought to affect initial motion, relative mobility and selective entraiment of different particles.

8.8 FURTHER WORK AND RESEARCH

Although the present investigation was specific to the Upper Tees and Trout Beck catchments bedload transport system, the implications are more widely applicable to coarse-bed rivers. From this project several further research objectives can be identified:

1. The present study demonstrated that apart from particle size, shape also has important influence on bedload transport in gravel-bed rivers. However, the magnetic tracers used for the present study were deliberately selected. Whereas, as mentioned in earlier sections, in coarse-bed rivers natural bed material deviates considerably from ideal shapes and does not comply exactly to sphere, blade, rod and disc-shaped particles. The majority of earlier studies (e.g. Carling *et al.*, 1992; Schmidt and Ergenzinger, 1992; Schmidt and Gintz, 1995) used well-shaped artificial or natural tracers. Thus a similar field investigation based on bed material with a wide natural range of shape and size may give important information on how clast shape and size of transported bedload varies during a range of storm events.

2. Gravel-bed rivers generally have rough beds and the bed morphology varies considerably. Although the influence of bed roughness on the initial motion of particles of various shape and size has been investigated using friction angle measurements, further is required to assess influence of bed morphology (e.g. step-pool systems, bars) on initial motion, travel lengths and transport of different shape and size classes (Hassan and Church, 1990; Hassan and Reid, 1990; Ergenzinger and Schmidt, 1990; Schmidt and Ergenzinger, 1992).

3. At the outset of the present study it was decided that it would not be possible in the initial experiments to visit the sites after every flood, therefore bedload movement

events could not be related to individual floods, instead the main interest was on the relative movement between different shape classes. In a future experiment, it would be important to relate mean transport of clasts of various shape and size to individual floods. This would enable virtual transport rates to be calculated (Hassan and Church, 1992; Hassan *et al.*, 1992).

4. Although both the tilting table and visualisation experiments have highlighted several important aspects of shape and size on initial motion, a series of flume experiments is required to determine how critical shear stress interacts with natural particles of different shapes and sizes over different bed roughnesses. Using the results of flume experiments a range of threshold values for various combination of shape, orientation and bed roughness could be determined. In addition, flume experiments also give further visual information on how the hydraulic behaviour of a particles varies during transport (Carling *et al.*, 1992).

5. It has been pointed out that, that compared to spherical forms, flat-shaped particles are easily lifted and transported in temporary suspension. The lifting mechanisms, probability of lifting over various bed roughness types and also in different flow conditions need to be investigated in further detail in a flume study (Carling *et al.*, 1992).

6. Using a pit trap across a stream channel, shape and size characteristics of natural trapped bedload may be determined and the percentages of particles in each size and shape groups may be compared to river discharges and also natural surface bed material adjacent to the trap. A more rigorous sampling programme could be established to better investigate such a relationship (Ashworth and Ferguson, 1989; Ferguson *et al.*, 1998).

7. Finally, the empirical results provided in these experiments and from the field observations could also be used to develop a model to simulate shape effects in bedload transport. Using appropriate empirical values the relative importance of particle shape at entrainment and in the transport process could be conceptualised and a simple model developed. This would provide a further means of uniting the various threads of research presented in this thesis.

APPENDICES

Appendix 1 Size and shape characteristics of magnetic tracers used in the field experiments.

Appendix 2 Summary of the magnetic tracer movements at the three sites over the observation period

Appendix 3 Results of friction angle experiments

Appendix 4 Results of the photographic visualisation experiments for artificial and natural particles.

APPENDIX 1: SIZE AND SHAPE CHARACTERISTICS OF MAGNETIC TRACERS USED IN THE FIELD EXPERIMENTS.

A1.1 INTRODUCTION

The purpose of this Appendix is to compare the shape and size properties of the magnetic tracers used in the field experiments. The chapter first examines and compares mean particle size and weight in three size groups and for four shape classes at the three sites (sections 2 and 3). It then deals mainly with b/a (the ratio of the intermediate axis of a particle to its longest axis) and c/b (the ratio of the shortest axes of a particle to its intermediate axis) ratios of the test particles respectively (Section 4 and section 5). For each site, the degree of roundness of the tracers are examined and compared (sections 6). The final two sections (7 and 8) summarize sphericity and flatness properties of the tracers in respect to their importance on the hydraulic behavior of a particle during transport. In each section mean values and frequency distributions of the particles are examined and compared statistically to determine whether there is a significant difference between the different sites. Table A1.15A, B and C provides a detailed summary of the size and shape characteristics of the magnetic tracers used at the three sites. Summary statistics are presented for each size and shape class.

A1.2 MEAN PARTICLE SIZE (b-axis)

In order to replicate similar conditions at each of the experimental stations it was decided to equalize b axes for 3 sizes in all shape classes. In terms of their b axes, tracers were classified into three size ranges (32-64, 64-128, and >128mm). This section tests whether similar conditions were achieved at the three sites.

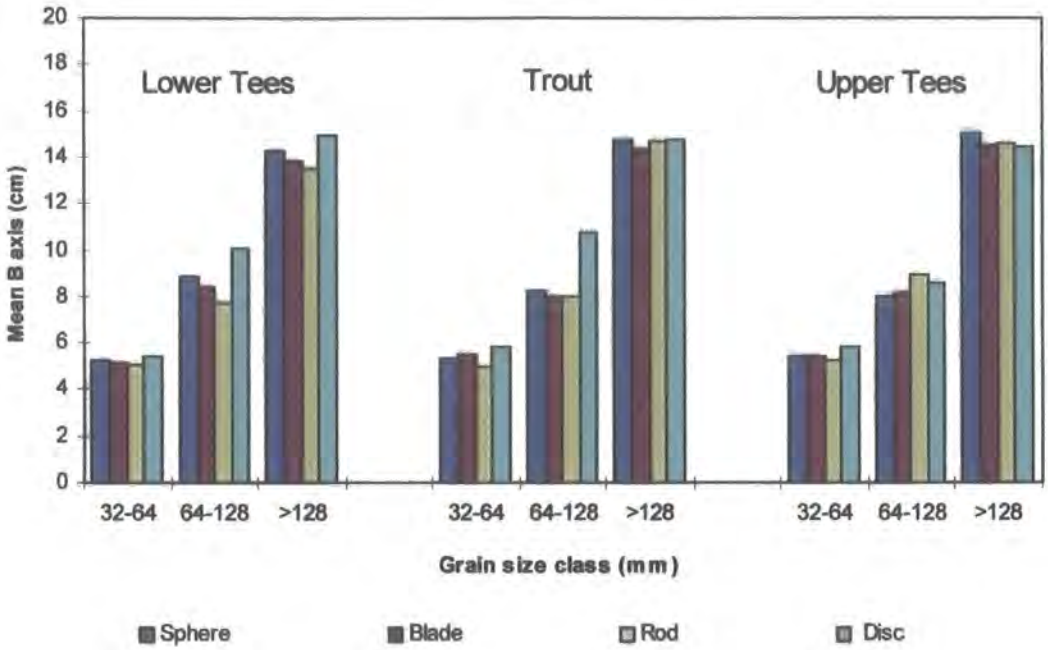

Figure A1.1. Mean distributions of b axis in three size categories for four shape classes at the Upper Tees, Trout Beck and the Lower Tees.

Mean particle sizes (b-axes) at the three sites vary between 8.9 cm and 9.6 cm. Figure A1.1 indicates an overall similarity between the three sites. There is no greater difference between the mean size of particles of four shape classes in small size groups. The distributions vary between 5.1 and 5.8 cm. Mean size of disc-shaped particles is slightly greater than other shapes at Lower Tees and Trout Beck sites, while at the Upper Tees site the four shapes have very similar mean values in all size groups. In the small size group, at all three sites, rod-shaped particles have the lowest value (5.0 cm at Trout Beck), while discs have greatest mean value (5.8 cm at the Trout Beck and Upper Tees sites). In the medium size group, the distribution varies between 7.3 mm (rods at the Lower Tees) and 10.7 mm (discs at Trout Beck) (Table A1 1). Lower Tees and Trout Beck sites, disc and rod-shaped particles have similar distribution. Table A1.1 shows that at the Lower Tees and Trout Beck discs have the greatest mean value, and rods have the lowest value, while at the Upper Tees site differences between the four shape classes decrease. In the large size group, however, the variation between the four shape classes is relatively small at all the three sites. It varies between 13.4 cm (rod at Lower Tees) and 19.9 cm (sphere at Upper Tees).

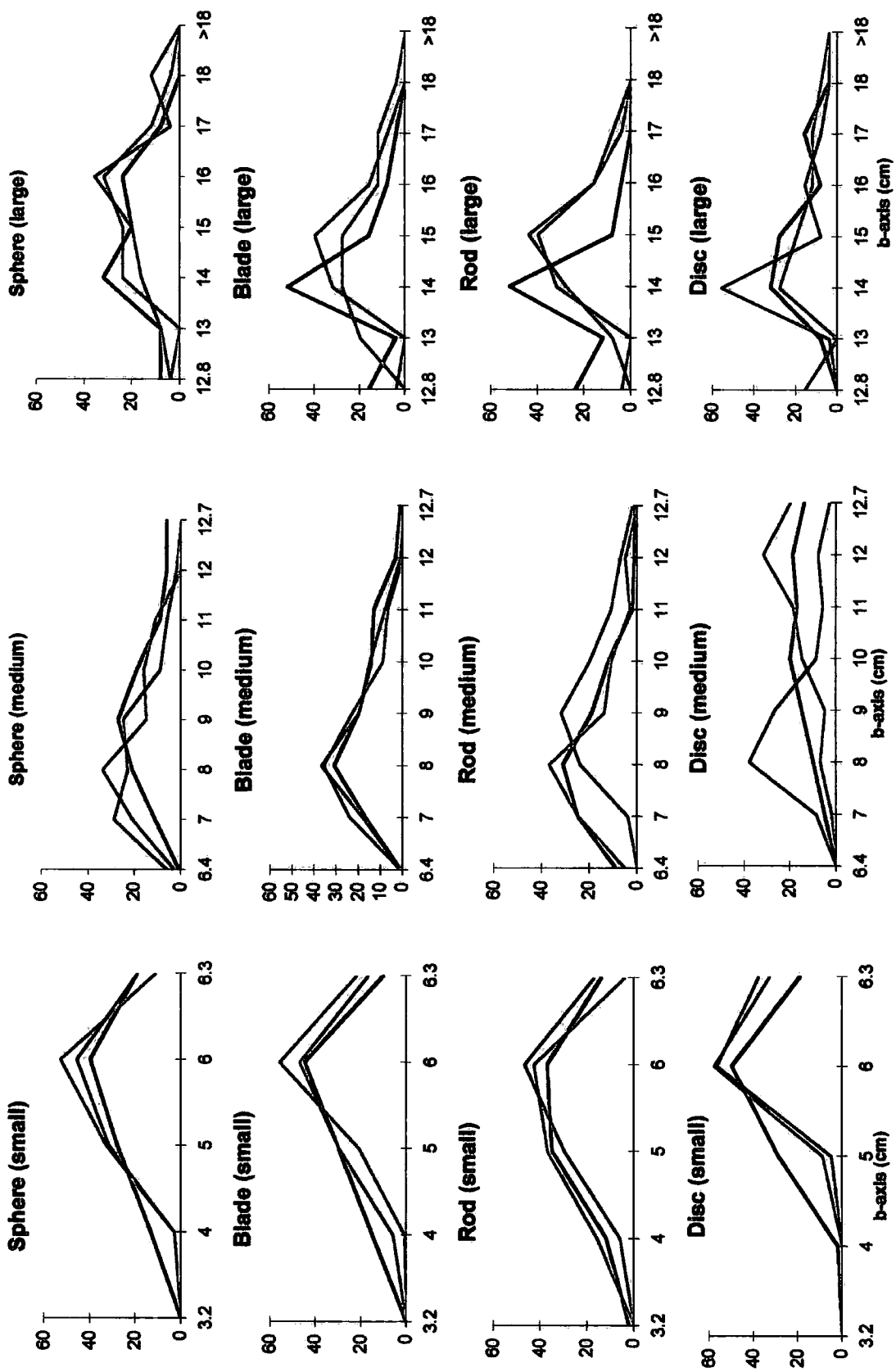

Figure A1.2 Frequency distributions of b-axes for four shapes and three size groups Lower Tees, Trout Beck and Upper Tees.

Comparison of the three sites shows that there is some degree of statistical difference in the mean b axis values of four shape groups in all shape classes, but the difference increases slightly in the medium size (the lowest value is 7.3 cm for the rods at Trout Beck and the highest value is 10.7 cm for the discs at Trout Beck) (Tables A1.1, A.1.2 and Figure A1.1).

Table A1.1. Mean particle size (b axis) distribution in three size groups for four shape classes at three sites

	Small (32-64 mm)			Medium (64-128 mm)			Large (>128 mm)		
	L.T	T.B	U.T	L.T	T.B	U.T	L.T	T.B	U.T
Sphere	5.2	5.3	5.3	8.8	8.2	7.9	14.2	14.8	14.9
Blade	5.1	5.5	5.3	8.3	7.9	8.1	13.8	14.3	14.5
Rod	5.1	5.0	5.2	7.7	8.0	9.0	13.4	14.7	14.5
Disc	5.3	5.8	5.8	10.0	10.7	8.5	14.9	14.7	14.2

Note: L.T: Lower Tees, U.T: Upper Tees, T.B: Trout Beck

In terms of particle size distributions, in general, Figure A1.2 and Table A1.15 show that, in small size group, particles of all shapes are negatively skewed with different degrees of kurtosis. This indicates that at each site and in the small size group (32-64 mm), the majority of particles are larger than the mean value. However, in the medium size group (64-128 mm), except for disc-shaped clasts, distributions are positively-skewed, indicating that majority of the particles are distributed between 7.0 and 10.0 cm. In the large size group, distributions at all the three sites show a tendency to positive skewness, but many classes are fairly normal. The majority of the particles have b axis values between 13.0 and 17.0 cm. (Figure A1.2 and Table A1.15).

Analysis of variance (ANOVA) techniques were used to investigate variability in the tracer sets. The sample variance is separated into two components of within–sample and between–sample variance, and compared using the F-test. Statistical comparisons of the three sites show that frequency distributions of sphere-shaped classes are quite similar and also statistically there is no significant difference between them in the small and large size groups (Table A1.2 and Figure A1.2). However, in the medium size class the differences between the three sites increase. This is because the Lower Tees site has greater mean value and also shows a larger standard deviation value (hence larger variation) than Trout Beck and Upper Tees. In the large size, there is some

irregularity in the frequency distributions of sphere-shaped particles, but this is not statistically significant (Table A1.2).

Table A1.2 Calculated values of F (F-ratio test) for the comparison of size-frequency distributions of four shape classes, three size groups at the three sites.

SHAPES	Small size (32-64 mm)	Medium size (64-128) mm	Large size (>128 mm)
SPHERE	1.71	**11.57**	2.02
BLADE	**8.02**	3.01	3.36
ROD	2.58	25.47	**9.28**
DISC	**30.94**	**52.43**	0.70

(Note: The critical values of F at the 0.01significance level for small and medium size groups is 7.07 and for large size group is 7.61. The values shown in bold indicate a statistical significant difference between the compared parameters.)

In terms of blade-shaped particles, however, Table A1.2 shows that there is a slightly significant difference between the frequency distribution of three sites in the small size group. However, both Figure A1.2 and Table A1.15 indicate that this difference is due probably to Lower Tees having a greater mean value and higher standard deviation than the other sites. In the medium and large-sizes of blades, however, there is no significant difference between the three sites (Table A1.2).

For rod-shaped particles, Figure A1.2 and Table A1.2 show that there is no significant difference between the three sites in the small size group, but in the medium and large size groups the similarity decreases significantly between sites (Table A1.2). In the medium size group the Upper Tees site shows a very different frequency distribution than Lower Tees and Trout Beck sites. Although the three sites have positively-skewed frequency distributions, the degree of skewness is less for the Upper Tees site. This implies that the size (b value) of the particles in the distribution at Upper Tees is greater than the other sites (Figure A1.2). For the large size, the Trout Beck and Upper Tees sites have almost normal frequency distributions with lower positive-skewness, lower kurtosis (*platykurtic*) and high standard deviation value. This indicates that they have a relatively wide range of size distributions in comparison with the Lower

Tees site, which has a lower standard deviation with relatively positive skewness (Table A1.15).

In the case of disc-shaped particles, Table A1.2 and Figure A1.2 show that for the small and medium size groups differences between the three sites are highly significant compared to that of larger size group. In the small size group, Trout Beck and Upper Tees sites show a high degree of negative skewness, while the Lower Tees shows almost normal distributions with lower degree of negative skewness and kurtosis. The Lower Tees also has a greater standard deviation than the other sites (Table A1.15). These differences indicate that variations in size at the Lower Tees site are greater than at Trout Beck and Upper Tees sites. It also signifies that at the Lower Tees site, the majority of the particles in the distribution have smaller b axes than Trout Beck and Upper Tees sites (Figure A1.2). In the medium size, at the Lower Tees and Trout Beck sites distributions are relatively flat, while the Upper Tees has highly positively-skewed distribution. Both relatively flat size distributions and hence high standard deviations values at the Lower Tees and Trout Beck sites clearly indicates that they have very wide spread of sizes around their mean values. In the large size group (Table A1.2) there is no significant difference between the three sites, though Upper Tees has a very high (*leptokurtic*) degree of kurtosis indicating that most of the particles are distributed around the mean.

A1.3 WEIGHT

Beside other factors particle weight is considered to be an important influence on the dynamic behaviour of a particle during transport and deposition. Within the same shape class (especially for flat particles), difference in particles weight may be important in that lighter particles tend to be lifted and transported further downstream by turbulent flow than heavier ones, which move close to the bed in a rolling or sliding. Lighter particles also have lower settling velocities than those of heavier ones.

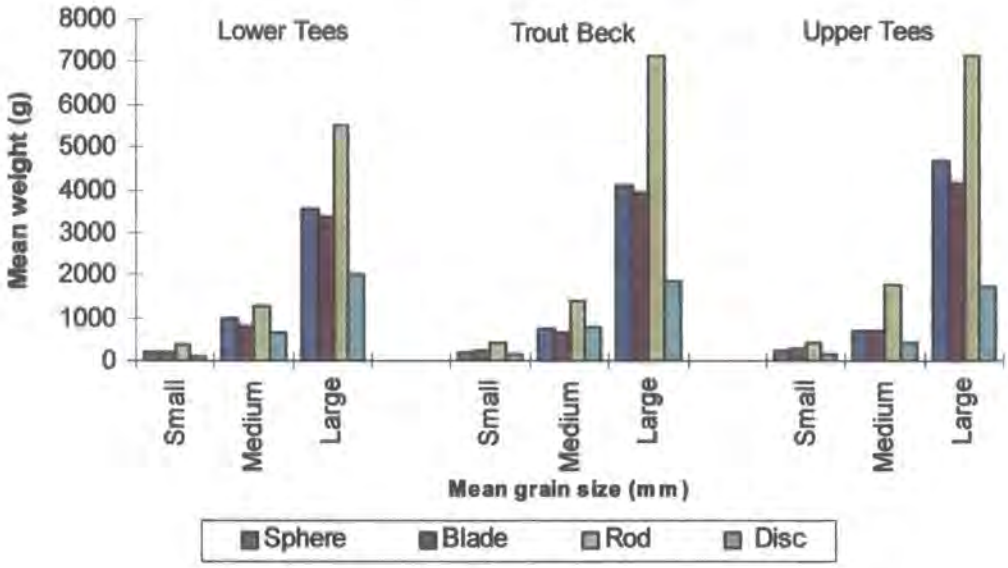

Figure A1.3. Mean weight distribution of clasts in three size groups for four shape classes at the Lower Tees, Trout Beck and the Upper Tees sites.

Generally, the three sites have very similar mean weight distributions (Figure A1.3). In all three size groups together mean weight values of the three sites vary between 1588 (Lower Tees) and 1862 grams (Upper Tees) Overall, there are no very significant differences in mean weight values between the Trout Beck and the Upper Tees, but it increases greatly between Lower Tees, Trout Beck and the Upper Tees sites (Table A1.3). In each shape class differences in mean weight between the medium and large size groups at all three sites are significantly greater than those between the small and medium size groups. At all three sites for the small size group, the differences in the distributions of mean weight values between the four shape classes are very small, but differences increase noticeably with particle size (Table A1.3). This is because, regardless of shape, size classification was based on the diameter of the "b" axes of each particle. In other words, length and thickness of particles were not taken into consideration. Thus for similar sizes, shape consistently influences the weights and this is more pronounced at larger sizes. Figure A1.3 shows that although it is not very significant in the small size group rod-shaped particles in the medium and large size groups at all three sites always have greater mean values. Disc shaped particles, on the other hand, have the lowest mean values, while blade and sphere shapes have very similar values at all three sites. The decreasing order of the mean weight distributions for the medium and large size groups is rod, sphere, blade and disc at each site.

Table A1.3 Mean weights of the four shape classes in three size groups at the Lower Tees, Trout Beck and the Upper Tees sites.

	Lower Tees				Trout Beck				Upper Tees			
	S	M	L	Mean	S	M	L	Mean	S	M	L	Mean
Sphere	207	968	3556	1577	209	764	4108	1694	222	708	4657	1862
Blade	191	798	3365	1451	233	657	3939	1610	265	687	4158	1703
Rod	387	1275	5522	2395	400	1391	7145	2979	402	1773	7175	3117
Disc	110	669	2007	929	140	794	1855	930	147	418	1734	766
Mean	224	927	3612	1588	246	902	4262	1803	259	897	4431	1862

Note: S: small size, M: medium size, L: large size

Figure A1.4 shows that there are no major differences between the three sites in the frequency distributions of the weights of the particles within the three size groups. In the small size group distributions are very similar and also relatively symmetrical with lower degrees of skeweness and kurtosis. This indicates that distributions are clustered around their means, and tend to be normal. In the medium size group, however, the three sites show positive skeweness and slightly greater kurtosis. In the large size group the three sites show some irregular variations, and lower values of skeweness and kurtosis. Sphere-shaped particles show no major differences between the three sites in three size groups (Table A1.4). In general, in the small and medium size groups distributions are more symmetrical and also peaky compared with large size group. This indicates that distributions tend to be relatively normal. In the small size group Lower Tees and Trout Beck have very similar means (207.3 and 208.6), and lower standard deviations (89.8 and 82.7), while the Upper Tees shows a slightly greater mean (221.7) and standard deviation (110.3) values with a higher positively skeweness (Table A1.15c). In the medium size group all sites tend to be very similar in the sense they have similar degree of positive skewnesses and kurtosis indicating relatively peaked distributions. In the large size group, however, distributions are remarkably flat, indicating wide but irregular distributions around the means. The higher standard deviation values also clearly suggest that there is a wide spread of values in weight for each site.

In terms of blade shaped particles, Table A1.4 and Figure A1.4 show that, except for the Lower Tees in the small size group, there is no statistically significant difference between the sites in the three size groups. In the small size group, slight

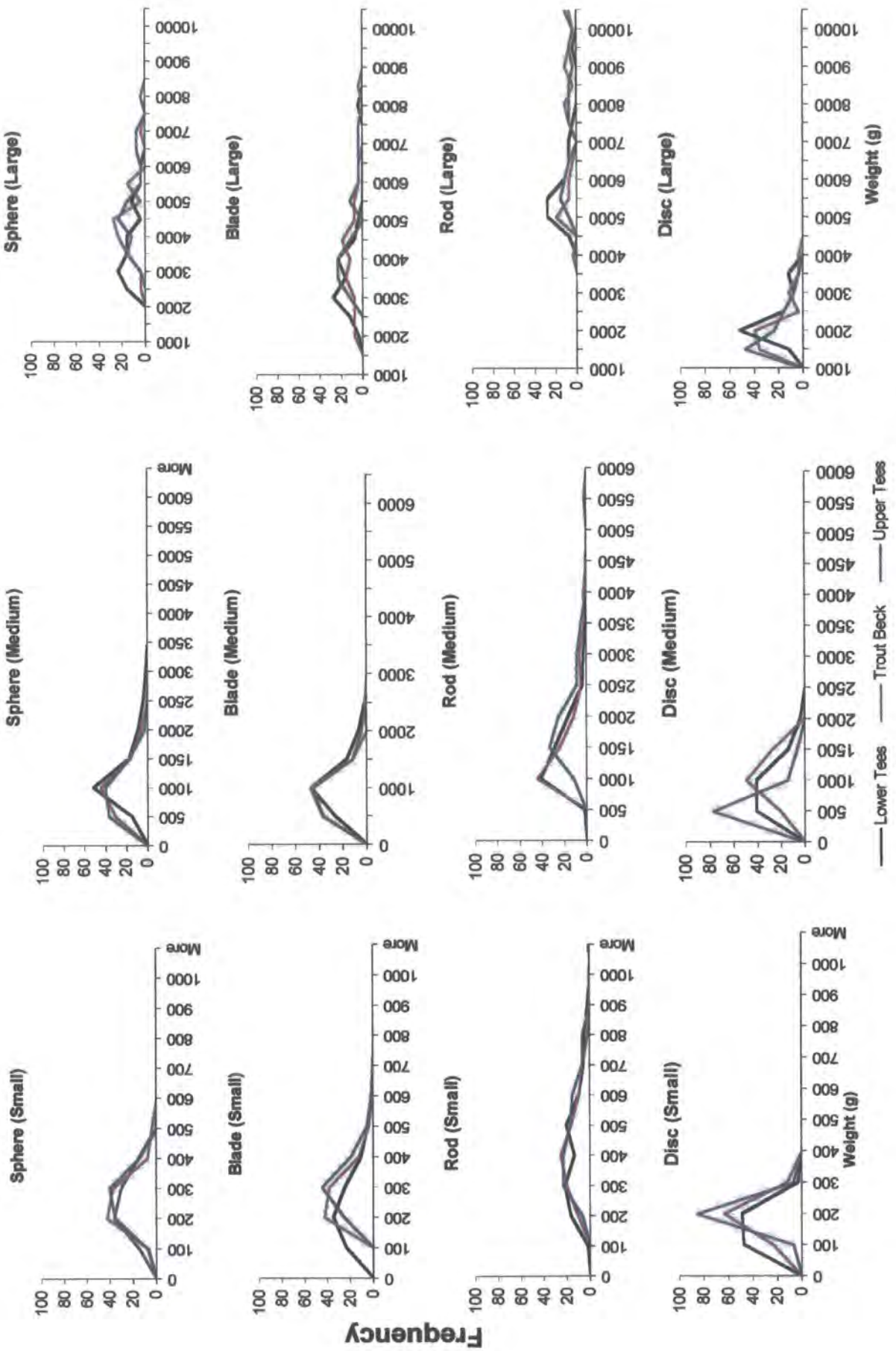

Figure A1.4 Frequency distributions of weight for four shapes and three size groups t Lower Tees, Trout Beck and Upper Tees.

kurtosis and minor positive skewness values at the Lower Tees site shows that the distributions of the particles cluster less around their mean value, while Trout Beck and the Upper Tees cluster more and are positively skewed and show a greater degree of kurtosis. In the medium size group at all three sites, distributions are similar with positive skewness and kurtosis values indicating that the weight of most particles is lower than the mean. In the large size group, the three sites have positive kurtosis and skewness values reflecting very wide but irregular frequency distributions, which are similar to these of sphere-shaped particles in the same size group. The higher standard deviation values of each distribution also suggests that there is a wide spread of values in weight for each site (Table A1.15).

Rod-shaped particles show no statistically significant differences between the three sites in the small and large size groups (Table A1.3). In the small size group, the Trout Beck and Upper Tees sites show very similar normal distributions with a lower degree of kurtosis and smaller standard deviation values, while Lower Tees has slightly higher positive kurtosis and skewness with longer tails (hence higher standard deviation). This indicates that the distribution of the particles by weight at the Lower Tees site is more dispersed than at the other sites (Figure A1.3 and Table A1.15). In the medium size group, however, all the sites show a greater degree of positive skewness and kurtosis. A slight statistical difference between the three sites is due probably to the fact that Upper Tees has greater mean values than the other sites. Although the three sites have positive skewness and kurtosis distributions, The Lower Tees has very high kurtosis which indicates that distributions cluster more around mean value and have shorter tails than at the other sites.

There is no significant difference between the three sites in the large size group and all sites have irregular frequency distributions. The Lower Tees and Trout Beck sites have comparable positive kurtosis, indicating a wider distribution than at the Upper Tees site.

In general, in all size groups, disc-shaped particles can be considered similar in the sense that they have a more symmetrical and a similar peaky *(leptokurtic)* frequency distribution as compared with other shapes (Figure A1.4). Table A1.4 shows that, except for the large size group, there are statistically significant differences between the three sites in the small and medium size groups. In the small size group all sites have almost normal frequency distributions with lower standard deviations and less kurtosis (Table A1.15). Statistically significant differences between the three sites might be

attributed to the fact that the Lower Tees has a lower mean and slightly wider distribution (slightly higher kurtosis) than the other sites (Table A1.15). In the medium size group, however, difference between the three sites occur because the Upper Tees site has a lower mean, higher positive-skewness and greater kurtosis (hence wider) than Lower Tees and Trout Beck. The Lower Tees and Trout Beck tend to be very similar in the sense that they have similar mean value and kurtosis.

Table A1.4 Calculated values of F (F ratio test) for comparison of size frequency distributions of weight for four shape classes in three size groups at the Lower Tees, Trout Beck and the Upper Tees sites.

	WEIGHT (g)		
SHAPES	Small	Medium	Large
SPHERE	0.22	**9.90**	4.60
BLADE	**14.88**	3.97	2.46
ROD	0.20	**9.88**	6.86
DISC	**22.49**	**37.13**	1.15

(The critical values of F at the 0.01significance level for small and medium size groups is 7.07 and for large size group is 7.61. The values shown in bold indicate a statistical significant difference between the compared parameters)

A1.4 b/a RATIO

The determination of the shape of a particle is conventionally based on the measurement of the three prime axes: the a (long), b (intermediate) and c (short) axes. From these three axes b/a and c/b ratios are determined. Using these ratios the shape of a particle is determined (e.g. form, sphericity,) (Krumbein, 1941). The b/a ratios (together with c/b ratio) can be used to calculate the degree of the sphericity of a particle, which is fundamentally important in both mode of transport (sliding, rolling etc.) and as well as settling velocity of a particle in a fluid flow (Sneed and Folk, 1958). The surface area of a particle depends on its b/a ratio (the ratio of the intermediate axis to the long axis). A particle with a greater b/a ratio and a lower c/b ratio tends have a relatively flat shape and therefore moves in a sliding mode. Flat-shaped particles also

tend to settle slowly compared to spherical ones. The b/a ratio of a particle also affects resting position (orientation) and imbrication. Apart from other factors such as shape and size, particle orientation is also considered to be one of the important controlling factors in the initial motion and the entrainment of a particle sitting on various beds. Investigations have shown that particles with low b/a ratios (either rod or blade shaped-particles), placed parallel to the flow, have threshold shear velocities nearly double those for the transverse situation (Carling *et al.*, 1992). Particle with a high b/a ratio and low c/b ratio tend to take-up an imbricated position more easily than spherical ones.

Table A1.5 Mean b/a ratios of four shape classes in three size groups at the Lower Tees, Trout Beck and the Upper Tees sites.

	Lower Tees				Trout Beck				Upper Tees			
	S	M	L	Mean	S	M	L	Mean	S	M	L	Mean
Sphere	0.85	0.86	0.88	0.86	0.87	0.86	0.84	0.86	0.87	0.87	0.85	0.86
Blade	0.50	0.52	0.53	0.52	0.48	0.52	0.51	0.50	0.44	0.52	0.52	0.49
Rod	0.45	0.44	0.50	0.46	0.42	0.46	0.51	0.46	0.44	0.48	0.53	0.48
Disc	0.85	0.86	0.88	0.86	0.85	0.84	0.88	0.86	0.83	0.84	0.86	0.84
Mean	0.66	0.67	0.70	**0.68**	0.66	0.67	0.69	**0.67**	0.65	0.68	0.69	**0.67**

Note: S: small size, M: medium size , L: large size

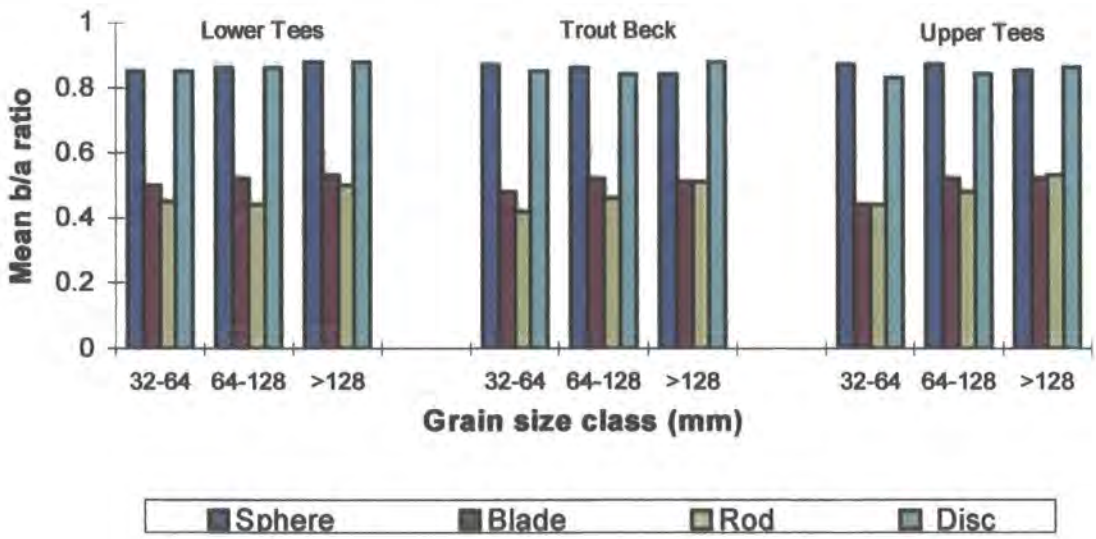

Figure A1.5 Mean distribution of b/a ratio of clasts in three size groups for four shape classes at the Lower Tees, Trout Beck and the Upper Tees sites.

Table A1.5 and Figure A1.5 show that there is little difference in mean b/a ratio among three sites (Lower Tees, 0.68; the Trout Beck and Upper Tees sites, 0.67). Within each size group and at each site, sphere-and disc-shaped particles have greater mean b/a ratios than blade-and rod-shaped particles.

Sphere-shaped particles at the three sites have the same b/a ratio, while in the blade-shaped category the ratios decrease from the Lower Tees to the Upper Tees. This indicates that the projected area of the blade-shaped particles tends to decrease from the Lower Tees to the Upper Tees, which affect their mode of transport (increasing settling velocity and imbrication). For rod-shaped particles, Lower Tees and Trout Beck have same ratio which is slightly smaller than for the Upper Tees. The disc-shaped particles show a similar distribution to the rod-shaped-particles at all three sites.

Table A1.6 Comparison of frequency distributions of b/a ratios in four shape classes and in three size groups at the three sites

SHAPES		Small	Medium	Large
SPHERE	F	2.47	0.76	2.45
	P	0.086	0.468	0.093
BLADE	F	**18.6**	0.18	0.76
	P	2.28E-08	0.827	0.471
ROD	F	5.32	7.03	1.66
	P	0.005	0.000	0.197
DISC	F	4.54	1.63	0.47
	P	0.011	0.198	0.627

(The critical values of F at the 0.01significance level for small and medium size groups is 7.07 and for large size group is 7.61. The values shown in bold indicate a statistical significant difference between the compared parameters)

Frequency distributions of sphere-shaped particles in all size groups are very similar and there is no statistically significant difference between the three sites (Table A1.6). Indeed, except for Trout Beck in the small size group, which has a moderate degree of peakiness (*mesokurtic*), within each size group, all sites show greater similarity with a common negative degree of kurtosis (*platykurtic*), indicating wide distribution of b/a ratios around the means (Table A1.15 and Figure A1.6). Except for Trout Beck and the Upper Tees sites in the small size group, positive-skewness is common at all sites in

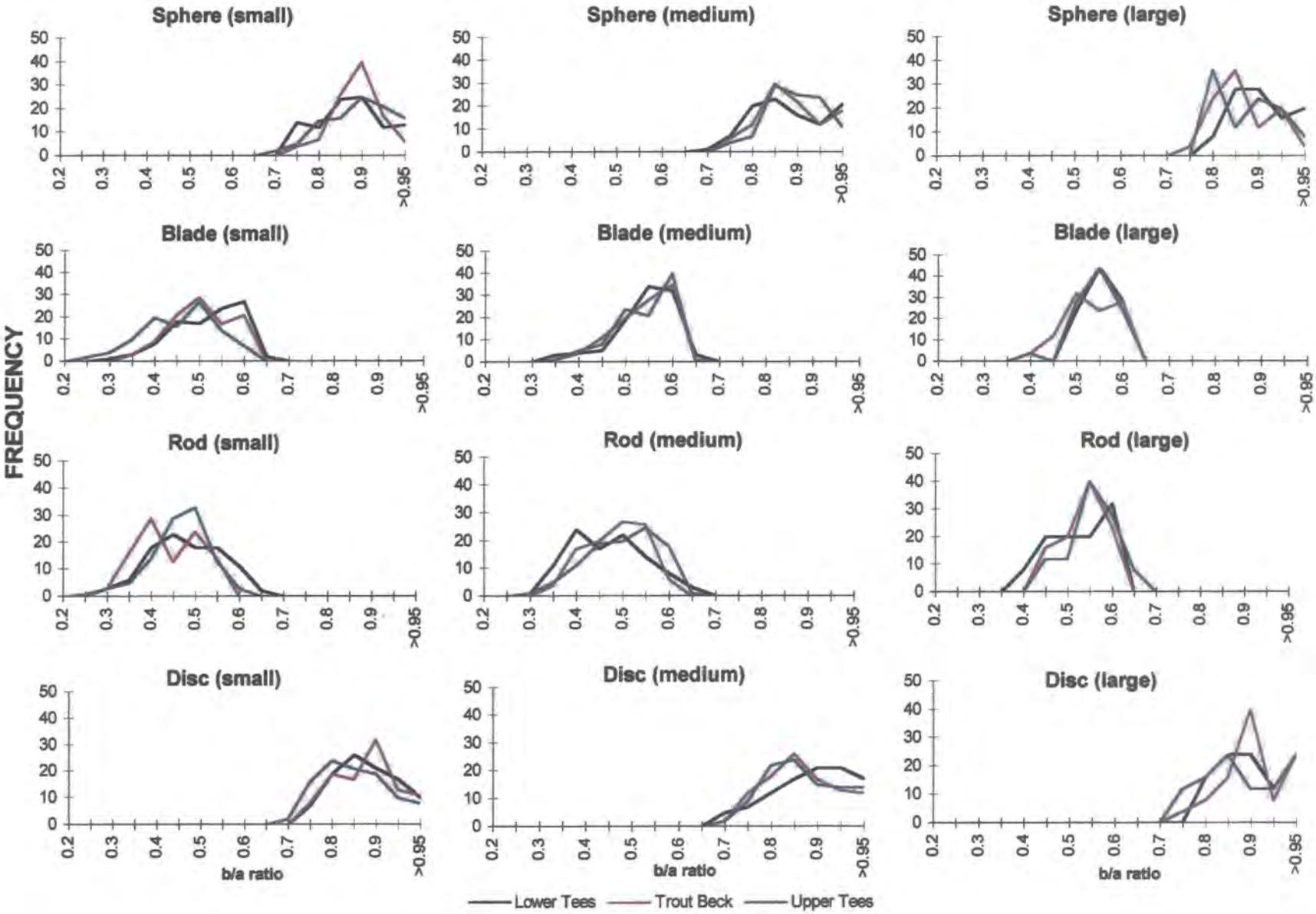

Figure A1.6 Frequency distributions of b/a ratios for four shaped classes within three size groups at Lower Tees, Trout Beck and Upper Tees.

the three size groups, showing that the b/a ratio of the majority of the particles is smaller than the mean. In the blade-shaped particles, all sites have negatively-skewed and also some irregular (bi-modal) distributions. However, Table A1.6 shows that there is no major difference between the three sites in both the medium and the large size groups. In the small size group, however, Table A1.15 shows that, in terms of their mean, median and mode values, there is a significant difference between the three sites. The Lower Tees and Trout Beck sites have very similar mean, mode and median values and within each site there is no major differences between these values. On the other hand, the Upper Tees has a lower mean value than The Lower Tees and Trout Beck sites and there is also a significant difference between mean, median and mode values. This indicates that, although the average value for b/a ratio at Upper Tees is 0.44, the most frequently occurring b/a ratio value in the distribution is 0.50 and thus the Upper Tees has a wider frequency distribution than the Lower Tees and Trout Beck.

For the rod-shaped particles, Table A1.6 indicates that there is no statistical difference for all size groups between the three sites. In the small size group all sites show negatively-skewed distributions, indicating that most frequently occurring b/a ratio values within each distribution greater than their mean value. The mean values of the b/a ratios are 0.42, 0.44 and 0.45 for the Trout Beck, Upper Tees and Lower Tees sites respectively (Table A1.5). The Lower Tees and Trout Beck sites tend to have wider and relatively flat (*platykurtic*) distributions, while the Upper Tees has a moderate degree of peakiness with a lower standard deviation (Table A1.15 and Figure A1.6). In the medium size group, means of the b/a ratios tend to increase from Lower Tees (0.44) to Upper Tees (0.48). All sites have some degree of negative kurtossis, which indicate relatively flat distributions. The Trout Beck and Upper Tees sites show negative skewness, while the Lower Tees shows positive skeweness but an irregular frequency distribution. This indicates that b/a ratios Trout Beck and Upper Tees tend to be greater than at the Lower Tees site (Figure A1.6). In the large size group, however, Table A1.6 reveals no significant difference between the three sites. Small standard deviations indicate that distributions are clustered around the means (Table A1.15).

In terms of disc-shaped particles, at all sites all three size groups have very similar distributions and there is no statistically difference between them. Figure A1.6 and Table A1.15 clearly show that all sites have somewhat flatter and wider frequency distributions when compared to the other shape categories. Table A1.6 reveals that there is no statistically significant difference between the three sites in the medium size

category.

A1.5 c/b RATIO

The ratio of particle short axis "c" to intermediate axis "b" describes the degree of flattening which influences significantly a particle's rolling or sliding capability (Krumbein, 1942; Sneed and Folk, 1958; Carling *et al.*, 1992). There is a positive relationship between particle c/b ratio and rolling capability. Particles with a low c/b ratio tend to slide, whereas those with high c/b ratios tend to roll in a fluid flow. Therefore the c/b ratio is an important factor for the hydraulic behavior of a particle and should be examined in bedload studies.

Table A1.7. Mean C/B ratios of the four shape classes in three size groups at the Lower Tees, Trout Beck and the Upper Tees sites.

	Lower Tees				Trout Beck				Upper Tees			
	S	M	L	Mean	S	M	L	Mean	S	M	L	Mean
Sphere	0.84	0.85	0.81	0.83	0.84	0.84	0.84	0.84	0.85	0.85	0.87	0.86
Blade	0.40	0.41	0.41	0.41	0.37	0.37	0.42	0.39	0.37	0.34	0.42	0.38
Rod	0.84	0.82	0.80	0.82	0.83	0.83	0.82	0.83	0.85	0.80	0.81	0.82
Disc	0.40	0.37	0.36	0.38	0.38	0.33	0.33	0.35	0.4	0.35	0.33	0.36
Mean	0.62	0.61	0.60	0.61	0.61	0.59	0.60	0.60	0.62	0.59	0.61	0.60

Note: S: small size, M: medium size, L: large size

Figure A1.7, Tables A1.7 and A1.8 show that there is no significant difference in mean c/b ratios between the three sites (the Lower Tees site, 0.61; Trout Beck and Upper Tees sites, 0.60). Not surprisingly, within each size group and at each site, sphere-and rod-shaped particles always have greater mean c/b ratio than blade and disc-shaped particles (Table A1.7). In terms of sphere-shaped particles at the Lower Tees site, it is clear that there is no significant difference between the mean c/b ratio of the small and medium size groups but mean ratios are slightly smaller in the large size group. This may indicate that the larger size sphere-shaped particles tend to have less rolling capability than that of small and medium size groups due to their more irregular shape.

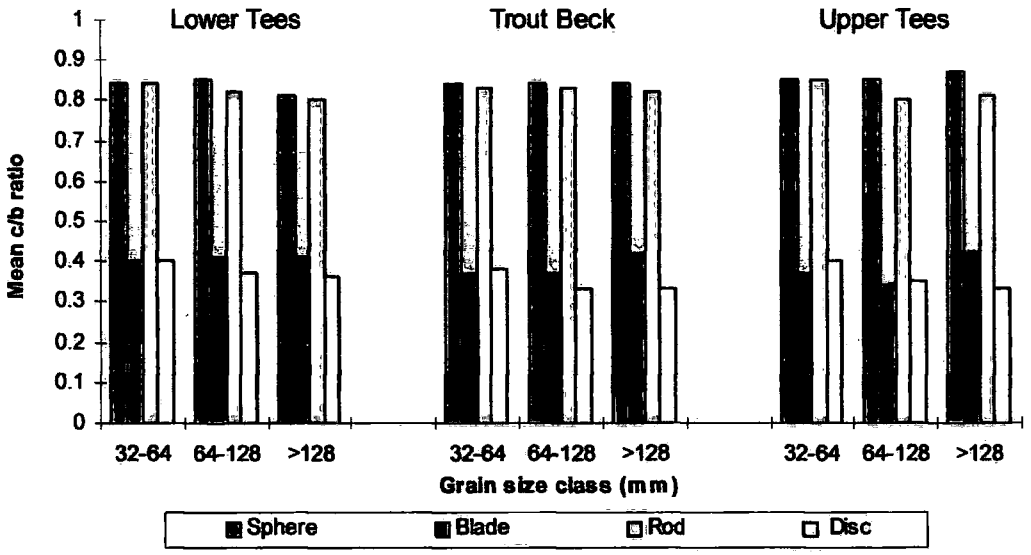

Figure A1.7 Mean distribution of c/b ratio of clasts in three size groups for four shape classes at the Lower Tees, Trout Beck and the Upper Tees sites.

For blade-shaped particles, the three size groups have exactly the same mean values at the Lower Tees site but at the Trout Beck and Upper Tees sites the largest sized particles have greater mean c/b ratio than the smaller and median size group of blades. For rod-shaped particles the small size groups have greater mean b/a ratios. This suggests that particles in the small size groups can roll more easily than those of the larger sizes. Disc-shaped particles show greater c/b ratios in the small size group and as particle size increases the c/b decreases gradually. Decreasing c/b ratio of a particle primarily affects its weight. In other words particles with lower c/b ratio are generally lighter than those with higher c/b ratios. Several investigators have pointed out that disc-shaped particles with a low c/b ratio but high b/a ratio, which makes them lighter, can preferably be lifted and transported further downstream than other shaped particles (Bradley *et al.*, 1972).

Table A1.8 Comparison frequency distributions of c/b ratios in the four shape classes and in the three size groups at three sites

SHAPES		c/b ratio		
		Small	Medium	Large
SPHERE	F	1.39	0.45	3.51
	P	0.25	0.640	0.034
BLADE	F	5.28	**12.01**	0.45
	P	0.005	9.59E-06	0.639
ROD	F	2.06	3.50	0.64
	P	0.129	0.031	0.530
DISC	F	1.66	**7.43**	1.92
	P	0.191	0.000	0.155

The critical values of F at the 0.01significance level for small and medium size groups is 7.07 and for large size group is 7.61. The values shown in bold indicate a statistical significant difference between the compared parameters)

The frequency distributions of sphere-shaped particles in all size groups show similarity between the three sites (Figure A1.8 and Table A1.8). Although there is no significant statistical difference between the three sites, in the large size group, the three sites show some minor differences. The Lower Tees site has a bi-modal distribution, while Trout Beck tends to have a normal distribution with a low standard deviation and a slight positive skew. The Upper Tees site has a negatively-skewed distribution, indicating that the majority of particles have greater c/b ratio than the mean. For blade-shaped particles, there is no statistical difference between the three sites in small and large size groups. In the small size group, all sites have positive skewness and a relatively flat (platykurtic) distribution. For the large size group, the Trout Beck and Upper Tees sits show rather flat, slightly bi-modal distributions, while the Lower Tees is very peaky and negatively skewed (Figure A1.8). In the medium size group, there is statistical difference between the three sites. Despite their similar skewnsses, the three sites show some degree of differences in their kurtosis degrees. The Lower Tees shows a very platykurtic distribution compared to the other sites (Table A1.15).

In the rod-shaped clasts, the common similarity between the three sites is that all sites have relatively flat distributions in all size classes. However, in the large sizes the flatness of the distribution decreases in a way similar to the distributions of sphere and

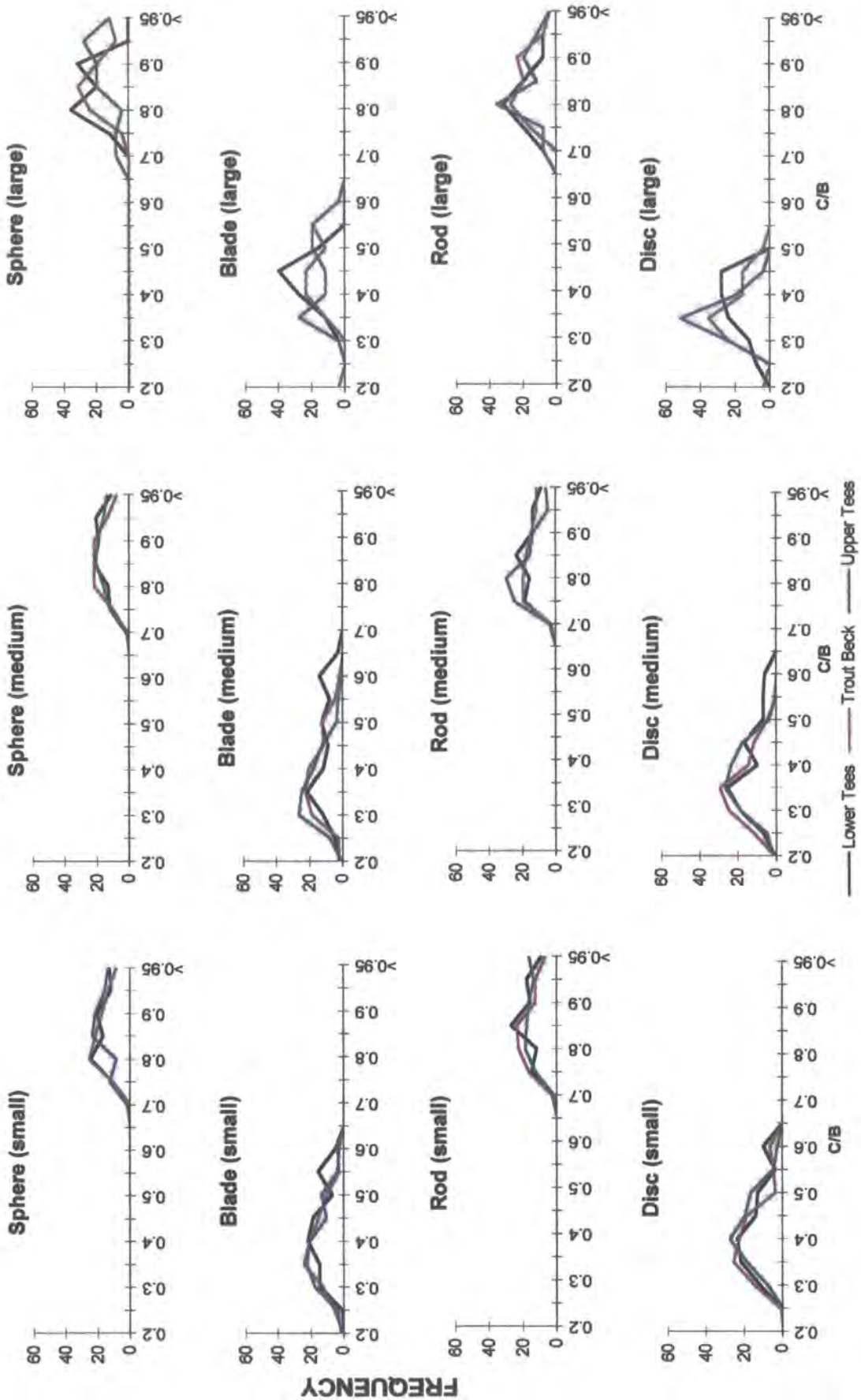

Figure A1.8 Frequency distributions of c/b ratios for four shaped classes within three size groups at Lower Tees, Trout Beck, Upper Tees.

blade-shaped particles. Nevertheless, Table A1.8 indicates that there are no statistically significant differences between the three sites in the various size groups.

In the small and medium size groups, all disc-shaped particles show wide platykurtic distributions, which are similar to those of rod-shaped particles. There are no significant differences among them (Figure A1.8 and Table A1.8). In large size group there is no statistically significant difference between the three sites, but Figure A1.8 and Table A1.15 indicate that Lower Tees has very low kurtosis with a negatively skewed distribution, while Trout Beck and the Upper Tees have positively-skewed distributions. This indicates that at the Lower Tees site there is a wide distribution of c/b ratios around their mean and most of the ratios are between 0.20 and 0.55. On the other hand at the Trout Beck and Upper Tees sites it varies between 0.25 and 0.60 and distributions of c/b ratios are more clustered around their means.

A1.6 ROUNDNESS

Roundness is the relationship of the outline or image of the particle to a circle, often defined as the ratio between the radius of curvature of the particle and that of an inscribed circle (Briggs, 1977). Roundness relates to the sharpness of the corners and the edges of a particle. In a fluid flow and between the similar shapes, particles with high roundness are said to have a greater rolling potential than those of low roundness. A comprehensive review of roundness, including the means by which roundness values are determined, is given in Chapter 2.

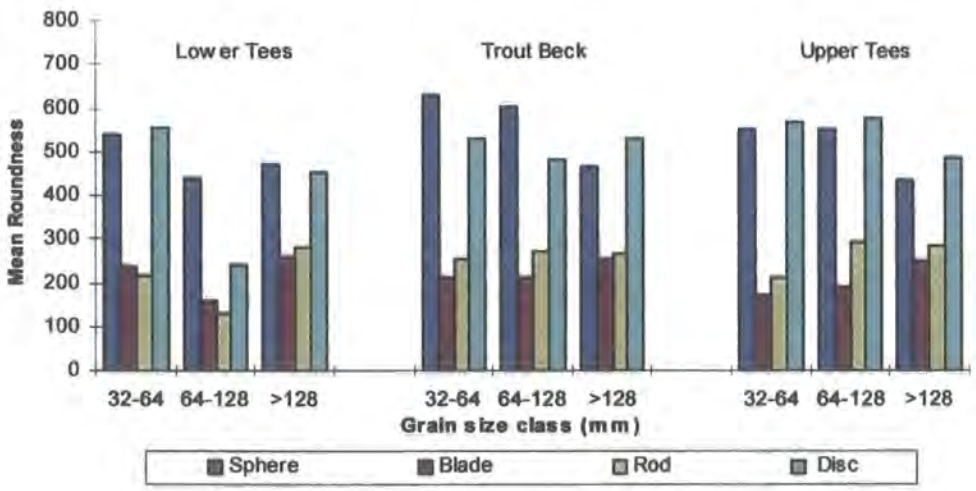

Figure A1.9 Mean roundness distributions of particles in the three size groups and for the four shape classes at the Lower Tees, Trout Beck and the Upper Tees sites.

In all three-size groups, mean roundness values at the three sites vary between 322 (Lower Tees) and 392 (Trout Beck). There is a small difference between the Trout Beck and Upper Tees sites, but an even greater difference between these sites and the Upper Tees. Figure A1.9 shows the roundness distributions of particles in three size groups for four shape classes at the three sites. This shows that within each size group, sphere-and disc-shaped particles have greater mean roundness values than rods and blades. In general, The decreasing order of mean roundness values at the Lower Tees site are spheres, discs, blades and rods respectively. At the Trout Beck Upper Tees sites the order is spheres, discs, rods and blades (Table A1.9). Figure A1.9 and Table A1.10 also suggest that, although there is no significant difference in the mean roundness values between sphere-and disc-shaped particles within each size group for three sites, the differences increases noticeably between sphere and the other-shaped particles. Table A1.9 also reveals that there is no pattern to changes in the mean roundness values between rod and blade-shape particles from one size group to another, though spheres and discs in the small size group always have greater mean values than the medium and large sizes. This is particularly important for sphere-shaped particles. Because particles with higher roundness in the small size group may roll much more easily than larger ones that have lower roundness and therefore irregular shape.

Table A1.9. Mean roundness values for four shapes in the three size groups at the Lower Tees, Trout Beck and the Upper Tees sites.

	Lower Tees				Trout Beck				Upper Tees			
	S	M	L	Mean	S	M	L	Mean	S	M	L	Mean
Sphere	537	439	468	481	626	601	465	564	553	550	435	513
Blade	238	158	260	219	211	211	254	225	173	189	248	203
Rod	214	127	279	207	252	273	266	264	212	293	282	262
Disc	554	239	453	415	531	481	531	514	568	578	488	545
Mean	386	241	365	331	405	392	379	392	377	403	363	381

Note: S: small size, M: medium size , L: large size.

Frequency distributions of roundness show some irregularities with different degree of skewness and kurtosis in the three sizes and four shape classes at the sites

(Figure A1.10). In general, sphere and disc-shaped particles in each size group and at all sites show wider roundness distributions (hence lower kurtosis) than blade and rod-shaped particles (Figure A1.10). This implies that particles are not very similar in terms of their roundness and, therefore, even within one size range, there would be some differences in mode of movement due to variations in roundness of particles. At all three sites and for all three size categories, blade and rod-shaped particles have lower roundness values and also lower standard deviations than discs and spheres. This indicates that roundness values of blade and rod-shaped particles are closely distributed around the mean (Table A1.15) and that such particles tend to move in a sliding mode due to low roundness.

Table A1.10 Calculated values of F (the F ratio test) for comparison of three means in roundness for four shape classes and in three size groups at the three sites.

SHAPES		Small	Medium	Large
SPHERE	F	6.63	**18.52**	0.33
	P	0.001	2.63E-0.8	0.722
BLADE	F	**13.04**	**8.06**	0.07
	P	3.71E-06	0.000	0.932
ROD	F	4.08	**69.24**	0.15
	P	0.017	2.07E-25	0.855
DISC	F	0.95	**79.02**	1.21
	P	0.387	3.03E-28	0.301

(The critical values of F at the 0.01significance level for small and medium size groups is 7.07 and for large size group is 7.61. The values shown in bold indicate a statistical significant difference between the compared parameters)

Table A1.10 reveals that, except blade-shaped particles in the small size group, there is no statistically significant difference between the three sites in small and large size groups. Sphere-shaped particles in almost each size group show somewhat irregular roundness distributions. Despite a similar distribution in the small size group, in the medium size, Lower Tees shows a highly positively skewed distribution, while Trout Beck has negative skewness and Upper Tees shows a wide but normal distributions. This distributions indicate that due to its positively skewness particles at the Lower Tees site are less rounded than the other sites, while at the Upper Tees site, because of negative skeweness, they are more rounded (Figure A1.10 and Table A1.9).

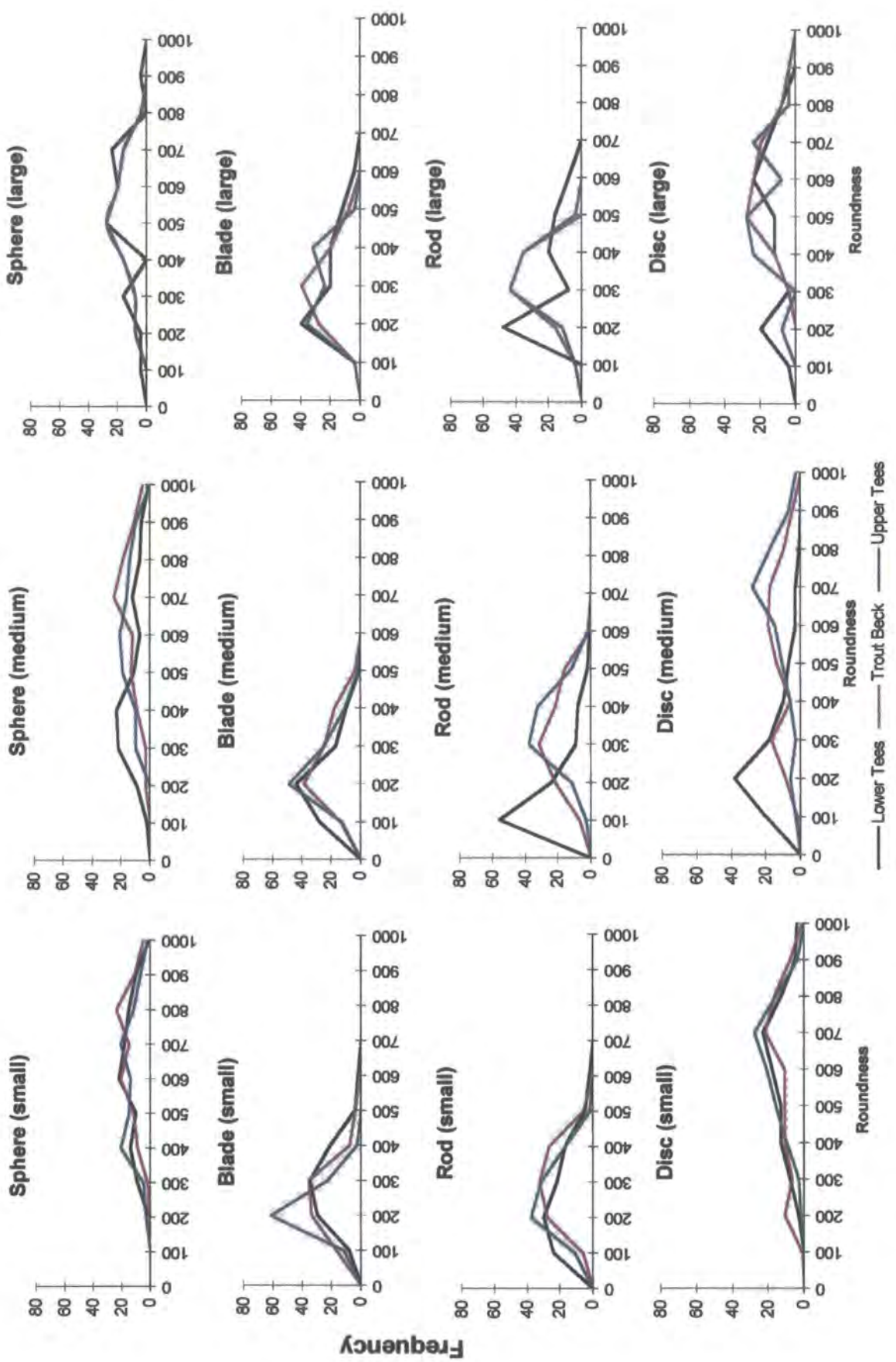

Figure A1.10 Roundness frequency distributions of the tracers in three size groups and for four shape classes at Lower Tees, Trout Beck, Upper Tees.

In the larger size group the three sites have relatively similar distributions and therefore there is no statistically significant difference between the three sites (Table A1.10). Median values of the distributions vary between 434 (Upper Tees) and 497 (Lower Tees), indicating that most of the particles have roundness values around 400 despite their wider distributions at the three sites (Figure A1.10 and Table A1.9).

In terms of blade-shaped particles, Figure A1.10 shows that, generally, at all the sites frequency distributions are narrower and more peaked than those of sphere and disc-shaped particles. Narrower ranges of distributions imply that particles in each of the distributions have very similar roundness values. They also all have positively-skewed distributions with different degrees ranging from 0.18 (Upper Tees) to 0.88 (Lower Tees) (Table A1.15), which indicate lower roundness values than those of negative skewness. Comparison of the three sites indicates that, in the small and medium size groups, there are statistically significant differences between the three sites. In the small size group, Upper Tees shows a very high degree of kurtosis (*leptocurtic*), while The Lower Tees and Trout Beck sites have comparable distributions with a moderate degree of kurtosis (*mesokurtic*). These various distributions signify that The Lower Tees and Trout Beck sites have relatively large range roundness distributions (between <100 and >700), while at Upper Tees the range is relatively narrow (between 100 and 400) and most of the particles are clustered around their mean (Figure A1.10). In the medium-size blade class, however, a significant difference between the three sites is probably due to different standard deviations (Table A1.15). Most of the particles are distributed between a range of 200 and 300 roundness (Figure A1.10). Table A1.10 also shows no significant differences between three sites in the large size, though Figure A1.10 reveals some dissimilarity between the distributions of three sites. The Lower Tees tends to have greater positive skeweness as compared to Trout Beck and Upper Tees, while Trout Beck has an almost normal distribution and the Upper Tees shows an almost bi-modal distribution.

Frequency distributions of rod-shaped particles in the medium-size group show large differences in roundness between the three sites. In the small and large size classes, however, there is no statistical a difference (Table A1.10). In the medium size groups, the Lower Tees has a higher positive-skew than Trout Beck and Upper Tees. This indicates that at the Lower Tees site the majority of the particles in the distribution have lower roundness values than the mean value. On the other hand, Trout Beck and Upper Tees show similar distribution with lower kurtosis and greater standard

deviations (Figure A1.10 and Table A1.15).

In terms of disc-shaped particles, Table A1.10 and Figure A1.10 show that, despite small differences in the mean roundness values as well as similar frequency distributions among the three sites in the small size group, variations between the three sites are more significant in the medium size group. In the medium size group the Lower Tees site shows a low mean roundness, high kurtosis and strong positively skewed frequency distribution when compared to Trout Beck and Upper Tees. In the large size group, the distributions tend to be uneven with varying degrees of skeweness and kurtosis Table A1.10 and Figure A1.10).

A1.7 SPHERICITY

The rollability of a particle is primarily related to its degree of sphericity and roundness. Spherical particles tend to roll faster than non-spherical ones (e.g. Krumbein, 1942b; Sneed and Folk, 1958). The greater the departure of a particle from a spherical shape, the greater is the reduction in its rolling capability and the more irregular is its motion during transport (Komar and Reimers, 1978, Pye, 1994). Sphericity also has an important influence on particle settling velocity. Particles with higher sphericity settle more rapidly (Wadell, 1932). The possible range in sphericity values varies from 0 for a perfectly flat disc to 1 for a perfect sphere (Krumbein, 1941; Sneed and Folk, 1958). The more the departure from a spherical shape the lower its sphericity values. However, in nature it is very difficult to find a perfect sphere with a value 1.0 (for more detail see Chapter 2).

For the three size groups, regardless of shape, mean sphericity values vary between 0.59 and 0.62 at the three sites (Table A1.11). Generally, small and medium size particles tend to have greater mean sphericity values than the larger ones. In terms of shape, not surprisingly, within each size group sphere-shaped particles always have greater mean sphericity values, while disc and blade-shaped tracers have the lowest values (Figure A1.11, Table A1.11). Mean sphericity values are very similar and vary between 0.84 and 0.86 in the sphere-shaped particles in all size groups at the three sites. Large size spheres, at Trout Beck and Lower Tees have slightly lover sphericity values than that those of small and medium size. With blade-shaped particles the lowest value is 0.30 at the Upper Tees site in the large size group and the highest value is 0.48 at Lower Tees in the small size group. At Lower Tees and Trout Beck sites particles in

large size groups have greater mean sphericity values than that of small and medium size groups. For the rod-shaped particles, regardless of size, the Upper Tees has greater mean sphericity values (0.58) than the Lower Tees and Trout Beck sites, which have the same sphericity (0.56). There tends to be an increase in sphericity as particle size increase at all the sites (Table A1.11). This indicates that particles in the large size group tend to roll easier than those of smaller one. For disc-shaped particles, however, regardless of shape, ranges of mean sphericity vary between 0.58 (Upper Tees) and 0.65 (Upper Tees). Lower Tees and Trout Beck sites show much greater mean sphericity values (0.65 and 0.63) than the Upper Tees site (0.58). This implies that particles at Lower Tees and Trout Beck sites may have greater rolling capability than at the Upper Tees site. In general, at each of the sites small discs are slightly more spherical than those of larger sizes. (Table A1.11). For all the three size groups at Lower Tees and Trout Beck sites the increasing orders of mean sphericity values are blade, rod, discs and sphere. Upper Tees also shows a similar trend, except for the medium size group in which disc-shaped particles have a lower mean value than rod-shaped particles.

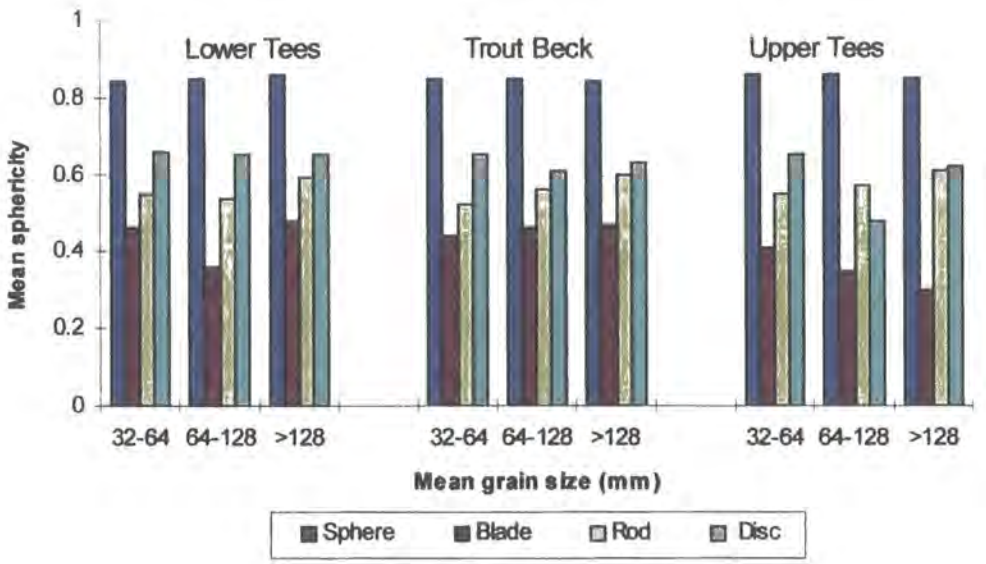

Figure A1.11 Mean sphericity distributions of clasts in three size groups and for four shape classes at the Lower Tees, Trout Beck and Upper Tees sites.

Table A1.11. Mean sphericity values of four shape classes in three size groups separately and three sizes group all together at Lower Tees, Trout Beck and Upper Tees sites.

	Lower Tees				Trout Beck				Upper Tees			
	S	M	L	Mean	S	M	L	Mean	S	M	L	Mean
Sphere	0.84	0.85	0.86	0.85	0.85	0.85	0.84	0.85	0.86	0.86	0.85	0.86
Blade	0.46	0.36	0.48	0.43	0.44	0.46	0.47	0.46	0.41	0.35	0.30	0.35
Rod	0.55	0.54	0.59	0.56	0.52	0.56	0.60	0.56	0.55	0.57	0.61	0.58
Disc	0.66	0.65	0.65	0.65	0.65	0.61	0.63	0.63	0.65	0.48	0.62	0.58
Mean	0.63	0.60	0.65	0.62	0.62	0.62	0.64	0.62	0.62	0.57	0.60	0.59

Note: S: small size, M: medium size , L: large size.

Table A1.11 shows that, in general, there is no major difference between three sites in the mean sphericity values of sphere-and rod-shaped particles, while in the blade-shaped it varies between 0.35 and 0.46 and for disc-shaped the range is 0.58 and 65. Table A1.12 and Figure A1.12 show that frequency distributions of sphere-shaped particles in each size group at all three sites are virtually the same at each site. Small differences in the mean and medium values indicate that they have normal or bell-shaped distributions (Table A1.15).

Table A1.12. Comparison of sphericity frequency distributions in four shape classes for three size groups at three sites

SHAPES		Sphericity		
		Small	Medium	Large
SPHERE	F	3.18	1.18	0.99
	P	0.043	0.308	0.373
BLADE	F	**27.57**	**225.92**	**280.45**
	P	1.04E-11	2.28E-60	1.04E-34
ROD	F	6.49	5.69	1.51
	P	0.001	0.003	0.227
DISC	F	1.12	**220.88**	1.93
	P	0.327	1.7E-59	0.152

(The critical values of F at the 0.01significance level for small and medium size groups is 7.07 and for large size group is 7.61. The values shown in bold indicate a statistical significant difference between the compared parameters)

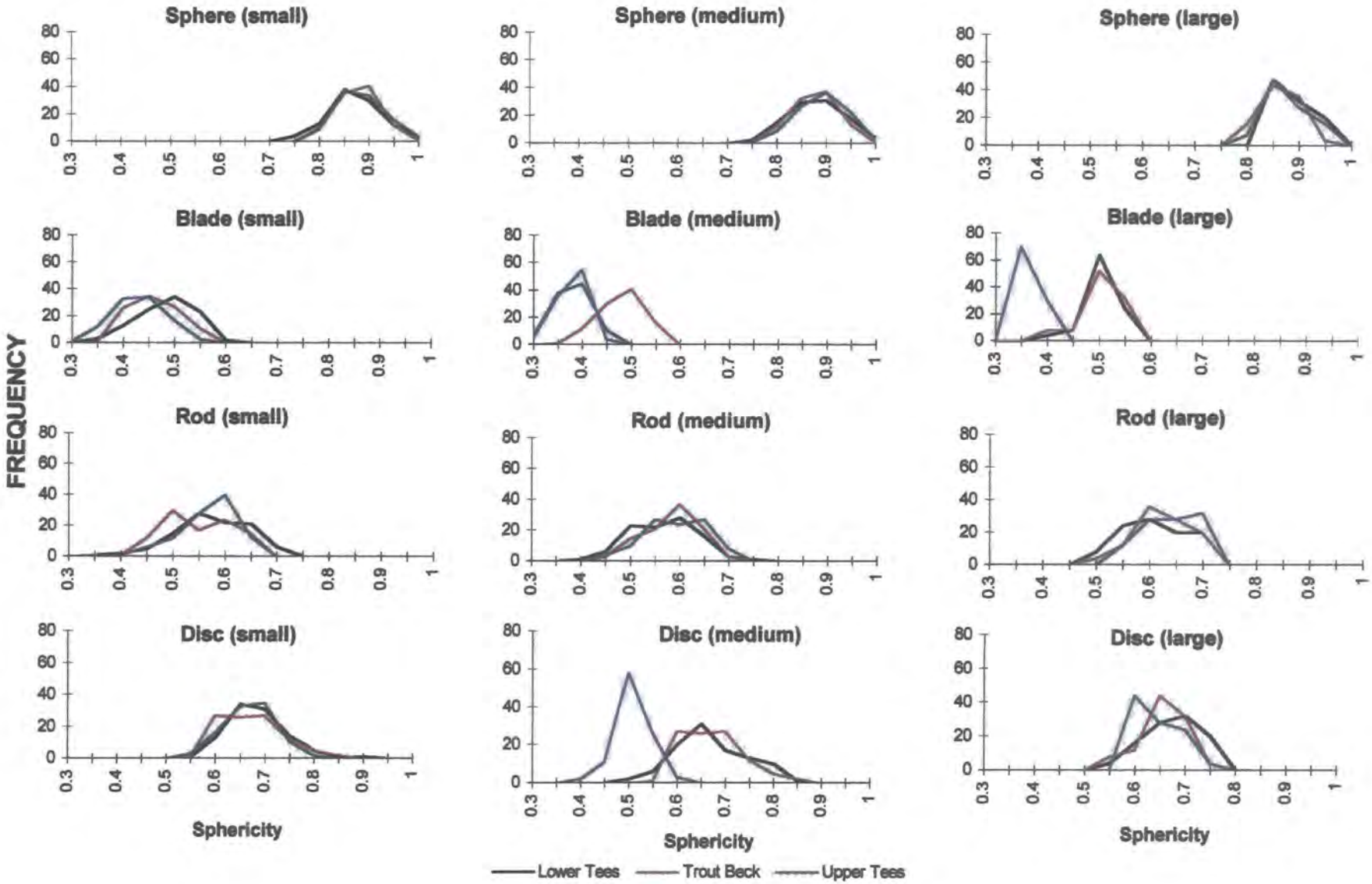

Figure A1.12 Frequency distributions of the sphericity of the tracers in three size groups and for four shape classes at Lower Tees, Trout Beck, Upper Tees.

For blade-shaped particles the difference between the three sites shows much greater variation both within size groups as well as between size groups. In the small size class there is statistically significant difference in the frequency distribution of the three sites (Table A1.12). Though the Trout Beck and Upper Tees sites show almost normal distributions, the Lower Tees site shows a slightly negatively skewed distribution indicating a slightly greater mean sphericity value than the other sites. However, for the medium size particles, marked differences occur between the three sites. Although there is no major difference between the Lower Tees and Upper Tees sites, it increases significantly between Trout Beck and the Lower and Upper Tees sites. With a negative skewness, Trout Beck shows a greater mean sphericity (0.46) and thus represents a significant difference in the frequency distribution in comparison with the Lower Tees and Upper Tees sites which have similar distributions and mean values of 0.36 and 0.35 respectively (Table A1.11 and Figure A1.11). For the large size blade-shaped particles there is also a major difference between the three sites. This is because the three sites have different degrees of skewness, indicating different ranges of sphericity values. Indeed, Figure A1.12 and Table A1.11 reveal that though the Lower Tees and Trout Beck sites have very similar frequency distributions (the range varies between 0.40 and 0.55) and also similar mean sphericity values (Lower Tees: 0.48 and Trout Beck: 0.47), Upper Tees shows a relatively lower mean sphericity value (0.30) and also a lower range of sphericity values (0.30).

The frequency distributions of rod-shaped particles, in all three size groups, have similar distributions, which are wider than for sphere and blade particles. Comparison of the three sites indicates there is no major statistical differences between the three sites in all size groups. Disc-shaped particles (Figure A1.12) show frequency distributions which have a high degree of kurtosis (leptokurtic distributions) (Table A1.15). However, in the medium size group, Upper Tees has a much lower mean sphericity and a very peaked (leptocurtic) frequency distribution (Table A1.11). This may indicate that the particles at Upper Tees may have less rolling capability than the other sites.

A1.8 FLATNESS

Flatness is conventionally based on the relationship between the three primary axes of a particle and ranges from 100 to infinity. The minimum value relates to a perfectly equidimensional particle, and the flatter the particle the higher is the flatness index. This is also essentially the inverse of Krumbein's sphericity (Briggs, 1977).

Comparison of Tables A1.11 A1.and 13 clearly show that in almost each size group flatness index has a very high inverse correlation with sphericity. Not surprisingly, there is a strong inverse relationship between a particle's rolling capability and its flatness value. The flatter a particle is the more likely the particle will be to slide, instead of roll. In addition, many investigators have already examined the influence of the flattening on the settling velocity of a particle (see Chapter 7). These studies have clearly shown that the more particles are flattened, the slower they will settle compared with a sphere of the same volume and density.

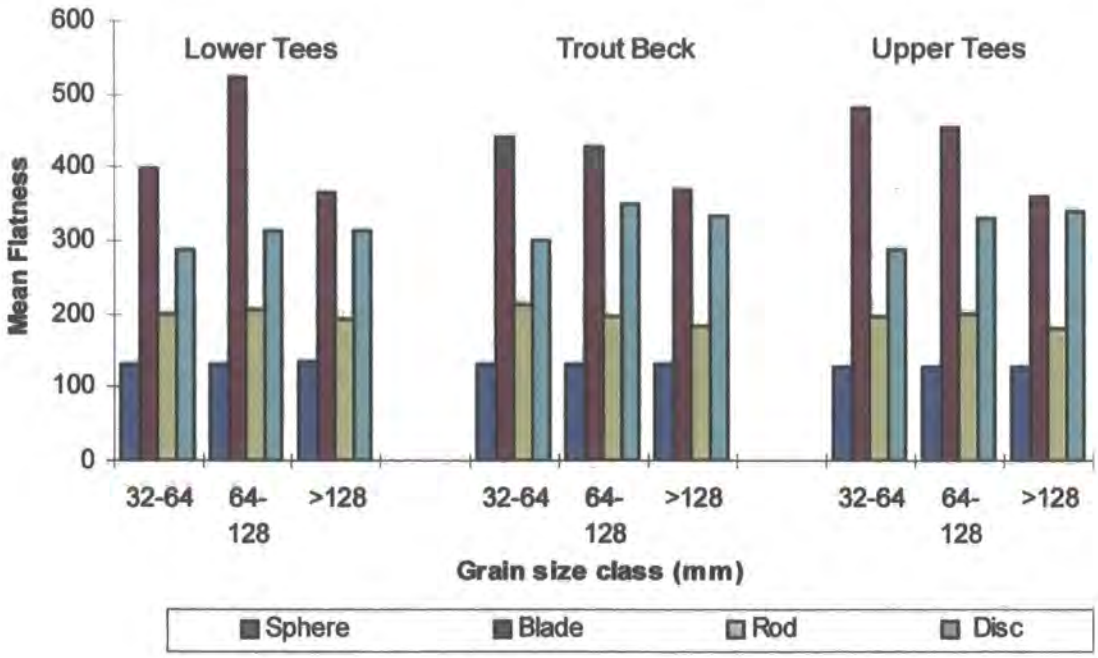

Figure A1.13 Mean flatness distributions of the tracers for the three sites.

Table A1.13. Mean flatness values of four shape classes in three size groups at the Upper Tees, Lower Tees and Trout Beck.

	Lower Tees				Trout Beck				Upper Tees			
	S	M	L	Mean	S	M	L	Mean	S	M	L	Mean
Sphere	131	129	132	131	130	130	131	130	127	128	127	127
Blade	396	523	365	428	441	427	370	413	480	453	359	431
Rod	198	205	191	198	212	195	182	197	197	197	180	192
Disc	288.5	313	313	304	300	350	334	328	287	328	338	318
Mean	253	293	251	265	271	276	254	267	273	277	251	267

Note: S: small size, M: medium size , L: large size.

Generally, the three sites have very similar mean flatness values, which vary from 265 (Lower Tees) to 267 (Trout Beck and Upper Tees) (Table A1.13). Figure A1.13 shows that, except for blade-shaped particles at Lower Tees, all shapes have similar mean flatness values for the three size groups. At each site blade-shaped particles have the greatest flatness values, while, not surprisingly, sphere-shaped have the lowest flatness. In rank order flatness increases from sphere, rod, disc through blade-shapes. Although it is not very important for the sphere and rod shaped-particles, mean flatness values of blade and disc-shaped particles in the small and medium size groups varies. As particle size increases the mean flatness decreases for blade-shaped particles and the difference between blades and discs also decreases (Figure A1.13).

Table A1.14. Comparison in frequency distributions of flatness in four shape classes for three size groups at three Sites

SHAPES		Flatness		
		Small	Medium	Large
SPHERE	F	2.30	0.75	1.43
	P	0.102	0.472	0.245
BLADE	F	16.25	14.37	0.14
	P	1.98E-07	1.1E-06	0.87
ROD	F	6.05	2.81	1.32
	P	0.002	0.062	0.273
DISC	F	1.65	5.70	1.01
	P	0.194	0.004	0.366

(The critical values of F at the 0.01significance level for small and medium size groups is 7.07 and for large size group is 7.61. The values shown in bold indicate a statistical significant difference between the compared parameters)

Figure A1.14 shows that sphere and rod shaped-particles always have very symmetrical leptokurtic normal frequency distributions, whereas blade and disc-shaped particles have relatively 'flat' distributions, In the sphere and rod shaped groups most of the particles are distributed mainly between 100 and 300 flatness values, while for blade and disc shape groups the ranges vary between 100 and 1000 (Figure A1.14).

Table A1.14 shows that there is no statistically significant difference between the three sites within each size group in the sphere, rod and disc-shaped categories. For the sphere and rod-shaped particles almost all sites have relatively normal frequency distributions with low standard deviations (Table A1.15). For the disc-shaped particles, however, the standard deviation values increase. In terms of blade-shaped-particles, Figure A1.14 clearly shows that all sites have very wide distributions in all three size groups. Table A1.14 also indicates that there are statistically significant differences between the sites in the small and medium size categories. It is clear in Figure A1.14 and Table A1.15 that as particle size increases, the differences between the mode and mean decreases (lower lesser standard deviation) and the distribution becomes narrower.

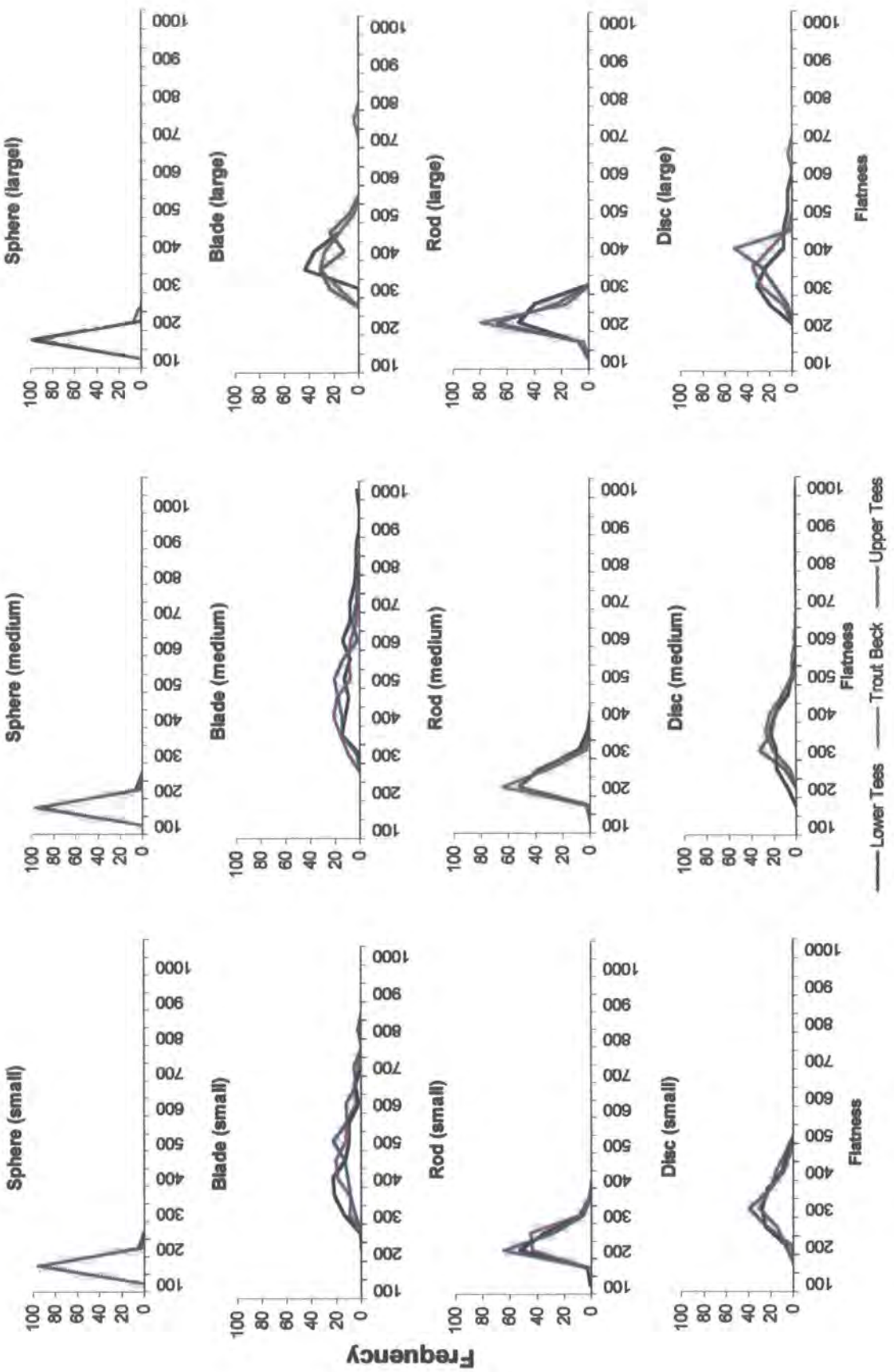

Figure A1.14 Frequency distributions of flatness of the clasts for four shape classes and in three size groups at Lower Tees, Trout Beck, Upper Tees.

Table A1.15a. Summary of the size and shape characteristics of magnetic tracers used at the Lower Tees site.

SPHERE										
Number of clasts: 100				32-64 mm						
	a-axis	b-axis	c-axis	Radius	b/a	c/b	Round-ness	Spheri-city	Flat ness	Weight (g)
Mean	6.16	5.20	4.39	1.65	0.85	0.84	537	0.84	131	207
median	6.20	5.35	4.40	1.50	0.85	0.84	566	0.84	130	197
mode	6.40	6.00	4.00	2.00	0.86	0.79	351	#N/A	136	87
skewness	-0.15	-0.32	-0.09	0.27	0.06	0.13	-0.18	0.19	0.1	0.2
Kurtosis	-0.48	-1.28	-0.81	-0.72	-0.60	-0.91	-0.96	-0.24	-0.4	-0.9
Stn. Dev.	1.06	0.86	0.83	0.64	0.08	0.08	185.0	0.05	12.2	89.8
Number of clasts: 100				64-128 mm						
Mean	10.39	8.88	7.51	2.30	0.86	0.85	439	0.85	129	968
median	10.20	8.70	7.30	2.00	0.85	0.85	379	0.86	127	822
mode	9.80	8.70	7.40	2.00	0.84	0.87	625	0.88	143	587
skewness	0.62	0.68	0.83	0.88	0.06	-0.29	0.58	0.06	0.4	1.5
Kurtosis	0.08	-0.12	0.48	0.15	-1.03	-0.71	-0.59	-0.69	-0.4	2.1
Stn. Dev.	1.85	1.57	1.36	1.20	0.08	0.08	205.7	0.05	12.8	540.4
Number of clasts: 25				>128 mm						
Mean	16.26	14.25	11.57	3.85	0.88	0.81	468	0.86	132	3556
median	16.10	14.10	11.40	4.00	0.88	0.80	497	0.86	129	3451
mode	16.20	13.30	11.10	4.50	0.86	0.86	#N/A	#N/A	#N/A	#N/A
skewness	0.53	0.31	0.48	-0.49	0.37	-0.07	-0.65	0.30	0.1	1.0
Kurtosis	0.12	-0.20	-0.42	-0.10	-1.10	-1.01	0.31	-1.25	-1.2	0.5
Stn. Dev.	2.04	1.32	1.34	1.59	0.06	0.06	178.2	0.04	9.1	1179.0
BLADE										
Number of clasts: 100				32-64 mm						
	a-axis	b-axis	c-axis	Radius	b/a	c/b	Round-ness	Spheri-city	Flat-ness	Weight (g)
Mean	10.65	5.14	2.06	1.19	0.50	0.40	238	0.46	396	191
median	10.40	5.30	2.00	1.10	0.51	0.40	229	0.47	376	177
mode	11.00	5.60	2.00	1.00	0.50	0.30	182	#N/A	375	150
skewness	0.73	-0.47	0.56	-0.15	-0.64	0.27	0.28	-0.37	0.6	0.6
Kurtosis	0.22	-0.91	0.00	-0.47	-0.32	-0.92	0.11	-0.65	-0.4	-0.3
Stn. Dev.	2.62	0.81	0.49	0.47	0.075	0.09	107.7	0.05	94.4	100.1
Number of clasts: 100				64-128 mm						
Mean	16.39	8.39	3.37	1.28	0.52	0.41	158	0.36	522	798
median	15.80	8.00	3.30	1.00	0.53	0.39	151	0.36	505	653
mode	13.00	7.20	2.00	1.00	0.56	0.58	133	0.38	400	1096
skewness	0.91	0.67	0.31	0.74	0.01	0.15	0.56	-0.37	1.1	1.5
Kurtosis	1.18	-0.42	-0.57	0.02	4.53	-0.97	-0.07	-0.44	2.5	2.0
Stn. Dev.	3.32	1.43	0.99	0.81	0.07	0.12	93.6	0.04	166.6	437.1
Number of clasts: 25				>128 mm						
Mean	26.50	13.80	5.60	3.40	0.53	0.41	260	0.48	365	3365
median	26.10	13.50	5.60	3.00	0.50	0.40	222	0.50	360	3186
mode	25.00	12.80	5.50	2.50	#N/A	0.39	#N/A	#N/A	#N/A	#N/A
skewness	1.42	1.28	-0.02	0.50	-0.89	-0.54	0.88	-0.91	1.0	2.2
Kurtosis	2.92	1.72	1.62	-0.50	2.00	0.01	0.30	2.19	0.4	7.4
Stn. Dev.	3.36	0.99	0.66	1.50	0.05	0.05	124.9	0.03	50.5	1161.0

Continued overleaf

ROD										
Number of clasts: 100				32-64 mm						
	a-axis	**b-axis**	**c-axis**	**Radius**	**b/a**	**c/b**	**Round-ness**	**Spheri-city**	**Flat-ness**	**Weight (g)**
Mean	11.73	5.10	4.29	1.15	0.45	0.84	214	0.55	198	387
median	11.00	5.20	4.20	1.00	0.45	0.84	193	0.55	195	369
mode	11.00	5.00	4.20	1.00	0.50	0.78	273	0.68	172	234
skewness	1.26	-0.51	0.17	0.52	-0.16	0.93	0.53	0.08	0.8	1.4
Kurtosis	2.42	-0.53	0.04	-0.38	-0.10	3.41	-0.38	0.77	1.4	3.9
Stn. Dev.	3.25	0.82	0.77	0.68	0.08	0.09	137.0	0.08	36.4	210.4
Number of clasts: 100				64-128 mm						
Mean	17.96	7.73	6.36	1.09	0.44	0.82	127	0.54	205	1275
median	18.00	7.40	6.10	0.75	0.44	0.82	88	0.54	198	1052
mode	20.00	6.40	6.00	0.50	0.40	0.92	176	0.52	195	829
skewness	0.46	1.20	1.31	1.57	0.25	-0.25	1.50	0.01	1.2	2.7
Kurtosis	0.15	1.52	3.21	2.44	-0.36	0.04	2.15	-0.09	1.7	11.7
Stn. Dev.	3.55	1.19	1.18	0.98	0.08	0.09	115.4	0.07	35.1	723.8
Number of clasts: 25				>128 mm						
Mean	27.10	13.44	10.73	3.67	0.50	0.80	279	0.59	191	5521
median	26.00	13.20	10.40	3.50	0.50	0.78	248	0.58	190	5289
mode	26.40	12.80	9.50	5.50	0.50	0.78	468	#N/A	#N/A	5784
skewness	1.04	1.66	0.60	0.09	-0.36	0.63	0.40	0.00	0.1	1.8
Kurtosis	0.51	3.81	-0.60	-1.62	-0.98	-0.03	-1.25	-1.01	-0.6	4.0
Stn. Dev.	3.63	0.69	1.25	1.77	0.07	0.07	149.3	0.07	28.7	1100.9
DISC										
Number of clasts: 100				32-64 mm						
	a-axis	**b-axis**	**c-axis**	**Radius**	**b/a**	**c/b**	**Round-ness**	**Spheri-city**	**Flat-ness**	**Weight (g)**
Mean	6.31	5.37	2.13	1.75	0.85	0.40	554	0.66	288	110
median	6.20	5.35	2.00	1.80	0.85	0.38	563	0.65	290	103
mode	6.20	5.30	1.80	2.00	0.79	0.38	625	#N/A	300	92
skewness	0.32	-0.41	0.57	-0.08	0.45	0.53	-0.09	0.69	0.3	0.8
Kurtosis	-0.32	-0.38	-0.06	-0.59	0.71	-0.56	-0.55	0.77	-0.6	0.4
Stn. Dev.	0.74	0.62	0.53	0.62	0.07	0.09	190.4	0.06	63.2	42.5
Number of clasts: 100				64-128 mm						
Mean	11.75	10.02	3.69	1.35	0.86	0.37	239	0.65	313	669
median	11.85	10.00	3.55	1.00	0.88	0.35	194	0.64	312	586
mode	13.00	10.00	4.00	1.00	0.70	0.31	189	#N/A	349	#N/A
skewness	0.34	-0.21	0.58	1.35	-0.46	0.43	1.40	0.17	0.7	0.9
Kurtosis	0.00	-1.07	-0.24	1.56	-0.64	-0.65	1.82	-0.33	0.8	0.5
Stn. Dev.	2.25	1.69	1.05	0.99	0.08	0.10	182.3	0.07	85.6	359.7
Number of clasts: 25				>128 mm						
Mean	16.98	14.94	5.31	3.83	0.88	0.36	453	0.65	313	2007
median	16.50	14.30	5.60	4.00	0.87	0.37	510	0.66	291	1763
mode	16.20	12.90	3.50	1.50	#N/A	#N/A	#N/A	#N/A	#N/A	#N/A
skewness	0.23	0.70	-0.03	-0.35	0.08	-0.33	-0.25	-0.45	1.1	1.2
Kurtosis	-0.75	-0.65	-0.80	-1.19	-1.25	-0.72	-1.07	-0.63	0.8	0.5
Stn. Dev.	1.46	1.58	1.07	1.79	0.07	0.07	215.4	0.06	74.0	603.1

Table A1.15b. Summary of the size and shape characteristics of magnetic tracers used at the Trout Beck site.

				SPHERE						
Number of clasts: 100				32-64 mm						
	a-axis	**b-axis**	**c-axis**	**Radius**	**b/a**	**c/b**	**Round-ness**	**Spheri-city**	**Flat-ness**	**Weight (g)**
Mean	6.15	5.30	4.44	1.91	0.87	0.84	626	0.85	130	209
median	6.00	5.40	4.40	2.00	0.87	0.83	633	0.85	132	201
mode	5.40	6.00	4.00	2.00	0.89	0.80	741	#N/A	138	156
skewness	0.18	-0.34	0.51	-0.10	-0.32	0.29	-0.24	0.09	-0.07	0.7
Kurtosis	-0.41	-0.85	-0.19	-0.67	0.07	-0.81	-0.56	-0.19	-0.72	0.3
Stn. Dev.	0.85	0.65	0.70	0.55	0.06	0.07	170.4	0.04	11.05	82.7
Number of clasts: 100				64-128 mm						
Mean	9.57	8.22	6.89	2.90	0.86	0.84	601	0.85	130	764
median	9.35	8.00	6.70	3.00	0.85	0.84	628	0.85	129	657
mode	8.20	8.00	6.00	3.00	0.83	0.90	610	0.82	136	461
skewness	0.52	0.43	0.75	0.22	0.07	0.14	-0.35	0.10	0.34	1.3
Kurtosis	-0.61	-1.01	0.17	-0.46	-0.64	-0.82	-0.42	-0.58	0.02	1.1
Stn. Dev.	1.59	1.29	1.16	1.13	0.07	0.08	193.2	0.05	11.27	379.5
	9.57	8.22	6.89	2.90	0.86	0.84	601	0.85	130	764
Number of clasts: 25				>128 mm						
Mean	17.66	14.80	12.45	4.05	0.84	0.84	464.51	0.84	131	4108
median	17.10	15.00	12.20	4.00	0.82	0.83	484.85	0.83	129	4027
mode	16.30	15.20	12.00	4.50	#N/A	#N/A	674.85	#N/A	#N/A	#N/A
skewness	0.88	0.00	0.89	-0.51	0.40	0.46	-0.35	0.47	0.13	0.7
Kurtosis	-0.42	-0.77	0.45	-0.15	-1.04	-0.26	-0.29	0.60	0.13	0.8
Stn. Dev.	1.56	1.15	1.30	1.29	0.06	0.07	158.5	0.04	10.68	925.0
				BLADE						
Number of clasts: 100				32-64 mm						
	a-axis	**b-axis**	**c-axis**	**Radius**	**b/a**	**c/b**	**Round-ness**	**Spheri-city**	**Flat-ness**	**Weight (g)**
Mean	11.59	5.53	2.05	1.20	0.48	0.37	211	0.44	441	233
median	11.20	5.60	2.00	1.00	0.48	0.36	200	0.44	421	215
mode	11.20	6.20	1.80	1.00	0.50	0.50	196	#N/A	450	170
skewness	0.92	-0.55	0.65	0.19	-0.14	0.44	0.50	0.01	0.67	1.1
Kurtosis	0.96	-0.50	0.12	-0.27	-0.71	-0.20	0.25	-0.80	0.20	1.4
Stn. Dev.	1.59	0.58	0.53	0.51	0.07	0.09	98.0	0.05	104.13	86.1
Number of clasts: 100				64-128 mm						
Mean	15.70	7.95	2.92	1.61	0.52	0.37	211	0.46	427	1311
median	15.30	7.70	2.80	1.50	0.53	0.36	195	0.46	405	1297
mode	13.00	6.60	2.60	1.00	0.57	0.27	185	#N/A	375	798
skewness	1.08	0.84	0.40	0.75	-0.70	0.39	0.33	-0.26	0.83	2.1
Kurtosis	1.03	-0.03	-0.38	0.65	-0.39	-0.49	-0.67	-0.30	0.26	12.1
Stn. Dev.	3.27	1.14	0.80	0.79	0.06	0.09	101.3	0.05	107.0	741.0
Number of clasts: 25				>128 mm						
Mean	28.53	14.35	6.08	3.55	0.51	0.42	254	0.47	370	3939
median	28.30	14.30	6.00	3.50	0.51	0.43	250	0.48	352	3723
mode	30.60	13.00	6.10	2.00	#N/A	0.36	294	#N/A	#N/A	#N/A
skewness	0.20	0.65	-0.26	0.12	-0.49	-0.34	0.21	-0.46	2.31	0.9
Kurtosis	-1.26	-0.09	1.05	-0.83	-0.13	0.51	-0.50	0.22	8.05	1.8
Stn. Dev.	3.74	1.15	1.32	1.41	0.05	0.09	106.8	0.04	96.9	1490.5

Continued overleaf

ROD										
Number of clasts: 100				32-64 mm						
	a-axis	**b-axis**	**c-axis**	**Radius**	**b/a**	**c/b**	**Round-ness**	**Spheri-city**	**Flat-ness**	**Weight (g)**
Mean	12.27	5.01	4.14	1.49	0.42	0.83	252	0.52	212	400
median	12.00	5.00	4.05	1.50	0.41	0.82	243	0.52	205	368
mode	10.20	5.00	4.00	1.50	0.50	0.80	224	#N/A	192	247
skewness	0.69	-0.41	0.10	-0.43	-0.12	0.24	-0.04	-0.25	0.87	0.8
Kurtosis	0.03	-0.55	-0.80	0.04	-0.91	-0.87	-0.19	-0.69	0.86	0.4
Stn. Dev.	2.51	0.74	0.72	0.54	0.07	0.08	102.1	0.06	34.72	172.0
Number of clasts: 100				64-128 mm						
Mean	17.53	7.95	6.60	2.32	0.46	0.83	273	0.56	195	1391
median	16.40	7.60	6.40	2.25	0.47	0.83	265	0.56	189	1108
mode	13.40	7.20	5.40	2.00	0.44	0.71	253	0.54	200	649
skewness	0.83	1.20	0.74	0.51	-0.23	0.23	0.10	-0.34	0.56	1.9
Kurtosis	0.02	0.77	-0.14	0.19	-0.51	-1.01	-0.91	-0.48	-0.52	4.0
Stn. Dev.	3.96	1.36	1.36	0.94	0.06	0.09	113.1	0.05	27.7	863.6
Number of clasts: 25				>128 mm						
Mean	28.90	14.71	12.06	3.80	0.51	0.82	265	0.60	182.22	7144.6
median	29.60	14.90	12.00	4.00	0.52	0.81	258	0.60	180.00	7489.0
mode	34.50	13.50	14.00	4.50	#N/A	0.74	250	#N/A	179.17	#N/A
skewness	0.03	0.19	0.12	-0.73	-0.10	0.27	-0.38	-0.11	0.66	0.2
Kurtosis	-0.88	-1.03	-0.31	0.47	-0.81	-0.72	-0.21	-0.52	0.75	-0.9
Stn. Dev.	3.68	1.36	1.39	1.26	0.05	0.07	93.6	0.05	21.97	2073.4
DISC										
Number of clasts: 100				32-64 mm						
	a-axis	**b-axis**	**c-axis**	**Radius**	**b/a**	**c/b**	**Round-ness**	**Spheri-city**	**Flat-ness**	**Weight (g)**
Mean	6.84	5.80	2.20	1.82	0.85	0.38	531	0.65	301	140
median	6.90	5.80	2.10	2.00	0.86	0.36	571	0.65	300	136
mode	7.20	6.30	2.00	2.50	0.90	0.39	694	0.68	300	101
skewness	0.21	-0.67	0.84	-0.31	-0.04	0.74	-0.37	0.54	0.18	0.6
Kurtosis	-0.14	-0.23	0.30	-1.07	-0.73	-0.03	-1.02	0.01	-0.44	-0.3
Stn. Dev.	0.71	0.42	0.53	0.78	0.07	0.09	221.9	0.06	65.0	46.6
Number of clasts: 100				64-128 mm						
Mean	12.87	10.74	3.52	3.10	0.84	0.33	481	0.61	350	794
median	13.00	11.10	3.35	3.00	0.84	0.33	511	0.61	342	795
mode	13.40	12.00	3.70	4.50	0.94	0.33	672	0.55	360	1149
skewness	-0.33	-0.86	0.43	-0.06	0.14	0.29	-0.30	-0.06	0.88	0.2
Kurtosis	0.25	0.10	-0.84	-1.06	-0.80	-0.41	-0.94	-0.36	1.31	-0.7
Stn. Dev.	2.05	1.49	0.90	1.43	0.08	0.07	203.8	0.06	78.1	318.6
Number of clasts: 25				>128 mm						
Mean	16.80	14.76	4.90	4.46	0.88	0.33	531	0.63	334	1855
median	16.30	14.30	5.00	4.50	0.88	0.33	537	0.63	323	1643
mode	16.10	12.80	5.50	5.00	0.87	#N/A	435	#N/A	#N/A	#N/A
skewness	1.11	1.17	0.11	0.12	-0.30	-0.32	0.31	0.11	2.05	1.7
Kurtosis	1.56	1.87	0.63	-0.88	0.14	0.53	-0.22	0.70	6.45	2.9
Stn. Dev.	1.89	1.68	0.99	1.22	0.07	0.07	135.51	0.05	76.50	676.9

Table A1.15c. Summary of the size and shape characteristics of magnetic tracers used at the Upper Tees site.

SPHERE										
Number of clasts: 100				32-64 mm						
	a-axis	b-axis	c-axis	Radius	b/a	c/b	Round-ness	Spheri-city	Flat-ness	Weight (g)
Mean	6.24	5.39	4.60	1.72	0.87	0.85	553	0.86	127	222
median	6.30	5.40	4.60	1.75	0.88	0.85	561	0.86	127	213
mode	6.60	6.20	5.00	2.00	0.94	0.93	606	0.89	125	145
skewness	0.06	-0.38	0.10	-0.06	-0.37	-0.23	0.11	0.26	0.18	3.1
Kurtosis	-0.27	-0.69	-0.65	-0.86	-0.70	-0.80	-0.72	-0.41	-0.32	-0.7
Stn. Dev.	0.81	0.67	0.69	0.62	0.07	0.08	199.9	0.05	11.33	110.3
Number of clasts: 100				64-128 mm						
Mean	9.19	7.98	6.79	2.48	0.87	0.85	550	0.86	128	708
median	8.95	7.65	6.60	2.50	0.87	0.85	536	0.86	127	579
mode	8.60	7.00	6.00	2.00	0.95	0.81	500	#N/A	125	787
skewness	0.62	0.86	0.47	0.36	-0.07	-0.01	0.00	-0.10	0.24	1.2
Kurtosis	0.04	0.18	-0.54	-0.56	-0.63	-0.90	-0.93	-0.25	-0.42	1.3
Stn. Dev.	1.49	1.25	1.24	0.79	0.06	0.08	177.3	0.05	12.42	361.0
Number of clasts: 25				>128 mm						
Mean	17.72	14.99	12.94	3.78	0.85	0.87	435	0.85	127	4657
median	17.60	15.10	13.00	4.00	0.86	0.89	452	0.84	123	4398
mode	14.60	15.30	13.10	4.00	0.89	#N/A	#N/A	#N/A	#N/A	#N/A
skewness	-0.22	0.69	0.34	0.24	0.12	-0.71	0.10	0.25	0.98	0.8
Kurtosis	-0.92	0.05	-0.54	0.13	-1.31	-0.55	-0.84	-0.79	-0.20	0.0
Stn. Dev.	2.20	1.56	1.63	1.16	0.07	0.09	146.6	0.05	12.9	1295.7
BLADE										
Number of clasts: 100				32-64 mm						
	a-axis	b-axis	c-axis	Radius	b/a	c/b	Round-ness	Spheri-city	Flat-ness	Weight (g)
Mean	12.67	5.39	1.97	1.08	0.44	0.37	173	0.41	480	265
median	12.45	5.55	2.00	1.00	0.45	0.36	170	0.41	471	247
mode	13.00	6.00	2.00	1.00	0.50	0.36	154	0.41	465	398
skewness	0.87	-0.55	0.60	0.52	-0.28	0.35	0.55	0.09	0.38	1.0
Kurtosis	1.09	-0.66	1.01	0.28	-0.55	-0.38	1.22	-0.42	-0.08	1.1
Stn. Dev.	2.08	0.69	0.47	0.35	0.08	0.09	56.9	0.05	111.1	99.8
Number of clasts: 100				64-128 mm						
Mean	15.91	8.18	2.78	1.46	0.52	0.34	189	0.35	453	687
median	15.30	7.85	2.65	1.30	0.53	0.33	164	0.36	444	579
mode	14.60	7.80	2.20	1.00	0.50	0.40	287	0.37	483	774
skewness	0.48	0.74	0.70	1.00	-0.63	0.66	0.60	-0.17	0.77	1.3
Kurtosis	-0.28	-0.08	0.01	1.09	0.12	0.41	-0.55	0.09	0.43	1.1
Stn. Dev.	2.76	1.21	0.70	0.67	0.06	0.08	88.1	0.03	106.79	342.8
Number of clasts: 25				>128 mm						
Mean	28.12	14.50	6.11	3.47	0.52	0.42	248	0.30	359	4158
median	27.80	14.50	6.30	3.50	0.53	0.45	259	0.30	343	3759
mode	27.00	13.70	5.10	2.00	#N/A	#N/A	259	0.30	#N/A	#N/A
skewness	0.95	0.42	-0.03	0.11	-0.92	-0.03	0.18	-0.60	0.60	1.1
Kurtosis	1.79	-0.27	-1.55	-1.12	0.99	-1.35	-1.05	1.82	-0.73	0.4
Stn. Dev.	2.65	0.92	1.14	1.51	0.05	0.08	109.3	0.01	63.3	1244.4

Continued overleaf

ROD										
Number of clasts: 100				32-64 mm						
	a-axis	**b-axis**	**c-axis**	**Radius**	**b/a**	**c/b**	**Round-ness**	**Spheri-city**	**Flat-ness**	**Weight (g)**
Mean	12.08	5.25	4.45	1.24	0.44	0.85	212	0.55	197	402
median	11.80	5.40	4.40	1.30	0.45	0.84	205	0.56	191	376
mode	11.80	4.80	4.60	1.50	0.38	0.83	200	0.58	175	451
skewness	0.57	-0.38	0.22	0.27	-0.32	0.02	0.38	-0.69	1.23	0.7
Kurtosis	0.30	-0.80	-0.31	-0.50	0.03	-1.06	-0.53	0.34	1.45	0.4
Stn. Dev.	2.18	0.70	0.69	0.49	0.06	0.08	90.0	0.05	30.18	161.9
Number of clasts: 100				64-128 mm						
Mean	18.97	8.96	7.15	2.71	0.48	0.80	293	0.57	197	1773
median	18.40	8.70	7.00	2.50	0.49	0.78	296	0.57	197	1540
mode	14.00	8.40	6.20	2.50	0.50	0.75	217	#N/A	186	#N/A
skewness	0.59	0.72	0.90	-0.30	-0.37	0.78	0.00	-0.39	0.52	1.7
Kurtosis	-0.33	0.04	1.26	1.02	-0.59	0.04	0.10	-0.62	0.0	3.9
Stn. Dev.	3.76	1.33	1.14	0.81	0.07	0.07	98.3	0.06	29.6	892.3
Number of clasts: 25				>128 mm						
Mean	27.57	14.59	11.88	3.82	0.53	0.81	282	0.61	180	7175
median	26.70	14.30	11.90	4.00	0.55	0.79	291	0.63	182	7108
mode	25.50	13.50	12.20	3.50	0.59	0.81	#N/A	#N/A	#N/A	#N/A
skewness	1.04	0.44	0.39	-0.56	-0.75	0.36	-0.64	-0.57	0.51	0.4
Kurtosis	0.94	-0.75	-0.73	0.51	-0.10	-0.79	0.80	-0.53	-0.50	-1.0
Stn. Dev.	3.59	1.31	1.74	0.98	0.06	0.08	77.8	0.06	26.9	2080.8
DISC										
Number of clasts: 100				32-64 mm						
	a-axis	**b-axis**	**c-axis**	**Radius**	**b/a**	**c/b**	**Round-ness**	**Spheri-city**	**Flatn-ess**	**Weight (g)**
Mean	7.16	5.87	2.35	2.03	0.83	0.40	568	0.65	287	147
median	7.20	6.00	2.40	2.00	0.82	0.40	585	0.65	278	147
mode	7.40	6.20	2.40	2.50	0.79	0.33	714	0.71	225	143
skewness	-0.15	-1.07	0.25	-0.69	0.38	0.33	-0.50	-0.01	0.49	0.2
Kurtosis	-0.24	0.88	-0.35	0.01	-0.68	-0.41	0.07	-0.46	-0.37	0.2
Stn. Dev.	0.76	0.37	0.44	0.54	0.07	0.07	150.8	0.05	53.31	35.0
Number of clasts: 100				64-128 mm						
Mean	10.17	8.55	2.98	2.94	0.84	0.35	578	0.48	328	418
median	9.80	8.10	2.95	3.00	0.83	0.35	625	0.48	312	354
mode	9.80	8.00	3.40	3.00	0.80	0.33	625	0.53	375	353
skewness	1.38	1.08	0.70	-0.14	0.27	0.12	-0.76	0.00	0.87	1.9
Kurtosis	2.36	0.54	1.69	0.15	-0.65	-0.19	0.17	0.45	1.10	3.4
Stn. Dev.	1.82	1.44	0.76	1.16	0.08	0.07	201.7	0.04	70.81	256.0
Number of clasts: 25				>128 mm						
Mean	16.83	14.42	4.69	4.05	0.86	0.33	488	0.62	338	1734
median	16.70	13.70	4.60	4.10	0.85	0.32	479	0.62	352	1590
mode	16.70	13.50	4.30	4.50	0.96	#N/A	#N/A	#N/A	#N/A	#N/A
skewness	0.37	1.19	0.96	-0.06	0.07	0.95	-0.18	0.37	-0.76	1.1
Kurtosis	-0.55	0.59	1.19	0.39	-1.41	0.82	-0.33	-0.86	-0.25	0.9
Stn. Dev.	2.16	1.48	0.74	1.3583	0.085	0.04	168.8	0.04	38.7	630.0

APPENDIX 2: SUMMARY OF THE MAGNETIC TRACER MOVEMENTS AT THE THREE SITES OVER THE OBSERVATION PERIOD.

Table A2.1 Summary of the number of magnetic tracers transported at the two experimental reaches in four shapes classes and three size groups during the monitoring period of 26th November-19th December 1997 (S: small size, M: medium size, L: large size).

19.12.1997

Site	Total tracers	Sphere				Blade				Rod				Disc			
		S	M	L	All	S	M	L	All	S	M	L	All	S	M	L	All
Upper Tees	15	3	4	1	8	0	0	0	0	2	3	0	5	1	1	0	2
Lower Tees	no stones	no stones				no stones				no stones				no stones			
Trout Beck	134	29	39	4	72	1	0	0	1	17	16	6	39	19	2	1	22
Total	149	32	43	5	80	1	0	0	1	19	19	6	44	20	3	1	24

Summary of the mean travel distances of the magnetic tracers in four shapes classes and three size groups during the monitoring period of 26th November-19th December 1997 at Upper and Lower Tees and Trout Beck (MS: medium sphere).

Site	Sphere				Blade				Rod				Disc				Max. dis. (m)
	S	M	L	All	S	M	L	All	S	M	L	All	S	M	L	All	
Upper Tees	6.3	6.2	8.6	6.5	0	0	0	0	4.4	4.5	0	4.8	7.8	5.8	0	6.8	MS 9.96
Lower Tees	no stones				no stones				no stones				no stones				no stones
Trout Beck	15.5	14.6	12.3	14.8	3.3	0	0	3.3	10.4	10.8	5.6	14.1	10.9	*4.2*	7.8	10.2	MS 62.46
Average	14.6	13.8	10.1	14.0	3.3	0	0	3.3	9.7	9.8	5.6	9.2	10.8	4.7	7.7	9.9	

Table A2.2.Summary of the number of magnetic tracers transported at the three experimental reaches in four shapes classes and three size groups during the monitoring period of 19th December 1997-18th March 1998. (S: small size, M: medium size, L: large size).

Site	Total tracers	Sphere				Blade				Rod				Disc			
		S	M	L	All	S	M	L	All	S	M	L	All	S	M	L	All
Upper Tees	43	7	15	1	23	0	0	0	0	11	4	0	15	2	3	0	5
Lower Tees	230	37	35	6	78	10	6	1	17	33	34	3	67	44	20	1	65
Trout Beck	177	41	43	4	88	3	0	0	3	19	24	8	51	30	4	1	35
Total	450	85	93	11	189	13	6	1	20	63	62	11	133	76	27	2	105

Summary of the mean travel distances of the magnetic tracers at the three experimental reaches in four shapes classes and three size groups during the monitoring period of 19th December 1997-18th March 1998at Upper and Lower Tees and Trout Beck (MS: medium sphere, MR: medium rod).

Site	Sphere				Blade				Rod				Disc				Maximum distance (m)	
	S	M	L	All	S	M	L	All	S	M	L	All	S	M	L	All		
Upper Tees	14.8	21.2	23.8	19.4	0.0	0 0	0.0	0.0	13.8	5.4	0.0	11.5	13.3	8.8	0.0	10.6	MS	93.4
Lower Tees	15.6	11.9	5.5	13.1	6.9	6.0	5.7	7.4	9.8	8.9	4.5	9.4	11.3	5.6	3.4	9.4	MR	71.1
Trout Beck	19.6	21.6	14.9	20.4	6.8	0.0	0.0	6.8	13.5	10.4	9.6	11.4	12.1	3.9	7.8	11.0	MS	127.0
Average all	17.5	17.9	10.6	17.3	6.7	5.9	5.7	6.4	11.6	9.3	8.2	10.3	11.7	5.7	5.6	10.0		

Table A2.3.Summary of the number of magnetic tracers transported at the three experimental reaches in four shapes classes and three size groups during the monitoring period of 18th March –21 August 1998. (S: small size, M: medium size, L: large size).

Site	Total tracers	Sphere				Blade				Rod				Disc				Maximum Distance (m)	
		S	M	L	All	S	M	L	All	S	M	L	All	S	M	L	All		
Upper Tees	51	7	19	2	28	1	0	0	1	10	5	0	15	2	5	0	7	MS	93.6
Lower Tees	335	50	50	9	109	6	14	1	21	47	50	9	106	47	41	1	89	SS	106.0
Trout Beck	238	52	54	9	115	6	2	0	8	28	28	10	66	41	6	2	49	MS.	116.5
Total	624	109	123	20	252	13	16	1	30	85	83	19	187	90	52	3	145		

Summary of the mean travel distances of the magnetic tracers at the three experimental reaches in four shapes classes and three size groups during the monitoring period of 18th March –21 August 1998 at Upper and Lower Tees and Trout Beck (MS: medium sphere, SS: small sphere).

Site	Sphere				Blade				Rod				Disc				Maximum distance (m)	
	S	M	L	All	S	M	L	All	S	M	L	All	S	M	L	All		
Upper Tees	15.8	19.7	13.6	18.3	25.8	0	0	0	16.	5.5	0	12.9	13.0	7.4	0	9.0	MS	93.6
Lower Tees	24.7	16.2	7.6	19.4	8.0	6.1	3.0	7.0	11.9	11.9	3.9	11.2	14.8	6.5	3.0	10.8	SS	106.5
Trout Beck	25.0	24.2	14.0	22.7	9.9	4.5	0	8.5	13.9	12.6	10.7	12.9	14.8	4.7	5.8	13.2	MS	116.5
Average all	24.3	20.2	11.1	21.3	9.2	5.9	3.0	7.7	13.0	11.7	7.5	12.0	14.8	6.4	4.9	11.6		

Table A2.4 Summary of the number of magnetic tracers transported at the three experimental reaches in four shapes classes and three size groups during the monitoring period of 21 August-24 September 1998. (S: small size, M: medium size, L: large size).

Site	Total tracers	Sphere				Blade				Rod				Disc				Maximum Distance (m)	
		S	M	L	All	S	M	L	All	S	M	L	All	S	M	L	All		
Upper Tees	190	30	41	10	81	5	5	1	11	31	23	6	60	17	20	1	38	MS	93.6
Lower Tees	506	58	76	14	148	23	39	2	64	61	75	19	155	61	71	7	139	SS	131.8
Trout Beck	413	55	85	14	154	19	23	6	48	49	61	15	125	54	23	9	86	MS	159.9
Total	1109	143	202	38	383	47	67	9	123	141	159	40	340	132	114	17	263		

Summary of the mean travel distances of the magnetic tracers at the three experimental reaches in four shapes classes and three size groups during the monitoring period of 21 August-24 September 1998at Upper and Lower Tees and Trout Beck.

Site	Sphere				Blade				Rod				Disc				Maximum distance (m)	
	S	M	L	All	S	M	L	All	S	M	L	All	S	M	L	All		
Upper Tees	14.4	22.0	20.1	19.0	8.8	8.7	8.4	8.7	18.4	11.1	7.0	14.4	17.7	13.8	4.5	13.9	MS	93.6
Lower Tees	35.1	26.2	18.8	29.0	11.2	15.0	6.1	13.3	21.8	22.1	13.2	20.9	25.4	15.2	7.8	19.3	SS	131.8
Trout Beck	45.2	35.7	24.2	38.0	7.4	6.0	7.4	6.7	25.5	19.2	14.6	21.3	20.5	12.2	6.9	16.9	MS	159.9
Average all	34.7	29.3	21.1	30.5	9.4	11.4	7.2	10.4	22.3	19.4	12.8	19.8	22.0	14.4	7.1	17.7		

Table A2.5 Summary of the number of magnetic tracers transported at the three experimental reaches in four shapes classes and three size groups during the monitoring period of 24 September 1998-6 July 1999. (S: small size, M: medium size, L: large size).

Site	Total tracers	Sphere				Blade				Rod				Disc				Maximum Distance (m)	
		S	M	L	All	S	M	L	All	S	M	L	All	S	M	L	All		
Upper Tees	203	33	41	8	82	7	5	1	13	36	25	7	68	15	24	1	40	SR	146
Lower Tees	589	65	88	19	172	35	43	4	82	69	82	23	174	71	80	10	161	MR	361
Trout Beck	429	55	82	20	157	22	21	9	52	47	70	19	136	43	31	10	84	MS.	116.5
Total	1221	153	211	47	411	64	69	14	147	152	177	49	378	129	135	21	285		

Summary of the mean travel distances of the magnetic tracers at the three experimental reaches in four shapes classes and three size groups during the monitoring period of 24 September 1998-6 July 1999 at Upper and Lower Tees and Trout Beck.

Site	Sphere				Blade				Rod				Disc				Maximum distance (m)	
	S	M	L	All	S	M	L	All	S	M	L	All	S	M	L	All		
Upper Tees	17.2	23.7	19.7	20.7	9.0	8.9	8.5	9.0	20.8	12.3	8.7	16.4	15.6	13.8	4.1	14.2	MS	17.2
Lower Tees	67.4	66.3	30.3	62.7	18.8	26.7	5.3	22.3	50.4	39.6	19.8	41.3	59.0	32.2	10.5	42.6	MS	45.3
Trout Beck	71.3	54.2	25.8	56.6	9.0	7.0	7.4	7.9	42.2	25.4	24.3	31.1	43.6	9.3	9.1	20.8	MS	36.8
Average all	58.0	53.3	26.6	52.0	14.4	19.4	6.9	16.0	40.8	30.1	20.0	33.1	48.8	23.6	9.5	33.4		

APPENDIX 3: RESULTS OF FRICTION ANGLE EXPERIMENTS

Table A3.1 Percentage of friction angle distributions for 3 test grains and six shape/orientations classes on four different bed roughness (S: sphere, B.T: blade transverse blade, B.P: blade with long axis parallel to the slope, R.T: rod with transverse orientation, R.P: rod with long axis parallel to the slope, D: disc).

Roughness 1

Test grain size: 24 mm

	S	*B.T*	*B.P*	*R.T*	*R.P*	*D*
10°	0	0	0	0	0	0
20°	2	0	0	2	0	0
30°	12	6	0	32	0	0
40°	48	8	8	52	12	6
50°	22	40	20	12	24	26
60°	14	26	22	2	20	40
70°	2	20	36	0	42	24
80°	0	0	14	0	2	4
90°	0	0	0	0	0	0
100°	0	0	0	0	0	0

Test grain size: 48 mm

	S	*B.T*	*B.P*	*R.T*	*R.P*	*D*
10°	0	0	0	0	0	0
20°	10	0	0	22	0	0
30°	62	16	6	62	10	0
40°	28	26	38	14	46	16
50°	0	40	30	2	16	24
60°	0	4	14	0	22	40
70°	0	14	10	0	6	20
80°	0	0	2	0	0	0
90°	0	0	0	0	0	0
100°	0	0	0	0	0	0

Test grain size: 96 mm

	S	B.T	B.P	R.T	R.P	D
10°	0	0	0	0	0	0
20°	48	0	0	66	0	0
30°	40	20	22	32	6	4
40°	12	54	66	2	54	42
50°	0	18	10	0	18	24
60°	0	6	2	0	22	22
70°	0	2	0	0	0	6
80°	0	0	0	0	0	2
90°	0	0	0	0	0	0
100°	0	0	0	0	0	0

Roughness 2

Test grain size: 24 mm

	S	B.T	B.P	R.T	R.P	D
10°	0	0	0	0	0	0
20°	0	0	0	3	0	0
30°	7	1	0	10	0	0
40°	12	9	0	18	6	3
50°	14	14	10	12	17	13
60°	9	20	20	5	12	18
70°	8	5	13	2	15	7
80°	0	1	7	0	0	9
90°	0	0	0	0	0	0
100°	0	0	0	0	0	0

Test grain size: 48 mm

	S	B.T	B.P	R.T	R.P	D
10°	0	0	0	2	0	0
20°	5	0	0	11	0	0
30°	21	0	0	21	3	0
40°	18	11	4	11	12	2
50°	5	14	13	5	18	13
60°	1	16	9	0	12	22
70°	0	8	16	0	5	12
80°	0	1	8	0	0	1
90°	0	0	0	0	0	0
100°	0	0	0	0	0	0

Test grain size: 96 mm

	S	B.T	B.P	R.T	R.P	D
10°	3	0	0	1	0	0
20°	22	0	0	29	0	0
30°	22	8	5	18	7	6
40°	3	23	19	2	27	22
50°	0	8	19	0	8	15
60°	0	6	4	0	7	3
70°	0	5	3	0	1	4
80°	0	0	0	0	0	0
90°	0	0	0	0	0	0
100°	0	0	0	0	0	0

Roughness 3

Test grain size: 24 mm

	S	B.T	B.P	R.T	R.P	D
10°	0	0	0	0	0	0
20°	0	0	0	1	0	0
30°	4	1	0	7	0	0
40°	8	5	1	13	1	6
50°	12	5	9	19	11	8
60°	10	18	17	4	25	12
70°	11	13	14	3	12	7
80°	5	8	9	3	1	17
90°	0	0	0	0	0	0
100°	0	0	0	0	0	0

Test grain size: 48 mm

	S	B.T	B.P	R.T	R.P	D
10°	0	0	0	0	0	0
20°	6	0	0	1	0	0
30°	15	2	0	17	1	1
40°	12	11	15	26	13	5
50°	11	17	12	5	20	19
60°	5	12	13	1	11	16
70°	1	7	5	0	5	8
80°	0	1	5	0	0	1
90°	0	0	0	0	0	0
100°	0	0	0	0	0	0

Test grain size: 96 mm

	S	B.T	B.P	R.T	R.P	D
10°	0	0	0	0	0	0
20°	9	0	0	4	0	0
30°	27	10	15	25	9	6
40°	8	20	18	19	21	16
50°	4	15	12	2	12	10
60°	2	3	4	0	7	5
70°	0	2	1	0	1	12
80°	0	0	0	0	0	1
90°	0	0	0	0	0	0
100°	0	0	0	0	0	0

ROUGHEST BED

Test grain size: 24 mm

	S	B.T	B.P	R.T	R.P	D
10°	0	0	0	0	0	0
20°	0	0	0	0	0	0
30°	0	0	0	0	0	0
40°	0	0	0	4	1	1
50°	3	1	0	8	4	0
60°	16	8	7	20	10	0
70°	10	14	11	10	25	6
80°	8	17	18	6	10	15
90°	6	10	12	2	0	21
100°	7	0	2	0	0	7

Test grain size: 48 mm

	S	B.T	B.P	R.T	R.P	D
10°	0	0	0	0	0	0
20°	0	0	0	0	0	0
30°	2	0	0	5	0	0
40°	11	0	1	23	2	1
50°	20	6	13	14	12	12
60°	14	23	17	8	16	4
70°	3	18	13	0	17	19
80°	0	3	5	0	3	11
90°	0	0	1	0	0	1
100°	0	0	0	0	0	2

Test grain size: 96 mm

	S	B.T	B.P	R.T	R.P	D
10°	0	0	0	0	0	0
20°	1	0	0	0	0	0
30°	15	0	2	23	1	0
40°	23	14	16	19	13	8
50°	10	19	17	7	11	12
60°	1	8	8	1	23	24
70°	0	6	4	0	2	4
80°	0	3	3	0	0	2
90°	0	0	0	0	0	0
100°	0	0	0	0	0	0

Table A3.2 Friction angle frequency distributions for the test particles of equal weight but differing shapes/orientations on various bed roughnesses.

Roughness 1

Friction angle (φ)	S	B.T	B.P	R.T	R.P	D
10°	0	0	0	0	0	0
20°	31	0	0	27	0	0
30°	19	6	6	22	1	11
40°	0	24	38	1	27	20
50°	0	12	4	0	19	14
50°	0	6	2	0	3	2
70°	0	2	0	0	0	3
80°	0	0	0	0	0	0
90°	0	0	0	0	0	0

Roughness 2

Friction angle (φ)	S	B.T	B.P	R.T	R.P	D
10°	0	0	0	0	0	0
20°	8	0	1	2	0	0
30°	26	7	5	31	2	5
40°	15	14	26	16	10	19
50°	1	22	10	1	17	13
50°	0	5	3	0	16	7
70°	0	2	4	0	5	6
80°	0	0	1	0	0	0
90°	0	0	0	0	0	0

Roughness 3

Friction angle (φ)	S	B.T	B. P	R.T	R.P	D
10°	0	0	0	0	0	0
20°	22	0	0	9	0	0
30°	21	2	15	32	6	10
40°	7	19	15	9	19	23
50°	0	23	13	0	9	7
50°	0	5	6	0	16	6
70°	0	1	1	0	0	3
80°	0	0	0	0	0	1
90°	0	0	0	0	0	0

Roughness 4

Friction angle (φ)	S	B.T	B.P	R.T	R.P	D
10°	0	0	0	0	0	0
20°	1	0	0	0	0	0
30°	16	0	1	15	0	0
40°	28	1	7	26	2	7
50°	5	22	24	7	11	16
50°	0	17	15	2	26	17
70°	0	9	2	0	11	10
80°	0	1	0	0	0	0
90°	0	0	1	0	0	0

Table A3.3 Friction angle frequency distributions for natural test particles of four different shapes on various bed roughnesses.

Roughness 1							Roughness 2						
Friction angle	S	B.T	B.P	R.T	R.P	D	Friction angle	S	B.T	B.P	R.T	R.P	D
10°	0	0	0	0	0	0	10°	0	0	0	0	0	0
20°	27	0	0	11	0	0	20°	9	0	0	4	0	0
30°	22	4	3	33	3	7	30°	27	1	2	20	7	0
40°	1	22	45	6	30	21	40°	12	9	30	20	26	18
50°	0	21	2	0	14	20	50°	2	26	16	6	14	25
50°	0	3	0	0	3	1	50°	0	11	2	0	2	5
70°	0	0	0	0	0	1	70°	0	3	0	0	1	2
80°	0	0	0	0	0	0	80°	0	0	0	0	0	0
90°	0	0	0	0	0	0	90°	0	0	0	0	0	0

Roughness 3							Roughness 4						
Friction angle	S	B.T	B.P	R.T	R.P	D	Friction angle	S	B.T	B.P	R.T	R.P	D
10°	0	0	0	0	0	0	10°	0	0	0	0	0	0
20°	7	0	0	0	0	0	20°	2	0	0	0	0	0
30°	23	0	2	13	2	2	30°	14	0	0	11	0	0
40°	17	4	24	29	6	4	40°	30	3	5	25	1	0
50°	3	18	18	8	25	32	50°	4	19	27	14	12	12
50°	0	16	1	0	16	8	50°	0	13	10	0	31	22
70°	0	8	4	0	1	3	70°	0	12	7	0	6	12
80°	0	4	1	0	0	1	80°	0	2	0	0	0	4
90°	0	0	0	0	0	0	90°	0	1	1	0	0	0

(S: sphere, B.T: Blade in transverse orientation, B.P: blade in parallel orientation, R.T: blade in transverse orientation, R.P: rod in parallel orientation, D: disc).

Table A3.4 Friction angle distributions for three test grain sizes and six shape/orientation classes on the reconstructed natural bed types.
(Data represents friction angle values in degrees. S: sphere, B.T: Blade in transverse orientation, B.P: blade in parallel orientation, R.T: rod in transverse orientation, R.P: rod in parallel orientation, D: disc).

	Small (24 mm)							**Medium (48 mm)**							**Large (96 mm)**					
(°)	S	B.T	B.P	R.T	R.P	D	(°)	S	B.T	B.P	R.T	R.P	D	(°)	S	B.T	B.P	R.T	R.P	D
10°	0	0	0	0	0	0	**10°**	0	0	0	0	0	0	**10°**	0	0	0	0	0	0
20°	0	0	0	0	0	0	**20°**	0	0	0	0	0	0	**20°**	0	0	0	1	0	0
30°	0	0	0	0	0	0	**30°**	0	0	0	3	0	0	**30°**	19	0	0	5	0	0
40°	4	0	0	0	1	0	**40°**	10	2	4	7	0	1	**40°**	22	1	2	27	3	0
50°	0	7	1	18	10	0	**50°**	15	8	10	21	8	13	**50°**	7	9	5	9	12	10
50°	1	10	14	25	29	2	**50°**	16	19	21	11	25	15	**50°**	2	20	22	3	27	23
>70°	45	33	35	5	10	48	**>70°**	9	21	15	8	17	21	**>70°**	0	20	21	5	8	17

Table A3.5 Friction angle distributions for particles of equal weights in six shapes/orientation classes on the reconstructed natural bed

Friction angle	S	B.T	B.P	R.T	R.P	D
10^0	0	0	0	0	0	0
20^0	0	0	0	0	0	0
30^0	8	0	0	4	0	0
40^0	22	2	6	22	0	0
50^0	48	30	28	30	14	12
60^0	16	48	26	26	42	30
$>70^0$	6	20	40	18	44	58

Table A3.6 Friction angle distributions for naturally-formed test particles in six shapes/orientation classes on the reconstructed natural bed.

Friction angle	S	B.T	B.P	R.T	R.P	D
10^0	0	0	0	0	0	0
20^0	1	0	0	0	0	0
30^0	6	0	0	5	0	0
40^0	19	1	5	17	10	0
50^0	8	9	28	16	15	2
60^0	11	28	12	5	8	14
$>70^0$	5	12	5	7	17	34

Table A3.7 Friction angle distributions for sphere and rod test particles of various roundness on different bed roughnesses. (VA: very angular, A: angular, SA: sub angular, R: round, VR: very round)

Sphere

	Roughness 1					Roughness 2					Roughness 3					Roughness 4					Natural bed				
	VR	R	SA	A	VA		VR	R	SA	A	VA		VR	R	SA	A	VA		VR	R	SA	A	VA		VR	R	SA	A	VA
10°	0	0	0	0	0	10°	0	0	0	0	0	10°	0	0	0	0	0	10°	0	0	0	0	0	10°	0	0	0	0	0
20°	40	20	10	4	2	20°	0	10	4	0	0	20°	4	0	0	2	0	20°	0	0	0	0	0	20°	0	0	0	0	0
30°	50	64	62	40	22	30°	34	38	28	24	22	30°	38	26	36	18	24	30°	12	2	2	0	2	30°	28	18	8	14	0
40°	10	16	24	54	50	40°	56	40	52	52	38	40°	34	54	42	48	42	40°	30	46	28	30	38	40°	40	22	38	10	4
50°	0	0	4	2	26	50°	10	12	14	24	38	50°	14	20	16	32	26	50°	36	34	34	46	30	50°	16	30	34	54	42
60°	0	0	0	0	0	60°	0	0	2	0	2	60°	10	0	6	0	8	60°	12	18	26	12	20	60°	10	26	10	18	32
>'70°	0	0	0	0	0	>'70°	0	0	0	0	0	>'70°	0	0	0	0	0	>'70°	10	0	10	12	10	>'70°	6	4	10	4	22

Transverse rod

	VR	R	SA	A	VA		VR	R	SA	A	VA		VR	R	SA	A	VA		VR	R	SA	A	VA		VR	R	SA	A	VA
10°	0	0	0	0	0	10°	0	0	0	0	0	10°	0	0	0	0	0	10°	0	0	0	0	0	10°	0	0	0	0	0
20°	64	40	24	8	0	20°	4	12	4	0	0	20°	4	2	0	0	0	20°	0	0	0	0	0	20°	0	0	0	0	0
30°	34	56	54	60	24	30°	62	70	50	48	30	30°	38	32	14	22	24	30°	6	10	2	4	2	30°	14	4	8	10	2
40°	2	4	22	32	70	40°	32	16	40	46	50	40°	34	44	60	48	42	40°	44	52	48	58	20	40°	68	46	20	26	28
50°	0	0	0	0	6	50°	2	2	6	6	18	50°	14	20	24	28	32	50°	40	28	40	24	60	50°	18	30	38	8	46
60°	0	0	0	0	0	60°	0	0	0	0	2	60°	10	2	2	2	2	60°	8	10	8	14	18	60°	0	6	28	38	10
>'70°	0	0	0	0	0	>'70°	0	0	0	0	0	>'70°	0	0	0	0	0	>'70°	2	0	2	0	0	>'70°	0	14	6	18	14

Parallel rod

	VR	R	SA	A	VA		VR	R	SA	A	VA		VR	R	SA	A	VA		VR	R	SA	A	VA		VR	R	SA	A	VA
10°	0	0	0	0	0	10°	0	0	0	0	0	10°	0	0	0	0	0	10°	0	0	0	0	0	10°	0	0	0	0	0
20°	0	0	0	0	0	20°	2	0	0	0	0	20°	0	0	0	0	0	20°	0	0	0	0	0	20°	2	0	0	0	0
30°	8	4	14	2	12	30°	2	0	0	0	2	30°	2	2	0	0	4	30°	0	0	0	0	0	30°	2	0	0	0	4
40°	50	34	50	36	50	40°	16	34	20	16	26	40°	16	32	16	18	16	40°	0	16	4	8	2	40°	6	12	4	6	4
50°	16	28	30	36	24	50°	52	34	38	46	34	50°	50	28	40	34	36	50°	26	38	32	40	30	50°	26	36	26	22	28
60°	22	30	6	20	12	60°	22	26	40	30	36	60°	22	28	34	40	28	60°	56	36	50	36	50	60°	32	34	46	36	32
>'70°	4	4	0	6	2	>'70°	6	6	2	8	2	>'70°	10	10	10	8	16	>'70°	18	10	14	16	18	>'70°	32	18	24	36	32

APPENDIX 4: RESULTS OF PHOTOHGRAPHIC VISUALISATION EXPERIMENTS FOR ARTIFICIAL AND NATURAL PARTICLES

Table A4.1 Results of settling and transport velocities experiments carried out with artificial test particles in four shape classes. Note: W_o: fall velocity, D: medium axis of particle, V: Kinematic viscosity. (R: rolling mode, S sliding mode)

Photo No	Shape of test particle	Settling Velocity cm s^{-1}	Reynolds Number (W_o D/V)	Transport velocity on bed cm s^{-1}	Reynolds Number (W_o D/V)	Dominant mode of Transport
15	Sphere	33.3	3333	13.3	1333	R
16	Sphere	33.3	3333	14.3	1429	R
17	Sphere	33.3	3333	12.5	1250	R
18	Sphere	33.3	3333	13.3	1333	R
19	Sphere	33.3	3333	13.3	1333	R
20	Sphere	40.0	4000	13.3	1333	R
21	Sphere	40.0	4000	13.3	1333	R
22	Sphere	33.3	3333	12.5	1250	R
23	Sphere	40.0	4000	13.3	1333	R
24	Sphere	50.0	5000	14.3	1429	R
Mean		**37.0**	**3700**	**13.4**	**1336**	R
S. Dev.		**5.5**		**0.6**		
27	Blade	12.5	1250	11.8	1176	S
28	Blade	11.8	1176	12.5	1250	S
29	Blade	13.3	1333	12.5	1250	S
30	Blade	15.4	1538	12.5	1250	S
31	Blade	15.4	1538	11.1	1111	S
32	Blade	13.3	1333	10.0	1000	S
33	Blade	13.3	1333	11.8	1176	S
34	Blade	18.2	1818	-	-	S
35	Blade	40.0	4000	9.1	909	S
36	Blade	14.3	1429	-	-	S
Mean		**16.8**	**1675**	**11.7**	**1144**	
S. Dev.		**8.4**		**0.9**		
1	Rod	28.6	2857	12.5	1250	R
2	Rod	33.3	3333	11.8	1176	R
3	Rod	28.6	2857	13.3	1333	R
4	Rod	40.0	4000	11.1	1111	R
5	Rod	28.6	2857	11.1	1111	R
6	Rod	33.3	3333	11.8	1176	R
7	Rod	28.6	2857	10.0	1000	R
8	Rod	22.2	2222	10.5	1053	R
9	Rod	22.2	2222	12.5	1250	R
10	Rod	28.6	2857	11.8	1176	R
Mean		**29.4**	2940	**11.6**	1164	
S. Dev.		**5.3**		**0.9**		
11	Disc	13.3	1333	10.0	1000	S
12	Disc	13.3	1333	11.1	1111	S
13	Disc	25.0	2500	10.0	1000	S
14	Disc	13.3	1333	-	-	S
15	Disc	13.3	1333	11.1	1111	S
16	Disc	14.3	1429	-	-	S
17	Disc	12.5	1250	11.8	1176	S
19	Disc	13.3	1333	12.5	1250	S
20	Disc	14.3	1429	11.1	1111	S
21	Disc	13.3	1333	11.8	1176	S
Mean	Disc	**14.6**	1461	**11.2**	**1117**	S
S. Dev.	Disc	**3.7**		**0.9**		

Table A4.2 Results of settling and transport velocities experiments carried out with natural particles in four shape classes. (W_o: fall velocity, D: medium axis of particle, V: Kinematic viscosity)

Photo No	Shape of test particle	Settling velocity	Reynolds Number (W_o D/V)	Transport velocity	Reynolds Number (W_o D/V)	Dominant mode of transport
1	Sphere	68.8	6875	25.0	2500	R
2	Sphere	68.8	6875	28.6	2857	R
3	Sphere	68.8	6875	28.6	2857	R
4	Sphere	68.8	6875	28.6	2857	R
5	Sphere	45.8	4583	28.6	2857	R
6	Sphere	68.8	6875	28.6	2857	R
7	Sphere	45.8	4583	25.0	2500	R
8	Sphere	68.8	6875	25.0	2500	R
9	Sphere	45.8	4583	28.6	2857	R
10	Sphere	68.8	6875	28.6	2857	R
	Mean	**61.9**	**6188**	**27.5**	**2750**	
	Stn. Dev.	**11.1**		**1.7**		
11	Blade	22.9	2292	20.0	2000	S
12	Blade	34.4	3438	25.0	2500	S
13	Blade	15.3	1528	28.6	2857	S
14	Blade	22.9	2292	18.2	1818	S
15	Blade	34.4	3438	16.7	1667	S
16	Blade	27.5	2750	16.7	1667	S
17	Blade	27.5	2750	20.0	2000	S
18	Blade	68.8	6875	18.2	1818	S
19	Blade	34.4	3438	16.7	1667	S
20	Blade	22.9	2292	22.2	2222	S
	Mean	**31.1**	**3109**	**20.2**	**2022**	
	Stn. Dev.	**14.6**		**4.0**		
22	Rod	34.4	3438	22.2	2222	R
23	Rod	68.8	6875	22.2	2222	R
24	Rod	34.4	3438	20.0	2000	R
25	Rod	45.8	4583	20.0	2000	R
26	Rod	45.8	4583	22.2	2222	R
27	Rod	45.8	4583	20.0	2000	R
28	Rod	45.8	4583	22.2	2222	R
29	Rod	68.8	6875	20.0	2000	R
30	Rod	45.8	4583	20.0	2000	R
31	Rod	45.8	4583	20.0	2000	R
	Mean	**48.1**	**4813**	**20.9**	**2089**	
	Stn. Dev.	**11.8**		**1.1**		
33	Disc	22.9	2292	18.2	1818	S
34	Disc	19.6	1964	14.3	1429	S
35	Disc	22.9	2292	18.2	1818	S
36	Disc	22.9	2292	13.3	1333	S
1	Disc	22.9	2292	18.2	1818	S
2	Disc	22.9	2292	15.4	1538	S
3	Disc	22.9	2292	12.5	1250	S
4	Disc	34.4	3438	15.4	1538	S
6	Disc	19.6	1964	15.4	1538	S
7	Disc	22.9	2292	20.0	2000	S
	Mean	**23.4**	**2341**	**16.1**	**1608**	
	Stn. Dev.	**4.1**		**2.4**		

REFERENCES

Abbott, J.E. & Francis, J.R.D., 1977, Saltation and suspension trajectories of solid grains in a water stream. *Philosophy of Transactions Royal Society of London.*, 284A: 225-254.

D'Agostino, V. & Lenzi, M.A., 1999, Bedload transport in the instrumented catchment of the Rio Cordon; Part II: Analyses of the bedload rate. *Catena*, 36, 191-204.

Alger, G., 1964, *Terminal fall velocity of particles of irregular shapes as affected by surface area.* PhD thesis, Colorado State University, Fort Collins, Colorado, 99pp.

Allen, J.R.L., 1969, The maximum slope angle attainably surfaces underlain by bulked equal spheroids with variable dimensional ordering. *Bulletin Geological Society of America*, 80, 1923-1930.

Allen, J.R.L., 1981, *Particle size measurement.* 2nd edn. London: Chapman and Hall.

Allen, J.R.L., 1982, *Sedimentary structures*, Volume, 1. Elsevier, Amsterdam, 593p.

Allen, J.R.L., 1985, *Principles of physical sedimentology.* Allen and Unwin, London.

Andel, TJ. H., Wiggers, A.J. & Maarleveld, G., 1954, Roundness and shape of marine gravels from Urk (Netherlands), a comparison of several methods of investigation. *Journal of Sedimentary Petrology*, 24, 100-116.

Archer, D.R., 1989, Flood wave attenuation due to channel and floodplain storage and effects on flood frequency. In Beven, K. & Carling, P. (Eds.) *Floods: Hydrological, sedimentological & geomorphological implications.* John Wiley & Sons, Chichester, 37-46.

Archer, D., 1992, Land of Singing Waters: Rivers and Great Floods of Northumbria. Spreddon Press, Northumbria, 217p.

Arkell, P.L., Leeks G., Newson, M. and Oldfield, F., 1983, Trapping and tracing: some recent observations on supply and transport of coarse sediment from Wales. In: Modern and Ancient Fluvial Systems (J.D. Collinson and J. Lewin, eds). *International Association of Sedimentologists Special Publication* 6, 107-119.

Aschenbrenner, B.C., 1956, A new method of expressing particle sphericity. *Journal of Sedimentary Petrology*, 26, 15-31.

Ashworth, P.J. & Ferguson, R.I., 1989, Size selective entrainment of bedload in gravel bed streams. *Water Resources Research*, 25, 627-634.

Baba, J. & Komar, P.D., 1981a, Measurements and analysis of settling velocities of natural quartz sand grains. *Journal of Sedimentary Petrology.* 51, 631-640.

Baba, J. & Komar, P.D., 1981b, Settling velocities of irregular grains at low Reynolds numbers. *Journal of Sedimentary Petrology*, 51, 121-128.

Bagnold, R.A., 1941, *The physics of blown sand and desert dunes*. Methuen & Co. Ltd., London, 265p.

Bagnold, R.A., 1966, An approach to the sediment transport problem from general physics. *United States Geological Survey, Professional Paper* 442-I.

Bagnold, R.A., 1973, The nature of saltation and of 'bed-load' transport in water. *Proceedings Royal Society of London*. A 332, 473-504.

Bagnold, R.A., 1980, An empirical correlation of bedload transport rates in flume and natural rivers. *Proceedings of the Royal Society of London*, 372-A: 453-473.

Ballantyne, C.K., 1982, Aggregate clast form characteristics of deposits near the margins of four glaciers in the Jotumheimen Massif, Norway, *Norsk Geografisk Tidsskrift*, 36, 103-113.

Barrett, J.P., 1980, The shape of rock particles, a critical review. *Sedimentology* 27, 291-203.

Bathurst, J.C., 1987, Measuring and modelling bedload transport in channels with coarse-bed materials. In Richards, K.S. (editor). *River Channels: Environment and Process,* Oxford: Basil Blackwell, 272-294.

Benn, D.I. & Ballantyne, C.K., 1993, Short communication: The description and representation of particle shape. *Earth Surface Processes and Landforms*, 18, 665-672.

Bergesen, O.F., 1973, The roundness analysis of stones. A neglected aid in till studies. *Bulletin of the Geological Institutions of the University of Upsala* N.S. 5, 69-79.

Blenk, M., 1960, Ein Beitrag zur morphometrishchen Schotteranalyse. *Zeitschift Fur Geomorphologie* N.F. 4, 202-242.

Bluck, B.J., 1969, Particle rounding in beach gravels. *The Geological Magazine*, 106, 1-14.

Boon, J.D., Evans, D.A. & Hennigar, H.F., 1982, Spectral information from Fourier analyses of digitized quartz grain profiles. *Mathematical Geology*, 14, 589-605.

Bott, M.H.P., 1967, Geophysical investigation of the northern Pennine basement rocks. *Proceedings of the Yorkshire Geological Society,* 36, 139-168.

Boulton, G.S., 1978, Boulder shapes and grain-size distribution of debris as indicators of transport paths through a glacier and till genesis. *Sedimentology,* 25, 773-799.

Bovee, K.D. & Milhous, R., 1978, Hydraulic simulation in instream flow studies: theory and techniques. *Instream Flow Information Paper 5, FWS/OBS-78/33, US Fish and Wildlife Service, Office of Biological Sciences.*

Du Boys, M.P., 1879, Le Rhone et les rivieres a lit affouillable (The Rhone and alluvial rivers). *Mem. Doc. Ann. Ponts Chaussees*, 5th Series, 18, 141-195.

Bradley, W.C., 1970, Effect of weathering on abrasion of granitic gravel, Colorado River, Texas. *Geological Society of America Bulletin*, 81, 61-80.

Bradley, W. C., Fahnestock, R.K. & Rowekamp, E.T., 1972, Coarse sediment transport by flood flow on Knik River, Alaska. *Geological Society of America Bulletin*, 83, 1261-1284.

Bradshaw, M.E., 1976, (Ed.)The natural history of Upper Teesdale. *Durham County Conservation Trust*. 75p.

Brayshaw, A.C., 1983, *Bed microtopography and bedload transport in coarse-grained alluvial channels*. Unpublished PhD Thesis, University of London, 415 p.

Brayshaw, A.C., Frostick, L.E. & Reid, I., 1983, The hydrodinamics of particle clusters and sediment entrainment in coarse alluvial channels. *Sedimentology*, 30, 137-143.

Brewer, R., 1964, *Fabric and mineral analysis of soils*, John Wiley & Sons, Chichester, 470p.

Bridgland, D.R., 1986, (ed) *Clast Lithological Analysis*. Quaternary Research Association. Technical Guide No. 3, 207p.

Brierley, G.J. & Hickin, E.J., 1985, The downstream gradation of particle sizes in the Squamish River, British Columbia. *Earth Surface Processes and Landforms*, 10, 597-606.

Briggs, D.J., 1977, *Sources and methods in geography*: S*ediment*. Butterworth, London.

Buffington, J.M., Dietrich, W.E. & Kirchner, J.W., 1992, Friction angle measurements on a naturally formed gravel streambed: implications for critical boundary shear stress. *Water Resources Research*, 28, 411-425.

Bunte, K. & Ergenzinger, P., 1989, New tracer techniques for particles in gravel-bed rivers. *Bulletin dela Societe Geographique de Liege* 25, 85-90.

Burgess, I.C. & Wadge, A.J., 1974, The Geology of the Cross Fell Area. *British Geological Survey*, HMSO, London, 92p.

Burt, T.P., Holden, J. and Evans, M.G., 1998. The hydrology of blanket peat with special referenceto the Moor House NNR. *Geomorphological studies in the North Pennines: Field Guide.* British Geomorphological Research Group, 104p.

Busskamp, R. & Hasholt, B., 1996, Coarse bedload transport in a glacial valley, Sermilik, sout east Greenland. *Zeitschrift fur Geomorphologie*, 40, 349-358.

Butler, R.P., 1977, Movement of cobbles in a gravel bed stream during a flood season. *Geological Society of America, Bulletin* 88, 1072-1074.

Cailleux, A., 1947, L'indice d'emousse: Definition et premi`ere application: *Comptes Rendus de Science, Societe Geolojique de la France*, 250-252.

Cailleux, A., 1952, Morphoskopischeanalyse der geschiebe und sandkorner und ihre bedutung fur die palaoklimatologie. *Geologice Rundschau*, 40, 11-19.

Carling, P.A., 1983, Threshold of coarse sediment transport in broad and narrow natural streams. *Earth Surface Processes & Landforms*, 8, 1-18.

Carling, P.A., 1986, The Noon Hill flash floods; July 17th 1983. Hydrological and geomorphological aspects of a major formative event in an upland landscape. *Transaction of the Institute of British Geographers*, 11, 105-118.

Carling, P.A., 1987, "Bed stability in gravel streams, with reference to stream regulation and ecology" in River channels; Environmental and Process, Richards, K. (ed.). Institute of British Geographers, *Special Publication* 17, 321-347.

Carling, P.A., 1989, Bedload transport in two gravel-bedded streams. *Earth Surface Processes and Landforms*, 14, 27-39.

Carrigy, M.A., 1970, Experiments on the angles of repose of granular materials. *Sedimentology*, 14, 147-158.

Carling, P.A., Kelsey, A. & Glaister, M.S., 1992, Effect of bed roughness, particle shape and orientation on initial motion criteria. *Dynamics of Gravel-bed Rivers*, Billi, P., Hey, R.D., Thorne, C.R. & Taconni, P. (eds), Wiley, Chicester pp. 23-39.

Carson, M.A. & Kirkby, M.J., 1972, *Hillslope form and process*. Cambridge University Press. Chambridge.

Chepil, W.S., 1959, Equilibrium of soil grains at the threshold of movement by wind. *Proc. Soil Sci. Soc. Am.* 23, 422-428.

Church, M. & Gilbert, R., 1975, Proglacial fluvial and lacustrine environments. A reprint in in Glaciofluvial and Glaciolacustrine sedimentation. *Society of Economic and Palaeontologists and Mineralogists*, Special Publocation No. 23, 29-99.

Church, M. & Hassan, M.A., 1992, Size and distance of travel of unconstrained clasts on a streambed. *Water Resources Research,* 28, 299-303.

Church, M., McLean, D.G. & Wolcott, J.F., 1987, *River bed gravels: Sampling and analysis*, In Sediment Transport in Gravel-bed Rivers, edited by C.R. Thorne, J.C. Bathurst, and R.D. Hey, pp. 43-88, Wiley Interscience, New York,, 1987.

Clark, M.W., 1981, Quantitative shape analysis: a review. *Mathematical Geology*, 13, 303-320.

Clark, N.N., 1987, A new scheme for particle shape characterisation based on fractal harmonics and fractal dimension. *Powder Technology*, 51, 243-249.

Clayton, C.L., 1951, The problem of gravel in highland water courses. *Journal of the Institute of Water Engineering* 5, 400-406.

Corey, A.T., 1949, *Influence of shape on the fall velocity of sand grains*. Unpublished MS Thesis, A&M College, Colorado.

Cox, N.J., 1992, Precipitation statistics for Geomorphologists: variations on a theme by Frank Ahnert. *Catena Supplement*, 23, 189-212.

Crickmore, M.J., 1967, Measurement of sand transport in rivers with special reference to tracer methods. *Sedimentology* 8, 175-228.

Cui, B., Komar, P.D. & Baba, J., 1983, Settling velocities of natural sand grains in air. *Journal of Sedimentary Petrology*, 53, 1205-1211.

Daubree, A., 1879, *Etudes synthetiques de geologie experimentale*. Two volumes, Paris, Dunod.

Davis, A.P., 1900, Hydrography of Nicaragua. *US Geological Survey 20th Annual Report*, 1898-99, 20: 563-637.

Davies, T.R. H. & Pearce, A.J., 1981, Proc. Christchurch symposium on erosion and sediment transport in pasifirim steeplands. *International Association of Hydraulic Science Special Publication,* No. 132.

Dawson, M., 1988, Sediment size variation in a braided reach of the Sunwapta River, Alberta Canada. *Earth Surface Processes and Landforms*, 13, 599-618.

Diepenbroek, M., Bartholoma, A. & Ibbeken, H., 1992, How round is round? A new approach to the topic "roundness" by Fourier grain shape analyses. *Sedimentology*, 39, 411-422.

Dietrich, W.E., 1982, Settling velocity of natural particles. *Water Resources Research*, 18, 1615-1626.

Dietrich, W.E. & Kirchner, J.W., 1992, Friction angle measurements on a naturally formed gravel streambed: implications for critical boundary shear stress. *Water Resources Research*, 28, 411-425.

Dingman, S.L., 1984, *Fluvial hydrology*, New York, USA 383pp.

Dobkins, J.E., Jr & Folk, R.L., 1970, Shape development on Tahiti-nui. *Journal of Sedimentary Petrology,* 40, 1167-1203.

Dowdeswell, J.A., Osterman, L.E. & Andrews, J.T., 1985, Quartz sand grain shape and other criteria used to distinguish glacial and non-glacial events in a marine core from Forbisher Bay, Baffin Island, NWT, Canada. *Sedimentology,* 32, 119-132.

Drake, L.D., 1972, Mechanisms of clast attrition in basal till. *Geological Society of America Bulletin*, 83, 2159-2165.

Duff, P.M. & Smith, A.J., 1992, (Eds), *Geology of England and Wales*. The Geological Society, London, 651p.

Dunham, K.C., 1990, *Geology of the Northern Pennine Orefield*, Volume 1, Tyne to Stainmore. Economic Memoir of the British Geological Survey (2nd Edition). HMSO, London, 299p.

Eagleson, P.S. & Dean, R.G., 1961, Wave-induced motion of sediment particles. *Transactions of the American Society of Civil Engineering,* 126, 1162-1186.

Edward, F., Chacho, J.R., Robert, L. & William M.E., 1988, Detection of coarse sediment movement using radio transmitters. *U.S. Geological Survey, Water Resources Division, Denver, Colorado, USA*, pp. B-366-B-373.

Ehrenberger, R., 1932, Geschiebemessungen an Flussenmittels Auffanggeraten und Modellversuche mitletzeren (Bedload measurements in rivers by means of sediment traps and model experiments on the latter). *Wasserwirtschaft*, Heft 34.

Ehrlich, R. & Weinberg, B., 1970, An exact method for the characterisation of grain shape. *Journal of Sedimentary Petrology*, 40, 205-212.

Ehrlich, R., Orzeck, J. and Weinberg, B., 1974, Detrital quartz as a natural tracer-Fourier grain shape analysis. *Journal of Sedimentary Petrology*, 44, 145-150.

Ehrlich, R., Brown, P.J., Yarus, J.M. & Przygocki, R.S., 1980, The origin of shape frequency distribution and the relationship between shape and size. *Journal of Sedimentary Petrology*, 50, 475-483.

Einstein, H.A., 1950, The bedload function for sediment transportation in open channel flows. *US Department of Agriculture Soil Conservation Service Technical Bulletin, 1026.*

Emery, K.O., 1960, *The sea of the southern California a modern habitat of petroleum.* Wiley, New York, 366p.

Emmet, W. W., 1980a, A field calibration of the sediment-trapping characteristics of the Helley-Smith bedload sampler. *US Geological Survey Professional Paper*, 1139.

Emmet, W.W., 1980b, Bedload sampling in Rivers. *Proceeding of the International Symposium on River Sedimentation.* Beijing, China, Vol. 2: 991-1017.

Ergenzinger, P. & Conrady, J., 1982, A new tracer technique for measuring bedload in natural channels. *Catena*, 9, 77-80.

Ergenzinger, P.J. & Custer, S.G., 1982, First experiences measuring coarse material bedload transport with a magnetic device. *Mechanics of sediment transport (Proc. of Euromech.* 156, Summer, B.M. & Muller, A., Eds), 223-227.

Ergenzinger, P.J. & Custer, S.G., 1983, Determination of bedload transport using natural magnetic tracers: first experience at Squaw Creek, Gallatin Country, Montana. *Water Resource Research*, 19: 187-193.

Ergenzinger, P., Schmidt, K.H. & Busskamp, R., 1989, The Pebble Transmitter System (PETS) first result of a technique for studying coarse material erosion, transport and deposition. *Zeitschrift fur Geomorphologie* N.F., 33, 503-508.

Ergenzinger, P. & Schmidt, K.-H., 1990, Stochastic elements of bedload transport in a step-pool mountain river. in *Hydrology in Mountainous Regions.* II. *Artificial Reservoirs*; *Water & slopes*. Proc. Of Symposia, Lausanne, August, IAHS Publication, 194, 39-46.

Ergenzinger, P., 1992, Riverbed adjustments in a step-pool system: Lainbach, Upper Bavaria. In: Hey, R.D., Billi, P., Thorne, C.R. & Taconni, P. (eds), *Dynamic of Gravel-Bed Rivers*, Wiley, Chichester, pp. 415-430.

McEwan, I.K., Jefcoate, B.J. & Willetts, B.B., 1999, The grain-fluid interaction as a self-stabilising mechanism in fluvial bedload transport. *Sedimentology*, 46, 407-416.

Federal Inter-Agency River Basin Committee, 1940, Equipment used for sampling bedload and bed material. *Federal-Inter Agency River Basin Committee*, Report No. 2, 57 p.

Ferguson, R.I., 1981, Channel form and channel changes. In Lewin, J. (Ed), *British Rivers*, Allen & Unwin, London, 90-125.

Ferguson, R.I. & Ashworth, P.J., 1992, Spatial patterns of bedlaod transport and channel change in braided and near-braided rivers. *Dynamics of Gravel-bed Rivers*, Billi, P., Hey, R.D., Thorne, C.R. & Tacconi, P. (eds), Wiley, Chicester, pp. 477-496.

Ferguson, R.I., Hoey, T.B., Wathen, S.J., Werrity, A., Hardwick, R.I. & Sambrook Smith, G.H., 1998, Downstream fining of river gravels: integrated field, laboratory and modelling study. Gravel Bed Rivers in the Environment, Kingeman, P.C, Beschta, R.L., Komar, P.D. & Bradley, J.B. (eds), *Water Resources Publications,* Colorado, U.S.A. pp. 85-113.

Folk, R.L., 1968, *Petrology of sedimentary rocks*, Hemphill, Austin 170pp.

Folk, R.L., 1972, Experimental error in pebble roundness determination by the modified Wentworth method. *Journal of Sedimentary Petrology*, 42, 973-974..

Folk, R.L., 1977, A morphometric analysis of terrace gravels, California: comments. *Sedimentary Geology*, 19, 233-234.

Francis, J.R.D., 1973, Experiments on the motion of solitary grains along the bed of a water-stream. *Proceedings of the Royal Society of London*, A.332, 443-471.

Fripp, J.B. & Diplas, P., 1993, Surface sampling in gravel streams. *Journal of Hydraulic Engineering*, ASCE, 119, 473-4902.

Froehlich, W., 1982, Mechanizm transportu fluwialnego I dostawyzwietrzelin do koryta w gorskiej zlewni fliszowej (The mechanism of fluvial transport and waste supply into the stream channel in a mountainous flysch catchment). *Prace Geograficzne* 143.

Frostick, L.E. & Reid, I., 1982, Alluvial processes, mass wasting and slope evolution in arid environments. *Zeitschrift Fur Geomorph.* 44, 53-67.

Frostick, L.E., Lucas, P.M. & Reid, I., 1984, The infiltration of fine matrices into coarse-grained alluvial sediments and its implications for stratigraphical interpretation. *Journal Geological Society London*, 141, 955-965.

Gale, S.J., 1990, The shape of beach gravels. *Journal of Sedimentary Petrology*, 60, 787-789.

Gale, S.J. & Hoare, P.G., 1991, *Quaternary sediments: petrographic methods for the study of unlithified rocks*. Belhaven Press, London.

Garnett, P.W., 1966, Particle roundness and surface texture effects on fall velocity. *Journal of Sedimentology Petrology*, 36, 255-259.

Gary, M., McAfee, Jr, R. & Wolf, C.L. (Eds) 1972, *Glossary of Geology*. American Geological Institute, Washington, D.C.

Gintz, D. & Schmidt, K.-H., 1991, Grobgeschiebetranspor in einem Gebirgsbach als funktion von Gerinnebettform und Geschiebemorphometrie. *Zeitschrift fur Geomorphologie*, Supplementband, 89, 63-72.

Goldbery, R. & Richardson, D., 1989, The influence of bulk shape factors on settling velocities of natural sand-sized sedimentary suites. *Sedimentology*, 36, 125-136.

Gomez, B., 1983, Temporal variation in bedload transport rates: the effect of progressive bed armouring. *Earth Surface Processes and Landforms*, 8, 41-54.

Gomez, B., 1991, Bedload Transport. *Earth Science Reviews*, 31, 89-132.

Gomez, B & Church, M., 1989a, An assessment of bedload sediment transport formulae for gravel bed rivers. *Water Resources Research*, 25, 1161-1186.

Gomez, B. & Church, M., 1989b, A catalogue of equilibrium bedload transport data for sand and gravel-bed channels. *University of British Colombia, Department of Geography report*, 45.

Goossens, D., 1987, Interference phenomena between particle flattening and particle rounding in free vertical sedimentation processes. *Sedimentology*, 34, 155-167.

Gordon, N.D., McMahon, T.A. & Finlayson, B.L., 1992, *Stream Hydrology: An Introduction for Ecologists*. Wiley, Chichester, 526p.

Goudie, A. & Gardner, R., 1985, High Force: a remarkable cataract. In *Discovering the Landscape in England & Wales*. George Allen & Unwin, London, 18-19.

Graf, W.H., 1971, *Hydraulics of sediment transport*. McGraw-Hill, New York 513pp.

Gregory, K.J., 1977, (Ed), *River channel changes*. Wiley, Chichester, 448pp.

Gregory, K.J., 1979a, Fluvial Geomorphology. *Progress in Physical Geography* 3 (2) 274-282.

Gregory, K.J., 1979b, *River channels*. In Gregory K.G. & Walling, D.E. (Eds), Man and Environmental Processes; A physical geography Perspective, Dawson, Folkestone, 123-143.

Gregory, K.J. & Cullingford, R.A., 1974, Lateral variations in pebble shape in northwest Yorkshire. *Sediment Geology*, 12, 237-248.

Grogan, R.M., 1945, Shape variation of some Lake Superior beach pebbles. *Journal of Sedimentary Petrology*, 15, 3-10.

Haines, J. & Mazzullo, J.M., 1988, The original shape of quartz silt grains. *Marine Geology*, 78, 227-240.

Hallermieier, R.J., 1981, Terminal settling velocity of commonly occuring sand grains. *Sedimentology*, 28, 859-865.

Hassan, M. & Church, M., 1990, The movement of individual grains on bed streambed. *Dynamics of Gravel-bed Rivers*, Billi, P., Hey, R.D., Thorne, C.R. & Tacconi, P. (eds), Wiley, Chicester, pp. 159-175.

Hassan, M.A. & Reid, I., 1990, The influence of microform bed roughness elements on flow & sediment transport in gravel bed rivers. *Earth Surface Processes & Landforms*, 15, 739-750.

Hassan, M. & Church, M., 1992, The movement of individual grains on the streambed. In. Dynamics of Gravel-bed Rivers. *Dynamics of Gravel-bed Rivers*, Billi, P., Hey, R.D., Thorne, C.R. & Tacconi, P. (eds), Wiley, Chicester, pp. 159-173.

Hassan, M., Schick, A.P. & Laronne, J.B., 1984, The recovery of flood dispersed coarse sediment particles-a three-dimensional magnetic tracing method. *Catena Supplement*, 5, 153-162.

Hassan, M.A, Church, M. & Schick, 1991, Distance of movement of coarse particles in gravel bed streams. *Water Resources Research*. 27, No:4, 503-511.

Hassan, M.A., Church, M. & Ashworth, P.J., 1992, Virtual rate and mean distance of travel of individual clasts in gravel-bed channels. *Earth Surface Processes and Landforms*, 17, 617-627.

Hassan, M., Schick, A.P. & Shaw, P.A., 1999, The transport of gravel in an ephemeral sandbed river. *Earth Surface Processes and Landforms*, 24, 623-640.

Hayward, J.A., 1980, *Hydrology and stream sediment from Torlesse Stream Catchment.* Special Publication 17, Tussock Grasslands and Mountain Lands Institute, Lincoln College, Canterbury, New Zealand, 236pp.

Helley, E.J., 1969, Field measurement of the initation of large motion in Blue Creek near Klamath, California. *United States Geological Survey Professional paper* 256-G.

Helley, E.J. & Smith, W., 1971, Development and calibration of a pressure-difference bedload sampler. *U.S. Geological Survey Open-file Report.*

Herschy, R.W.(Ed.), 1999, *Hydrometry.* Wiley, Chichester, England, 376pp.

Hey, R.D., Bathurst, J.C. & Thorne, C.R., 1982, *Gravel-bed rivers: fluvial processes, engineering and management.* Chichester: John Willey & Sons Ltd. 875p.

Hockey, B., 1970, An improved coordinate system for particle shape representation. *Journal of Sedimentary Petrology*, 40, 1054-1056.

Hoey, T.B., 1989, Reconstruction of the recent flow history of a braided gravel river. *Journal of Hydrology of New Zealand,* 28, 76-97.

Hoey, T.B., 1992, Temporal variations in bedload transport rates and sediment storage in gravel-bed rivers. *Progress in Physical Geography*, 16,3, 319-338.

Hoey, T.B. & Ferguson, R.I., 1994, Numerical modelling of downstream fining by selective transport in gravel bed rivers: model development and illustration. *Water Resources Research*, 30, 2251-2260.

Hooke, J.M., 1995, Processes of channel planform change on meandering channels in the UK. In Gurnell, A. and Petts, G. (Eds) *Changing River Channels.* Wiley, Chichester, Britain.

Hottovy, J.D. & Sylvester, N.D., 1979, Drag coefficient for irregularly shaped particles. *Ind. Engng Chem. Processes Des. Dev.* 18, 433-436.

Hubbel, D.W., 1964, Apparatus and techniques for measuring bedload. *US Geological Survey Water-Supply Paper*, 1748.

Hubbel, D.W. & Sayre, W.W., 1964, Sand transport studies with radioactive tracers. *Journal of Hydraulic Division*, 90, 39-68.

Huddart, D., 1994, Rock-type controls on downstream changes in clast parameters in sandur systems in Southeast Iceland. *Journal of Sedimentary Research*, 64, 2, 215-225.

Iseya, F. & Ikeda, H., 1987, Pulsations in bedload transport rates induced by a longitudinal sediment sorting: a flume study using sand and gravel mixtures. *Geografiska Annaler*, 69A, 15-27.

Jackson, W.L. & Beschta, R.L., 1982, A model of two-phase bedload transport in an Oregon Coast Range stream. *Earth Surface Processes and Landforms*, 7, 517-528.

Johansson, C.E., 1976, Structural studies of frictional sediments. *Geografiska Annaler*, 58 210-301.

Johnson, G.A.L. & Dunham, K.C., 1963, The geology of Moor House. *Monographs of the Nature Conservancy Council Number Two*. HMSO, London, 182p.

Johnson, G.A.L. & Hickling, G., 1970, Geology of Durham County. *Transactions of the Natural History Society of Northumberland, Durham and Newcastle upon Tyne.* 41, 1.

Jong, C. & Ergenzinger, P., 1995, The interrelationship between mountain valley form and river-bed arrangement. In Hickin, E.J. (Ed.) *River Geomorphology*. Wiley, Chichester, Britain.

Kaye, B.H., 1978, Specification of the ruggedness and/or texture of a fine particle profile by its fractal dimension. *Powder Technology*, 21, 207-213.

Keller, E.A., 1970, Bedload movement experiments, Dry Creek, California. *Journal of Sedimentary Petrology*, 40, 1339-1344.

Kennedy, S.K. & Ehrlich, R., 1985, Origin of shape changes of sand and silt in a high-gradient stream system. *Journal of Sedimentary Petrology*, 55, 57-64.

Kennedy, S.K. & Lin, W.H., 1991, A comparison of Fourier and Fractal techniques in the analysis of closed forms. *Journal of Sedimentary Petrology*, 62, 842-848.

King, C.A.M., 1966, *Techniques in Geomorphology*. Arnold, London, 342 p.

King, C.A.M. & Buckley, J.T., 1968, Analysis of stone size and shape in Arctic environments. *Journal of Sedimentary Petrology*, 38, 200-214.

Kirchner, J.W., Dietrich, W.E., Iseya, F. & Ikeda, H., 1990, The variability of critical shear stress, friction angle, and grain protrusion in water-worked sediments. *Sedimentology*, 37, 647-672.

Klein, M., 1976, The influence of drainage area in producing threshold for the hydrological regime and channel characteristics of natural rivers. *Working Paper* No. 147, Department of Geography, University of Leeds, 97 pp.

Klingeman, P.C. & Emmett, W.W., 1982, Gravel bedload transport processes. In Gravel-bed Rivers, Hey, R.D., Bathurst, J.C. & Thorne, C.R. (eds), Wiley, Chichester, pp. 141-169.

Knighton, A.D., 1980, Longitudinal changes in size and sorting of stream-bed material in four English Rivers. *Geological Society of America, Bulletin,* 91, 55-62.

Knighton, A.D., 1982, Longitudinal changes in the size and shape of stream bed material: evidence of variable transport conditions. *Catena*, 9, 25-34.

Knighton, D., 1998, *Fluvial form and processes*. Wiley, London, 383p.

Kodama, Y., 1992, *Effect of abrasion on downstream gravel-size reduction in the Waterase River, Japan: fieldwork and laboratory experiments*. Environmental Research Center, The University of Tsukuba, Japan, pp. 88.

Komar, P.D., 1987, Selective grain entrainment by a current from a bed of mixed sizes: a reanalysis: Journal of Sedimentary Petrology, 57, 203-211.

Komar, P.D. & Reimers, C.E., 1978, Grain shape effects on settling rates. *Journal of Geology*, 86, 193-205.

Komar, P.D. & Li, Z., 1986, Pivoting analyses of the selective entrainment of sediments by shape and size with application to gravel threshold. *Sedimentology,* 33, 425-436.

Komar, P.D. & Li, Z., 1988, Applications of grain pivoting and sliding analysis to selective entrainment of gravel and to flow-competence evaluations. *Sedimentology*, 35, 681-695.

Komar, P.D. & Carling, P.A., 1991, Grain sorting in gravel-bed streams and the choice of particle sizes for flow-competence evaluations. *Sedimentology*, 38, 489-502.

Komar, P.D. & Wang, C., 1984, Processes of selective grain transport and the formation of placers on beaches. *Journal of Geology*, 92, 637-655.

Krumbein, W.C., 1941a, The effect of abrasion on the size, shape, and roundness of rock fragments. *Journal of Geology*, 49, 482-520.

Krumbein, W., 1941b, Measurenents and geological significance of shape and roundness of sedimentary particles. *Journal of Sedimentary Petrology,* 11, 64-72.

Krumbein, W., 1942, Settling-velocity and flume-behaviour of non-spherical particles. *Transactions of the American Geophysical Union*, 65, 621-633.

Krumbein, W.C. & Sloss, L.L., 1955, *Stratigraphy and sedimentation*. W.H. Freeman, San Fransisco. 660pp.

Kuenen, P.H., 1956, Experimental abrasion of pebbles. 2. Rolling by current. *Journal of Geology*, 64, 336-368.

Lane, E.W., 1938, Notes on the formation of sand. *Transaction American Geophysics Union. 18, 505-508.*

Lane, E.W. & Borland, W.M., 1951, Estimation of bedload. *Transaction American Geophysics Union*, 32 (1), 121-123.

Lane, E.W. & Carlson, E.J., 1954, Some observations on the effect of particle shape on the movement of coarse sediments. *Transaction, American Geophysical Union*, 35, 453-462.

Lane, S.N. & Richards, K.S., 1995, Within-reach spatial patterns of process and channel adjustment. In Hickin, E.J. (Ed.) *River Geomorphology*. Wiley, Chichester, Britain.

Laronne, J.B. & Carson, M.A., 1976, Interrelationship between bed morphology and bed material transport for a small gravel-bed channel. *Sedimentology*, 23, 67-85.

Laronne, J.B. & Duncan, M.J., 1992, Bedload transport paths and gravel bar formation. *Dynamics of Gravel-bed Rivers*, Billi, P., Hey, R.D., Thorne, C.R. & Taconni, P. (eds), Wiley, Chicester, pp. 177-202.

Lauffer, H. & Sommer, N., 1982, Studies on sediment transport in mountain streams of the eastern Alps. *Proc 14 Congress International Commission on Large Dams*. Rio De Janeiro, Brazil, pp. 431-453.

Lechalas, M., 1871, Sur les rivieres a fond de sable (on sand bed rivers). *Mem. Doc. Ann. Ponts Chaussees*, 5th, Ser., 1: 381-431.

Lees, G., 1964, A new method for determining the angularity of particles. *Sedimentology*, 3, 2-21.

Lenzi, M.A., D'Agostino, V. & Billi, P., 1999, Bedload transport in the instrumented catchment of the Rio Cordon; Part I: Analyses of the bedload records, conditions and threshold of bedload entrainment. *Catena*, 36, 171-190.

Leopold, L. B. & Emmet, W.W., 1981, Some observations on the movement of cobbles on a streambed. *Int. Ass. Hydr. Sci., Proc. Florence Symp.*, 22-26 June 1981, pp. 49-59.

Leopold, L.B., Wolman, M.G. and Miller, J.P., 1964, *Fluvial processes in geomorphology*. Freeman, San Fransisco, pp. 522.

Leopold, L. B., Emmet, W.W. and Myrick, R.W. 1966, Channel and hillslope processes in a semi-arid area, New Mexico. *U.S. Geological Survey Professional Paper*, 352G.

Lewin, J., 1981, (ed.) *British Rivers*. Wiley, Chichester, pp. 35-55, Chapters 2 and 3.

Li, Z. & Komar, P., 1986, Laboratory measurements of pivoting angles for applications to selective entrainment of gravel in a current. *Sedimentology,* 33, 413-423.

Li, M.Z. & Komar, P.D., 1992a, Longshore grain sorting and beach placer formation adjacent to the Colombia River. *Journal of Sedimentary Petrology*, 62, 429-441.

Li, M.Z. & Komar, P.D, 1992b, Selective entrainment and transport of mixed size and density sands: flume experiments simulating the formation of the black sand placers. *Journal of Sedimentary Petrology*, 62, 584-590.

Macklin, M.G., 1997, Fluvial Geomorphology of north-east England. In Gregory, K.J. (Ed.) Fluvial Geomorphology of Great Britain. *Geological conservation Review series.* Chapman Hall, London, Chapter 5, 203-238

Macklin, M.G. & Rose, J., 1986, *Quaternary river landforms and sediments in Northern Pennines, England: Field Guide,* British Geomorphological Research Group / Quaternary Research Association, 88p.

Manley, G., 1942, Meteorological observations on Great Dunn Fell, a mountain station in northern England. *Quarterly Journal of the Royal Meteorological Society*, 68, 151-165.

Manley, G., 1943, Further climatological averages from the northern Pennines, with a note on topographical effects. *Quarterly Journal of the Royal Meteorological Society*, 69, 251-261.

Mandelbrot, B.B., 1967, How long is the coastline of Britain? Statistical self-similarity and frictional dimension. *Science*, 155, 636-638.

Mandelbrot, B.B., 1977, *Fractals: form, Change and Dimensoin.* W.H. Freeman, San Fransisco.

Mandelbrot, B.B., 1982, *The fractal geometry of nature.* W.H. Freeman, San Francisco. 460pp.

Marshall, P., 1927, The wearing of beach gravels. *New Zealand Institution Transaction,* 58, 507-532.

Mazzullo, J.M., Ehrlich, R. & Pilkey, O.H., 1983, Local and distal origin of sands in the Hatteras Abyssal Plain. *Marine Geology*, 48, 75-88.

Mazzullo, J.M., Sims, D. & Cunningham, D., 1986, The effects of eolian sorting and abrasion on the shapes of fine quartz and sine grains. *Journal of Sedimentary Petrology*, 56, 45-56.

Mazzullo, J.M., Alexander, A., Tieh, T. & Menglin, D., 1992, The effect of wind transport on the shapes of quartz silt grains. *Journal of Sedimentary Petrology*, 62, 961-971.

McNown, J.S. & Malaika, J., 1950, Effect of particle shape on settling velocity at low Reynolds numbers. *Transaction American Geophysics Union.* 31, 74-82.

Meade, R.H., Yuzyk, T.R. & Day, J.T., 1990, Movement and storage of sediment in rivers of the United States and Canada. In: M.G. Wolman and H.C. Riggs (Eds), Geology of North America: Surface Water Hydrology. *Geological Society of America.*, Boulder, CO, 255-280.

Meland, N. & Norrman, J.O., 1966, Transport velocities and single particles in bedload motion. *Geografiska Annaler.* 48, 165-182.

Meland, N. & Norrman, J.O., 1969, Transport velocities of individual size fractions in heterogeneous bed load *Geografiska Annaler*, 51, 127-144.

Meyer-Peter, E. & Muller, R., 1948, Formulas for bedload transport. *Intl. Assoc. for Hydraulic Structures Research, Report of the Second Meeting, Stockholm*, 1948, pp. 39-64.

Middleton, G.V. & Southard, J.B., 1978, *Mechanics of sediment transport.* Lecture notes for short course No. 3. McMaster University, Binghampton, New York, 120pp.

Milhous, R.T., 1972, The movement of individual particles in a gravel bottomed stream. Paper presented at *the Northwest Regional American Geophysical Union Meeting*, Vancouver, B.C., October 1972.

Miller, R.L., & Byrne, R.J., 1966, The angle of repose for a single grain on a fixed rough bed. *Sedimentology*, 6, 303-314.

Mills, H.H., 1979, Downstream rounding of pebbles a quantitative review. *Journal of Sedimentary Petrology*, 49, 0295-0302.

Mitchell, W.A., 1991, Western Pennines: *Field Guide.* Quaternary Research Association, London, 124p.

Morisawa, M., 1968, *Streams: Their dynamics and morphology.* McGraw-Hill, London, 175pp.

Moriwaki, H., Nogami, M., Hatsumi. & Inoue, Y., 1985, Relationship between size characteristics of the Yahagi River bed materials and rock-forming mineral grains of source rocks in the drainage basin. *Geological Review of Japan*, 53, 557-573. (in Japanese with English abstract).

Naden, P., 1988, Models of sediment transport in natural streams, in Anderson, M.G. (Ed), *Modelling Geomorphological System*, 217-258.

Nelson, D.E. & Coakley, J.P., 1974, Techniques for tracing sediment movement. Inland Waterws. *Dir., Con. Sci. Ser.Rep.*, 32.

Nesper, F., 1937, Ergebnisse der Messunger uber die Geschiebe- und Schlammfuhrung des Rheins an der Brugger Rheinbrucke [Results of bedload and silt movement observations on the Rhine at the Brugg Bridge]. *Schweiz. Bauz.*, Heft 110.

Newson, M.D., 1979, Framework for field experiments in mountain areas of Great Britain. *Studia Geomorphologica Carpatho-Balcanica*, 13, Krakow.

Newson, M.D., 1980, The geomorphological effectiveness of floods - a contribution stimulated by two recent events in mid-Wales. *Earth Surface Processes & Landforms*, 5, 1-16

Newson, M.D., 1981, Mountain streams, in *British Rivers*, Lewin, J. (Ed), Wiley, Chichester, pp. 59-89.

Nir, D., 1964, Les processus erosifs dans le Nahal Zine (Neguev septentrional) pendant les saisons pluvieuses. *Annales de geographie*, 73, 8-20.

O'Leary, S.J. & Beschta, R.L., 1981, Bedload transport in an Oregon Coast Range stream. *American Water Resources Association, Water Resources Bulletin.* 17 (5), 886-894.

Oldfield, P., Thompson, F.R. & Dickson, D.P.E., 1981, Artificial enhancment of stream bedload: a hydrological application of superparamagnetism. *Physics of the Earth and Planetary Systems* 26, 107-124.

Orford, J.D., 1981, Particle form. 86-90 In Goudie, A. (ed) *Geomorphological Techniques.* George Allen and Unwin, London. 395pp.

Orford, J.D. & Whalley, W.B., 1983, The use of fractal dimensions to quantify the morphology of irregular-shaped particles. *Sedimentology*, 30, 655-668.

Orford, J.D. & Whalley., W.B., 1991, *Quantitative grain form analysis . In Syvitzki J. (ed.) Principles, Methods and Application of Particle Size analysis,*. Cambridge University Press, Cambridge, pp. 88-108.

Park, C.C., 1995, *Channel cross-section change.* In Gurnell, A. and Petts, G. (Eds) Changing River Channels. Wiley, Chichester, Britain.

Parker, G., 1991a, Selective sorting and abrasion of river gravel. I : Theory. *Journal of Hydraulic Engineering,* 117, 131-149.

Parker, G., 1991b, Selective sorting and abrasion of river gravel. II : Application. *Journal of Hydraulic Engineering,* 117, 150-171.

Parker, G. & Klingeman, P.C., 1982, On why gravel bed streams are paved. *Water Resources Research*, 18, 1409-1423.

Parker, G., Klingeman, P.C. & McLean, D.G., 1982, Bedload and size distribution in paved gravel-bed streams, *Journal of Hydraulic Division, American Society of Civil Engineering*, 108: 544-571.

Pashinskiy, A.F., 1964, Experience of the study of alluvial deposits of the Psezuapse River. *Soviet Hydrology*, 3, 156-173.

Pearce, A.J. & Watson, A., 1983, Medium-term effects of two landsliding episodes on channel storage of sediment. *Earth Surface Processes and Landforms.* 8, 29-40.

Peel, R.F., 1949, A study of two Northumbrian spillways. *Transactions of the Institute of British Geographers*, 15. 13-89.

Pettijohn, F.J., 1957, *Sedimentary rocks. (Second Edition)*, Harper and Bros., New York. 718p.

Petts, G.E., 1983, *Rivers*. Butterworths, London. pp. 228.

Pitty, A.F., 1971, *Introduction to Geomorphology*. London: Methuen.pp.526.

Plumley, W.J., 1948, Blackhills terrace gravels: a study in sediment transport. *Journal of Geology*, 56, 526-577.

Potter, P.E., 1955, The petrology and origin of the Lafayette gravel. *Journal of Geology*, 63, 1-38.

Pounder, E., 1989, *Classic landforms of the Northern Dales*. Classic Landforms Guides No.10. Geomorphological Association, 48p.

Powers, M.C., 1953, A new roundness scale for sedimentary particles. *Journal of Sedimentary Petrology*, 23, 117-119.

Proffit, G.T. & Sutherland, A.J., 1983, Transport of non-uniform sediments. *Journal of Hydraulic Research*, 21, 33-43.

Pryor, W.A., 1971, Grain Shape. 131-150 in Carver, R.E. (ed) *Procedures in Sedimentary Petrology*. John Wiley, New York. 653pp.

Pye, K., 1994a, *Properties of sediment particles in*: Sediment transport and depositional processes. Blackwell Scientific Publications. Oxford, pp.1-24.

Pye, K., 1994b, Shape sorting during wind transport of quartz silt grains-discussion. *Journal of Sedimentary Research*, A64, 704-705.

Proffit, G.T. & Sutherland, A.J., 1983, Transport of non-uniform sediments. *Journal of Hydraulic Research*, 21, 33-43.

Rayleigh, L., 1942, The ultimate shapes of pebbles, natural and artificial. *Proceedings of the Royal Society of London*, 181, 107-118.

Rayleigh, L., 1944, Pebbles, natural and artificial. Their shape under various conditions of abrasion. *Proceedings of the Royal Society of London*, Series A., 182, 321-335.

Reichelt, G., 1961, Uber Schotterformen und Rundungsgradanalyse als Feldmethode. *Petermanns Geogr. Mitt.*, 105, 15-24.

Reid, I., Layman, J.T. & Frostick, L.E., 1980, The continuous measurement of bedload discharge. *Journal of Hydrological Research*, 18, 243-249.

Reid, I., Brayshaw, A.C. & Frostick, L.E., 1984, An electromagnetic device for automatic detection of bedload motion and its field applications. *Sedimentology*, 31, 269-276.

Reid, I., Frostick, L.E. & Layman, J.T., 1985, The incidence and nature of bedload transport during flood flows in coarse-grained alluvial channels. *Earth Surface Processes and Landforms*, 10, 33-44.

Reid, I., Frostick, L.E. & Brayshaw, A.C., 1992, Microform roughness elements and the selective entrainment and entrapment of particles in gravel-bed rivers', *Dynamics of Gravel-bed Rivers*, Billi, P., Hey, R.D., Thorne, C.R. & Tacconi, P. (eds), Wiley, Chichester, pp. 253-275.

Reid, I., Bathurst, J.C., Carling, P.A., Walling, D.E. & Webb, B.W., 1997, Sediment erosion, transport and deposition. *Applied Fluvial Geomorphology for River Engineering and Management*. Thorne, C.R., Hey, R.D. & Newson, M.D. (eds), Wiley, Chichester, pp. 95-135.

Rittenhouse, G., 1943, A visual method of estimating two dimentional sphericity. *Journal of Sedimentary Petrology*, 13, 79-81.

Ritter, J.R., 1967, Bed-Material movement, Middle Fork Eel River, California. *United States Geological Survey Professional Paper* 423-C.

Robert, A., 1990, Boundary roughness in coarse-grained alluvial channels. *Progress in Physical Geography,* 14, 42-70.

Romanovskij, V.V., 1966, A study of the fall velocity of coarse sediment. *Soviet. Hydrology,* 5, 47-62.

Rosenfeld, M.A. & Griffiths, J.C., 1953, An experimental test of visual comparision techniques in estimating two dimensional sphericity and roundness of quartz grains. *American Jeological Science*, 251, 553-585.

Rummery, T.A., 1981, *The effects of fire on soil and sediment magnetism.* Unpublished PhD. Thesis, University of Liverpool.

Rummery, T.A., Bloemendal, J., Oldfield, F. & Thompson, R., 1979, The persistence of fire-induced magnetic oxides in soil and lake sediments. *Annaler Geophysics*, 35: 103-107.

Russell, R. D. & Taylor, R.E., 1937, Roundness and shape of Mississippi River sands. *Journal of Geology*, 43, 225-267.

Sames, C.W., 1966, Morphometic data of some recent pebble associations and their application to ancient deposits. *Journal of Sedimentary Petrology*, 36, 126-142.

Sarmiento, A., 1945, *Experimental study of pebble abrasion.* Unpublished Master's dissertation, Department of Geology, University of Chicago.

Schick, A.P., 1970, Desert floods: interim result of observations in the Nahal Yael research watershed, Southern Israel, 1965-1970. *International Association of Scientific Hydrology, Publication* 96, 478-493.

Schick, A.P. & Sharon, D., 1974, *Geomorphology and Climatology of an Arid Watershed.* Department of Geography, Hebrew University of Jerusalem, 161pp.

Schick, A.P., Hassan, M.A. & Lekach, J., 1998, A vertical exchange model for coarse bedload movement – numerical considerations. *Catena Supplement*, 10, 73-83.

Schmeeckle, M.W., 1998, *Mechanics of bedload sediment transport.* PhD thesis, University of Colorado, 181pp.

Schmidt, H.K. & Ergenzinger, P., 1990, Magnettracer und Radiotracer – Die Leistungen neuer Meßsysteme in der fluvialen Dynamik. *Die Geowissenschaften*, 8, 96-102.

Schmidt, H.K. & Ergenzinger, P., 1992, Bedload entrainment travel lengths, step lengths, rest periods - studied with passive (iron, magnetic) and active (radio) tracer techniques. *Earth Surface Processes and Landforms*, 17, 147-165.

Schmidt, H.K. & Gintz, D., 1995, Results of bedload tracer experiments in a mountain river. River Geomorphology. In Hickin, E.J. (Ed.) River Morphology. John Wiley & Sons Ltd, Chichester.

Schneiderhohn, P., 1954, Eine vergleichende studie uber methoden zur quantitativen Bestimmung von Abrundung und Form an Sandcornern. *Heidelberger Beitrage Zur Min. u. Pet.* 4, 172-191.

Schoklitsch, A., 1962, *Handbuch des Wasserbaues*, 3rd edn, Springer-Verlag, Vienna.

Schwarcz, H.P. & Shane, K.C., 1969, Measurement of particle shape by fourier analysis. *Sedimentology,* 13, 213-231.

Sear, D.A., Lee, M.W.E., Collins, M.B. & Carling, P.A., 1998, Development in coarse sediment tracing: A review, Paper presented at the British Geomorphological Research Group Annual Conference, *Tracers in Geomorphology*, 18th-20th September 1998, Coventry University, 33 pp.

Shakesby, R.A., 1980, Field measurement of roundness: a review. *Universit College of Swansea, 11, 27-36*

Shakesby, R.A., 1989, A simple device for measuring the primary axes of clasts. *British Geomorphological Research Group, Technical Bulletin*, 24.

Shamov, G.I., 1935, Kratkoye soobshshyeniye o resultatakh laborarornikh isslyedovahii batomyetrov [Brief information regarding the results of laboratory testing of silt samplers]. *Trans. Sci. Res. Inst. Hydrotech.*, USSR, 16: 218-220.

Shaw, E.M., 1994, *Hydrology in practice* (2nd Edition). Chapman & Hall, London, 569p.

Shields, A., 1936, Anwendungder Ahnlichkeitsmechanik und der Turbulenzforschung auf die Geschiebebewegung. *Mitt. Preuss. Vers. Anst. Wasserb. Schiffb*, 36, 26pp (translated by W.P. Ott & J. C. van Uchelen, U.S. Department of Agriculture, Soil Conservation Servise Coop Laboratory, California Institute of Technology).

Shih, S.M. & Komar, P.D., 1990, Differential bedload transport rates in a gravel bed stream: A grain size distribution aproach. *Earth Surface Processes and Landforms*, 15, 539-552.

Simithson, P.A., 1985, The present climate of the Northern Pennines. In Boardman, J. (Ed.) *Field Guide to the Periglacial Landforms of Northern England.* Quaternary Research Association, Cambridge, 1-3.

Simons, D.B. & Senturk, F., 1977, *Sediment Transport Technology*. Water Resources Publications, Fort Collins, Colorado, 807pp.

Simons, D.B. & Simons, R.K., 1987, Differences between gravel- and sand bed rivers. in *Sediment Transport in Gravel-bed Rivers*, Thorne, C.R. Thorne, J.C. & Hey, R.D. (eds), Wiley, Chichester, pp. 3-15.

Slaymaker, H.O., 1972, Patterns of present sub-aerial erosion and landforms in mid-Wales. *Transactions Institute of British Geographers*, 55, 47-68.

Slingerland, R.L., 1977, The effects of entrainment on the hydraulic equivalence relationship of light and heavy minerals in sands. *Journal of Sedimentary Petrology*, 47, 753-770.

Smalley, I.J., 1966, The expected shape of blocks and grains. *Journal of sedimentary Petrology*, 36, 626-629.

Sneed, E.D. & Folk, R.L., 1958, Pebbles in the lower Colorado River, Texas: a study in particle morphogenesis. *Journal of Geology*, 66, 114-150.

Sorby, H.C., 1980, On the structure and origin of non-calcareous stratified rocks. *Quaterly Journal Geological Society of London*, 36, 46-92.

Steidtmann, J.R., 1982, Size-density sorting of sand-size spheres during deposition from bedload transport and implications concerning hydraulic equivalence. *Sedimentology*, 29, 877-883.

Stott, T. & Sawyer, A., 1998, Clast travel distances and abrasion rates in coarse upland channels determined using magnetically tagged bedload tracers. Paper presented at the British Geomorphological Research Group Annual Conference, *Tracers in Geomorphology*, 18th-20th September 1998, Coventry University.

Stratten, T., 1974, Notes on the application of shape paramaters to differentiate between beach and river deposits in southern Africa. *Transactions of the Geological society South Africa*, 77, 59-64.

Stringham, G.E. & Guy, H.P., 1969, The behaviour of large particles falling in quiescent liquids. *U.S. Geological Survey Professional Paper*, 562-C, 36.

Summerfield, M.A., 1991, *Global Geomorphology*. Longman Scientific and Technical, Wiley, England, 537pp.

Sundborg, A., 1956, The River Klaralven a study of fluvial processes. *Geografiska Annaler*, 38 127-316.

Swan, B., 1974, Measures of particle roundness: a note. *Journal of Sedimentary Petrology*, 44, 572-577.

Swanson, F.J., Janda, R.J., Dunne, T. & Swanston, D.N. (eds) 1982, Sediment butchet and routing in forested drainage basins. Report PNW-141, *US Department of Agriculture Forest Service, Pacific Northwest Forest and Range Experiment Station*, 165pp.

Swiss Federal Authority for Water Utilization, 1939, Untersuchungen in der Natur uber Bettbildung, Geschiebe- und Schwebestoffuhrung [Fieald research on bed formations, bedload and suspended load movement]. *Mitt. Nr.* 33 Amtes Wasserwirtschaft.

Szadeczky-Kardoss, E.V., 1933, Die bestimmung des abrollungsgrades. *Zentbl. Miner.*, B, 389-401.

Taconni, P. & Billi, P., 1987, Bedload transport measurement by the vortex trap on Virginio Creek, Italy. In: C.R. Thorne, J.C. Bathurst and R.D. Hey (Editors), *Sediment Transport in Gravel-bed Rivers*. Wiley, Chichester, pp. 583-616.

Takayama, S., 1965, Bedload movement in torrential mountain streams. *Tokyo Geographical paper* 9, 169-188 (Japanese).

Taylor, B.J., Burgess, I.C., Mills, D.A.C., Smith, D.B. & Warren, M.A., 1971, *Northern England* (Fourth Edition). British Regional Geology. Natural Environment Research Council, Institute of Geological Sciences, HMSO, London, 125p.

Thompson, R.D., Mannion, A.M., Mitchell, C.W., Parry, M. & Townshend, J.R.G., 1992, *Processes in physical geography*. Longman Scientific and Technical, Wiley, England, 380pp.

Thorne, C.R. & Lewin, J., 1982, Bank processes, bed material movement and planform development in a meandering river. In: *Adjustments of the Fluvial System* (Ed. by D. D. Rhodes and G. P. Williams), pp. 117-137. Allen & Unwin, London.

Tonnard, V., 1963, Criteres de sensibilite appliques aux indices de formes des grains de sable, *in Developments in Sedimentology* (ed. van Straaten), 1, 410-416.

Unrug, R., 1957, Recent transport and sedimentation of gravels in the Dunajec valley (western Carpathians). *Acta Geologica Polonica,* 7, 217-257.

Wadell, H., 1932, Volume shape, and roundness of rock particles. *Journal of Geology,* 40, 443-451.

Wadell, H., 1934, The coefficient of resistance as a function of Reynolds number for solids of various shapes. *Journal of Franklin Institution*, 217, 459-490.

Wadell, H., 1935, Volume, shape and roundness of quartz particles. *Journal of Geology,* 43, 250-280.

Warburton, J., 1998, General description of the north Pennine upland region *Geomorphological studies in the North Pennines: Field Guide.* British Geomorphological Research Group, 104p.

Warburton, J. & Evans, M.G., 1998, Preliminary estimates of bedload yield from the Moor House National Reserve. *Geomorphological studies in the North Pennines: Field Guide.* British Geomorphological Research Group, 104p.

Wentworth, C.K., 1919, A laboratory and field study of cobble abrasion. *Journal of Geology,* 27, 507-522.

Wentworth, C.K., 1922a, A method of measuring and plotting the shapes of pebbles. U.S. *Geological Survey Bulletin,* 730. pp. 91-102.

Wentworth, C.K., 1922b, A field study of the shapes of river pebbles. *U.S. Geological Survey Bulletin,* 730. pp. 103-114.

Whalley, W.B., 1972, The description and measurement of sedimentary particles and the concept of form. *Journal of Sedimentary Petrology*, 4, 961-965.

Whalley, W.B. & Orford., 1983, Analysis of S.E.M. images of sedimentary particles and the concept of form by fractal dimension and Fourier analysis methods. *Scanning Electron Microscope* 1982, II, 961-965.

White, C.M., 1940, The equilibrium of grains on the bed of a stream. *Proceeding Royal Society of London*, A174, 332-338.

White, W.A. & Day, T.J., 1982, *Transport of graded gravel bed material.* In: R.D. Hey, J.C. Bathurst and C.R. Thorne (eds), Gravel-Bed Rivers. Wiley, Chichester, pp.181-213.

Whiting, P.J., Dietrich, W.E., Leopold, L.B., Shreve, R.L. & Drake, T., 1988, Bedload sheets in heterogeneous sediment. *Geology*, 16, 105-108.

Wiberg, P.L. & Smith, J.D., 1987, Calculations of critical shear stress for motion of uniform and heterogeneous sediments. *Water Resources Research*, 23, 1417-1480.

Wilcock, D.N., 1971, Investigation into the relations between bedload transport and channel shape. *Geological Society of America, Bulletin* 82, 2159-2176.

Wilcock, P.R., 1988, Methods for estimating the critical shear stress of individual fractions in mixed-sized sediment. *Water Resources Research*, 24, 1127-1135.

Wilcock, P.R. & Southard, J.B., 1989, Experimental study of incipient motion in mixed-sized sediment. *Water Resources Research*, 24, 1137-1151.

Wilde, R.H., 1952, *Effect of shape on the fall velocity of grain-sized particles*. MSc thesis, Colorado, 86pp.

Willetts, B.B. & Rice, A., 1983, Practical representation of characteristic grain shape of sand: a comparison of methods. *Sedimentology,* 30, 557-565.

Willmarth, W.W., Hawk, N.E., & Harvey, R.L., 1964, Steady and unsteady motions and wakes of freely falling discs. *Physical Fluids*, 7, 197-208.

Wilson, L. & Huang, T.C., 1979, The influence of shape on the atmospheric settling velocity of volcanic ash particles. *Earth and Planetary Science Letters*, 44, 311-324.

Wilson, P. & Clark, R., 1995, Landforms associated with a Loch Lomond Stadial glacier at Cronkley Scar, Teesdale, northern Pennines. *Proceedings of the Yorkshire Geological Society*, 50, 4, 277-283.

WMO (1980), *Manual on Stream Gaugin, Volume I: Fieldwork, Volume II: Computation of Discharge*. Operational Hydrology Report No. 13, WMO No. 519, Secretariat of the World meteorological Organisation, Geneva, Switzerland.

Wolman, M.G., 1954, A method of sampling coarse river-bed material. *Transactions of the American Geophysical Union*, 35, 951-955.

Zingg, T.H., 1935, Beitrag zur Schotteranalyse: Schweizische *Mineralogie und Petrographie Mitteilungen*, 15, 39-140.